Neural Plasticity

Hearing Loss: Reestablish the Neural Plasticity in Regenerated Spiral Ganglion Neurons and Sensory Hair Cells

Guest Editors: Renjie Chai, Genglin Li, Jian Wang, and Jing Zou

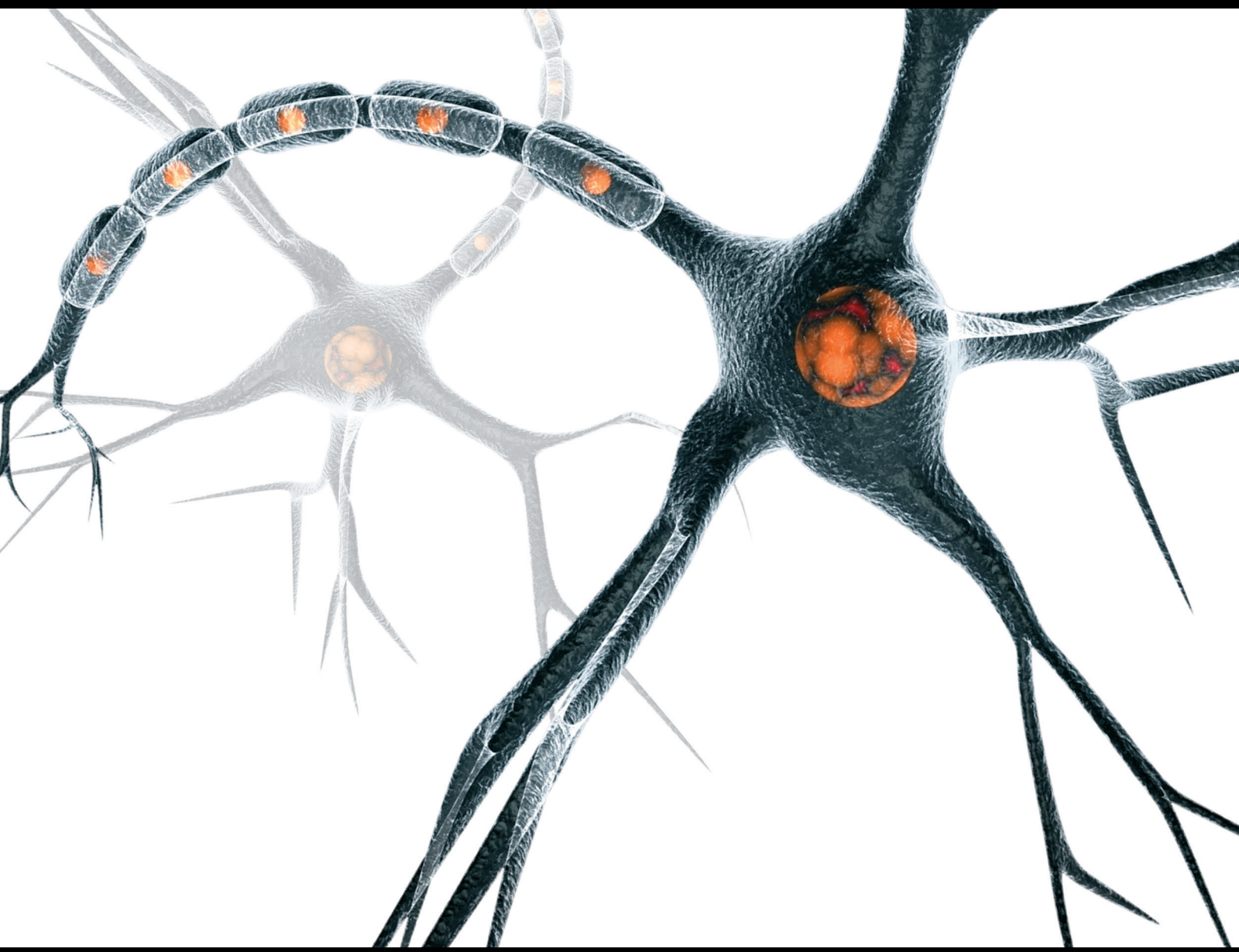

Hearing Loss: Reestablish the Neural Plasticity in Regenerated Spiral Ganglion Neurons and Sensory Hair Cells

Neural Plasticity

Hearing Loss: Reestablish the Neural Plasticity in Regenerated Spiral Ganglion Neurons and Sensory Hair Cells

Guest Editors: Renjie Chai, Genglin Li, Jian Wang, and Jing Zou

Editorial Board

Contents

Hindawi Publishing Corporation
Neural Plasticity
Volume 2017, Article ID 1807581, 2 pages
http://dx.doi.org/10.1155/2017/1807581

Editorial

Hearing Loss: Reestablish the Neural Plasticity in Regenerated Spiral Ganglion Neurons and Sensory Hair Cells

Renjie Chai,[1,2] Geng-Lin Li,[3] Jian Wang,[4] and Jing Zou[5,6]

[1]*MOE Key Laboratory of Developmental Genes and Human Disease, Institute of Life Sciences, Southeast University, Nanjing 210096, China*
[2]*Co-Innovation Center of Neuroregeneration, Nantong University, Nantong 226001, China*
[3]*Biology Department, University of Massachusetts Amherst, Amherst, MA 01003, USA*
[4]*School of Human Communication Disorders, Dalhousie University, 1256 Barrington Street, Halifax, NS, Canada B3J1Y6*
[5]*Department of Otolaryngology-Head and Neck Surgery, Changhai Hospital, Second Military Medical University, Shanghai 200433, China*
[6]*Hearing and Balance Research Unit, School of Medicine, University of Tampere, Lääkärinkatu 1, Room E222, 33520 Tampere, Finland*

Correspondence should be addressed to Renjie Chai; renjiec@seu.edu.cn

Received 29 January 2017; Accepted 29 January 2017; Published 20 February 2017

Hearing loss is considered as the most common sensory disorder in human population that occurs at all ages worldwidely and sensorineural hearing loss (SNHL) is the most common type of hearing loss. Various insults could induce SNHL, including acoustic trauma, ear and brain tumors, aging, noise exposure, or ototoxic medications or chemicals. SNHL is caused by irreversible loss of sensory hair cells and/or degeneration of spiral ganglion neurons. SNHL is not yet curable due to the lack of automatic regeneration of hair cells and spiral ganglion neurons in the cochlea. In recent years, exciting animal studies on signaling pathway manipulation, gene therapy, and stem cell transplantation as well as pharmaceutical agents have demonstrated that hair cells and spiral ganglion neurons could be triggered to regenerate, suggesting that hearing loss might be curable eventually in the future. Neural plasticity is the key feature for hair cells and spiral ganglion neurons, and it is especially important for the newly regenerated hair cells and spiral ganglion neurons to be functionally integrated into auditory pathways. In this special issue on neural plasticity of hair cells and spiral ganglion neurons, we are pleased to present a series of articles that represent the latest advances in hair cell development, protection and regeneration, spiral ganglion neuron development and protection, and inherited hearing loss.

Hair Cell Development. J. Hang et al. ("Synchronized Progression of Prestin Expression and Auditory Brainstem Response during Postnatal Development in Rats") report that the onset time of hearing may require the expression of prestin and is determined by the functional maturation of outer hair cells. H. Nie et al. ("Plasma Membrane Targeting of Protocadherin 15 Is Regulated by the Golgi-Associated Chaperone Protein PIST") report that PIST regulates the intracellular trafficking and membrane targeting of the tip-link proteins CDH23 and PCDH15 in hair cells.

Hair Cell Damage and Hair Cell Protection. X. Liu et al. ("Analysis of the Damage Mechanism Related to CO_2 Laser Cochleostomy on Guinea Pig Cochlea") report that enhanced cell-cell adhesion and activation of β-catenin-related canonical Wnt signaling pathway may play a role in the protection of the cochlear from further damage. M. Fu et al. ("The Effects of Urethane on Rat Outer Hair Cells") report that urethane anesthesia is expected to decrease the responses of outer hair cells, whereas the frequency selectivity of the cochlea remains unchanged. X. Fu et al. ("Loss of Myh14 Increases Susceptibility to Noise-Induced Hearing loss in CBA/CaJ Mice") report that Myh14 may play a beneficial role in the protection of the cochlea after acoustic overstimulation in CBA/CaJ mice. L. Shi et al. ("Cochlear Synaptopathy

and Noise-Induced Hidden Hearing Loss") provide a brief review to address several critical issues related to NIHHL: mechanisms of noise-induced synaptic damage, reversibility of synaptic damage, functional deficits in NIHHL animal models, evidence of NIHHL in human subjects, and peripheral and central contributions of NIHHL.

Hair Cell Regeneration. Y. Shu et al. ("Adenovirus Vectors Target Several Cell Subtypes of Mammalian Inner Ear *In Vivo*") report that adenovirus vectors are capable of efficiently and specifically transfecting different cell types in the mammalian cochlea and therefore provide useful tools to study inner ear gene functions and evaluate gene therapies for treating hearing loss and vestibular dysfunction. X. Lu et al. ("Mammalian Cochlear Hair Cell Regeneration and Ribbon Synapse Reformation") review recent research progress in hair cell regeneration, synaptic plasticity, and reinnervation of new regenerated hair cells in the mammalian cochlea. C. Wang et al. ("Evaluation of the Hair Cell Regeneration in Zebrafish Larvae by Measuring and Quantifying the Startle Responses") report the capability of a behavioral assay in noninvasively evaluating hair cell functions of fish larvae and its potential as a high-throughput screening tool for auditory-related gene and drug discovery.

Spiral Ganglion Neuron Development and Protection. P. Chen et al. ("NLRP3 Is Expressed in the Spiral Ganglion Neurons and Associated with Both Syndromic and Nonsyndromic Sensorineural Deafness") report that NLRP3 may have specific functions in spiral ganglion neurons that are altered in both syndromic and nonsyndromic sensorineural deafness. X. Bai et al. ("Protective Effect of Edaravone on Glutamate-Induced Neurotoxicity in Spiral Ganglion Neurons") investigated the toxicity of glutamate in spiral ganglion neurons and they found that the protection of edaravone is related to the PI3K pathway and Bcl-2 protein family.

Inherited Hearing Loss. X. Gu et al. ("Massively Parallel Sequencing of a Chinese Family with DFNA9 Identified a Novel Missense Mutation in the LCCL Domain of COCH") identified a missense mutation in the LCCL domain of COCH that is absent in 100 normal hearing controls and cosegregated with impaired hearing. J. Chen et al. ("Identification of a Novel ENU-Induced Mutation in Mouse *Tbx1* Linked to Human DiGeorge Syndrome") confirm the pathogenic basis of *Tbx1* in DGS, point out the crucial role of DNA binding activity of *Tbx1* for the ear function, and provide additional animal model for studying mechanisms underlying the DGS disease. Y. Guo et al. ("The Relative Weight of Temporal Envelope Cues in Different Frequency Regions for Mandarin Sentence Recognition") report that, for Mandarin Chinese, a tonal language, the temporal E cues of Frequency Region 1 (80–502 Hz) and Region 3 (1,022–1,913 Hz) contribute more to the intelligence of sentence recognition than other regions, particularly the region of 80–502 Hz, which contains fundamental frequency (*F*0) information. L. He et al. ("Mutation in the Hair Cell Specific Gene *POU4F3* Is a Common Cause for Autosomal Dominant Nonsyndromic Hearing Loss in Chinese Hans") report that mutations in *POU4F3* are a relatively common cause (3/16) for ADNSHL in Chinese Hans, which should be routinely screened in such cases during genetic testing. C. Zhang et al. ("A Novel Nonsense Mutation of *POU4F3* Gene Causes Autosomal Dominant Hearing Loss") report the first nonsense mutation of *POU4F3* associated with progressive hearing loss and explored the possible underlying mechanism.

The articles in this special issue provide valuable insights into development, protection, and regeneration of hair cells and spiral ganglion neurons. By highlighting findings in these articles, we hope this special issue will provide not only new perspectives for future directions in hearing research but also potential therapeutic strategies for treating hearing loss.

Renjie Chai
Geng-Lin Li
Jian Wang
Jing Zou

Hindawi Publishing Corporation
Neural Plasticity
Volume 2017, Article ID 8283075, 8 pages
http://dx.doi.org/10.1155/2017/8283075

Research Article

Evaluation of the Hair Cell Regeneration in Zebrafish Larvae by Measuring and Quantifying the Startle Responses

Changquan Wang,[1] Zhenmin Zhong,[1] Peng Sun,[1] Hanbing Zhong,[1] Hongzhe Li,[2,3] and Fangyi Chen[1]

[1]*Department of Biomedical Engineering, South University of Science and Technology of China, Guangdong, China*
[2]*Research Service, VA Loma Linda Healthcare System, Loma Linda, CA 92357, USA*
[3]*Department of Otolaryngology, Head & Neck Surgery, Loma Linda University School of Medicine, Loma Linda, CA 92350, USA*

Correspondence should be addressed to Hanbing Zhong; zhonghb@sustc.edu.cn, Hongzhe Li; hongzhe.li@va.gov, and Fangyi Chen; chenfy@sustc.edu.cn

Received 9 September 2016; Revised 10 November 2016; Accepted 5 December 2016; Published 29 January 2017

Academic Editor: Renjie Chai

The zebrafish has become an established model organism for the study of hearing and balance systems in the past two decades. The classical approach to examine hair cells is to use dye to conduct selective staining, which shows the number and morphology of hair cells but does not reveal their function. Startle response is a behavior closely related to the auditory function of hair cells; therefore it can be used to measure the function of hair cells. In this study, we developed a device to measure the startle response of zebrafish larvae. By applying various levels of stimulus, it showed that the system can discern a 10 dB difference. The hair cell in zebrafish can regenerate after damage due to noise exposure or drug treatment. With this device, we measured the startle response of zebrafish larvae during and after drug treatment. The results show a similar trend to the classical hair cell staining method. The startle response was reduced with drug treatment and recovered after removal of the drug. Together it demonstrated the capability of this behavioral assay in evaluating the hair cell functions of fish larvae and its potential as a high-throughput screening tool for auditory-related gene and drug discovery.

1. Introduction

Due to its miniature size, prolific reproduction, and the external development of the transparent embryo, the zebrafish is a leading model for developmental and genetic studies, as well as in toxicology and omics-based research [1–6]. Despite being genetically more distant from humans than other models, the vertebrate zebrafish has comparable organs and tissues, such as heart, kidney, pancreas, bone, cartilage, and even hearing organs [7, 8]. Indeed, the zebrafish is nowadays an established animal model for gene and drug screening in auditory research and has become a popular model organism for the study of hearing and balance system over the past 20 years [9–12].

The zebrafish carries numerous valuable features as a model in auditory research. For instance, several dozens of hearing-related genes have been discovered in zebrafish and many of them similarly influence the inner ear of humans and other vertebrates [7, 8]. In addition, the sensitivities to a variety of ototoxins, otoprotectants, and otoregeneratives are comparable to those in the zebrafish and in humans [6, 10]. The hair cells in the lateral line system are homologous with the ones in a human's inner ear, only located superficially on zebrafish's skin, with excellent permeability of various dyes and chemicals [13]. Recent advances in studying the biophysical properties of the zebrafish hair cell provided evidence on how to relate the findings in the zebrafish hair cell to their mammalian counterpart [14, 15].

Loss of sensory hair cells is the leading cause resulting in deafness or hearing deficits, and the process is not reversible in mammalian vertebrates. There is no or very limited hair cell regeneration after hair cell damage or death. Postnatal hair cell death in humans is often induced by bacterial infections, damage from prolonged noise exposure, and

treatments with certain ototoxic drugs such as aminoglycoside antibiotics or chemotherapeutic agents. In contrast to mammalian vertebrates, robust hair cell regeneration occurs in most nonmammalian vertebrates, including zebrafish [16, 17]. In combination with the advantageous technical nature of zebrafish, this animal model is positioned to become a unique research tool to study hair cell regeneration, as well as development [18]. Ongoing efforts are underway to identify regeneration specific genes and pathways that are regulated during particular stages of hair cell regeneration.

The hair cell regeneration in zebrafish is usually assessed through staining the hair cells and microscopically counting the cell number. In brief, the drug dose-dependent hair cell death can be examined with a particular ototoxin, such as neomycin, and subsequent time-lapsed cell regeneration can be investigated with borderline-hair cell death that is achieved by appropriate drug dose [17, 19].

Functional examination of zebrafish hair cell is difficult due to the lack of reliable quantification methods, compared to the electrophysiological measurement of auditory brainstem response, or otoacoustic emissions in mice. Zebrafish do harbor a rich repertoire of motor behaviors neurologically initiated by their sensory organs, either the lateral line system or the auditory system [20]. For instance, the startle response has some definitive and stable traits and can be simply triggered by a tap on the zebrafish container [21]. The startle response is intense and rapid and typically is comprised of two stages. The fish body first bends into a characteristic C-shape away from the intense stimulus within 10 msec. Afterwards, the body exhibits a small reversed curve, followed by fast swimming. The startle response can be triggered by acoustic stimuli from 5 dpf and throughout adulthood, with similar intensity threshold and frequency range [22]. These traits allow us to utilize the startle response as a behavioral tool to reliably assess hair cell damage and pertinent intervening effects. Compared to the hair cell counting method, this behavioral assay is noninvasive, so that the same fish can be examined multiple times and at various stages of the process. This system measures dozens of fish larvae each time, so that it can be used as a high-throughput drug or gene screening assay.

Deviant from previous systems for startle response measurement, significant improvement has been made to increase the accuracy. Using the system, we have successfully quantified the startle response in zebrafish (1) immediately after, (2) one day after, and (3) three days after drug exposure. The hair cells in the lateral line were also stained and counted at stages (1) and (3) to verify the damage and regeneration. The startle response results showed similar trends as what hair cell counting did but with much less effort. It demonstrated that this system can facilitate regenerative research in the zebrafish and improve and expedite our understandings in regenerative pathways and regulations in hair cell development and regeneration.

2. Materials and Methods

2.1. Animals. Wild-type TU fish line was raised and maintained in a recirculating aquaculture system according to standards described by Kimmel et al. [21]. Zebrafish larvae were maintained in embryo medium containing 0.002% Methylene Blue as a fungicide. Larvae were fed with dry food (Zeigler Bros Inc., PA, USA) starting at 5 dpf.

2.2. Staining and Imaging. Neomycin was used to induce damage in neuromast hair cells. It was applied to 7-dpf zebrafish larvae in the culture medium for duration of 24 hours. At the end of drug treatment, 8-dpf zebrafish were incubated in 8 μM Yo-Pro-1 dye (Y3603, Molecular Probes, OR, USA) dissolved in culture medium for 1 hour at 28.5°C. After rinsing 3 times, fish were anaesthetized with 0.01% tricaine and mounted with methylcellulose in a depression slide for observation. Stained neuromasts in the lateral trunk were quantified with stereomicroscope (SMZ18, Nikon) using a 13.5x objective. For confocal imaging, fish were embedded with 1.5% low melting agarose gel. Lateral line neuromasts in the trunk region were visualized by a Leica confocal microscope TCS SP8.

2.3. Instrumentation for Startle Response. An instrument system was developed to measure the startle responses of the fish larvae. The schematic of the system was shown in Figure 1(a). The fish was contained in a Petri dish within a thin layer (2 mm) of water. This assures that every fish is within the focal range of the lens and the magnification is identical. The dish was illuminated with a light guide panel, providing evenly distributed illumination, an improvement from the previous practice with beam lighting from the side [22]. This illumination improved the image quality, resulting in better accuracy for the image processing process. The Petri dish was glued on the light guide panel with transparent glue and the light panel was glued on a mini vibrator, which generates acoustic vibrations with varying frequency and amplitude under the control of electrical signal input. The stimulus vibration is conducted to the Petri dish via the light guide panel. A MEMS-based accelerometer was also glued on the panel. This is applied to monitor the stimulus in real time. In addition, a laser Doppler vibrometer was used to measure the vibration of the water surface under various stimulations prior to the test. This step provided a direct measure of the stimulus that would be applied to the fish. Thus, stimulus parameters had been confirmed prior to the actual measurement and stimulus precision was guaranteed.

A digital camera system was mounted on a microscope frame to monitor the Petri dish and zebrafish from the top. With the transillumination, the fish larva body appears as dark region in each image frame and the fish larvae were segmented from the background with in-house software, developed within MATLAB (MathWorks, MA, USA). With the segmented fish body, the position of the fish within the Petri dish can be located. By connecting the position in each frame for a fish larva, its movement during each experiment can be extracted from the recorded video. As proposed in [22], the moving distance of the fish larvae under a short tone burst stimulus can be used as a measure of its auditory startle response. Figure 1(b) shows the trace of 10 fish larvae after a stimulus. The mean distance of the fish can be calculated from the trace. A potentially more

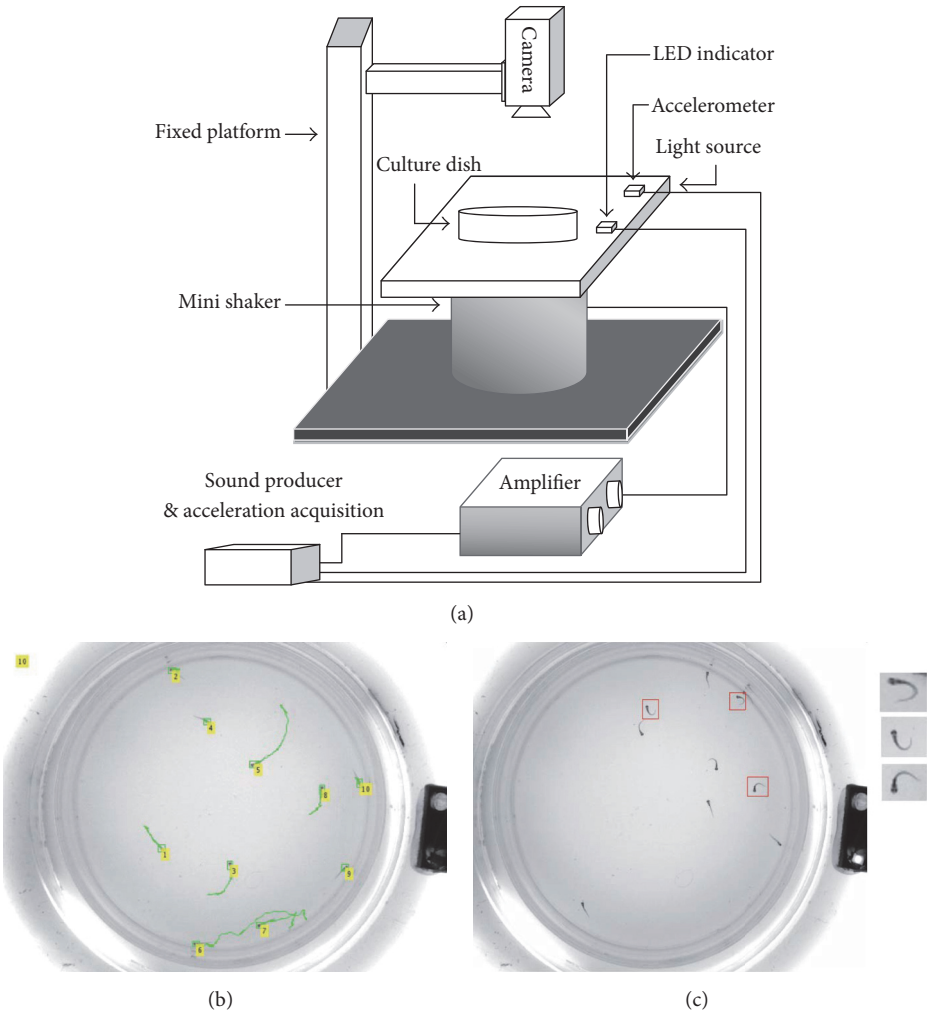

Figure 1: Recording the startle response in zebrafish. (a) Instrumentation for the measurement of startle response. (b) Moving traces identified from multiple picture frames after delivering a stimulus. (c) Characteristic C-bend motion identified in a single picture frame from a subset of zebrafish.

accurate but less sensitive measure is to count the number of fish larvae that demonstrate a C-shape motion right after the auditory stimulus. The C-shape motion is specific to the auditory startle response and lasts less than 10 ms upon stimulation [22]. The speed of the camera is 500 fps, which allows capturing the fast C-shape motion of each fish larva inside the dish. The number of fish with C-shape motion after each stimulus was calculated from several frames of the video. Both the mean distance and the number of fish with C-bend motion were calculated and used to quantify the startle responses. Here in this report we only showed the mean distance results. Figure 1(c) shows that three fish larvae demonstrated the C-bend motion in one single frame.

2.4. Verification of Instrument System. To verify the efficacy of the instrument system, an experiment was performed to measure the startle responses of zebrafish larvae to sound stimulus with different intensity in fish that were treated with or without ototoxic drug. To test the relationship between the startle response and stimulus level, 400 Hz tone bursts with 3 different sound levels were applied to the amplifier to drive the vibrator. The stimulus mid-level was chosen by visually observing that more than 5 larvae (without drug treatment) showed significant movement. The high level is about 10 dB above and the low level is about 10 dB below the mid-level. For each stimulus level, 10 repeats were performed to achieve the statistical significance. Between each stimulus, 100 sec of break was applied to avoid the adaptation, as suggested in [22]. To test the sensitivity of the system to ototoxic drug, 7-dpf zebrafish larvae were treated with neomycin of 3 different levels of concentration, 0, 0.16, and 1.6 μM, for 24 hours. Higher concentration of 8 μM neomycin resulted in high death rate; thus it was only used in the staining experiment for hair cell survival and recovery. The startle responses were measured with the system right after rinsing the larvae at 8 dpf, with the tone burst stimulus of 400 Hz of the same sound level.

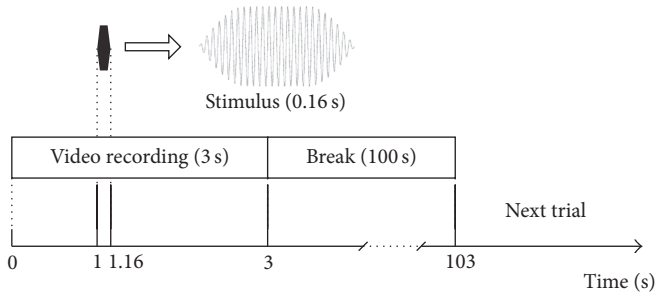

Figure 2: Time course for the measurement of startle response in zebrafish.

2.5. Recovery of Zebrafish Larvae from Drug Exposure. With the instrument system introduced earlier, we performed the startle responses as well as the traditional hair cell counting technique to monitor the recovery of the auditory function of the zebrafish larvae. In each test, 10 larvae were placed in the Petri dish. Two testing systems were used in parallel so that in total 20 larvae were tested for each experiment. The stimulus waveform was a tone burst of 160 ms with 30 ms rise and fall time, as shown in Figure 2. The stimulus frequency was 400 Hz and the stimulus level was 39 mm/s as the vibration velocity of the water surface. The absolute sound pressure level of this stimulus was impractical to measure due to the shallow water (~2 mm). Therefore, the vibration of the water surface at this sound level was measured by a laser Doppler interferometer to ensure the consistency.

One hundred zebrafish larvae were used in the present study. At 7 dpf, larvae were divided into three groups: control (i.e., 0) and 0.16 μM and 1.6 μM neomycin treatment. The startle responses of 20 larvae were tested before adding the drug. The larvae were merged in culture medium with neomycin for 24 hours and then rinsed with clean culture medium for three times. At 8 dpf, right after rinsing, 20 larvae from each group were tested with the startle response. The same test was again performed at 9 and 11 dpf (24 hrs and 72 hrs after rinsing) to monitor potential recovery due to expected hair cell regeneration.

In parallel with the startle response test, the hair cell damage by neomycin treatment was confirmed by observing and counting the hair cell with staining. As in previous test, the larvae were divided into three groups, with neomycin concentration of 0, 0.16, or 1.6 μM. The hair cells on the lateral line were stained and counted at 8 dpf right after drug treatment to check the damage and at 11 dpf, 72 hrs after the treatment, to check the regeneration.

3. Results

3.1. Characterizing Startle Response. We quantified the startle response by zebrafish larvae's moving distance upon sound stimulation. Figure 3(a) shows that the mean moving distance increased with rising sound levels, in a range of 20 dB, that is, 10-fold. Figure 3(b) shows the startle responses versus ototoxic drug concentration. The concentration of neomycin was at 0, 0.16 μM, or 1.6 μM. The sound stimulus was 400 Hz tone bursts.

3.2. Regeneration of Neuromast Hair Cells after Neomycin-Induced Hair Cell Damage. Previous studies have mostly demonstrated that neomycin exposure ablated hair cells in the lateral line in a dose-dependent manner [10, 16]. Here in this study, Yo-Pro-1 was used to identify hair cells from posterior neuromasts in the lateral line. After 24-hour neomycin treatment, neuromasts in the trunk region dorsal to the pelvic fin were observed and hair cells were counted. Figure 4(a) illustrates that a high dose of 8 μM neomycin led to loss of most hair cells; the Yo-Pro-1 positive residues were random and dispersed, unlike the cluster-like organization observed with lower neomycin dosing. Compared to the control group, a smaller and less number of hair cells were observed with either 0.16 or 1.6 μM neomycin treatment (Figure 4(b)). Three-day recovery enabled robust regeneration of hair cells (Figure 4(b)), which is consistent with previous reports investigating the precursor pool maintenance in lateral line hair cells [23].

3.3. Startle Responses of the Same Procedure. Using the same experimental condition with neomycin treatment, we also evaluated the startle response with our in-house instrument system. The tone burst attributes were the same as previously described and the tone frequency was 400 Hz. The startle responses were checked 24 hrs and 72 hrs after the drug treatment. The mean moving distance of the control group is used as a reference at each checkpoint. The responses of the drug treatment groups were normalized by that of the control group to eliminate the possible variation in startle responses between different days. At 8 dpf (0 h in Figure 5), the responses of the drug treatment group are significantly smaller than that of the control. With drug treatment, the startle responses at 24 h and 72 h showed gradual growth of moving distance, compared to that at 0 h, indicating time-lapsed functional recovery.

4. Discussion

4.1. Efficacy of Using the Vibrator. In this study, a mini shaker was used as the driver to deliver acoustic vibration to the Petri

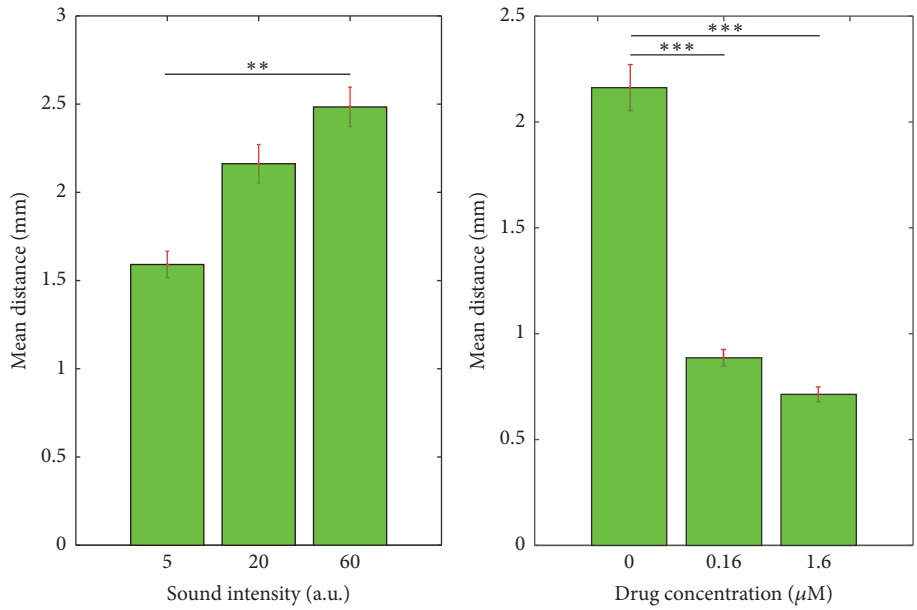

FIGURE 3: Characterizing the startle response. (a) Mean moving distance of larvae with 400 Hz sound of intensity linearly grown from 5 to 60 with an arbitrary unit. This results in a sound level in about 20 dB. The values are 1.59 ± 0.23, 2.16 ± 0.34, and 2.48 ± 0.35. There is statistically significant difference between the 1st column and 3rd column ($p < 0.01$) but not between adjacent columns. (b) Mean moving distance as function of the neomycin concentration. The values are 2.16 ± 0.34, 0.89 ± 0.12, and 0.71 ± 0.11. There is statistically significant difference between the 1st column and 2nd column ($p < 0.001$) but not between 2nd and 3rd columns ($p = 0.09$). The error bar is standard error.

dish and produce the sound stimulus to fish larvae. Although this is not a direct sound generation, it is an effective way of delivering sound stimulus. Using a load speaker in air is not efficient because of the air-water interface, where 95% of sound energy is reflected back. An aquatic speaker can be used underwater but it is not practical in this setup because the water level is only a few millimeters inside the Petri dish. The mini shaker was previously used in [24] and was experimentally effective.

4.2. Interference between Fish. In one of the previous systems [24], the fish larvae were placed in a multiwell plate. The design made it easier to identify each individual fish during image processing. However, the setup resulted in the uneven sound pressure level of stimulus in each well, causing inaccuracy in data collection. In the present setup, all the fish were placed in the same Petri dish. Due to the shallow water level, the sound level is evenly distributed and thus stimulus to each fish is identical. One concern on this setup is that fish larvae can sense each other in this setup without the segregation by the individual well wall. Theoretically, some fish may move after seeing others' quick motion. Yet, we doubt that visual cue contributes to the measured startle response and contaminates our data collection. In our setup, the fish are mostly distanced (see Figure 1(c)), which largely reduced the visual interference among them. In addition, if a C-bend motion was triggered by a visual cue on other fish's startle response, the latency of this motion would be extended, causing desynchronized "startle responses" among fish. However, this desynchronization was not observed. The concern on interanimal interference can also be further evaluated by using infrared illumination during the experiment [25].

4.3. Behavioral Test Sensitivity Based on the Startle Response. With the experimental protocol in the present study, the test sensitivity was comparable between the morphological hair cell counting method in Figure 4 and the behavioral method testing the startle response in Figure 5. Both methods were able to detect the ototoxic neomycin caused damage with the lowest tested concentration (0.16 μM). With higher neomycin concentration, extended hair cell loss was observed and so was the further shortened swimming distance after the startle stimuli. Although the behavioral test produced satisfactory outcome, we believe the test sensitivity is likely further improved with modification in experiment design. For instance, prepulse inhibition was shown to increase the sensitivity by about 40 dB in a startle response test system [26], while sound pressure level of 60 dB above the hearing threshold is required to directly induce the startle response.

5. Conclusion

In this study, we developed a behavioral assay to evaluate the auditory function of hair cells by measuring the startle

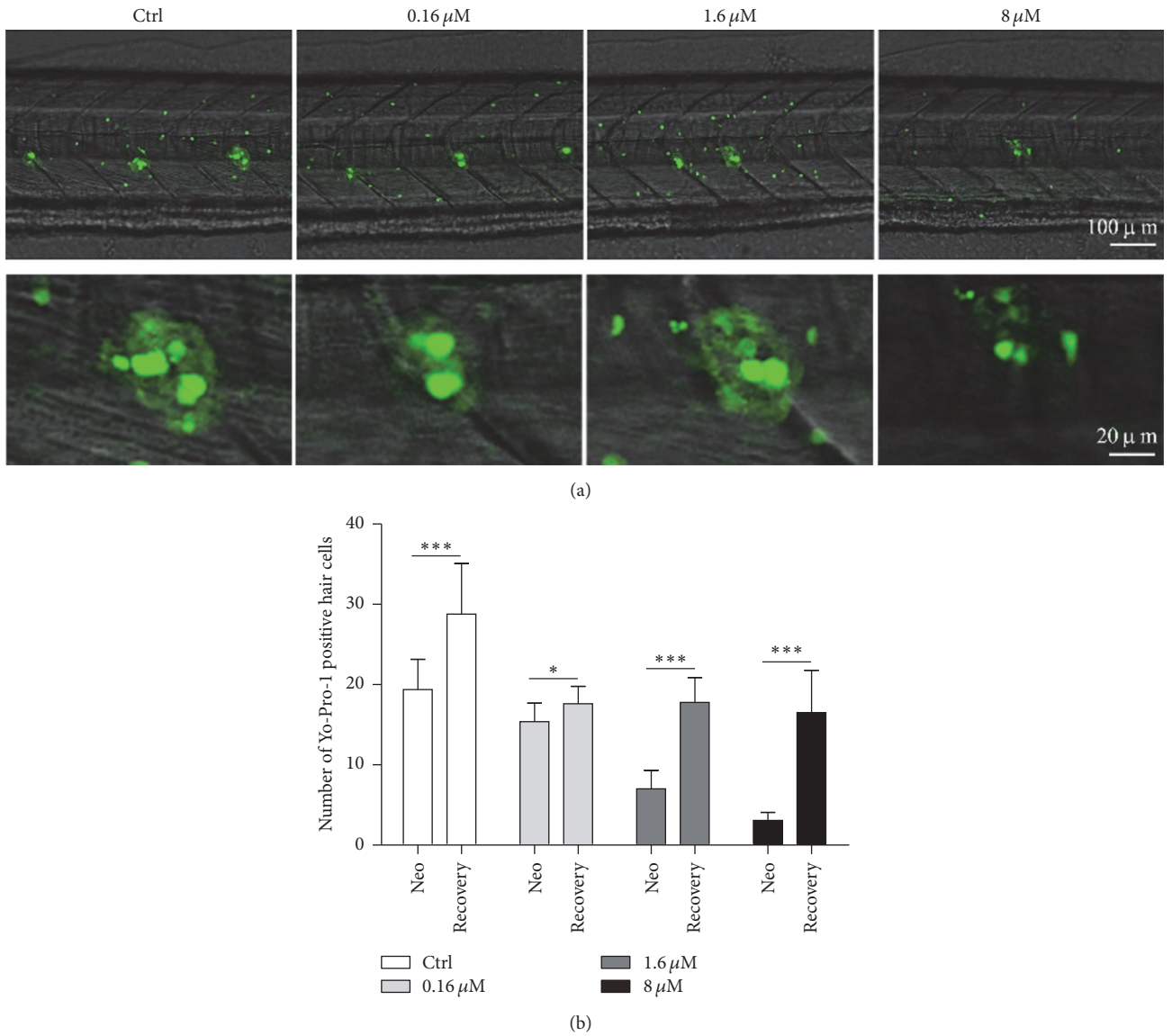

Figure 4: Neomycin-induced neuromast hair cell damage and regeneration. (a) Confocal image of lateral line neuromasts under neomycin treatment in wild-type zebrafish. (b) Average number of neuromast hair cells in each group. Each group consists of 10 7 dpf zebrafish larvae treated with respective concentration for 24 h and then allowed to recover for 72 h to assess hair cell regeneration. All neomycin-treated larvae showed decreased number of hair cells to some extent; statistical analyses were performed using Student's t-test ($^{*}p < 0.05$; $^{***}p < 0.001$). Error bars are standard deviation.

response of zebrafish larvae. By applying various level of stimulus, results showed that the system can discern a 10 dB sound level difference. Using the system, we investigated the hair cell damage and regeneration in the lateral line neuromasts of zebrafish larvae. The result from this system shows similar trend to the traditional hair cell counting methods. The startle response was reduced with neomycin treatment and recovered with hair cell regeneration. These results demonstrated the capability of this behavioral assay in evaluating the hair cell functions of zebrafish larvae and its potential as a high-throughput screening tool for auditory-related gene and drug discovery.

Competing Interests

The authors declare that there are no competing interests regarding the publication of this paper.

Acknowledgments

This work was supported by the National Natural Science Foundation of China (Grant no. 81470701), the Shenzhen Overseas Talents Innovation Plan (Grant no. KQCX20140522150857838) awarded to FC, and the US

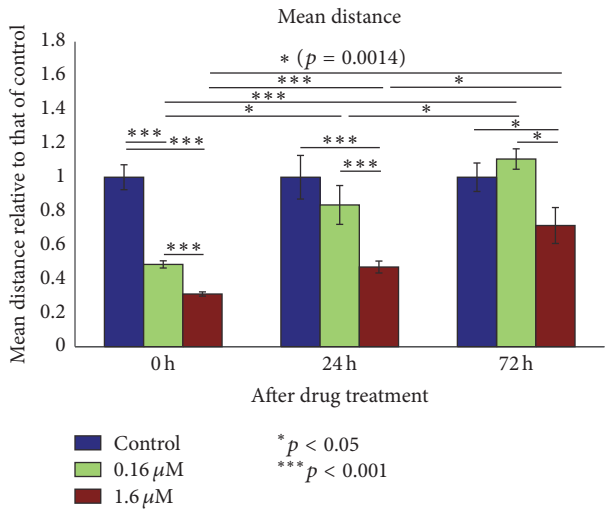

Figure 5: Startle response of fish larvae with neomycin treatment of different level of concentration and subsequent recovery period after drug removal. Mean moving distance after sound stimulation was used as the quantification parameter. To eliminate the variation of different days, the values are scaled by that of the control group in each day. The value in each column from left to right is 1 ± 0.23, 0.48 ± 0.06, 0.31 ± 0.03, 1 ± 0.41, 0.84 ± 0.36, 0.47 ± 0.11, 1 ± 0.27, 1.10 ± 0.19, or 0.72 ± 0.34 in the format of mean ± standard deviation. The unpaired t-test on adjacent columns in each day is shown to be mostly significant, except for between control and 0.16 μM at 24 h or at 72 h. For the same drug concentration (e.g., 0.16 μM at 0 h, 24 h, and 72 h), unpaired t-test shows significant ($p < 0.05$) difference between days for both 0.16 and 1.6 μM cases.

Army Medical Research and Materiel Command (Grant no. W81XWH1410006) awarded to HL.

References

[1] Y. He, C. Cai, D. Tang, S. Sun, and H. Li, "Effect of histone deacetylase inhibitors trichostatin A and valproic acid on hair cell regeneration in zebrafish lateral line neuromasts," *Frontiers in Cellular Neuroscience*, vol. 8, no. November, 2014.

[2] X. Shen, F. Liu, Y. Wang et al., "Down-regulation of msrb3 and destruction of normal auditory system development through hair cell apoptosis in zebrafish," *International Journal of Developmental Biology*, vol. 59, no. 4–6, pp. 195–203, 2015.

[3] T. M. Stawicki, R. Esterberg, D. W. Hailey, D. W. Raible, and E. W. Rubel, "Using the zebrafish lateral line to uncover novel mechanisms of action and prevention in drug-induced hair cell death," *Frontiers in Cellular Neuroscience*, vol. 9, article 46, 2015.

[4] A. B. Steiner, T. Kim, V. Cabot, and A. J. Hudspeth, "Dynamic gene expression by putative hair-cell progenitors during regeneration in the zebrafish lateral line," *Proceedings of the National Academy of Sciences of the United States of America*, vol. 111, no. 14, pp. E1393–E1401, 2014.

[5] L. Y. Zamora and Z. Lu, "Alcohol-induced morphological deficits in the development of octavolateral organs of the zebrafish (*Danio rerio*)," *Zebrafish*, vol. 10, no. 1, pp. 52–61, 2013.

[6] H. C. Ou, F. Santos, D. W. Raible, J. A. Simon, and E. W. Rubel, "Drug screening for hearing loss: using the zebrafish lateral line to screen for drugs that prevent and cause hearing loss," *Drug Discovery Today*, vol. 15, no. 7-8, pp. 265–271, 2010.

[7] K. Howe, M. D. Clark, C. F. Torroja et al., "The zebrafish reference genome sequence and its relationship to the human genome," *Nature*, vol. 496, no. 7446, pp. 498–503, 2013.

[8] T. Nicolson, "The genetics of hearing and balance in zebrafish," *Annual Review of Genetics*, vol. 39, pp. 9–22, 2005.

[9] J. Kanungo, E. Cuevas, S. F. Ali, and M. G. Paule, "Zebrafish model in drug safety assessment," *Current Pharmaceutical Design*, vol. 20, no. 34, pp. 5416–5429, 2014.

[10] C. Ton and C. Parng, "The use of zebrafish for assessing ototoxic and otoprotective agents," *Hearing Research*, vol. 208, no. 1-2, pp. 79–88, 2005.

[11] T. T. Whitfield, B. B. Riley, M.-Y. Chiang, and B. Phillips, "Development of the zebrafish inner ear," *Developmental Dynamics*, vol. 223, no. 4, pp. 427–458, 2002.

[12] S. W. Baxendale and T. Tanya, "Zebrafish inner ear development and function," in *Development of Auditory and Vestibular Systems*, R. Romand and I. Varela-Nieto, Eds., Elsevier, Amsterdam, The Netherlands, 4th edition, 2014.

[13] B. Fritzsch and K. W. Beisel, "Evolution and development of the vertebrate ear," *Brain Research Bulletin*, vol. 55, no. 6, pp. 711–721, 2001.

[14] A. J. Ricci, J.-P. Bai, L. Song, C. Lv, D. Zenisek, and J. Santos-Sacchi, "Patch-clamp recordings from lateral line neuromast hair cells of the living zebrafish," *The Journal of Neuroscience*, vol. 33, no. 7, pp. 3131–3134, 2013.

[15] J. Olt, S. L. Johnson, and W. Marcotti, "In vivo and in vitro biophysical properties of hair cells from the lateral line and inner ear of developing and adult zebrafish," *Journal of Physiology*, vol. 592, no. 10, pp. 2041–2058, 2014.

[16] J. A. Harris, A. G. Cheng, L. L. Cunningham, G. MacDonald, D. W. Raible, and E. W. Rubel, "Neomycin-induced hair cell death and rapid regeneration in the lateral line of zebrafish (*Danio rerio*)," *Journal of the Association for Research in Otolaryngology*, vol. 4, no. 2, pp. 219–234, 2003.

[17] F. Pinto-Teixeira, M. Muzzopappa, J. Swoger, A. Mineo, J. Sharpe, and H. López-Schier, "Intravital imaging of hair-cell development and regeneration in the zebrafish," *Frontiers in Neuroanatomy*, vol. 7, article 33, 2013.

[18] J. Wang, Q. Song, D. Yu et al., "Ontogenetic development of the auditory sensory organ in zebrafish (*Danio rerio*): changes in hearing sensitivity and related morphology," *Scientific Reports*, vol. 5, Article ID 15943, 2015.

[19] M. Tanimoto, Y. Ota, M. Inoue, and Y. Oda, "Origin of inner ear hair cells: morphological and functional differentiation from ciliary cells into hair cells in zebrafish inner ear," *Journal of Neuroscience*, vol. 31, no. 10, pp. 3784–3794, 2011.

[20] M. Wolman and M. Granato, "Behavioral genetics in larval zebrafish: learning from the young," *Developmental Neurobiology*, vol. 72, no. 3, pp. 366–372, 2012.

[21] C. B. Kimmel, J. Patterson, and R. O. Kimmel, "The development and behavioral characteristics of the startle response in the zebra fish," *Developmental Psychobiology*, vol. 7, no. 1, pp. 47–60, 1974.

[22] D. G. Zeddies and R. R. Fay, "Development of the acoustically evoked behavioral response in zebrafish to pure tones," *Journal of Experimental Biology*, vol. 208, no. 7, pp. 1363–1372, 2005.

[23] I. A. Cruz, R. Kappedal, S. M. Mackenzie et al., "Robust regeneration of adult zebrafish lateral line hair cells reflects continued precursor pool maintenance," *Developmental Biology*, vol. 402, no. 2, pp. 229–238, 2015.

[24] T. Nicolson, A. Rüsch, R. W. Friedrich, M. Granato, J. P. Ruppersberg, and C. Nüsslein-Volhard, "Genetic analysis of vertebrate sensory hair cell mechanosensation: the zebrafish circler mutants," *Neuron*, vol. 20, no. 2, pp. 271–283, 1998.

[25] M. Niihori, T. Platto, S. Igarashi et al., "Zebrafish swimming behavior as a biomarker for ototoxicity-induced hair cell damage: a high-throughput drug development platform targeting hearing loss," *Translational Research*, vol. 166, no. 5, pp. 440–450, 2015.

[26] A. A. Bhandiwad, D. G. Zeddies, D. W. Raible, E. W. Rubel, and J. A. Sisneros, "Auditory sensitivity of larval zebrafish (*Danio rerio*) measured using a behavioral prepulse inhibition assay," *Journal of Experimental Biology*, vol. 216, no. 18, pp. 3504–3513, 2013.

Hindawi Publishing Corporation
Neural Plasticity
Volume 2017, Article ID 7416727, 7 pages
http://dx.doi.org/10.1155/2017/7416727

Research Article

The Relative Weight of Temporal Envelope Cues in Different Frequency Regions for Mandarin Sentence Recognition

Yang Guo, Yuanyuan Sun, Yanmei Feng, Yujun Zhang, and Shankai Yin

Department of Otolaryngology Head and Neck Surgery, Shanghai Jiao Tong University Affiliated Sixth People's Hospital, No. 600, Yishan Road, Xuhui District, Shanghai 200233, China

Correspondence should be addressed to Yanmei Feng; feng.yanmei@126.com

Received 8 September 2016; Accepted 4 January 2017; Published 19 January 2017

Academic Editor: Genglin Li

Acoustic temporal envelope (E) cues containing speech information are distributed across the frequency spectrum. To investigate the relative weight of E cues in different frequency regions for Mandarin sentence recognition, E information was extracted from 30 contiguous bands across the range of 80–7,562 Hz using Hilbert decomposition and then allocated to five frequency regions. Recognition scores were obtained with acoustic E cues from 1 or 2 random regions from 40 normal-hearing listeners. While the recognition scores ranged from 8.2% to 16.3% when E information from only one region was available, the scores ranged from 57.9% to 87.7% when E information from two frequency regions was presented, suggesting a synergistic effect among the temporal E cues in different frequency regions. Next, the relative contributions of the E information from the five frequency regions to sentence perception were computed using a least-squares approach. The results demonstrated that, for Mandarin Chinese, a tonal language, the temporal E cues of Frequency Region 1 (80–502 Hz) and Region 3 (1,022–1,913 Hz) contributed more to the intelligence of sentence recognition than other regions, particularly the region of 80–502 Hz, which contained fundamental frequency (F_0) information.

1. Introduction

Speech is an indispensable process for communicating in everyday life; it is transmitted through the cochlea to the brain and then becomes understood. The cochlea is commonly referred to as a series of overlapping auditory filters that divide the normal frequency range of speech into narrow bands, with center frequencies corresponding to specific positions on the basilar membrane [1]. As the high-frequency sound causes maximum displacement of the basilar membrane near the base, the basilar membrane close to the apex vibrates strongest in response to the low-frequency sound. The speech signal within a narrow band is a compound signal consisting of two different kinds of information: the slowly varying amplitude, known as the temporal envelope (E), and rapid variations with rates close to the central frequency of the band, called the temporal fine structure (TFS) [2–4]. Acoustic E cues can provide sufficient information for nearly perfect speech recognition in a quiet environment, while the TFS is needed for a noisy background and for pitch and tonal recognition [3, 5, 6].

The redundant nature of speech, based on spectral and temporal cues, guarantees the intelligence of speech even under temporally and spectrally degraded conditions. Under these conditions, listeners use different strategies to make comprehension possible, such as temporal [7, 8] and spectral integration [9–11]. To understand the relative importance of the different spectral regions, much effort has been made over the years.

By changing the location of the spectral "hole" in the tonotopic representation of the cochlea in an orderly manner, Shannon et al. [12] suggested that a hole in the apical region was more detrimental to speech perception using temporal E information than a hole in the basal or middle regions. Ardoint and Lorenzi [3] adopted high-pass and low-pass method to show that the temporal E information in frequency regions of 1-2 kHz conveys important phonetic cues, while the synergistic effect [13] across frequency regions was not considered.

Taking the synergistic effect across frequency regions into account, Apoux and Bacon [14] used both the hole and the

correlational methods to investigate the relative weight of temporal E information across spectral regions. However, they consistently found that temporal E cues contained in the highest frequency region (>3.5 kHz) were more important in a noisy environment. Subsequently, another recognition task with bandpass-filtered speech was conducted to evaluate the ability to use temporal E in different frequency regions of English [15]. The recognition scores of consonants were measured with only 1 frequency region or 2 disjointed or 2 adjacent regions. The performance increased as the region-center frequency increased consistently for both the processed single region and pairs of regions in a quiet environment, showing that E cues in higher frequency regions (1.8–7.3 kHz) contributed most to consonant recognition [15].

As mentioned above, most reported studies have explored the features of English, a nontonal language, while limited attention has been paid to Mandarin, a tonal language spoken by many people. Luo et al. [16, 17] showed that periodic fluctuation cues (50–500 Hz) in the highest frequency region (3043–6000 Hz) contributed the most to Mandarin tone recognition, while vowel recognition was not significantly affected by the availability of periodic fluctuation cues. For recognition of Mandarin sentence, however, little is known about the ability to use temporal E cues in different frequency regions and to combine the temporal E from various frequency regions. As a tonal language, the same phoneme with different tones has various meanings. For example, the syllable /ma/ can have different meanings depending on the F_0 contours. Additionally, Mandarin-speaking listeners rely more on F_0 variations to discriminate Thai lexical tones than do French-speaking listeners [18]. It has been established that changes in fundamental frequency (F_0) play essential roles in tone identification [19, 20], which, in turn, contribute to Mandarin sentence recognition [17, 21].

Fogerty [22] suggested that acoustic TFS cues in the middle-frequency region (528–1,941 Hz) weigh most for English recognition while those in the low-frequency (80–528 Hz) and high-frequency (1,941–6,400 Hz) regions were much less important [22]. However, the findings from our previous study indicated that the acoustic TFS cues in the low-frequency region contributed more to Mandarin sentence recognition than English. For Mandarin, the relative weight of the acoustic TFS in the low-frequency region (~0.4) was slightly lower than that of the middle-frequency region (~0.5) [10].

Considering these apparent differences in the TFS weight distribution between English and Mandarin and the contribution of F_0 to tone recognition, it is possible that the frequency-weighting functions of temporal E for Mandarin differ from those for English. The goal of this study was to investigate the relative weight of temporal E in different frequency regions for Mandarin sentence recognition in a quiet environment.

2. Materials and Methods

2.1. Participants. In total, 40 normal-hearing listeners (20 males, 20 females) were recruited in this study. Their ages ranged from 21 to 28 (average = 24.9) years. All subjects were native Mandarin speakers with no reported history of ear disease or hearing difficulty. All subjects were recruited from graduates of Shanghai Jiao Tong University and were tested at Shanghai Jiao Tong University Affiliated Sixth People's Hospital. In all participants, audiometric thresholds were at the ≤25 dB hearing level (HL), bilaterally, at octave intervals from 0.25 to 8 kHz. Pure-tone audiometric thresholds were recorded with a GSI-61 audiometer (Grason-Stadler, Madison, WI) using standard audiometric procedures [23]. No subject had any preceding exposure to the sentence materials.

This study was approved by the Ethics Committee of Shanghai Jiao Tong University Affiliated Sixth People's Hospital. Signed consent forms were obtained from all participants before testing, and they were compensated on an hourly basis for their participation.

2.2. Signal Processing. The Mandarin version of the hearing in noise test (MHINT), provided by the House Ear Institute, was used as original material, which was recorded digitally by a male speaker [24]. The MHINT materials consist of 12 lists, each comprising 20 sentences. With each sentence containing 10 key words, there are 240 key words in one list.

The sentences were filtered into 30 contiguous frequency bands using zero-phase, third-order Butterworth filters (36 dB/oct slopes), ranging from 80 to 7,562 Hz. Each band was an equivalent rectangular bandwidth (ERB_N) for normal-hearing listeners, simulating the frequency selectivity of the normal auditory system [25]. E information was extracted from each band using the Hilbert decomposition and low-pass filter at 64 Hz using third-order Butterworth filters. Then E was used to modulate the amplitude of a white noise. The envelope-modulated noise was bandpass-filtered using the same filter parameters as before, after which the modulated noise bands were summed across frequency bands to produce the frequency regions of acoustic E cues as follows: Bands 1–8, 9–13, 14–18, 19–24, and 25–30 were summed to form Frequency Regions 1–5, respectively (Table 1).

To investigate the role of the frequency regions in sentence recognition, the acoustic E information from 1 frequency region (5 conditions), 2 adjacent frequency regions (4 conditions), 2 nonadjacent frequency regions (6 conditions), and all frequency regions (1 condition) was presented to subjects. To prevent the possible use of information from the transition bands [4, 26], frequency regions containing sentence E information were combined with complementary frequency regions containing noise masker that was presented at a speech-to-noise ratio (SNR) of +16 dB. As with the preparation of the frequency regions of the sentence E cues, the white noise was filtered into 30 contiguous frequency bands and summed to produce the frequency regions of noise. For example, the condition of "Region 1" means that the stimulus presented to the listeners consisted of sentence E information from Frequency Region 1 and noise from the other frequency regions (Regions 2–5). Similarly "Region 1 + 2" refers to a stimulus consisting of acoustic E information from Frequency Regions 1 and 2 and noise from the rest of the frequency regions (Regions 3–5). The "Full Region" stimulus consisted of E from all five frequency regions (Regions 1–5) with no added noise.

Table 1: Cutoff frequency for extracting temporal envelope information.

Frequency regions	Bands	Lower frequency (Hz)	Upper frequency (Hz)
1	1	80	115
	2	115	154
	3	154	198
	4	198	246
	5	246	300
	6	300	360
	7	360	427
	8	427	502
2	9	502	585
	10	585	677
	11	677	780
	12	780	894
	13	894	1022
3	14	1022	1164
	15	1164	1322
	16	1322	1499
	17	1499	1695
	18	1695	1913
4	19	1913	2157
	20	2157	2428
	21	2428	2729
	22	2729	3066
	23	3066	3440
	24	3440	3856
5	25	3856	4321
	26	4321	4837
	27	4837	5413
	28	5413	6054
	29	6054	6767
	30	6767	7562

As there are 12 lists in the MHINT materials, there were 16 experimental conditions to be tested. The same list was not used in two different test conditions on one subject to avoid any learning effect. Thus, the 16 test conditions were divided into two groups. Group 1 completed 5 conditions with 1 frequency region, 4 conditions with 2 adjacent frequency regions, and 1 condition with the full frequency regions. Group 2 completed 4 conditions with 2 adjacent frequency regions and 6 conditions with 2 nonadjacent frequency regions. Thus, there were 10 conditions in each group, and the 4 experimental conditions with 2 adjacent frequency regions in the 2 groups were the same. Accordingly, there were 10 lists in each group of MHINT materials.

2.3. Procedures. The 40 participants were divided randomly and equally into groups 1 and 2, each comprising 10 males and 10 females. The participants were tested individually in a double-walled, sound-attenuated booth. Stimuli were presented binaurally to the participants through Sennheiser HD 205 II circumaural headphones at the most comfortable level for each subject, usually at 65 dBSPL. Each key word in a sentence was scored as correct or incorrect, and the performances were expressed as the percentage of correct words for the different conditions.

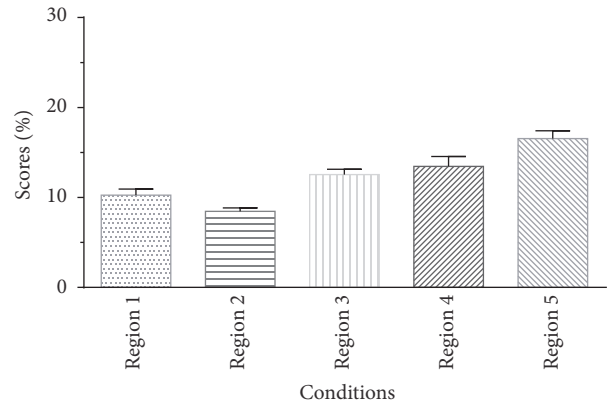

Figure 1: Averaged percent-correct scores for sentence recognition using acoustic temporal envelope as a function of condition in Group 1. The error bars indicate standard errors.

About 30 min of practice was provided prior to the formal test. The practice stimuli consisted of 40 sentences (two lists) of MHINT materials and were first presented under "Full Region" conditions and then processed in the same manner as the experimental stimuli. Feedback was provided during practice. To familiarize the participants with the processed stimuli, they could repeat a sentence as many times as they wished before moving on to the next sentence until their performance reached a plateau.

In the formal tests, the participants were permitted to listen to the sentence as many times as they wished. All 10 conditions, corresponding to 10 lists of MHINT materials, were presented in a random order across subjects to avoid any order effect. Participants were instructed to repeat the sentences as accurately as possible and were encouraged to guess if uncertain of the words in a sentence. No feedback was given during the test period. The subject could take a break whenever needed. The total duration of testing was ~2 h for each listener.

3. Results

3.1. Percent-Correct Scores for Sentence Recognition across Conditions Using Temporal E. The mean percent-correct sentence recognition scores with acoustic E from one frequency region obtained from Group 1 are shown in Figure 1. The scores range from ~8.2% to ~16.3%, with the Region 5 condition scores being highest and the Region 2 scores being the lowest. Indeed, the listeners could not understand the meaning of the sentences under such adverse conditions. However, the intelligibility of sentences using temporal E approached perfect when all five regions were presented to the listener simultaneously (Figure 2). The data were transformed to rationalized arcsine units (RAU) for the

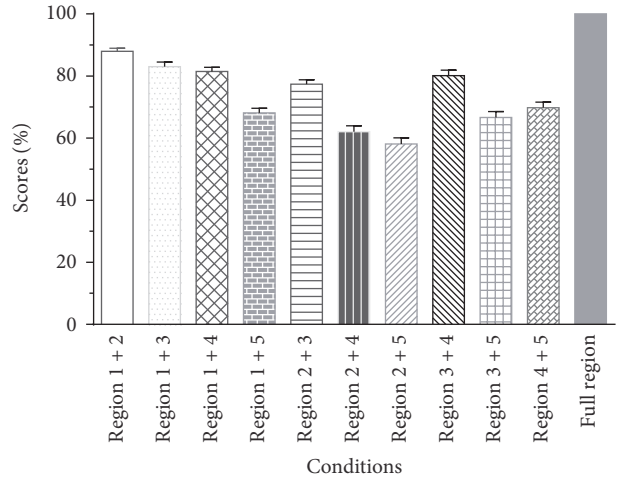

Figure 2: Averaged percent-correct scores for sentence recognition using acoustic temporal envelope as a function of conditions in Group 2 and the condition with a full frequency region in Group 1. The error bars indicate standard errors.

Table 2: Comparison of percent-correct scores for conditions with two adjacent frequency regions in two groups.

Conditions	Scores of Group 1	Scores of Group 2	t-test
Region 1 + 2	89.6 ± 5.4 (%)	87.7 ± 4.3 (%)	$p = 0.219$
Region 2 + 3	74.0 ± 5.0 (%)	77.2 ± 6.4 (%)	$p = 0.091$
Region 3 + 4	79.2 ± 6.7 (%)	79.9 ± 7.9 (%)	$p = 0.764$
Region 4 + 5	68.8 ± 9.2 (%)	69.7 ± 7.7 (%)	$p = 0.746$

purposes of statistical analyses [27]. A one-way repeated-measures analysis of variance (ANOVA) was used for the results from different conditions with one frequency region, showing a significant main effect of condition on sentence recognition ($F(4, 76) = 21.781$, $p < 0.001$). The post hoc analysis (Tukey's test) revealed that the scores differed significantly between any two conditions ($p < 0.05$), except for the scores obtained from the Region 3 and Region 4 conditions.

As the conditions with two adjacent regions were the same in both subject groups, we compared the performance of these conditions in the two groups first (Table 2). Independent samples t-tests showed that the percent-correct score differences obtained from the same conditions in two groups were not significant (all $p > 0.05$). Therefore, the data obtained from the two groups were combined to calculate the relative weights of the five frequency regions.

As shown in Figure 2, under all conditions with two frequency regions, the score was >55%, and the Region 1 + 2 condition scores were the highest, ~87.7%, while Region 2 + 5 scores were the lowest, ~57.9%. Generally, the intelligence scores for conditions with two frequency regions tended to decrease as the distance between the two regions increased. The results were subjected to a one-way repeated-measures ANOVA, which showed a significant main effect of conditions ($F(9, 171) = 56.094$, $p < 0.001$). The post hoc analysis (Tukey's test) showed that the performance using temporal E of the Region 1 + 2 condition was significantly better than the performances under all other conditions with two frequency regions, and the performance using temporal E of the Region 1 + 3, Region 1 + 4, and Region 3 + 4 conditions was better than that under the other conditions with two frequency regions. If one frequency region was combined with another frequency region, the scores obtained from conditions combined with Frequency Region 1 would be higher than those obtained from conditions combined with other regions. For example, if the Frequency Region 2 was combined with another Frequency Region, the score of Region 1 + 2 condition was significantly higher than scores of any other combinations with Frequency Region 2, such as Region 2 + 3, Region 2 + 4, and Region 2 + 5 conditions. However, the difference between scores of conditions is not significant when Region 1 + 3 or Region 1 + 4 was compared with Region 3 + 4 and when Region 1 + 5 was compared with Region 3 + 5 or Region 4 + 5.

3.2. Relative Weights of the Five Frequency Regions. To calculate the relative weight of the different frequency regions for Mandarin sentence recognition using acoustic temporal E, the least-squares approach described by Kasturi et al. (2002) was used. First, the strength of each region was defined to be a binary value which is either 0 or 1 depending on whether the region is presented or not. Then a linear combination of the strength of each region was applied to predict the responses of the listeners, and the weight of each region was calculated by minimizing the sum of all the squared prediction errors. The raw weights for the five regions of each listener were transformed to relative weights by summing their values and each region's weight was expressed as the raw weight divided by this sum. Therefore, the sum of the weights of the five regions was equal to 1.0. As shown in Figure 3, the mean weights of Regions 1–5 were 0.25, 0.18, 0.22, 0.20, and 0.15, respectively. The one-way ANOVA showed a significant main effect of region on weight for sentence recognition ($F(4, 76) = 60.129$, $p < 0.001$). The post hoc tests (Tukey's test) showed that the relative weights differed significantly between any two frequency regions. The temporal E of Frequency Regions 1 and 3 contributed more to the intelligence of sentence recognition in Mandarin Chinese than the E cues of the other frequency regions.

4. Discussion

By systematically altering the stimuli presented to listeners, recognition scores with different frequency regions using acoustic E cues were recorded. Frequency-weighting functions were obtained using a least-squares approach to assess the relative contributions of temporal E cues across different frequency regions in Mandarin sentence perception. While the relative contribution of the temporal envelope across different frequency regions in English perception has been studied thoroughly [13, 15, 28], this is the first report to discuss the issue for Mandarin sentence, a tonal language.

As can be seen from Figure 2, the intelligence performance was very good when the temporal E cues of all frequency regions were presented (full region); indeed,

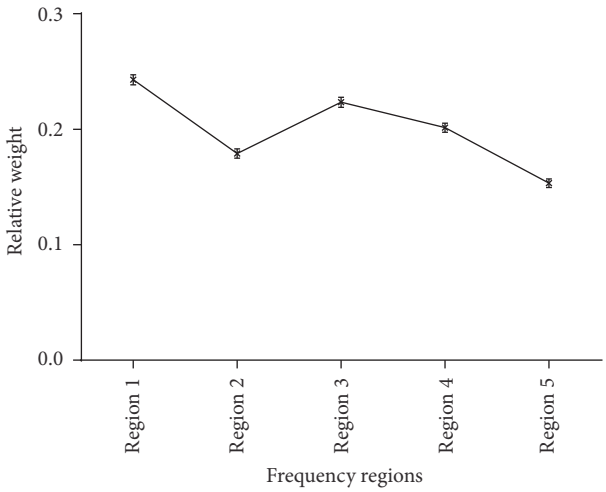

Figure 3: The relative weights of different frequency regions for Mandarin sentence recognition using acoustic temporal envelope. The error bars indicate standard errors.

all listeners scored perfectly. This result is consistent with previous results showing that envelope information alone is sufficient for speech intelligibility in a quiet environment [3, 29, 30]. Nevertheless, the sentence recognition correct scores were only about ~10% when the acoustic E cue from one frequency region was presented alone (Figure 1). When the acoustic E cues from any two frequency regions were presented, the performances were better than the simple sum of the scores obtained with the acoustic E cues of two corresponding frequency regions presented individually. This synergistic effect has been observed previously [11, 13, 31]. Warren et al. [11] found that the regions centered at 370 and 6,000 Hz interacted synergistically when integrated but provided little information when presented individually. Healy and Warren [31] also showed that unintelligible individual speech regions became intelligible when combined, and this effect is similar to the CI simulation results that showed a performance improvement when the number of channels increased from 1 to 2. However, Healy and Warren focused only on pair regions that had equal logarithmic separation from the frequency at 1,500 Hz. In this paper, we recorded the performance under various conditions, with all potential combinations between frequency regions, to drive the relative weight of acoustic E cues in different frequency regions.

The frequency-weighting functions indicated that the five frequency regions contributed to sentence recognition differently. Regions 1 (80–502 Hz) and 3 (1,022–1,913 Hz) were more important than the other regions. The importance of the middle-frequency range (similar to Region 3 in this study) is consistent with previous studies. The Articulation Index (AI) [32] suggested that the 1,500–2,000 Hz frequency region was most important, and Kasturi et al. [33] found that the recognition of vowels and consonants was reduced if the frequency region centered at 1,685 Hz was removed. Moreover, the mean crossover frequencies for temporal envelope speech, an indication of the frequency region providing the most information, were estimated to be 1,421 and 1,329 Hz for male and female speakers, respectively [3]. All of these results indicated that the frequency region around 1,500 Hz is important for speech recognition.

However, the relative weight of acoustic E in the low-frequency region (80–502 Hz) was highest in the present study, in contrast to the study of Ardoint et al. [15], which showed that the E information from the 1.8–7.3 kHz frequency region was more important than other regions for English recognition. Regarding the differences observed between that study and the present study, we suggest four possible reasons. First, Ardoint et al. used vowel-consonant-vowel (VCV) stimuli as test materials, while Mandarin sentences in conversational style were presented in this experiment. The context of the sentence, which is absent in the VCV stimuli, may play a role in this difference. Second, the temporal E information used by Ardoint et al. was extracted from each 2-ERB_N-wide band and then summed in the stimuli presented to the listeners. To better model the frequency selectivity of the normal cochlea, the temporal E information presented in this paper was extracted from 30 continuous 1-ERB_N-wide frequency bands. Third, there were obvious synergistic effects of acoustic E cues between different frequency regions in this study, especially when E cues from Frequency Region 1 were combined with any other frequency region. Thus, the temporal E cues of Frequency Region 1 (80–502 Hz) weighed most heavily here. In contrast, Ardoint et al. suggested that the performance with the E information from two frequency regions could be predicted by the performances when only one frequency region was available. Although no evident synergistic effect was observed, the sentence recognition scores with the E cues from 2 frequency regions tended to be higher if Region 4 (1,845–3,726 Hz) was selected as 1 of the 2 frequency regions [15]. Thus, their results actually showed that E cues from frequency regions above 1.8 kHz transmitted more information. Therefore, synergistic effects should have contributed to the high weight of the low-frequency region in Mandarin recognition.

Indeed, the most important difference was likely the difference in languages. As a tonal language, the recognition of tones contributes significantly to Mandarin recognition because the tonality of a monosyllable is lexically meaningful [20, 21, 34]. It is generally accepted that the tone recognition relies mainly on the variation in F_0 [19, 20, 35]. Kuo et al. [36] showed that the explicit F_0 cue contributed to tone recognition the most, with which listeners could consistently score >90% correct. And the temporal coding of F_0 and the amplitude envelope could contribute to tone recognition more or less in the absence of explicit F_0. Studies have also found a significant correlation between amplitude modulation processing and Mandarin tone recognition without explicit F_0. Also, Mandarin tone recognition has been shown to improve with enhanced similarity between the amplitude and F_0 contour [17, 35, 37].

Considering the essential role of F_0 in tone perception and the importance of tone recognition in Mandarin sentence recognition, it seems reasonable to expect a higher weight for the low-frequency region (Region 1) for Mandarin sentence perception than nontonal English recognition. Similarly,

Wong et al. [38] found that the frequency importance weight for Cantonese was inconsistent with English, due to language differences. Compared with English, the low-frequency information contributes more to Cantonese recognition, which was attributed to the tonal nature of Cantonese. Moreover, the one-third octave band (<180 Hz), which contained F_0 of male speakers, weighed more than each of the four one-third octave bands between 180 and 450 Hz [38]. Furthermore, Kong and Zeng [39] found a relationship between the formant 1 (F_1) frequency and the four Mandarin lexical tones. Therefore, the partial F_1 in Frequency Region 1 may also contribute to tone recognition.

Knowledge of the extent to which each frequency region contributes to Mandarin sentence perception may allow us to modify the programing strategy to maximize the benefit of a cochlear implant by taking advantage of electrodes mapping to the frequency regions that weigh the most. Similar to the "normal weighting functions" for English described by Turner et al. [28], the frequency-weighting functions in this paper indicate a "normal" pattern for Mandarin perception. Based on the comparable effect of the "hole" on the performance of normal-hearing listeners and those with cochlear implants [12], knowledge of the higher weights of Frequency Regions 1 and 3 for some normal-hearing listeners here may have clinical implications for both those with cochlear implants and hearing-impaired listeners, shedding some light on the development of rehabilitation treatment for Chinese patients. The speech signals in the frequency regions with higher weights might be gained before being transmitted to the corresponding electrodes of cochlear implant. And the high weight of the Region 1 suggested the potential of the bimodal hearing [40], which would take good advantage of the speech information in the low-frequency regions, to help the cochlear implanters perform better in Mandarin speech recognition.

However, we concentrated only on the recognition of Mandarin sentences in normal listeners, and the unique frequency-weighting functions for hearing loss and cochlear implants remain unknown. Mehr et al. [41] showed that the relative weights of different regions for cochlear implant users differed from those of normal listeners. In comparison with normal-hearing listeners, Wang et al. [42] suggested that the listeners with hearing loss suffered from a lack of the ability to use spectral envelope cues for lexical tone recognition due to a reduction in frequency selectivity. Turner et al. [43] indicated that listeners with hearing impairment could not compare and integrate the temporal patterns in different frequency regions as effectively as normal hearers. Using the same speech stimuli and the region division of Turner et al. [28], Apoux and Bacon [14] suggested that a severe reduction in frequency resolution led to an increased weight of the high-frequency region. Moreover, patients with sensorial hearing loss generally suffered from reduced frequency selectivity; their frequency-weighting functions may differ from those with normal hearing. Thus, further studies are needed to address the relative importance of the different frequency regions in Chinese speakers with hearing impairment.

5. Conclusions

Frequency-weighting functions for temporal E information were obtained to evaluate the different contributions of various frequency regions to Mandarin sentence recognition. The results indicated that the temporal E cues of Frequency Regions 1 (80–502 Hz) and 3 (1,022–1,913 Hz) were more important than other regions. Compared with the recognition of English, the low-frequency region defined using the parameter conditions here contributed more to Mandarin sentence perception due to the tonal nature of Mandarin.

Competing Interests

The authors declare that there are no competing interests relevant to the publication of this paper.

Acknowledgments

This study was supported by Shanghai Municipal Education Commission-Gaofeng Clinical Medicine Grant Support (Grant no. 20152526) and the National Natural Science Foundation of China (Grant no. 81300820) to Yanmei Feng and the National Natural Science Foundation of China (Grant no. 81530029) to Shankai Yin.

References

[1] Z. M. Smith, B. Delgutte, and A. J. Oxenham, "Chimaeric sounds reveal dichotomies in auditory perception," *Nature*, vol. 416, no. 6876, pp. 87–90, 2002.

[2] C. Lorenzi, G. Gilbert, H. Carn, S. Garnier, and B. C. J. Moore, "Speech perception problems of the hearing impaired reflect inability to use temporal fine structure," *Proceedings of the National Academy of Sciences of the United States of America*, vol. 103, no. 49, pp. 18866–18869, 2006.

[3] M. Ardoint and C. Lorenzi, "Effects of lowpass and highpass filtering on the intelligibility of speech based on temporal fine structure or envelope cues," *Hearing Research*, vol. 260, no. 1-2, pp. 89–95, 2010.

[4] B. Li, L. Hou, L. Xu et al., "Effects of steep high-frequency hearing loss on speech recognition using temporal fine structure in low-frequency region," *Hearing Research*, vol. 326, pp. 66–74, 2015.

[5] B. C. J. Moore, "The role of temporal fine structure processing in pitch perception, masking, and speech perception for normal-hearing and hearing-impaired people," *Journal of the Association for Research in Otolaryngology*, vol. 9, no. 4, pp. 399–406, 2008.

[6] S. Wang, L. Xu, and R. Mannell, "Relative contributions of temporal envelope and fine structure cues to lexical tone recognition in hearing-impaired listeners," *Journal of the Association for Research in Otolaryngology*, vol. 12, no. 6, pp. 783–794, 2011.

[7] B. C. J. Moore, "Temporal integration and context effects in hearing," *Journal of Phonetics*, vol. 31, no. 3-4, pp. 563–574, 2003.

[8] J. A. Bashford, K. R. Riener, and R. M. Warren, "Increasing the intelligibility of speech through multiple phonemic restorations," *Perception & Psychophysics*, vol. 51, no. 3, pp. 211–217, 1992.

[9] R. M. Warren, K. R. Hainsworth, B. S. Brubaker, J. A. Bashford Jr., and E. W. Healy, "Spectral restoration of speech: intelligibility is increased by inserting noise in spectral gaps," *Perception & Psychophysics*, vol. 59, no. 2, pp. 275–283, 1997.

[10] B. Li, H. Wang, G. Yang et al., "The importance of acoustic temporal fine structure cues in different spectral regions for Mandarin sentence recognition," *Ear and Hearing*, vol. 37, no. 1, pp. e52–e56, 2016.

[11] R. M. Warren, K. R. Riener, J. A. Bashford, and B. S. Brubaker, "Spectral redundancy: intelligibility of sentences heard through narrow spectral slits," *Perception & Psychophysics*, vol. 57, no. 2, pp. 175–182, 1995.

[12] R. V. Shannon, J. J. Galvin III, and D. Baskent, "Holes in hearing," *JARO - Journal of the Association for Research in Otolaryngology*, vol. 3, no. 2, pp. 185–199, 2002.

[13] R. M. Warren, J. A. Bashford Jr., and P. W. Lenz, "Intelligibilities of 1-octave rectangular bands spanning the speech spectrum when heard separately and paired," *Journal of the Acoustical Society of America*, vol. 118, no. 5, pp. 3261–3266, 2005.

[14] F. Apoux and S. P. Bacon, "Relative importance of temporal information in various frequency regions for consonant identification in quiet and in noise," *Journal of the Acoustical Society of America*, vol. 116, no. 3, 2004.

[15] M. Ardoint, T. Agus, S. Sheft, and C. Lorenzi, "Importance of temporal-envelope speech cues in different spectral regions," *Journal of the Acoustical Society of America*, vol. 130, no. 2, pp. EL115–EL121, 2011.

[16] X. Luo, Q.-J. Fu, and R.-H. Wang, "Contributions of periodicity fluctuation cues in individual frequency channels to the perception of Chinese vowels and tones," *Technical Acoustics*, vol. 24, no. 4, pp. 254–258, 2005.

[17] X. Luo and Q.-J. Fu, "Enhancing Chinese tone recognition by manipulating amplitude envelope: implications for cochlear implants," *Journal of the Acoustical Society of America*, vol. 116, no. 6, pp. 3659–3667, 2004.

[18] L. Cabrera, F.-M. Tsao, D. Gnansia, J. Bertoncini, and C. Lorenzi, "The role of spectro-temporal fine structure cues in lexical-tone discrimination for French and Mandarin listeners," *Journal of the Acoustical Society of America*, vol. 136, no. 2, pp. 877–882, 2014.

[19] D. H. Whalen and Y. Xu, "Information for Mandarin tones in the amplitude contour and in brief segments," *Phonetica*, vol. 49, no. 1, pp. 25–47, 1992.

[20] L. Xu and N. Zhou, "Tonal languages and cochlear implants," in *Auditory Prostheses*, pp. 341–364, 2011.

[21] Q.-J. Fu, F.-G. Zeng, R. V. Shannon, and S. D. Soli, "Importance of tonal envelope cues in Chinese speech recognition," *Journal of the Acoustical Society of America*, vol. 104, no. 1, pp. 505–510, 1998.

[22] D. Fogerty, "Perceptual weighting of individual and concurrent cues for sentence intelligibility: frequency, envelope, and fine structure," *Journal of the Acoustical Society of America*, vol. 129, no. 2, pp. 977–988, 2011.

[23] ANSI, *American National Standards Specifications for Audiometers (ANSI S3.6-2004)*, American National Standards Institute, New York, NY, USA, 2004.

[24] L. L. N. Wong, S. D. Soli, S. Liu, N. Han, and M.-W. Huang, "Development of the mandarin hearing in noise test (MHINT)," *Ear and Hearing*, vol. 28, no. 2, pp. 70S–74S, 2007.

[25] B. R. Glasberg and B. C. J. Moore, "Derivation of auditory filter shapes from notched-noise data," *Hearing Research*, vol. 47, no. 1-2, pp. 103–138, 1990.

[26] R. M. Warren, J. A. Bashford Jr., and P. W. Lenz, "Intelligibility of bandpass filtered speech: steepness of slopes required to eliminate transition band contributions," *Journal of the Acoustical Society of America*, vol. 115, no. 3, pp. 1292–1295, 2004.

[27] G. A. Studebaker, "A 'rationalized' arcsine transform," *Journal of Speech & Hearing Research*, vol. 28, no. 3, pp. 455–462, 1985.

[28] C. W. Turner, B. J. Kwon, C. Tanaka, J. Knapp, J. L. Hubbartt, and K. A. Doherty, "Frequency-weighting functions for broadband speech as estimated by a correlational method," *Journal of the Acoustical Society of America*, vol. 104, no. 3, part 1, pp. 1580–1585, 1998.

[29] R. V. Shannon, F.-G. Zeng, V. Kamath, J. Wygonski, and M. Ekelid, "Speech recognition with primarily temporal cues," *Science*, vol. 270, no. 5234, pp. 303–304, 1995.

[30] F.-G. Zeng, "Trends in cochlear implants," *Trends in Amplification*, vol. 8, no. 1, pp. 1–34, 2004.

[31] E. W. Healy and R. M. Warren, "The role of contrasting temporal amplitude patterns in the perception of speech," *Journal of the Acoustical Society of America*, vol. 113, no. 3, pp. 1676–1688, 2003.

[32] ANSI, *American National Standards Methods for the Calculation of the Articulation Index*, American National Standards Institute, New York, NY, USA, 1969.

[33] K. Kasturi, P. C. Loizou, M. Dorman, and T. Spahr, "The intelligibility of speech with 'holes' in the spectrum," *Journal of the Acoustical Society of America*, vol. 112, no. 3, pp. 1102–1111, 2002.

[34] C.-G. Wei, K. Cao, and F.-G. Zeng, "Mandarin tone recognition in cochlear-implant subjects," *Hearing Research*, vol. 197, no. 1-2, pp. 87–95, 2004.

[35] Q. Fu and F. Zeng, "Identification of temporal envelope cues in Chinese tone recognition," *Asia Pacific Journal of Speech, Language & Hearing*, vol. 5, no. 1, pp. 45–57, 2013.

[36] Y.-C. Kuo, S. Rosen, and A. Faulkner, "Acoustic cues to tonal contrasts in Mandarin: implications for cochlear implants," *Journal of the Acoustical Society of America*, vol. 123, no. 5, pp. 2815–2824, 2008.

[37] X. Luo, Q.-J. Fu, C.-G. Wei, and K.-L. Cao, "Speech recognition and temporal amplitude modulation processing by Mandarin-speaking cochlear implant users," *Ear and Hearing*, vol. 29, no. 6, pp. 957–970, 2008.

[38] L. L. N. Wong, A. H. S. Ho, E. W. W. Chua, and S. D. Soli, "Development of the Cantonese speech intelligibility index," *Journal of the Acoustical Society of America*, vol. 121, no. 4, pp. 2350–2361, 2007.

[39] Y.-Y. Kong and F.-G. Zeng, "Temporal and spectral cues in Mandarin tone recognition," *Journal of the Acoustical Society of America*, vol. 120, no. 5, pp. 2830–2840, 2006.

[40] X. Luo, Y.-P. Chang, C.-Y. Lin, and R. Y. Chang, "Contribution of bimodal hearing to lexical tone normalization in Mandarin-speaking cochlear implant users," *Hearing Research*, vol. 312, pp. 1–8, 2014.

[41] M. A. Mehr, C. W. Turner, and A. Parkinson, "Channel weights for speech recognition in cochlear implant users," *Journal of the Acoustical Society of America*, vol. 109, no. 1, pp. 359–366, 2001.

[42] S. Wang, R. Mannell, P. Newall, and D. Han, "Contribution of spectral cues to mandarin lexical tone recognition in normal-hearing and hearing-impaired mandarin Chinese speakers," *Ear and Hearing*, vol. 32, no. 1, pp. 97–103, 2011.

[43] C. W. Turner, S.-L. Chi, and S. Flock, "Limiting spectral resolution in speech for listeners with sensorineural hearing loss," *Journal of Speech, Language, & Hearing Research*, vol. 42, no. 4, pp. 773–784, 1999.

Hindawi Publishing Corporation
Neural Plasticity
Volume 2016, Article ID 2523458, 9 pages
http://dx.doi.org/10.1155/2016/2523458

Review Article

Mammalian Cochlear Hair Cell Regeneration and Ribbon Synapse Reformation

Xiaoling Lu,[1] Yilai Shu,[1] Mingliang Tang,[2,3] and Huawei Li[1,4,5,6,7]

[1]*Otorhinolaryngology Department of Affiliated Eye and ENT Hospital, State Key Laboratory of Medical Neurobiology, Fudan University, Shanghai 200031, China*
[2]*Key Laboratory for Developmental Genes and Human Disease, Ministry of Education, Institute of Life Sciences, Southeast University, Nanjing 210096, China*
[3]*Co-Innovation Center of Neuroregeneration, Nantong University, Nantong 226001, China*
[4]*Institutes of Biomedical Sciences, Fudan University, Shanghai 200032, China*
[5]*Key Laboratory of Hearing Medicine of NHFPC, Shanghai 200031, China*
[6]*Shanghai Engineering Research Centre of Cochlear Implant, Shanghai 200031, China*
[7]*The Institutes of Brain Science and the Collaborative Innovation Center for Brain Science, Fudan University, Shanghai 200032, China*

Correspondence should be addressed to Mingliang Tang; mingliangtang@seu.edu.cn and Huawei Li; huaweili611@126.com

Received 9 September 2016; Revised 29 November 2016; Accepted 1 December 2016

Academic Editor: Genglin Li

Hair cells (HCs) are the sensory preceptor cells in the inner ear, which play an important role in hearing and balance. The HCs of organ of Corti are susceptible to noise, ototoxic drugs, and infections, thus resulting in permanent hearing loss. Recent approaches of HCs regeneration provide new directions for finding the treatment of sensor neural deafness. To have normal hearing function, the regenerated HCs must be reinnervated by nerve fibers and reform ribbon synapse with the dendrite of spiral ganglion neuron through nerve regeneration. In this review, we discuss the research progress in HC regeneration, the synaptic plasticity, and the reinnervation of new regenerated HCs in mammalian inner ear.

1. Introduction

Mammalian HCs loss by noise trauma, ototoxic drugs, or infection is a major cause of deafness [1]. HCs in mammalian inner ear, unlike invertebrate animals such as birds and fish, do not undergo spontaneous regeneration, even though vestibular supporting cells (SCs) retain a limited capacity to divide [2, 3]. There are two approaches of HC regeneration: (1) direct transdifferentiation of surrounding SCs that directly change cell fate and become HCs and (2) induction of a proliferative response in the SCs which mitotically divide and further differentiate to replace damaged HCs [4–6]. There are various numbers of genes and cell signaling pathways involved in these two mechanisms that remain challenging to understand the molecular mechanism underneath hair cell regeneration. Several studies showed reinnervation of the regenerated HCs after HC regeneration [6–8]. However, innervation of new regenerated HCs still needs to be determined in all kinds of hearing loss.

2. The Anatomy and Function of the Organ of Corti

The organ of Corti, also called the spiral organ, is the spiral structure on the basement membrane of the cochlear duct. The sensory epithelium of the organ of Corti is made up of HCs and SCs. HCs, which can be divided into inner HCs and outer HCs, are sensory receptor cells whose mechanically sensitive hair bundles convert mechanical force produced by sound waves into neural impulses. HCs are surrounded by SCs and connected with cochlear nerve fibers by forming synaptic connection. There are several types of SCs, such as pillar cells and phalangeal cells. Pillar cells can be divided into inner and outer pillar cells found in the middle of

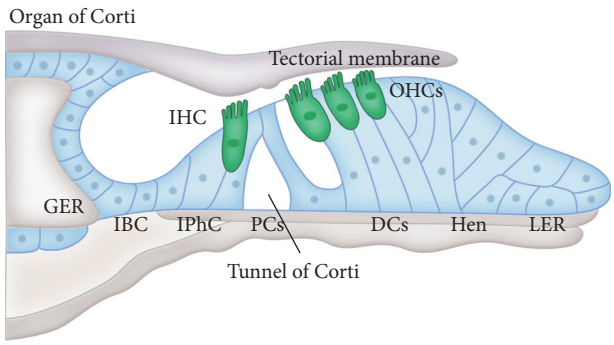

Figure 1: Schematic model of the organ of Corti. IHC: inner hair cell; OHCs: outer hair cells; PCs: inner and outer pillar cells; IPhC: inner phalangeal cell; DCs: Deiters' cells; IBC: inner border cell; Hen: Hensen's cell; GER: greater epithelial ridge; LER: lesser epithelial ridge.

the inner and outer HCs separately. The top and bottom of the inner and outer pillar cells are combined, but the middle of them is separated, forming the two edge sides of the triangular tunnel. In the lateral of inner and outer HCs rows, inner and outer phalangeal cells (also called the Deiters' cells) reside, respectively. The finger like projection of Deiters' cells are tightly connected with the apical of outer pillar cells forming a thin, hard reticular membrane, also called reticular layer. The stereocilium of outer HCs is tightly bounded trough the mesh of reticular layer. The reticular layer constitutes fiber and matrix and is found below the tectorial membrane. HCs are sensory cells, and they do not contain axons and dendrites. Instead, the basolateral surface of HCs form afferent synaptic contacts with the axonal terminals of the eighth nerve and receive efferent contacts from neurons in the brainstem. There are about 25,000 to 30,000 auditory nerve fibers connected with HCs. These fibers originate from bipolar spiral ganglion neurons in the modiolus, whose axonal terminals form synaptic connections with the ribbons at HCs and the dendrite forms connection with cochlear nucleus neuron (Figure 1).

The organ of Corti acts as an auditory receptor. Acoustic wave passes through the external auditory canal and reaches the tympanic membrane; the tympanic membrane transmitted these vibrations to the oval window by auditory ossicles, causing the perilymph in scala vestibuli to further pass these vibrations to the vestibular membrane and endolymph in cochlear duct. At the same time, the vibration of perilymph in scala vestibuli can be transmitted to the scala tympani through helicotrema, causing the basement membrane to resonance. Due to the different length and diameter of hearing fiber in different parts of the basement membrane results in the different frequency of acoustic wave resonance in the different parts of the basement membrane. The vibration of corresponding parts causes the HCs to contact with the tectorial membrane, the stereocilia bends, and HCs become excited to translocate the mechanical vibration into electrical excitation, which further transmit to the central auditory nerve to eventually producing the sense of hearing.

3. Hair Cell Regeneration

The organ of Corti harbors HCs, which are vulnerable to infections and many pharmaceutical drugs such as aminoglycoside antibodies, for example, streptomycin and neomycin, and the chemotherapeutic agent cisplatin. Most importantly, HCs can be damaged by acoustic trauma. In nonmammalian vertebrates such as birds, after ototoxic drugs or damaged by noise, the inner ear sensory HCs can regenerate spontaneously and eventually replace the damaged HCs, thus maintaining and restoring the function of sensory epithelium [5, 9]. However, in mammals, spontaneous HC regeneration in vivo has only been identified in neonatal cochleae and also the number of regenerated HCs is quite low; as a result the hearing loss is permanent in mammals [10, 11]. It is thought that the mammalian inner ear HCs and SCs originate from the common precursor cells and some of the reported studies suggested that some SCs become HCs when the microenvironment changes, such as damage to HCs and activation of particular genes; SCs can continue to differentiate to form HCs [12, 13]. Thus, currently some of the SCs are more commonly recognized as progenitor cells in regenerating HCs. At present, in view of the origin and regeneration of mammalian HCs, there are mainly two mechanisms of HCs regeneration from SCs, one is mitotic division of SC and the other is transdifferentiation [4–6]. In mitotic division, the SCs can divide and then their daughter cells undergo differentiating into HCs in some portions. In transdifferentiation, the SCs directly undergo phenotypic conversion and thus transdifferentiate into a HC without mitosis. Many studies have been done that illustrated the important factors, which are involved in the process of HC differentiation, such as Atoh1, p27Kip1, and Rb. Also, the cell signaling pathways, such as Notch, Wnt, and FGF signaling pathway, play important roles in HC regeneration (Figure 2).

Atoh1, the bHLH differentiation factor, was relating to the formation of mechanoreceptor and photoreceptor in *Drosophila* [14, 15]. During the embryonic development of mice cochlea, the upregulation of Atoh1 causes an increase number of HCs [7, 16]. In the neonatal cochlea of mice, the upregulation of Atoh1 can activate the SCs to differentiate to form more HCs [17–19]. However, in the undamaged and mature cochleae, the differentiation capacity of SCs is significantly decreased when assessed in transgenic mice or via direct viral inoculation [20]. In consideration of the crucial role of Atoh1 gene during the development of HCs, various studies focused on the regulation of Atoh1 to produce HCs in the damaged and mature cochlear. It is reported that, after ototoxic injury in guinea pigs, immature HCs were regenerated through regulating the ectopic expression of Atoh1, and the hearing function was rescued to a certain extent [21]. However, other studies also found that the efficacy of this approach to regenerate HCs might be limited, and the regulation time of Atoh1 expression after damage is dependent [22, 23]. Moreover, it has been revealed that the H3K4me3/H3K27me3 bivalent chromatin structure is crucial for the function of Atoh1, which is observed at the Atoh1 locus of SCs, and might give an explanation for why these cells can keep the capacity to transdifferentiate into HCs [24].

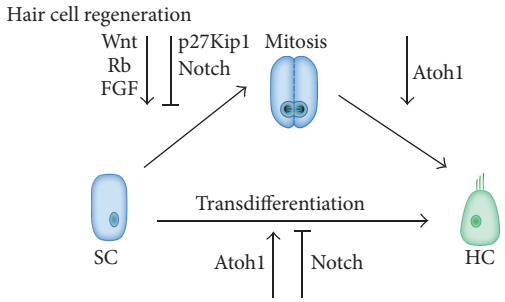

Figure 2

Several cyclin/cyclin-dependent-kinases (CDKs), including p27Kip1, are dynamically expressed in the sensory epithelial [25, 26]. During the embryonic development of mammalian cochlea, the prosensory cells begin to express p27Kip1 from the apex to the base [25, 26]. Disruption of p27Kip1 gene in the mouse cochlea results in ongoing cell proliferation in the postnatal and adult mouse organ of Corti [25, 27]. Although this approach partially keep the capacity of prosensory cells to proliferate, the cell overproduction will cause dysfunction in the organ of Corti, which results in hearing loss [25]. These studies indicated that the proper expression level of p27Kip1 is necessary for maintaining the normal quantity of HCs and SCs. In contrast to the non-mammals, the mammalian organ of Corti completely lacks the phenomenon through which SCs reenter cell cycle [28–30]. One reason why the mature mammalian organ of Corti cannot reproduce HCs is because the SCs are mitotically quiescent after birth. When p27Kip1 is genetically deleted in the SCs in the neonatal cochlear, these SCs proliferate but do not differentiate into HCs [31–33]. The number of mitotic cells significantly decreased in the mature cochlea when compared to that in the neonatal cochlea [31–33]. When p27Kip is deleted in the HCs of neonatal cochlea, these HCs autonomously reenter into the cell cycle and regenerate new HCs; also these newly generated HCs survived till adult age without compromising hearing function [34]. These findings revealed a new route to directly induce regeneration by renewing the proliferation capacity of surviving HCs in mammalian organ of Corti.

pRb is a retinoblastoma protein, which is encoded by the retinoblastoma gene Rb1. It plays a role in cell cycle exit, differentiation, and survival [35, 36]. It has been shown that the targeted deletion of Rb1 allowed them to undergo cell cycle and become highly differentiated and functional indicating that the differentiation of the sensory epithelia and cell division are not mutually exclusive [6, 37]. However, the proliferation due to Rb1 deletion is age dependent and eventually the cochlear HCs undergo apoptosis [38, 39]. Moreover, the transient downregulation of Rb1 is necessary to induce proliferation in adult cochlea, also together with Rb1 deletion some other strategies such as epigenetic modifications and reprogramming need to be further studied in order to regenerate HCs in mature cochlea.

The Notch signaling pathway plays multiple roles during the development of mammalian cochlea. The precise formation of mosaic structure of the HC and SC is medi ated by lateral inhibition through dynamic expression of the Notch signaling pathway [40–42]. As the process of HCs differentiation begins, a prosensory cell chooses to become a HC or a SC under the precise regulation of lateral inhibition through Notch pathway. The HCs undergoing the differentiation express the Notch ligands and activate Notch signaling pathway in the neighboring SCs, thus preventing them from obtaining a HC fate. Eventually, the mosaic structure of HC and SC is formed. Moreover, in the germline deletion of the Notch ligand Jag2 or Delta-like 1 (Dll1), the HC number is increased at the cost of SCs [43, 44]. In a similar manner, when Notch/Jag2 and Dll1 are suppressed during early embryonic development, the prosensory cells proliferation becomes prolonged comparing with the normal control in the inner ear [43, 44]. On the contrary, the formation of prosensory domain is prevented when the Notch receptor Notch1 is conditionally knocked out; meanwhile, there is increased number of HCs and a concomitant deceased number of SCs [43]. These findings demonstrated that the Notch pathway plays important roles in the specification of normal prosensory domain and regulates the differentiation of HCs in different levels through different combination of Notch ligands and receptors. Furthermore, the effects of Notch inhibition have also been explored on the regeneration process of HC. It is reported that the SCs can transdifferentiate into HCs when treated with Notch inhibitor in the undamaged neonatal mammalian cochlea [45–47]. Coincidently, this pharmacological approach produces significantly less number of HCs in the damaged and mature cochlea of mammals [48, 49] and these newly regenerated HCs are acquired through direct transdifferentiation of SCs [45–49]. Taken together, these findings suggests that both the proliferation of SCs and HC differentiation including their coordination might require the regeneration and function recovery of the organ of Corti.

Wnt are widely expressed and evolutionary conserved in the vertebrates and invertebrates animal tissues. Wnt play important roles in several biological processes, such as development, proliferation, metabolism, and regulation of stem cells. The activation of Wnt signaling pathway through beta-catenin overexpression protects HCs against neomycin insult [50]. When cochleae are cultured in vitro, the addition of Wnt inhibitors prevents the proliferation of prosensory cells and also the differentiation into HCs [51]. On the contrary, when supplied with Wnt signaling activators result in increased proliferation of prosensory cells and HCs [51]. These studies revealed that the canonical Wnt signaling pathway plays important roles in regulating the proliferation of prosensory cells and differentiation of HCs during cochlea development. Furthermore, when beta-catenin is ablated during cochlear development, which is a key gene of canonical Wnt signaling pathway, the proliferation of prosensory cells is significantly decreased and the large number of HCs was diminished [52]. Recent studies have found that Lgr5 positive SCs are the precursor cells with the capacity to regenerate HCs under certain conditions [13, 53]. In the neonatal cochleae of mammals, the Wnt target gene Lgr5 is expressed in a subset of SCs (the pillar cells, inner phalangeal cells, and Deiters' cells) [54], and

these endogenous Lgr5+ cells maintain mitotic quiescence. The expression level of Wnt signaling pathway including Lgr5 regulated via the expression of Bmi1 [55]. When isolated as single cells using flow cytometry and cultured in vitro, they become proliferative and converted into HC-like cells [13]. In addition, the isolated Lgr5+ SCs significantly increase the Atoh1 expression and the number of HC-like cells after the addition of Wnt signaling pathway agonist [53]. Moreover, it is reported that the proliferation capacity of the Lgr5 positive cells in the apical turn is higher than the basal turn [56]. The conditional overexpression of beta-catenin in the neonatal transgenic mouse cochlea significantly increased the percentage of proliferative supporting cells [13, 53]. Prior study reveals that the inner pillar cells are more sensitive to the beta-catenin overexpression and can also upregulate the expression level of Atoh1 [57]. These studies suggested that the Wnt/beta-catenin signaling pathway participated in the proliferative response in the SCs of neonatal mammals and the interaction between Wnt and Notch signaling pathway is important in the inner ear [46, 58]. More excitingly, extensive SCs proliferation followed by mitotic HCs generation can be achieved through a genetic reprogramming process involving beta-catenin activation, Notch1 deletion, and Atoh1 overexpression. [59].

The FGF signaling pathway is important during inner ear development and morphogenesis. It is related to the induction of otic placode and the development of otic vesile [60–62]. When the FGF receptor 1 (Fgfr1) is genetically deleted in the inner ear, the number of proliferative prosensory cells decreases resulting in decreased number of HCs and SCs [63, 64]. It is reported that Fgf20, which is the candidate ligand for Fgfr1, might be the downstream target of Notch signaling pathway [42]. The addition of Ffg20 rescues the abnormal prosensory specification caused by Notch inhibition [42]. Moreover, downregulation of Fgf20 expression does not cause vestibular dysfunction, which indicates that the Fgf20 might be related to HCs specification in the cochlea. Moreover, it is identified that Fgf8 and Fgf3 are necessary for the development of pillar cells [65, 66]. So far, the function of FGF signaling pathway on HC regeneration is explored in the utricle of chicken and lateral line of zebrafish. When SCs robustly proliferate, the expression level of Fgf20 and Fgfr3 decreases [67]. It is found that the expression level of Fgfr3 is decreased in the cochlea of chicken and the lateral line of zebrafish [68, 69]. However, in the damaged and undamaged mammalian cochlea increased Fgfr3 expression was observed [70]. Taken together, these studies indicated that FGF signaling pathway plays an important role in the specification of prosensory cells and differentiation of HCs and SCs during development, but the function of FGF signaling on HC regeneration is still remain unknown.

4. Ribbon Synapse Reforming and Reinnervation in Regenerated Hair Cells

It is true that the regeneration of HCs is predominantly important and the pivotal issue for restoring hearing and balance function. The regeneration of synaptic connection between newly generated HCs and spiral ganglion neurons is also required. It is reported that when exposed to excessive noise, both HCs and spiral ganglion neuron are sensitive. In mammals, spiral ganglion neurons are hardly recovered from injury [71, 72] and the auditory nerve fibers often degenerate after ototoxic insult, including noise damage and ototoxic drugs. The process of degeneration has been revealed. At first, the unmyelinated terminal dendrites within the organ of Corti disappear (within hours to days), followed by the slow degeneration of peripheral axons in the osseous spiral lamina (within days to weeks). Then, the cell bodies in the spiral ganglion and their central axons that compose the cochlear nerve (over weeks to months and longer) degenerate in the last. Thus the regeneration of ribbon synapses and spiral ganglion neurons in combination with HCs are important for treating hearing loss.

The innervation of HCs is complex process. In the mammalian cochlea, the inner HCs are key component in the sound perception. The inner HC transmits signal to the nerve fibers of spiral ganglion neuron through transforming the mechanical signals induced by sound into electrochemical signal. On the other hand, the outer HC is related to the amplification of audible signals. In the auditory nervous system, there are two kinds of functional neuron population that works differently to convey sound information. In the adult mouse cochlea, there are approximately 800 inner HCs, which are exclusively innervated by 5–30 type I spiral ganglion neuron fibers. These type I spiral ganglion neurons are the main encoders of the auditory signal, which constitute almost 95 percent of the total neuron population [73–75]. In contrast, the type II spiral ganglion neurons constituting approximately 5 percent of the total neuron population innervate the approximately 2,600 outer HCs (almost 1-2 outer HCs per fiber) [76] (Figure 3). The innervation of type II spiral ganglion neuron to the outer HCs is likely to give sensory feedback as a component of the neural control loop, which includes the inhibitory olivocochlear efferent innervation of both outer HC and the postsynaptic region of the type I spiral ganglion neuron at the inner HC region. The mature organ of Corti receives extensive efferent innervation via the lateral olivocochlear (LOC) input to the boutons and dendrites of type I spiral ganglion neurons in the inner spiral plexus region and via the medial olivocochlear (MOC) bundle projection to the outer HCs [76] (Figure 3). This reorganization occurs just before the onset of hearing during the first postnatal week. There are three distinct stages in the formation and development of the afferent nerve fiber innervation to the inner and outer HCs [77]. From embryonic day 18 to postnatal day 0, two kinds of afferent nerve fibers begin to extend and the neurite grows towards HCs. From postnatal day 0 to day 3, the neurite of these afferent fibers begins to refine to form outer spiral bundles, which innervate outer HCs. From postnatal day 3 to day 6, the neurite and synapse structure of type I spiral ganglion neuron retract towards outer HCs and prune to eliminate the innervation between outer HCs and type I spiral ganglion neuron, while the innervation of inner HC is retained by type I spiral ganglion neuron. Also, multiple factors and

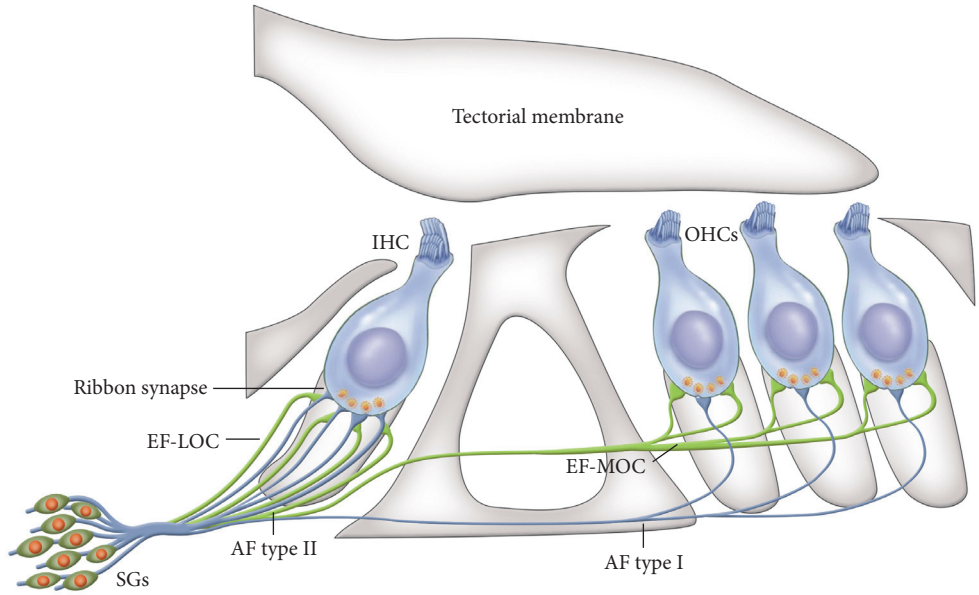

Figure 3: Schematic drawing of the innervation of hair cells. IHC: inner hair cell; OHCs: outer hair cells; AF: afferent fiber; EF: efferent fiber; LOC: lateral olivary complex; MOC: medial olivary complex.

signaling pathways have been studied in the development and regeneration processes in inner HC ribbon synapses, such as neurotrophins, hormonal signaling, thrombospondins, Gata3-mafb, and Foxo3 networks [78, 79].

The neurotransmission between inner HCs and type I spiral ganglion neurons and outer HCs and type II spiral ganglion neurons are conveyed by the ribbon synapses, which are crucial for the accurate encoding of acoustic information [76, 80]. The key component of the ribbon synapse is the glutamatergic synaptic complexes, which are composed of presynaptic ribbons and postsynaptic densities. This kind of afferent ribbon synapse is capable of releasing neurotransmitter quickly and synchronously [81]. The presynaptic ribbons in the inner ear basolateral membrane was found in the opposite side of the postsynaptic glutamate receptors on the dendrite of afferent fibers. The presynaptic ribbons are settled in the active zone of HCs by electron-dense ribbon configuration. When responding to different acoustic signals, the presynaptic ribbons release multiple vesicles quickly and synchronously with high temporal resolution [82–84]. In the postsynaptic dendrite of afferent fibers, the excitatory neurotransmission is mediated by AMPA-type glutamate receptors [85].

In recent years, HC regeneration has made certain achievements; thus, the reinnervation of newly generated HCs and reformation of ribbon synapses are urgently needed for restoring hearing and balance function. Cochlear ribbon synapses have limited intrinsic capacity to spontaneously regenerate [86–88]. Prior study reported that when cochleae is damaged in neonatal mice, the HCs spontaneously regenerate from the SCs, but the inner cell marker vesicular glutamate transporter VGlut3 was not detected in these newly regenerated HCs [10]. When the Notch1 signaling pathway overactivated to induce the ectopic HCs, the neural fiber marker Tuj1 was detected in the lateral edge of spiral ganglion neuron, while the synaptic marker synaptophysin was detected between the new HCs and neuronal cells in the spiral ganglion regions, but the synaptophysin signals adjacent to new HCs were weaker indicating that the synaptic structures among new HCs and neuronal cells were not fully mature [89]. The deletion of p27Kip1 induced regeneration of new HCs and these HCs were stained with espin (stereociliary bundles), C-terminal binding protein-2 (Ctbp2; ribbon synapses), and class III beta-tubulin (Tuj1; innervating nerve fibers). However, a portion of the postnatal derived inner HCs was negative for VGlut3 (synaptic transmission) marker [34]. Deletion of p27Kip1 reforms "synaptic structure" to some extent. Although hearing function was normal in adult mice, the functional reformation of synaptic contacts still remained unclear. The ectopic expression of Atoh1 induced HC regeneration, the synaptic markers, CSP, synaptophysin, and synaptotagmin 1 detected at the basal of the newly generated HCs. Although some synaptic markers were found at the site of newly regenerated HCs and neuron contacts, the normal synaptic ribbons were still absent [18].

To achieve a better innervation of the newly generated HCs, the regeneration of ribbon synapses is predominantly important. Recently, many factors and signaling pathways have been found to play a role in promoting axonal regeneration and synapse reformation [90, 91]. The synaptotrophic factors are the most well-known factors. The members of the neutrophin family, such as the nerve growth factor (NGF), brain-derived neurotrophic factor (BDNF), neurotrophin-3 (NT3), and neurotrophin-4/5 (NT-4/5), are participated in

the formation of ribbon synapse and promote the synaptic regeneration process [92–95]. BDNF and its congenital receptor TrkB and the NT-3 and its congenital receptor were detected in the cochlea [96]. It has been reported that BDNF and NT-3 are critical factors for the survival of sensory neurons and the initiation of nerve fibers extending towards the sensory epithelial in the cochlea and vestibule [97]. In the neonatal inner ear of mammals, the deletion of BDNF or NT-3 causes specific loss of ribbon synapses in the cochlea and vestibule, respectively, causing hearing loss and vestibular dysfunction [98, 99]. After ototoxic drug damage, the addition of BDNF and NT-3 promotes the reinnervation of spiral ganglion neurons in cultured cochleae and expresses the postsynaptic markers [100]. Moreover, it is likely that the NT-3 is more significant for ribbon synapses after noise exposure than BDNF [99]. Supporting cell-derived NT-3 promotes the regeneration of ribbon synapses and is helpful in the recovery of cochlear function [78, 100] indicating that the neurotrophins are important for the formation of postsynaptic densities and ribbon synapse regeneration after injury. Glutamate is another important synaptotrophic factor [100]. In the deafferented organ of Corti, the number of newly generated synaptic contacts at the dendrite of spiral ganglion neurons was significantly decreased in the Vglut3 deletion mice when compared to normal controls, indicating that the proper releasing of glutamate transmitter is important for the regeneration of synaptic contacts in vitro [100]. However, the in vivo role of glutamate in synaptic regeneration still remains unclear. Furthermore, the contacts generated between cultured spiral ganglion neurons and denervated HCs were evaluated and found that the postsynaptic density protein PSD-95 was immunopositive and directly facing the HC ribbons [100]. The neurotrophins, BDNF and NT-3, significantly increase the number of new synapses. In consideration of the synapse formation activities, these neurotrophins reveal a potential to promote synapse regeneration in the newly regenerated HCs.

5. Conclusions

In the recent years, there is growing concern about the HC regeneration and synaptic plasticity around the globe and the great achievements have been made in revealing the mechanism and strategies to recover hearing function in mammals [10, 13, 59, 101]. Different levels of HC regeneration could be achieved through the regulation of factors and signaling pathways, which play important roles during the development of mammalian inner ear [23, 34, 48, 59]. Synapse and nerve fiber related markers are detected around the newly regenerated HCs [10, 34, 89]. However, we are still quite far from restoring the hearing function in the damaged inner ear. The maturation and survival of newly generated HCs are still challenging. Furthermore, the maturation of reinnervation of the regenerated HCs and the function of the reformed ribbon synapse remain open to question, such as the contact between stereocilium and tectorial membrane, reorganization of the innervation of afferent Type I and Type II spiral ganglion neuron, and the integral interplay of outer hair cell based cochlear amplification. To obtain a viable treatment option for future hair cell regeneration of patients suffering from hearing loss, the understanding of reinnervation of the regenerated hair cells and the function of the reformed ribbon synapse is essential and it remains to be explored and open to question.

Competing Interests

The authors have declared that no competing interests exist.

Authors' Contributions

Xiaoling Lu and Yilai Shu contributed equally to this work.

References

[1] J. V. Brigande and S. Heller, "Quo vadis, hair cell regeneration?" *Nature Neuroscience*, vol. 12, no. 6, pp. 679–685, 2009.

[2] A. Forge, L. Li, J. T. Corwin, and G. Nevill, "Ultrastructural evidence for hair cell regeneration in the mammalian inner ear," *Science*, vol. 259, no. 5101, pp. 1616–1619, 1993.

[3] M. E. Warchol, P. R. Lambert, B. J. Goldstein, A. Forge, and J. T. Corwin, "Regenerative proliferation in inner ear sensory epithelia from adult guinea pigs and humans," *Science*, vol. 259, no. 5101, pp. 1619–1622, 1993.

[4] Y. Raphael, "Evidence for supporting cell mitosis in response to acoustic trauma in the avian inner ear," *Journal of Neurocytology*, vol. 21, no. 9, pp. 663–671, 1992.

[5] J. S. Stone and D. A. Cotanche, "Hair cell regeneration in the avian auditory epithelium," *International Journal of Developmental Biology*, vol. 51, no. 6-7, pp. 633–647, 2007.

[6] C. Sage, M. Huang, K. Karimi et al., "Proliferation of functional hair cells in vivo in the absence of the retinoblastoma protein," *Science*, vol. 307, no. 5712, pp. 1114–1118, 2005.

[7] S. P. Gubbels, D. W. Woessner, J. C. Mitchell, A. J. Ricci, and J. V. Brigande, "Functional auditory hair cells produced in the mammalian cochlea by in utero gene transfer," *Nature*, vol. 455, no. 7212, pp. 537–541, 2008.

[8] M. W. Kelley, "Regulation of cell fate in the sensory epithelia of the inner ear," *Nature Reviews Neuroscience*, vol. 7, no. 11, pp. 837–849, 2006.

[9] B. M. Ryals and E. W. Rubel, "Hair cell regeneration after acoustic trauma in adult coturnix quail," *Science*, vol. 240, no. 4860, pp. 1774–1776, 1988.

[10] B. C. Cox, R. Chai, A. Lenoir et al., "Spontaneous hair cell regeneration in the neonatal mouse cochlea in vivo," *Development*, vol. 141, no. 7, pp. 1599–1599, 2014.

[11] P. M. White, A. Doetzlhofer, Y. S. Lee, A. K. Groves, and N. Segil, "Mammalian cochlear supporting cells can divide and trans-differentiate into hair cells," *Nature*, vol. 441, no. 7096, pp. 984–987, 2006.

[12] T. A. Jan, R. Chai, Z. N. Sayyid et al., "Tympanic border cells are Wnt-responsive and can act as progenitors for postnatal mouse cochlear cells," *Development*, vol. 140, no. 6, pp. 1196–1206, 2013.

[13] R. Chai, B. Kuo, T. Wang et al., "Wnt signaling induces proliferation of sensory precursors in the postnatal mouse cochlea," *Proceedings of the National Academy of Sciences of the United States of America*, vol. 109, no. 21, pp. 8167–8172, 2012.

[14] A. P. Jarman, Y. Grau, L. Y. Jan, and Y. N. Jan, "Atonal is a proneural gene that directs chordotonal organ formation in the

Drosophila peripheral nervous system," *Cell*, vol. 73, no. 7, pp. 1307–1321, 1993.

[15] A. P. Jarman, E. H. Grell, L. Ackerman, L. Y. Jan, and Y. N. Jan, "*Atonal* is the proneural gene for *Drosophila* photoreceptors," *Nature*, vol. 369, no. 6479, pp. 398–400, 1994.

[16] C. Woods, M. Montcouquiol, and M. W. Kelley, "Math1 regulates development of the sensory epithelium in the mammalian cochlea," *Nature Neuroscience*, vol. 7, no. 12, pp. 1310–1318, 2004.

[17] M. C. Kelly, Q. Chang, A. Pan, X. Lin, and P. Chen, "Atoh1 directs the formation of sensory mosaics and induces cell proliferation in the postnatal mammalian cochlea *in vivo*," *Journal of Neuroscience*, vol. 32, no. 19, pp. 6699–6710, 2012.

[18] Z. Liu, J. A. Dearman, B. C. Cox et al., "Age-dependent in vivo conversion of mouse cochlear pillar and Deiters' cells to immature hair cells by Atoh1 ectopic expression," *Journal of Neuroscience*, vol. 32, no. 19, pp. 6600–6610, 2012.

[19] Z. Liu, J. Fang, J. Dearman, L. Zhang, and J. Zuo, "In vivo generation of immature inner hair cells in neonatal mouse cochleae by ectopic Atoh1 expression," *PLoS ONE*, vol. 9, no. 2, Article ID e89377, 2014.

[20] K. Kawamoto, S.-I. Ishimoto, R. Minoda, D. E. Brough, and Y. Raphael, "Math1 gene transfer generates new cochlear hair cells in mature guinea pigs in vivo," *The Journal of Neuroscience*, vol. 23, no. 11, pp. 4395–4400, 2003.

[21] M. Izumikawa, R. Minoda, K. Kawamoto et al., "Auditory hair cell replacement and hearing improvement by Atoh1 gene therapy in deaf mammals," *Nature Medicine*, vol. 11, no. 3, pp. 271–276, 2005.

[22] M. Izumikawa, S. A. Batts, T. Miyazawa, D. L. Swiderski, and Y. Raphael, "Response of the flat cochlear epithelium to forced expression of Atoh1," *Hearing Research*, vol. 240, no. 1-2, pp. 52–56, 2008.

[23] P. J. Atkinson, A. K. Wise, B. O. Flynn, B. A. Nayagam, and R. T. Richardson, "Hair cell regeneration after ATOH1 gene therapy in the cochlea of profoundly deaf adult guinea pigs," *PLoS ONE*, vol. 9, no. 7, Article ID e102077, 2014.

[24] Z. P. Stojanova, T. Kwan, and N. Segil, "Epigenetic regulation of Atoh1 guides hair cell development in the mammalian cochlea," *Development*, vol. 143, article 1632, 2016.

[25] P. Chen and N. Segil, "p27(Kip1) links cell proliferation to morphogenesis in the developing organ of Corti," *Development*, vol. 126, no. 8, pp. 1581–1590, 1999.

[26] R. J. Ruben, "Development of the inner ear of the mouse: a radioautographic study of terminal mitoses," *Acta Oto-Laryngologica*, supplement 220, pp. 221–244, 1967.

[27] H. Lowenheim, D. N. Furness, J. Kil et al., "Gene disruption of p27(Kip1) allows cell proliferation in the postnatal and adult organ of corti," *Proceedings of the National Academy of Sciences of the United States of America*, vol. 96, no. 7, pp. 4084–4088, 1999.

[28] J. A. Harris, A. G. Cheng, L. L. Cunningham, G. MacDonald, D. W. Raible, and E. W. Rubel, "Neomycin-induced hair cell death and rapid regeneration in the lateral line of zebrafish (*Danio rerio*)," *Journal of the Association for Research in Otolaryngology*, vol. 4, no. 2, pp. 219–234, 2003.

[29] P. P. Hernández, F. A. Olivari, A. F. Sarrazin, P. C. Sandoval, and M. L. Allende, "Regeneration in zebrafish lateral line neuromasts: expression of the neural progenitor cell marker sox2 and proliferation-dependent and-independent mechanisms of hair cell renewal," *Developmental Neurobiology*, vol. 67, no. 5, pp. 637–654, 2007.

[30] J. I. Matsui, E. C. Oesterle, J. S. Stone, and E. W. Rubel, "Characterization of damage and regeneration in cultured avian utricles," *Journal of the Association for Research in Otolaryngology*, vol. 1, no. 1, pp. 46–63, 2000.

[31] Z. Liu, B. J. Walters, T. Owen et al., "Regulation of $p27^{Kip1}$ by Sox2 maintains quiescence of inner pillar cells in the murine auditory sensory epithelium," *Journal of Neuroscience*, vol. 32, no. 31, pp. 10530–10540, 2012.

[32] J. C. Maass, F. A. Berndt, J. Cánovas, and M. Kukuljan, "P27Kip1 knockdown induces proliferation in the organ of Corti in culture after efficient shRNA lentiviral transduction," *Journal of the Association for Research in Otolaryngology*, vol. 14, no. 4, pp. 495–508, 2013.

[33] E. C. Oesterle, W. M. Chien, S. Campbell et al., "p27(Kip1) is required to maintain proliferative quiescence in the adult cochlea and pituitary," *Cell Cycle*, vol. 10, no. 8, pp. 1237–1248, 2011.

[34] B. J. Walters, Z. Liu, M. Crabtree, E. Coak, B. C. Cox, and J. Zuo, "Auditory hair cell-specific deletion of p27Kip1 in postnatal mice promotes cell-autonomous generation of new hair cells and normal hearing," *The Journal of Neuroscience*, vol. 34, no. 47, pp. 15751–15763, 2014.

[35] M. Classon and E. Harlow, "The retinoblastoma tumour suppressor in development and cancer," *Nature Reviews Cancer*, vol. 2, no. 12, pp. 910–917, 2002.

[36] M. M. Lipinski and T. Jacks, "The retinoblastoma gene family in differentiation and development," *Oncogene*, vol. 18, no. 55, pp. 7873–7882, 1999.

[37] C. Sage, M. Huang, M. A. Vollrath et al., "Essential role of retinoblastoma protein in mammalian hair cell development and hearing," *Proceedings of the National Academy of Sciences of the United States of America*, vol. 103, no. 19, pp. 7345–7350, 2006.

[38] J. Mantela, Z. Jiang, J. Ylikoski, B. Fritzsch, E. Zacksenhaus, and U. Pirvola, "The retinoblastoma gene pathway regulates the postmitotic state of hair cells of the mouse inner ear," *Development*, vol. 132, no. 10, pp. 2377–2388, 2005.

[39] Y. Yu, T. Weber, T. Yamashita et al., "In vivo proliferation of postmitotic cochlear supporting cells by acute ablation of the retinoblastoma protein in neonatal mice," *Journal of Neuroscience*, vol. 30, no. 17, pp. 5927–5936, 2010.

[40] R. Brooker, K. Hozumi, and J. Lewis, "Notch ligands with contrasting functions: Jagged1 and Delta1 in the mouse inner ear," *Development*, vol. 133, no. 7, pp. 1277–1286, 2006.

[41] A. E. Kiernan, J. Xu, and T. Gridley, "The Notch ligand JAG1 is required for sensory progenitor development in the mammalian inner ear," *PLoS Genetics*, vol. 2, no. 1, article no. e4, 2006.

[42] V. Munnamalai, T. Hayashi, and O. Bermingham-McDonogh, "Notch prosensory effects in the mammalian cochlea are partially mediated by Fgf20," *Journal of Neuroscience*, vol. 32, no. 37, pp. 12876–12884, 2012.

[43] A. E. Kiernan, R. Cordes, R. Kopan, A. Gossler, and T. Gridley, "The Notch ligands DLL1 and JAG2 act synergistically to regulate hair cell development in the mammalian inner ear," *Development*, vol. 132, no. 19, pp. 4353–4362, 2005.

[44] P. J. Lanford, Y. Lan, R. Jiang et al., "Notch signalling pathway mediates hair cell development in mammalian cochlea," *Nature Genetics*, vol. 21, no. 3, pp. 289–292, 1999.

[45] A. Doetzlhofer, M. L. Basch, T. Ohyama, M. Gessler, A. K. Groves, and N. Segil, "*Hey2* regulation by fgf provides a *Notch*-independent mechanism for maintaining pillar cell fate in the

organ of corti," *Developmental Cell*, vol. 16, no. 1, pp. 58–69, 2009.

[46] W. Li, J. Wu, J. Yang et al., "Notch inhibition induces mitotically generated hair cells in mammalian cochleae via activating the Wnt pathway," *Proceedings of the National Academy of Sciences of the United States of America*, vol. 112, no. 1, pp. 166–171, 2015.

[47] N. Yamamoto, K. Tanigaki, M. Tsuji, D. Yabe, J. Ito, and T. Honjo, "Inhibition of Notch/RBP-J signaling induces hair cell formation in neonate mouse cochleas," *Journal of Molecular Medicine*, vol. 84, no. 1, pp. 37–45, 2006.

[48] K. Mizutari, M. Fujioka, M. Hosoya et al., "Notch inhibition induces cochlear hair cell regeneration and recovery of hearing after acoustic trauma," *Neuron*, vol. 77, no. 1, pp. 58–69, 2013.

[49] Y. Tona, K. Hamaguchi, M. Ishikawa et al., "Therapeutic potential of a gamma-secretase inhibitor for hearing restoration in a guinea pig model with noise-induced hearing loss," *BMC Neuroscience*, vol. 15, article 66, 2014.

[50] L. Liu, Y. Chen, J. Qi et al., "Wnt activation protects against neomycin-induced hair cell damage in the mouse cochlea," *Cell Death and Disease*, vol. 7, no. 3, article e2136, 2016.

[51] B. E. Jacques, C. Puligilla, R. M. Weichert et al., "A dual function for canonical Wnt/β-catenin signaling in the developing mammalian cochlea," *Development*, vol. 139, no. 23, pp. 4395–4404, 2012.

[52] F. Shi, L. Hu, B. E. Jacques, J. F. Mulvaney, A. Dabdoub, and A. S. B. Edge, "β-catenin is required for hair-cell differentiation in the cochlea," *Journal of Neuroscience*, vol. 34, no. 19, pp. 6470–6479, 2014.

[53] F. Shi, J. S. Kempfle, and A. S. B. Edge, "Wnt-responsive Lgr5-expressing stem cells are hair cell progenitors in the cochlea," *Journal of Neuroscience*, vol. 32, no. 28, pp. 9639–9684, 2012.

[54] R. Chai, A. Xia, T. Wang et al., "Dynamic expression of *Lgr5*, a Wnt target gene, in the developing and mature mouse cochlea," *Journal of the Association for Research in Otolaryngology : JARO*, vol. 12, no. 4, pp. 455–469, 2011.

[55] X. Lu, S. Sun, J. Qi et al., "Bmi1 regulates the proliferation of cochlear supporting cells via the canonical Wnt signaling pathway," *Molecular Neurobiology*, pp. 1–14, 2016.

[56] M. Waqas, L. Guo, S. Zhang et al., "Characterization of Lgr5+ progenitor cell transcriptomes in the apical and basal turns of the mouse cochlea," *Oncotarget*, vol. 7, no. 27, pp. 41123–41141, 2016.

[57] F. Shi, L. Hu, and A. S. B. Edge, "Generation of hair cells in neonatal mice by β-catenin overexpression in Lgr5-positive cochlear progenitors," *Proceedings of the National Academy of Sciences of the United States of America*, vol. 110, no. 34, pp. 13851–13856, 2013.

[58] M. Waqas, S. Zhang, Z. He, M. Tang, and R. Chai, "Role of Wnt and Notch signaling in regulating hair cell regeneration in the cochlea," *Frontiers of Medicine*, vol. 10, no. 3, pp. 237–249, 2016.

[59] W. Ni, C. Lin, L. Guo et al., "Extensive supporting cell proliferation and mitotic hair cell generation by in vivo genetic reprogramming in the neonatal mouse cochlea," *Journal of Neuroscience*, vol. 36, no. 33, pp. 8734–8745, 2016.

[60] U. Pirvola, B. Spencer-Dene, L. Xing-Qun et al., "FGF/FGFR-2(IIIb) signaling is essential for inner ear morphogenesis," *The Journal of Neuroscience*, vol. 20, no. 16, pp. 6125–6134, 2000.

[61] T. Schimmang, "Expression and functions of FGF ligands during early otic development," *International Journal of Developmental Biology*, vol. 51, no. 6-7, pp. 473–481, 2007.

[62] T. J. Wright and S. L. Mansour, "Fgf3 and Fgf10 are required for mouse otic placode induction," *Development*, vol. 130, no. 15, pp. 3379–3390, 2003.

[63] K. Ono, T. Kita, S. Sato et al., "FGFR1-Frs2/3 signalling maintains sensory progenitors during inner ear hair cell formation," *PLOS Genetics*, vol. 10, no. 1, Article ID e1004118, 2014.

[64] U. Pirvola, J. Ylikoski, R. Trokovic, J. M. Hébert, S. K. McConnell, and J. Partanen, "FGFR1 is required for the development of the auditory sensory epithelium," *Neuron*, vol. 35, no. 4, pp. 671–680, 2002.

[65] J. S. Colvin, B. A. Bohne, G. W. Harding, D. G. McEwen, and D. M. Ornitz, "Skeletal overgrowth and deafness in mice lacking fibroblast growth factor receptor 3," *Nature Genetics*, vol. 12, no. 4, pp. 390–397, 1996.

[66] B. E. Jacques, M. E. Montcouquiol, E. M. Layman, M. Lewandoski, and M. W. Kelley, "Fgf8 induces pillar cell fate and regulates cellular patterning in the mammalian cochlea," *Development*, vol. 134, no. 16, pp. 3021–3029, 2007.

[67] Y.-C. Ku, N. A. Renaud, R. A. Veile et al., "The transcriptome of utricle hair cell regeneration in the avian inner ear," *The Journal of Neuroscience*, vol. 34, no. 10, pp. 3523–3535, 2014.

[68] O. Bermingham-McDonogh, J. S. Stone, T. A. Reh, and E. W. Rubel, "FGFR3 expression during development and regeneration of the chick inner ear sensory epithelia," *Developmental Biology*, vol. 238, no. 2, pp. 247–259, 2001.

[69] L. Jiang, A. Romero-Carvajal, J. S. Haug, C. W. Seidel, and T. Piotrowski, "Gene-expression analysis of hair cell regeneration in the zebrafish lateral line," *Proceedings of the National Academy of Sciences of the United States of America*, vol. 111, no. 14, pp. E1383–E1392, 2014.

[70] U. Pirvola, Y. Cao, C. Oellig, Z. Suoqiang, R. F. Pettersson, and J. Ylikoski, "The site of action of neuronal acidic fibroblast growth factor is the organ of Corti of the rat cochlea," *Proceedings of the National Academy of Sciences of the United States of America*, vol. 92, no. 20, pp. 9269–9273, 1995.

[71] K. Liu, X. Jiang, C. Shi et al., "Cochlear inner hair cell ribbon synapse is the primary target of ototoxic aminoglycoside stimuli," *Molecular Neurobiology*, vol. 48, no. 3, pp. 647–654, 2013.

[72] L. Shi, K. Liu, H. Wang et al., "Noise induced reversible changes of cochlear ribbon synapses contribute to temporary hearing loss in mice," *Acta Oto-Laryngologica*, vol. 135, no. 11, pp. 1093–1102, 2015.

[73] E. M. Keithley and M. L. Feldman, "Hair cell counts in an age-graded series of rat cochleas," *Hearing Research*, vol. 8, no. 3, pp. 249–262, 1982.

[74] N. B. Slepecky and Y. Ogata, "Immunohistochemical labeling of inner ear tissues embedded in polyethylene glycol 4000—comparative study with araldite and unicryl embedded sections," *Nippon Jibiinkoka Gakkai kaiho*, vol. 99, no. 3, pp. 361–369, 1996.

[75] H. Burda and M. Branis, "Postnatal development of the organ of Corti in the wild house mouse, laboratory mouse, and their hybrid," *Hearing Research*, vol. 36, no. 1, pp. 97–105, 1988.

[76] W. B. Warr and J. J. Guinan Jr., "Efferent innervation of the organ of corti: two separate systems," *Brain Research*, vol. 173, no. 1, pp. 152–155, 1979.

[77] L. C. Huang, P. R. Thorne, G. D. Housley, and J. M. Montgomery, "Spatiotemporal definition of neurite outgrowth, refinement and retraction in the developing mouse cochlea," *Development*, vol. 134, no. 16, pp. 2925–2933, 2007.

[78] Q. Wang and S. H. Green, "Functional role of neurotrophin-3 in synapse regeneration by spiral ganglion neurons on inner hair cells after excitotoxic trauma in vitro," *Journal of Neuroscience*, vol. 31, no. 21, pp. 7938–7949, 2011.

[79] W. Singer, R. Panford-Walsh, and M. Knipper, "The function of BDNF in the adult auditory system," *Neuropharmacology*, vol. 76, pp. 719–728, 2014.

[80] C. Weisz, E. Glowatzki, and P. Fuchs, "The postsynaptic function of type II cochlear afferents," *Nature*, vol. 461, no. 7267, pp. 1126–1129, 2009.

[81] S. Safieddine, A. El-Amraoui, and C. Petit, "The auditory hair cell ribbon synapse: from assembly to function," *Annual Review of Neuroscience*, vol. 35, pp. 509–528, 2012.

[82] P. A. Fuchs, "Time and intensity coding at the hair cell's ribbon synapse," *Journal of Physiology*, vol. 566, no. 1, pp. 7–12, 2005.

[83] D. Khimich, R. Nouvian, R. Pujol et al., "Hair cell synaptic ribbons are essential for synchronous auditory signalling," *Nature*, vol. 434, no. 7035, pp. 889–894, 2005.

[84] R. Nouvian, D. Beutner, T. D. Parsons, and T. Moser, "Structure and function of the hair cell ribbon synapse," *Journal of Membrane Biology*, vol. 209, no. 2-3, pp. 153–165, 2006.

[85] R. T. Fremeau Jr., S. Voglmaier, R. P. Seal, and R. H. Edwards, "VGLUTs define subsets of excitatory neurons and suggest novel roles for glutamate," *Trends in Neurosciences*, vol. 27, no. 2, pp. 98–103, 2004.

[86] S. F. Maison, H. Usubuchi, and M. Charles Liberman, "Efferent feedback minimizes cochlear neuropathy from moderate noise exposure," *Journal of Neuroscience*, vol. 33, no. 13, pp. 5542–5552, 2013.

[87] R. Martinez-Monedero, C. E. Corrales, M. P. Cuajungco, S. Heller, and A. S. B. Edge, "Reinnervation of hair cells by auditory neurons after selective removal of spiral ganglion neurons," *Journal of Neurobiology*, vol. 66, no. 4, pp. 319–331, 2006.

[88] M. Matsumoto, T. Nakagawa, K. Kojima, T. Sakamoto, F. Fujiyama, and J. Ito, "Potential of embryonic stem cell-derived neurons for synapse formation with auditory hair cells," *Journal of Neuroscience Research*, vol. 86, no. 14, pp. 3075–3085, 2008.

[89] Z. Liu, T. Owen, J. Fang, and J. Zuo, "Overactivation of notch1 signaling induces ectopic hair cells in the mouse inner ear in an age-dependent manner," *PLoS ONE*, vol. 7, no. 3, Article ID e34123, 2012.

[90] K. A. Deyst, J. Ma, J. R. Fallon, R. G. Dacey, and C. J. Hodge Jr., "Agrin: toward a molecular understanding of synapse regeneration," *Neurosurgery*, vol. 37, no. 1, pp. 71–77, 1995.

[91] P. R. Gordon-Weeks and A. E. Fournier, "Neuronal cytoskeleton in synaptic plasticity and regeneration," *Journal of Neurochemistry*, vol. 129, no. 2, pp. 206–212, 2014.

[92] L. T. Alto, L. A. Havton, J. M. Conner, E. R. Hollis II, A. Blesch, and M. H. Tuszynski, "Chemotropic guidance facilitates axonal regeneration and synapse formation after spinal cord injury," *Nature Neuroscience*, vol. 12, no. 9, pp. 1106–1113, 2009.

[93] L.-X. Deng, P. Deng, Y. Ruan et al., "A novel growth-promoting pathway formed by GDNF-overexpressing Schwann cells promotes propriospinal axonal regeneration, synapse formation, and partial recovery of function after spinal cord injury," *Journal of Neuroscience*, vol. 33, no. 13, pp. 5655–5667, 2013.

[94] K. J. M. Marler, E. Becker-Barroso, A. Martínez et al., "A TrkB/EphrinA interaction controls retinal axon branching and synaptogenesis," *The Journal of Neuroscience*, vol. 28, no. 48, pp. 12700–12712, 2008.

[95] H. Park and M.-M. Poo, "Neurotrophin regulation of neural circuit development and function," *Nature Reviews Neuroscience*, vol. 14, no. 1, pp. 7–23, 2013.

[96] D. Ramekers, H. Versnel, W. Grolman, and S. F. L. Klis, "Neurotrophins and their role in the cochlea," *Hearing Research*, vol. 288, no. 1-2, pp. 19–33, 2012.

[97] B. Fritzsch, L. Tessarollo, E. Coppola, and L. F. Reichardt, "Neurotrophins in the ear: their roles in sensory neuron survival and fiber guidance," *Progress in Brain Research*, vol. 146, pp. 265–278, 2004.

[98] M. E. Gómez-Casati, J. C. Murtie, C. Rio, K. Stankovic, M. C. Liberman, and G. Corfas, "Nonneuronal cells regulate synapse formation in the vestibular sensory epithelium via erbB-dependent BDNF expression," *Proceedings of the National Academy of Sciences of the United States of America*, vol. 107, no. 39, pp. 17005–17010, 2010.

[99] G. Wan, M. E. Gómez-Casati, A. R. Gigliello, M. Charles Liberman, and G. Corfas, "Neurotrophin-3 regulates ribbon synapse density in the cochlea and induces synapse regeneration after acoustic trauma," *eLife*, vol. 3, Article ID e03564, 2014.

[100] M. Tong, A. Brugeaud, and A. S. B. Edge, "Regenerated synapses between postnatal hair cells and auditory neurons," *Journal of the Association for Research in Otolaryngology*, vol. 14, no. 3, pp. 321–329, 2013.

[101] L. L. Cunningham and D. L. Tucci, "Restoring synaptic connections in the inner ear after noise damage," *The New England Journal of Medicine*, vol. 372, no. 2, pp. 181–182, 2015.

Hindawi Publishing Corporation
Neural Plasticity
Volume 2016, Article ID 9409846, 8 pages
http://dx.doi.org/10.1155/2016/9409846

Research Article

Adenovirus Vectors Target Several Cell Subtypes of Mammalian Inner Ear *In Vivo*

Yilai Shu,[1,2,3] Yong Tao,[1] Wenyan Li,[1,2,3] Jun Shen,[4,5] Zhengmin Wang,[2,3] and Zheng-Yi Chen[1]

[1]*Department of Otolaryngology, Harvard Medical School and Eaton-Peabody Laboratories, Massachusetts Eye & Ear Infirmary, Boston, MA 02114, USA*
[2]*Department of Otolaryngology-Head and Neck Surgery, Eye and ENT Hospital, Shanghai Medical College, Fudan University, Shanghai, China*
[3]*Key Laboratory of Hearing Medicine, National Health and Family Planning Commission, Shanghai, China*
[4]*Department of Pathology, Brigham and Women's Hospital, Harvard Medical School, Boston, MA 02115, USA*
[5]*Laboratory for Molecular Medicine, Partners Personalized Medicine, Cambridge, MA 02139, USA*

Correspondence should be addressed to Zhengmin Wang; fjswzm2015@126.com
and Zheng-Yi Chen; zheng-yi_chen@meei.harvard.edu

Received 9 September 2016; Accepted 8 November 2016

Academic Editor: Genglin Li

Mammalian inner ear harbors diverse cell types that are essential for hearing and balance. Adenovirus is one of the major vectors to deliver genes into the inner ear for functional studies and hair cell regeneration. To identify adenovirus vectors that target specific cell subtypes in the inner ear, we studied three adenovirus vectors, carrying a reporter gene encoding green fluorescent protein *(GFP)* from two vendors or with a genome editing gene Cre recombinase *(Cre)*, by injection into postnatal days 0 (P0) and 4 (P4) mouse cochlea through scala media by cochleostomy *in vivo*. We found three adenovirus vectors transduced mouse inner ear cells with different specificities and expression levels, depending on the type of adenoviral vectors and the age of mice. The most frequently targeted region was the cochlear sensory epithelium, including auditory hair cells and supporting cells. Adenovirus with *GFP* transduced utricular supporting cells as well. This study shows that adenovirus vectors are capable of efficiently and specifically transducing different cell types in the mammalian inner ear and provides useful tools to study inner ear gene function and to evaluate gene therapy to treat hearing loss and vestibular dysfunction.

1. Introduction

Irreversible hair cell loss is a major cause of permanent sensorineural hearing loss with no effective treatment. Pathogenic variants in hundreds of genes are responsible for many forms of hereditary hearing loss. The development of strategies for hair cell regeneration and for gene delivery has become a major focus in the search for potential therapeutic approaches to restoring hearing [1–3].

Lower vertebrates including birds and fish can regenerate hair cells throughout life after hair cell loss by two mechanisms. First, inner ear supporting cells and remaining hair cells may reenter the cell cycle and differentiate into new hair cells. Second, surrounding cells located under the lost hair cells may also directly transdifferentiate into new hair cells [4–6]. However, the mammalian inner ear has lost the capacity to regenerate hair cells spontaneously. One strategy to regenerate hair cells in mammals to restore hearing is to induce surrounding cells especially supporting cells to transdifferentiate into hair cells directly. Another approach is to induce remaining hair cells or supporting cells to reenter the cell cycle and for supporting cells to further differentiate to hair cells [1, 7]. Either approach requires efficient delivery of genes necessary for the induction of these processes into mammalian inner ear cells.

The inner ear is a particularly attractive organ for targeted gene therapy, because vectors can be locally delivered to the enclosed structure, which significantly reduces systemic side

effects. One of the major hurdles to achieve hair cell regeneration or gene correction by gene therapy is the lack of efficient and specific vehicle to deliver genes into mammalian inner ear cells. Adenovirus (Ad) and Adeno-associated virus (AAV) are the most common vectors used for inner ear gene delivery. Both have been used to successfully transfer functional genes into the mammalian inner ear for gene therapy [8–23]. Ad vector is a good choice due to its high transfection efficiency in diverse tissues and cell types, with high level of expression soon after infection. Furthermore, Ad vector has low immunogenicity and toxicity [15–23]. Comparing to AAV vectors, Ad vectors have the capacity to accommodate larger inserts. For example, the most commonly used adenovirus vectors, which are E1/E3 deletion mutants, allow the insertion of up to 10 kb of foreign DNA into the viral vector genome, while an AAV can only carry up to 4.7 kb of foreign DNA [13, 24].

Previous studies have demonstrated the ability of Ad vectors to transduce cochlear hair cells and supporting cells [5–13]. In mammalian inner ear, transduction by Ad vectors is organ (cochlea versus vestibule), cell type (inner hair cells (IHCs), outer hair cells (OHCs), and supporting cells (SCs)), region (base, middle, and apical turns), and age dependence. The transduction patterns of Ad vectors in the inner ear vary. In order to use Ad vectors to effectively deliver genes into specific inner ear cell subtypes, it is important to characterize the transduction patterns of viral vector subtypes under various experimental conditions, including animal age, route of inoculation, viral preparations, volume, and number of viral particles.

To identify commercially available Ad vectors for their inner ear delivery patterns, we analyzed Ad vectors carrying a GFP from Baylor College of Medicine (Ad-GFP-Baylor) and from Vector Biolabs (Ad-GFP-VB) and an Ad vector carrying GFP linked with a genome editing gene Cre recombinase (Cre) from Baylor College of Medicine (Ad-Cre-GFP-Baylor) *in vivo* for their potential for inner ear gene delivery in P0 and P4 mouse cochleae.

2. Material and Methods

2.1. Ad Vectors. We obtained three commercially available Ad vectors: Ad-GFP-Baylor (Baylor College of Medicine, Houston, TX, USA), Ad-GFP-VB (Vector Biolabs, Malvern, PA, USA), and Ad-Cre-GFP-Baylor (Baylor College of Medicine, Houston, TX, USA). The titers of Ad-GFP-Baylor, Ad-GFP-VB, and Ad-Cre-GFP-Baylor were 2.5×10^{10}–5×10^{11} plaque-forming unit (pfu)/ml, 1×10^{10} pfu/ml, and 1.7×10^{11} pfu/ml, respectively. We consider the titer of Ad-GFP-Baylor as 10×10^{10} pfu/ml for dilution. We diluted all Ads to 1×10^{10} pfu/ml with storage buffer according to the vectors instructions from two vendors for microinjection.

2.2. Microinjection of Ad Vectors into Mouse Inner Ear. P0 and P4 CD1 mice (Charles River Laboratory, Wilmington, MA, USA) were used for Ad-Cre-GFP-Baylor, Ad-GFP-Baylor, and Ad-GFP-VB injection, according to protocols approved by the Massachusetts Eye & Ear Infirmary IACUC committee. Mice were anesthetized by lowering their temperature on ice. Cochleostomies were performed by making an incision behind the right ear to expose the cochlea. Glass micropipettes (WPI, Sarasota, FL, USA) held by a Nanoliter Microinjection System (WPI, Sarasota, FL, USA) were used to deliver the Ad into the scala media, which allows access to inner ear cells. A total volume of ~0.2 μL was injected per cochlea on the right side and the release was controlled by a micromanipulator at the speed of 3 nL/sec. The left cochlea was left intact as an internal control.

2.3. Immunofluorescence and Quantification. Four days after injection, mice were sacrificed and cochleae were harvested by standard protocols [1, 17]. For whole-mount immunofluorescence, primary antibodies against HC (MYO7A, #25-6790, Proteus Biosciences) and SC (SOX2, #sc-17320, Santa Cruz Biotech) markers and fluorescent-labeled secondary antibodies (Invitrogen) were used following a previously described protocol [1]. To quantify the proportion of GFP positive cells after Ad injection, we counted the number of GFP positive IHCs, OHCs, and SCs, which were then divided by the total number of IHCs, OHCs, and SCs, respectively, in a region spanning 200 μm in the apical, middle, or basal turn of the cochlea.

3. Results

We injected Ad vectors into the neonatal mouse inner ear at P0 or P4 via cochleostomy, because previous studies have shown that injection of AAV into the neonatal mouse cochlea by cochleostomy resulted in efficient transduction *in vivo* without adversely affecting hearing [8]. Four days after injection of any of the three Ad vectors into P0 or P4 mouse inner ears, cochlear structures remained intact and hair cells and supporting cells survived, indicating that the injection and Ad transduction did not damage inner ear cells (Figures 1–7).

We assessed the transduction efficiency of the viral vectors by calculating the proportion of GFP positive cells, because all three Ad vectors carried the *GFP* gene. Whole-mount immunofluorescence labeling of HC and SC markers Myo7a and Sox2 identified hair cells and supporting cells, respectively. We found that the Ad-Cre-GFP-Baylor transduction was restricted to the injected side and no GFP expression was observed in the uninjected inner ear (Figure 1(d)). Same was true for Ad-GFP-Baylor and Ad-GFP-VB (data not shown). Our results confirmed that targeted delivery of Ad vectors via cochleostomy was confined within the injected inner ear.

Our results showed that three different Ad vectors injected at two different ages transduced different cell types in different cochlear regions with varying efficiencies (Table 1). Ad-Cre-GFP-Baylor, when injected at P0, efficiently transduced more than 70% of SCs but not HCs in the basal and middle turns (Figures 1(a) and 1(b)). It transduced few cells in the apical turn (Figure 1(c)). Comparing to injection at P0, injected at P4, Ad-Cre-GFP-Baylor transduced fewer SCs in the basal and middle turns, but more SCs in the apical turn (Figure 4).

A similar trend of transduction efficiency in SCs was observed for Ad-GFP-Baylor (Table 1). It transduced inner

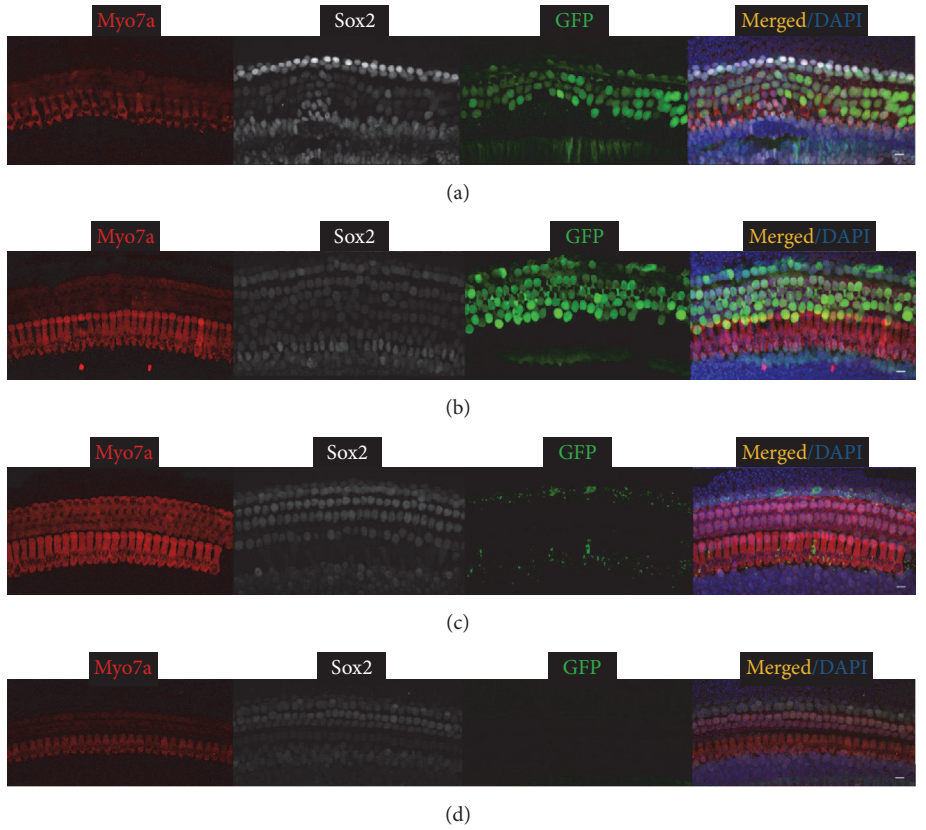

Figure 1: Ad-Cre-GFP-Baylor transduces supporting cells when injected into mouse cochlear at P0. Representative confocal images of whole-mount fluorescent immunolabeling of cochlea injected at P0 to illustrate the basal (a), middle (b), and apical turns (c), as compared to the contralateral uninjected middle turn of cochlea (d). Myo7a labels hair cells, and Sox2 labels supporting cells. Ad-Cre-GFP-Baylor mainly transduces supporting cells in basal and middle turns. Scale bars: 10 μm.

Table 1: Comparison of *in vivo* transduction efficiency in different cell types and cochlear regions four days after injection of three adenoviral vectors into P0 or P4 mouse cochleae. $N = 4$ per condition. Apical: apical turn of the cochlea, basal: basal turn of the cochlea, IHCs: inner hair cells, middle: middle turn of the cochlea, OHCs: outer hair cells, P0: injected at postnatal day 0, P4: injected at postnatal day 4, and SCs: supporting cells.

Transduction efficiency (%)		IHCs			OHCs			SCs		
		Basal	Middle	Apical	Basal	Middle	Apical	Basal	Middle	Apical
Ad-Cre-GFP-Baylor	P0							74.5 ± 8.6	70.6 ± 7.8	
	P4							54.4 ± 6.8	52.4 ± 6.9	3.8 ± 1.2
Ad-GFP-Baylor	P0	9.1 ± 1.2					80.0 ± 12.0	90.8 ± 9.2	84.7 ± 10.6	
	P4		13.6 ± 2.9				17.4 ± 4.2	79.1 ± 10.6	74.3 ± 11.2	42.3 ± 6.1
Ad-GFP-VB	P0		9.1 ± 1.5	15.0 ± 4.8	9.8 ± 1.8	29.0 ± 4.9	27.8 ± 4.1	41.5 ± 8.1	7.7 ± 2.9	
	P4						2.9 ± 0.9	51.1 ± 6.2	33.1 ± 4.2	

ear cells more efficiently than Ad-Cre-GFP-Baylor when injected at either P0 (Figure 2) or P4 (Figure 5). Furthermore, it also transduced a majority of OHCs in the apical turn and some IHCs in the basal turn when injected at P0 and IHCs in the middle turn and OHCs in the apical turn when injected at P4.

In contrast, Ad-GFP-VB transduced fewer SCs than either of the Ad-GFP-Baylor vectors with an opposite temporal trend: more efficiently when injected at P4 than at P0 (Table 1, Figures 3 and 6). Further, it more consistently transduced IHCs in the middle and apical turns and OHCs along the whole cochlear coil when injected at P0 (Table 1).

Ad-GFP-Baylor and Ad-GFP-VB transduced vestibular HCs and SCs with similar patterns when injected at either P0 or P4 (Figure 7), whereas Ad-Cre-GFP-Baylor transduced no utricular HCs or SCs.

In summary, we compared the transduction patterns of three Ad vectors injected at two different ages. All three Ad vectors consistently transduced SCs, with Ad-GFP-Baylor exhibiting the highest transduction rate across the whole

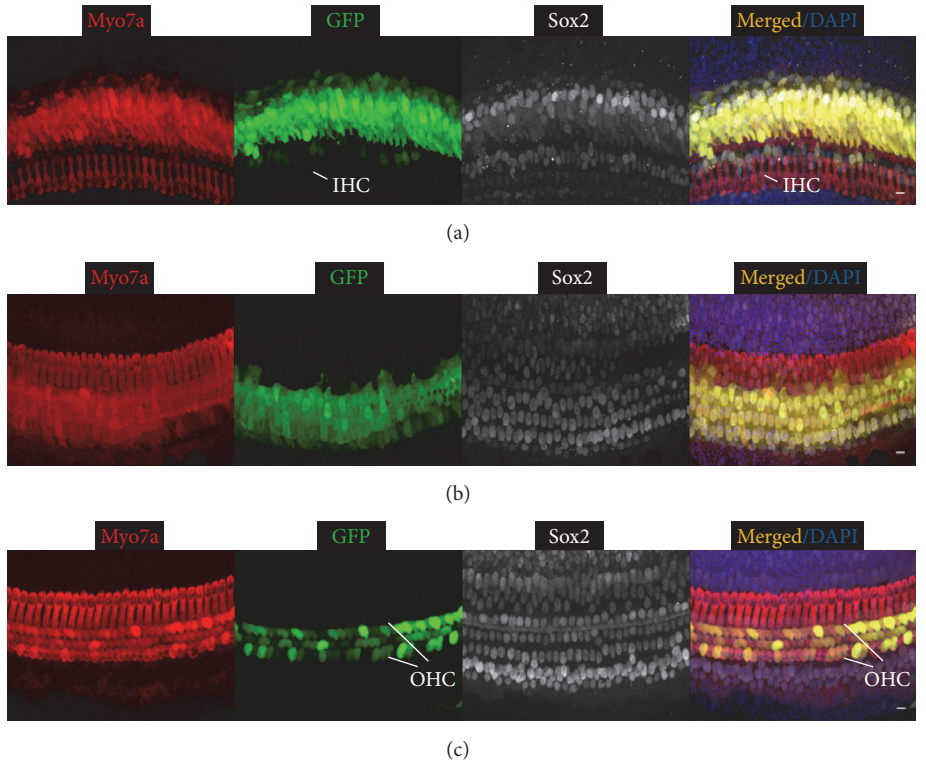

Figure 2: Ad-GFP-Baylor transduces diverse cochlear cell types when injected at P0. Representative confocal images of whole-mount fluorescent immunolabeling of cochlea injected at P0 to illustrate the basal (a), middle (b), and apical turns (c). Ad-GFP-Baylor transduces supporting cells (SCs) and inner hair cells (IHCs) at basal (a), SCs at middle (b), and outer hair cells (OHCs) at apical turns (c). IHC: inner hair cell, OHC: outer hair cell, and SC: supporting cell. Scale bars: 10 μm.

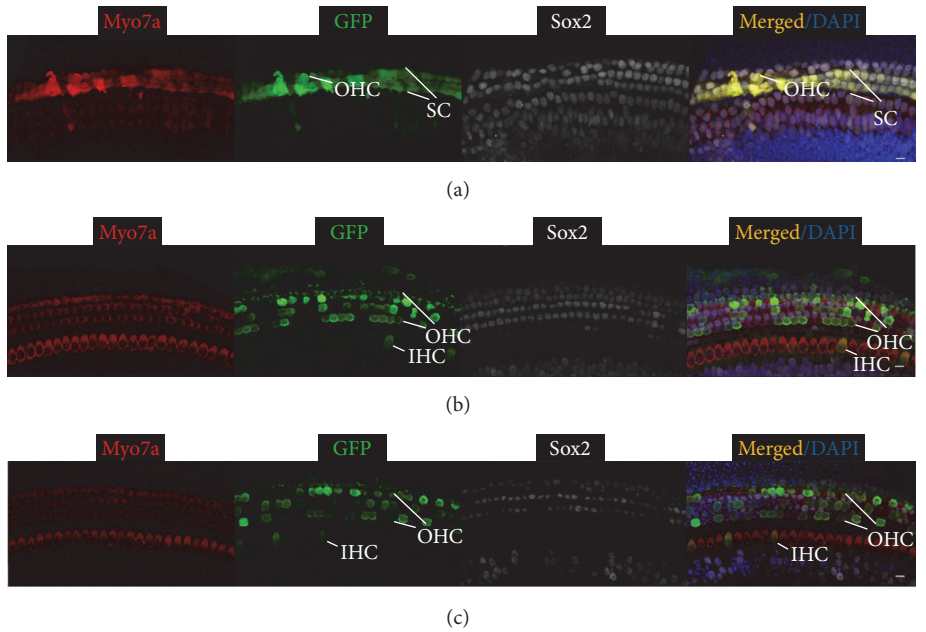

Figure 3: Ad-GFP-VB transduces diverse cell types in mouse cochlea when injected at P0. Representative confocal images of whole-mount fluorescent immunolabeling of the cochlea injected with adenovirus at P0 to illustrate the basal (a), middle (b), and apical turns (c). Ad-GFP-VB transduces SCs and OHCs at basal (a), OHCs, IHCs, and SCs at middle (b), and OHCs and IHCs at apical turns (c). IHC: inner hair cell, OHC: outer hair cell, and SC: supporting cell. Scale bars: 10 μm.

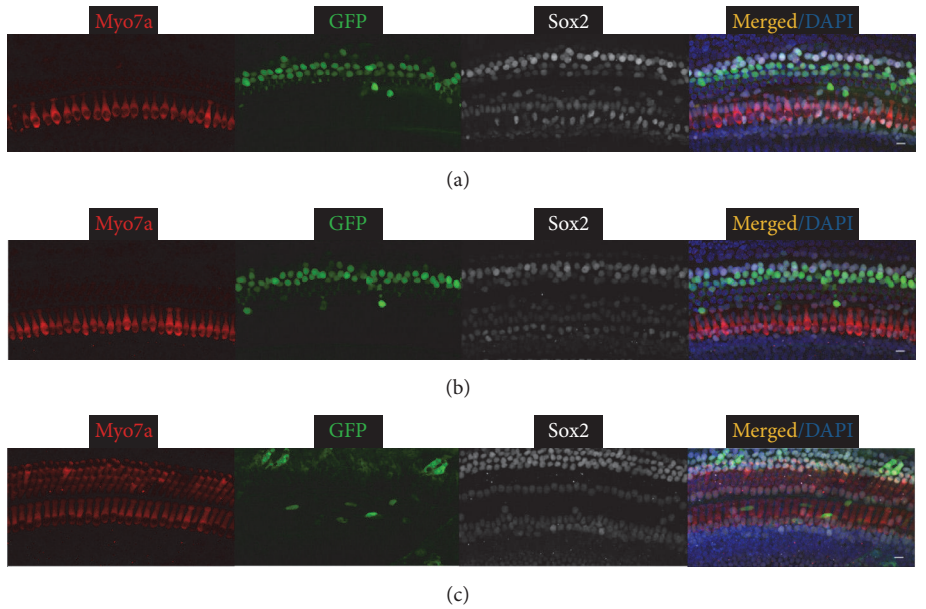

Figure 4: Ad-Cre-GFP-Baylor transduces supporting cells in the mouse cochlear when injected at P4. Representative confocal images of whole-mount fluorescent immunolabeling mouse cochlea to illustrate the basal (a), middle (b), and apical turns (c). Ad-Cre-GFP-Baylor transduces SCs at basal and middle turns efficiently. It transduces some SCs at the apical turn. Scale bars: 10 μm.

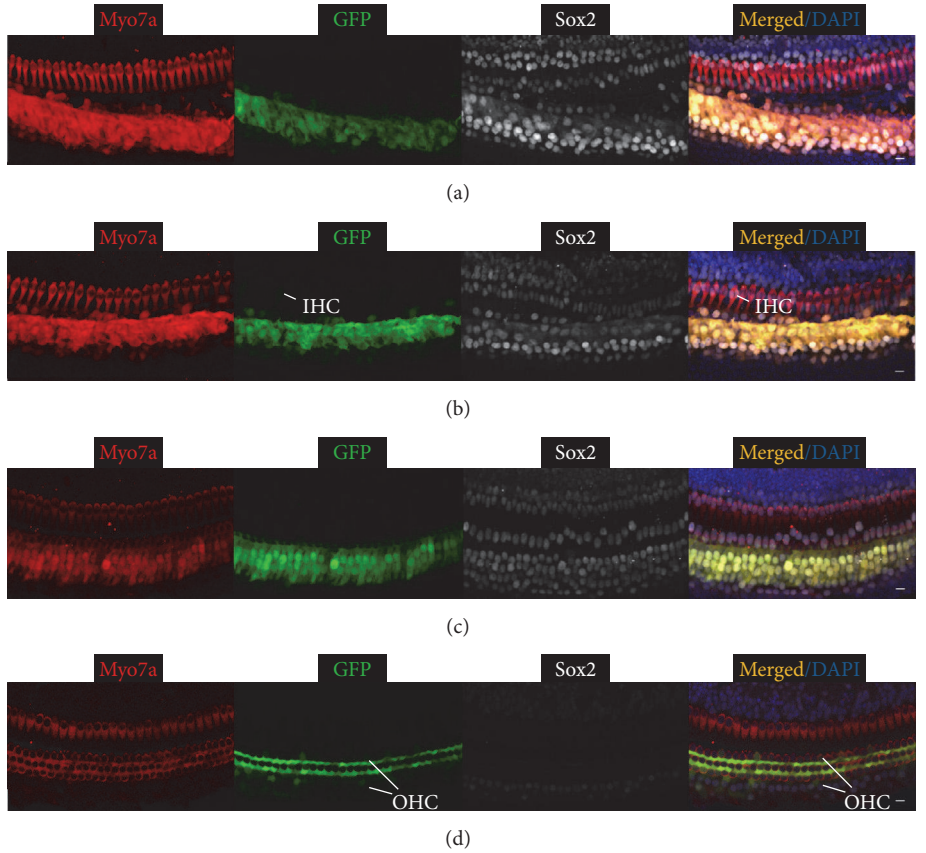

Figure 5: Ad-GFP-Baylor transduces mouse cochlea when injected at P4. Representative confocal images of whole-mount fluorescent immunolabeling P0 cochlea to illustrate the basal (a), middle (b), and apical turns (c, d). Ad-GFP-Baylor transduces SCs at basal (a), SCs and IHCs at middle (b), and SCs and OHCs at apical turns (c). Outer hair cells are transduced at the apical turn (d). IHC: inner hair cell; OHC: outer hair cell.

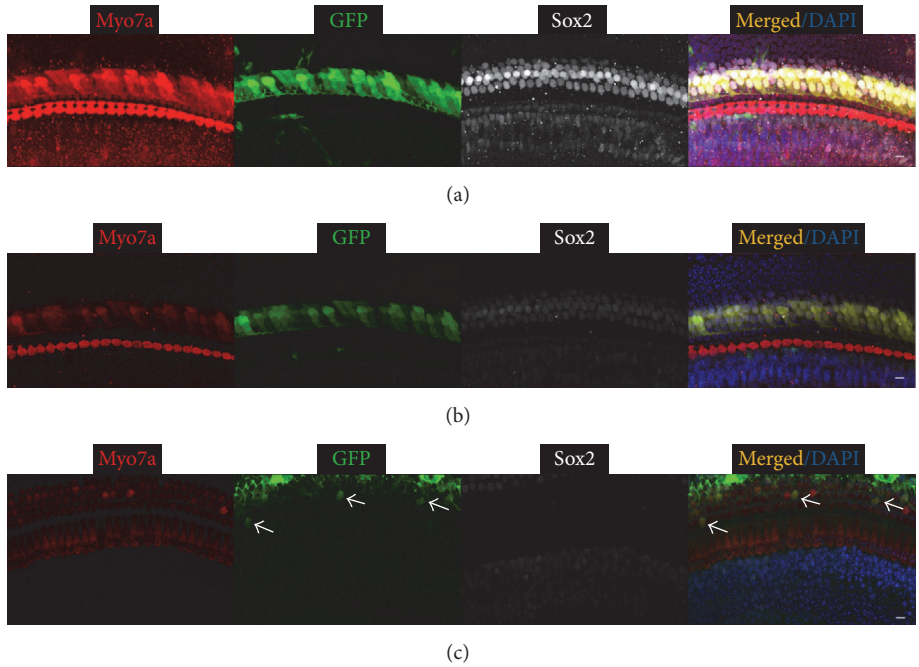

Figure 6: Ad-GFP-VB transduces supporting cells and OHCs in the mouse cochlear when injected at P4. Representative confocal images of whole-mount fluorescent immunolabeling of the cochlea to illustrate the basal (a), middle (b), and apical turns (c). Ad-GFP-VB transduces SCs at basal (a) and middle (b) and occasional OHCs at apical turns (arrows in (c)). Scale bars: 10 μm.

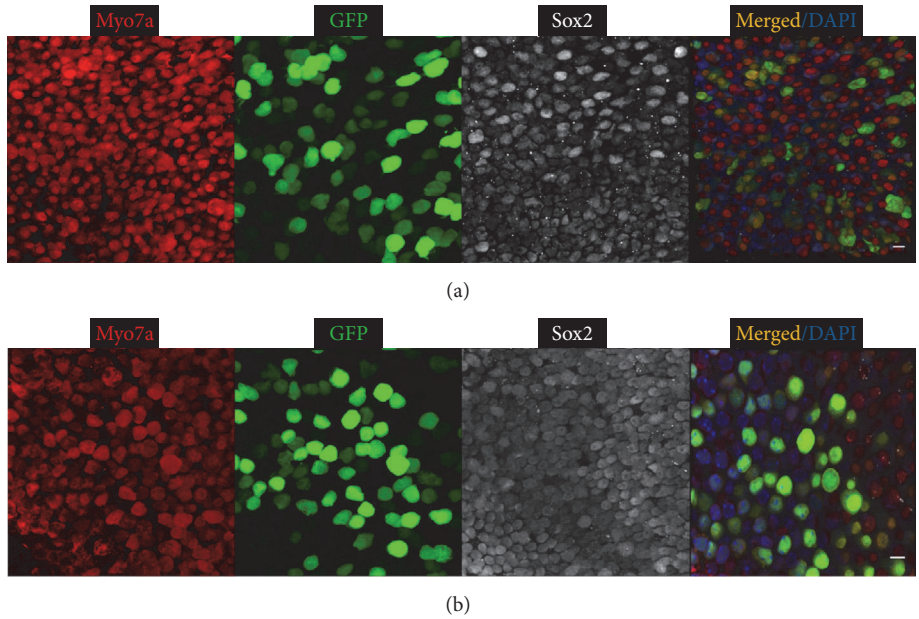

Figure 7: Ad-GFP-Baylor (a) and Ad-GFP-VB (b) transduce supporting cells and hair cells in the mouse utricle when injected at P0. Representative confocal images of whole-mount fluorescent immunolabeling of the utricle. Scale bars: 10 μm.

cochlea. Ad-Cre-GFP-Baylor transduced only SCs in the basal and middle turns. Ad-GFP-Baylor and Ad-GFP-VB also transduced some HCs including both IHCs and OHCs (Table 1). The overall transduction efficiency was lower for Ad-GFP-Baylor vectors when injected at P4 than at P0 but higher for Ad-GFP-VB in SCs. Furthermore, Ad-GFP-VB had a broader transduction pattern when injected at P0 as it transduced OHCs along the whole cochlea and IHCs at middle and apex turns, but it only transduced a few OHCs at the apical turn when injected at P4.

4. Discussion

This study identified commercial adenovirus viral vectors that target mouse inner ear cell subtypes for gene delivery. Three adenovirus vectors transduced P0 and P4 inner ear, with different specificities and expression levels that are dependent on the type of adenoviral vectors and the age of mice. The cochlear sensory epithelium, which harbors auditory hair cells and supporting cells, is transduced with higher efficiency. The adenovirus with GFP alone transduced utricular supporting cells. The infected cells survived at the time of the study (four days after injection). The study shows that Ad vectors are capable of transducing mammalian inner ear efficiently and provides useful tools to evaluate gene therapy and to study inner ear gene function.

There are two approaches of hair cell regeneration: (1) direct transdifferentiation of surrounding cells especially supporting cells to change cell fate to become hair cells and (2) induction of cell cycle re-entry in cells such as supporting cells, which then further differentiate to replace damaged hair cells [1, 25, 26]. Thus, supporting cells are ideal candidates for hair cell regeneration by direct transdifferentiation or by renewed proliferation with subsequent transdifferentiation. Moreover, remaining hair cells can divide to generate new hair cells. Many cases of sensorineural hearing loss and vestibular dysfunction are caused by a primary pathology in the sensory epithelium [17, 18]. It is therefore important to express transgenes in the sensory epithelial cells such as supporting cells specifically. Three Ad vectors transduced SCs efficiently, an indication that they could be useful for potential hair cell regeneration studies. Ad-Cre-GFP-Baylor transduced SCs only at middle and base turns when injected at P0. The lack of transduction of the apical SCs was likely due to limited diffusion of the viral particles. Ad-Cre-GFP-Baylor transduces only SCs, whereas Ad-GFP-Baylor transduced 80% OHCs at apex turn and some IHCs at base turn at P0. Ad-GFP-VB transduces SCs and OHCs. Each Ad vector can therefore be selected to deliver genes to only SCs, HCs, or both.

The volume and titer of vector inoculation influence the cell types and location of cells transduced by the virus. To compare the difference of three virus infection, we use the same titer of three Ads. It is interesting that Ad-GFP-Baylor and Ad-Cre-GFP-Baylor had different transduction specificities. However, according to the instruction of Ad-GFP-Baylor from Baylor College of Medicine, the virus particle (vp) to plaque-forming unit (pfu) ratio is in a range of 1 : 10 to 1 : 200 and the titer is 2.5×10^{10}–5×10^{11} pfu/ml. We used the titer of 10×10^{10} pfu/ml for dilution, which may be an underestimate of the actual titer as it had the highest transduction efficiency.

Injection into mouse cochlea through scala media by cochleostomy maximizes the efficiency as it allows virus to have access to many cochlear cell types. Previous studies suggested that, a better outcome of cell survival, mice younger than P5 should be used, as OHCs will generally die due to surgery in mice older than P5, especially at adult stage [8, 9, 13]. Future study needs to focus on identification of a route by which injection can be performed in adult without causing cell death or hearing loss.

Combining a therapeutic transgene with a reporter gene would be informative for easy identification of the cell types targeted. The human inner ear is much larger in size and would facilitate a more accurate delivery, which could help with the development of gene therapy in patients.

5. Conclusions

The present study explored commercial three Ad vectors into the mouse inner ear *in vivo*. The results show the feasibility of gene transfer into mouse inner ear via Ad vectors with different specificity and efficiency. Future application of gene delivery for the inner ear may include the induction of hair cell regeneration and treatment of hereditary deafness and vestibular dysfunction. The ability of the cochleostomy to deliver reporter transgenes into a variety of cell types in the inner ear, including the sensory epithelium, makes this method attractive to target inner ear cell subtypes. Continuous improvement in identification of highly efficient vectors targeting inner ear cell subtypes would advance their eventual use to treat hearing loss in human.

Competing Interests

The authors declare that there is no conflict of interests regarding the publication of this paper.

Authors' Contributions

Yilai Shu and Yong Tao contributed equally to this work.

Acknowledgments

Zheng-Yi Chen was supported by US National Institutes of Health (R01 DC006908). Yilai Shu, Yong Tao, and Wenyan Li were supported by the Frederick and Ines Yeatts Hair Cell Regeneration Grant and Yilai Shu by the National Nature Science Foundation of China (NSFC81300824) and Science and Technology Commission of Shanghai Municipality (15pj1401000).

References

[1] C. Sage, M. Huang, K. Karimi et al., "Proliferation of functional hair cells in vivo in the absence of the retinoblastoma protein," *Science*, vol. 307, no. 5712, pp. 1114–1118, 2005.

[2] J. V. Brigande and S. Heller, "Quo vadis, hair cell regeneration?" *Nature Neuroscience*, vol. 12, no. 6, pp. 679–685, 2009.

[3] J. A. Zuris, D. B. Thompson, Y. Shu et al., "Cationic lipid-mediated delivery of proteins enables efficient protein-based genome editing in vitro and in vivo," *Nature Biotechnology*, vol. 33, no. 1, pp. 73–80, 2014.

[4] J. M. Jørgensen and C. Mathiesen, "The avian inner ear. Continuous production of hair cells in vestibular sensory organs, but not in the auditory papilla," *Naturwissenschaften*, vol. 75, no. 6, pp. 319–320, 1988.

[5] J. T. Corwin and D. A. Cotanche, "Regeneration of sensory hair cells after acoustic trauma," *Science*, vol. 240, no. 4860, pp. 1772–1774, 1988.

[6] B. M. Ryals and E. W. Rubel, "Hair cell regeneration after acoustic trauma in adult coturnix quail," *Science*, vol. 240, no. 4860, pp. 1774–1776, 1988.

[7] P. M. White, A. Doetzlhofer, Y. S. Lee, A. K. Groves, and N. Segil, "Mammalian cochlear supporting cells can divide and trans-differentiate into hair cells," *Nature*, vol. 441, no. 7096, pp. 984–987, 2006.

[8] Y. Shu, Y. Tao, Z. Wang et al., "Identification of Adeno-associated viral vectors (AAV) that target neonatal and adult mammalian inner ear cell subtypes," *Human Gene Therapy*, vol. 27, no. 9, pp. 687–699, 2016.

[9] L. A. Kilpatrick, Q. Li, J. Yang, J. C. Goddard, D. M. Fekete, and H. Lang, "Adeno-associated virus-mediated gene delivery into the scala media of the normal and deafened adult mouse ear," *Gene Therapy*, vol. 18, no. 6, pp. 569–578, 2011.

[10] O. Akil, R. P. Seal, K. Burke et al., "Restoration of hearing in the VGLUT3 knockout mouse using virally mediated gene therapy," *Neuron*, vol. 75, no. 2, pp. 283–293, 2012.

[11] C. Askew, C. Rochat, B. Pan et al., "Tmc gene therapy restores auditory function in deaf mice," *Science Translational Medicine*, vol. 7, no. 295, Article ID 295ra108, 2015.

[12] W. W. Chien, K. Isgrig, S. Roy et al., "Gene therapy restores hair cell stereocilia morphology in inner ears of deaf whirler mice," *Molecular Therapy*, vol. 24, no. 1, pp. 17–25, 2016.

[13] Q. Yu, Y. Wang, Q. Chang et al., "Virally expressed connexin26 restores gap junction function in the cochlea of conditional Gjb2 knockout mice," *Gene Therapy*, vol. 21, no. 1, pp. 71–80, 2014.

[14] Y. Wang, Y. Sun, Q. Chang et al., "Early postnatal virus inoculation into the scala media achieved extensive expression of exogenous green fluorescent protein in the inner ear and preserved auditory brainstem response thresholds," *Journal of Gene Medicine*, vol. 15, no. 3-4, pp. 123–133, 2013.

[15] Y. Raphael, J. C. Frisancho, and B. J. Roessler, "Adenoviral-mediated gene transfer into guinea pig cochlear cells in vivo," *Neuroscience Letters*, vol. 207, no. 2, pp. 137–141, 1996.

[16] A. E. Luebke, J. D. Steiger, B. L. Hodges, and A. Amalfitano, "A modified adenovirus can transfect cochlear hair cells in vivo without compromising cochlear function," *Gene Therapy*, vol. 8, no. 10, pp. 789–794, 2001.

[17] K. Kawamoto, S.-H. Oh, S. Kanzaki, N. Brown, and Y. Raphael, "The functional and structural outcome of inner ear gene transfer via the vestibular and cochlear fluids in mice," *Molecular Therapy*, vol. 4, no. 6, pp. 575–585, 2001.

[18] S.-I. Ishimoto, K. Kawamoto, S. Kanzaki, and Y. Raphael, "Gene transfer into supporting cells of the organ of Corti," *Hearing Research*, vol. 173, no. 1-2, pp. 187–197, 2002.

[19] T. Iizuka, S. Kanzaki, H. Mochizuki et al., "Noninvasive in vivo delivery of transgene via adeno-associated virus into supporting cells of the neonatal mouse cochlea," *Human Gene Therapy*, vol. 19, no. 4, pp. 384–390, 2008.

[20] V. Lin, J. S. Golub, T. B. Nguyen, C. R. Hume, E. C. Oesterle, and J. S. Stone, "Inhibition of notch activity promotes nonmitotic regeneration of hair cells in the adult mouse utricles," *Journal of Neuroscience*, vol. 31, no. 43, pp. 15329–15339, 2011.

[21] H. Staecker, D. Li, B. W. O'Malley, and T. R. Van De Water, "Gene expression in the mammalian cochlea: a study of multiple vector systems," *Acta Oto-Laryngologica*, vol. 121, no. 2, pp. 157–163, 2001.

[22] A. E. Luebke, P. K. Foster, C. D. Muller, and A. L. Peel, "Cochlear function and transgene expression in the guinea pig cochlea, using adenovirus- and adeno-associated virus-directed gene transfer," *Human Gene Therapy*, vol. 12, no. 7, pp. 773–781, 2001.

[23] J. L. Zheng and W.-Q. Gao, "Overexpression of Math1 induces robust production of extra hair cells in postnatal rat inner ears," *Nature Neuroscience*, vol. 3, no. 6, pp. 580–586, 2000.

[24] A. K. Lalwani, J. Jero, and A. N. Mhatre, "Current issues in cochlear gene transfer," *Audiology & Neurotology*, vol. 7, no. 3, pp. 146–151, 2002.

[25] Y. Raphael, "Evidence for supporting cell mitosis in response to acoustic trauma in the avian inner ear," *Journal of Neurocytology*, vol. 21, no. 9, pp. 663–671, 1992.

[26] J. S. Stone and D. A. Cotanche, "Hair cell regeneration in the avian auditory epithelium," *International Journal of Developmental Biology*, vol. 51, no. 6-7, pp. 633–647, 2007.

Hindawi Publishing Corporation
Neural Plasticity
Volume 2016, Article ID 5310192, 4 pages
http://dx.doi.org/10.1155/2016/5310192

Research Article

Massively Parallel Sequencing of a Chinese Family with DFNA9 Identified a Novel Missense Mutation in the LCCL Domain of COCH

Xiaodong Gu,[1,2] Wenling Su,[3] Mingliang Tang,[4,5] Luo Guo,[1,2,6] Liping Zhao,[1,2,6] and Huawei Li[1,2,7,8,9]

[1]*Otorhinolaryngology Department, Affiliated Eye and ENT Hospital, State Key Laboratory of Medical Neurobiology, Fudan University, Shanghai 200031, China*
[2]*Key Laboratory of Hearing Medicine of National Health and Family Planning Commission, Shanghai 200031, China*
[3]*Department of Otolaryngology-Head and Neck Surgery, The First Affiliated Hospital, Xiamen University, Xiamen, China*
[4]*Key Laboratory for Developmental Genes and Human Disease, Ministry of Education, Institute of Life Sciences, Southeast University, Nanjing 210096, China*
[5]*Co-Innovation Center of Neuroregeneration, Nantong University, Nantong 226001, China*
[6]*Central Laboratory, Affiliated Eye and ENT Hospital, Fudan University, Shanghai 200031, China*
[7]*Institutes of Biomedical Sciences, Fudan University, Shanghai 200032, China*
[8]*The Institutes of Brain Science and the Collaborative Innovation Center for Brain Science, Fudan University, Shanghai, China*
[9]*Shanghai Engineering Research Center of Cochlear Implant, Shanghai 200031, China*

Correspondence should be addressed to Huawei Li; hwli@shmu.edu.cn

Received 9 September 2016; Revised 16 November 2016; Accepted 23 November 2016

Academic Editor: Jian Wang

DFNA9 is a late-onset, progressive, autosomal dominantly inherited sensorineural hearing loss with vestibular dysfunction, which is caused by mutations in the *COCH* (coagulation factor C homology) gene. In this study, we investigated a Chinese family segregating autosomal dominant nonsyndromic sensorineural hearing loss. We identified a missense mutation c.T275A p.V92D in the LCCL domain of *COCH* cosegregating with the disease and absent in 100 normal hearing controls. This mutation leads to substitution of the hydrophobic valine to an acidic amino acid aspartic acid. Our data enriched the mutation spectrum of DFNA9 and implied the importance for mutation screening of *COCH* in age related hearing loss with vestibular dysfunctions.

1. Introduction

As the most common sensory impairment, hearing loss (HL) affects one of every 500 newborn infants, and its prevalence rises to 2.7 per 1000 children before the age of 5 and 3.5 per 1000 during adolescence [1, 2]. HL is a genetically and clinically heterozygous disorder and can be classified according to pattern of inheritance (autosomal dominant, autosomal recessive, or X-linked recessive, and mitochondrial inheritance), the absence (nonsyndromic) or presence (syndromic) of other clinical features, and age at onset (prelingual or postlingual) [3]. To date, researchers have identified 98 genes associated with nonsyndromic hearing loss (NSHL) (Hereditary Hearing Loss Homepage, http://hereditaryhearingloss.org). Most of the mutations in the autosomal dominant loci cause postlingual hearing impairments [4].

Mutations in the *COCH* gene are responsible for the late-onset, progressive ADNSHL with incomplete penetrance of vestibular malfunction known as DFNA9 [5]. The COCH gene encodes a 550-aa extracellular protein cochlin that is the most highly expressed protein in the human and mouse inner ear [6]. The cochlin amino acid sequence contains an N-terminal signal peptide, an LCCL domain highly homologous to factor C, a serine proteinase involved in immune response

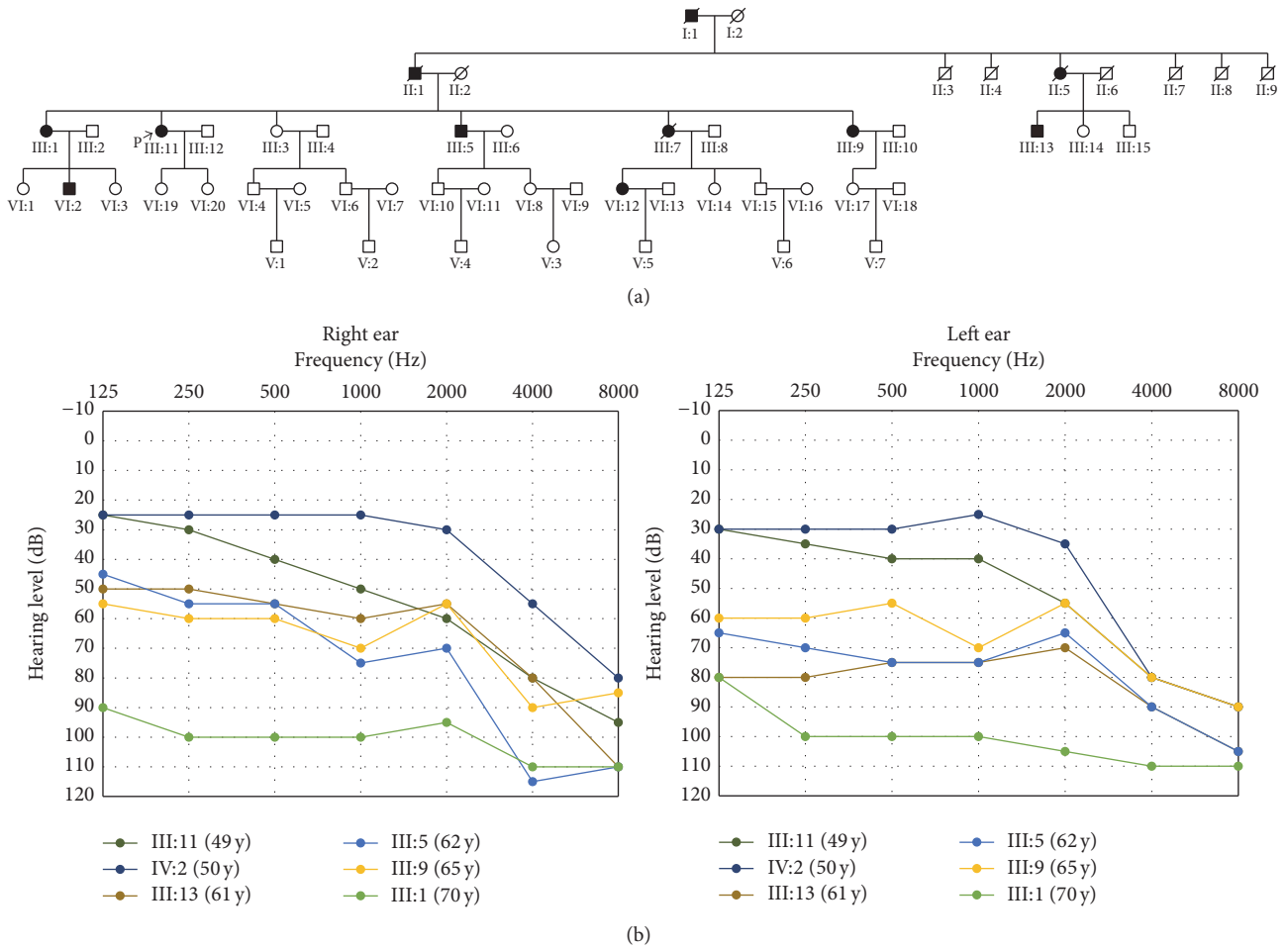

FIGURE 1: (a) Pedigree of the family with nonsyndromic autosomal recessive hearing loss. Darkened symbols denote affected individuals. (b) Audiograms of all affected individuals in the family.

of the *Limulus*, and two von Willebrand factor A (vWFA) domains [7]. So far, twenty-three DFNA9 mutations were identified in the LCCL domain, vWFA domain, and intervening domain [8–15]. Individuals with DFNA9 manifest late-onset progressive HL with onset usually before the fourth or fifth decade [16]. Onset of HL is initially in high frequencies, progressing to include lower frequencies, and usually leads to severe HL by the sixth decade of life. COCH mutations also result in vestibular dysfunction and balance problems in many affected individuals [16].

In this study, we performed massively parallel sequencing on a nonconsanguineous Chinese family segregating autosomal dominant sensorineural HL and identified a novel missense mutation in the LCCL domain.

2. Results

2.1. Clinical Phenotype. Seven individuals in family G405 were diagnosed with sensorineural hearing loss by otologic and audiometric analysis (Figure 1(a)). Affected family members showed moderate to severe bilateral sensorineural hearing loss initially affected high frequencies and, with increasing age, developed to mid- and low-frequencies, which resulted in a flat or downward sloping audiogram (Figure 1(b)). The self-reported age at onset of hearing loss was in the 2nd or 3rd decade. Vertigo, dizziness, and tinnitus have been reported or diagnosed in all affected family members except for VI:12.

2.2. Massively Parallel Sequencing. Targeted MPS aiming 131 deafness-associated genes was applied to proband of family G123. A mean depth of coverage of 176 was achieved with more than 98.6% of the targeted bases covered by more than 10 reads. Variants were called and filtered using strategies described previously. Briefly, variants meeting the following criteria were filtered out: (1) variants covered by less than 10 sequencing reads; (2) intronic and synonymous variants; (3) variants with allele frequencies below 0.01 in 1000 genome database, ESP6500 database, or ExAC database. Consequently, the COCH mutation c.T275A p.V92D (NM_001135058) was the only candidate variant that passed all filtering steps.

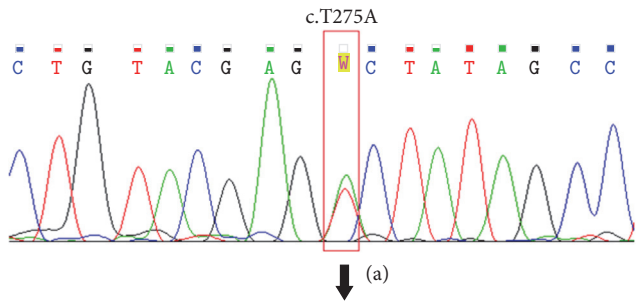

	SIFT	PolyPhen2	LRT	MutationTaster
p.V92D	0(D)	0.903(D)	0.999998(D)	0.999978(D)

(c)

Figure 2: (a) Sanger sequencing chromatograms showing the c.T275A p.V92D mutation of the family. (b) Protein sequence alignment showing conservation of the V92 residue in cochlin across human (*H. sapiens*), chimpanzee (*P. troglodytes*), macaca (*M. mulatta*), mouse (*M. musculus*), chicken (*G. gallus*), and zebrafish (*D. rerio*). (c) Pathogenicity prediction using computational programs. D in the parentheses stands for deleterious.

2.3. Mutation Analysis. Segregation analysis of candidate variants was carried out by Sanger sequencing. The novel COCH mutation c.T275A:p.V92D (NM_001135058) (Figure 2(a)) was present in all affected individuals but not in the normal family members that are above 40 years of age. This mutation caused an amino acid substitution in the LCCL domain of cochlin protein. Sequence alignment analysis of COCH from different species revealed that this amino acid is highly conserved (Figure 2(b)). The mutation was predicted to be deleterious by four computational programs (Figure 2(c)). Then, we scanned exon 4 of *COCH* gene in 100 unrelated Chinese control individuals. Consequently, no variants were detected.

3. Methods

3.1. Subjects and Clinical Diagnosis. A Chinese nonconsanguineous family, G405, with late-onset progressive hearing loss was recruited from the Department of Otolaryngology, Affiliated Eye and ENT Hospital, Fudan University, Shanghai, China. Family G405 has five generations and segregated late-onset autosomal dominant sensorineural hearing loss by otologic and audiometric analysis. Twenty-five family members, including seven affected individuals, were recruited. Otoscopy and pure tone audiometry (including frequencies from 250 to 8000 Hz) were applied to identify the phenotype. Vestibular function was assessed in some family members by caloric testing and electronystagmography. Blood samples were drawn from the participants. Written informed consent was obtained from all participating individuals in accordance with the ethics committee of Fudan University.

3.2. Massively Parallel Sequencing. Genomic DNA was extracted from whole blood using genomic DNA isolation kit (Qiagen, Hilden, Germany). Exome capture was carried out using TruSeq Exome Enrichment Kit according to the manufacturer's protocols. Captured libraries were then loaded onto the Hiseq2000 platform, and sequencing was performed 100 bp paired-end, providing at least 80-fold coverage for each sample. Raw image files were processed by Illumina's Cassava pipeline for base-calling with default parameters. The proband of family G123 was subjected to a gene panel containing 131 deafness genes. Capture and MPS of the coding exons plus ~100 bp of the flanking intronic sequences for the 131 deafness genes on a HiSeq2000 (Illumina) were performed by Otogenetics Corporation (Norcross, GA). A total of 3 μg genomic DNA was used as input material for NimbleGen capture methods to generate 2 × 100 paired-end reads. Sequencing reads were aligned to human reference genome (hg19/NCBI 37) using the Burrows-Wheeler Aligner (BWA) program, refined using the Genome Analysis Tool Kit (GATK) software and Picard. The genotypes in target regions were identified using the GATK Unified Genotyper; quality scores of the variants were recalibrated. Functional annotations of the variants were performed by Annovar [17].

3.3. Mutational Analysis. Segregation analysis of the candidate mutation identified by MPS was performed in available members of family G405 using PCR followed by bidirectional Sanger sequencing of the amplified fragments (ABI 3730XL; Applied Biosystems, Foster City, CA). In addition, sequences from 100 ethnicity-matched samples with normal hearing were examined.

4. Discussion

In this study, we identified a novel heterozygous missense mutation within the LCCL domain of cochlin in a large Chinese family with late-onset progressive sensorineural HL and vestibular dysfunction. The mutations cosegregated with the disease and were not observed in public databases or 100 ethnicity-matched controls.

The p.V92D mutation identified in this study resides within the N-terminal LCCL domain of cochlin, which leads to substitution of the hydrophobic valine to an acidic amino acid aspartic acid. Mutations of this domain have been shown to cause misfolding and aggregation of the cochlin protein in a dominant-negative fashion and lead to cytotoxicity [7, 16]. It is noteworthy that most of the patients carrying mutations in the LCCL domain manifested vestibular dysfunctions. Our study supported this genotype-phenotype correlation because nearly all affected patients of family G405 exhibit vestibular dysfunction.

The pathogenic mechanisms of DFNA9 mutations have not been fully revealed; recent studies suggested several possible mechanisms. Several studies suggest that mutations in the LCCL domain induce misfolded LCCL domain and demonstrate cytotoxicity leading to inner ear damage [6, 18]. Others demonstrated that mutant cochlin forms a stable dimer that is sensitive to reducing agent. The mutant cochlin can stabilize wild type cochlin in the dimer conformation,

providing a possible explanation for the dominant nature of DFNA9 mutations [19]. A recent study indicates that amino acid substitutions in cochlin lessened cochlin susceptibility to cleavage enzyme induced by aggrecanase, which caused reduced secretion of the LCCL domain to the extracellular compartment [8]. It is possible that the p.V92D mutation in our study may also lead to cochlin misfolding.

In conclusion, our findings enriched the mutation and genotype-phenotype correlation spectrum of DFNA9 and implied the importance for mutation screening of COCH in late-onset hearing loss with vestibular dysfunctions.

Competing Interests

The authors declare that they have no competing interests.

Authors' Contributions

Xiaodong Gu, Wenling Su, Mingliang Tang, and Luo Guo contributed equally to this work.

Acknowledgments

This work was supported by grants from the Major State Basic Research Development Program of China (2016YFC0905200 and 973 Program Grant 2015CB965000), the National Natural Science Foundation of China (Grants 81470687, 81230019, and 81500801), the Construction Program of the Shanghai Committee of Science and Technology (Grant 12DZ2251700), and the Xiamen Science and Technology Planning Project (Grant 3502z2014013).

References

[1] C. C. Morton and W. E. Nance, "Newborn hearing screening—a silent revolution," *The New England Journal of Medicine*, vol. 354, no. 20, pp. 2151–2164, 2006.

[2] N. G. Robertson, A. B. Skvorak, Y. Yin et al., "Mapping and characterization of a novel cochlear gene in human and in mouse: a positional candidate gene for a deafness disorder, DFNA9," *Genomics*, vol. 46, no. 3, pp. 345–354, 1997.

[3] A. E. Shearer and R. J. Smith, "Genetics: advances in genetic testing for deafness," *Current Opinion in Pediatrics*, vol. 24, no. 6, pp. 679–686, 2012.

[4] N. Hilgert, R. Smith, and G. Camp, "Function and expression pattern of nonsyndromic deafness genes," *Current Molecular Medicine*, vol. 9, no. 5, pp. 546–564, 2009.

[5] N. G. Robertson, L. Lu, S. Heller et al., "Mutations in a novel cochlear gene cause DFNA9, a human nonsyndromic deafness with vestibular dysfunction," *Nature Genetics*, vol. 20, no. 3, pp. 299–303, 1998.

[6] T. Ikezono, A. Omori, S. Ichinose, R. Pawankar, A. Watanabe, and T. Yagi, "Identification of the protein product of the *Coch* gene (hereditary deafness gene) as the major component of bovine inner ear protein," *Biochimica et Biophysica Acta (BBA)—Molecular Basis of Disease*, vol. 1535, no. 3, pp. 258–265, 2001.

[7] N. G. Robertson, C. W. R. J. Cremers, P. L. M. Huygen et al., "Cochlin immunostaining of inner ear pathologic deposits and proteomic analysis in DFNA9 deafness and vestibular dysfunction," *Human Molecular Genetics*, vol. 15, no. 7, pp. 1071–1085, 2006.

[8] J. Jung, H. S. Kim, M. G. Lee, E. J. Yang, and J. Y. Choi, "Novel COCH p.V123E mutation, causative of DFNA9 sensorineural hearing loss and vestibular disorder, shows impaired cochlin post-translational cleavage and secretion," *Human Mutation*, vol. 36, no. 12, pp. 1168–1175, 2015.

[9] D.-Y. Chen, Y.-C. Chai, T. Yang, and H. Wu, "Clinical characterization of a novel COCH mutation G87V in a Chinese DFNA9 family," *International Journal of Pediatric Otorhinolaryngology*, vol. 77, no. 10, pp. 1711–1715, 2013.

[10] T. Makishima, C. I. Rodriguez, N. G. Robertson, C. C. Morton, C. L. Stewart, and A. J. Griffith, "Targeted disruption of mouse Coch provides functional evidence that DFNA9 hearing loss is not a COCH haploinsufficiency disorder," *Human Genetics*, vol. 118, no. 1, pp. 29–34, 2005.

[11] I. Nagy, M. Horváth, M. Trexler, G. Répássy, and L. Patthy, "A novel COCH mutation, V104del, impairs folding of the LCCL domain of cochlin and causes progressive hearing loss," *Journal of Medical Genetics*, vol. 41, no. 1, article no. e9, 2004.

[12] M. Kamarinos, J. McGill, M. Lynch, and H. Dahl, "Identification of a novel COCH mutation, I109N, highlights the similar clinical features observed in DFNA9 families," *Human Mutation*, vol. 17, no. 4, p. 351, 2001.

[13] R. J. Pauw, P. L. M. Huygen, R. W. J. Collin et al., "Phenotype description of a novel DFNA9/COCH mutation, I109T," *Annals of Otology, Rhinology and Laryngology*, vol. 116, no. 5, pp. 349–357, 2007.

[14] J. Gao, J. Xue, L. Chen, X. Ke, Y. Qi, and Y. Liu, "Whole exome sequencing identifies a novel DFNA9 mutation, C162Y," *Clinical Genetics*, vol. 83, no. 5, pp. 477–481, 2013.

[15] V. A. Street, J. C. Kallman, N. G. Robertson, S. F. Kuo, C. C. Morton, and J. O. Phillips, "A novel DFNA9 mutation in the vWFA2 domain of COCH alters a conserved cysteine residue and intrachain disulfide bond formation resulting in progressive hearing loss and site-specific vestibular and central oculomotor dysfunction," *American Journal of Medical Genetics A*, vol. 139, no. 2, pp. 86–95, 2005.

[16] A. M. L. C. Bischoff, P. L. M. Huygen, M. H. Kemperman et al., "Vestibular deterioration precedes hearing deterioration in the P51S COCH mutation (DFNA9): an analysis in 74 mutation carriers," *Otology & Neurotology*, vol. 26, no. 5, pp. 918–925, 2005.

[17] X. Gu, L. Guo, H. Ji et al., "Genetic testing for sporadic hearing loss using targeted massively parallel sequencing identifies 10 novel mutations," *Clinical Genetics*, vol. 87, no. 6, pp. 588–593, 2015.

[18] R. Grabski, T. Szul, T. Sasaki et al., "Mutations in COCH that result in non-syndromic autosomal dominant deafness (DFNA9) affect matrix deposition of cochlin," *Human Genetics*, vol. 113, no. 5, pp. 406–416, 2003.

[19] J. Yao, B. F. Py, H. Zhu, J. Bao, and J. Yuan, "Role of protein misfolding in DFNA9 hearing loss," *The Journal of Biological Chemistry*, vol. 285, no. 20, pp. 14909–14919, 2010.

Hindawi Publishing Corporation
Neural Plasticity
Volume 2016, Article ID 5836143, 10 pages
http://dx.doi.org/10.1155/2016/5836143

Research Article

Identification of a Novel ENU-Induced Mutation in Mouse *Tbx1* Linked to Human DiGeorge Syndrome

Jiaofeng Chen,[1] Xue Zhang,[2] Jie Li,[1] Chenmeng Song,[1] Yichang Jia,[2] and Wei Xiong[1]

[1]*School of Life Sciences, Tsinghua University, Beijing, China*
[2]*School of Medicine, Tsinghua University, Beijing, China*

Correspondence should be addressed to Yichang Jia; yichangjia@tsinghua.edu.cn and Wei Xiong; wei_xiong@tsinghua.edu.cn

Received 9 September 2016; Revised 22 November 2016; Accepted 28 November 2016

Academic Editor: Renjie Chai

The patients with DiGeorge syndrome (DGS), caused by deletion containing dozens of genes in chromosome 22, often carry cardiovascular problem and hearing loss associated with chronic otitis media. Inside the deletion region, a transcription factor *TBX1* was highly suspected. Furthermore, similar DGS phenotypes were found in the *Tbx1* heterozygous knockout mice. Using ENU-induced mutagenesis and G1 dominant screening strategy, here we identified a nonsynonymous mutation p.W118R in T-box of TBX1, the DNA binding domain for transcription activity. The mutant mice showed deficiency of inner ear functions, including head tossing and circling, plus increased hearing threshold determined by audiometry. Therefore, our result further confirms the pathogenic basis of *Tbx1* in DGS, points out the crucial role of DNA binding activity of TBX1 for the ear function, and provides additional animal model for studying the DGS disease mechanisms.

1. Introduction

The two major types of hearing loss, both conductive and sensorineural, are caused by gene mutations that affect the structure and function of the auditory system. Currently, more than 70 nonsyndromic deafness genes have been identified [1]. Usually the nonsyndromic deafness genes participate more specifically in auditory functions such as transduction, ciliogenesis, cell metabolism, and ion homeostasis [2]. For example, *GJB2* is a major deafness gene [3] that encodes for a component of gap junctions specifically in the supporting cells of the cochlea and governs potassium recycling [4]. *Lhfpl5* was found expressed specifically in hair bundle of cochlear hair cells [5] that modulate the transduction complex location and channel gating [6]. In addition, many more loci have been linked to nonsyndromic deafness though the causative genes have not been characterized yet [1].

However, it is more prevalent that a deafness phenotype always accompanies with other types of disorder(s), which is considered as a syndromic deafness. For example, Pendred syndrome is the most common deaf syndrome that manifests cochlear development abnormalities and sensorineural hearing loss, in parallel with diffuse thyroid enlargement [7]. The Pendred syndrome is caused by a chloride-iodide transport protein malfunction [8]. Patients with Usher syndrome hold both profound hearing loss and retinitis pigmentosa [9]. Hence, the identification of novel deafness gene and the annotation thereafter are appreciated greatly in the research field and clinical community. Strategically the forward genetics and reverse genetics based approaches are widely applied to search novel deafness genes.

For all characterized deafness genes, a large number of them are encoding structural proteins or homeostasis modulators that are mostly linked to nonsyndromic deafness. It may not be difficult to understand, considering that cochlea is such a sophisticated tissue machine endowing ear the hearing function. More importantly, the transcription factors and noncoding RNA molecules are broadly manipulating the development of the ear that often cause syndromic deafness. It has been characterized that a bunch of transcription factors mainly are involved in neural development in addition to inner ear development and morphogenesis. For example, transcription factors including *Bmb4*, *Jag1*, *Islet1*, *Lfng*, *Fgf16*, *Prox1*, and *Tbx1* regulate specification of prosensory patches [10]. These transcription factors are expressed in specified

temporal and spatial patterns with intermingled interaction to each other.

Mice with *Tbx1* mutation showed a reduced expression of *Bmp4* and thus resulted in deficiency of sensory epithelia formation [11]. In early inner ear development, *Tbx1* is a very important transcription factor [12] that is also one of the candidate genes in pathogenesis of del22q11/DiGeorge syndrome (DGS)/velocardiofacial syndrome (VCFS) (for short DGS below) [13–15]. Usually, DGS patients carry a hemizygous deletion for a 1.5–3 Mb region on human chromosome 22, which includes 24 genes. DGS is complex and manifested by lots of phenotypes including craniofacial anomalies such as external ear defects and hearing impairment in addition to cardiovascular problem [16, 17]. It has been reported that most of the DGS patients carry conductive hearing loss associated with chronic otitis media [18, 19]. However, a minor (15%) of hearing loss is of the sensorineural type with unknown mechanisms [18]. In addition, balance problem was observed in DGS patients [20]. Recent study has given strong evidence that *Tbx1* is a critical gene in the pathogenesis of DGS [21–23].

In this study, we have utilized a chemical mutagenesis based N-ethyl-N-nitrosourea (ENU) screening and characterized a mouse line called *ENU706* that carried phenotype of deafness and imbalance in a fashion of dominant inheritance. Audiometric analysis demonstrated that the hearing threshold of *ENU706* heterozygous mice was elevated around 30 dB SPL by average comparing to control mice. However, the hearing threshold in each heterozygous mouse was randomly elevated for each ear. The genetic analysis pointed out that *Tbx1* was the causative gene for the ear problem. A previously unreported nonsynonymous mutation, p.W118R, hits a conserved amino acid in the T-box region of TBX1, a DNA binding domain responsible for the *Tbx1* transcription activity. In T-box domain, very close to our mouse mutation, the other 2 human DGS mutations, p.F148Y and p.H194Q, were previously found in familial cases. Therefore, our data further confirm the pathogenic roles of *Tbx1* in DGS, pinpoint the mechanistic association of its DNA binding activity and hearing loss, and provide additional animal model for studying the DGS disease mechanisms.

2. Materials and Methods

All procedures were performed in accordance with research guidelines of the institutional animal care and use committee of Tsinghua University. Mice of either sex were used in this study.

2.1. Generation of ENU Mutant Mice. The ENU-mutagenesis protocol and primary phenotypic screen have been described previously [25]. Briefly, C57BL/6J male mice were injected with ENU at the dose of 100 mg/kg according to body weight once every week for three weeks. After recovery of fertility, the mice were mated to female naive C57BL/6J. The offspring G1 mice were applied for neurological phenotypic assays, including learning and memory, movement impairment, hearing loss, and gait analysis. The affected G1 founders were bred to naive C57BL/6J to set up mutant family. The offspring mice carrying the inherited phenotypes were sent for whole exon capture to identify the responsible mutations.

2.2. Whole-Exome Analysis. Exonic single nucleotide polymorphism (SNP) was examined at whole genome level [26]. In brief, the exome captured sequencing library was produced by SeqCap EZ Library SR (Roche). The DNA-seq data was subjected to bioinformatics analysis to recognize the potential variants caused by ENU by comparing mutant (affected) with C57BL/6J database. All the candidates must meet four criteria: (1) the number of supporting reads > 4; (2) the number of supporting reads/the depth of this locus > 0.2; (3) the variant appeared heterozygous in the affected sample but not in the unaffected sample; (4) according to the annotation by ANNOVAR it is a nonsynonymous exonic mutation.

2.3. Audiometry. Auditory brainstem response (ABR) measurement was used to evaluate the hearing threshold of mice in this study as previously described [27]. The measurement was applied on mice with age older than 30 days. To examine developmental effect on hearing progression, the mice were tested with age up to 300 days. Before measurement, the mouse was anesthetized by i.p. injection of pentobarbitone. Then the mouse was transferred into a sound-proof chamber (Shengnuo, Shanghai) for audiometry. The audiometric evaluation was done with a TDT RZ6 system (Tucker-Davis Technologies). The electrodes were placed into the mouse subdermally. The ground electrode was inserted in the back near the hind leg, and the reference electrode was just behind the pinna, and the active electrode was inserted at the vertex. An EC1 close-field speaker was placed onto the external ear canal through a conduct tube. A balanced click stimuli were applied per second, each with a duration of 0.1 ms, starting at 90 dB SPL and decreasing at 10 dB SPL step in intensity. Stimuli and recordings were performed with the BioSigRZ software provided with the TDT workstation. The number of acquisition trials was set at 512 for averaging. Auditory thresholds were analyzed for both ears of mutant mice and single ears of wild-type mice. Wild-type mice were examined for another ear if there was an abnormal hearing. The hearing threshold was defined once a visible ABR emerged in recorded traces with graded click stimuli. Our setup determined the median threshold of wild-type C57BL/6J as 20 dB SPL. This baseline was elevated a bit with aging of mice.

2.4. Scanning Electron Microscopy. Inner ears were dissected out in phosphate buffer (0.1 M $Na_2HPO_4{\cdot}12H_2O$, 0.1 M $NaH_2PO_4{\cdot}2H_2O$, PH 7.4) and transferred into fixative buffer (2.5% glutaraldehyde, 0.1 M phosphate buffer). A hole was poked at the apex to let the fixative flush through the cochlear labyrinth before the sample was fixed overnight at 4°C. The inner ears were washed by phosphate buffer for 10 minutes with 3 times and fine-dissected to remove the spiral ligament, Reissner's membrane, and tectorial membrane. Samples were dehydrated by 30-minute incubation in 10/20/30/50/70/80/95/100% ethanol, followed by freeze drying (Hitachi ES-2030) and gold coating (Hitachi E-1010). The samples were imaged with FEI Quanta 200.

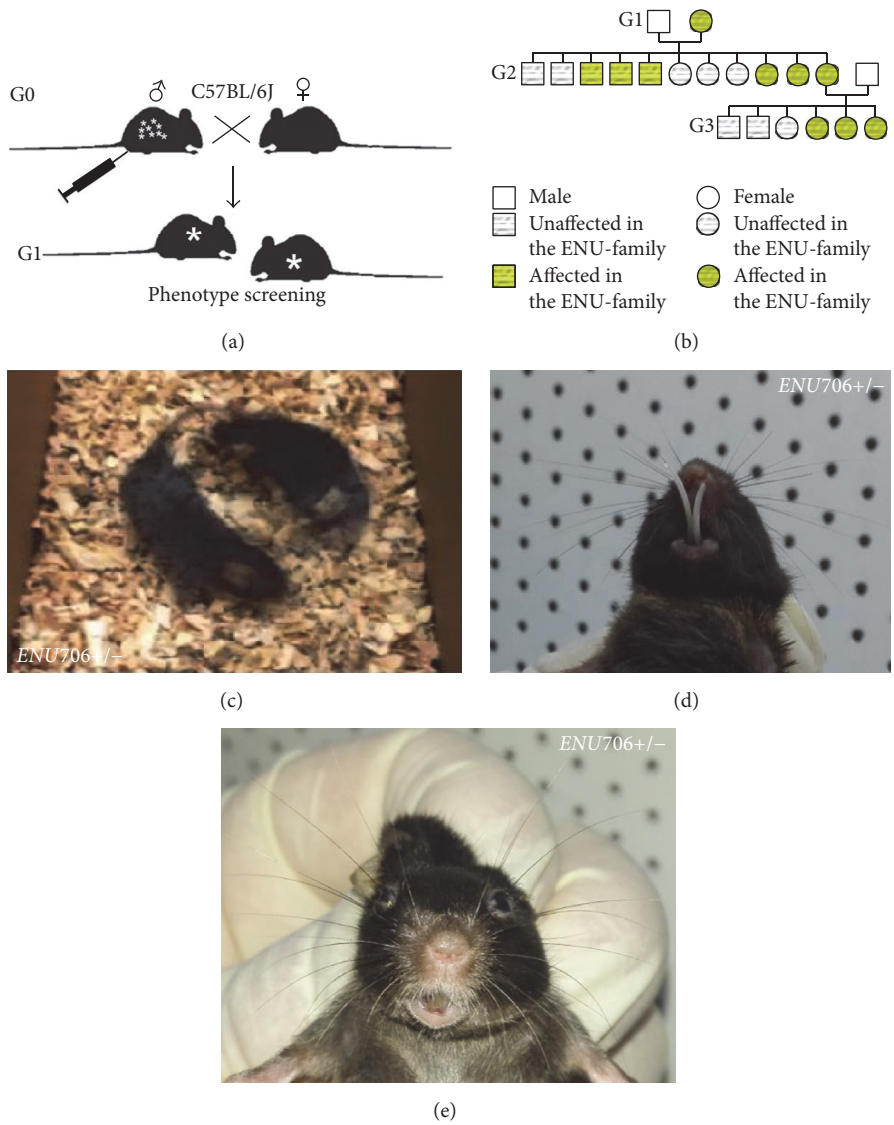

Figure 1: Identification of a mutant line *ENU706* by ENU-mutagenesis screening. (a) The strategy for our ENU screen on C57BL/6J mice. The male founder mouse was injected with mutagen and cross with female mice. The G1 mice were sent for phenotype screening for dominant phenotypes. (b) The family pedigree for the *ENU706* line. (c) Representative image of circling behavior in a heterozygous *ENU706* mouse. The syndromic traits were inherited in a dominant manner. Some of the heterozygous mutant mice showed abnormal craniofacial development including (d) elongated teeth and (e) asymmetrical face.

2.5. Electrophysiology. Cochlear hair cells were observed with an upright microscope (Olympus BX51WI). Borosilicate glass with filament (Sutter) was pulled with a PC-10 pipette puller (Narishige) and polished with MF-830 microforge (Narishige) to resistance of 3–5 MOhm. Hair bundles were deflected with a glass pipette mounted on a P-885 piezoelectric stack actuator (Physik Instrumente). Whole cell currents were sampled at 100 KHz with an EPC 10 USB patch-clamp amplifier operated by Patchmaster software (HEKA). Extracellular solution contains (in mM) 144 NaCl, 0.7 NaH_2PO_4, 5.8 KCl, 1.3 $CaCl_2$, 0.9 $MgCl_2$, 5.6 glucose, and 10 H-HEPES, pH 7.4. Intracellular solution contains (in mM) 140 KCl, 1 $MgCl_2$, 0.1 EGTA, 2 Mg-ATP, 0.3 Na-GTP, and 10 H-HEPES, pH 7.2. Hair cells were voltage-clamped at −70 mV.

2.6. Data Analysis. Data analysis was performed by software including Excel (Microsoft), Prism (GraphPad), and Igor Pro 6 (WaveMetrics).

3. Results and Discussion

3.1. Generation and Genetic Mapping of ENU706 Mouse Line. In order to identify the inherited mutations responsible for the mouse neurological phenotypes, we have set up a G1 dominant mutagenesis screening (Figure 1(a)). The *ENU706* line appeared obvious circling phenotype in the G1 founders (Figure 1(c)). After crossing to the naive C57BL/6J, we found that the dominant inherited phenotype reoccurred in the family (Figure 1(b)), which met the expected Mendelian ratio (Figure 4(c)).

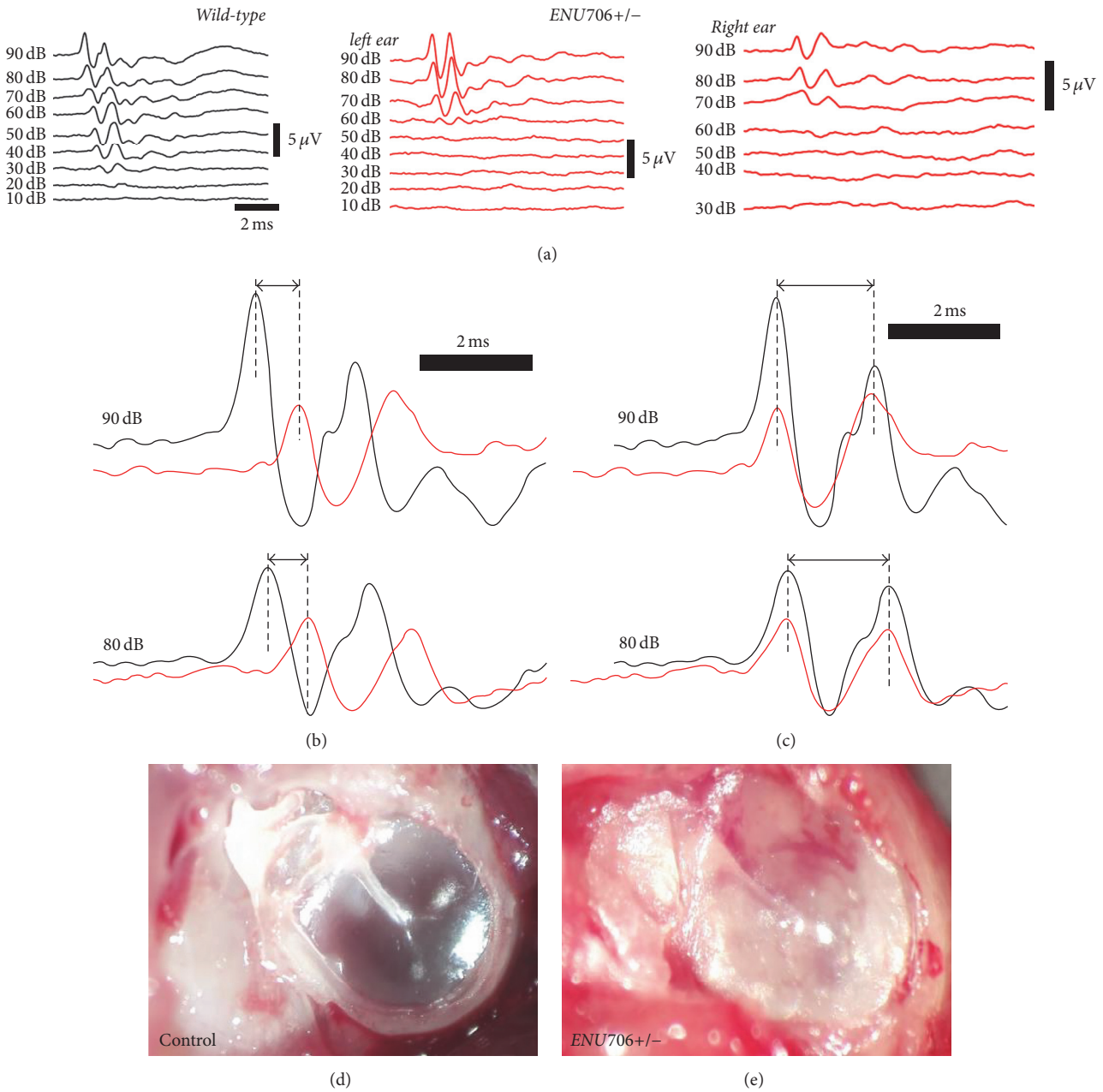

Figure 2: The *ENU706* mice possessed moderate hearing loss. (a) A representative case showed the click ABR test in control and *ENU706* mice. A control mouse possessed a hearing threshold as low as 20 dB SPL. An *ENU706* mouse had 50 dB SPL hearing threshold at the left ear and 60 dB SPL hearing threshold at the right ear. (b) The onset of ABR responses was 0.36 milliseconds later in mutant than that in control mouse. (c) The duration between peaks I and II was not altered obviously in mutant compared to the control. The traces analyzed in (b) and (c) were from the same recordings shown in (a). In (a), (b), and (c), control was shown in black and *ENU706* in red. In difference with the control (d), the heterozygous *ENU706* mice with elevated ABR responses were found to have otitis media (e).

3.2. ENU706 Line Possessed Moderate Hearing Loss. *ENU706* heterozygous mice had circling (Figure 1(c)) and head tossing behavior observed as early as 1-month old that was a typical phenotype of vestibular problem. In general, one-half of the mice were circling (Figure 4(c), left bar), which further confirmed the mutation caused imbalance in a dominant inheritance style. Circling is often accompanied with hearing loss in animals suffering from deficit of the inner ear function. We then assessed the hearing threshold for the colony of *ENU706* mice. Click ABR test was applied to evaluate the threshold of hearing. A control wild-type mouse started to respond to click sound as low as 20 dB SPL (Figure 2(a), left), which is a typical value for normal hearing. While in an *ENU706* heterozygous mouse, the hearing threshold was 50 dB SPL for the left ear and 60 dB SPL for the right ear (Figure 2(a), right). It suggested that this mutant mouse had a moderate hearing loss and might be differentially affected in each ear. Notably, the different hearing threshold for either

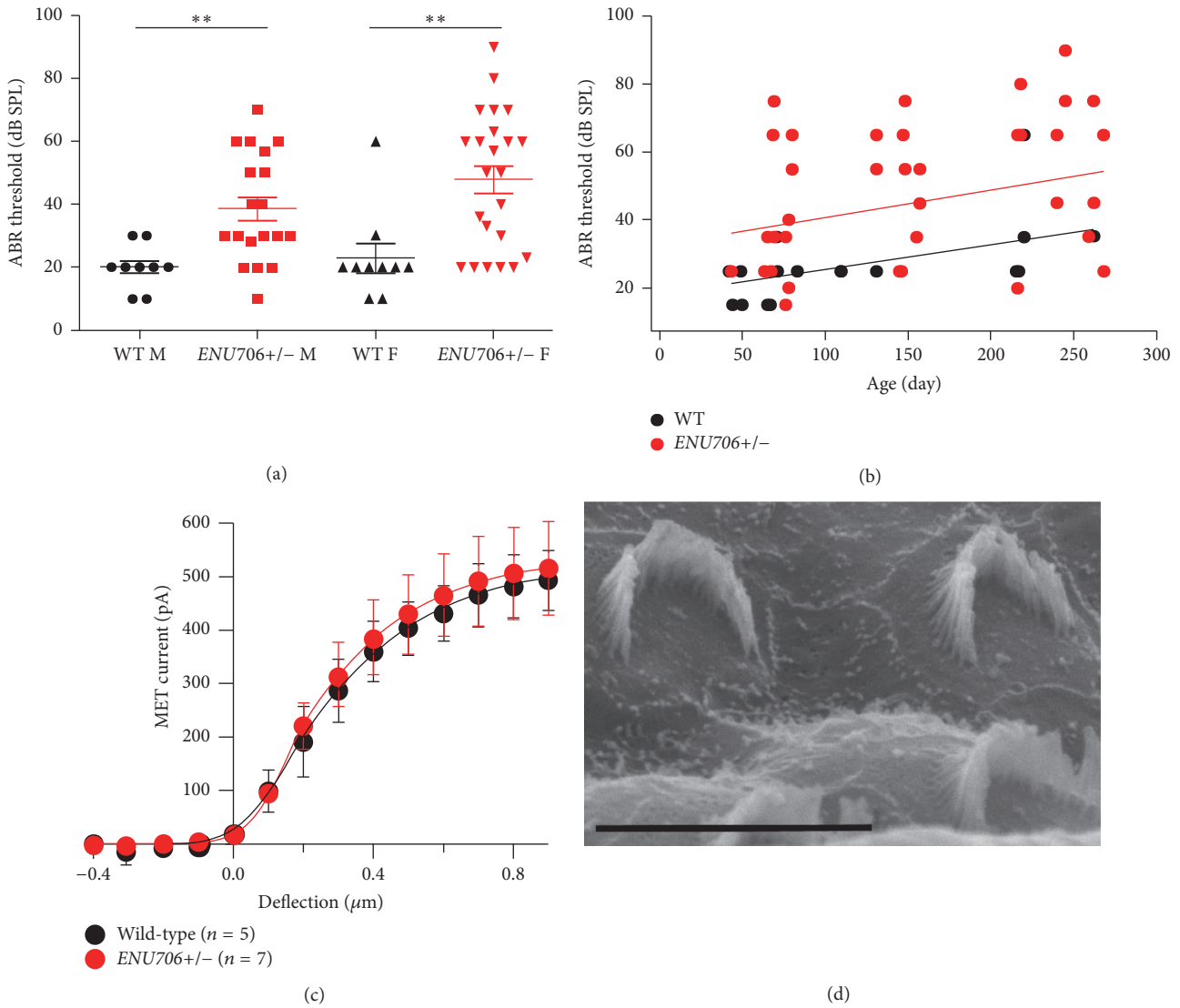

Figure 3: The *ENU706* mice had no obvious defects in hair cell mechanotransduction. (a) The ABR threshold was box-whisker plotted in 4 categories: wild-type male (WT M, 20.0 ± 2.4 dB SPL, 8 males tested, 8 right ears plus 1 left ear), heterozygous male (*ENU706*+/− M, 38.7 ± 3.9 dB SPL, 11 males tested, 11 right ears, and 8 left ears), wild-type female (WT F, 23.0 ± 4.5 dB SPL, 8 females tested, 9 right ears, and 1 left ear), and heterozygous female (*ENU706*+/− F, 47.9 ± 4.5 dB SPL, 13 females tested, 13 right ears, and 10 left ears). The "*n*" numbers were counted twice if both ears were measured. Data shown as mean ± SEM. Statistical significance ($^{**}p < 0.01$) was determined by Student's two-tailed unpaired *t*-test. (b) The ABR threshold was plotted against age. The data pooled from left and right ear were shown (WT, 20 mice tested, 20 right ears, and 3 left ears; *ENU706*+/−, 24 mice tested, 24 right ears, and 19 left ears). (c) The mechanotransduction currents were measured in outer hair cells of *ENU706* heterozygous mice and control littermates (cell number shown in the panel). Data shown as mean ± SD. A set of mechanical deflections from −400 nm to 900 nm at 100 nm step were applied to hair bundle to generate mechanotransduction currents in hair cells. In all panels, control was shown in black and *ENU706* in red. (d) Scanning electron microscopy showed the hair bundles of apical-middle outer hair cells were relatively normal in an *ENU706* heterozygous mouse. Scale bar: 5 μm.

ear of one mouse was often not identical. We observed in some extreme case that the mouse had one ear normal (20 dB SPL) but with another ear profoundly deaf (70 dB SPL). To determine whether the hearing loss was conductive or sensorineural, the latencies of the ABR responses were analyzed. The onset of ABR was submillisecond slower in the *ENU706* heterozygous mouse (Figure 2(b)), but the interpeak seemed not altered (Figure 2(c)). Surgical examinations showed otitis media in *ENU706* heterozygous mice if they had hearing loss (Figures 2(d) and 2(e)). In general, this sporadic hearing loss was not related with gender (Figure 3(a)) or age (Figure 3(b)) in *ENU706* mice. Indeed, the hearing threshold was significantly elevated about 20 dB by average in *ENU706* mice (Figure 3(a)). Consistently, *ENU706* mice also shared a parallel trend of progression with wild-type animals but with elevated hearing threshold (Figure 3(b)). To further investigate whether any of sensorineural factors was involved in the hearing loss, we examined mechanotransduction response in cochlear hair cells. Our electrophysiological data showed no obvious change of mechanotransduction currents in *ENU706*

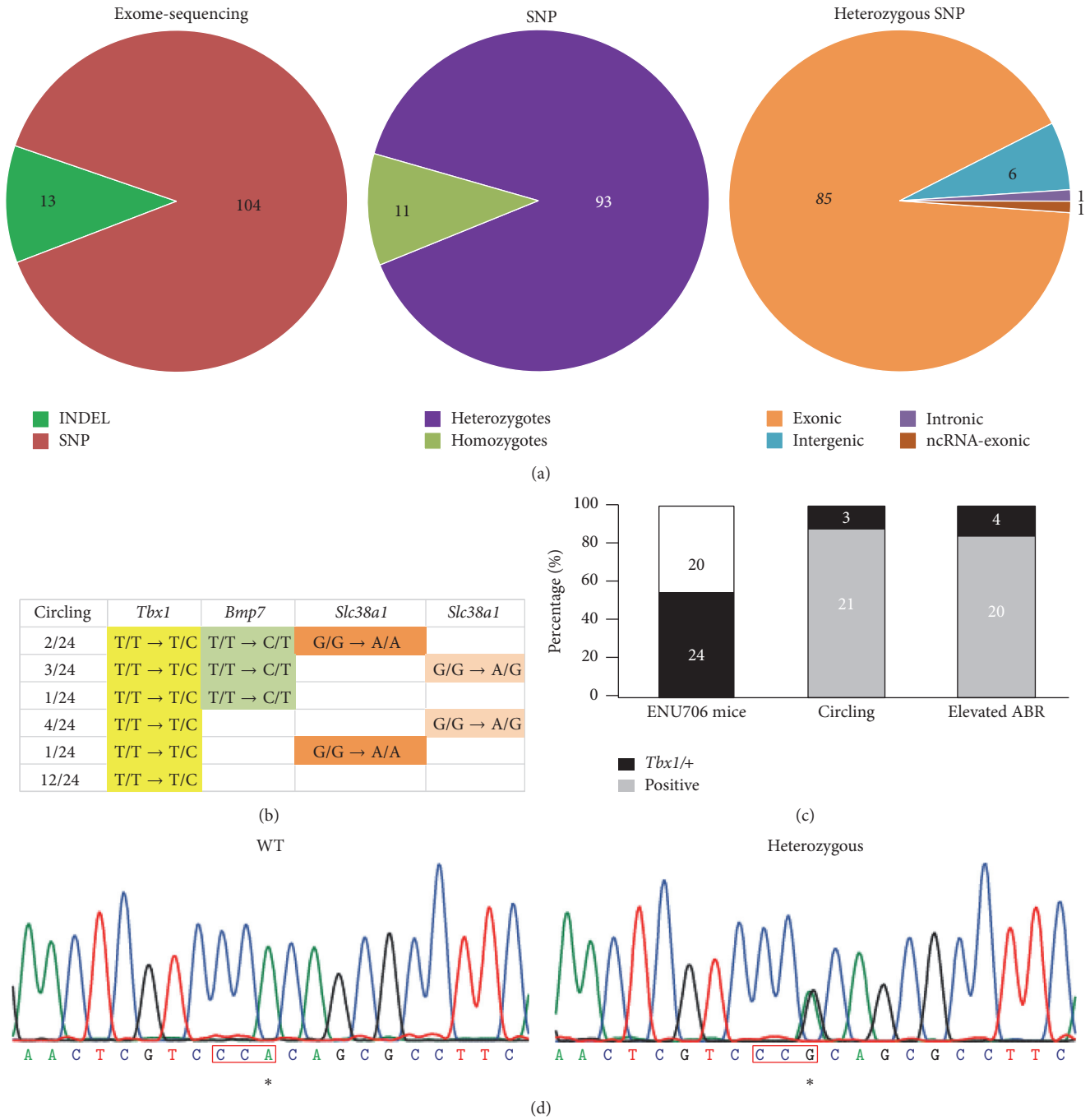

Figure 4: Genetic analysis of target gene in *ENU706* phenotypes. (a) Whole genome sequence identified 104 SNPs in one circling *ENU706* mutant mouse, among which 93 SNPs were heterozygous and 85 SNPs were exonic. (b) Top 3 candidate genes were *Tbx1*, *Bmp7*, and *Slc38a1*. The T-to-C mutation in *Tbx1* had the high penetration in *ENU706* heterozygous mice with the circling phenotype. (c) The genotyping for the T-to-C mutation in *Tbx1* showed there were 24 heterozygous mice out of all the 44 mice in this colony. And phenotypic assays showed 21 *ENU706* heterozygous mice were circling and 20 *ENU706* heterozygous mice had elevated ABR in all the 24 *Tbx1*+/− mice. (d) A typical DNA chromatogram showing the T-to-C mutation in an *ENU706* heterozygous mouse. Note a reverse primer was used for sequencing. ∗ refers to the T-to-C mutation.

heterozygous mouse (Figure 3(c)), so did their hair bundle (Figure 3(d)).

3.3. Tbx1 Gene Is Linked to the Inner Ear Problem. To identify the causative gene linked to the dominant hearing loss and circling phenotype, we performed a whole-exome sequencing. The preliminary analysis indicated that there are 104 SNPs plus 13 insertions and deletions (indels) at the gene coding regions. Considering that the inherited trait is consistent with Mendel's law (Figure 4(c), the 1st bar), the homozygous SNPs were rule out. Then 85 out of 93 heterozygous SNPs were presented in the preliminary

analysis to be validated to link to the hearing loss. Based on our previous data-mining experience, 31 out of the 85 SNPs were selected to be studied (Figure 4(a)). We then applied the PCR sequencing to validate each SNP transversion for the 31 candidate genes. It turned out that 3 out of the 31 SNPs were the top candidates that emerged with a high consistency between the genotype and the phenotype. The 3 genes were *Tbx1*, *Bmp7*, and *Slc38a1*, in which *Tbx1* and *Bmp7* have been previously linked to hearing impairment. *Tbx1* has been proposed as a candidate gene for pathogenesis of DGS including hearing impairment [28]. We found a T→C transversion in *Tbx1* gene in most of circling *ENU706* heterozygous mice. *Bmp7* has also been found to relate with development of inner ear and specify the tonotopic cochlea axis [29]. A T→C transversion was found in *Bmp7* gene in few *ENU706* heterozygous mice. For Slc38a1 gene, there was a G→A mutation and sometimes homozygous mutations were observed at both alleles (Figure 4(b)). With comparison of PCR sequencing result and circling phenotype, we speculated that *Tbx1* was the highly possible target gene that carried the mutation T/T→T/C in *ENU706* mice (23 out of the 24 circling mice). Among all the 44 mice in breeding, 24 had the T/T→T/C SNP change in *Tbx1* gene (Figures 4(c) and 4(d)). In the 24 *Tbx1*+/− mice, 21 were circling and 20 had elevated ABR (Figure 4(c)). The mutation caused a W to R change at the 118 amino acid in T-box region of TBX1 protein (Figure 5(a)), which is very conserved in different species (Figure 5(b)) and TBX paralogues (Figure 5(c)).

4. Discussion

All the evidence in this study indicated *Tbx1* was linked to the hearing problem of *ENU706* mice we generated. *ENU706* mice carried a moderate auditory threshold elevation plus vestibular problem, which was induced by a hemizygous SNP transversion in T-box region of *Tbx1*. *Tbx1*, as a transcription factor, has been associated to middle and inner ear development and morphogenesis, including conductive and sensorineural hearing loss [18, 19]. It was also the candidate gene concerning the pathogenesis of del22q11/DGS/VCFS [14]. More recent studies indicate that *Tbx1* was very likely linked to the hearing defect in DGS patients and engineered mutant mice [21–23]. Moreover, we did notice some syndromic phenotypes in a few *ENU706* heterozygous mice (Figures 1(d) and 1(e)) mimicking DGS traits reported in humans and mice. The *ENU706* homozygous mice were not found alive in our breeding colony, which also happened in *Tbx1* knockout mice [15].

During our gene identification, mutations in *BMP7* and *Slc38a1* genes had occasionally emerged; *BMP7* especially was previously identified critical for cochlear axis specification. These two genes were not likely the causative genes in *ENU706* mice. *BMP7* is in chromosome 2 and Slc38a1 is in chromosome 15, while Tbx1 is in chromosome 16. The late crossed ENU706 mice, from the 4th generation, did not carry *BMP7* and *Slc38a1* mutations anymore but still possess the DGS phenotypes. The mechanisms underlying the hearing defect including both conductive and sensorineural hearing loss has been tackled by our audiometry (Figures 2(b) and 2(c)) and electrophysiological recordings (Figure 3(c)). These data indicated that it was a more likely conductive hearing loss in *ENU706* mutants. To study the accurate gene function, chromosomally engineered *Df1*/+ mice and single gene knockout *Tbx1*/+ mice were used. Heterozygous loss of *Tbx1* resulted in major structural abnormalities of the heart similar to those observed in *Df1*/+ mice and *Lgdel*/+ mice [16]. Chronic otitis media was also a feature in clinical diagnosis of DGS [28]. The pathogenesis of otitis media is considered resulting from multiple causes, such as deficits of the inflammatory clearance [30, 31] or the mucosa in the middle-ear cavity [32, 33]. Our work was a reminiscent of the study on *Df1*/+ and *Tbx1*/+ mice, including dominant inheritance, circling, and partial hearing loss. A recent report further described that a defect in early myogenesis thus resulted in otitis media in mouse models of DGS [23]. Their data showed that the *Tbx1* heterozygous mice showed the hearing loss mainly by Eustachian tube problem related with muscle problem. Then it made sense that the hearing thresholds were different between the two ears of a given *ENU706* mouse (Figure 2(a)). It also coincided with the observation that the hearing loss in *ENU706* mice was moderate and sporadic (Figures 3(a) and 3(b)). Nevertheless, our work pointed out that a single point mutation was responsible for most of the hearing features of DGS. Interestingly, another gene, *Comt*, in the deleted region of chromosome in DGS patients has also been linked to hearing loss [34].

In early development, *Tbx1* as a transcription factor is expressed in the endodermal lining of the first pharyngeal pouch and in the meiosis of the pharyngeal arches [28]. T-box domain has been proposed to be important for T-box protein dimerization and DNA binding activity. It has been reported that F148Y and H194Q in the T-box domain actually induced a gain-of-function effect, plus G310S at the boundary of the T-box [35]. We speculated that W118R in ENU706 mice might also have a gain-of-function as other T-box mutations. More interestingly, recent study indicated that it also binds to chromatin that may function epigenetically [36]. Another study proposed that cortical development was regulated by mesodermal expression of *Tbx1* [37]. That raised the complexity of the TBX1 function. This *ENU706* mice hence provided a new line of mouse model to finely dissect TBX1 function in development and physiology.

5. Conclusion

To further understand the molecular and physiological relevance of hearing sensation and hearing impairment, we have set out to establish a forward genetics based deafness gene screen in mice. And it was also a major goal in our collaborative effort to identify disease genes linked to neurological disorders. In this study, we characterized a novel mutation in *Tbx1* gene, which caused a W118R amino acid change in T-box region of TBX1 protein. This single point missense mutation in the highly conserved region induced a robust phenotype of imbalance in affected mice that also carried moderate hearing loss. More interestingly, the deficiency was in a dominant inherited manner that was consistent with previous study in *Tbx1* deficient *Df1*/+ mice and *Tbx1*/+ mice. Our study

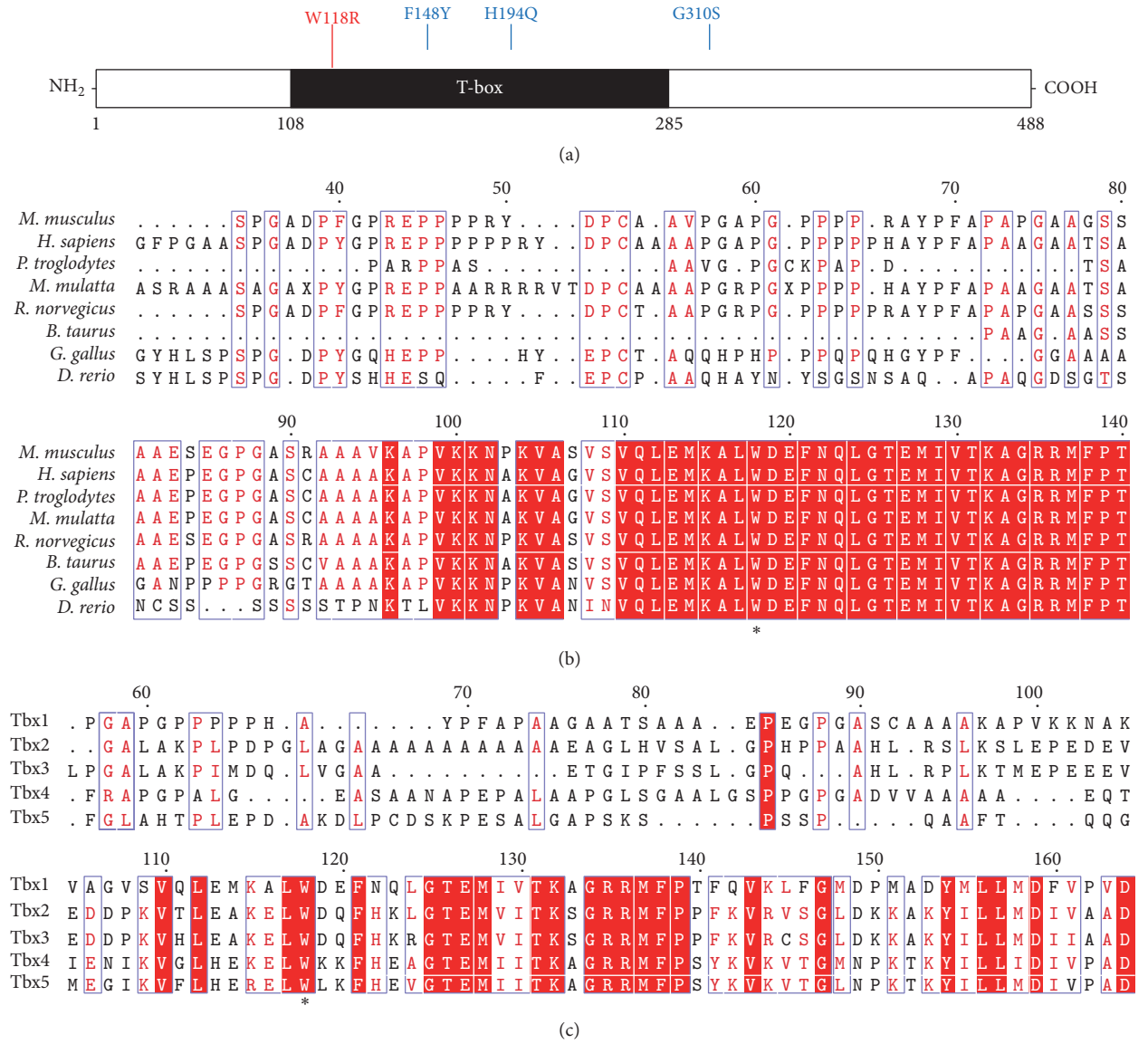

Figure 5: Conservation analysis of nonsynonymous mutation in TBX1 found in the *ENU706* mutant mouse. (a) The *ENU706* mutation caused a W118R conversion. F148Y, H194Q, and G310S mutations, previously reported in DGS patients, are also indicated [24]. (b) The W118 is highly conserved across the species. The protein NCBI IDs, NP_035662.1 (*M. musculus*), NP_542377.1 (*H. sapiens*), XP_016795078.1 (*P. troglodytes*), XP_015005141.1 (*M. mulatta*), NP_001101792.1 (*R. norvegicus*), XP_002694701.2 (*B. taurus*), XP_015131167.1 (*G. gallus*), and NP_899182.1 (*D. rerio*). (c) The Trp amino acid is also highly conserved in 5 TBX paralogues. The protein NCBI IDs, NP_542377.1 (Tbx1), NP_005985.3 (Tbx2), NP_005987.3 (Tbx3), NP_001308049.1 (Tbx4), and NP_000183.2 (Tbx5). ∗ refers to the W118 in (b) and Trp amino acid in (c).

thus provided an alternative model to study *Tbx1* function and might help to dissect domain-specific and tissue-specific TBX1 function in the DGS study.

Competing Interests

The authors declare that there is no conflict of interests regarding the publication of this paper.

Authors' Contributions

Jiaofeng Chen and Xue Zhang contributed equally to this work.

Acknowledgments

This work was funded by the National Natural Science Foundation of China (31571080 and 31522025 to Wei Xiong; 31571097 and 81371361 to Yichang Jia) and the Research Funds of Tsinghua University (to Wei Xiong and Yichang Jia).

References

[1] A. E. Shearer and R. J. H. Smith, "Genetics: advances in genetic testing for deafness," *Current Opinion in Pediatrics*, vol. 24, no. 6, pp. 679–686, 2012.

[2] G. P. Richardson, J. B. De Monvel, and C. Petit, "How the genetics of deafness illuminates auditory physiology," *Annual Review of Physiology*, vol. 73, pp. 311–334, 2011.

[3] S. W. Lee, C. Tomasetto, D. Paul, K. Keyomarsi, and R. Sager, "Transcriptional downregulation of gap-junction proteins blocks junctional communication in human mammary tumor cell lines," *Journal of Cell Biology*, vol. 118, no. 5, pp. 1213–1221, 1992.

[4] R. Rabionet, P. Gasparini, and X. Estivill, "Molecular genetics of hearing impairment due to mutations in gap junction genes encoding beta connexins," *Human Mutation*, vol. 16, no. 3, pp. 190–202, 2000.

[5] C. M. Longo-Guess, L. H. Gagnon, S. A. Cook, J. Wu, Q. Y. Zheng, and K. R. Johnson, "A missense mutation in the previously undescribed gene Tmhs underlies deafness in hurry-scurry (hscy) mice," *Proceedings of the National Academy of Sciences of the United States of America*, vol. 102, no. 22, pp. 7894–7899, 2005.

[6] W. Xiong, N. Grillet, H. M. Elledge et al., "TMHS is an integral component of the mechanotransduction machinery of cochlear hair cells," *Cell*, vol. 151, no. 6, pp. 1283–1295, 2012.

[7] L. A. Everett, B. Glaser, J. C. Beck et al., "Pendred syndrome is caused by mutations in a putative sulphate transporter gene (PDS)," *Nature Genetics*, vol. 17, no. 4, pp. 411–422, 1997.

[8] D. A. Scott, R. Wang, T. M. Kreman, V. C. Sheffield, and L. P. Karniski, "The Pendred syndrome gene encodes a chloride-iodide transport protein," *Nature Genetics*, vol. 21, no. 4, pp. 440–443, 1999.

[9] C. G. Möller, W. J. Kimberling, S. L. H. Davenport et al., "Usher syndrome: an otoneurologic study," *The Laryngoscope*, vol. 99, no. 1, pp. 73–79, 1989.

[10] M. W. Kelley, "Regulation of cell fate in the sensory epithelia of the inner ear," *Nature Reviews Neuroscience*, vol. 7, no. 11, pp. 837–849, 2006.

[11] S. Raft, S. Nowotschin, J. Liao, and B. E. Morrow, "Suppression of neural fate and control of inner ear morphogenesis by *Tbx1*," *Development*, vol. 131, no. 8, pp. 1801–1812, 2004.

[12] D. L. Chapman, N. Garvey, S. Hancock et al., "Expression of the T-box family genes, Tbx1-Tbx5, during early mouse development," *Developmental Dynamics*, vol. 206, no. 4, pp. 379–390, 1996.

[13] R. Goldberg, B. Motzkin, R. Marion, P. J. Scambler, and R. J. Shprintzen, "Velo-cardio-facial syndrome: a review of 120 patients," *American Journal of Medical Genetics*, vol. 45, no. 3, pp. 313–319, 1993.

[14] B. Morrow, R. Goldberg, C. Carlson et al., "Molecular definition of the 22q11 deletions in velo-cardio-facial syndrome," *The American Journal of Human Genetics*, vol. 56, no. 6, pp. 1391–1403, 1995.

[15] L. A. Jerome and V. E. Papaioannou, "DiGeorge syndrome phenotype in mice mutant for the T-box gene, Tbx1," *Nature Genetics*, vol. 27, no. 3, pp. 286–291, 2001.

[16] S. Merscher, B. Funke, J. A. Epstein et al., "TBX1 is responsible for cardiovascular defects in velo-cardio-facial/DiGeorge syndrome," *Cell*, vol. 104, no. 4, pp. 619–629, 2001.

[17] B. Funke, J. A. Epstein, L. K. Kochilas et al., "Mice overexpressing genes from the 22q11 region deleted in velo-cardio-facial syndrome/DiGeorge syndrome have middle and inner ear defects," *Human Molecular Genetics*, vol. 10, no. 22, pp. 2549–2556, 2001.

[18] M. C. Digilio, C. Pacifico, L. Tieri, B. Marino, A. Giannotti, and B. Dallapiccola, "Audiological findings in patients with microdeletion 22q11 (di George/velocardiofacial syndrome)," *British Journal of Audiology*, vol. 33, no. 5, pp. 329–333, 1999.

[19] M. R. T. Reyes, E. M. LeBlanc, and M. K. Bassila, "Hearing loss and otitis media in velo-cardio-facial syndrome," *International Journal of Pediatric Otorhinolaryngology*, vol. 47, no. 3, pp. 227–233, 1999.

[20] A. Swillen, K. Devriendt, E. Legius et al., "The behavioural phenotype in velo-cardio-facial syndrome (VCFS): from infancy to adolescence," *Genetic Counseling*, vol. 10, no. 1, pp. 79–88, 1999.

[21] H. Yagi, Y. Furutani, H. Hamada et al., "Role of TBX1 in human del22q11.2 syndrome," *The Lancet*, vol. 362, no. 9393, pp. 1366–1373, 2003.

[22] J. S. Arnold, E. M. Braunstein, T. Ohyama et al., "Tissue-specific roles of Tbx1 in the development of the outer, middle and inner ear, defective in 22q11DS patients," *Human Molecular Genetics*, vol. 15, no. 10, pp. 1629–1639, 2006.

[23] J. C. Fuchs, J. F. Linden, A. Baldini, and A. S. Tucker, "A defect in early myogenesis causes Otitis media in two mouse models of 22q11.2 deletion syndrome," *Human Molecular Genetics*, vol. 24, no. 7, Article ID ddu604, pp. 1869–1882, 2014.

[24] T. Ogata, T. Niihori, N. Tanaka et al., "TBX1 mutation identified by exome sequencing in a Japanese family with 22q11.2 deletion syndrome-like craniofacial features and hypocalcemia," *PLoS ONE*, vol. 9, no. 3, Article ID e91598, 2014.

[25] F. J. Probst and M. J. Justice, "Mouse mutagenesis with the chemical supermutagen ENU," *Methods in Enzymology*, vol. 477, pp. 297–312, 2010.

[26] H. Fairfield, G. J. Gilbert, M. Barter et al., "Mutation discovery in mice by whole exome sequencing," *Genome Biology*, vol. 12, no. 9, article R86, 2011.

[27] M. Schwander, A. Sczaniecka, N. Grillet et al., "A forward genetics screen in mice identifies recessive deafness traits and reveals that pejvakin is essential for outer hair cell function," *Journal of Neuroscience*, vol. 27, no. 9, pp. 2163–2175, 2007.

[28] J. Liao, L. Kochilas, S. Nowotschin et al., "Full spectrum of malformations in velo-cardio-facial syndrome/DiGeorge syndrome mouse models by altering Tbx1 dosage," *Human Molecular Genetics*, vol. 13, no. 15, pp. 1577–1585, 2004.

[29] Z. F. Mann, B. R. Thiede, W. Chang et al., "A gradient of Bmp7 specifies the tonotopic axis in the developing inner ear," *Nature Communications*, vol. 5, article 3839, 2014.

[30] C. J. MacArthur, S. H. Hefeneider, J. B. Kempton, and D. R. Trune, "C3H/HeJ mouse model for spontaneous chronic otitis media," *Laryngoscope*, vol. 116, no. 7, pp. 1071–1079, 2006.

[31] A. Z. Rivkin, S. D. Palacios, K. Pak, T. Bennett, and A. F. Ryan, "The role of Fas-mediated apoptosis in otitis media: observations in the lpr/lpr mouse," *Hearing Research*, vol. 207, no. 1-2, pp. 110–116, 2005.

[32] J. M. Hilton, M. A. Lewis, M. Grati et al., "Exome sequencing identifies a missense mutation in Isl1 associated with low penetrance otitis media in dearisch mice," *Genome Biology*, vol. 12, no. 9, article R90, 2011.

[33] M. T. Cheeseman, H. E. Tyrer, D. Williams et al., "HIF-VEGF pathways are critical for chronic otitis media in Junbo and Jeff mouse mutants," *PLoS Genetics*, vol. 7, no. 10, Article ID e1002336, 2011.

[34] X. Du, M. Schwander, E. M. Moresco et al., "A catechol-O-methyltransferase that is essential for auditory function in mice and humans," *Proceedings of the National Academy of Sciences of the United States of America*, vol. 105, no. 38, pp. 14609–14614, 2008.

[35] C. Zweier, H. Sticht, I. Aydin-Yaylagül, C. E. Campbell, and A. Rauch, "Human TBX1 missense mutations cause gain of

function resulting in the same phenotype as 22q11.2 deletions," *American Journal of Human Genetics*, vol. 80, no. 3, pp. 510–517, 2007.

[36] F. G. Fulcoli, M. Franzese, X. Liu, Z. Zhang, C. Angelini, and A. Baldini, "Rebalancing gene haploinsufficiency in vivo by targeting chromatin," *Nature Communications*, vol. 7, Article ID 11688, 2016.

[37] G. Flore, S. Cioffi, M. Bilio, and E. Illingworth, "Cortical development requires mesodermal expression of Tbx1, a gene haploinsufficient in 22q11.2 deletion syndrome," *Cerebral Cortex*, Article ID bhw076, 2016.

Hindawi Publishing Corporation
Neural Plasticity
Volume 2016, Article ID 6720420, 16 pages
http://dx.doi.org/10.1155/2016/6720420

Research Article

Loss of Myh14 Increases Susceptibility to Noise-Induced Hearing Loss in CBA/CaJ Mice

Xiaolong Fu,[1] Linqing Zhang,[1] Yecheng Jin,[1] Xiaoyang Sun,[1] Aizhen Zhang,[1] Zongzhuang Wen,[1] Yichen Zhou,[1] Ming Xia,[2] and Jiangang Gao[1]

[1]*School of Life Science and Key Laboratory of the Ministry of Education for Experimental Teratology, Shandong University, Jinan 250100, China*
[2]*Department of Otolaryngology-Head and Neck Surgery, The Second Hospital of Shandong University, Jinan 250033, China*

Correspondence should be addressed to Jiangang Gao; jggao@sdu.edu.cn

Received 31 July 2016; Revised 8 October 2016; Accepted 7 November 2016

Academic Editor: Jian Wang

MYH14 is a member of the myosin family, which has been implicated in many motile processes such as ion-channel gating, organelle translocation, and the cytoskeleton rearrangement. Mutations in MYH14 lead to a DFNA4-type hearing impairment. Further evidence also shows that MYH14 is a candidate noise-induced hearing loss (NIHL) susceptible gene. However, the specific roles of MYH14 in auditory function and NIHL are not fully understood. In the present study, we used CRISPR/Cas9 technology to establish a Myh14 knockout mice line in CBA/CaJ background (now referred to as Myh14$^{-/-}$mice) and clarify the role of MYH14 in the cochlea and NIHL. We found that Myh14$^{-/-}$mice did not exhibit significant hearing loss until five months of age. In addition, Myh14$^{-/-}$mice were more vulnerable to high intensity noise compared to control mice. More significant outer hair cell loss was observed in Myh14$^{-/-}$mice than in wild type controls after acoustic trauma. Our findings suggest that Myh14 may play a beneficial role in the protection of the cochlea after acoustic overstimulation in CBA/CaJ mice.

1. Introduction

Noise-induced hearing loss (NIHL) has now become one of the most prevalent occupational injuries reported [1]. Long-term exposure to high intensity noise can cause this sensorineural hearing disorder. Currently, it has been estimated that about 500 million individuals suffer from this hazard in the world [2]. NIHL is a preventable deficit, but it is difficult to reverse it once it occurs since the lost mammalian sensory cells cannot regenerate [3–6]; therefore, understanding its pathogenesis has become a very important task for researchers. Moreover, there have been great efforts to clarify the molecular and biochemical mechanisms involved in NIHL.

Studies have shown that acoustic overstimulation could lead to the pathogenesis and biochemical changes that result in hearing loss [7, 8]. The continued and evolving research involving NIHL has determined that there is a close relationship between the occurrence of noise-induced deafness and changes in some genes, cell metabolism, cell apoptosis [9], and so forth. The pathogenesis of NIHL is very complicated, and the exact mechanism is unknown. Generally, it is the outcome of the interaction between genetic and environmental factors [9–11]. In spite of many efforts, the research progress of NIHL has been slow, and it is difficult to study NIHL in humans. No heritability studies have been performed because families exposed to identical noise conditions are almost impossible to collect [12]. Gene modified mice are good models for studying the mechanism of NIHL. In recent years, some genes have been found to affect the susceptibility to noise in animal models [13, 14]. Several of the knockout mouse lines that have been developed, including Pjvk$^{-/-}$ [15], *PMCA2*$^{+/-}$ [16], *P2RX2*$^{-/-}$ [17], and *CDH23*$^{+/-}$ [18], were determined to be more sensitive to noise than their wild type controls. Meanwhile, more studies are beginning to search for new NIHL susceptibility genes, and hundreds of single nucleotide polymorphism (SNP) loci have been found in genes involved in different pathways of the inner ear. An

extended analysis of 644 SNPs in 53 candidate genes was performed in two independent (Swedish and Polish) populations; and two SNPs (rs667907 and rs588035) in MYH14 resulted in a positive association in the Polish sample set and significant interaction with noise exposure level in the Swedish sample set [19, 20]. This result suggested that MYH14 is likely to be a NIHL susceptibility gene [4, 19].

MYH14, also known as nonmuscle II heavy chain (NMHCII-C), together with two other nonmuscle chains (MYH9 and MYH10), is a member of the myosin family, which have been implicated in many motile processes such as ion-channel gating, organelle translocation, and cytoskeleton rearrangement [21, 22]. Mutations in MYH14 lead to a DFNA4-type hearing impairment. Interestingly, MYH14 shares great similarities with MYH9 and MYH10 in structure [22]. MYH14 has been shown to play roles in neuritogenesis and maintenance of apical cell junctions in epithelial cells within the cochlea [23, 24]. However, the relationship between MYH14 and NIHL is still obscure, and the role they play in NIHL needs further analysis [12].

In our study, we applied the CRISPR/Cas9 technology to establish a Myh14 knockout mouse line ($Myh14^{-/-}$) using the CBA/CaJ background strain. Then, we investigated the hearing threshold and morphological changes in these mice under normal conditions or under noise exposure. We found that $Myh14^{-/-}$ mice did not exhibit significant hearing loss until five months of age. Moreover, $Myh14^{-/-}$ mice were more vulnerable to high intensity noise compared to control mice. More significant outer hair cell (OHC) loss was observed in $Myh14^{-/-}$ mice after acoustic trauma. These data indicate that the absence of Myh14 may increase susceptibility to NIHL and that Myh14 may play a beneficial role in the protection of the cochlea after acoustic stimulation in the CBA/CaJ mouse line.

2. Materials and Methods

2.1. Ethical Statement. The use of animals in this study and the experimental procedures were approved by the Animal Ethics Review Committee of Shandong University. Animal management was performed strictly in accordance with the standards of the Animal Ethics Committee of Shandong University (Permit Number: ECAESDUSM 20123004).

2.2. Generation of $MYH14^{-/-}$ Mice. Myh14-deficient mice were generated using the CRISPR-Cas9 genome-editing technology and were maintained on the CBA/CaJ background. Both pX330 and pST1374 were obtained from Addgene (Plasmid ID: #42230, #44758, resp.). The CRISPR-Cas9 genome-editing technology in mice was used as previously described [25, 26]. In brief, a pair of oligonucleotides for the target sequence (5′-CCTGAAGAAAGAGCGCAATA-3′) was annealed and ligated to PX330 digested with *BbsI*. Then sgRNA was produced by in vitro transcription (T7 as promoter) using the MEGAshortscript kit (Ambion, Am1354, USA). The hCas9 mRNA was derived from pST1374-N-NLS-flag-linker-cas9, synthesized using the mMESSAGE mMACHINE T7 kit (Ambion, Am1345, USA), and polyadenylated with a polyA tailing kit (Life Technologies, USA). Both the sgRNA and the Cas9 mRNA were purified using the MEGAclear kit (Ambion, AM1908, USA) and eluted in RNase-free water.

CBA/CaJ female mice were superovulated and mated with CBA/CaJ male mice. Then, the female mice were sacrificed and the fertilized eggs were removed from the oviducts. The purified sgRNAs (50 ng/μL) and *hCas9* mRNAs (100 ng/μL) were coinjected into the cytoplasm of pronuclear stage eggs. Following the injected pronuclear stage, eggs were incubated for ten minutes. Then, the eggs were transferred into the oviducts of pseudopregnant CD1 female mice. Genomic DNA was extracted from the tails of the newborn pups. The genomic DNA fragment around the gRNA target site was amplified by PCR using two sets of primers: Myh14 forward, 5′-ACCTCGTGCTTGTTCAG-3′, and Myh14 reverse 5′-TGTCTTCAGCAGGGTGT-3′. The PCR products obtained were sequenced directly or cloned using the T/A cloning method and then sequenced to identify the mutation.

2.3. Analysis of Potential off-Target Mutations. Off-target effects may exist in CRISPR/Cas9 technology. In response to this possibility, we used the CRISPR design tool available on the web (http://crispr.mit.edu), to search for the off-target locus. Five potential off-target sites for the Myh14 gene were found. The primers for the off-target analysis were as follows: Sin3b 5′-GCCAGGAGGTATATG-AGAAC-3′ and 5′-GAAATTTCCCCAGGAATGGACTGA-CA-3′; Pcdh9 5′-GTGTACTTATAGCACTCACC-3′ and 5′-CTAACGCGGAAACACCTCAC-3′; Patl1 5′-CCACTG-AGCCTTTCCTACCTTC-3′ and 5′-GTAAATTTAGAA-ATTTTATTTT-3′; Arhgap27 5′-GAAGCTAGGCCAGCG-GGCGAAAG-3′ and 5′-CTGCCCATGGGCGGGGCTG-3′; and Olfr1333 5′-GCGCTATACTGTCATCCTCAAC-3′ and 5′-GCAAGCCAAGCTACGCACTG-3′. The genomic DNA fragment from the newborn pups was amplified using the PCR primers mentioned above. Then, the PCR products obtained were sequenced directly or cloned using the T/A cloning method and sequenced to identify the mutation.

2.4. Preparation of Protein Extracts and Western Blot Analysis. Mice were decapitated; the cochlea were quickly removed from the skull and homogenized in ice-cold cell lysis buffer (10 mM Tris, pH = 7.4, 1% Triton X-100, 150 mM NaCl, 1 mM EDTA, and 0.2 mM PMSF), then lysed for 30 min on ice, and centrifuged at 10,000 ×g at 4°C for 30 min. The supernatant was then collected, and the protein concentration was measured using a BCA kit. The samples were mixed with loading buffer and heated at 100°C for 5 min and stored at −20°C. Protein samples were separated by a 10% sodium dodecyl sulfate (SDS) polyacrylamide gel and transferred onto a PVDF membrane. The membrane was blocked in 5% nonfat dry milk in TBS-T at room temperature for 1 h and incubated with primary antibodies at 4°C overnight. After washing with TBS-T (three times for 10 min each at room temperature), membranes were incubated with an anti-rabbit HRP-conjugated secondary antibody (1 : 8000, Cell Signaling,

USA) diluted in 5% nonfat dry milk in TBS-T at room temperature for 1 h. Next, membranes were washed in TBS-T (three times for 10 min each) and bands were detected using ECL Western blot detection kit (Thermo, USA). Membranes were incubated with the following primary antibodies diluted in 5% bovine serum albumin (BSA): rabbit anti-Myosin-IIa (1 : 1000, Cell Signaling, USA), rabbit anti-Myosin-IIb (D8H8) (1 : 1000, Cell Signaling, USA), rabbit anti-Myosin-IIc (D4A7) (1 : 1000, Cell Signaling, USA), and rabbit anti-β-actin (1 : 5000, Bioworld, China).

2.5. Auditory Brainstem Response (ABR) Measurement. Mice were deeply anesthetized with pentobarbital sodium (50 mg/kg body weight) by intraperitoneal injection and the body temperature was maintained at 37°C using a heat pad. Testing was performed in a sound-isolated room. Three needle electrodes were inserted subcutaneously in the anesthetized mice: one was inserted between the ears at the forehead, one was underneath the left external ear, and one was at the back near the tail. Click and tone burst stimuli at frequencies of 4, 8, 16, and 32 kHz were generated and responses were recorded using a Tucker-Davis Technologies System (TDT, USA) workstation running the SigGen32 software (TDT, USA). Auditory thresholds (dB SPL) were defined by reducing the sound intensity in5 dB steps from 90 dB to 10 dB. The ABR threshold was defined as the lowest sound intensity sufficient to elicit the first wave clearly.

2.6. RNA Isolation and Real-Time PCR. In parallel experiments, total RNA was extracted from mouse cochleae at a defined time point after noise exposure using TRIzol Reagent (Invitrogen) according to the provided directions. Total RNA yield and purity were assessed with Eppendorf BioPhotometer plus. All samples had A260/280 ratios of 1.9–2.1 and showed two sharp peaks corresponding to the 18S and 28S RNA on electropherograms. Then cDNA was synthesized using PrimeScript RT reagent kit with gDNA Eraser (Takara). Quantitative PCR was performed on a Bio-Rad real-time thermal cycling system with Power SYBR Green PCR Master Mix (Takara). The amplification reaction mixture (20 μL) contained 800 nmol of each primer in the SYBR Green system. The quality control for the mRNA quantification was performed using three integrated control assays in the PCR array: a reverse transcription control, a positive PCR control, and a genomic DNA control. All PCR runs passed the control tests. Data were analyzed using Bio-Rad CFX manager software. The primers utilized in this study are shown as follows: Myh9 F: ACAATGGAGGCCATGAGAAT, Myh9 R: GAGATGACCCGCAGCAAG, Myh10 F: GGAGGACACCCTAGACACCA, and Myh10 R: CCACTTCCTGCTCACGTTTT

2.7. Noise Exposure. Mice were kept awake and placed in a stainless steel wire cage in the center of an open-field acoustic chamber. Then, they were exposed to 2–10 kHz band noise at an intensity of 105 dB SPL for 4 h to induce a temporary change in auditory threshold shifts. The sound was generated by a noise generator (SF-06, Random Noise Generator, RION, USA), amplified by a power amplifier (CDi 1000 Power Amplifier, Crown, USA), and delivered to microphones. The noise sound files were created and equalized with audio editing software (audacity portable). Sound levels were calibrated at multiple locations within the sound chamber to ensure uniformity of the stimulus.

2.8. Immunostaining. Immunostaining of the cochleae was performed as previously described [27]. Cochlea were fixed in 4% formaldehyde in 10 mM phosphate-buffered saline (PBS) at 4°C overnight and decalcified in 10% EDTA in 10 mM PBS at room temperature for at least one day. For sectioning, the cochleae were dehydrated with 15% sucrose for 2 h and then 30% sucrose overnight at 4°C. Samples were embedded in Tissue-Tek OCT compound and frozen in liquid nitrogen and then sectioned into 10 μm thick slices. For whole-mount immunostaining, the organ of Corti's sensory epithelium was isolated from the cochleae and divided into apical, middle, and basal turn sections to then permeabilize the samples in 0.5% Triton X-100 in PBS at room temperature for 15 min. The sections or cochlea samples were washed in PBS and then blocked in 10% goat serum in PBS at 37°C for 30 min. The samples were incubated with a primary antibody at 4°C overnight. After washing with PBS, followed by further incubation with an anti-rabbit TRITC-conjugated secondary antibody diluted in PBS at 37°C for 1 h, followed by Alexa Fluor 488-conjugated phalloidin (Sigma-Aldrich, USA) at 37°C for 30 min and 4′,6-diamidino-2-phenylindole (DAPI) at 37°C for 10 min, immunofluorescence images were collected using a confocal laser-scanning microscope. Cochleae were incubated with the following primary antibodies diluted in PBS: rabbit anti-Myosin-IIa (1 : 100, Cell Signaling, USA), rabbit anti-Myosin-IIb (D8H8) (1 : 100, Cell Signaling, USA), rabbit anti-Myosin-IIc (D4A7) (1 : 50, Cell Signaling, USA), rabbit anti-ZO-1 (1 : 400, Invitrogen, USA), and rabbit anti-E-cadherin (1 : 200, Cell Signaling, USA). Goat anti-rabbit TRITC-conjugated secondary antibodies (1 : 200) were from Invitrogen, USA.

2.9. Histological Analysis. Cochlea samples were fixed and decalcified using a procedure similar to that used for the immunostaining assay, dehydrated by an ethanol series ranging from 30% to 100%, and embedded in paraffin to then be sectioned at a thickness of 10 μm. Sections were deparaffinized by an ethanol series ranging from 100% to 30%, stained with hematoxylin and eosin (H&E), and viewed under light microscopy (Nikon YS100, Japan).

2.10. Quantitative Assessment of HC Loss. Mice were sacrificed 2 weeks after noise exposure and the cochlear epithelia were immunostained for HC counts. Briefly, the apical, middle, and basal parts of the basilar membrane were counted and labeled with Alexa Fluor 488-conjugated phalloidin to outline HCs and their stereocilia for quantitative assessment. The numbers of missing OHCs were counted and the ratio of missing OHCs was expressed as a percentage.

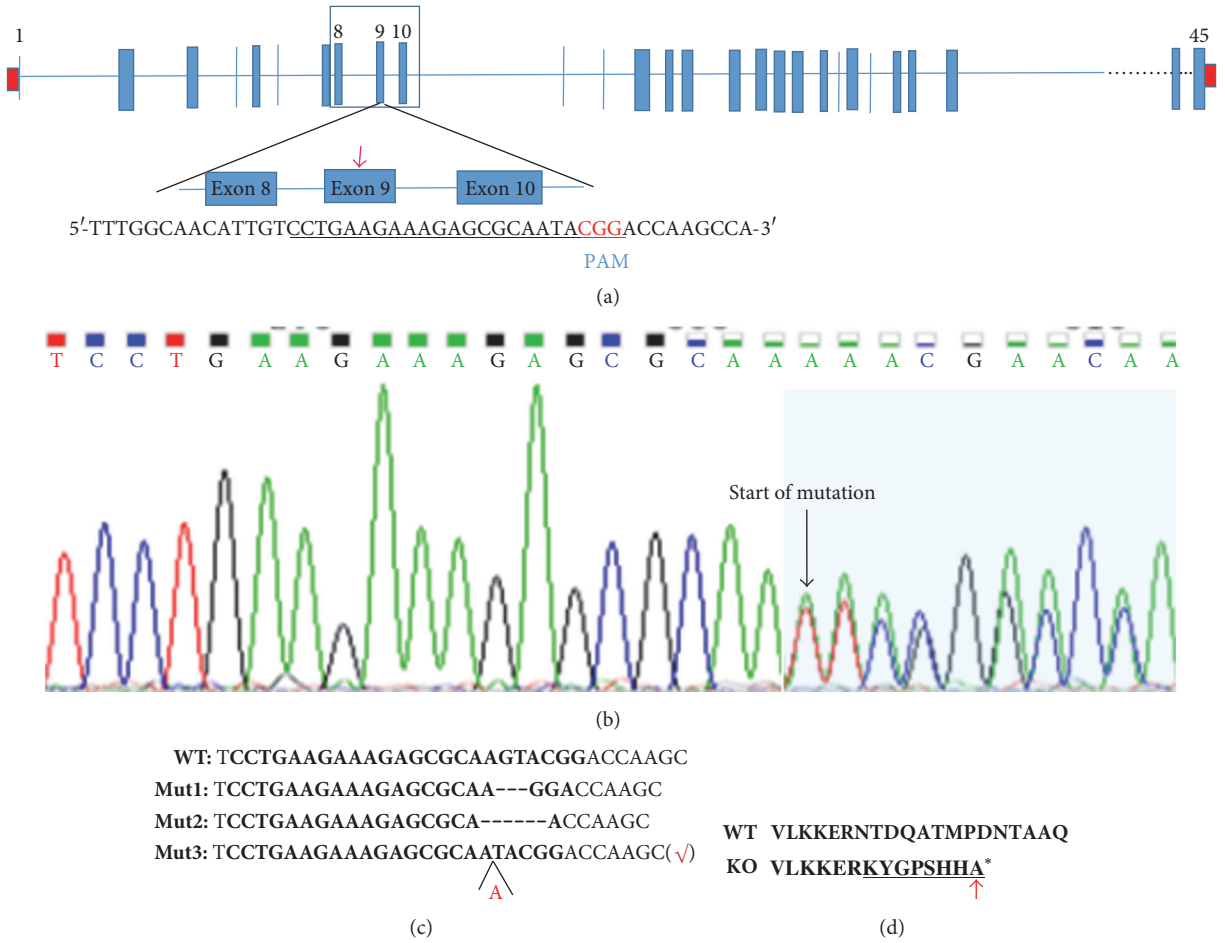

Figure 1: CRISPR/Cas9-mediated generation of Myh14 knockout mice. (a) Schematic diagram of sgRNA at Myh14 Exon 9 locus (indicated by the red arrow). The sgRNA sequence is underlined in black, and the PAM sequence is shown in red. (b) Sequencing chromatograms of Myh14$^{-/-}$ mice. The sequence at the start of the mutated site becomes scrambled. (c) Three types of mutations (3, 6 bp deletions and 1 bp insertion) were produced. Type 3 frameshift mutation was chosen for further analysis. (d) Frameshift mutation of Myh14$^{-/-}$ mice. The mutation is underlined in black. "∗" indicates a premature stop codon. The translation of the protein is terminated at the point of the arrow.

2.11. Statistical Analysis. All experiments were performed at least three times. Data are expressed as mean ± SD. Repeated-measures ANOVA was performed to evaluate the difference in ABR threshold shifts, one-way ANOVA or t-test was selected to test the MYH14 expression and cochlear hearing loss, and statistical analysis was performed using GraphPad software. For all tests, a value of $P < 0.05$ was considered to be statistically significant.

3. Results

3.1. CRISPR/Cas9-Mediated Generation of the Myh14$^{-/-}$ Mice Line. To investigate the functions of MYH14 in hearing, the CRISPR/Cas9 genome-editing technology was used to destroy the Myh14 gene in mice. In brief, a single guide RNA (sgRNA) containing a 20 nt target sequence and the endonuclease Cas9 are essential for successful targeting. When the sgRNA guides Cas9 to the target sequence, a double-strand break will be generated. The double-strand break produces indels (insertions and deletions), which then produce frameshift mutations. Exon 9 of the Myh14 gene is the CRISPR-amenable target, as shown in Figure 1(a). The Cas9 mRNA and the sgRNA, which were produced by in vitro transcription, were microinjected into the pronuclear stage of mouse embryos. Eighteen days after transplantation, 37 pups were born. These mice were designated as F0. Among these 37 pups, 16 pups contained the mutation, as determined by genotyping sequence analysis, and surprisingly, all of them had heterozygous mutations. Then, TA clones of the PCR products were analyzed by DNA sequencing, where a total of three types of mutations were shown (Figures 1(b) and 1(c)). We chose the third-type mutation as our research subject, as this type of mutation can cause a frameshift mutation and a stop codon will appear eight amino acids later (Figure 1(d)). Concurrently, we performed the off-target analysis using the mouse line mentioned above. The results showed no off-target effect in our experiment (data not shown). In order to produce a Myh14 homozygous mutant, F0 male mice with a 1 bp insertion were bred with wild type CBA/CaJ female,

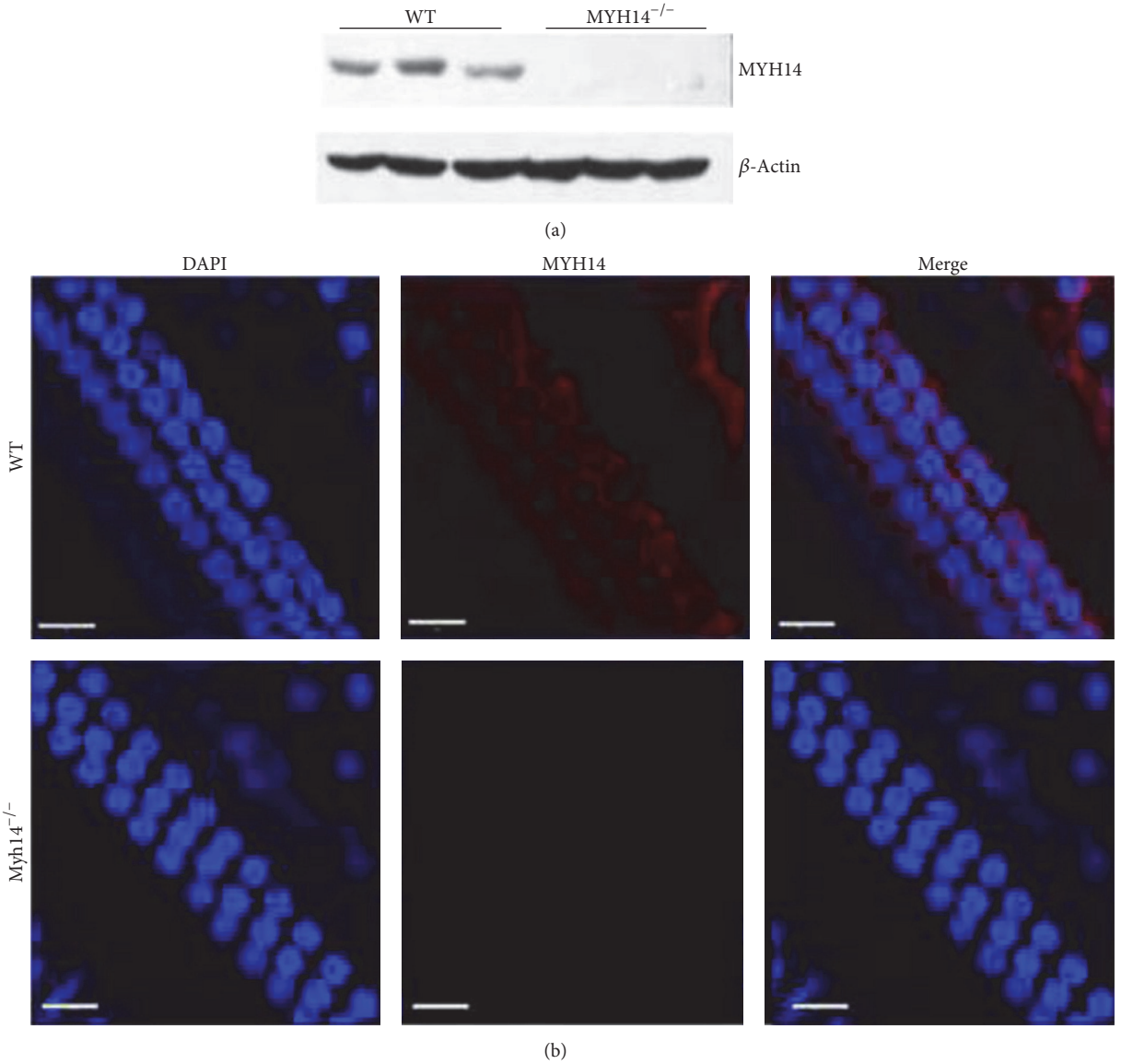

Figure 2: Validation of MYH14 protein knockout in mutant mice. (a) Western blot analysis validation of MYH14 protein knockout in the cerebellums of mutant mice ($n = 3$ for each group). (b) Confocal images of the basilar membrane in wild type and Myh14$^{-/-}$mice. The fluorescence was observed in wild type mice, but no fluorescence was seen in Myh14$^{-/-}$mice. Scale bar, 20 μm.

thus generating F1 mice. Then, the F1 heterozygous mice were inbred for one generation, obtaining a mouse strain homozygous for the Myh14 gene.

To confirm that the MYH14 protein in the Myh14 mutant mice was abolished, we performed a Western blot analysis on the cerebellum (where MYH14 expression is high) using specific antibodies. As showed in Figure 2(a), MYH14 protein expression in the cerebellum was completely abolished in the homozygous mutants. Finally, we performed immunocytochemistry experiments on cochlea whole mounts (Figure 2(b)). It has been reported that MYH14 is primarily expressed in or near the reticular lamina [21]. In our study, MYH14 immunoreactivity in the apical junctional complexes (AJCs) was completely abolished in Myh14 homozygous mutants. These results consistently show the successful generation of a Myh14 knockout mouse using the CBA/CaJ strain.

3.2. Elevation of ABR Thresholds in Myh14$^{-/-}$ Mice Aged Five Months. Tracking analysis of Myh14$^{-/-}$ mice was performed to determine that there were no significant differences in the appearance of Myh14$^{-/-}$ mutant mice and wild type mice. H&E staining was performed to investigate the cochlear morphology of Myh14$^{-/-}$ mice. The cochleae of three-month old Myh14$^{-/-}$ mice showed no differences (Figure 3). No abnormalities were seen in either the HCs or the SGN (spiral ganglion). ABR measurements were performed in Myh14$^{-/-}$ mice and were compared to wild type mice. Wild type

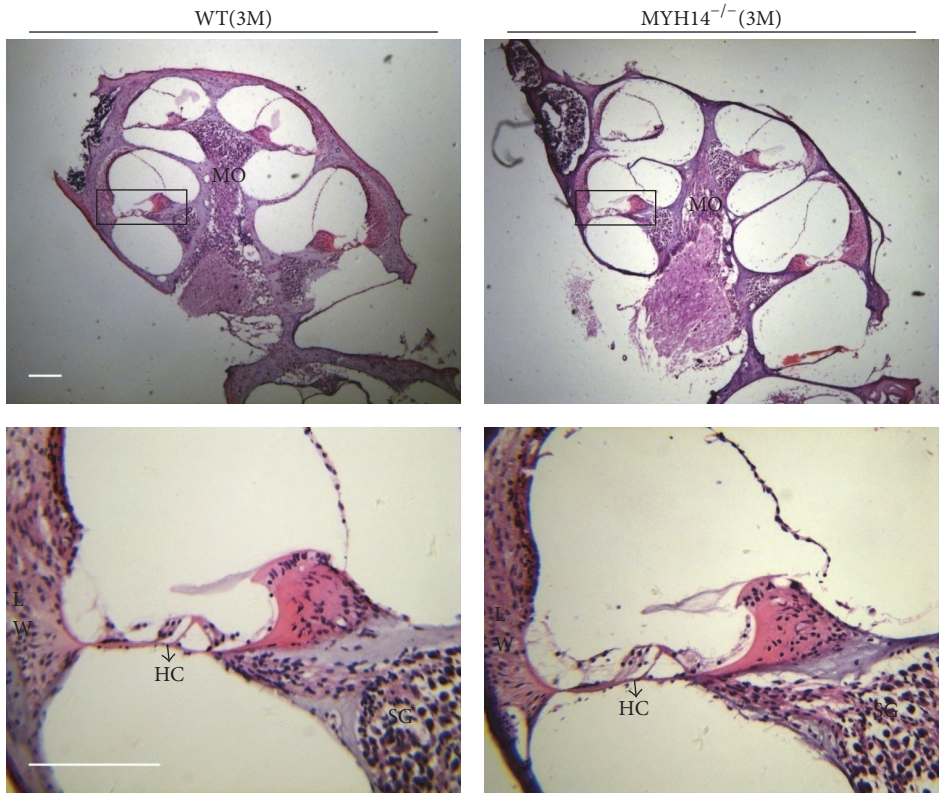

Figure 3: Myh14$^{-/-}$ mice showed normal cochlear morphology. Cochlear morphology is normal in Myh14$^{-/-}$ mutant mice. Cochlea stained with hematoxylin and eosin from 3-month-old control and Myh14$^{-/-}$ mice. No prominent differences, including spiral ganglion (SGN) in modiolus (MO) and hair cells (HC), were found between wild type and mutant mice. Scale bar, 100 μm.

mice ($n = 10$) and Myh14$^{-/-}$ mice ($n = 10$) showed no statistical differences in ABR thresholds until five months of age (Figure 4(a)). Tone burst ABR showed that 5-month-old Myh14$^{-/-}$ mice have high-frequency hearing loss, and the statistics show that there are significant differences. Consistent with the ABR results, immunofluorescence results showed no loss of HC and no change of SGN at three months; however, a 4%–10% HC loss was found in the cochlea basal turn of 5-month-old mutants. Sporadic OHCs were also lost in the middle and apical turn of the cochleae (Figures 4(b), 4(c), and 4(d)).

The small effect of Myh14 loss on hearing thresholds raised the possibility that other related genes might compensate for the absence of Myh14. Evidence shows that MYH14 and MYH10 are colocalized in cell-cell junctions and that MYH14 shares great similarities with both MYH9 and MYH10 in structure; therefore, they may have complementary effects in auditory function. An immunoblot analysis was performed to clarify changes in the expression of MYH10 and MYH9. Results showed that the expression of MYH10 in the cochleae of Myh14$^{-/-}$ mice was prominent increased, but changes in the expression of MYH9 were not obvious (Figures 5(a) and 5(b)). Immunofluorescence results further verified the results of the immunoblot analysis (data not shown).

3.3. Expression of MYH14 Is Noise Exposure-Dependent. To investigate the response of MYH14 in mouse cochleae (2 months old) to noise exposure, Western blot analysis and immunofluorescent staining ($n = 3$ for each group) were performed to evaluate MYH14 protein levels at different time points: before (2 h), during, and after (2 and 4 h, 1, 2, and 7 days) noise exposure (Figure 6). We found that MYH14 protein expression was largely dependent on noise exposure (Figures 7(a) and 7(b)). The expression levels of MYH14 were significantly upregulated by acoustic stimuli, and they reached the highest peak 2 h after noise treatment. The results of immunofluorescence also showed that the upregulation of MYH14 was most obvious 2 h after noise treatment in the HCs of the cochlea (Figure 7(c)). However, this upregulation gradually disappeared until seven days after noise exposure, when the expression of MYH14 was restored to basal levels (before noise exposure). All these results showed that MYH14 is upregulated after noise exposure and that this change is time-dependent.

3.4. Myh14$^{-/-}$ Mice Are Less Capable of Recovering from Noise Damage. To determine the effect of Myh14 knockout on NIHL, we examined the response to acoustic trauma in Myh14$^{-/-}$ mice in comparison to wild type controls (4 months of age, $n = 8$ for each group). The ABR was recorded before and after acoustic trauma. The results showed that ABR thresholds were almost comparable between the two genotypes before acoustic stimuli. Then, animals were exposed to 2–10 kHz band noise at 105 db SPL for 4 h. ABR

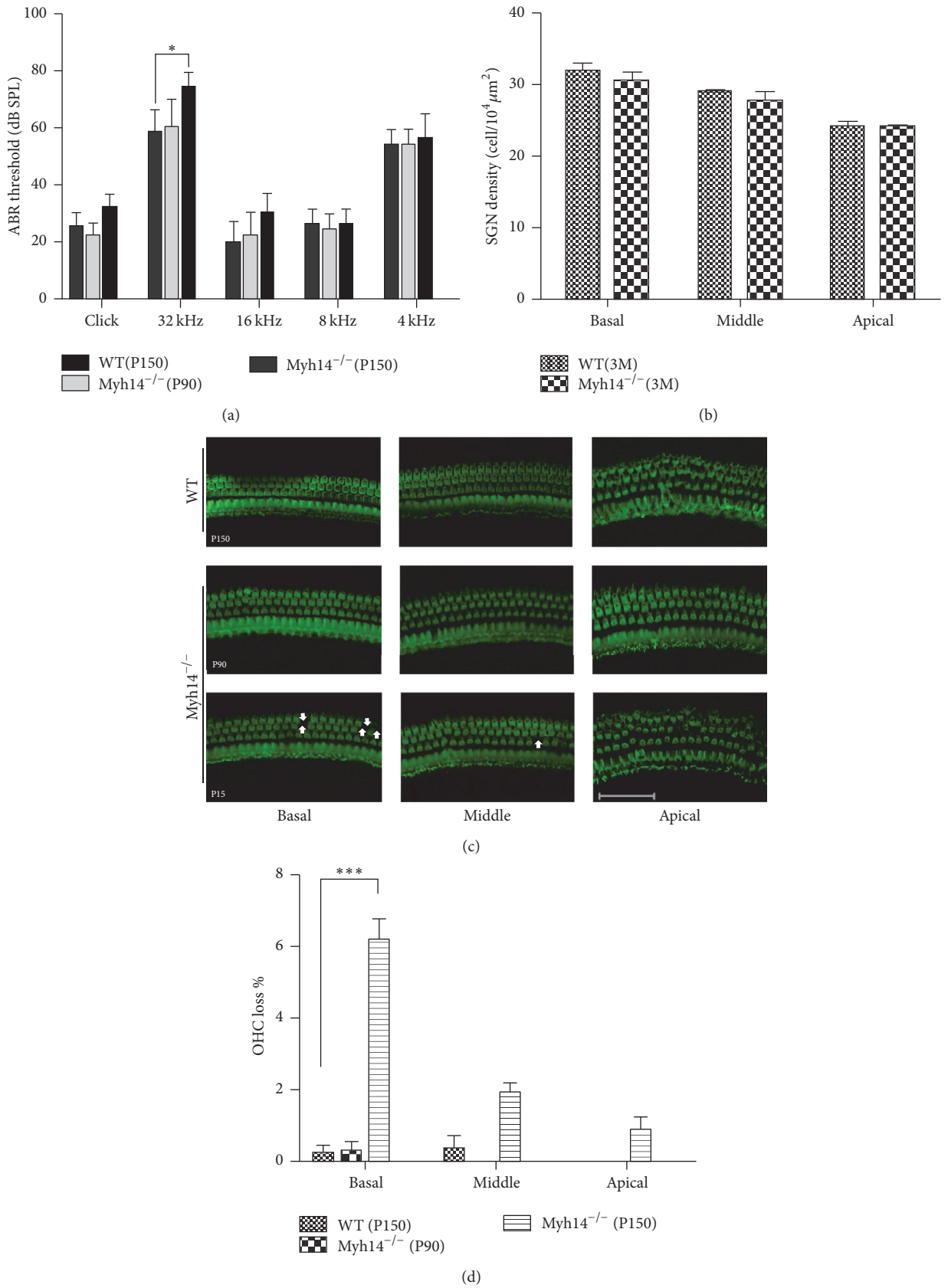

Figure 4: ABR measurement and cell loss patterns in cochleae of the mutant mice. (a) ABR threshold between control and Myh14$^{-/-}$ mice ($n = 10$ for each group). $^{*}P < 0.05$ compared to the controls. (b) No significant difference in the SGN density between wild type and mutant mice. (c) Hair cell loss (white arrows) was found in 5-month-old experimental groups ($n = 8$). (d) Quantifications of OHC loss at specific locations in control and experimental groups. $^{***}P < 0.001$ compared to the control group.

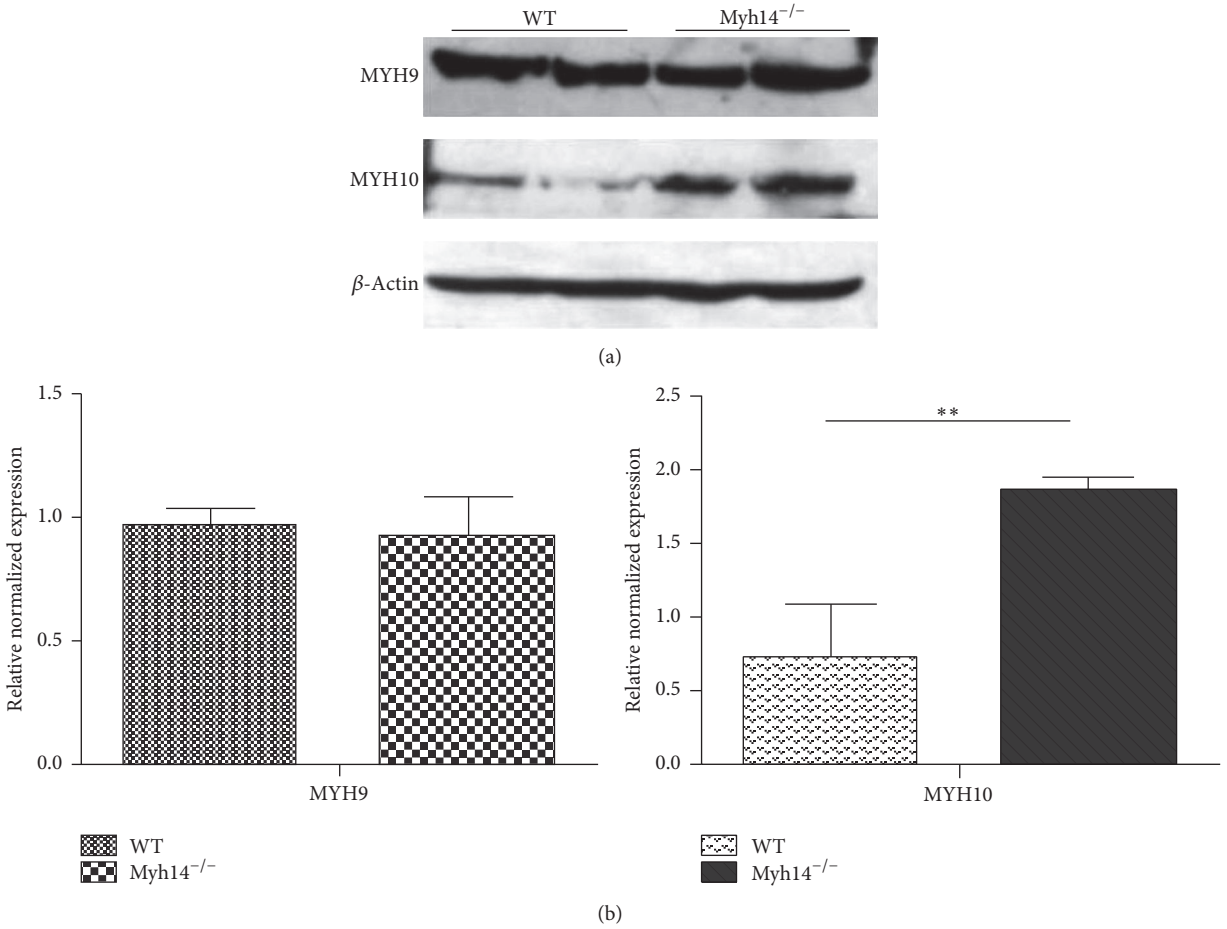

Figure 5: Expression of MYH10 is upregulated in the cochleae of Myh14$^{-/-}$ mice. ((a), (b)) Western blot analysis of 3-month-old mice indicates that the expression of MYH10, not MYH9, is upregulated in the cochleae of Myh14$^{-/-}$ mice compared to controls ($n = 3$ for each group). $^{**}P < 0.01$ by Student's t-test.

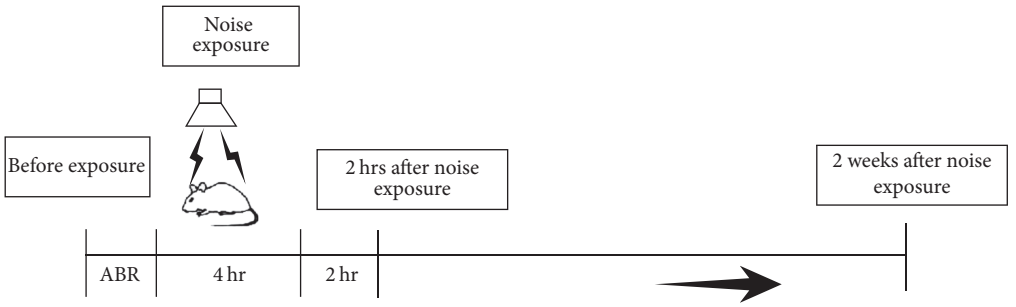

Figure 6: Experimental design for noise exposure and ABR test. Wild type and Myh14$^{-/-}$ mice were exposed to noise at 105 dB for 4 h. ABR thresholds were tested at the following time points: 2 h before, 2 h after, and 7 days after noise exposure.

recordings 2 h after exposure showed that acoustic overstimulation induced great hearing loss (temporary threshold shift, TTS) in both Myh14$^{-/-}$ mice and control groups; moreover, there were no significant differences between the two genotypes. The ABR test showed that wild type mice fully recovered two weeks after acoustic trauma. However, the hearing of mutant mice failed to recover two weeks after the acoustic trauma. ABR thresholds of the mutants were significantly increased compared to the controls two weeks after the high-level noise exposure (Figures 8(a), 8(b), 8(c), 8(d), and 8(e)). These results suggest that Myh14$^{-/-}$ mice are less capable of recovering from NIHL than controls.

3.5. OHC Loss Was Significantly Increased 2 Weeks after Acoustic Trauma in Myh14$^{-/-}$ Mice. In order to compare the degree of damage to HCs after noise exposure in Myh14$^{-/-}$ mice and control groups, immunofluorescence staining (phalloidin)

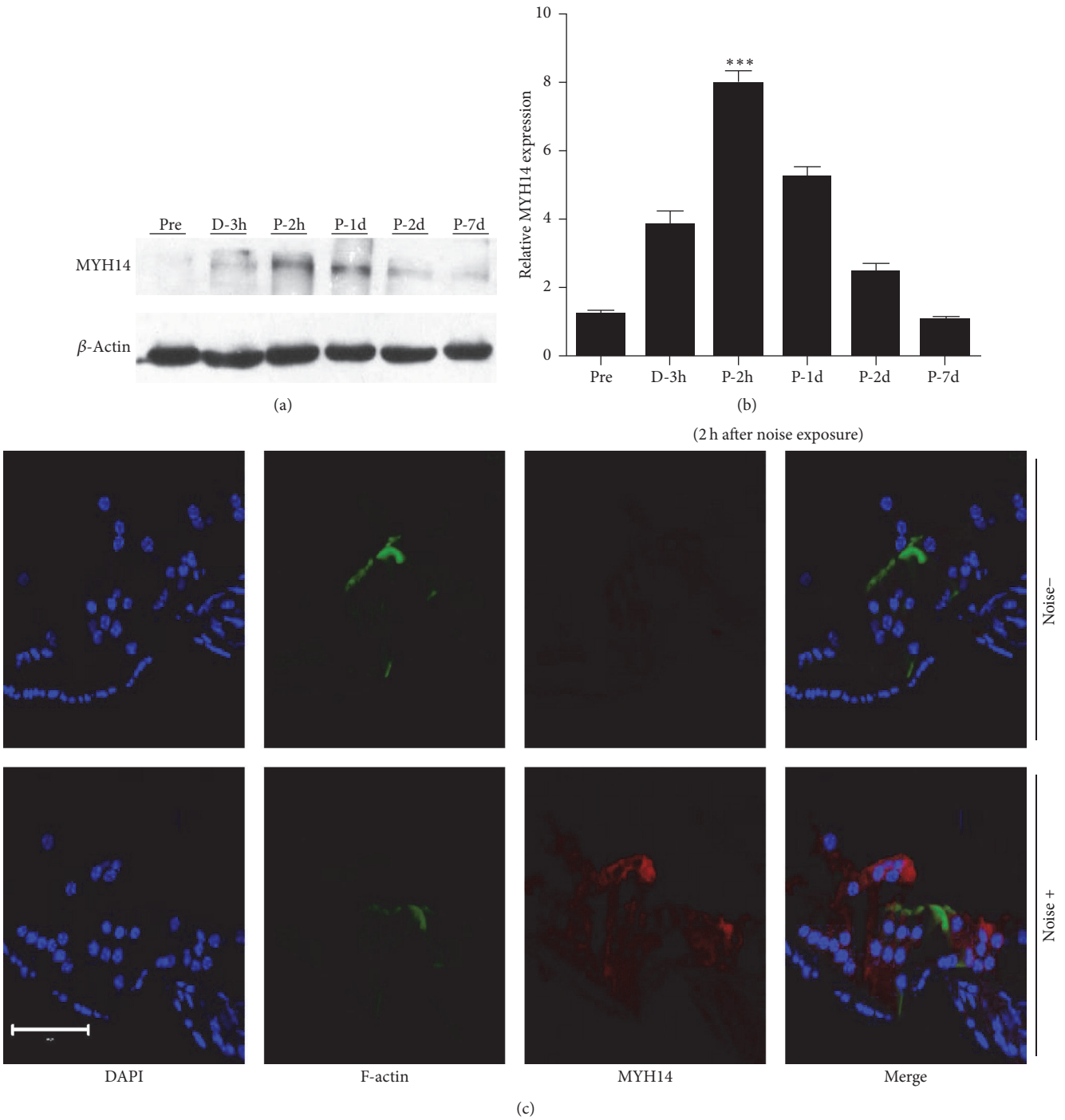

Figure 7: Expression of MYH14 is noise exposure-dependent. ((a) and (b)) Western blots analysis was performed at different time points (before, during, and after noise exposure) to show the expression levels of MYH14 ($n = 3$ for each group). The expression of MYH14 reached its highest peak 2 h after noise exposure (P-2h) and then gradually returned to basal levels (P-7d). $^{***}P < 0.001$ by Student's t-test compared to the pre-noise exposure levels. (c) Confocal images showing the expression of MYH14 before and 2 h after noise exposure in the organ of Corti. The organ of Corti was labeled with Alexa 488-conjugated phalloidin (green); red, MYH14; blue, DAPI. Scale bar, 50 μm.

was performed to compare HC losses of cochleae two weeks after noise exposure. The results showed that the HC loss mainly happened in the OHCs, and loss of OHCs was more significant in Myh14$^{-/-}$ mice compared to controls (Figures 9(a) and 9(b)). However, the number of inner hair cells (IHCs) showed no obvious differences between the two groups of mice. Additionally, we did not observe defects in the spiral ganglion of either Myh14$^{-/-}$ or control mice (data not shown). Because Myh14 is positioned at the apical junctions in mouse HCs, we examined the expression of tight-junction

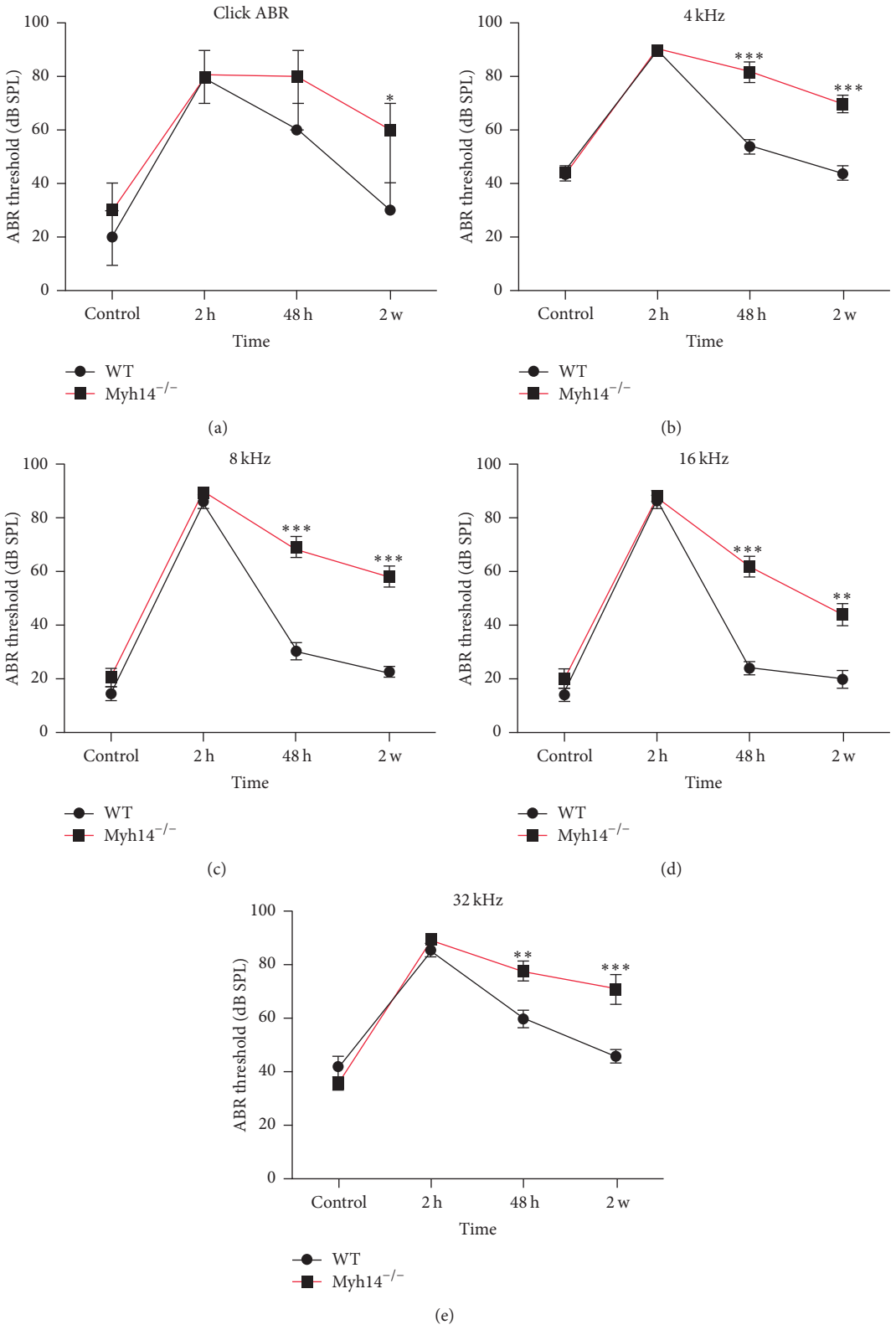

FIGURE 8: ABR threshold shifts following noise exposure between Myh14$^{-/-}$mice and controls. The ABR threshold shift was tested on Myh14$^{-/-}$mice and controls before noise exposure and 2 h, 48 h, and 2 weeks after noise exposure ($n = 8$ for each group). $^{*}P < 0.05$ compared to the controls. $^{**}P < 0.01$ by Student's t-test. $^{***}P < 0.001$ by Student's t-test compared to the control group. ABR measurements were reproducible.

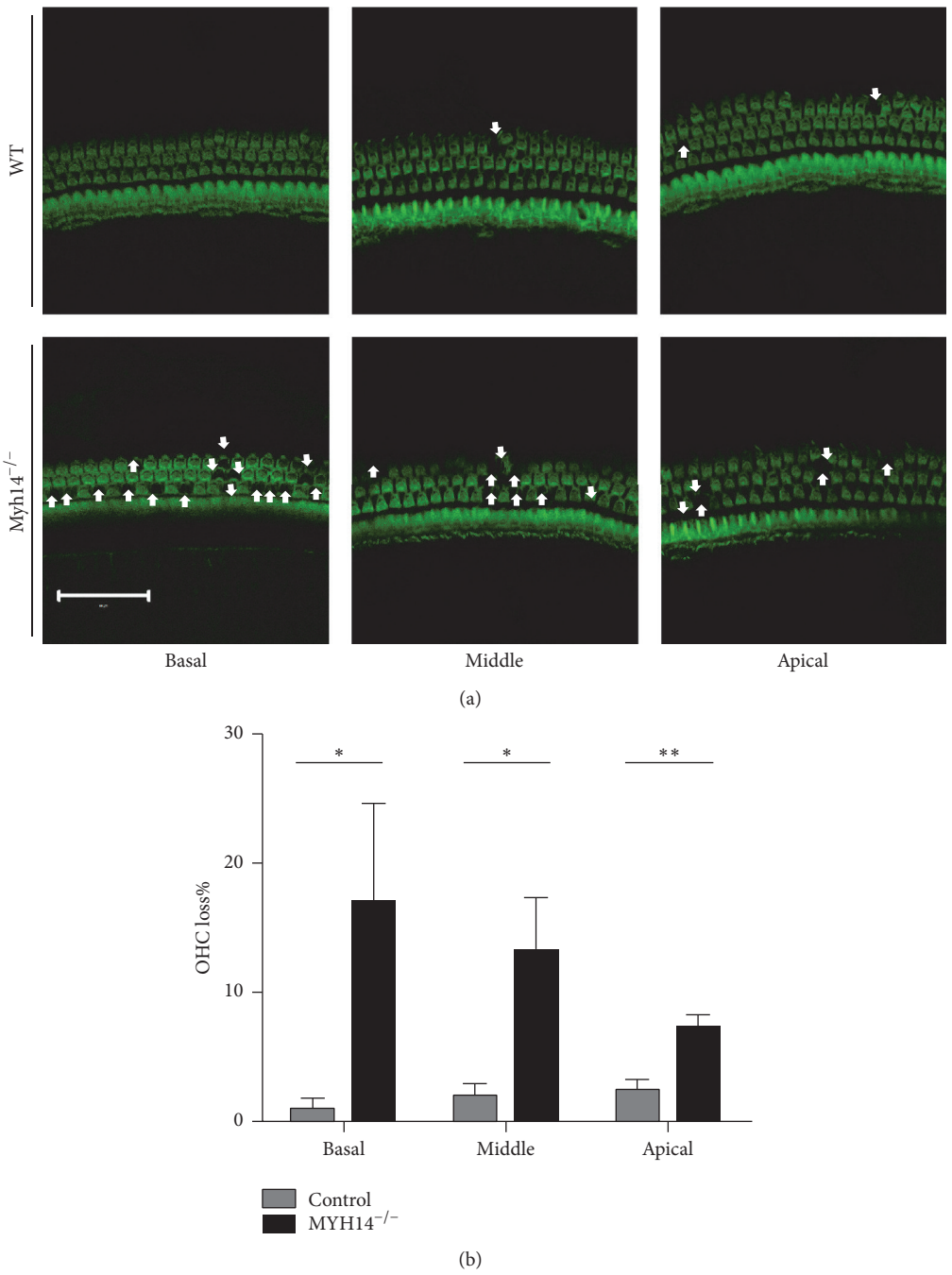

Figure 9: Myh14$^{-/-}$mice show more outer hair cell loss after noise exposure compared to controls. (a) Confocal images of outer hair cells (OHCs) in wild type and Myh14$^{-/-}$mice 2 weeks after noise exposure. More OHC loss (white arrow) is seen in Myh14$^{-/-}$mice. All of the experiments were performed at least three times. Scale bar, 20 μm. (b) Percentage of OHC loss at different cochlea locations in control and Myh14$^{-/-}$mice. $^{*}P < 0.05$ compared to the controls. $^{**}P < 0.01$ compared to the controls ($n = 5$).

proteins, ZO1 and E-cadherin, in Myh14$^{-/-}$ mice and controls after noise exposure. The immunofluorescence staining assay showed that the expressions of ZO1 and E-cadherin were not altered (data not shown). Immunoblot analysis and qRT-PCR were performed to examine if there is change in the expression level of MYH9 and MYH10. The results showed that the expression of MYH10 in the cochleae of noise-exposed Myh14$^{-/-}$ mice was significantly increased compared with the wild type mice, while there was no obvious change in the expression of MYH9 (Figures 10(a) and 10(b)).

In summary, Myh14$^{-/-}$ mice are less capable of recovering from noise exposure, and more HCs are lost after acoustic

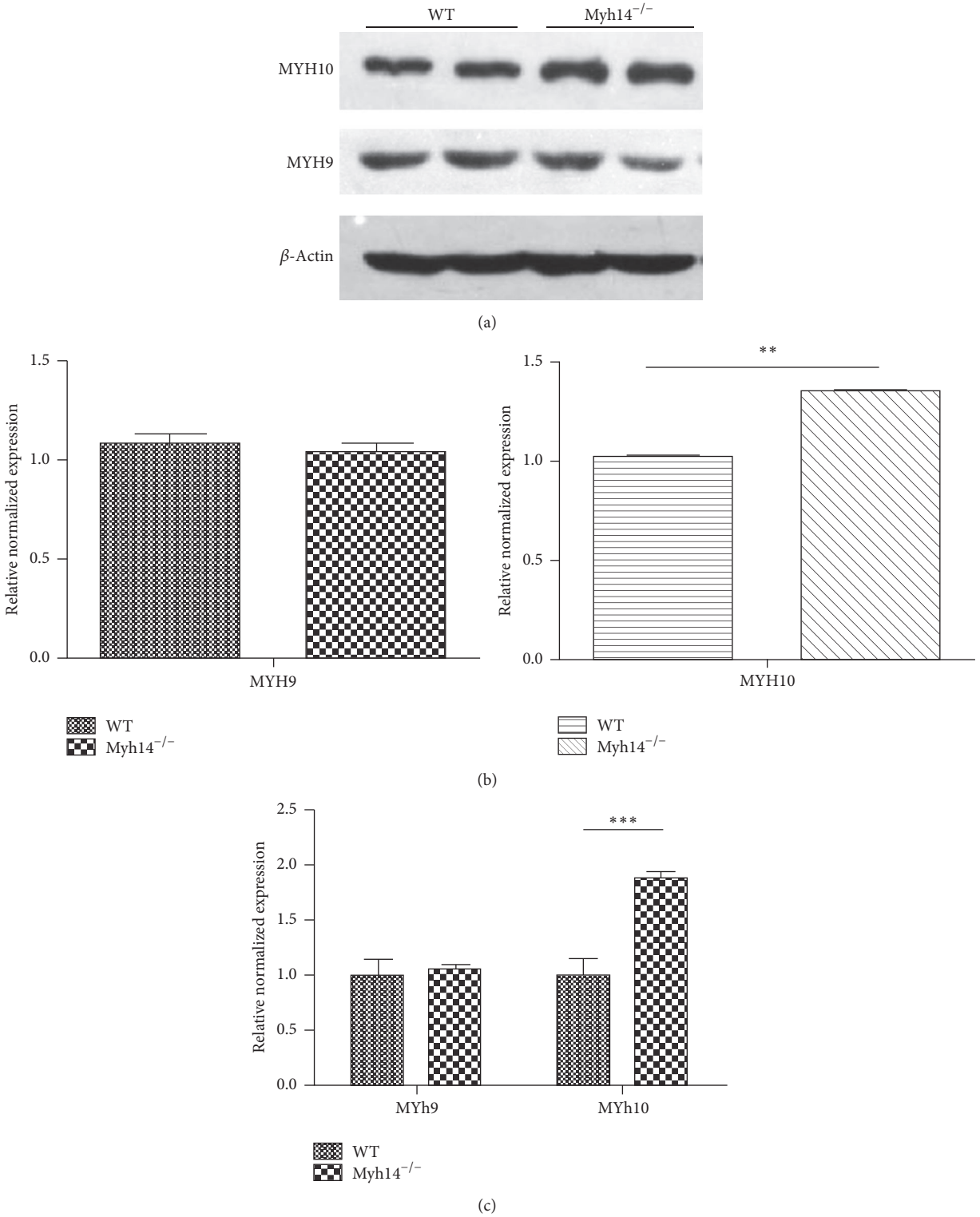

Figure 10: The expression level of MYH9 and MYH10 after the noise exposure. ((a), (b)) Western blots analysis was performed to show the expression level of MYH9 and MYH10 after the noise exposure ($n = 3$ for each group). (c) The consequence of Western blots was verified by real-time PCR. $^{**}P < 0.01$ compared to the controls. $^{***}P < 0.001$ by Student's t-test compared to the control group.

trauma. Our data indicate that Myh14$^{-/-}$ mice are more vulnerable to high-level noise exposure and that Myh14 plays a protective role in noise-induced damage of OHCs.

4. Discussion

According to the World Health Organization (WHO) survey results, NIHL has become a very serious problem; thus, numerous efforts are being focused on understanding the mechanism of NIHL and on the treatment of hearing loss (updated February 2015). A relationship between NIHL and various genes has been established. In recent years, many NIHL susceptibility candidate genes, including MYH14, have been discovered. MYH14, which belongs to the myosin family, is required for normal hearing in humans. To this date, many mutations of the human MYH14 gene have been reported to cause DFNA4-type hearing impairment. However, the specific roles of MYH14 in auditory function and NIHL are not fully understood. In our current study, we generated a Myh14$^{-/-}$ mice strain to clarify the role of MYH14 in the auditory system and in NIHL. Our results suggest that MYH14 plays a beneficial role after acoustic trauma.

4.1. CBA/CaJ Mice Are an Ideal Model for Performing NIHL and Other Hearing-Related Research. Caused by exposure to high-level noise, NIHL is one of the most common forms of sensorial hearing loss. Several experimental animal studies have reported morphological and physiological changes in the inner ear of mice after excessive noise exposure.

NIHL has a relationship with many genes. Great progress has been made in NIHL-related gene research. Currently, there are two main ways to study NIHL susceptibility genes: one is mass screening of population and the other is animal experiments. Mass screening is a commonly used method for the study of susceptibility genes in NIHL. However, population based study does not allow for the acquisition of auditory organs. In addition, to perform a study of NIHL susceptibility genes in a population, it is necessary to carry out a large-scale field survey to identify NIHL-susceptible persons. Compared with human groups, knockout mice are a good model for studying the mechanism of NIHL. In the past years, various animal knockout models have been developed. However, the establishment of traditional gene-knockout animal models must be based on traditional stem-cell methods. It is impossible to avoid using 129 and C57BL/6 background mice, which have a problem of age-related hearing loss (AHL) [20, 28]. Evidence shows that AHL and NIHL have common molecular mechanisms [29, 30], and both C57BL/6 and some 129 mice tend to be more susceptible to NIHL than CBA/CaJ mice [31]. C57BL/6 mice lose hair cells and show significant hearing loss by 6 months of age [32], and several 129 substrains except for 129Sv/Ev also show age-related hearing loss [33, 34]. Thus, this will interfere with our study of the pathogenesis of NIHL. Therefore, C57BL/6 and some 129 mice are not suitable strains for studying delayed hearing loss and NIHL. In contrast, CBA/CaJ mice retain normal hearing up to ≥18 months of age, and there is no AHL in this strain. Consequently, the CBA/CaJ mouse becomes one of the most ideal mouse strains for performing hearing-related research in the 80 inbred strains [35]. The CRISPR/Cas9 technology developed in the past three years makes the manipulation of CBA/CaJ mouse genes possible [35]. In our current study, we combined the CRISPR/Cas9 technology in the CBA/CaJ mouse strain to generate the Myh14 knockout model, thus avoiding the influence of an adverse genetic background on the experimental results.

A previous study by Ma et al. established a Myh14$^{-/-}$ mouse using C57/B6 and 129/Sv strains. They found that there were no obvious differences between Myh14$^{-/-}$ mice and wild type mice [23, 36]. In our current study, we generated a Myh14$^{-/-}$ mouse using the CBA/CaJ background. In this model, no obvious differences in appearance were found; the cochleae of Myh14$^{-/-}$ mice develop normally. However, our Myh14$^{-/-}$ mice have high-frequency hearing loss at five months; furthermore, moderate HC loss was also found in the cochlea from the basal turn of the mutants, which also started during this time period. It is understandable that these two mouse models may have different phenotypes; a possible explanation is that the mouse strain used in this study is not the same as the one used in the previous study, and the susceptibility to NIHL is different between strains [37, 38].

4.2. MYH10 May Compensate for the Absence of MYH14 in the Cochleae. Myosin is a superfamily of proteins related to the movement of molecules that are present in all eukaryotic cells; it binds to actin and uses ATP to move along the actin filament. The myosin superfamily is divided into two major categories: traditional myosin (nonmuscle myosin II; NM II) and nonconventional myosin (myosins I and III–VII). The distribution of the myosin families in the cochlea is different, and there is a difference in their normal physiological functions in the cochlea. NM II is thought to be involved in mediating epithelial tissue morphogenesis and tensional homeostasis, regulating force within epithelial apical junctions [39–41]. There are three isoforms of NM II in the cochlea, encoded by *myh9*, *myh10*, and *myh14* in mice [21]. The three NM II isoforms share very similar molecular structures [22]. Therefore, the slight effect of MYH14 loss on hearing thresholds raised the possibility that the other two genes may compensate for its absence [36]. The immunoblot analysis result showed that only the expression of MYH10 was significantly increased, and there was no obvious change in the expression of MYH9. A previous study reported that MYH10 is the major isoform regulating Schaffer collateral inputs [42]; thus, it is likely that the increase in MYH10, but not MYH9, can compensate for most of the functions of MYH14 in cochlea. The results from the MYH14 gene screening revealed one nonsense mutation. The affected individuals exhibited progressive hearing impairment beginning in the 1st decade of life with profound hearing loss in the 4th decade. This is to contrast with our Myh14$^{-/-}$ mice where onset of progressive hearing loss began at 5 months of age. This milder phenotype observed with our Myh14$^{-/-}$ mice could be explained by a more pronounced compensatory effect of MYH10 on MYH14 in the murine model. However,

MYH10 cannot completely replace the function of MYH14 because loss of HCs in Myh14$^{-/-}$ mice was still observed from five months. Moreover, we cannot exclude the possibility that other unidentified molecules may compensate for MYH14.

4.3. Loss of MYH14 Promotes NIHL. Evidence from several mouse mutants showed that the pathogenesis of AHL and NIHL is highly similar in most cases [17, 18]. In our study, Myh14$^{-/-}$ mice were used to investigate the role of MYH14 in the mechanism of NIHL. We found that abrogation of Myh14 increased the mouse susceptibility to acoustic trauma. In the wild type mice, 105 dB SPL noise exposure for 4 h caused a TTS, and their ABR thresholds recovered two weeks after noise exposure. However, mutant mice exhibited impaired recovery of ABR thresholds. In addition, more HC loss (mainly OHCs) was observed in mutant mice compared to controls two weeks after noise exposure. Consistent with previous reports [43–45], our results indicated that OHCs are more vulnerable to noise compared to IHCs. Failed recovery of ABR thresholds in mutant mice may be partially caused by permanent HC loss in the cochlea.

In addition, we found no obvious differences in the spiral ganglion and lateral wall (two other places easily affected by noise exposure) between Myh14$^{-/-}$ and control mice after noise exposure. Thus, our results indicated that MYH14 plays an indispensable role in HCs, when compared to that in other parts of the cochlea. Together, these findings suggest that MYH14 may play a beneficial role in the protection of the cochlea after acoustic stimulation in the CBA/CaJ mouse line.

We tried to determine the mechanism through which Myh14$^{-/-}$ mice were susceptible to NIHL. Because MYH14 is positioned at the apical junctions in the mouse HCs, we studied the expression of ZO-1 and E-cadherin cell junction proteins in Myh14$^{-/-}$ mice after noise exposure using immunofluorescence analysis to then compare them to the control group. We found that there were no statistically significant differences between both of these proteins in the Myh14$^{-/-}$ mice when compared to the controls. Then, how does a MYH14 deficiency cause more HC loss after noise exposure? A possible explanation is that loss of MYH14 can damage the permeability of ions in a noisy environment. Under normal conditions, MYH10 can partially compensate for the function of MYH14, but the absence of MYH14 makes it easier for mutant mice to be damaged in AJCs compared to the controls in a noisy environment. AJCs with long-term damage may cause changes in ion concentration, which eventually induced more HC loss in Myh14$^{-/-}$ mice [46, 47]. However, the specific mechanism of this hypothesis needs to be further analyzed.

5. Conclusion

We used the CRISPR/Cas9 technology in the CBA/CaJ mouse strain to generate a MYH14 knockout model. Myh14$^{-/-}$ mice were more vulnerable to high intensity noise compared to control mice. MYH14 may play beneficial role in NIHL. Additional experiments are necessary to identify the mechanism through which MYH14 contributes to NIHL.

Competing Interests

The authors declare that there is no conflict of interests regarding the publication of this paper.

Acknowledgments

This work was supported by grants from the Natural Science Foundation of China (31171194), the National 973 Basic Research Program of China (2014CB541703), and the Shandong Provincial Science and Technology Key Program (2009GG10002039).

References

[1] C. E. Graham, J. Basappa, and D. E. Vetter, "A corticotropin-releasing factor system expressed in the cochlea modulates hearing sensitivity and protects against noise-induced hearing loss," *Neurobiology of Disease*, vol. 38, no. 2, pp. 246–258, 2010.

[2] J. Lavinsky, M. Ge, A. L. Crow et al., "The genetic architecture of noise-induced hearing loss: evidence for a gene-by-environment interaction," *G3: Genes/Genomes/Genetics*, vol. 116, no. 032516, 2016.

[3] J. E. Hawkins Jr., "Comparative otopathology: aging, noise, and ototoxic drugs," *Advances in Oto-Rhino-Laryngology*, vol. 20, pp. 125–141, 1973.

[4] H. Spoendlin, "Retrograde degeneration of the cochlear nerve," *Acta Oto-Laryngologica*, vol. 79, no. 3–6, pp. 266–275, 1975.

[5] D. W. Roberson and E. W. Rubel, "Cell division in the gerbil cochlea after acoustic trauma," *Otology & Neurotology*, vol. 15, no. 1, pp. 28–34, 1994.

[6] A. J. Hudspeth, "How hearing happens," *Neuron*, vol. 19, no. 5, pp. 947–950, 1997.

[7] J. J. Finneran, "Noise-induced hearing loss in marine mammals: a review of temporary threshold shift studies from 1996 to 2015," *Journal of the Acoustical Society of America*, vol. 138, no. 3, pp. 1702–1726, 2015.

[8] R. de Iriarte Rodríguez, M. Magariños, V. Pfeiffer, U. R. Rapp, and I. Varela-Nieto, "C-Raf deficiency leads to hearing loss and increased noise susceptibility," *Cellular and Molecular Life Sciences*, vol. 72, no. 20, pp. 3983–3998, 2015.

[9] P.-I. Carlsson, L. Van Laer, E. Borg et al., "The influence of genetic variation in oxidative stress genes on human noise susceptibility," *Hearing Research*, vol. 202, no. 1-2, pp. 87–96, 2005.

[10] M. Pawlaczyk-Luszczynska, A. Dudarewicz, K. Zaborowski, M. Zamojska, and M. Sliwinska-Kowalska, "Noise induced hearing loss: research in central, eastern and south-eastern Europe and newly independent states," *Noise and Health*, vol. 15, no. 62, pp. 55–66, 2013.

[11] A. Konings, L. Van Laer, M. Pawelczyk et al., "Association between variations in CAT and noise-induced hearing loss in two independent noise-exposed populations," *Human Molecular Genetics*, vol. 16, no. 15, pp. 1872–1883, 2007.

[12] M. Sliwinska-Kowalska and M. Pawelczyk, "Contribution of genetic factors to noise-induced hearing loss: a human studies

review," *Mutation Research/Reviews in Mutation Research*, vol. 752, no. 1, pp. 61–65, 2013.

[13] X. Zhou, S. Chen, L. Xie et al., "Reduced connexin26 in the mature cochlea increases susceptibility to noise-induced hearing lossin mice," *International Journal of Molecular Sciences*, vol. 17, no. 3, p. 301, 2016.

[14] D. Yan, Y. Zhu, T. Walsh et al., "Mutation of the ATP-gated P2X2 receptor leads to progressive hearing loss and increased susceptibility to noise," *Proceedings of the National Academy of Sciences of the United States of America*, vol. 110, no. 6, pp. 2228–2233, 2013.

[15] S. Delmaghani, J. Defourny, A. Aghaie et al., "Hypervulnerability to sound exposure through impaired adaptive proliferation of peroxisomes," *Cell*, vol. 163, no. 4, pp. 894–906, 2015.

[16] P. J. Kozel, R. R. Davis, E. F. Krieg, G. E. Shull, and L. C. Erway, "Deficiency in plasma membrane calcium ATPase isoform 2 increases susceptibility to noise-induced hearing loss in mice," *Hearing Research*, vol. 164, no. 1-2, pp. 231–239, 2002.

[17] G. D. Housley, R. Morton-Jones, S. M. Vlajkovic et al., "ATP-gated ion channels mediate adaptationto elevated sound levels," *Proceedings of the National Academy of Sciences*, vol. 110, no. 18, pp. 7494–7499, 2013.

[18] R. H. Holme and K. P. Steel, "Progressive hearing loss and increased susceptibility to noise-induced hearing loss in mice carrying a Cdh23 but not a Myo7a mutation," *Journal of the Association for Research in Otolaryngology*, vol. 5, no. 1, pp. 66–79, 2004.

[19] A. Konings, L. Van Laer, A. Wiktorek-Smagur et al., "Candidate gene association study for noise-induced hearing loss in two independent noise-exposed populations," *Annals of Human Genetics*, vol. 73, no. 2, pp. 215–224, 2009.

[20] M. Sliwinska-Kowalska and M. Pawelczyk, "Contribution of genetic factors to noise-induced hearing loss: a human studies review," *Mutation Research—Reviews in Mutation Research*, vol. 752, no. 1, pp. 61–65, 2013.

[21] E. Golomb, X. Ma, S. S. Jana et al., "Identification and characterization of nonmuscle myosin II-C, a new member of the myosin II family," *The Journal of Biological Chemistry*, vol. 279, no. 4, pp. 2800–2808, 2004.

[22] N. Billington, A. Wang, J. Mao, R. S. Adelstein, and J. R. Sellers, "Characterization of three full-length human nonmuscle myosin II paralogs," *The Journal of Biological Chemistry*, vol. 288, no. 46, pp. 33398–33410, 2013.

[23] S. Ebrahim, T. Fujita, B. A. Millis et al., "NMII forms a contractile transcellular sarcomeric network to regulate apical cell junctions and tissue geometry," *Current Biology*, vol. 23, no. 8, pp. 731–736, 2013.

[24] S. R. Wylie and P. D. Chantler, "Myosin IIC: a third molecular motor driving neuronal dynamics," *Molecular Biology of the Cell*, vol. 19, no. 9, pp. 3956–3968, 2008.

[25] H. Yang, H. Wang, and R. Jaenisch, "Generating genetically modified mice using CRISPR/Cas-mediated genome engineering," *Nature Protocols*, vol. 9, no. 8, pp. 1956–1968, 2014.

[26] Y. Fujihara and M. Ikawa, "CRISPR/Cas9-based genome editing in mice by single plasmid injection," *Methods in Enzymoogy*, vol. 546, no. 2, pp. 319–336, 2014.

[27] Y. Jin, N. Ren, S. Li et al., "Deletion of Brg1 causes abnormal hair cell planer polarity, hair cell anchorage, and scar formation in mouse cochlea," *Scientific Reports*, vol. 6, Article ID 27124, 2016.

[28] A. M. Jimenez, B. B. Stagner, G. K. Martin, and B. L. Lonsbury-Martin, "Susceptibility of DPOAEs to sound overexposure in inbred mice with AHL," *Journal of the Association for Research in Otolaryngology*, vol. 2, no. 3, pp. 233–245, 2001.

[29] K. K. Ohlemiller, "Contributions of mouse models to understanding of age- and noise-related hearing loss," *Brain Research*, vol. 1901, no. 1, pp. 89–102, 2006.

[30] A. Bahloul, M.-C. Simmler, V. Michel et al., "Vezatin, an integral membrane protein of adherens junctions, is required for the sound resilience of cochlear hair cells," *EMBO Molecular Medicine*, vol. 1, no. 2, pp. 125–138, 2009.

[31] L. C. Erway, Y.-W. Shiau, R. R. Davis, and E. F. Krieg, "Genetics of age-related hearing loss in mice. III. Susceptibility of inbred and F1 hybrid strains to noise-induced hearing loss," *Hearing Research*, vol. 93, no. 1-2, pp. 181–187, 1996.

[32] S. Hequembourg and M. C. Liberman, "Spiral ligament pathology: a major aspect of age-related cochlear degeneration in C57BL/6 mice," *Journal of the Association for Research in Otolaryngology*, vol. 2, no. 2, pp. 118–129, 2001.

[33] N. Yoshida, S. J. Hequembourg, C. A. Atencio, J. J. Rosowski, and M. C. Liberman, "Acoustic injury in mice: 129/SvEv is exceptionally resistant to noise-induced hearing loss," *Hearing Research*, vol. 141, no. 1-2, pp. 97–106, 2000.

[34] Q. Y. Zheng, K. R. Johnson, and L. C. Erway, "Assessment of hearing in 80 inbred strains of mice by ABR threshold analyses," *Hearing Research*, vol. 130, no. 1-2, pp. 94–107, 1999.

[35] H. Wang, H. Yang, C. Shivalila et al., "One-step generation of mice carrying mutations in multiple genes by CRISPR/Cas-mediated genome engineering," *Cell*, vol. 153, no. 4, pp. 910–918, 2013.

[36] X. Ma, S. S. Jana, M. A. Conti, S. Kawamoto, W. C. Claycomb, and R. S. Adelstein, "Ablation of nonmuscle myosin II-B and II-C reveals a role for nonmuscle myosin II in cardiac myocyte karyokinesis," *Molecular Biology of the Cell*, vol. 21, no. 22, pp. 3952–3962, 2010.

[37] K. K. Ohlemiller, J. S. Wright, and A. F. Heidbreder, "Vulnerability to noise-induced hearing loss in 'middle-aged' and young adult mice: a dose-response approach in CBA, C57BL, and BALB inbred strains," *Hearing Research*, vol. 149, no. 1-2, pp. 239–247, 2000.

[38] J. G. Turner, J. L. Parrish, L. F. Hughes, L. A. Toth, and D. M. Caspary, "Hearing in laboratory animals: strain differences and nonauditory effects of noise," *Comparative Medicine*, vol. 55, no. 1, pp. 12–23, 2005.

[39] C. Bertet, L. Sulak, and T. Lecuit, "Myosin-dependent junction remodelling controls planar cell intercalation and axis elongation," *Nature*, vol. 429, no. 6992, pp. 667–671, 2004.

[40] M. A. Conti, S. Even-Ram, C. Liu, K. M. Yamada, and R. S. Adelstein, "Defects in cell adhesion and the visceral endoderm following ablation of nonmuscle myosin heavy chain II-A in mice," *The Journal of Biological Chemistry*, vol. 279, no. 40, pp. 41263–41266, 2004.

[41] N. Yamamoto, T. Okano, X. Ma, R. S. Adelstein, and M. W. Kelley, "Myosin II regulates extension, growth and patterning in the mammalian cochlear duct," *Development*, vol. 136, no. 12, pp. 1977–1986, 2009.

[42] E. D. Ozkan, M. Aceti, T. K. Creson et al., "Input-specific regulation of hippocampal circuit maturation by non-muscle myosin IIB," *Journal of Neurochemistry*, vol. 134, no. 3, pp. 429–444, 2015.

[43] H. Yuan, X. Wang, K. Hill et al., "Autophagy attenuates noise-induced hearing loss by reducing oxidative stress," *Antioxidants & Redox Signaling*, vol. 22, no. 15, pp. 1308–1324, 2015.

[44] E. Borg, "Loss of hair cells and threshold sensitivity during prolonged noise exposure in normotensive albino rats," *Hearing Research*, vol. 30, no. 2-3, pp. 119–126, 1987.

[45] G. D. Chen and L. D. Fechter, "The relationship between noise-induced hearing loss and hair cell loss in rats," *Hearing Research*, vol. 177, no. 1-2, pp. 81–90, 2003.

[46] H. P. Zenner, G. Reuter, U. Zimmermann, A. H. Gitter, C. Fermin, and E. L. LePage, "Transitory endolymph leakage induced hearing loss and tinnitus: depolarization, biphasic shortening and loss of electromotility of outer hair cells," *European Archives of Oto-Rhino-Laryngology*, vol. 251, no. 3, pp. 143–153, 1994.

[47] G. Nayak, S. I. Lee, R. Yousaf et al., "Tricellulin deficiency affects tight junction architecture and cochlear hair cells," *Journal of Clinical Investigation*, vol. 123, no. 9, pp. 4036–4049, 2013.

Hindawi Publishing Corporation
Neural Plasticity
Volume 2016, Article ID 4545826, 10 pages
http://dx.doi.org/10.1155/2016/4545826

Research Article

Synchronized Progression of Prestin Expression and Auditory Brainstem Response during Postnatal Development in Rats

Jianfeng Hang,[1,2] Wenlu Pan,[1] Aoshuang Chang,[1] Shun Li,[3] Cuixian Li,[1] Mingyu Fu,[1] and Jie Tang[1]

[1]*Department of Physiology, School of Basic Medical Sciences, Southern Medical University, Guangzhou 510515, China*
[2]*Department of Laboratory Medicines, General Hospital of Guangzhou Military Command of PLA, Guangzhou 510010, China*
[3]*Affiliated High School of South China Normal University, Guangzhou 510630, China*

Correspondence should be addressed to Jie Tang; jietang@smu.edu.cn

Received 8 September 2016; Revised 8 November 2016; Accepted 30 November 2016

Academic Editor: Jian Wang

Prestin is the motor protein expressed in the cochlear outer hair cells (OHCs) of mammalian inner ear. The electromotility of OHCs driven by prestin is responsible for the cochlear amplification which is required for normal hearing in adult animals. Postnatal expression of prestin and activity of OHCs may contribute to the maturation of hearing in rodents. However, the temporal and spatial expression of prestin in cochlea during the development is not well characterized. In the present study, we examined the expression and function of prestin from the OHCs in apical, middle, and basal turns of the cochleae of postnatal rats. Prestin first appeared at postnatal day 6 (P6) for basal turn, P7 in middle turn, and P9 for apical turn of cochlea. The expression level increased progressively over the next few days and by P14 reached the mature level for all three segments. By comparison with the time course of the development of auditory brainstem response for different frequencies, our data reveal that prestin expression synchronized with the hearing development. The present study suggests that the onset time of hearing may require the expression of prestin and is determined by the mature function of OHCs.

1. Introduction

Mammalian hearing is characterized by incredible sensitivity and exquisite frequency selectivity. However, in many species including rodents, auditory function is developed after birth. In rats, action potential cannot be obtained from neurons in primary auditory cortex before postnatal days 10 to 11 (P10-P11) [1, 2]. Therefore, this period at approximately P10 is an important stage of rat auditory development and is described as "hearing onset." During the following several days, the hearing sensitivity rapidly increases, and the minimal threshold for hearing decreases by approximately 30–50 dB during P11–P14, reaching the adult level [2, 3]. The maturation of auditory perception requires completion of the structural and functional development of both the auditory periphery and the central auditory system. Some important studies have investigated the maturation of central neurons and the refinement of the synaptic connections [4, 5]. In vivo patch-clamp data show that subthreshold auditory inputs were observed in cortical neurons before hearing onset [3, 6]. These reports suggest that cochlear function develops before hearing onset.

The morphological and functional development of the cochlea has been widely studied. Inner hair cells (IHCs) and outer hair cells (OHCs) are two types of sensory cells in the mammalian cochlea. OHCs convert sound vibration into electrical signals and change their cell length at acoustic frequencies [7, 8]. These shape changes, termed electromotility, are assumed to be part of the mechanical feedback process that amplifies low-level sound [7, 9]. The cochlear amplification derived from the motility of OHCs increases the sensitivity of weak sound by 40–60 dB [9, 10]. OHC electromotility is powered by a motor protein called prestin, which resides in the lateral membrane of OHCs. Driven by changes in membrane voltage, intracellular chloride ions move in or out of the prestin molecule, thereby triggering

a switch in the conformation of prestin between the long and short states [10, 11]. Interestingly, the morphological and functional maturation of OHCs occurs at postnatal ages [12, 13]. Belyantseva et al. reported that prestin expression increases progressively after birth in a time course coinciding with that of electromotility [14]. These findings imply that the electromotility of IHCs is likely to be an important limiting factor in the development of mature hearing.

Auditory brainstem responses (ABRs) are likely an important manifestation of the global neural response to sound stimulation and are generally believed to be associated with in vivo hearing function. Therefore, in the present study, we investigated the development of the ABR and the expression of prestin in postnatal rats. Our results suggest that the expression and function of prestin coincide with the time course of ABR development.

2. Materials and Methods

2.1. Experimental Animals. Adult (2 to 3 months old) Sprague-Dawley rats and rat pups ranging from postnatal day 0 (P0) to P14 were used in this study. The animals were maintained on a 12-hour light/12-hour dark schedule and had free access to water and a standard diet. All of the studies were performed in accordance with the Chinese Prevention of Cruelty to Animals Act and permission was obtained from the Southern Medical University Laboratory Animal Center.

2.2. ABR Recording. Experiments were carried out on rat pups aged P0–P14 and on adult rats. Briefly, each animal was anesthetized with an intraperitoneal injection of sodium pentobarbital (22 mg/kg for pups and 30 mg/kg for adults). Then, the animal was placed on an antivibration table in a soundproof chamber. The animal's body temperature was maintained at 37.5°C with a heating pad during ABR recording. A subdermal needle electrode was placed over the skull vertex. The ground was placed ventrolateral to the left external pinna, and the reference was placed ventrolateral to the right external pinna. Calibrated stimuli were generated using TDT SigGenRP software (Tucker-Davis Technologies). Tone bursts (1 ms rise/fall, 3 ms plateau) of various frequencies (1, 2, 4, 8, 16, 24, and 32 kHz) and intensities (0–90 dB SPL at 5 dB intervals) were presented using a calibrated TDT ES1 speaker located 50 cm away from the animal. The frequency-amplitude scan was computer controlled (TDT System 3, Tucker-Davis Technologies) and was delivered in a randomized sequence. Each frequency-amplitude combination was repeated 256 times at a rate of 10 bursts/s. The ABR signals were filtered (100–1000 Hz), amplified and averaged using TDT hardware (TDT System 3, Tucker-Davis Technologies), and recorded using BioSigRP software (Tucker-Davis Technologies). Hearing thresholds were determined by visual inspection of ABR waveforms and defined as the minimum intensity at which averaged waveforms could be distinguished. Data were stored for offline analysis. The entire recording for one animal spanned about 40 minutes.

2.3. Immunofluorescence Staining. The temporal bones of pups and adult Sprague-Dawley rats were isolated and placed into L-15 media (Invitrogen, Carlsbad, CA). The Organ of Corti was isolated and cut evenly into three pieces representing the basal, middle, and apical turns. Tissues were fixed with 4% paraformaldehyde in 0.1 M PBS (pH 7.4) at 25°C for 2 hours. After being washed with PBS, the tissues were incubated in a blocking solution (10% goat serum and 1% BSA in PBS) with 0.3% Triton X-100 for 20 min at room temperature and then incubated with a primary antibody against the prestin C-terminus (1 : 200, Santa Cruz Biotech Inc., Santa Cruz, CA) at 4°C overnight. After the primary antibodies were completely washed out with PBS, the tissue samples were incubated with Alexa Fluor 488-conjugated secondary antibodies (1 : 600; Invitrogen, Carlsbad, CA) in blocking solution at room temperature for 1 h. Counterstaining of stereocilia was performed using phalloidin labeled with tetramethyl rhodamine isothiocyanate (TRITC-phalloidin, 1 : 200; Sigma, St. Louis, MO, USA) for 20 min at room temperature. After being washed three times in PBS, samples were mounted between a slide and a coverslip using ProLong antifade reagent (Invitrogen, Carlsbad, CA). Fluorescence images were obtained with a Nikon microscope (Nikon, A1+, Japan) using 20x or 40x objectives.

2.4. Western Blot. Western blot was performed as described in our previous study [15]. In brief, the apical turn of the Organ of Corti was isolated and homogenized in lysis buffer (50 mM Tris-HCl, pH 7.4, 150 mM NaCl, 1% Triton X-100, 1% sodium deoxycholate, and 0.1% SDS) supplemented with cOmplete™ protease inhibitor (Roche). After incubation on ice for 30 min, samples were centrifuged at 12,000 rpm for 15 min at 4°C, and the supernatant was collected for further analysis. Subsequently, 20 μg of total cochlear protein was separated using 8% SDS-PAGE and transferred to a nitrocellulose membrane (Millipore). After blocking with 5% nonfat milk in TBS containing 0.1% Tween 20, the membrane was incubated with primary antibodies (Sigma, St. Louis, MO, USA) overnight at 4°C on a shaking platform, followed by horseradish peroxidase-conjugated secondary antibodies (Invitrogen, Carlsbad, CA) for 1 h at room temperature. Immunoreactive bands were detected by enhanced chemiluminescence and visualized with the Amersham Imager™ 600 (GE Healthcare). Prestin and GAPDH bands were quantified using ImageQuant™ TL Image Analysis software (GE Healthcare) according to the manufacturer's instructions.

2.5. Patch-Clamp Recording and Nonlinear Capacitance Measurement. The animals were anesthetized by CO_2 inhalation and decapitated. The cochlea was rapidly removed from the temporal bone and placed in a Petri dish filled with ice-cold Leibovitz's L-15 media (Invitrogen, Carlsbad, CA). The Organ of Corti was isolated from the apical turn of the cochlea and underwent mild enzymatic digestion with collagenase for 5 min (2 mg/mL collagenase IV, Sigma, St. Louis, MO). After gentle pipetting, the cells were transferred to a small plastic chamber filled with enzyme-free L-15 medium (~1.5 mL) supplemented with 10 mM HEPES (pH 7.35 and 300 mOsm).

The chamber then was placed on the stage of a Nikon inverted microscope (Eclipse Ti-S, Nikon, Japan) with a video camera (DS-Fi1c, Nikon, Japan). Healthy-appearing isolated OHCs were selected for the electrophysiological experiments. Cells showing any signs of shrinkage, swelling, or damage were excluded from the patch-clamp recording. Nonlinear capacitance (NLC) was measured as described in our previous publications [16–19]. The recording patch pipette was pulled by a pipette puller (P97, Sutter) and back-filled with the intracellular solution (140 CsCl, 10 EGTA, 2 $MgCl_2$, and 10 HEPES in mM, 305 mOsm and pH 7.35). Usually, the initial resistance of patch pipette was 2.5–3.5 MΩ in bath solution. Classical patch-clamp recording was performed under the whole-cell configuration using an Axopatch 200B amplifier and a 1440 A/D converter (Molecular Devices, CA, USA). The membrane capacitance of OHCs was measured using a two-sine-wave voltage stimulus protocol with a holding potential of 0 mV [20]. The stimuli were controlled and the data were acquired using jClamp software (Scisoft, New Haven, CT). Software OriginPro (OriginLab Corporation, Northampton, MA) was used for offline analysis of the data. The NLC can be fitted with a two-state Boltzmann function and can reflect the nonlinear charge movements to membrane voltage [21]. The Boltzmann function for capacitance fitting is described as

$$C_m = C_{\text{lin}} + \frac{Q_{\max}\alpha}{\exp\left[\alpha\left(V_m - V_{1/2}\right)\right]\left(1+\exp\left[-\alpha\left(V_m - V_{1/2}\right)\right]\right)^2}. \quad (1)$$

Four parameters ($Q_{\max}$, $V_{1/2}$, C_{lin}, and z) from the equation were related for the functional activity of prestin: $Q_{\max}$ is the maximum charge transfer across the membrane; $V_{1/2}$ (or V_h) is the membrane voltage at which the maximum charge movement occurs, or, equivalently, the peak of the capacitance-voltage function; C_{lin} is the linear capacitance; and α represents the slope of the voltage dependence ($\alpha = ze/kT$, where k is the Boltzmann constant, T is the absolute temperature, z is the valence of the charge movement, and e is the electron charge). C_{lin} is determined by the surface area of the cell membrane. To compare the magnitude values of the NLC obtained from OHCs with various cell sizes, we normalized NLC and $Q_{\max}$ to C_{lin}.

2.6. OHC Length Measurement. OHCs were isolated from the Organ of Corti as described above. In brief, the Organ of Corti was rapidly removed from the cochlea and cut evenly into three pieces in ice-cold L-15 medium. After mild enzymatic digestion for 5 min (2 mg/mL collagenase IV, Sigma, St. Louis, MO), the tissues were transferred to a small plastic chamber filled with enzyme-free L-15 medium (7.35 pH, 300 mOsm). Hair cells were separated by gentle trituration of the tissue with a 100 μL Hamilton syringe and a 25 G needle. By using this technique, a fairly large number of isolated hair cells can be obtained. The chamber containing the hair cells was placed on the stage of a Nikon inverted microscope (Eclipse Ti-S, Nikon, Japan) equipped with a video camera (DS-Fi1c, Nikon, Japan). Because of their morphology, in most preparations, IHCs and OHCs are easy to recognize. Usually, OHCs show a larger axis-diameter ratio, whereas IHCs have a tight neck [22]. The angle between the cuticular plate and the axis of the cell is another important landmark for identifying OHCs versus IHCs. Images of healthy-appearing solitary OHCs were captured using a video camera. The cell lengths of OHCs were measured offline.

2.7. Statistical Analysis. Results are presented as the mean ± SD. Student's t-test was used to examine the significance of the difference between the data obtained from different postnatal ages. Significance was defined as $p < 0.05$. The programs Excel and OriginPro were used for calculation, data fitting, and plotting.

3. Results

ABR waveforms were recorded from rat pups at various postnatal ages from day 0 (P0) to P14. During the first several days after birth, no ABR signal was observed, regardless of the frequency of sound stimulation and type of acoustic stimulus utilized (tone bursts, clicks, or noise). ABR for high-frequency tone bursts was detectable as early as P6. Responses were only found for stimuli of frequencies higher than 20 kHz with relatively high intensity (thresholds > 75 dB SPL; 5 of 6 animals). Rapid changes occurred over the three subsequent days, and, by P9, the ABR could be readily identified for all frequencies tested. Figure 1(a) shows the representative ABR recordings to tone bursts at 1, 16, and 32 kHz frequencies obtained from a rat pup at P9. Because wave I was the most consistent and robust component, it was used to estimate the ABR threshold (Figure 1(a), arrows). Thresholds for tone stimuli at different postnatal ages are shown in Figure 1(b). From P9 to P14, the ABR thresholds decreased progressively with increasing age, but the thresholds for different tone frequencies were affected differently. For frequencies higher than 24 kHz, the ABR responses were present as early as P6 in five of six animals. Mean thresholds (±SD) in response to 32 kHz tones at P6, P7, P9, P11, and P14 were 76.3 ± 2.5, 73.0 ± 2.7, 72.5 ± 2.8, 69.0 ± 2.5, and 51 ± 2.2 dB SPL, respectively (Figure 1(c)), and the threshold at P14 did not differ significantly from that in adult animals (47.5 ± 5 dB SPL, $p > 0.05$, t-test). ABRs for middle frequencies (4–16 kHz) were firstly observed at P7 in 7 of 7 animals. The mean thresholds (±SD) in response to 16 kHz tones at P7, P9, P11, and P14 were 74.0 ± 2.2, 67.5 ± 2.8, 62.5 ± 2.8, and 40 ± 2.2 dB SPL, respectively (Figure 1(c)). The adult threshold (17.1 ± 2.6 dB SPL) was significantly lower than that observed at P14 ($p < 0.01$, t-test). ABRs for low frequencies (<2 kHz) appeared as late as P9. The mean thresholds (±SD) in response to 1 kHz tones at P9, P11, and P14 were 75 ± 2.5, 71.3 ± 2.5, and 63.4 ± 2.7 dB SPL, respectively (Figure 1(c)), and thresholds at P14 did not differ from that in adults (60.7 ± 3.5 dB SPL, $p > 0.05$, t-test). Our data show that, for most frequencies tested, the ABR thresholds at P14 were close to the adult levels. The arrows in Figure 1(c) indicate the first day when ABR appeared for different frequencies.

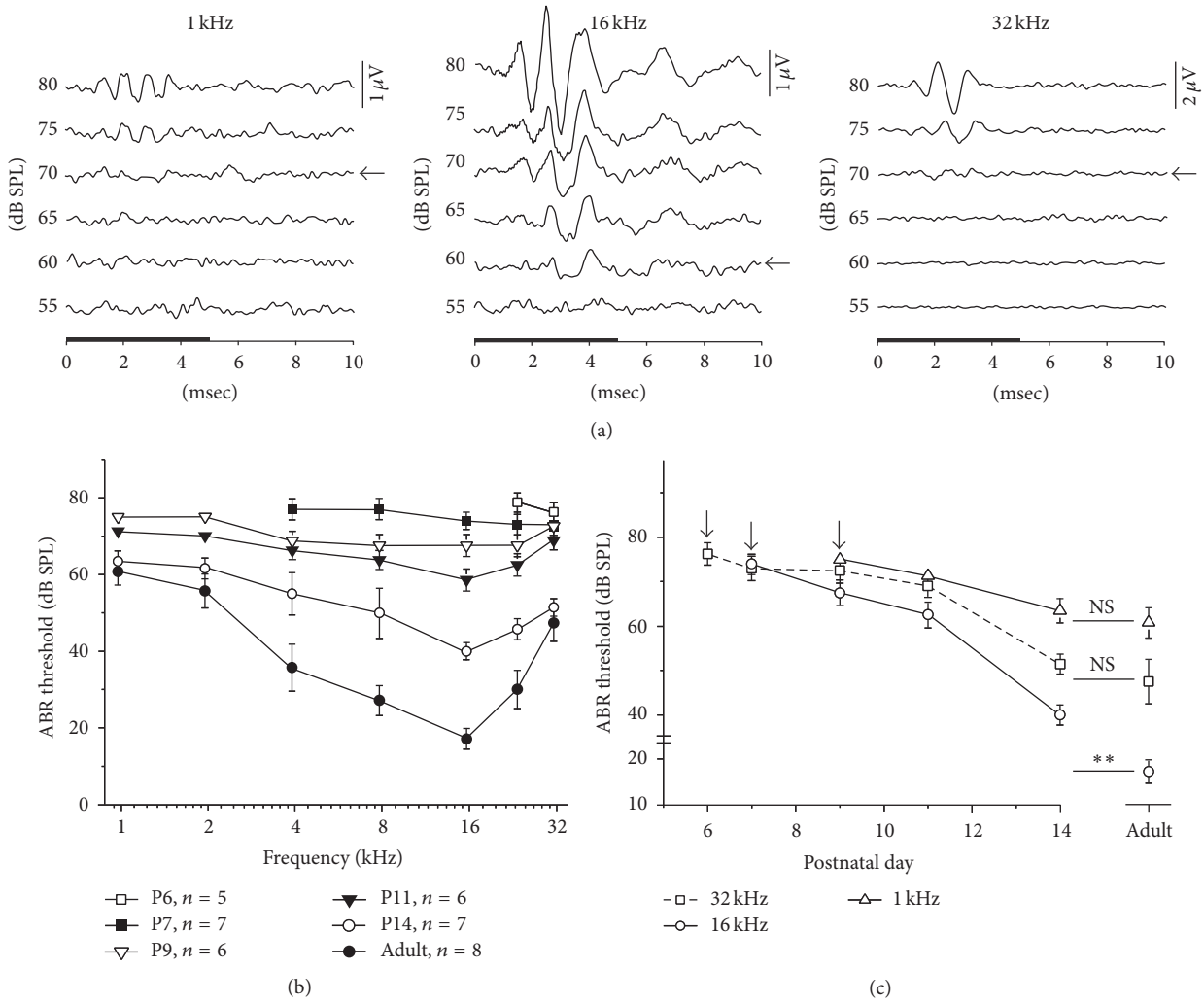

Figure 1: The ABR threshold changes during postnatal development. (a) The ABR waveforms recorded from a P9 rat pup. Arrows indicate ABR thresholds for 1 kHz, 16 kHz, and 32 kHz tones. The black horizontal bar on the x-axis denotes the 5 ms of the stimulus. (b) The ABR tuning curve changes during development. Data are expressed as the mean ± SD. n indicates the number of animals assessed. (c) The ABR thresholds decreased with time during postnatal development. Arrows indicate the first day on which the ABR appeared for different frequencies. $^{**}p < 0.01$; $^{NS}p > 0.05$ (Student's t-test).

Because the waveform I of the ABR represents the response elicited from the cochlea, our data show that cochlear functions developed between P6 and P14. The electromotility of OHCs contributes significantly to the cochlear response. Our result implies that, during this period, the OHCs are very likely involved in the response to sound stimulation as the cochlear amplifier. The electromotility of OHCs is produced by the motor protein prestin, which is located on the lateral membrane. To investigate the density and position of prestin in the developing OHCs, immunolabeling of prestin was performed and images were collected along the length of cochlea by confocal microscopy. Figure 2 shows confocal micrographs of OHCs from the apical, middle, and basal turns of cochleae from P5 to P14 rat pups. For P5 and P7 apical turns, rhodamine-phalloidin staining for hair bundles is shown to define the apical surface of the OHCs. DAPI staining for nucleus is shown to indicate the bottom region of the OHCs. As shown in Figure 2, no prestin was detected in the OHCs along the entire cochlea at P5. Expression of prestin was first labeled at P6 to P7 in OHCs located in basal cochlea and showed a continued increase over the next week. Prestin expression progressed both spatially and temporally, with basal OHCs showing prestin expression ~4 days earlier than apical OHCs. By P14, robust ring-shaped fluorescence was observed in all three segments.

In order to quantify the observed expression level changes of prestin during development, we measured the immunoband intensity of prestin in apical OHCs at different postnatal ages by using western blotting. As shown by the representative immunobands in Figure 3(a), the expression of prestin increased in an age-dependent manner. Figure 3(b) shows the mean (±SD) expression level from four independent experiments after normalization to GAPDH, the internal control protein. The expression of prestin remained

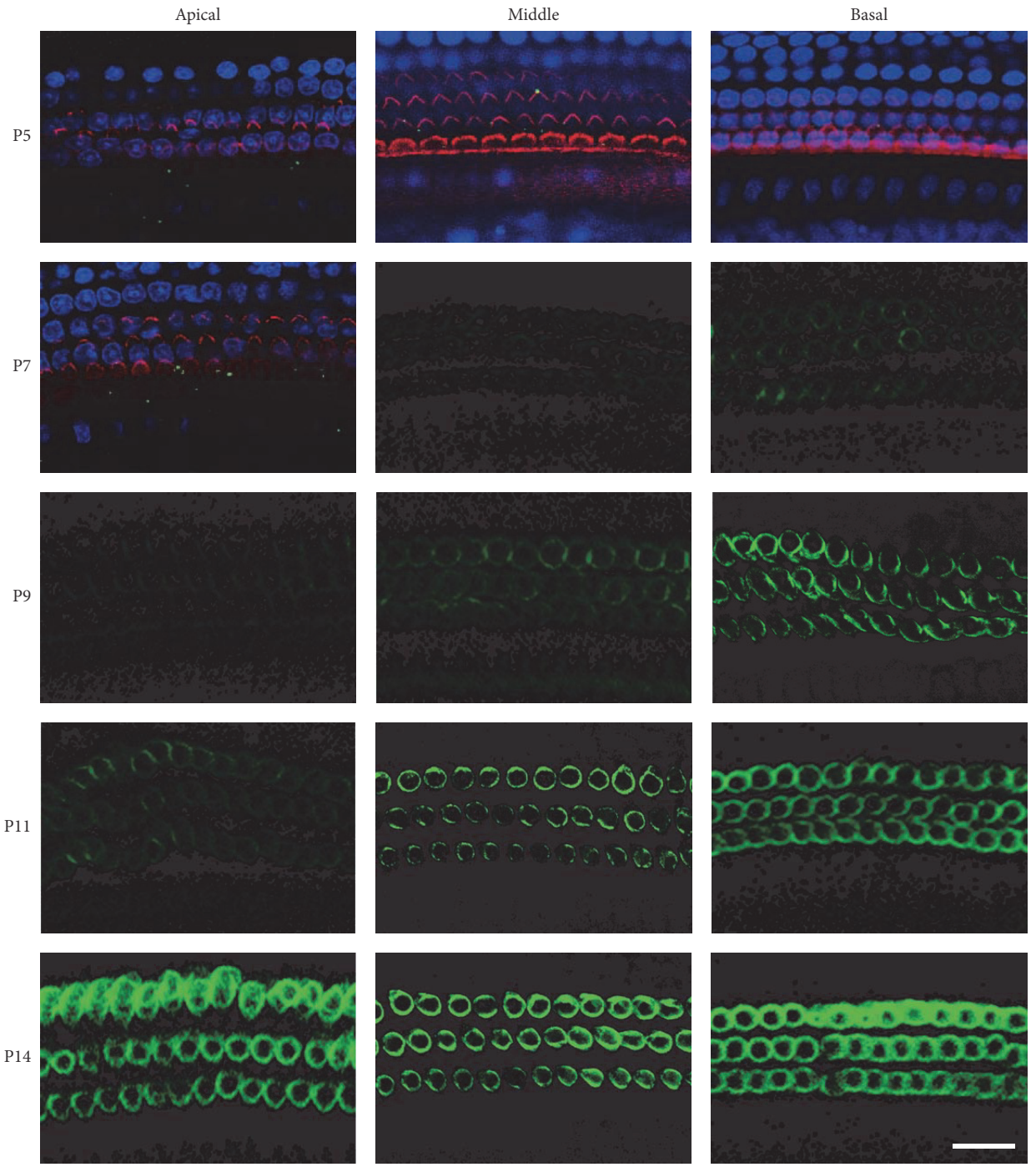

Figure 2: Confocal images of prestin expression in OHCs at various postnatal ages. Prestin immunoreactivity was measured from three segments (basal, middle, and apical) along the cochlea. For P5 and P7 apical turns, the hair bundles were labeled with rhodamine-phalloidin (red), the nuclei of hair cells were stained with DAPI (blue), and the prestin was labeled in green. Three images with different focal planes at hair bundle (to indicate the apical surface of the OHCs), the upper lateral wall of the HOCs, and nucleus were merged. No prestin fluorescence (green) was seen at P0–P5. To better illustrate the expression of prestin on the lateral wall of the OHCs, only green channel was shown after P7. Prestin expression progressed both spatially and temporally. Scale bar represents 20 μm.

low during the first five days after birth, and the most prominent increase in the prestin intensity occurred between P9 and P14. Although the prestin level increased slightly after P14, no significant difference was observed between the levels at P14 and adulthood.

Two essential electrophysiological properties are usually used to probe the function of prestin expressed in mammalian OHCs: NLC and electromotility. NLC and electromotility are fully coupled in mammals [21, 23, 24]. Because NLC can be easily and accurately measured experimentally, it

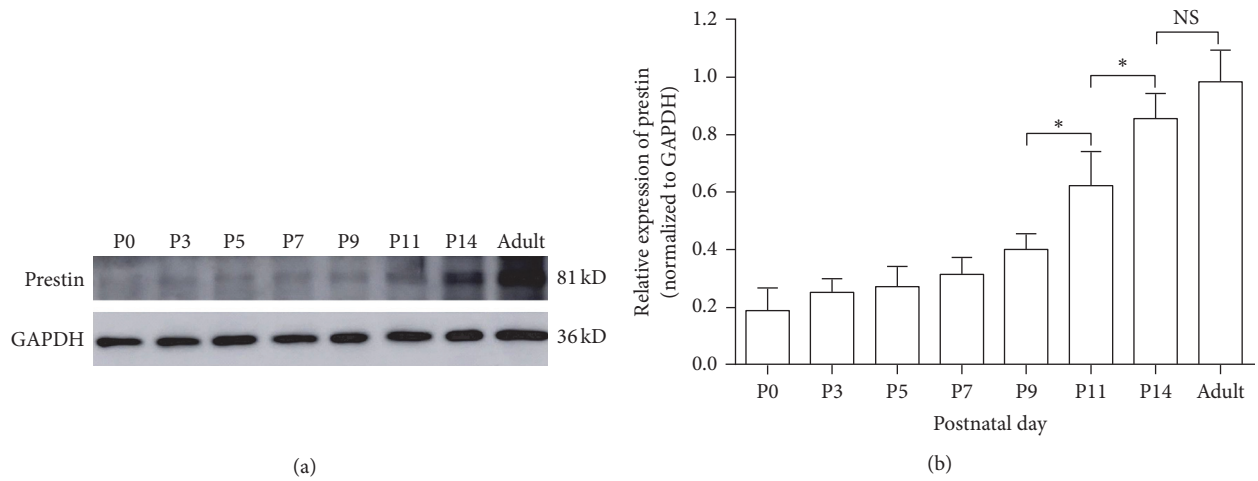

Figure 3: Expression of prestin in rats during cochlear development. (a) Representative prestin and GAPDH immunobands from western blots were detected at 81 kD and 36 kD. GAPDH was used as the internal control. (b) Relative expression of prestin (all normalized to GAPDH) at different postnatal ages. Comparisons are shown by the bars above the relevant columns. Data were obtained from four independent experiments and are expressed as mean ± SD. $^{*}p < 0.05$; $^{**}p < 0.01$; $^{NS}p > 0.05$ (Student's t-test).

is used as an assay to evaluate the functional development of prestin in the experiment described below. In OHCs of adult rodents, NLC is characterized by bell-shaped dependence on membrane potential with a peak at approximately −70 mV [21]. As shown in Figure 4, we compared the NLC recorded from apical OHCs from P6 to P14 with adult OHCs. To eliminate the influence of different cell sizes, the magnitude of NLC was normalized to C_{lin} (representing the surface area of OHC). Figure 4(a) shows that NLC responses were first detectable in 4 of 9 OHCs at P6, with very small magnitude (Figure 4(a), black line). Robust NLC responses were recorded in all OHCs measured from P9, and the responses increased throughout the developmental time period studied. At P14, the NLC reached a level comparable with that in adults. Parameters derived from the curve fitting with the two-state Boltzmann function are summarized in Figures 4(b)–4(e). It is apparent that $V_{1/2}$ during early development (P6) is relatively low (−83.96 ± 8.79 mV); however, at ages above P9, $V_{1/2}$ increases to the adult level (−66.46 ± 6.50 mV, Figure 4(b)). NLC/C_{lin} and Q_{max}/C_{lin} are both correlated with the moving charge density or with the amount of activated prestin. The larger the values, the more the charges translocated during voltage stimulation. As shown in Figures 4(c) and 4(d), both NLC/C_{lin} and Q_{max}/C_{lin} increase between P6 and P14, and these values reach maturity at P14. The voltage sensitivity or valence, z, remained stable at all ages studied (Figure 4(e), $p > 0.05$, t-test).

Because electromotility occurs along the longitudinal axis of OHCs, it is generally accepted that OHC length is critical for cochlear amplification. With the identical prestin expression level and activity, the longer OHCs could generate more significant motility and therefore conduct larger cochlear amplification. We measured the cell length of OHCs isolated from different segments along the basilar membrane. Figure 5 shows that the OHC length kept increasing and exhibited a sigmoidal rise from P0 to P14. The length of basal OHCs had minor changes over this period while the apical OHCs kept growing until approximately P11. Basal, middle, and apical OHCs reached their adult lengths at P5, P8, and P11, respectively (indicated by stars in Figure 5), and apical OHCs matured later than middle and basal OHCs.

4. Discussion

In this study, we used the ABR to measure the hearing sensitivity in developing rat pups. The ABR is a compound evoked potential derived from the acoustic responses of different stages along the ascending pathway of the auditory system. It is generally accepted that the peaks of ABR waveforms with different time delay are generated by distinct brainstem nuclei [25]. The responses of the cochlea and the auditory nerve are primarily responsible for peaks I and II, respectively. Peaks III to V (up to seven peaks were observed in some studies) represent the responses from the cochlear nucleus and other brainstem nuclei in higher level. Compared with recordings from adult animals, our data show that the ABR waveforms obtained from pups younger than P14 showed some special features. Only three to four distinct waves were identifiable within the first 8 ms after stimulus onset, as shown in Figure 1. The latency of peak I is very similar to previously published examples from adults (e.g., 1.4 ± 0.24 ms in P9 pups versus 1.2 ± 0.15 ms in adults for 32 kHz, 90 dB SPL tones) [26]. Therefore, our results suggest that the acoustic responses of higher level auditory nuclei are absent in developing rats. Although we did not examine the development of responses for individual nuclei in the central auditory system, our results imply that central auditory neurons reach functional maturity later than do cochleae and the cochlear signal inputs are required for the development of the auditory system. This hypothesis is supported by recent evidence from in vivo patch-clamp recording from cortical auditory neurons. The excitatory and inhibitory synaptic inputs are not cotuned

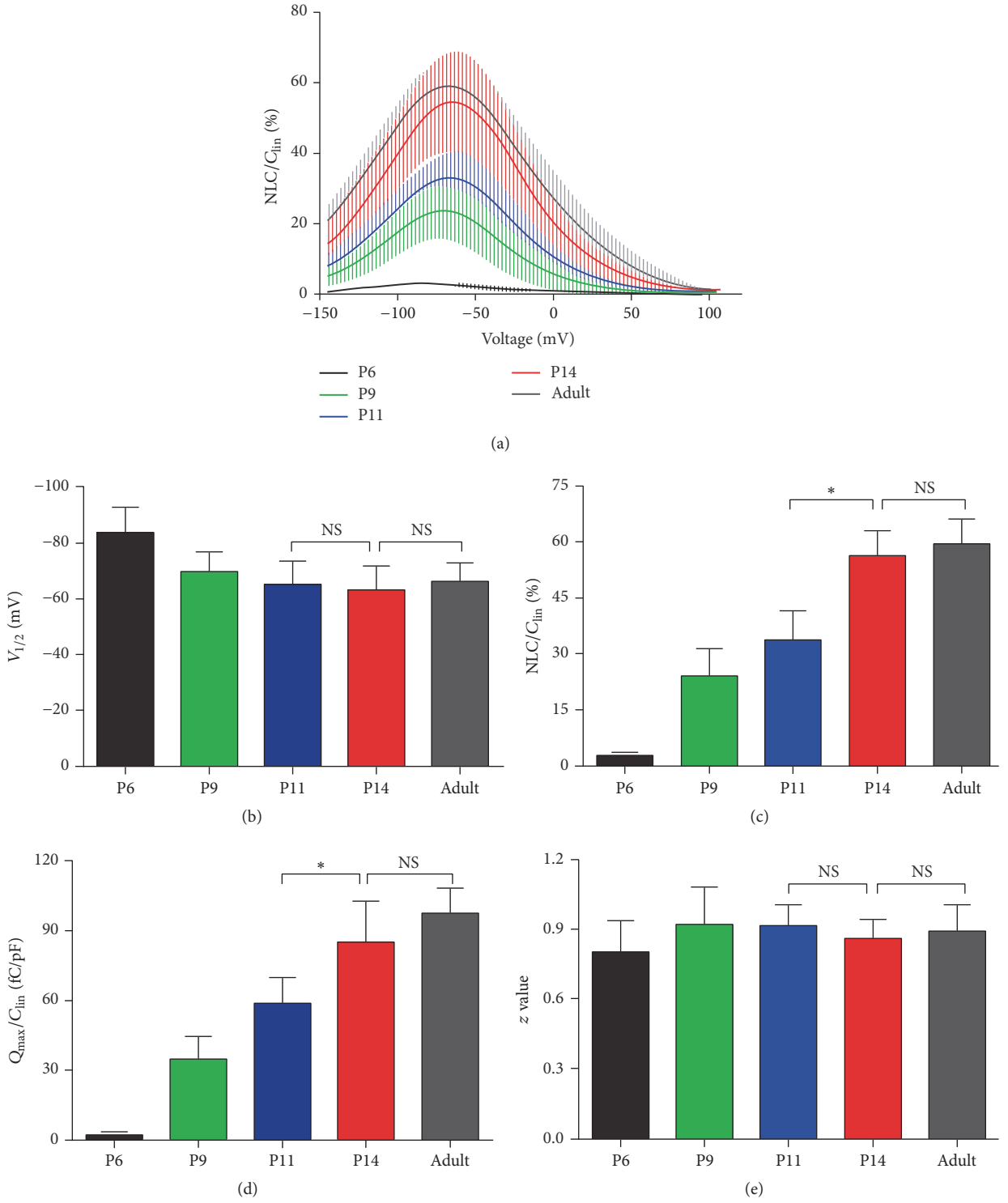

FIGURE 4: NLC measured from apical OHCs at various postnatal ages. (a) The mean NLC-voltage responses were fitted with the Boltzmann function (color coded heavy lines). NLC was normalized by C_{lin} and the curves were plotted as the mean ± SD. ((b)–(e)) Four parameters derived from curve fitting with Boltzmann's function. See results for details. Data are expressed as the mean ± SD. n = 4, 8, 8, 12, and 10 for P6, P9, P11, P14, and adult, respectively. $^{*}p < 0.05$; $^{NS}p > 0.05$ (Student's t-test).

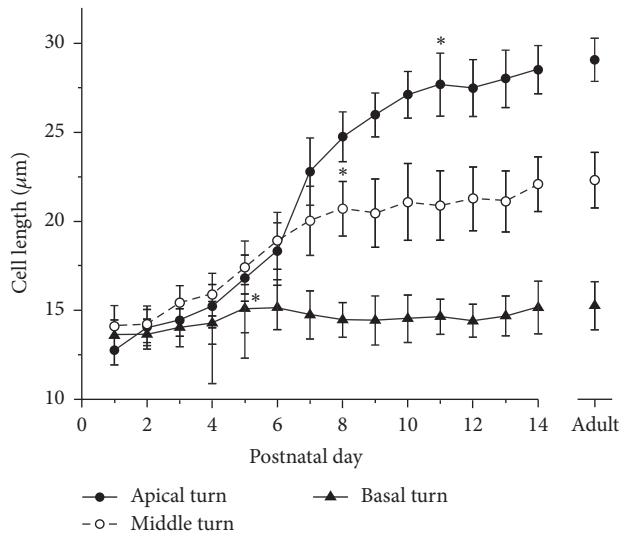

Figure 5: Changes in OHC length as a function of postnatal day. Each data point is plotted as the mean and SD of at least 50 OHCs. Stars indicate the earliest day at which cells reach the adult length ($p > 0.05$, Student's t-test).

and are temporally imbalanced before P12; therefore, action potentials were rarely recorded before hearing onset [3, 6]. These results suggest that the onset of cochlear responses occurs earlier than the synaptic refinement in the auditory cortex. Our results also show that the ABR response is detectable as early as P6–P9, although the time line is various for different frequencies (Figure 1).

However, the mechanisms responsible for the onset of the cochlear response and for determining the maturation time of cochlear function remain unclear. It is clear that substantial morphological and functional changes occur during cochlear development. In rats, the structure of the cochlea is formed at an early stage after birth; the middle ear is well developed and the ear canal is open before hearing onset [27–29]. The differentiation of hair cells and supporting cells, as well as the innervation of spiral ganglion neurons, is completed during the embryonic period [13, 30–35]. The morphological development of hair bundles and the functional maturation of mechanoelectrical transduction are completed before postnatal day 6 [13, 28, 29, 36, 37]. Because the cochlear response begins to appear at P6–P9 according to our ABR waveform analysis, the above processes are not likely to determine the onset of the cochlear response. In rats, action potentials of cortical neurons in response to sound stimulation are first recordable at P10-P11. Responses were found only for relatively high-intensity stimuli. Rapid changes occurred over the 3 subsequent days, and, by P14, the auditory cortex showed adult-like excitatory responses. The most significant change is the 40–50 dB threshold decreasing [1, 2]. This dramatic change in hearing sensitivity implies the involvement of a mechanism that modulates the sensitivity of the hearing system during this period.

Cochlear amplification confers extremely high sensitivity to our hearing with an enormous intensity range [38]. Mammalian cochlear amplification is attributed to OHCs, which can change their cell length in response to changes in membrane potential synchronized to sound waves [7]. This activity termed electromotility is powered by the unique motor protein prestin in the OHC lateral membrane [11]. Our study indicates that prestin is first expressed at P6 (Figure 2) and reaches the adult expression level at P14 (Figures 3 and 4). This period closely corresponds to the onset of cochlear function (Figure 1). The developmental expression pattern of prestin has been studied in two species, rat and mouse [14, 39]. Belyantseva et al. reported that prestin expression begins at postnatal day 0 and increases progressively in a time course coinciding with that of electromotility [14]. Our results do not appear to be consistent with these data. Expression of prestin in OHCs from different positions within the cochlea (basal, middle, and apical turns) is not synchronized: it reached the level of maturity in the basal turn at P9, in the middle turn at P10-P11, and in the apical turn at P12 (Figures 2 and 3). Our results are supported by function measurements of OHCs in other species. In mouse and gerbil, the NLC and electromotility of OHCs are first detected at P6 and reach adult levels at P12–P15 [12, 39]. In rats, however, the expression of prestin and the electromotility of OHCs are synchronous during development.

In the present study, we did not measure the motility of OHCs directly. NLC and electromotility are fully coupled in mammalian OHCs [21, 23, 24] and the former could be evaluated accurately [16–19]. Our NLC measurements show that, for apical OHCs, the function of prestin first appears at P9 and reached mature level at P14 (Figure 4). This result is consistent with the data recorded from mouse [39]. This functional measurement is also concordant with our immunofluorescence staining and western blot results (Figures 2 and 3). Thus, we proposed that the development of auditory central neural system, indicated by an increased sensitivity of ABR responses, occurs as the functional maturation of prestin, the motor protein of the OHCs.

Besides the expression level and functional activity, the cell length of OHCs is definitely an important factor that affects the overall motility magnitude of OHCs. As shown in Figure 5, the times at which mature cell lengths were reached are P5, P8, and P11 for basal, middle, and apical OHCs, respectively. These time points are earlier than those of the prestin expression. Therefore, we conclude that cell length development is not likely the limiting factor to determine the onset time of cochlear function. It is well established that the basal segments of the cochlea respond to high-frequency stimuli while more apical portions are tuned to low frequencies. Our data revealed that the spatial and temporal expression patterns of prestin and development of auditory brainstem response are highly concordant. It is more likely that the expression and functional development of prestin may play a critical role in the maturity of hearing.

5. Conclusions

In conclusion, our results indicate that the expression pattern of prestin and the NLC function of OHCs are synchronized

with the development of auditory brainstem responses. This finding suggests that the expression and functional development of prestin may determine the onset of hearing of rats.

Competing Interests

The authors declare that they have no competing interests.

Acknowledgments

This work was supported by grants from the 973 Program (2014CB943002) and the National Natural Science Foundation of China (31271179, 31500841).

References

[1] L. I. Zhang, S. Bao, and M. M. Merzenich, "Persistent and specific influences of early acoustic environments on primary auditory cortex," *Nature Neuroscience*, vol. 4, no. 11, pp. 1123–1130, 2001.

[2] E. de Villers-Sidani, E. F. Chang, S. Bao, and M. M. Merzenich, "Critical period window for spectral tuning defined in the primary auditory cortex (A1) in the rat," *The Journal of Neuroscience*, vol. 27, no. 1, pp. 180–189, 2007.

[3] Y. J. Sun, G. K. Wu, B.-H. Liu et al., "Fine-tuning of pre-balanced excitation and inhibition during auditory cortical development," *Nature*, vol. 465, no. 7300, pp. 927–931, 2010.

[4] D. H. Sanes and S. Bao, "Tuning up the developing auditory CNS," *Current Opinion in Neurobiology*, vol. 19, no. 2, pp. 188–199, 2009.

[5] R. C. Froemke and B. J. Jones, "Development of auditory cortical synaptic receptive fields," *Neuroscience & Biobehavioral Reviews*, vol. 35, no. 10, pp. 2105–2113, 2011.

[6] A. L. Dorrn, K. Yuan, A. J. Barker, C. E. Schreiner, and R. C. Froemke, "Developmental sensory experience balances cortical excitation and inhibition," *Nature*, vol. 465, no. 7300, pp. 932–936, 2010.

[7] W. E. Brownell, C. R. Bader, D. Bertrand, and Y. De Ribaupierre, "Evoked mechanical responses of isolated cochlear outer hair cells," *Science*, vol. 227, no. 4683, pp. 194–196, 1985.

[8] P. Dallos, B. N. Evans, and R. Hallworth, "Nature of the motor element in electrokinetic shape changes of cochlear outer hair cells," *Nature*, vol. 350, no. 6314, pp. 155–157, 1991.

[9] P. Dallos, "The active cochlea," *The Journal of Neuroscience*, vol. 12, no. 12, pp. 4575–4585, 1992.

[10] P. Dallos, "Cochlear amplification, outer hair cells and prestin," *Current Opinion in Neurobiology*, vol. 18, no. 4, pp. 370–376, 2008.

[11] J. Zheng, W. Shen, D. Z. Z. He, K. B. Long, L. D. Madison, and P. Dallos, "Prestin is the motor protein of cochlear outer hair cells," *Nature*, vol. 405, no. 6783, pp. 149–155, 2000.

[12] D. Z. Z. He, B. N. Evans, and P. Dallos, "First appearance and development of electromotility in neonatal gerbil outer hair cells," *Hearing Research*, vol. 78, no. 1, pp. 77–90, 1994.

[13] J. Waguespack, F. T. Salles, B. Kachar, and A. J. Ricci, "Stepwise morphological and functional maturation of mechanotransduction in rat outer hair cells," *The Journal of Neuroscience*, vol. 27, no. 50, pp. 13890–13902, 2007.

[14] I. A. Belyantseva, H. J. Adler, R. Curi, G. I. Frolenkov, and B. Kachar, "Expression and localization of prestin and the sugar transporter GLUT-5 during development of electromotility in cochlear outer hair cells," *The Journal of Neuroscience*, vol. 20, no. 24, Article ID RC116, 2000.

[15] C. Li, S. Chen, Y. Yu et al., "BIG1, a brefeldin A-inhibited guanine nucleotide-exchange factor, is required for GABA-gated Cl^- influx through regulation of $GABA_A$ receptor trafficking," *Molecular Neurobiology*, vol. 49, no. 2, pp. 808–819, 2014.

[16] X. Tan, J. L. Pecka, J. Tang et al., "From zebrafish to mammal: functional evolution of prestin, the motor protein of cochlear outer hair cells," *Journal of Neurophysiology*, vol. 105, no. 1, pp. 36–44, 2011.

[17] X. Tan, J. L. Pecka, J. Tang, S. Lovas, K. W. Beisel, and D. Z. Z. He, "A motif of eleven amino acids is a structural adaptation that facilitates motor capability of eutherian prestin," *Journal of Cell Science*, vol. 125, part 4, pp. 1039–1047, 2012.

[18] J. Tang, J. L. Pecka, X. Tan, K. W. Beisel, and D. Z. Z. He, "Engineered pendrin protein, an anion transporter and molecular motor," *The Journal of Biological Chemistry*, vol. 286, no. 35, pp. 31014–31021, 2011.

[19] J. Tang, J. L. Pecka, B. Fritzsch, K. W. Beisel, and D. Z. Z. He, "Lizard and frog prestin: evolutionary insight into functional changes," *PLoS ONE*, vol. 8, no. 1, Article ID e54388, 2013.

[20] J. Santos-Sacchi, M. Wu, and S. Kakehata, "Furosemide alters nonlinear capacitance in isolated outer hair cells," *Hearing Research*, vol. 159, no. 1-2, pp. 69–73, 2001.

[21] J. Santos-Sacchi, "Reversible inhibition of voltage-dependent outer hair cell motility and capacitance," *The Journal of Neuroscience*, vol. 11, no. 10, pp. 3096–3110, 1991.

[22] D. Z. Z. He, J. Zheng, R. Edge, and P. Dallos, "Isolation of cochlear inner hair cells," *Hearing Research*, vol. 145, no. 1-2, pp. 156–160, 2000.

[23] J. F. Ashmore, *Cochlear Mechanisms: Structure, Function, and Models*, Springer Science & Business Media, 1989.

[24] K. Homma and P. Dallos, "Evidence that prestin has at least two voltage-dependent steps," *The Journal of Biological Chemistry*, vol. 286, no. 3, pp. 2297–2307, 2011.

[25] A. Møller, *Hearing: Anatomy, Physiology, and Disorders of the Auditory System*, Elsevier, Oxford, UK, 2006.

[26] P. Scimemi, R. Santarelli, A. Selmo, and F. Mammano, "Auditory brainstem responses to clicks and tone bursts in C57 BL/6j mice," *Acta Otorhinolaryngologica Italica*, vol. 34, no. 4, pp. 264–271, 2014.

[27] M. Geal-Dor, S. Freeman, G. Li, and H. Sohmer, "Development of hearing in neonatal rats: air and bone conducted ABR thresholds," *Hearing Research*, vol. 69, no. 1-2, pp. 236–242, 1993.

[28] M. C. Kelly and P. Chen, "Development of form and function in the mammalian cochlea," *Current Opinion in Neurobiology*, vol. 19, no. 4, pp. 395–401, 2009.

[29] A. K. Groves and D. M. Fekete, "Shaping sound in space: the regulation of inner ear patterning," *Development*, vol. 139, no. 2, pp. 245–257, 2012.

[30] M. W. Kelley, "Regulation of cell fate in the sensory epithelia of the inner ear," *Nature Reviews Neuroscience*, vol. 7, no. 11, pp. 837–849, 2006.

[31] J. M. Appler and L. V. Goodrich, "Connecting the ear to the brain: molecular mechanisms of auditory circuit assembly," *Progress in Neurobiology*, vol. 93, no. 4, pp. 488–508, 2011.

[32] J. Defourny, F. Lallemend, and B. Malgrange, "Structure and development of cochlear afferent innervation in mammals," *American Journal of Physiology—Cell Physiology*, vol. 301, no. 4, pp. C750–C761, 2011.

[33] C. C. Lu, J. M. Appler, E. A. Houseman, and L. V. Goodrich, "Developmental profiling of spiral ganglion neurons reveals insights into auditory circuit assembly," *The Journal of Neuroscience*, vol. 31, no. 30, pp. 10903–10918, 2011.

[34] T. M. Coate, S. Raft, X. Zhao, A. Ryan, E. B. Crenshaw, and M. W. Kelley, "Otic mesenchyme cells regulate spiral ganglion axon fasciculation through a Pou3f4/EphA4 signaling pathway," *Neuron*, vol. 73, no. 1, pp. 49–63, 2012.

[35] S.-Z. Wang, L. A. Ibrahim, Y. J. Kim et al., "Slit/Robo signaling mediates spatial positioning of spiral ganglion neurons during development of cochlear innervation," *The Journal of Neuroscience*, vol. 33, no. 30, pp. 12242–12254, 2013.

[36] A. Dabdoub, M. J. Donohue, A. Brennan et al., "Wnt signaling mediates reorientation of outer hair cell stereociliary bundles in the mammalian cochlea," *Development*, vol. 130, no. 11, pp. 2375–2384, 2003.

[37] P. C. G. Rida and P. Chen, "Line up and listen: planar cell polarity regulation in the mammalian inner ear," *Seminars in Cell & Developmental Biology*, vol. 20, no. 8, pp. 978–985, 2009.

[38] P. Dallos, "Overview: cochlear neurobiology," in *The Cochlea*, P. Dallos, A. N. Popper, and R. R. Fay, Eds., vol. 8 of *Springer Handbook of Auditory Research*, pp. 1–43, Springer, New York, NY, USA, 1996.

[39] T. Abe, S. Kakehata, R. Kitani et al., "Developmental expression of the outer hair cell motor prestin in the mouse," *Journal of Membrane Biology*, vol. 215, no. 1, pp. 49–56, 2007.

Hindawi Publishing Corporation
Neural Plasticity
Volume 2016, Article ID 5982397, 8 pages
http://dx.doi.org/10.1155/2016/5982397

Research Article

Analysis of the Damage Mechanism Related to CO_2 Laser Cochleostomy on Guinea Pig Cochlea

Xiang Liu,[1,2,3] Xiao-qing Qian,[1,2,3] Rui Ma,[2,3,4] Fang-Lu Chi,[1,2,3] and Dong-Dong Ren[1,2,3]

[1]*Department of Otology & Skull Base Surgery, EYE & ENT Hospital of Fudan University, Shanghai 200031, China*
[2]*Shanghai Clinical Medical Center of Hearing Medicine, Shanghai 200031, China*
[3]*Key Laboratory of Hearing Medicine, Ministry of Health, Shanghai 200031, China*
[4]*Department of Research Center, EYE & ENT Hospital of Fudan University, Shanghai 200031, China*

Correspondence should be addressed to Fang-Lu Chi; dongdong_ren@163.com and Dong-Dong Ren; chifanglu@126.com

Received 8 September 2016; Accepted 14 November 2016

Academic Editor: Genglin Li

Different types of lasers have been used in inner ear surgery. Therefore, it is of the utmost importance to avoid damage to the inner ear (e.g., hyperthermia and acoustic effects) caused by the use of such lasers. The aim of this study was to use a high powered fibre-enabled CO_2 laser (10 W, 606 J/cm^2) to perform cochleostomies on guinea pig cochlea and to investigate the possible laser-induced damage mechanisms. The temperature changes in the round window membrane, auditory evoked brainstem response, and morphological of the hair cells were measured and recorded before and after laser application. All of the outcomes differed in comparison with the control group. A rise in temperature and subsequent increased hearing loss were observed in animals that underwent surgery with a 10 W CO_2 laser. These findings correlated with increased injury to the cochlear ultrastructure and a higher positive expression of E-cadherin and β-catenin in the damaged organ of Corti. We assume that enhanced cell-cell adhesion and the activated β-catenin-related canonical Wnt-signalling pathway may play a role in the protection of the cochlea to prevent further damage.

1. Introduction

The instruments used in surgical techniques for inner ear surgeries, such as stapedotomy and cochlear implantation, must be powerful enough to be efficient while, at the same time, preventing damage to the inner ear. Lasers with varying wavelengths, set to appropriate intensities, can fulfil two basic principal requirements: ablation of bone at a precise location and achievement of an ideal setting without penetrating deeply into the perilymph and causing injury to the sensory structures of the inner ear. The first laser stapedotomy was performed by Perkins in 1979 using an argon laser. Since then, different types of lasers, such as the erbium: yttrium aluminium garnet laser, potassium titanyl phosphate (KTP) laser, and CO_2 laser, have been used in inner ear surgery [1]. The use of different lasers has been described in both experimental and clinical studies [2–8].

However, each laser has advantages and disadvantages. The application of a laser to any medium leads to absorptive, reflective, thermal, and acoustic effects. Visible lasers (argon and KTP) have a short wavelength (0.5 μm) that can only be partially absorbed by the stapes footplate or the bone wall of the cochlea and readily passes through the perilymph to be absorbed by the tissues of the inner ear, leading to tissue damage [2]. The long wavelength of the invisible CO_2 laser (10.6 μm) is well-absorbed by water. Absorption results in the conversion of laser energy into heat [7]. In our previous study, positive expressions of iNOS and Hsp70 were observed in spiral ganglion cells, nerve fibres, supporting cells of the organ of Corti, and cells of the spiral ligament after serious irradiation injury of the cochlear ultrastructure [5]. Therefore, the degree of temperature increase and which molecules are affected by the application of a high-intensity CO_2 laser in a guinea pig cochlea model require further investigation.

This study aimed to explore how the thermal effect of lasers interferes with molecules in the damaged inner ear.

Table 1: Applied CO_2 laser mode and parameters.

Laser mode	Power	Spot diameter	Pulse duration/ interval	Working distances	Energy/impulse	Energy density	Number of pulses
SuperPulse	10 W	458 μm	100 ms/100 ms	3 mm	1 J	606 J/cm^2	2

W: watt; J: joule.

Guinea pigs were chosen as the animal model because the basal turn of the cochlea is easily accessible and the thickness of the cochlea wall (1 mm anterior to a round window of approximately 120–160 μm) is comparable to the dimensions of a slightly thickened otosclerotic footplate (150–200 μm) [3]. We used a new type of handheld fibre-enabled CO_2 laser, the 10 W (606 J/cm^2) CO_2 laser, to explore possible damage mechanisms in the inner ear.

2. Materials and Methods

2.1. Animals. Adult male albino guinea pigs (weight, 250–350 g) were used in this study. All 21 animals were obtained from the Animal Center of the Medical School of Fudan University and were housed under clear conditions. The Animal Research Control Committees of Fudan University approved the experimental protocols and procedures performed in this study.

An otoscopic examination was performed on all guinea pigs prior to surgery to ensure that the external auditory canals and tympanic membranes were normal. All animals had normal hearing with a positive Preyer reflex. Before each procedure, the guinea pigs were anaesthetised using ketamine (85 mg/kg body weight) and xylazine (7.5 mg/kg body weight). The left ear of each animal was chosen to be the experimental ear, and it received irradiation by a 10 W CO_2 laser. Each animal's right ear was classed as the control group and was irradiated on the temporal muscle close to the cochlea.

2.2. Laser Device. Perforation of the cochlear bone was performed with the new AcuPulse 40 WG CO_2 laser using the FiberLase flexible CO_2 laser waveguide (Lumenis, Santa Clara, CA, USA). This laser has a handheld energy delivery system with a flexible 2 m long waveguide and a variety of rigid and malleable microsurgical accessories with different lengths and flexibilities.

2.3. Surgery. After the induction of anaesthesia, we created a postauricular incision in the left ear, exposed the bulla, fractured and removed the bony shell of the bulla, and carefully exposed the basal turn of the cochlea under a microscope (OPMI 9-FC, Carl Zeiss, Jena, Germany). The left ear of each guinea pig underwent perforation of the cochlea with the laser 1 mm anterior to the round window niche. The 10 W SuperPulse laser mode was used at a working distance of up to 3 mm in noncontact mode. Two exposure times were selected. Each laser shot continued for 0.1 s and the time interval between each shot was 0.1 s (Table 1). Cochleostomy was recognised by an effusion of perilymph. An opening of approximately 0.5 mm in diameter was obtained. The control group underwent the same procedure but were irradiated by equal lasers on the temporal muscles to exclude the influence of noise caused by the application of the laser. The guinea pig cochleae with their bony coverage were photographed with the help of a digital camera coupled to a microscope (OPMI 9-FC, Carl Zeiss, Germany).

2.4. Temperature Measurement. Temperature changes were measured with a type K (chromium and aluminium) thermocouple (TM6801, Jingda, China). The detection procedure was well documented in our previous article [6]. A 0.8 mm diameter detecting head was placed onto the membrane of the round window to measure the temperature change at approximately one pulse per second during laser irradiation in vivo. The temperature was recorded manually by a digital thermometer.

2.5. Measurement of the Auditory Brainstem Response. Recordings of the auditory brainstem response (ABR) were performed before and immediately after laser irradiation. Animals were anaesthetised and then placed in a sound-isolated and electrically-shielded booth (Ningbo, Tonecon Acoustic Systems, Nanjing, China). Acoustic stimuli were delivered monaurally via an earphone (Bio-logic Systems Corp., Mundelein, IL, USA) attached to a customised plastic speculum inserted into the ear canal. Subdermal electrodes were inserted at the vertex of the skull, under the right (ground) and left ear. The Bio-Logic NAVPR2 hearing diagnostic system (Natus Medical Inc., San Carlos, CA, USA) was used to provide the stimuli (click stimuli; duration, 0.1 ms) and record the response. Up to 1,024 responses were averaged for each stimulus level. ABRs were determined by reducing the intensity in 10 dB increments and then in 5 dB steps close to the threshold until no organised responses were detected. Thresholds were estimated at the lowest stimulus level at which a response was observed, identified by the presence of recognisable and repeatable wave IIIs. All ABR measurements were evaluated by an expert blinded to the treatment conditions.

2.6. Scanning Electron Microscopy. Three guinea pigs from each group were sacrificed under deep anaesthesia after postoperative ABR evaluation. The tympanic bullae opened and the bony coverage of the cochlea was removed. The cochleae were fixed in a 2.5% solution of glutaraldehyde in a 0.1 mol/L sodium cacodylate buffer. After fixation, the dissected cochleae were dehydrated in 10%, 30%, 70%, 90%, and 100% (3x) concentrations of ethanol. A critical point dryer (EM CPD300, Leica, Wetzlar, Germany) was used to dry

the specimens with liquid carbon dioxide and the specimens were then sputter-coated with platinum-palladium (E-1045 ion sputter, Hitachi High Technologies Co., Tokyo, Japan). The surfaces of the organs of Corti were observed under a low-vacuum scanning electron microscope (SEM) (Nova NanoSEM 230, FEI Company, Hillsboro, OR, USA).

2.7. Immunofluorescent Staining. After the postoperative ABR evaluation, three additional guinea pigs from each group were sacrificed under deep anaesthesia for immunofluorescent staining. As outlined above, the tympanic bullae were removed and fixed in 4% paraformaldehyde in a phosphate-buffered saline solution (PBS) for a period of 24 h. Under magnification, the bony wall of the cochlea was removed with a pick and forceps to obtain the basilar membrane of the cochlea. The following staining procedure was performed as described previously [9]. The specimens were treated with 0.1% Triton X-100 plus 10% donkey serum for 30 min. They were then incubated overnight with primary antibodies at 4°C. The primary antibodies used were as follows: E-cadherin (1 : 200; BD Biosciences, Sparks, MD, USA) and β-catenin, (1 : 200; Santa Cruz Biotechnology, Inc., CA, USA). The preparation was rinsed 3–5 times in PBS and then incubated in the dark with secondary antibodies for 2 h at 37°C. The secondary antibodies used included donkey anti-mouse/rabbit Alexa Fluor 555 and/or donkey anti-mouse/rabbit/goat (H+L) Alexa Fluor 647 (1 : 1,000; Molecular Probes, Invitrogen Life Technologies, Carlsbad, CA, USA), and phalloidin (1 : 1000; Invitrogen). All specimens were examined with a Leica confocal laser-scanning microscope (Leica SP5, Leica Microsystems) and images were captured by the microscope.

2.8. Western Blot. Fifteen guinea pigs were sacrificed and separated into experimental and control groups. The basilar membranes were collected, as noted above, and lysed in a radioimmunoprecipitation assay buffer (50 mM Tris-HCl, 1% NP-40, 0.25% Na-deoxycholate, 150 mM NaCl, 1 mM Na_3VO_4 and NaF) containing protease inhibitors (1 μg/mL each of aprotinin, leupeptin, pepstatin, ethylenediaminetetraacetic acid, and phenyl methyl sulfonyl fluoride) in microcentrifuge tubes and were sonicated for 10 s. They were then centrifuged at 12,000g for 15 min at 4°C. The supernatant was transferred to a new microfuge tube, mixed with a sample buffer (12 mM Tris-HCl, 96 mM glycine, 10% SDS, 1% 2-mercaptoethanol, and 0.1% bromophenol blue, pH 6.8), and boiled for 5 min. The total protein was determined by the bicinchoninic acid assay protein assay (Beyotime, Beyotime Institute of Biotechnology, Jiangsu, China), and aliquots of 40 μg protein/lane for each sample were separated by electrophoresis in an 8% sodium dodecyl sulphate polyacrylamide gel using a 5% stacking gel. Resolved proteins were transferred to a nitrocellulose membrane and saturated for 30 min at room temperature with a blocking buffer (25 mM Tris (pH 8.0), 125 mM NaCl, 0.1% Tween 20, and 4% skim milk) and incubated with anti-E-cadherin (1 : 2500; BD Biosciences), anti-β-catenin (1 : 500; Santa Cruz Biotechnology), and anti-GAPDH (glyceraldehyde-3-phosphate dehydrogenase) (1 : 1000; Beyotime) antibodies for 1 h at room temperature and then overnight at 4°C, followed by incubation for 1 h in appropriate secondary antibodies conjugated with horseradish peroxidase (IgG-HRP; 1 : 1000; Beyotime, Beyotime). Immunoreactive bands were detected using an enhanced chemiluminescence system (Beyotime). Detection was performed by a Kodak imaging station 4000 MM Pro (Eastman Kodak, Rochester, NY, USA) and quantified using the ImageJ software.

2.9. Statistical Analysis. All statistical comparisons were performed with Student's t-test. Data analysis was undertaken using the SPSS software package (ver. 15.0; SPSS Inc., Chicago, IL, USA). A P value < 0.05 was taken to indicate statistical significance.

3. Results

3.1. Cochleostomy on Guinea Pig Cochlea. In this experiment, cochleostomy was performed in the basal turn near the round window. One cochlea of guinea pig with its bony coverage was shown in Figure 1. The perforation was clear and the membrane was delineated with dotted lines. The specimens from the basal membrane, suprabasal membrane, middle membrane, and apical membrane marked as the red arrows were collected and processed.

3.2. The Thermal Effect Was Intense in Animals Treated with a 10 W CO_2 Laser. Temperature changes were measured when applying the CO_2 laser. As shown in Figure 2(a), the temperature increase was significantly higher in the 10 W CO_2 laser group than in the control group (8.92 ± 2.13°C and 1.13 ± 0.32°C, respectively; $P < 0.01$).

3.3. Animals Had a Great Loss of Hearing When Treated with a 10 W CO_2 Laser. The ABR thresholds were recorded before and immediately after surgery. The mean rise in the ABR threshold after surgery was calculated and is shown in Figure 2(b). A higher ABR threshold equates to a greater degree of hearing loss. The average ABR threshold increase in the two groups was 2.5 ± 2.65 dB SPL (sound pressure level; control group) and 47.5 ± 10.5 dB SPL (10 W laser group). After surgery, when compared with the control group, the animals in the 10 W CO_2 laser group displayed a significantly large increase in their ABR threshold ($P < 0.01$).

3.4. Outer Hair Cell Collapse in Animals Treated with a 10 W CO_2 Laser. After surgery, the cochleae of each group were collected and processed for examination under SEM. Images of the basal turn of animals treated with a 10 W CO_2 laser are shown in Figure 3. The stereocilia and cuticular plates of the inner and outer hair cells and supporting cells showed a normal configuration in specimens in the control group (Figure 3(a)). In contrast, most of the outer hair cells had collapsed and derangements of the stereocilia were observed in the 10 W CO_2 laser group (Figure 3(b)) with part of them missing, especially those in the third row of the outer hair cells (arrow) in the basal turn. However, the inner hair cells showed a normal configuration. All ultrastructure in other

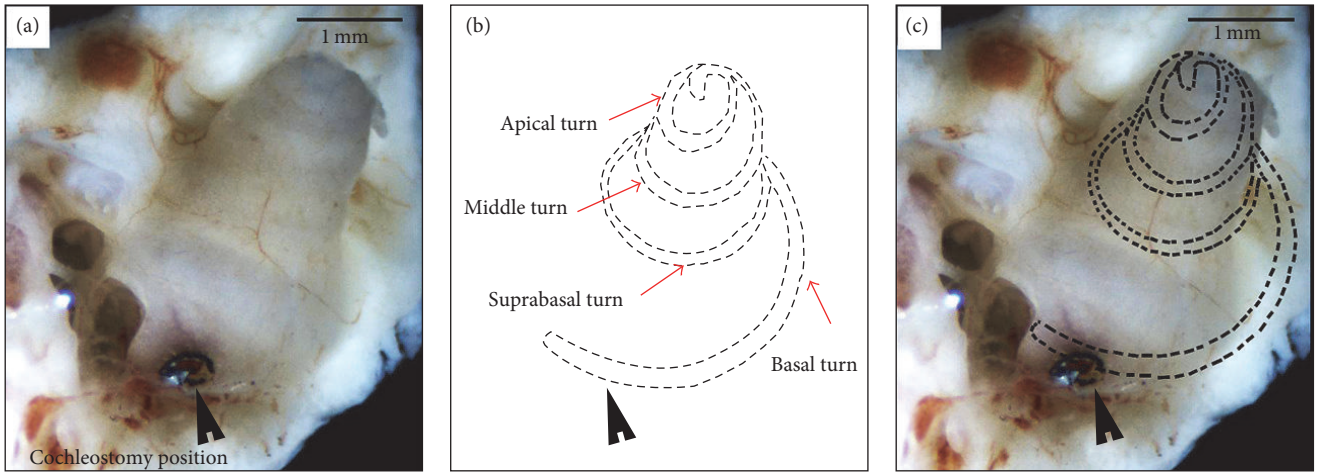

Figure 1: Cochleostomy was performed in the basal turn near the round window. (a) The perforation as the black arrow showed the cochleostomy position. (b) The cochlear membrane was delineated with dotted lines. The red arrows located the specimens from the basal turn, suprabasal turn, middle turn, and apical turn. (c) The site of the simulated cochlear membrane under the bone. Scale bar: 1 mm.

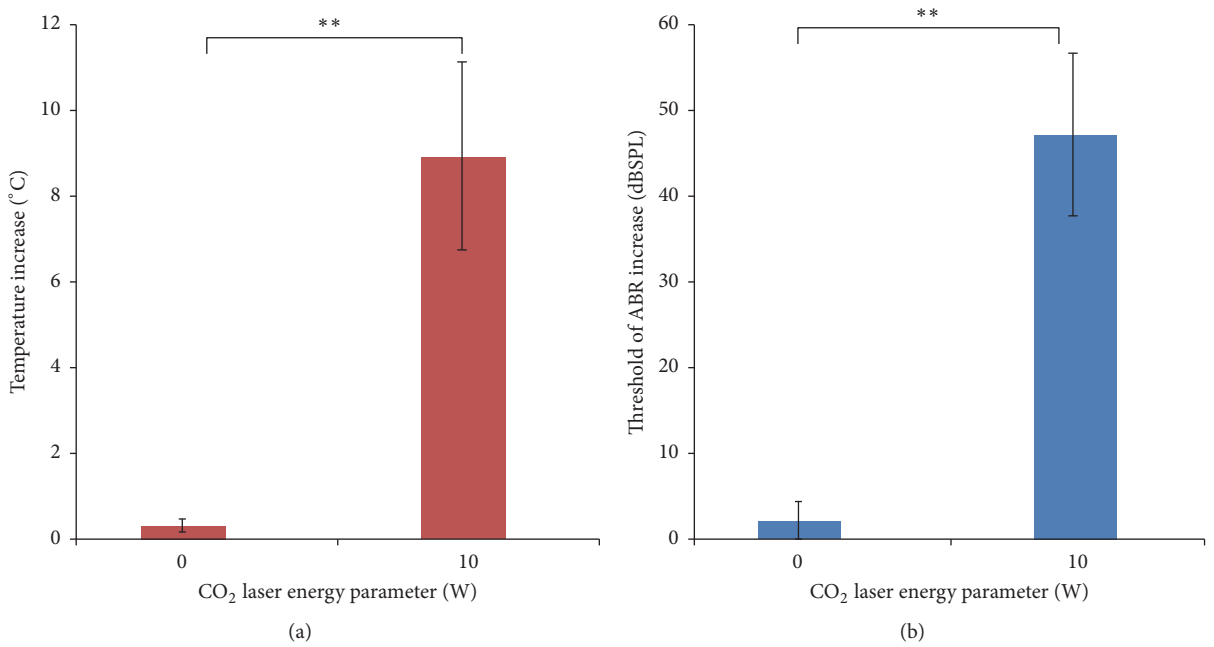

Figure 2: The temperature increase during surgery and mean incremental rise in the ABR threshold immediately after surgery by CO_2 laser irradiation (10 W laser and control groups). (a) The temperature rise in the 10 W CO_2 laser group was much higher than in the control group ($P < 0.01$). Data are presented as means + standard deviation (SD), $n = 21$, $^{**}P < 0.01$. (b) ABR threshold rise immediately after laser irradiation was higher in the 10 W laser group than the 0 W laser group ($P < 0.01$). Data are presented as means + SD, $n = 21$, $^{**}P < 0.01$.

turns showed normal appearance as the control (Data not shown).

3.5. Cell-Cell Adhesion Was Enhanced and the β-Catenin-Related Canonical Wnt-Signalling Pathway Was Activated following 10 W CO_2 Laser Treatment. The basilar membranes of basal turn on immunofluorescent staining showed positive E-cadherin and β-catenin, corresponding to cell-cell adhesion, after the application of a 10 W CO_2 laser. Images of the basal turn from the 10 W CO_2 laser group are shown in Figure 4. In the control group (Figures 4(a), 4(c), 4(e), and 4(g)), the inner and outer hair cells expressed almost no β-catenin (red, (e)) or E-cadherin (blue, (g)). However, in the 10 W laser group (Figures 4(b), 4(d), 4(f), and 4(h)), we observed strong expression of β-catenin (red) and E-cadherin (blue) in the damaged surface of the outer hair cells. The collapsed outer

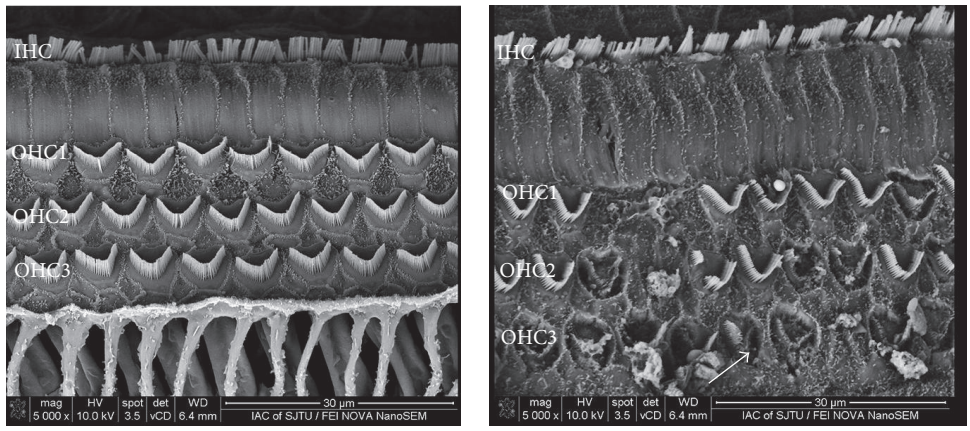

Control group (a) 10 W group (b)

FIGURE 3: SEM image of the basal turn of a cochlea immediately after applying CO_2 laser irradiation. (a) Image of the basal turn in the control group. The stereocilia and cuticular plates of the inner and outer hair cells and supporting cells showed a normal configuration. OHC1: first line of the outer hair cells; OHC2: second line of the outer hair cells; OHC3: third line of the outer hair cells; IHC: inner hair cells. Scale bar: 30 μm. (b) Image of the basal turn after applying 10 W CO_2 laser irradiation. Most of the outer hair cells had collapsed and derangements of the stereocilia were observed. Parts of the cells were missing, particularly in the third row of the outer hair cells (OHC3) in the basal turn (arrow), but the inner hair cells showed a normal configuration. Scale bar: 30 μm.

hair cell showed faint phalloidin (green, Figure 4(d)) and bold β-catenin (red, Figure 4(f)) and E-cadherin (blue) (Figure 4(h)). Western blot analysis of the proteins E-cadherin (Figure 4(i)) and β-catenin (Figure 4(j)) in the 10 W laser and control groups was quantified and is provided in Figure 4(k). The densities of the E-cadherin and β-catenin protein bands were normalised with housekeeping proteins GAPDH. The levels of E-cadherin (0.71 ± 0.14) and β-catenin (1.29 ± 0.16) were found to be significantly increased in CO_2 laser injuries (the 10 W laser group) compared with the control group (0.37 ± 0.01 and 0.89 ± 0.05, respectively; $P < 0.05$).

4. Discussion

The CO_2 laser used in this research has a handheld energy delivery system with a hollow-core fibre that can transfer the laser beam at various angles and distances and comes with various handheld accessories of differing lengths and flexibility. These devices expand the application of CO_2 lasers in ENT surgery [10–12]; fibre-enabled CO_2 has practical advantages, especially in cases with complex anatomical conditions [12]. In the guinea pig, a temporal bone study had already indicated that laser settings of between 4 and 10 W were sufficient for creating the cochleostomy [7]. In this study, we used a 10 W fibre-enabled CO_2 laser to establish an inner ear injury with hearing loss and damaged ultrastructure.

In our study, the 10 W CO_2 laser (606 J/cm^2) used for cochleostomy produced a rise in temperature of $8.92 \pm 2.13^{\circ}$C in the membrane of the round window. Kamalski et al. also observed such thermal effects when evaluating temperature increases during exposure to laser irradiation [8]. Along with an increase in temperature, the ABR threshold also increased by 47.5 ± 10.9 dB SPL in our 10 W CO_2 laser group. These findings demonstrated a strong relationship with the morphological changes observed within the cochleae. The ultrastructure of the basal turn of the cochlea in laser-treated animals showed various changes, whereas no obvious ultrastructure change was found in the rest parts of the cochlea. Changes in the outer hair cells were more evident than in the inner hair cells, particularly in the third row as seen in our SEM examinations. Most of the outer hair cells had collapsed, and derangements and even loss of the stereocilia were observed, while the outer hair cells acted as cochlear amplifier. Prestin on the outer hair cell membrane is the basis of cochlear amplification in mammals [13]. Okunade and Santos-Sacchi found that prestin is remarkably responsive to fast temperature jumps [14]. We assume the alteration of the prestin may partly explain the irreversible hearing loss.

The E-cadherin/β-catenin complex plays an important role in maintaining epithelial integrity, and disrupting this complex affects not only the adhesive repertoire of a cell but also the Wnt-signalling pathway [15]. However, the question of whether and how the Wnt-signalling pathway plays a role in thermal injuries of the inner ear following laser application remains unanswered. In our experiment, we observed that the areas of injured hair cells showed positive E-cadherin and β-catenin expressions after excessive laser irradiation. Furthermore, there were strong colocalised expressions of E-cadherin and β-catenin in the membrane of the injured hair cells and around the supporting cells. Karpowicz et al. showed that the overexpression of E-cadherin can aid the self-renewal of neural stem cells and increases their number in vitro [16]. In addition, the research of Chen et al. suggested that the overexpression of E-cadherin by viral transduction was sufficient to enhance the generation of induced pluripotent

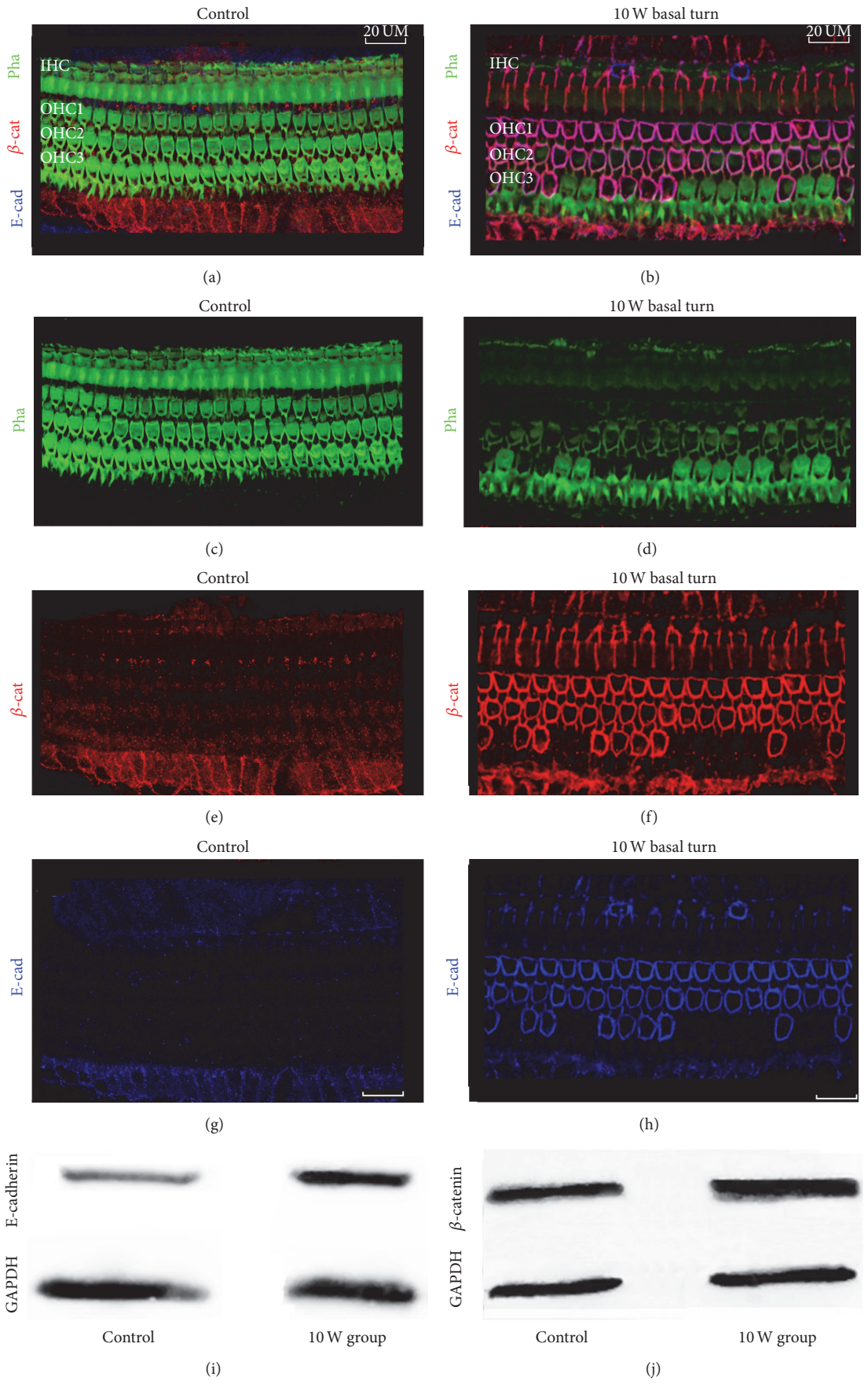

Figure 4: Continued.

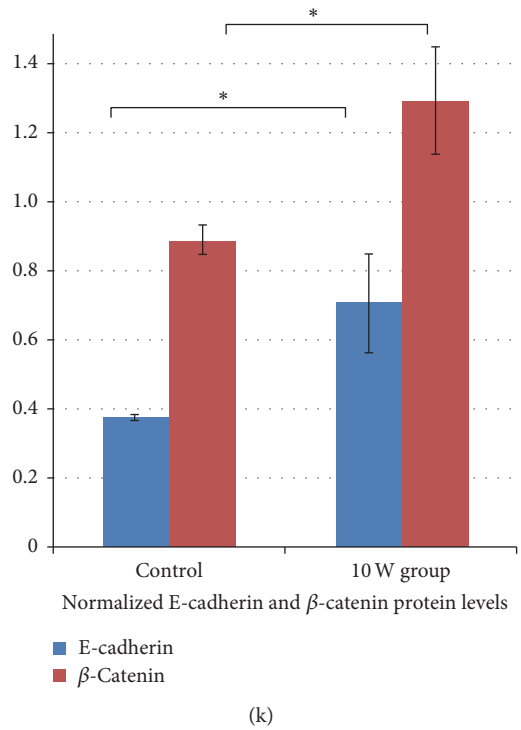

(k)

FIGURE 4: The expression of β-catenin and E-cadherin in the sensory epithelium changed after applying CO_2 laser irradiation. Surface views of the organ of Corti in the basal turn ((a), (c), (e), and (g)) in the control group and ((b), (d), (f), and (h)) in the 10 W laser group. The samples were stained for phalloidin (green, (c), (d)), β-catenin (red, (e), (f)), and E-cadherin (blue, (g), (h)). In the 10 W laser group, we observed overexpression of β-catenin (red) and E-cadherin (blue) in the damaged surface of the outer hair cells. ((i), (j)) Western blot analysis of E-cadherin (i) and β-catenin (j) proteins in the cochleae of the 10 W laser and control groups, which is quantified and plotted in (k). The densities of the E-cadherin and β-catenin protein bands were normalised with GAPDH ((i), (j)). Data are presented as means + SD; $n = 15$, $^*P < 0.05$. Scale bar: 20 μm. pha: phalloidin; E-cad: E-cadherin; β-cat: β-catenin. Scale bar: 20 μm.

stem cells [17]. That is to say, the upregulation of E-cadherin in the membrane may suggest stronger cell-cell adhesions in the surfaces of the injured hair cells to protect the hair cells from further damage or to enhance the self-rehabilitation of the injured cells after laser irradiation.

In our experiment, there was increased expression of β-catenin in the 10 W laser group, particularly in the membrane. We therefore assumed that β-catenin was redistributed on behalf of a rise in cell-cell adhesion following hair cell damage, and this may protect the hair cells from further damage by moving from the cytoplasm and nucleus to the membrane and activating the Wnt pathway synergistically with E-cadherin. It may be useful to explore the assumption that the Wnt pathway could lead to regeneration under some conditions, such as after damage. How β-catenin-related canonical Wnt signalling influences the rehabilitation or regeneration of damaged hair cells after thermal injury has not yet been demonstrated. Therefore, further studies are required in the future.

Results have shown that when the CO_2 laser exceeds the safe operating levels, this results in hair cell collapse and deranged stereocilia, particularly in the outer hair cells and, more surprisingly, causes the upregulation of E-cadherin and β-catenin in the injured hair cell membranes, suggesting that these could play a role in the overall injury mechanism. Stimulation of Wnt/β-catenin may be an avenue to explore for the replacement of adult cochlear hair cells, a sought-after goal for the treatment of sensorineural deafness, which is commonly caused by the loss of hair cells in humans.

Competing Interests

The authors report no competing interests pertaining to this work.

Authors' Contributions

All authors participated in the design, interpretation of the studies and analysis of the data, and review of the manuscript; Xiang Liu, Xiao-qing Qian, and Dong-Dong Ren conducted the experiments, Rui Ma and Dong-Dong Ren photographed and processed the figures, Xiang Liu and Dong-Dong Ren wrote the manuscript, and Fang-Lu Chi revised the manuscript. Xiang Liu and Xiao-qing Qian contributed equally to this work.

Acknowledgments

This study was supported by Key Project of Chinese National Programs (2016YFC0905200), the National Natural Science Foundation of China (NSFC) Grants nos. 81420108010

and 81271084 to Fang-Lu Chi and 81370022, 81570920, and 81000413 to Dong-Dong Ren, 973 Program (Grants nos. 2011CB504500 and 2011CB504506) and the Innovation Project of Shanghai Municipal Science and Technology Commission (Grant no. 11411952300) to Fang-Lu Chi, and the Training Program of the Excellent Young Talents of the Shanghai Municipal Health System (Grant no. XYQ2013084) and "Zhuo-Xue Plan" of Fudan University to Dong-Dong Ren.

References

[1] R. C. Perkins, "Laser stapedotomy for otosclerosis," *Laryngoscope*, vol. 90, no. 2, pp. 228–241, 1980.

[2] S. G. Lesinski and A. Palmer, "Lasers for otosclerosis: CO2 vs. Argon and KTP-532," *Laryngoscope*, vol. 99, no. 6, pp. 1–8, 1989.

[3] S. Jovanovic, U. Schönfeld, R. Fischer et al., "Thermic effects in the "vestibule" during laser stapedotomy with pulsed laser systems," *Lasers in Surgery and Medicine*, vol. 23, no. 1, pp. 7–17, 1998.

[4] J. Kiefer, J. Tillein, Q. Ye, R. Klinke, and W. Gstoettner, "Application of carbon dioxide and erbium:yttrium-aluminum-garnet lasers in inner ear surgery: an experimental study," *Otology & Neurotology*, vol. 25, no. 3, pp. 400–409, 2004.

[5] D. Ren, J. Sun, G. Wan, F. Yang, and F. Shen, "Influence of carbon dioxide laser irradiation on the morphology and function of guinea pig cochlea," *Journal of Laryngology and Otology*, vol. 119, no. 9, pp. 684–692, 2005.

[6] D.-D. Ren and F.-L. Chi, "Experimental study on thermic effects, morphology and function of guinea pig cochlea: a comparison between the erbium:yttrium-aluminum-garnet laser and carbon dioxide laser," *Lasers in Surgery and Medicine*, vol. 40, no. 6, pp. 407–414, 2008.

[7] A. J. Fishman, L. E. Moreno, A. Rivera, and C.-P. Richter, "CO_2 laser fiber soft cochleostomy: development of a technique using human temporal bones and a guinea pig model," *Lasers in Surgery and Medicine*, vol. 42, no. 3, pp. 245–256, 2010.

[8] D. M. A. Kamalski, R. M. Verdaasdonk, T. De Boorder, R. Vincent, F. Trabelzini, and W. Grolman, "Comparison of KTP, Thulium, and CO_2 laser in stapedotomy using specialized visualization techniques: thermal effects," *European Archives of Oto-Rhino-Laryngology*, vol. 271, no. 6, pp. 1477–1483, 2014.

[9] W.-W. Luo, J.-M. Yang, Z. Han et al., "Atoh1 expression levels define the fate of rat cochlear nonsensory epithelial cells in vitro," *Molecular Medicine Reports*, vol. 10, no. 1, pp. 15–20, 2014.

[10] A. E. Albers, W. Wagner, K. Stölzel, U. Schönfeld, and S. Jovanovic, "Laser stapedotomy," *HNO*, vol. 59, no. 11, pp. 1093–1102, 2011.

[11] M. Remacle, A. Ricci-Maccarini, N. Matar et al., "Reliability and efficacy of a new CO_2 laser hollow fiber: a prospective study of 39 patients," *European Archives of Oto-Rhino-Laryngology*, vol. 269, no. 3, pp. 917–921, 2012.

[12] C. Brase, J. Schwitulla, J. Künzel, T. Meusel, H. Iro, and J. Hornung, "First experience with the fiber-enabled CO2 laser in stapes surgery and a comparison with the "one-shot" technique," *Otology and Neurotology*, vol. 34, no. 9, pp. 1581–1585, 2013.

[13] L. Song and J. Santos-Sacchi, "Conformational state-dependent anion binding in prestin: evidence for allosteric modulation," *Biophysical Journal*, vol. 98, no. 3, pp. 371–376, 2010.

[14] O. Okunade and J. Santos-Sacchi, "IR laser-induced perturbations of the voltage-dependent solute carrier protein SLC26a5," *Biophysical Journal*, vol. 105, no. 8, pp. 1822–1828, 2013.

[15] X. Tian, Z. Liu, B. Niu et al., "E-Cadherin/β-catenin complex and the epithelial barrier," *Journal of Biomedicine and Biotechnology*, vol. 2011, Article ID 567305, 6 pages, 2011.

[16] P. Karpowicz, S. Willaime-Morawek, L. Balenci, B. Deveale, T. Inoue, and D. Van Der Kooy, "E-Cadherin regulates neural stem cell self-renewal," *Journal of Neuroscience*, vol. 29, no. 12, pp. 3885–3896, 2009.

[17] T. Chen, D. Yuan, B. Wei et al., "E-cadherin-mediated cell-cell contact is critical for induced pluripotent stem cell generation," *Stem Cells*, vol. 28, no. 8, pp. 1315–1325, 2010.

Hindawi Publishing Corporation
Neural Plasticity
Volume 2016, Article ID 8648297, 12 pages
http://dx.doi.org/10.1155/2016/8648297

Research Article

Effect of Endolymphatic Hydrops on Sound Transmission in Live Guinea Pigs Measured with a Laser Doppler Vibrometer

Chen-Ru Ding,[1,2,3] Xin-Da Xu,[1,2,3] Xin-Wei Wang,[1,2,3] Xian-Hao Jia,[1,2,3] Xiang Cheng,[1,2,3] Xiang Liu,[1,2,3] Lin Yang,[3,4] Bu-Sheng Tong,[5] Fang-Lu Chi,[1,2,3] and Dong-Dong Ren[1,2,3]

[1]*Department of Otology and Skull Base Surgery, Eye Ear Nose & Throat Hospital, Fudan University, Shanghai 200031, China*
[2]*Shanghai Auditory Medical Center, Shanghai, China*
[3]*Key Laboratory of Hearing Science, Ministry of Health, Shanghai, China*
[4]*Research Center, Eye Ear Nose & Throat Hospital, Fudan University, Shanghai 200031, China*
[5]*The First Affiliated Hospital of AnHui Medical University, Hefei, China*

Correspondence should be addressed to Fang-Lu Chi; chifanglu@126.com and Dong-Dong Ren; dongdong_ren@163.com

Received 28 July 2016; Revised 11 October 2016; Accepted 2 November 2016

Academic Editor: Renjie Chai

Objective. This study aimed at describing the mechanism of hearing loss in low frequency and the different dynamic behavior of the umbo, the stapes head, and the round window membrane (RWM) between normal guinea pigs and those with endolymphatic hydrops (EH), using a laser Doppler vibrometer (LDV). *Methods*. Cochlear sections were stained with hematoxylin and eosin (HE) to evaluate the hydropic ratio (HR). Auditory brainstem responses (ABR) and whole-mount immunostaining were measured. Displacement of the umbo, stapes head, and RWM in response to ear-canal sound was evaluated using a LDV. *Results*. Mean HR values in EH model of all the turns are larger than the control group. The ABR threshold of the EH group was significantly higher than that of the control. Strong positive correlation was found between HR at apical turn and ABR threshold elevation at 1000 Hz and at subapical turn and ABR threshold elevation at 2000 Hz. FITC-phalloidin immunostaining of the cochlear basilar membrane in the apical, subapical, and suprabasal turns showed missing and derangement stereocilia of third-row outer hair cells. The umbo, stapes head, and RWM displacement in ears with EH was generally lower than that of normal ears. The EH-induced differences in stapes head and RWM motion were significant at 0.5 kHz. *Conclusion*. The LDV results suggested that the higher inner ear impedance in EH affected the dynamic behavior of the two opening windows of the cochlea and then reduced the vibration of the ossicular chain by increasing the afterload, resulting in acoustic dysfunction. The vibration reduction mainly occurred at low frequencies, which has related with the morphology changes of the apical and subapical turns in EH model.

1. Introduction

In mammals, sound waves stimulate the cochlea via the vibration of the ossicular chain. The opposite vibrating phase between the round window and the oval window causes relative motion between the endolymph and perilymph and thus produces displacement waves travelling on the spirally basilar membrane. The motion of hair cell stereocilia created by basilar membrane (BM) vibration gates stereocilia transduction channels, leading to the generation of hair cell receptor potential and the excitation of afferent auditory nerve fibers [1]. Changes in cochlear lymphatic fluid homeostasis may result in cochlear acoustic dysfunctions, like endolymphatic hydrops (EH), semicircular canal dehiscence, labyrinthine fistulas, and so forth [2, 3].

Since Hallpike and Carins [4] described the presence of EH in the temporal bones of patients with Ménière's Disease (MD) in 1938, EH has generally been accepted as the basic histopathologic sign of this disease, which is an intractable disease that results in hearing loss that is often fluctuating and initially involves the low frequencies [5]. Wu et al. [6] reported that low-tone and middle-tone hearing thresholds were related to the severity of EH in the cochlea. In the study by Lee et al. [3], spontaneous low frequency air-bone gaps in evaluating hearing sensitivity were found in approximately 13.9% of patients with Ménière's Disease and may indirectly

reflect aggravation of the EH in the cochlear and the vestibular compartments. Yoshida et al. [7] suggested an association between endolymphatic hydrops and low frequency hearing loss in a 13-year-old girl with mutation of the SLC26A4 gene. Endolymphatic hydropic condition was described in certain cases of sudden deafness [8, 9]. Noguchi et al. [10] assumed that EH give rise to the pathogenesis of acute low-tone sensorineural hearing loss (ALHL) with little or no impairment of hair cells that resembles early-stage MD. It is widely hypothesized that the hydrops generates the clinical symptoms of this illness. Yet, there are few studies that have investigated how the dilated endolymph affects the middle ear acoustic transmission.

A laser Doppler vibrometer (LDV) is a noncontact, established optical technique that can be used to measure the displacement of middle ear components in response to sound stimulation [11–16]. It uses the Doppler-shift principle to determine the instantaneous velocity of a moving object by comparing the frequency of the laser's emitted light with the frequency of the light reflected from the moving object. This technique has been used to test the vibration of the round window membrane (RWM), the tympanic membrane (TM), and the stapes footplate in fresh and embalmed cadaveric human temporal bone and animal specimens. Moreover, animal models of different diseases have been created to investigate vibration changes in the ossicular chain and RWM, to explore the potential mechanism underlying the clinical symptoms of diseases. For instance, vibration of the RWM that is associated with acute otitis media is significantly decreased compared with those of the RWM from the ears of normal guinea pigs [15]. Moreover, middle ear effusion reduces the mobility of the TM, the incus tip, and the RWM at frequencies above 1 kHz in guinea pigs [17]. The mechanical properties of the incudostapedial joint directly affect the stapes movement or the middle ear transfer function for sound transmission [18]. However, no prior study has reported changes in the dynamic behavior of the umbo, the stapes head, and the RWM in association with EH.

To better understand how EH affects the sound transmission process and hearing loss in low frequency, we used guinea pigs to create EH models and measured the hydropic ratio (HR) and morphology in each turn, the vibration of the umbo, stapes head, and RWM, as well as the auditory-evoked brainstem response (ABR). The primary objective of this study was to compare the different dynamic properties of the ossicular chain and the RWM between normal and EH guinea pigs and explore the potential pathogenic mechanism underlying the associated hearing loss at low frequencies.

2. Material and Methods

2.1. Animals. All animal work conducted during the course of this study was approved by the institutional animal care and use committee at Eye Ear Nose & Throat Hospital, Fudan University, and conformed to the National Institutes of Health guide for care and use of laboratory animals.

Eighteen healthy albino male guinea pigs with an initial weight of 250 g–300 g and a positive Preyer reflex were used in this study. All animals were free of middle ear diseases, such as tympanic membrane perforation or otitis media, as evaluated by otoscopic examination. Identification of preexisting abnormalities of auditory function was made by a prerecruiting ABR measurement in each animal. If an abnormal response was found, the animal was excluded from the study. Guinea pigs were randomly allocated into two groups, the control group (9 guinea pigs with sham surgical procedure in the right ear) and the EH group (9 guinea pigs with obliteration of the endolymphatic sac in the right ear). Animals in the two groups were raised for 8 weeks postoperatively. Specimens from each group (control and EH) were used for histologic observations of paraffin sections (six ears) and whole-mount immunostaining (three ears).

2.2. Surgical Procedure

2.2.1. Creation of EH Model. The right ears of the nine animals in the EH group were prepared. The obliteration of the endolymphatic sac was performed surgically using an extradural posterior cranial fossa approach, under sterile conditions and under a surgical microscope (6030116204, Carl Zeiss, Jena, Germany). The right ears of the nine animals in the control group were subjected to sham operation. Exposure of the sigmoid sinus through the occipital bone was accomplished without obliteration of the endolymphatic sac. The temperature was maintained stably to keep animals warm during surgery, by using an electric heating pad. Anesthesia was induced with a combination of ketamine hydrochloride (35 mg/kg, intramuscular injection) and 1% xylazine hydrochloride (10 mg/kg, subcutaneous injection). Additional anesthesia was administered as required to maintain areflexia.

2.2.2. Preparation of the Umbo, Stapes Head, and RWM for LDV Measurement. The right ears from six animals in the control group as well as those from the EH group were prepared. After anesthesia (as also described above), the right auricles were cut off and the dorsal auditory bulla was opened into a square block under a surgical microscope (6030116204, Carl Zeiss, Jena, Germany), from which the incus-stapes complex, RWM, and the medial side of the umbo could be viewed clearly (Figure 1). A 0.25–0.5-mm^2 square (approximately 2–4 pieces, each piece with a mass of 40 μg) of laser reflective tape (3 M, Maplewood, MS, USA) was placed on the medial side of the umbo, the stapes head, and the middle of the RWM, as the laser-reflecting target (Figures 1(a)–1(d)). The mass of these pieces was deemed small enough not to affect the measurement. Membrane structures were not damaged during the preparation. Hemorrhagic spots were remedied through unipolar electrocoagulation.

2.3. ABR Measurement. ABR measurements in the control group and in the 8-week EH group were performed before the surgery and prior to the LDV measurement. After anesthesia, the ABR (Bio-Logic NAVPRO, 580-NAVPR2, Natus Medical Incorporated, Pleasanton, CA, USA) were tested in a sound-proofed booth to assess the auditory threshold. Needle electrodes were placed subcutaneously at the vertex for recording and behind the bilateral ears as reference and

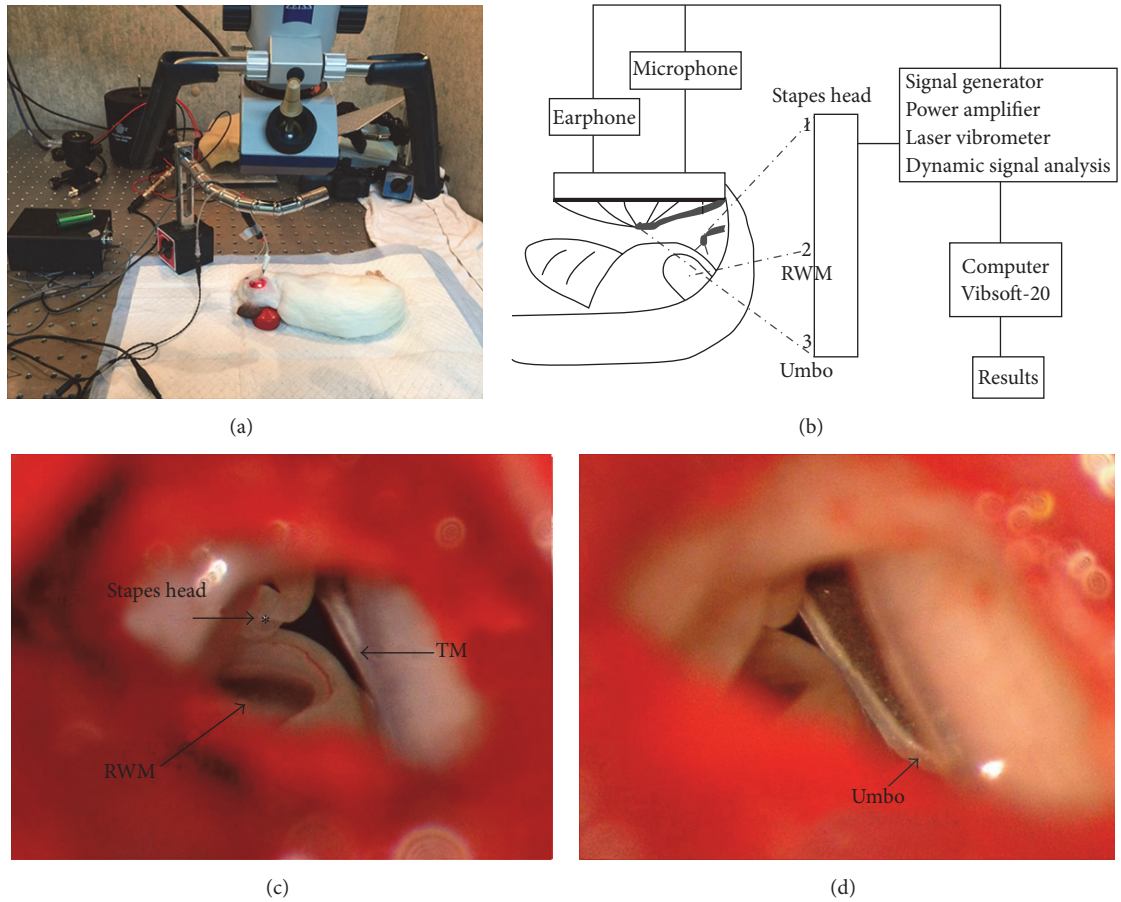

Figure 1: (a) the measurement system included a Compact Laser Vibrometer coupled with a microscope with a micromanipulator, signal generator, and power amplifier. (b) The schematic diagram of the laser Doppler vibrometer (LDV) detecting system. (c and d) The incus-stapes complex, round window membrane, and the medial side of the umbo, viewed from the opened middle ear cavity. The laser reflective tapes were placed at the location marked with an ∗ ((c) stapes head and middle of the RWM; (d) umbo).

ground electrodes. Stimulation was presented as tone bursts (5 ms duration, 0.5 ms rise-fall time, Blackman envelope) at a frequency of 0.5, 1, 2, 4, 6, and 8 kHz; the sound-intensity level was decreased in 10 dB steps from 80 to 20 dB SPL; 500 responses at each sound level were recorded and averaged. If I, III, and V waves disappeared, we increased the tone bursts by 5 dB repeatedly to judge the threshold by the waveform.

2.4. LDV Measurement. The measurement system included a Compact Laser Vibrometer (CLV-2534-4, Polytec, Wurzburg, Germany) coupled with a microscope (OPMI 1-FC, Carl Zeiss, Jena, Germany) with a micromanipulator (A-HLV-MM30, Polytec, Wurzburg, Germany), signal generator (33210A, Agilent, Santa Clara, CA, USA), and power amplifier (RMX 850, QSC, Costa Mesa, CA, USA) (Figure 1(a)). The intensity of each excitation frequency was calibrated to 85 dB SPL using a sound-level meter (AWA-5661-1B, AiHua, Yiyang City, China). An earphone associated with the microphone (ER-4PT, ER-7C, HLV-SPEC Adapter, Etymotic, Elk Grove Village, IL, USA) was inserted into the osseous external auditory canal to give signal stimuli and monitor sound pressure. The distance between the tympanic membrane and the earphone and microphone was maintained at 1 mm. The vibration of the moving surface was acquired through the reflective bead by the system and recorded on computer software (Vibsoft-20, Polytec, Wurzburg, Germany) for further analysis. The vibration amplitude of the moving surface was calculated from the voltage output of the laser vibrometer's velocity decoder. Appropriate anesthesia (subcutaneous injection of 10 mg/kg xylazine hydrochloride 1 h after normal anesthesia described above) was maintained to retain respiratory amplitude so as not to affect the test during the process. Testing was conducted in a sound-proofed booth to maintain a high signal-to-noise ratio. For each stimulus frequency, sound stimuli were repeated three times with a good signal-to-noise ratio, after which all data were averaged.

2.5. Section Processing. Six animals of each group were sacrificed by an overdose of anesthetic; intracardiac perfusion was performed with 150 mL of 0.2 M PBS, followed by 4% polymerized formaldehyde, and the temporal bones were then removed and fixed in 4% polymerized formaldehyde (pH = 7.4) for more than 24 h at 4°C. The temporal bones were decalcified in ethylenediaminetetraacetic acid, dehydrated

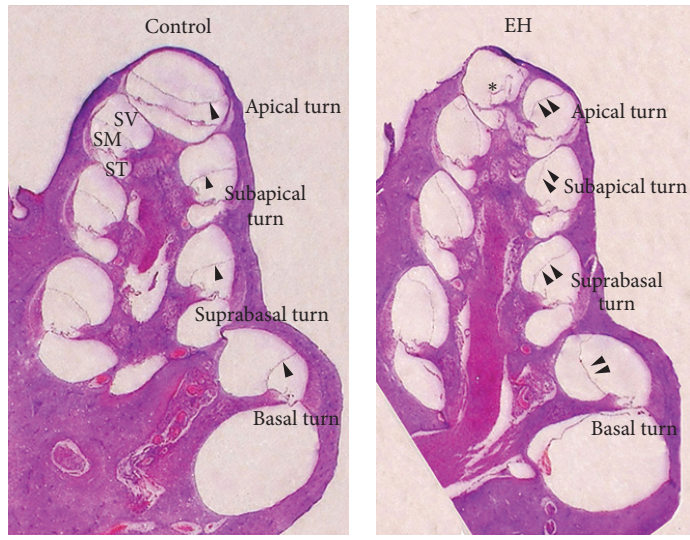

(a) (b)

Figure 2: Mid-modiolar hematoxylin and eosin-stained section of the cochlea in the right ears of the control group (a) and the 8-week endolymphatic hydrops (EH) group (b). SV: scala vestibuli; SM: scala media; ST: scala tympani; arrowhead: Reissner's membrane in the control group; double arrowheads: distention of Reissner's membrane in the 8-week EH group; ∗: rupture of Reissner's membrane due to artifact in the apical turn.

in increasingly higher concentrations of alcohol, embedded in paraffin, and sectioned serially at 10 μm in the plane parallel to the modiolus. Cochlear sections were stained with hematoxylin and eosin (HE) and then observed under a light microscope (6030116204, Carl Zeiss, Jena, Germany).

2.6. Whole-Mount Immunostaining. Three guinea pigs of each group were killed by means of decapitation by overdose anesthesia. Under magnification, the tympanic bullae were dissected from the surrounding tissues; the bony wall of the cochlea was removed with a pick and forceps to expose the upper aspect of the organ of Corti. Cochleae were fixed in a 4% paraformaldehyde (PFA) in phosphate-buffered saline (PBS) for 24 hours and then we dissected the cochlea and get the basilar membrane of the cochlea. The whole-mount tissues were incubated with Alexa Fluor 488-conjugated phalloidin (Invitrogen, USA, 1 : 1000) for 30 minutes to stain for F-actin prior to mounting. Confocal fluorescent microscope (Zeiss, LSM800, Germany) was used in scanning the surface image of Corti stained for stereocilia with green phalloidin.

2.7. Quantification of the Hydropic Ratio (HR) of the EH Models. In order to quantify the hydropic ratio (HR) of the EH models, a proportional measurement was conducted. Areas of scala media (SM) and scala vestibule (SV) (Figure 3(a)) were first obtained by using Photoshop CS6 and scala media area ratio (SMR) was calculated in formula

$$\mathrm{SMR} = \frac{\mathrm{SM}_{\mathrm{area}}}{\mathrm{SM}_{\mathrm{area}} + \mathrm{SV}_{\mathrm{area}}}. \quad (1)$$

As deviations in the plane of section and interanimal variability in anatomy cannot be avoided exactly, SMR is imprecise for representing hydropic degree of EH animals. Then we use the ratio of SMR in the EH ear divided by SMR in the contralateral ear to quantify the hydropic degree in the EH group, whose right ears were subject to obliteration of the endolymphatic sac. And this ratio was named as hydropic ratio (HR) here. In formula

$$\mathrm{HR} = \frac{\text{SMR in the EH ear}}{\text{SMR in the contralateral ear}} \quad (2)$$

a HR value of one suggests no hydrops in the given turn.

This is when hydropic ratio is close to 1; that to say, there is no hydrops in the given turn.

2.8. Statistical Analysis. Data are presented as mean ± standard error. All analysis was performed using the SPSS 19.0 statistical package. Two-tailed Students' t-tests were used to determine the confidence interval for comparison between two groups and p values ≤ 0.05 were considered significant. Spearman bivariate correlation analysis was taken to explore the relationship between ABR threshold elevation and endolymphatic hydropic ratio.

3. Results

3.1. Observation of Tissue Sections of the Cochlea in Ears with EH. The mid-modiolar HE-stained section of the cochlea showed that there was no displacement of Reissner's membrane in the control ear and the angle between Reissner's membrane and the osseous spiral lamina was almost 45°, suggesting that there was no EH in the control group (Figure 2(a)). Figure 2(b) illustrates that Reissner's membrane of each turn bulged significantly towards the scala vestibule in the 8-week EH group. Reissner's membrane was

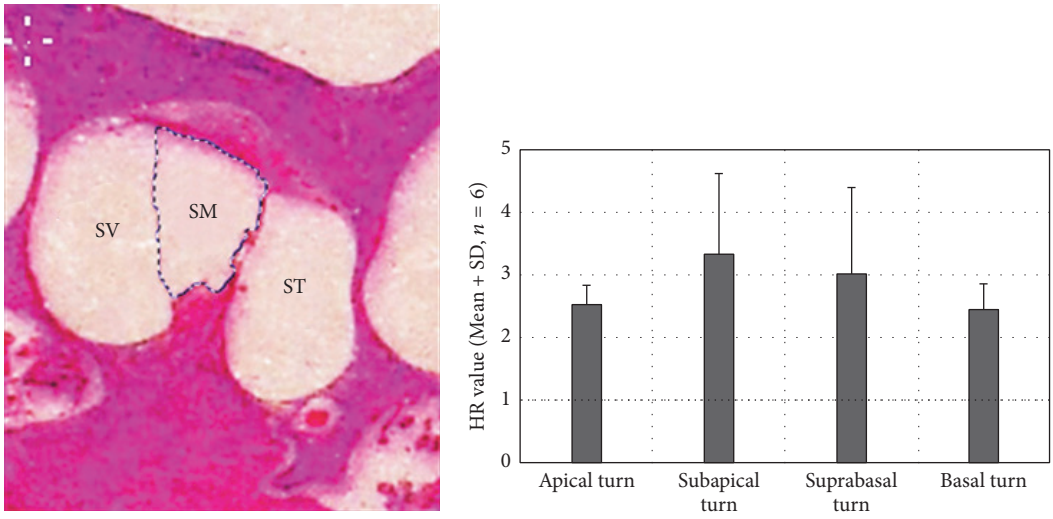

Figure 3: Mean HR value of each turn in the EH models. (a) HR was measured by the area of SM and SV. SM means the scala media, SV means scala vestibule, and ST means scala tympani. (b) Subapical turn had developed the most prominent hydrops with a mean HR value of 3.34, secondly followed by suprabasal turn. Mean HR values of all the turn are larger than 1 (dotted line: an indicator of no EH existence).

Table 1: HR for each turn in the EH models.

Animal number	HR for each turn			
	Apical turn	Subapical turn	Suprabasal turn	Basal turn
1	3.024615	3.167749	2.523004	2.537709
2	2.369168	3.506736	2.762338	1.780297
3	2.284045	1.856286	2.01498	2.967329
4	2.238242	5.37974	5.556607	2.300098
5	2.531883	2.139673	1.747295	2.373561
6	2.753971	4.046874	3.527099	2.790851
Mean ± SD	2.53 ± 0.30	3.34 ± 1.29	3.02 ± 1.38	2.45 ± 0.41

attached to the bony wall of the scala vestibule (SV) in the subapical turn of the cochlea. A high level EH was observed in the subapical turn, while the EH in the basal turn was markedly more moderate. These results agreed with those from a previous study by Chi and Liang [19] and indicated that the chronic EH model was successfully created.

3.2. Quantification of the Hydropic Ratio (HR) of the Four Turns in EH Models. In order to observe the extent of EH, we had quantified the HR in each turn of the cochlea. When hydropic ratio is close to 1, there is no labyrinthine hydrops in the given turn. The HR is much larger according to the most serious hydrops in the scala media. The results of the individual and average HR for each turn of all animals in the EH group are shown at Table 1 and Figure 3(b). HR values for all turns of the six EH models were obviously larger than 1 ($p < 0.05$), demonstrating that conspicuous hydrops was induced. The most serious labyrinthine hydrops is in the subapical turn, and the second is in the suprabasal turn.

3.3. Effect of EH on ABR Measurement. The auditory threshold of guinea pigs was assessed from the ABR threshold. The results of the ABR threshold in the control group and EH group are listed in Table 2 and Figure 4(a). Both the mean and standard deviation of each group were recorded. Elevation of the ABR threshold was observed in ears associated with EH. The ABR threshold was elevated in the EH group relative to the control group by more than 25 dB at 2, 4, 6, and 8 kHz and by less than 25 dB at 0.5 and 1 kHz. Student's t-tests revealed that the mean ABR threshold of the EH cases was significantly higher than that of the control group at 0.5, 1, 2, 4, 6, and 8 kHz ($p < 0.05$).

Spearman bivariate correlation analysis was taken to explore the relationship between ABR threshold elevation and extent of the endolymphatic hydrops. Strong positive correlation was found between HR at apical turn and ABR threshold elevation at 1000 Hz ($r = 0.82$, correlation is significant at the 0.01 level), as well as between HR at subapical turn and ABR threshold elevation at 2000 Hz ($r = 0.88$, correlation is significant at the 0.05 level). No significant correlations were found among the remainder. Results were presented in Figures 4(b) and 4(c).

3.4. Effect of EH on Movement of Umbo, Stapes Head, and RWM. The LDV measurements showed clear differences

Table 2: The ABR threshold of the control group and EH group at the frequency of 0.5, 1, 2, 4, 6, and 8 kHz.

Frequency (Hz)	Before surgery in control	8 weeks after surgery in control	Before surgery in EH	8 weeks after surgery in EH
	Mean ± Std. deviation (dB SPL)			
500	34.17 ± 4.91	35 ± 2.58	34.17 ± 5.84	54.17 ± 3.96
1000	25.8 ± 3.76	26.67 ± 2.1	31.67 ± 4.08	48.33 ± 3.33
2000	25.8 ± 2.04	24.17 ± 0.83	27.5 ± 4.18	49.17 ± 5.07
4000	24.17 ± 3.76	23.33 ± 1.67	25.8 ± 2.04	50 ± 5.32
6000	30.83 ± 5.84	31.67 ± 2.47	28.33 ± 2.58	57.5 ± 6.16
8000	33.33 ± 7.52	30.83 ± 3.75	31.67 ± 2.58	68.33 ± 8.23

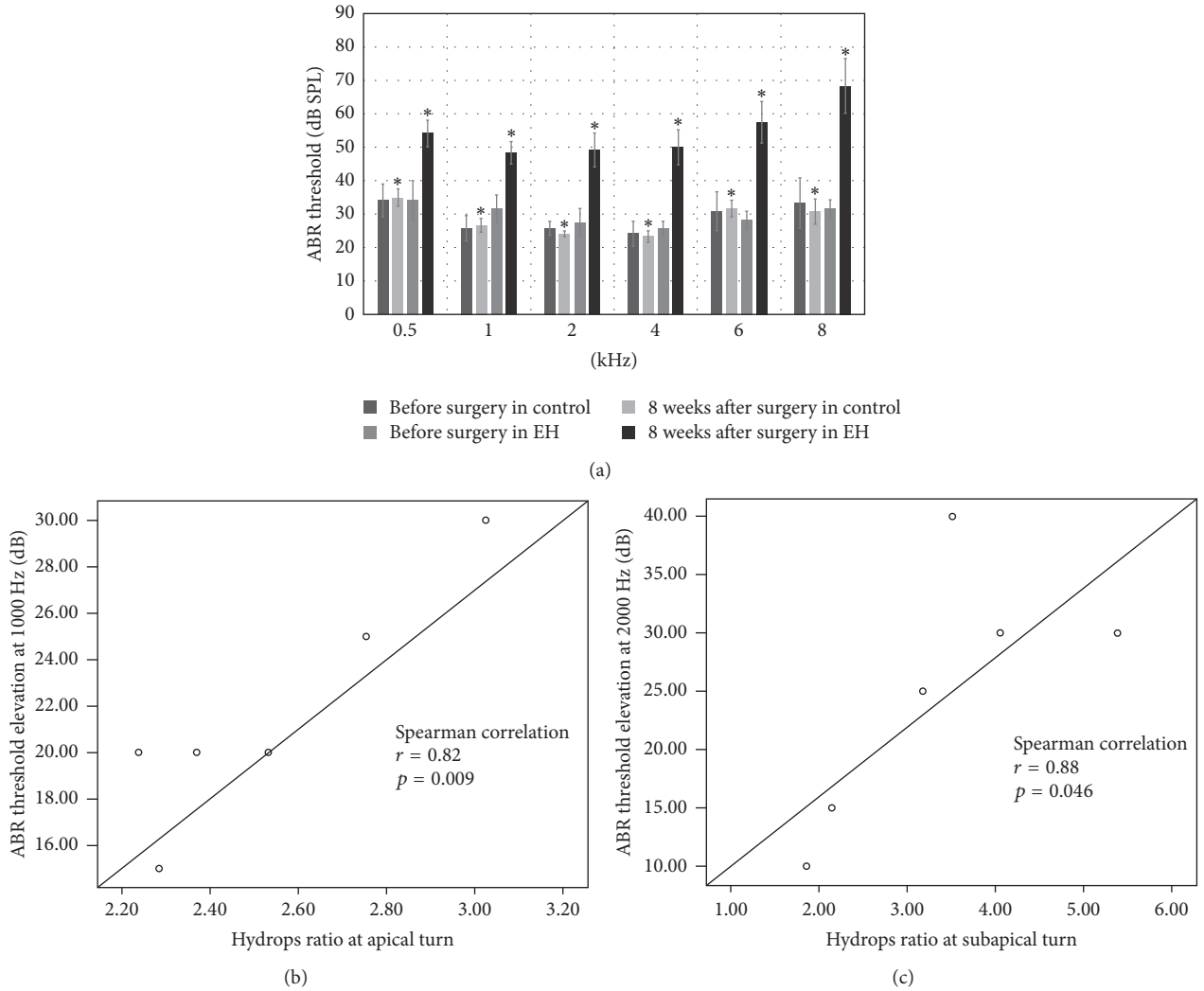

Figure 4: (a) The mean thresholds of ABR were recorded before surgery and 8 weeks after surgery in control and EH group. The mean ABR threshold of the EH cases was significantly higher than that of the control group at 0.5, 1, 2, 4, 6, and 8 kHz ($^{*}p < 0.05$) 8 weeks after surgery. (b) Correlation between HR at apical turn and ABR threshold elevation at 1 kHz. (c) Correlation between HR at subapical turn and ABR threshold elevation at 2 kHz.

between control and EH ears. These differences are shown in Figure 5. Figures 5(a) and 5(b) illustrate the peak-to-peak displacement amplitude-frequency curves of the umbo from the six control ears and that of the six EH ears, respectively, over the 0.5–8-kHz range in response to 85 dB SPL stimuli in the ear canal. The two groups possessed similar displacement-frequency curves for the 0.5–8-kHz range and the results of the EH ears were lower than that for the control ears overall (Figure 5(c)). A maximum displacement amplitude, almost 14 nm, presented at 0.5 kHz in the control group.

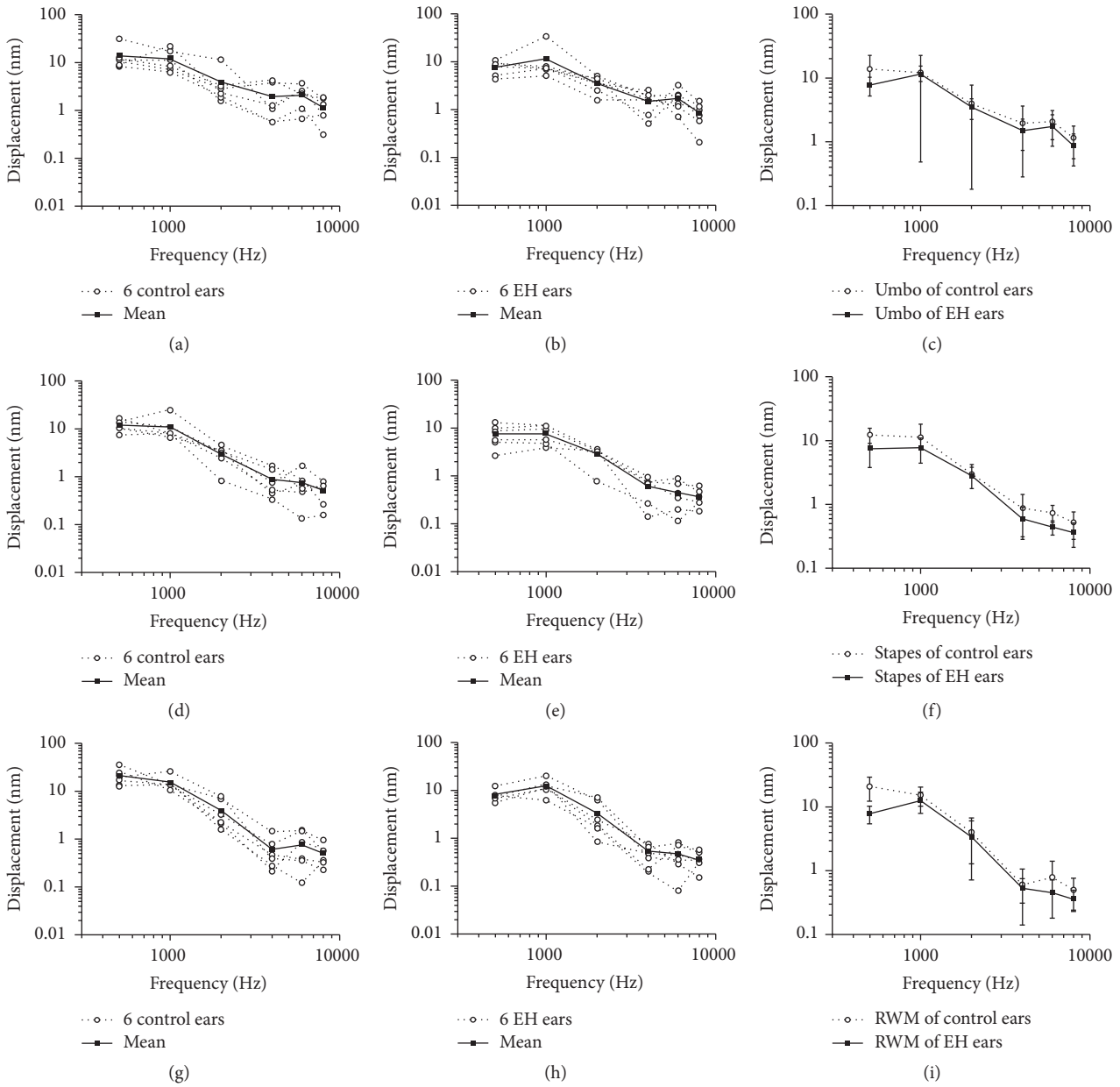

Figure 5: Peak-to-peak displacement-frequency curve of the umbo (a–c), stapes head (d–f), and round window membrane (RWM) (g–i) in response to 85 dB SPL sound stimuli at the ear canal. (a) Six individuals and their mean value in the control group (dotted line for the individuals and solid line for the mean value). (b) Six individuals and their mean value in the endolymphatic hydrops (EH) group (dotted line for the individuals and solid line for the mean value). (c) Mean ± SD ($n = 6$) of the control and EH groups, respectively: dotted line for the control group and solid line for the EH group. (d) Six individuals and their mean value in the control group (dotted line for the individuals and solid line for the mean value). (e) Six individuals and their mean value in the endolymphatic hydrops (EH) group (dotted line for the individuals and solid line for the mean value). (f) Mean ± SD ($n = 6$) of the control and EH groups (dotted line for the control group and solid line for the EH group). (g) Six individuals and their mean value in the control group (dotted line for the individuals and solid line for the mean value). (h) Six individuals and their mean value in the endolymphatic hydrops (EH) group (dotted line for the individuals and solid line for the mean value). (i) Mean ± SD ($n = 6$) of the control and EH groups (dotted line for the control group and solid line for the EH group).

In the EH group, peak displacement was found at 1 kHz (11.48 nm) and there was a sudden decrease in displacement amplitude between 1 and 2 kHz frequencies in both groups. Mean ± SD ($n = 6$) of the control and EH groups was compared in Figure 5(c) showing that there are no significant differences in each frequency; particularly the biggest reduction of displacement amplitude among the two groups was present at 0.5 kHz (6.05 nm, $p = 0.12$) and this reduction remained below 1 nm at frequencies above or equal to 1 kHz.

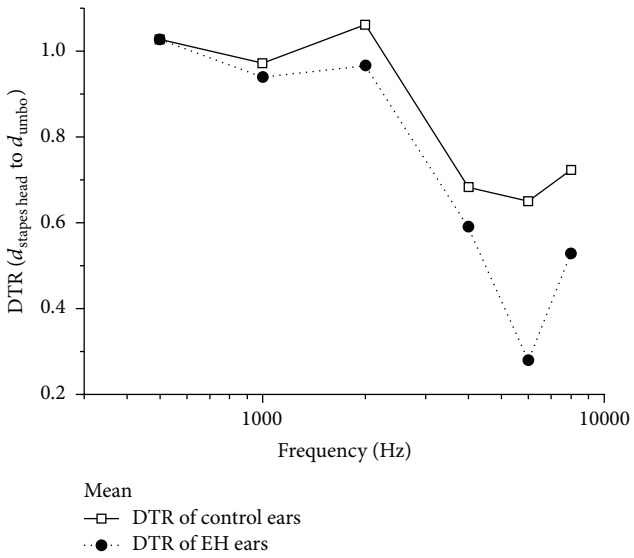

Figure 6: Displacement transmission ratio (DTR) of the stapes head to the umbo (mean value, $n = 6$) in control ears (solid line), and ears with endolymphatic hydrops (EH; dotted line).

Figures 5(d) and 5(e) display the peak-to-peak displacement curves of the stapes head in two groups. Displacements in the EH group were generally lower than those in the control group (Figure 5(f)). The displacement amplitude reached a maximum of 12.3 nm at 500 Hz and decreased gradually to 0.52 nm at 8 kHz in normal ears, while in the EH group the maximal displacement amplitude was 7.6 nm at 1 kHz. A statistically significant difference ($p < 0.05$) was found at 500 Hz and the reduction reached almost 4.82 nm.

Figures 5(g) and 5(h) show the peak-to-peak displacement curves of the RWM in both groups. Each curve shows a prominent displacement peak at 0.5, 1, 2, 4, 6, and 8 kHz. The displacement decreased along with the increase in frequency from 0.5 to 8 kHz in the two groups in response to 85 dB SPL input at the ear canal. The displacements of the EH group were generally lower than those in the control group (Figure 5(i)). There was a statistically significant difference ($p < 0.05$) at 0.5 and 6 kHz. For RMW, the best vibration response to displacement in the control ears was 20.79 nm at 500 Hz, while peak displacement in the EH group was 12.43 nm at 1 kHz.

The displacement transmission ratio (DTR) of the stapes head to the umbo was used to represent the middle ear transfer function under normal and EH conditions in this study. Figure 6 shows the mean DTR values ($n = 6$) at frequencies from 0.5 to 8 kHz. In the control ears, the displacement of the stapes head was slightly less than that of the umbo by factors of 0.64–0.72 at frequencies above 2 kHz and close to the umbo by factors of 0.9–1.06 at frequencies of 0.5–2 kHz. When EH was present in the cochlea, the displacement of the stapes head was much lower than that in the umbo, by factors of 0.2–0.5, at frequencies of 4–8 kHz. As for frequencies below 2 kHz, a factor of 0.9–1 suggested nearly equal displacement between stapes head and umbo (Figure 6). The lower DTR of the stapes head to the umbo in the EH group than in the control group suggested that vibration of the stapes head was reduced more than that of the umbo by EH.

3.5. The Morphology Changes of the EH Model. Three ears of two groups were dissected and stained with Alexa Fluor 488-conjugated phalloidin for F-actin of stereocilia. The hair cell bundles in each turn were shown to be normal in the control group 8 weeks later in Figure 6. In the EH group, we could observe the accidental loss of the stereocilia of outer hair cells (star in Figure 7) in the suprabasal, subapical, and apical turn. In the basal turn of EH model, the hair cell bundles were normal. Furthermore, the stereocilia in the third row of outer hair cells were sporadically collapsed and deranged in the suprabasal turn. Inner hair cells showed normal in each turn of the EH model. Interestingly, the most obvious morphology change in the apical and subapical turn of the EH group compared to the control group, which showed the high level extent of the labyrinthine hydrops and low frequency ABR threshold shift.

4. Discussion

We reported the effect of endolymphatic hydrops of live guinea pigs on the ABR threshold, morphology changes, and movements of the umbo, stapes head, and RWM under 85 dB SPL pure tone stimuli in the external auditory canal in this study. We had explored the mechanism of the hearing loss in EH model, which showed displacements reduction of the umbo, stapes head, and RWM was greater at low frequency (<1 kHz) and the stereocilia of outer hair cell were missing in apical and subapical turn, which was associated with the extent of the endolymphatic hydrops.

4.1. Dynamic Properties of the Umbo, Stapes Head, and RWM. Since the target location of laser beam along the TM affects data quality in terms of the signal-to-noise ratio and the TM is directly attached to the ossicular chain (the umbo and the lateral process of the malleus), TM movement in this study was measured on the medial side of the umbo to minimize variability. The umbo displacement was slightly decreased in the EH group compared with the control group at all measured frequencies and the differences were more notable at low frequencies. The biggest reduction in umbo displacement was 5.01 dB (ref = 1 pm) at 0.5 kHz. The control group shared a similar displacement amplitude-frequency curve of umbo with that reported by Guan and Gan [17] (Figure 3a in their paper). But data in this study was generally lower. This discrepancy may be explained by the different measurement sides and the subtle difference between angles of the laser beam in both studies. In the study by Guan and Gan, the target position was at the lateral side of umbo, while in this study the medial side of the umbo was taken as test point. Shinohara [20] and Murakami et al. [21] suggested that a positive inner ear fluid pressure weakened the vibration of the umbo mainly at low frequencies (≤1 kHz). Jang et al. [22] reported that the endolymphatic pressure load caused greater reduction in the umbo velocity than did the perilymphatic pressure load at frequencies below 1 kHz. All these findings supported the result in this study.

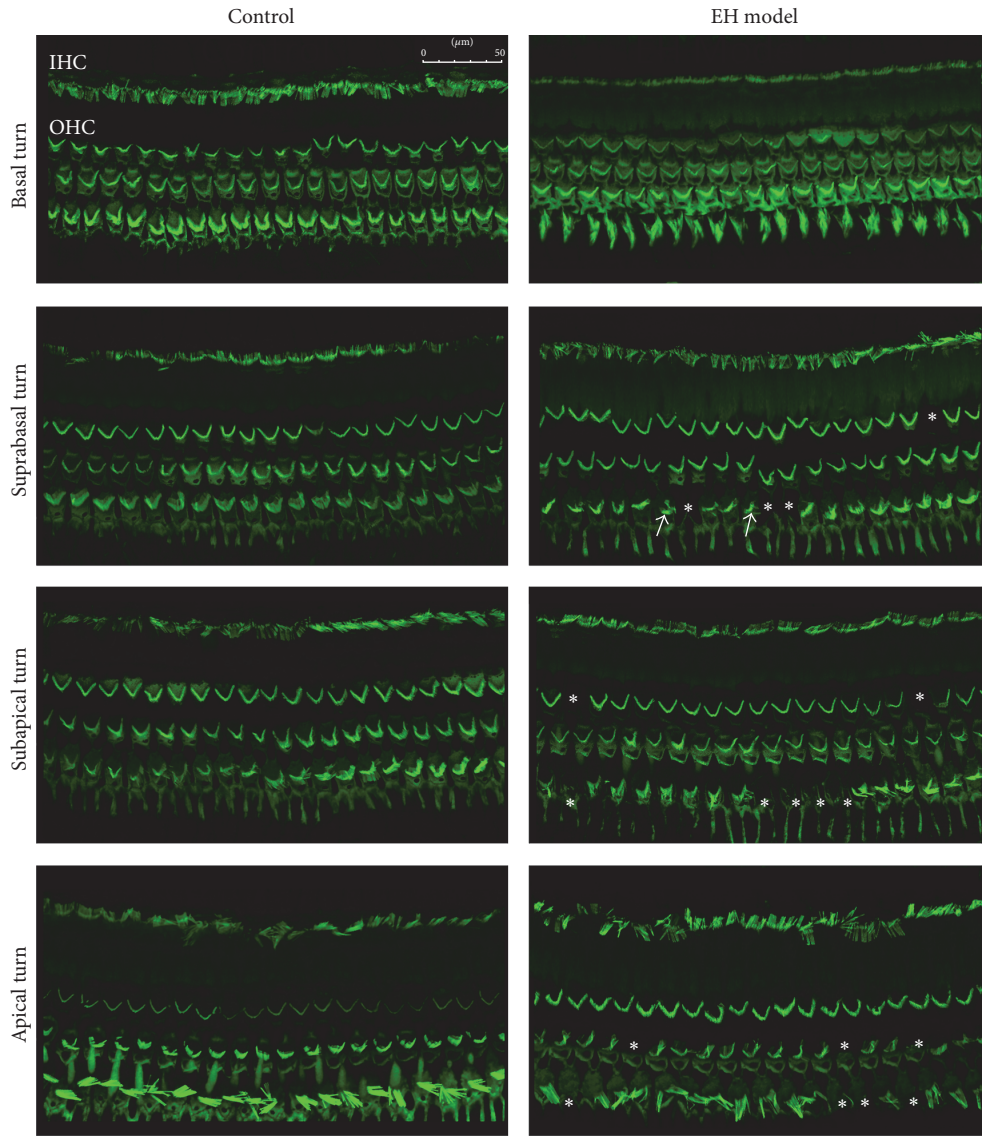

Figure 7: Confocal image of cochlea basilar membrane staining with FITC-conjugated phalloidin in the four turns of control group and EH model group. Accidental loss of stereocilia of outer hair cells (∗) in the suprabasal, subapical, and apical turns was observed. Sporadic collapse and derangement of stereocilia (white arrow) were found in the third row of outer hair cells. Inner hair cells showed normal.

The displacement of the incus tip in guinea pigs under 80 dB SPL acoustic stimulation in the ear canal was reported by Guan and Gan [17] and by Chen et al. [23]. The measurement of the stapes head in this study was recorded at a nearby site compared with the incus tip reported previously, both around the incudostapedial joint. The mean stapes head displacement of the control group in this study was in accordance with that reported by Guan and Gan [17] (Figure 4A in their paper) on the whole but was generally higher than that reported by Chen et al. [23]. Murakami et al. [21] reported that the stapes velocity decreased over 0.4–5.0 kHz in fresh human temporal bones with increased hydrostatic pressure of the inner ear under sound pressure of 114 dB SPL. And the effect was less marked at high frequencies than at low frequencies. Lord et al. [24] and Gyo et al. [25] found that the stapes motion changed at low frequencies when inner ear fluid was drained. In this study, the mean displacement amplitude of the stapes in the EH group decreased at all measured frequencies, with profound reduction below 1 kHz. All those findings suggested that cochlear fluid pressure/volume can affect inner ear impedance and cause changes in stapes displacement under acoustic stimulation.

The round window is one of the two openings into the cochlea from the middle ear. The RWM serves as a barrier between the middle ear cavity and the cochlea and plays an important role in the middle ear and cochlear mechanics. The mechanical response of the RWM can be indirect detection of acoustic dysfunction [15]. Compared with literature published by Guan and Gan [17] (Figure 5A in their paper), these two studies shared a parallel mean displacement amplitude-frequency curve and the data were

in the same order of magnitude. The data of RWM vibration from ears with EH have not yet been reported. The maximum reduction of the RWM displacement was 13.01 nm (8.5 dB ref = 1 pm) at 500 Hz. The difference between 1 kHz and 4 kHz was about 1–1.8 dB, which is relatively flat. A second difference-peak was found at 6 kHz (5 dB). Those findings suggested that EH has an influence on the vibration of the RWM and that changes occur mainly at low frequencies.

4.2. EH Effect on Transfer Function of the Middle Ear. Studies of motion of the ossicular chain revealed that it was more complicated than a simple piston-like motion and that the complexities increased with frequency. In order to evaluate the transfer function of middle ear approximately, DTR of single points (the TM to the footplate/incus tip) was calculated by researchers [17, 26]. Nevertheless, the DTR of the stapes head to the umbo may not reveal the exact middle ear transfer function. Through numerical conversion, the results of the control group from Guan and Gan [17] showed that the mean displacement of the incus tip was less than that of the TM by a factor of 0.2–0.34 at lower frequencies and low to 0.125 at higher frequencies. Results from this study do not correspond well with those reported by Guan and Gan [17]. As described before, the angle between the motion of the umbo and the laser beam in this study is different and this may be one reason for the discrepant findings between the two studies. Moreover, the complex motion of the stapes may increase the interindividual variations in the results of DTR and may underlie differences in the findings. When EH was present in the cochlea, the displacement of the stapes head was much lower than that of the umbo, by factors of 0.2–0.5, at frequencies of 4–8 kHz. The lower DTR in the EH group than in the control group suggested that vibration of the stapes head was reduced more than that of the umbo by EH. Both the umbo and stapes head vibration decreased due to the increased inner ear impedance, decreasing the stapes footplate movement. As the ossicular rotation axis and incudostapedial joint have some laxity, the increased inner ear impedance may not be wholly transmitted to the umbo. Therefore, the reduction of stapes head displacement should be greater, as described by the DTR.

4.3. The Endolymphatic Hydrops and Hearing Loss. Since the milestone findings on the temporal bones of Ménière's Disease (MD) patients [4, 27, 28], endolymphatic hydrops (EH) has been considered as the histopathological origin of MD, as characteristic morphological changes were reported previously by surgical obstruction of the endolymphatic sac (ES) in guinea pig [29]. Because surgical experiment induction procedure is still by far the most common method for producing experimental endolymphatic hydrops (EH), it is particularly important to characterize the pathologic changes in this model so that their relevance to Ménière's Disease can be fully appreciated. The simplest explanation for the hearing loss in the endolymphatic hydrops is initial loss of cochlear sensitivity, the shift in the cochlear microphonics (CM), and Distortion Product Otoacoustic Emission (DPOAE); increased SP (summating potential) amplitude, with a reduction in EP (endocochlear potential), is one which has been suggested by researchers who have performed acute endolymph injections [30]. Many authors have demonstrated that the significant correlation between the degree of hydrops and a reduction in the low frequency cochlear microphonic change was found in short- and long-standing surgically induced hydrops guinea pigs [31–33]. Because high-frequency hearing is ultimately affected in both the human and the animal conditions, these same studies imply a poor relationship between hair cell loss and the degree and nature of hearing loss. In our experiment, we have quantified the extent of hydrops in each turn of EH models. The most serious labyrinthine hydrops is in the subapical turn, and the second is in the suprabasal turn. Meanwhile, the mean ABR threshold of the EH cases was significantly higher than that of the control group at 0.5, 1, 2, 4, 6, and 8 kHz frequencies. Strong positive correlation was found between HR at apical turn and ABR threshold elevation at 1 kHz, as well as between HR at subapical turn and ABR threshold elevation at 2 kHz. In order to underline the morphology change of the hair cells stained with Alexa Fluor 488-conjugated phalloidin, we could observe the accidental loss of the outer hair cells and sporadic collapse of the stereocilia in the suprabasal, subapical, and apical turn. In the basal turn of EH model, there were almost normal hair cell bundles. Inner hair cells showed normal morphological features in each turn of the EH model. Interestingly, the most obvious morphology change in the apical and subapical turn of the EH group compared to the control group, which showed the high level extent of the labyrinthine hydrops and low frequency ABR threshold shift. We could not observe the serious hair cell damage in the basal and suprabasal turn with hydrops and higher frequency ABR threshold elevation, which should be needed for long-time EH model observation. Overall, the hearing loss of the surgical EH model in our experiment could be explained for two reasons: one is that the higher inner ear impedance in EH affected the dynamic behavior of the two opening windows of the cochlea and then reduced the vibration of the ossicular chain by increasing the afterload, resulting in acoustic dysfunction. The other is the morphological damage of the stereocilia of the outer hair cells especially in the apical and subapical turn with more serious labyrinthine hydrops.

5. Conclusions

In this study, an EH model was created in live guinea pigs by obliteration of the endolymphatic sac. It is the first time to detect the dynamic behaviors of the ossicular chain and the two opening windows by LDV in vivo guinea pigs. EH reduced the displacement of the umbo, stapes, and RWM mainly at lower frequencies. Elevation of the ABR threshold was noted at all measured frequencies. The LDV provides an accurate assessment of the dynamic properties of the middle ear and cochlear mechanics in EH animal models. The displacement of Reissner's membrane caused by EH indicates that the membranous cochlear duct reached a higher hydrostatic pressure. The LDV results suggested that abnormal endolymphatic pressure affects the dynamic behaviors of the two opening windows of the cochlea and that

this may be one of the major reasons for hearing loss at lower frequencies in EH-related conditions.

Competing Interests

None of the authors have potential conflict of interests to be disclosed.

Authors' Contributions

Chen-Ru Ding, Xin-Da Xu, Xin-Wei Wang, and Xian-Hao Jia contributed equally to this work.

Acknowledgments

This study was supported by Key Project of Chinese National Programs (2016YFC0905200); the National Natural Science Foundation of China (NSFC) Grant nos. 81420108010 and 81271084 to Fang-Lu Chi and nos. 81370022, 81570920, and 81000413 to Dong-Dong Ren; 973 Program (Grant nos. 2011CB504500 and 2011CB504506); the Innovation Project of Shanghai Municipal Science and Technology Commission (Grant no. 11411952300 to Fang-Lu Chi); the Training Program of the Excellent Young Talents of the Shanghai Municipal Health System (Grant no. XYQ2013084 to Dong-Dong Ren); and "Zhuo-Xue Plan" of Fudan University (Dong-Dong Ren).

References

[1] L. Robles and M. A. Ruggero, "Mechanics of the mammalian cochlea," *Physiological Reviews*, vol. 81, no. 3, pp. 1305–1352, 2001.

[2] A. A. Mikulec, M. J. McKenna, M. J. Ramsey et al., "Superior semicircular canal dehiscence presenting as conductive hearing loss without vertigo," *Otology and Neurotology*, vol. 25, no. 2, pp. 121–129, 2004.

[3] H. J. Lee, J. H. Jeon, S. Park, B. G. Kim, W.-S. Lee, and S. H. Kim, "Prevalence and clinical significance of spontaneous low-frequency air-bone gaps in Ménière's disease," *Otology and Neurotology*, vol. 35, no. 3, pp. 489–494, 2014.

[4] C. S. Hallpike and H. Cairns, "Observations on the Pathology of Meniere's Syndrome," *Section of Otology*, vol. 31, pp. 1317–1336, 1938.

[5] G. Ishiyama, I. A. Lopez, A. R. Sepahdari, and A. Ishiyama, "Meniere's disease: histopathology, cytochemistry, and imaging," *Annals of the New York Academy of Sciences*, vol. 1343, no. 1, pp. 49–57, 2015.

[6] Q. Wu, C. Dai, M. Zhao, and Y. Sha, "The correlation between symptoms of definite Meniere's disease and endolymphatic hydrops visualized by magnetic resonance imaging," *Laryngoscope*, vol. 126, no. 4, pp. 974–979, 2015.

[7] T. Yoshida, M. Sone, S. Naganawa, and T. Nakashima, "Patient with an SLC26A4 gene mutation who had low-frequency sensorineural hearing loss and endolymphatic hydrops," *Journal of Laryngology and Otology*, vol. 129, no. 1, pp. 95–97, 2015.

[8] R. Filipo, A. Cordier, M. Barbara, and G. A. Bertoli, "Electrocochleographic findings: Meniere's disease versus sudden sensorineural hearing loss," *Acta Oto-Laryngologica, Supplement*, no. 526, pp. 21–23, 1997.

[9] T. H. Yoon, M. M. Paparella, P. A. Schachern, and M. Alleva, "Histopathology of sudden hearing loss," *Laryngoscope*, vol. 100, no. 7, pp. 707–715, 1990.

[10] Y. Noguchi, H. Nishida, Y. Kawashima, H. Tokano, and K. Kitamura, "Comparison of acute low-tone sensorineural hearing loss versus Meniere's disease by electrocochleography," *Annals of Otology, Rhinology & Laryngology*, vol. 113, no. 3, pp. 194–199, 2004.

[11] R. L. Goode, G. Ball, S. Nishihara, and K. Nakamura, "Laser Doppler vibrometer (LDV)—a new clinical tool for the otologist," *American Journal of Otology*, vol. 17, no. 6, pp. 813–822, 1996.

[12] G. R. Ball, A. Huber, and R. L. Goode, "Scanning laser Doppler vibrometry of the middle ear ossicles," *Ear, Nose and Throat Journal*, vol. 76, no. 4, pp. 213–222, 1997.

[13] K. R. Whittemore Jr., S. N. Merchant, B. B. Poon, and J. J. Rosowski, "A normative study of tympanic membrane motion in humans using a laser Doppler vibrometer (LDV)," *Hearing Research*, vol. 187, no. 1-2, pp. 85–104, 2004.

[14] J. A. Beyea, S. A. Rohani, H. M. Ladak, and S. K. Agrawal, "Laser Doppler vibrometry measurements of human cadaveric tympanic membrane vibration," *Journal of Otolaryngology—Head and Neck Surgery*, vol. 42, article 17, 2013.

[15] R. Z. Gan, D. Nakmali, and X. Zhang, "Dynamic properties of round window membrane in guinea pig otitis media model measured with electromagnetic stimulation," *Hearing Research*, vol. 301, pp. 125–136, 2013.

[16] X. Zhang and R. Z. Gan, "Dynamic properties of human round window membrane in auditory frequencies running head: dynamic properties of round window membrane," *Medical Engineering and Physics*, vol. 35, no. 3, pp. 310–318, 2013.

[17] X. Guan and R. Z. Gan, "Effect of middle ear fluid on sound transmission and auditory brainstem response in guinea pigs," *Hearing Research*, vol. 277, no. 1-2, pp. 96–106, 2011.

[18] R. Z. Gan, B. Feng, and Q. Sun, "Three-dimensional finite element modeling of human ear for sound transmission," *Annals of Biomedical Engineering*, vol. 32, no. 6, pp. 847–859, 2004.

[19] F.-L. Chi and Q. Liang, "The quantification of endolymphatic hydrops in an experimental animal model with guinea pigs," *ORL*, vol. 66, no. 2, pp. 56–61, 2004.

[20] T. Shinohara, "Ossicular vibration changes associated with pressure changes in inner ear and cerebrospinal fluid in guinea pigs," *Journal of Otolaryngology of Japan*, vol. 100, no. 2, pp. 236–243, 1997.

[21] S. Murakami, K. Gyo, and R. L. Goode, "Effect of increased inner ear pressure on middle ear mechanics," *Otolaryngology—Head and Neck Surgery*, vol. 118, no. 5, pp. 703–708, 1998.

[22] C. H. Jang, H. Park, C. H. Choi, Y. B. Cho, and I. Y. Park, "The effect of increased inner ear pressure on tympanic membrane vibration," *International Journal of Pediatric Otorhinolaryngology*, vol. 73, no. 3, pp. 371–375, 2009.

[23] Y. Chen, X. Guan, T. Zhang, and R. Z. Gan, "Measurement of basilar membrane motion during round window stimulation in guinea pigs," *Journal of the Association for Research in Otolaryngology*, vol. 15, no. 6, pp. 933–943, 2014.

[24] R. M. Lord, E. W. Abel, Z. Wang, and R. P. Mills, "Effects of draining cochlear fluids on stapes displacement in human middle-ear models," *Journal of the Acoustical Society of America*, vol. 110, no. 6, pp. 3132–3139, 2001.

[25] K. Gyo, H. Aritomo, and R. L. Goode, "Measurement of the ossicular vibration ratio in human temporal bones by use of a

video measuring system," *Acta Oto-Laryngologica*, vol. 103, no. 1-2, pp. 87–95, 1987.

[26] R. Z. Gan, C. Dai, and M. W. Wood, "Laser interferometry measurements of middle ear fluid and pressure effects on sound transmission," *Journal of the Acoustical Society of America*, vol. 120, no. 6, pp. 3799–3810, 2006.

[27] K. Yamakawa, "Uber die pathologische Veranderung bei einem Meniere-Kranken," *Nihon Jibiinkoka Gakkai Kaiho*, vol. 44, pp. 2310–2312, 1938.

[28] C. S. Hallpike and H. Cairns, "Observations on the Pathology of Ménière's Syndrome," *The Journal of Laryngology & Otology*, vol. 53, no. 10, pp. 625–655, 1938.

[29] R. S. Kimura and H. Schuknecht, "Membranous hydrops in the inner ear of the guinea pig after obliteration of the endolymphatic sac," *Practica Oto-Rhino-Laryngologica*, vol. 27, no. 6, pp. 343–354, 1965.

[30] A. Kakigi, A. N. Salt, and T. Takeda, "Effect of artificial endolymph injection into the cochlear duct on perilymph potassium," *Journal for Otorhinolaryngology and Its Related Specialties*, vol. 71, supplement 1, pp. 16–18, 2010.

[31] S. F. Klis, J. Buijs, and G. F. Smoorenburg, "Quantification ofthe relation between electrophysiologic and morphologic changes in experimental endolymphatic hydrops," *Annals of Otology, Rhinology & Laryngology*, vol. 99, no. 7, part 2, pp. 566–570, 1990.

[32] M. E. Hott, M. Graham, L. J. Bonassar, and C. A. Megerian, "Correlation between hearing loss and scala media area in guinea pigs with long-standing endolymphatic hydrops," *Otology and Neurotology*, vol. 24, no. 1, pp. 64–72, 2003.

[33] D. J. Brown, Y. Chihara, I. S. Curthoys, Y. Wang, and M. Bos, "Changes in cochlear function during acute endolymphatic hydrops development in guinea pigs," *Hearing Research*, vol. 296, pp. 96–106, 2013.

Hindawi Publishing Corporation
Neural Plasticity
Volume 2016, Article ID 9890827, 6 pages
http://dx.doi.org/10.1155/2016/9890827

Research Article

Mutation in the Hair Cell Specific Gene *POU4F3* Is a Common Cause for Autosomal Dominant Nonsyndromic Hearing Loss in Chinese Hans

Longxia He,[1,2,3] Xiuhong Pang,[4] Penghui Chen,[1,2,3] Hao Wu,[1,2,3,5] and Tao Yang[1,2,3]

[1]*Department of Otolaryngology-Head and Neck Surgery, Xinhua Hospital, Shanghai Jiaotong University School of Medicine, Shanghai, China*
[2]*Ear Institute, Shanghai Jiaotong University School of Medicine, Shanghai, China*
[3]*Shanghai Key Laboratory of Translational Medicine on Ear and Nose Diseases, Shanghai, China*
[4]*Department of Otorhinolaryngology-Head and Neck Surgery, Taizhou People's Hospital, Jiangsu Province, China*
[5]*Department of Otorhinolaryngology-Head and Neck Surgery, Shanghai Ninth People's Hospital, Shanghai Jiaotong University School of Medicine, Shanghai, China*

Correspondence should be addressed to Hao Wu; wuhao622@sina.cn and Tao Yang; yangtfxl@sina.com

Received 8 September 2016; Revised 26 October 2016; Accepted 2 November 2016

Academic Editor: Renjie Chai

Autosomal dominant nonsyndromic hearing loss (ADNSHL) is extremely heterogeneous. So far the genetic etiological contribution of the gene *POU4F3* associated with ADNSHL has been rarely reported. In our previous study, a c.603_604delGG mutation in the hair cell specific gene *POU4F3* has been identified as the pathogenic cause in one of the seven Chinese Han ADNSHL families. In the present study, we performed targeted next-generation sequencing of 144 known deafness genes in another nine Chinese Han ADNSHL families and identified two more novel mutations in *POU4F3*, p.Leu311Pro and c.120+1G>C, as the pathogenic cause. Clinical characterization of the affected individuals in these three families showed that the three *POU4F3* mutations may lead to progressive hearing loss with variable ages of onset and degrees of severity. Our results suggested that mutations in *POU4F3* are a relatively common cause (3/16) for ADNSHL in Chinese Hans, which should be routinely screened in such cases during genetic testing.

1. Introduction

Hearing loss is one of the most common sensorineural defects, which may result from a great variety of genetic and environmental factors. Based on the inheritance patterns, the genetic hearing loss can be classified into autosomal recessive, autosomal dominant, and X-linked/mitochondrial, accounting for approximately 80%, 15%, and less than 5% of nonsyndromic hearing loss, respectively [1]. Both autosomal dominant (ADNSHL) and autosomal recessive (ARNSHL) nonsyndromic hearing loss have an extremely high degree of heterogeneity. For the former, 35 causative genes and over 60 loci have been reported for ADNSHL (The hereditary Hearing Loss Homepage, http://hereditaryhearingloss.org/). So far, mutations in most ADNSHL genes were reported based on studies of the individual cases or families. The etiological contribution of the ADNSHL gene *POU4F3* has been rarely studied. In recent years, however, the development of next-generation sequencing (NGS) has complemented the traditional Sanger sequencing method and made it possible to screen all deafness-associated genes in a high throughout manner [2–4].

Mutations in *POU4F3* have been reported to lead to ADNSHL named as DFNA15 [5]. This gene encodes a 338 amino acids' POU family transcription factor with two conserved DNA-binding domains (the POU-specific domain and the POU homeodomain, amino acids 179–256 and 274–333, resp.). In mouse inner ear, Pou4f3 is strongly expressed in both inner and outer hair cells [6–9]. It activates the transcription of a downstream target gene *Gfi1*, whose expression

is required for the maintenance of the outer hair cells [10]. To date, only eleven different mutations in *POU4F3* have been reported in Israeli Jewish, Dutch, Korean, Japanese, and Chinese ADNSHL families [5, 11–17]. The hearing loss caused by *POU4F3* mutations was highly variable in the age of onset, the progression course, and the severity of hearing impairment.

In the previous ($n = 7$) and the present ($n = 9$) studies [18], we preformed targeted NGS of known deafness genes in 16 Chinese Han ADNSHL families and identified novel mutations in *POU4F3* as the pathogenic cause in three of them. Characterization of the hearing phenotype was performed in the affected family members of these three families in the present study. Our results expanded the mutation spectrum of DFNA15 and suggested that mutations in *POU4F3* are a relatively common cause for ADNSHL in Chinese Hans.

2. Materials and Methods

2.1. Subjects. Probands of sixteen Chinese Han families segregating ADNSHL were recruited through Xinhua Hospital, Shanghai, China. The pedigrees of the families were shown in Figure 1(a) and Supplementary Figure S1 in Supplementary Material available online at http://dx.doi.org/10.1155/2016/9890827. For Families P1748, PD6, and P59 in which mutations in *POU4F3* were identified, 8, 10, and 13 additional family members were subsequently recruited, respectively. Informed consent was obtained from all subjects. This study was approved by the Ethics Committee of Xinhua Hospital, Shanghai Jiaotong University School of Medicine, Shanghai, China.

2.2. Clinical Evaluations. A detailed physical and medical history examination was performed in all probands of the ADNSHL families. The hearing levels were measured by pure tone audiometry (PTA) and shown as the average thresholds of 0.5, 1, 2, and 4 kHz from the better ear. The hearing levels were classified as normal (<20 dB), mild (20–40 dB), moderate (41–70 dB), severe (71–90 dB), and profound (>90 dB).

2.3. Mutation Analysis. Targeted NGS of 144 known deafness genes (see complete list in Supplementary Table S1) was performed using the MyGenotics gene enrichment system (MyGenotics, Boston, MD, USA) and the Illumina HiSeq 2000 sequencer (Illumina, San Diego, CA, USA) as previously described [18]. The raw data were first analyzed to filter out the low quality reads. NCBI37/hg19 assembly was used as the reference sequences. Nonsynonymous, on-target variants with maximum minor allele frequency (MAF) less than 0.001 in public databases NHLBI Exome Sequencing Project (ESP, http://evs.gs.washington.edu/EVS/) and the Exome Aggregation Consortium (ExAC, http://exac.broadinstitute.org/) were considered as the candidate pathogenic mutations in compliance with the ADNSHL inheritance. The pathogenicity of the candidate variants was predicted by computational programs Mutation Taster (http://www.mutationtaster.org/), PolyPhen-2 (http://genetics.bwh.harvard.edu/pph2/), PROVEAN, and SIFT (http://sift.jcvi.org/, cutoff scores set at −2.5 and 0.05, resp.). Cosegregation of the pathogenic mutations and the hearing phenotype was verified in members of Families P1748 and PD6 by Sanger sequencing.

3. Results

3.1. POU4F3 Mutations Identified in the ADNSHL Families. In our previous studies of 7 Chinese Han ADNSHL families, a c.603_604delGG (p.Leu201fs*12) mutation in *POU4F3* has been identified by targeted NGS as the pathogenic cause in Family P59 [18]. In the present study, we performed a comprehensive mutation screening in probands of another nine Chinese Han ADNSHL families (marked in asterisks in Figure 1(a) and Supplementary Figure S1) by targeted NGS of 144 known deafness genes. Interestingly, two novel heterozygous variants p.Leu311Pro (c.932T>C) and c.120+1G>C in *POU4F3* were identified as the candidate pathogenic variants in probands P1748-III-1 and PD6-IV-1, respectively (Table 1), along with a heterozygous *TECTA* p.Val1830Met and a heterozygous *TMC1* p.Ser697X variant in proband P1748-1 (Table 1). Sanger sequencing in the rest of the family members confirmed that p.Leu311Pro and c.120+1G>C were the only two candidate variants segregating with the hearing phenotype in Families P1748 and PD6 (Figures 1(a) and 1(b)), while the *TECTA* p.Val1830Met and the *TMC1* p.Ser697X variants were not seen in any other affected family members of P1748. The p.Leu311Pro (c.932T>C) and c.120+1G>C in *POU4F3* were not reported in previous studies, not present in the NHLBI ESP ($n = 6503$) and ExAC ($n = 60706$) database, and not seen in 300 Chinese Han normal hearing controls. The c.120+1G>C mutation was predicted to abolish the 5′ splice site of introns 1 of *POU4F3* (Figure 2(a)). The p.Leu311Pro mutation substituted a conserved amino acid Leu311 (Figure 2(b)) and was predicted to be deleterious by computational programs Mutation Taster, PolyPhen-2, PROVEAN, and SIFT (Table 1).

3.2. Clinical Characteristics of the Three ADNSHL Families with POU4F3 Mutations. Based on the audiograms and the self-description of the affected individuals with c.603_604delGG, p.Leu311Pro, and c.120+1G>C mutations in *POU4F3*, the hearing loss associated with the *POU4F3* mutations was typically progressive with considerable variability in ages of onset and degree of severity both interfamilially and intrafamilially. In Family P1748 with the p.Leu311Pro mutation, proband III-1 had notable hearing loss since age 10 years. The hearing loss affected high frequency most and gradually progressed to moderate hearing loss at age 29 years (Figure 1(c)). The affected individuals in the second generation of Family P1748 had hearing loss at the onset age of 10 years to 20 years and all eventually progressed to profound after age 50 years. Interestingly, all six female patients in the second generation had significantly decreased hearing levels after giving birth to their children. In Family PD6 with the c.120+1G>C mutation, proband IV-1 had congenital, moderate hearing loss with a relatively "flat" audiometric profile at age 23 years affecting all frequencies (Figure 1(c)). Other affected individuals in this family demonstrated progressive, moderate-to-profound deafness depending on their ages. The ages of onset

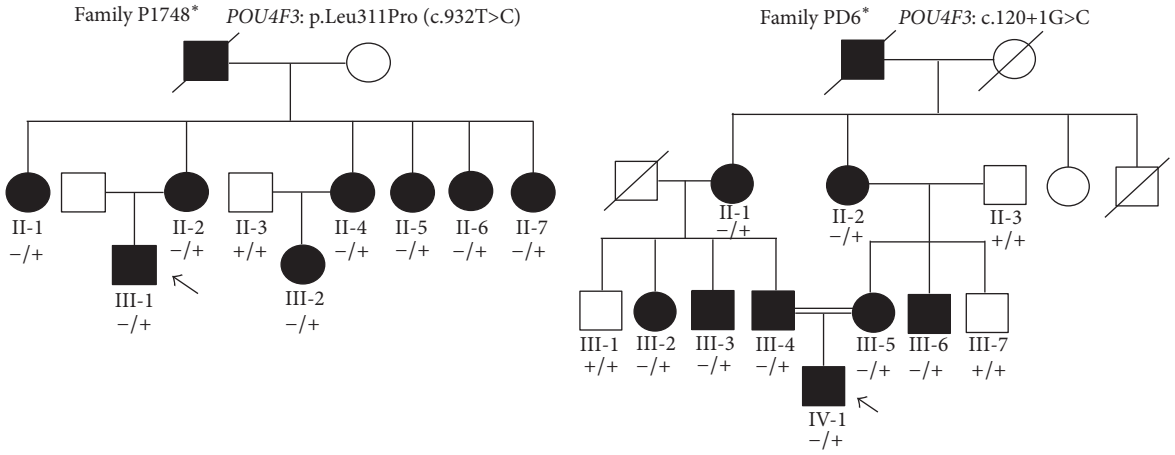

(a)

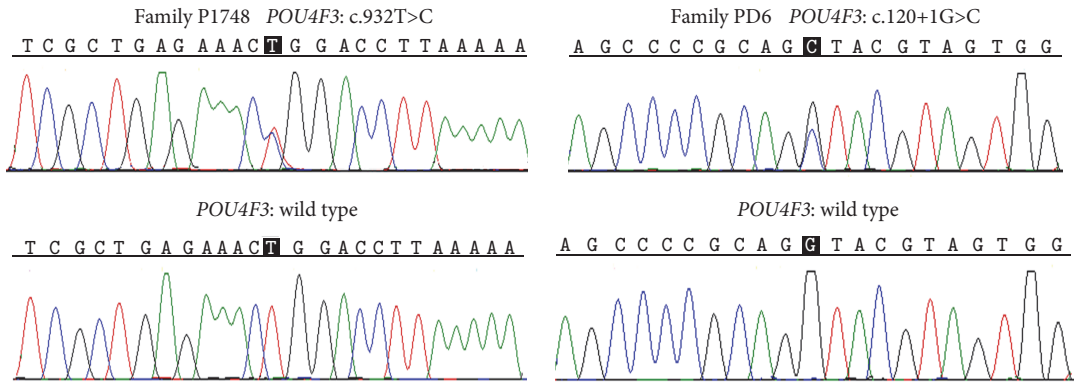

(b)

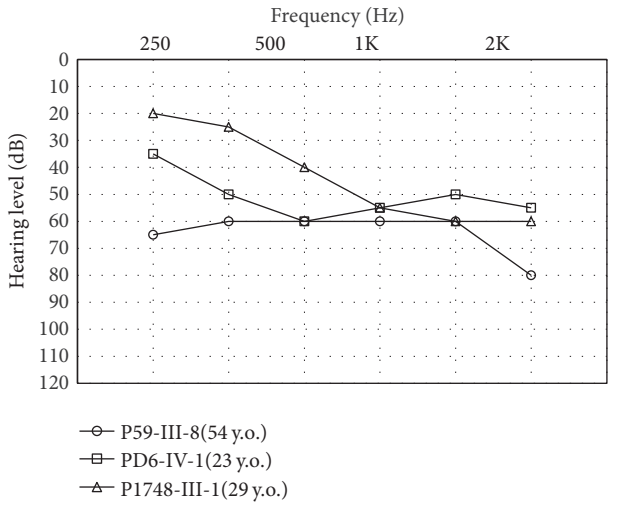

(c)

Figure 1: *POU4F3* mutations identified in the Chinese Han ADNSHL families. (a) Pedigrees and genotypes of the families with *POU4F3* mutations. Probands were pointed by arrows. – and + indicate the mutant and wild type alleles, respectively. Asterisks indicate the families with *POU4F3* mutations identified in the present study. (b) Chromatograms showing the c.932T>C (p.Leu311Pro) and the c.120+1G>C mutations in *POU4F3*. (c) Audiograms of the probands of the three families.

Table 1: Candidate pathogenic mutations identified in probands of Families P1748 and PD6 by targeted NGS.

Proband	Gene (reference sequence)	Mutation	MAF (ExAC)	MAF (NHLBI ESP)	Mutation Taster	PROVEAN (score)	SIFT (score)	PolyPhen-2 (HumVar score)	Intrafamilial phenotype cosegregation
P1748-III-1	POU4F3 (NM_002700)	p.Leu311Pro (c.932T>C)	0	0	Disease causing	Deleterious (−3.63)	Damaging (0)	Probably damaging (1)	Yes
	TECTA (NM_005422)	p.Val1830Met (c.5488G>A)	0.0003871	0	Disease causing	Neutral (−0.83)	Damaging (0.008)	Probably damaging (0.969)	No
	TMC1 (NM_138691)	p.Ser697X (c.2090C>G)	0	0	Disease causing	Deleterious (−10.26)	—	—	No
PD6-IV-1	POU4F3 (NM_002700)	c.120+1G>C	0	0	Disease causing	—	—	—	Yes

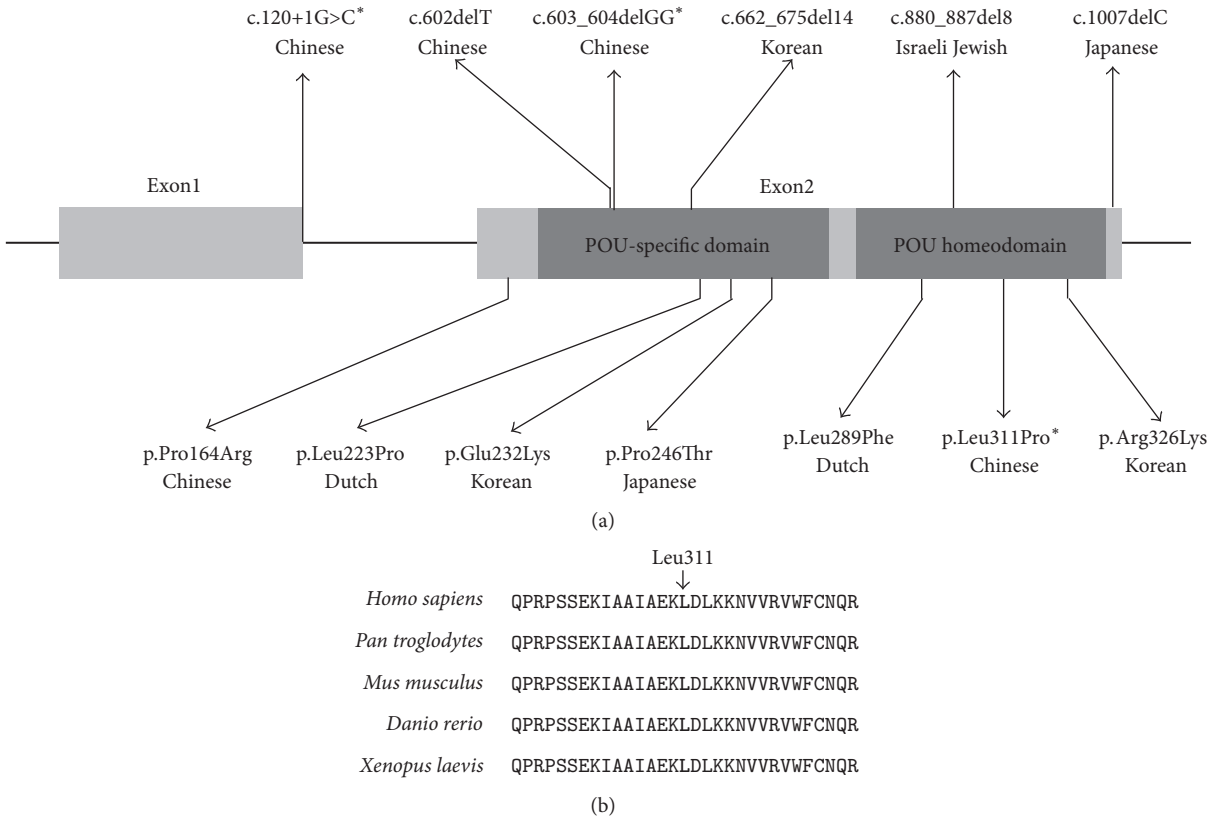

Figure 2: Summary and conservation of the *POU4F3* mutations. (a) Schematic illustration of the thirteen reported *POU4F3* mutations associated with DFNA15. Asterisks indicated the mutations reported in the present study. (b) Multispecies sequence alignment showing the evolutionary conserved amino acid Leu311.

ranged from congenital to 40 years. In Family P59 with the c.603_604delGG mutation, the proband III-8 had only moderate hearing loss at 54 years of age (Figure 1(c)) and all affected individuals in this family had a rather late age of onset around 40s. For other auditory symptoms, tinnitus has been complained by proband P1748-III-1. No vestibular dysfunction was shown in any affected individuals.

4. Discussion

Combined with our present and previous studies, we identified mutations in *POU4F3* as the pathogenic cause of deafness in 3 of the 16 (18%) Chinese Han ADNSHL families, suggesting that it is a relatively common cause for ADNSHL in Chinese Hans. Consistently, seven of the ten previously

reported *POU4F3* mutations from other research groups were also from the East Asians (three in Korean, two in Japanese, and two in Chinese, Figure 2(a)), suggesting that this gene should be routinely screened in ADNSHL cases of East Asian descent. In contrast, only three (one in Israeli Jewish and two in Dutch, Figure 2(a)) *POU4F3* mutations were previously reported from regions other than East Asia. The distinguished mutation spectrum among different ethnical groups has also been reported for other deafness genes such as *SLC26A4*, in which case biallelic *SLC26A4* mutations can be identified in 88.4% of deaf patients with nonsyndromic EVA in Chinese but only 15% in Caucasians [19, 20].

Our study also expanded the mutation spectrum of *POU4F3*. Figure 2(a) summarized the type, position, and associated ethnicity of the thirteen *POU4F3* mutations reported to date. Four of them, including the c.603_604delGG (p.Leu201fs*12) mutation reported in our previous study, were truncating mutations that were predicted to lead to prematurely stopped protein product or nonsense-mediated decay of the mRNA, while another seven *POU4F3* mutations, including the p.Leu311Pro mutation reported in the present study, were missense mutations leading to single amino acid substitutions. Notably, these twelve mutations were all located within or close to the POU-specific domain or the POU homeodomain, the two conserved DNA-binding domains of POU4F3 encoded in exon 2. On the contrary, the c.120+1G>C mutation identified in the present study is the only reported mutation outside exon 2 of *POU4F3*.

Consistent with previous reports [5, 11, 13–16], the *POU4F3* mutations identified in the present study were associated with progressive hearing loss with considerable variability in the ages of onset and the degrees of severity, and this variable hearing phenotype can be seen both interfamilially and intrafamilially. Apparently no simple genotype-phenotype correlation can be drawn based on the position or the truncating/nontruncating nature of the *POU4F3* mutations. In a previous study of the *Pou4f3* mutant deaf mice, deficiency of Pou4f3 has been found to result in reduced expression of its hair cell specific downstream target *Gfi1*, which was suggested as the direct cause of the outer hair cell degeneration in the *Pou4f3* mutant mice [10]. In future studies, therefore, it will be interesting to correlate the presumably reduced levels of the *Gfi1* transcription with different *POU4F3* mutations and the severity of the associated hearing loss.

5. Conclusions

Mutations in *POU4F3* are a relatively common cause for ADNSHL in Chinese Hans. The hearing loss associated with *POU4F3* mutations has considerable variability in the ages of onset and the degrees of severity.

Competing Interests

The authors declare no competing financial interests.

Authors' Contributions

Longxia He, Xiuhong Pang, and Penghui Chen contributed equally to this work.

Acknowledgments

This research was supported by grants from National Science Foundation of China (81570930 and 81371101 to Tao Yang; 81330023 to Hao Wu), Shanghai Municipal Science and Technology Commission (14DZ1940102 to Tao Yang; 14DZ2260300 and 14DJ1400201 to Hao Wu), and Shanghai Municipal Education Commission-Gaofeng Clinical Medicine Grant (20152519 to Tao Yang).

References

[1] R. J. H. Smith, A. E. Shearer, M. S. Hildebrand, and G. Van Camp, "Deafness and hereditary hearing loss overview," in *GeneReviews®*, R. A. Pagon, M. P. Adam, H. H. Ardinger et al., Eds., University of Washington, Seattle, Wash, USA, 1993.

[2] A. E. Shearer, A. P. DeLuca, M. S. Hildebrand et al., "Comprehensive genetic testing for hereditary hearing loss using massively parallel sequencing," *Proceedings of the National Academy of Sciences of the United States of America*, vol. 107, no. 49, pp. 21104–21109, 2010.

[3] A. E. Shearer and R. J. H. Smith, "Genetics: advances in genetic testing for deafness," *Current Opinion in Pediatrics*, vol. 24, no. 6, pp. 679–686, 2012.

[4] Z. Brownstein, Y. Bhonker, and K. B. Avraham, "High-throughput sequencing to decipher the genetic heterogeneity of deafness," *Genome Biology*, vol. 13, article 245, 2012.

[5] O. Vahava, R. Morell, E. D. Lynch et al., "Mutation in transcription factor *POU4F3* associated with inherited progressive hearing loss in humans," *Science*, vol. 279, no. 5358, pp. 1950–1954, 1998.

[6] L. Erkman, R. J. McEvilly, L. Luo et al., "Role of transcription factors Brn-3.1 and Brn-3.2 in auditory and visual system development," *Nature*, vol. 381, no. 6583, pp. 603–606, 1996.

[7] S. W. Wang, X. Mu, W. J. Bowers et al., "Brn3b/Brn3c double knockout mice reveal an unsuspected role for Brn3c in retinal ganglion cell axon outgrowth," *Development*, vol. 129, no. 2, pp. 467–477, 2002.

[8] M. Xiang, L. Gan, D. Li et al., "Essential role of POU-domain factor Brn-3c in auditory and vestibular hair cell development," *Proceedings of the National Academy of Sciences of the United States of America*, vol. 94, no. 17, pp. 9445–9450, 1997.

[9] M. Xiang, W.-Q. Gao, T. Hasson, and J. J. Shin, "Requirement for Brn-3c in maturation and survival, but not in fate determination of inner ear hair cells," *Development*, vol. 125, no. 20, pp. 3935–3946, 1998.

[10] R. Hertzano, M. Montcouquiol, S. Rashi-Elkeles et al., "Transcription profiling of inner ears from *Pou4f3*$^{ddl/ddl}$ identifies Gfi1 as a target of the Pou4f3 deafness gene," *Human Molecular Genetics*, vol. 13, no. 18, pp. 2143–2153, 2004.

[11] R. W. J. Collin, R. Chellappa, R.-J. Pauw et al., "Missense mutations in POU4F3 cause autosomal dominant hearing impairment DFNA15 and affect subcellular localization and DNA binding," *Human Mutation*, vol. 29, no. 4, pp. 545–554, 2008.

[12] H. Mutai, N. Suzuki, A. Shimizu et al., "Diverse spectrum of rare deafness genes underlies early-childhood hearing loss in Japanese patients: a cross-sectional, multi-center next-generation sequencing study," *Orphanet Journal of Rare Diseases*, vol. 8, article 172, 2013.

[13] H.-J. Kim, H.-H. Won, K.-J. Park et al., "SNP linkage analysis and whole exome sequencing identify a novel *POU4F3* mutation in autosomal dominant late-onset nonsyndromic hearing loss (DFNA15)," *PLoS ONE*, vol. 8, no. 11, Article ID e79063, 2013.

[14] H. K. Lee, H. J. Park, K. Y. Lee, R. Park, and U. K. Kim, "A novel frameshift mutation of POU4F3 gene associated with autosomal dominant non-syndromic hearing loss," *Biochemical and Biophysical Research Communications*, vol. 396, no. 3, pp. 626–630, 2010.

[15] X. Z. Cai, Y. Li, L. Xia et al., "Exome sequencing identifies *POU4F3* as the causative gene for a large Chinese family with non-syndromic hearing loss," *Journal of Human Genetics*, 2016.

[16] Q. Wei, H. Zhu, X. Qian et al., "Targeted genomic capture and massively parallel sequencing to identify novel variants causing Chinese hereditary hearing loss," *Journal of Translational Medicine*, vol. 12, article 311, 2014.

[17] M. Miyagawa, T. Naito, S.-Y. Nishio, N. Kamatani, and S.-I. Usami, "Targeted exon sequencing successfully discovers rare causative genes and clarifies the molecular epidemiology of Japanese deafness patients," *PLoS ONE*, vol. 8, no. 8, Article ID e71381, 2013.

[18] T. Yang, X. Wei, Y. Chai, L. Li, and H. Wu, "Genetic etiology study of the non-syndromic deafness in Chinese Hans by targeted next-generation sequencing," *Orphanet Journal of Rare Diseases*, vol. 8, no. 1, article 85, 2013.

[19] Q.-J. Wang, Y.-L. Zhao, A. Q. Rao et al., "A distinct spectrum of SLC26A4 mutations in patients with enlarged vestibular aqueduct in China," *Clinical Genetics*, vol. 72, no. 3, pp. 245–254, 2007.

[20] T. Yang, H. Vidarsson, S. Rodrigo-Blomqvist et al., "Transcriptional control of *SLC26A4* is involved in Pendred syndrome and nonsyndromic enlargement of vestibular aqueduct (*DFNB4*)," *American Journal of Human Genetics*, vol. 80, no. 6, pp. 1055–1063, 2007.

Hindawi Publishing Corporation
Neural Plasticity
Volume 2016, Article ID 3512098, 11 pages
http://dx.doi.org/10.1155/2016/3512098

Research Article

The Effects of Urethane on Rat Outer Hair Cells

Mingyu Fu,[1] Mengzi Chen,[1] Xiao Yan,[2] Xueying Yang,[3] Jinfang Xiao,[2] and Jie Tang[1]

[1]*Department of Physiology, School of Basic Medical Sciences, Southern Medical University, Guangzhou 510515, China*
[2]*Department of Anesthesiology, Nanfang Hospital, Southern Medical University, Guangzhou 510515, China*
[3]*Department of Anesthesiology, Sun Yat-sen Memorial Hospital, Guangzhou 510120, China*

Correspondence should be addressed to Jinfang Xiao; xiaojinfang718@163.com and Jie Tang; jietang@smu.edu.cn

Received 28 August 2016; Accepted 16 October 2016

Academic Editor: Renjie Chai

The cochlea converts sound vibration into electrical impulses and amplifies the low-level sound signal. Urethane, a widely used anesthetic in animal research, has been shown to reduce the neural responses to auditory stimuli. However, the effects of urethane on cochlea, especially on the function of outer hair cells, remain largely unknown. In the present study, we compared the cochlear microphonic responses between awake and urethane-anesthetized rats. The results revealed that the amplitude of the cochlear microphonic was decreased by urethane, resulting in an increase in the threshold at all of the sound frequencies examined. To deduce the possible mechanism underlying the urethane-induced decrease in cochlear sensitivity, we examined the electrical response properties of isolated outer hair cells using whole-cell patch-clamp recording. We found that urethane hyperpolarizes the outer hair cell membrane potential in a dose-dependent manner and elicits larger outward current. This urethane-induced outward current was blocked by strychnine, an antagonist of the $\alpha 9$ subunit of the nicotinic acetylcholine receptor. Meanwhile, the function of the outer hair cell motor protein, prestin, was not affected. These results suggest that urethane anesthesia is expected to decrease the responses of outer hair cells, whereas the frequency selectivity of cochlea remains unchanged.

1. Introduction

Under general anesthetics, decreased hearing sensitivity is common in both animal research and clinical settings. Several studies have demonstrated that different anesthetics increase auditory brainstem response thresholds [1–3] and depress neural excitability in the auditory midbrain [4, 5] and cortex [6–8]. The sensitivity of the auditory system could be changed by anesthetics at two levels: the cochlea and the auditory neurons. Because any change in cochlear function may influence the response of central auditory neurons, the effects on the cochlea are essential for the anesthetic-induced reduction in hearing sensitivity. However, the majority of studies have focused on the neural responses, whereas few have examined cochlear function [1]. Urethane has been widely used in animal research for more than a century because it exerts minimal effects on the cardiovascular and respiratory systems. Although urethane has been reported to depress the sound-evoked activity of the auditory system [4–6], its direct effect on the cochlea, particularly sensory hair cells, remains unknown.

Sensory hair cells in the cochlea not only translate sound vibration into electrical impulses but also amplify the signals of low-level sound. The latter process, defined as cochlear amplification, confers incredible sensitivity on mammalian hearing in a tremendous intensity range [9]. Cochlear amplification in mammals is attributed to outer hair cells (OHCs), which can alter their somatic length on the order of micrometers in response to membrane potential changes [10]. This electromotility is powered by the unique motor protein, prestin, on the OHC lateral membrane. The voltage-dependent structural conformation of prestin drives OHC somatic motility, which regulates cochlear amplification [11, 12]. However, the voltage-to-length change conversion function (ΔL-V) of OHCs is nonlinear and asymmetric: depolarization produces larger cell length changes than comparable hyperpolarization [13–15]. Therefore, the changes in the membrane potential may alter the operating point on the ΔL-V function and influence the overall level of cochlear amplification.

Because their electromechanical conversion occurs via a feedback mechanism, OHCs play a critical role in the efferent gain control of the cochlear amplifier. OHCs are

innervated by efferent fibers that originate in the superior olivary complex [16, 17]. These efferent fibers form synapses at the base of the OHCs and use acetylcholine (ACh) as their primary neurotransmitter [18, 19]. Nicotinic ACh receptors (AChR) have been identified on OHCs [18, 20, 21], and ACh hyperpolarizes the membrane potential of isolated OHCs [22]. The efferent activity of the olivocochlear nerve bundle during electrical stimulation has been shown to be inhibitory [23], thereby reducing the gain of the cochlear amplifier and providing protection to the ear against overstimulation [24]. A pharmacological study has indicated that urethane enhances the function of nicotinic AChRs while inhibiting the responses of NMDA and AMPA receptors [25]. We hypothesize that urethane influences the micromechanics of the organ of Corti via the OHCs and, in turn, the cochlear amplification process. If so, urethane anesthesia provides an alternative strategy to modulate cochlear amplification. By comparing the cochlear microphonic (CM) responses between awake and urethane-anesthetized rats, we found that the activity of OHCs was significantly reduced by urethane. We also measured the membrane potential and current as well as prestin activity in isolated OHCs in the presence of urethane. Our results indicate that urethane hyperpolarizes the OHC membrane potential, which is at least partially mediated by the AChR. However, prestin activity remains intact.

2. Materials and Methods

All experimental preparations, surgeries, and protocols used in this study were approved by the Animal Care and Use Committee of Southern Medical University of China. Healthy young Sprague Dawley rats of either sex (21–28 days old, body weight 40–70 g) exhibiting normal hearing were used for the experiments. The CM measurements and whole-cell patch recordings were performed as previously described [26, 27]. These methods are briefly described as follows.

2.1. CM Measurements in Awake Rats. Three days before recording, the rats were anesthetized using sodium pentobarbital. The scalp was removed, and a metal screw was mounted on the skull using glass ionomer cement. The animals were subcutaneously injected with 0.1 mg/kg buprenorphine and returned to their home cages to recover. During the recovery period, the animals were trained to become accustomed to being head-fixed in the recording setup. To fix the head, the screw was tightly clamped to a metal post. The rat was able to run freely on a plastic plate rotating around its center as described in our recent study [28]. On the day of recording, surgery was performed in a sound-proof chamber. The rats were anesthetized with 1.5% isoflurane. Then, the head was fixed to the metal post. A small incision was made via a dorsolateral approach to the pinna to expose the acoustic bulla. A silver wire recording electrode (tip diameter, ~500 μm) was placed near the round window membrane through an opening of 3 mm in diameter on the acoustic bulla (Figure 1(a)). The animal was allowed to recover from isoflurane anesthesia for at least 30 min. To acquire the CM under awake conditions, the recording was initiated after the animal exhibited normal running. Then, the animal was intraperitoneally injected with 1 g/kg urethane using a pipette to examine the effects of this anesthetic. The entire recording session lasted for approximately 5–10 hours.

Tone bursts (50 ms duration, 5 ms rise/fall time) of various frequencies (2, 4, 8, 16, or 32 kHz) and intensities (0–70 dB SPL at 5 dB intervals) were presented using a calibrated TDT ES1 speaker located 50 cm away from the recorded ear. The frequency-amplitude scan was computer controlled (TDT System 3, Tucker-Davis Technologies) and was delivered in a randomized sequence. Each frequency-amplitude combination was repeated 10 times. The CM responses to the tone bursts were amplified, filtered, and recorded using an A/D converter (1440A/700B system, Molecular Devices). The noise level of the recording system was approximately 10 μV. Customized MATLAB software was used for offline data processing, such as response averaging and response amplitude extraction.

2.2. Cell Isolation. The animals were anesthetized (CO_2 inhalation) and decapitated, and the inner ears were rapidly removed from the temporal bones and placed in Leibovitz's L-15 media (Invitrogen, Carlsbad, CA). The organ of Corti was isolated from the middle and apical turns of the cochlea. After mild enzymatic digestion for 5 min (2 mg/mL collagenase IV, Sigma, St. Louis, MO) and gentle pipetting, the cells were transferred to a small plastic chamber filled with enzyme-free culture medium (~1.5 mL). The standard medium was Leibovitz's L-15, supplemented with 10 mM HEPES (Invitrogen, Carlsbad, CA) and adjusted to pH 7.35 and 300 mOsm. Then, the chamber containing the cells was placed on the stage of an inverted microscope (Nikon, Eclipse FN1) equipped with a video camera. Healthy-appearing solitary OHCs were selected for the electrophysiological experiments if they displayed no obvious signs of shrinkage, swelling, damage, or deterioration such as granularity or translocation of the nucleus.

2.3. Whole-Cell Patch-Clamp Recordings. These experiments were performed at room temperature (22 ± 4°C) under video monitoring. The OHCs were bathed in L-15 medium buffered with 10 mM HEPES (pH 7.35, 300 mOsm). An Ag/AgCl ground electrode was installed in the bath. The patch electrodes were pulled from 1.5 mm glass capillary tubes at resistances between 3 and 6 MΩ using a horizontal micropipette puller (Model P-97, Sutter). The electrodes were back-filled with a solution containing (in mM) 145 KCl, 2 $MgCl_2$, and 10 HEPES. The access resistance typically ranged from 10 to 17 MΩ when the whole-cell recording configuration was established. At least 80% of the access resistance was compensated. In most of our recordings, the whole-cell currents were less than 3 nA.

Under computer control, hyperpolarizing and depolarizing voltage steps (250 ms duration and ranging from −140 to +94 mV in 13 mV increments) were used to elicit whole-cell currents. The low-pass-filtered currents (corner frequency of 5 kHz) were amplified using an Axopatch

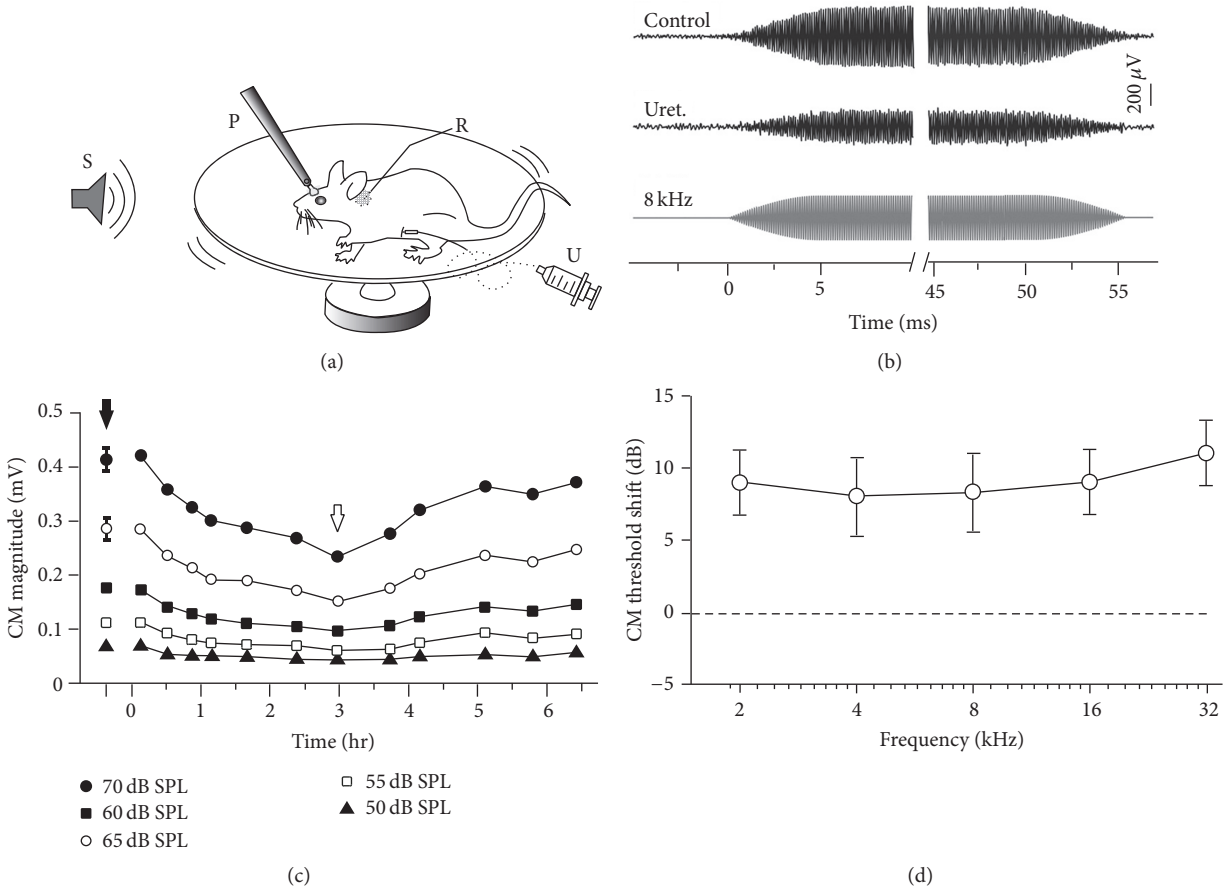

Figure 1: Reduction in the CM after urethane anesthesia. (a) A schematic of our CM recording setup. S, sound stimulation delivered by a speaker; P, metal post for head fixation; R, silver wire recording electrode; U, urethane delivery. The rat was awake and allowed to run freely on a rotatable plate. (b) Examples of the CM measured in response to an 8 kHz, 70 dB SPL tone burst (sound waveform shown in the bottom panel). The magnitude before urethane injection (upper panel, filled arrow in (c)) compared to that after anesthesia (middle panel, open arrow in (c)). (c) The time course of the CM magnitude changes after urethane injection. The curves shown are CM responses to different sound levels. Three CM measurements evoked before urethane injection were averaged as a control (mean ± SD) for each sound level. Time 0 indicates the time point of urethane injection. (d) CM threshold shifts for urethane application. Data presented as mean ± SD. Note the CM thresholds were elevated at all frequencies examined ($p < 0.05$, Student's t-test, $n = 5$).

200B amplifier (Axon Instruments). The urethane-evoked current responses were recorded in voltage-clamp mode. To obtain large urethane-evoked outward currents, the cells were typically held at 0 mV. The whole-cell currents and evoked current responses were acquired using pClamp 10 software (Molecular Devices) on a computer connected to an A/D converter (Digidata 1322A, Axon Instruments). The sampling frequency was between 5 and 10 kHz. The data were analyzed using the pClamp software package.

For nonlinear capacitance (NLC) measurements, the whole-cell patch-clamp technique was performed as described above. The membrane capacitance was measured using a two-sine-wave voltage stimulus protocol (10 mV peak at both 390.6 Hz and 781.2 Hz) with subsequent fast Fourier transform-based admittance analysis [29] at a holding potential of 0 mV. The data were acquired using jClamp software (Scisoft, New Haven, CT) and were analyzed using OriginPro software (OriginLab Corporation, Northampton, MA).

The NLC can be described as the first derivative of a two-state Boltzmann function of nonlinear charge movement to voltage [30]. The capacitance function is described as

$$C_m = C_{\text{lin}} + \frac{Q_{\max}\alpha}{\exp\left[\alpha\left(V_m - V_{1/2}\right)\right]\left(1 + \exp\left[-\alpha\left(V_m - V_{1/2}\right)\right]\right)^2}. \quad (1)$$

Four parameters ($Q_{\max}$, $V_{1/2}$, C_{lin}, and z) from the equation were obtained: $Q_{\max}$ is the maximum charge transfer; $V_{1/2}$ is the peak of the voltage-dependent capacitance; C_{lin} is the linear capacitance; and $\alpha = ze/kT$ is the slope of the voltage dependence of the charge transfer. Furthermore, k is the Boltzmann constant, T is absolute temperature, z is the valence of the charge movement, and e is the electron charge. C_{lin} is the linear capacitance representing the surface area of the membrane (i.e., the cell size). To compare the magnitude

of the NLC and Q_{max} obtained from different cells of varying size, we normalized the NLC and Q_{max} to C_{lin}.

2.4. Drug Application. The drugs were dissolved in standard medium (L-15) adjusted to pH 7.35 and 300 mOsm. All solutions were freshly prepared from stock solution before each experiment. Urethane was delivered via pressure ejection from a micropipette with a tip diameter of ~5 μm positioned 20–50 μm from the bottom of the cell. The duration and strength of the pressure were controlled using a homemade microinjector. Care was taken to assure that the application of a drug solution did not alter the position of the cell or influence the measurements. In the strychnine coapplication experiments, the strychnine solution was slowly perfused into the bath (1 mL/min) without disturbing the position of the cells. The entire bath was exchanged when strychnine was applied. Urethane was dissolved in strychnine solution and delivered via pressure ejection as described above. All of the drugs were applied to achieve a final concentration until a consistent response was observed and a washout was performed after each application.

2.5. Data Analysis. Results are presented as the mean ± SD. A Student's t-test was used to examine the significance of the difference between the responses obtained before and during the drug applications. Significance was determined as $p < 0.05$. Excel software and OriginPro software were used for calculating, data fitting, and plotting.

3. Results

3.1. The CM under Urethane Anesthesia. The inner and outer hair cells, which are the sensory receptor cells of the inner ear, function as a transducer by converting the mechanical movement of the basilar membrane into an alternating electrical voltage. This alternating voltage is defined as the CM, which mimics the waveform of a sound stimulus. Representative CM recordings are shown in Figure 1, in which the effects of urethane anesthesia are presented for the same rat. We performed CM recordings on head-fixed awake rats to monitor the receptor potential before and after urethane application (Figure 1(a)). To avoid the middle ear reflex, mild tone bursts (less than 70 dB SPL) were used to elicit the CM responses.

As shown in Figure 1(b), an 8 kHz tone (level at 70 dB SPL) evoked a CM at an amplitude of ~424 μV. The amplitude of the CM responses at saturation levels was reduced by 44% to 238 μV after the intraperitoneal injection of urethane. The proximity of the recording electrodes to the hair cells may affect the recorded amplitudes. To ensure that our control recordings were not influenced by the activity of the animal, we averaged at least three evoked CM measurements before the urethane injection. For the CMs measured from all five rats, urethane induced a significant decrease in the CM of 39.3% on average ($p < 0.01$, Student's t-test).

The time course of this urethane effect was examined in five rats that exhibited at least an 80% recovery in the CM amplitude. The representative changes in the CM over time after urethane injection are shown in Figure 1(c). The initial decrease in the CM was observed ~25 min after the urethane injection, reached its lowest value within ~3 hours, and then recovered gradually. The time of the peak reduction was highly variable between different rats, ranging from 45 min to 3 hours (45 min, 75 min, 90 min, 3 hours, and 3.2 hours, resp.). The CM responses to different sound levels were also measured. As shown in Figure 1(c), the changes in the CM amplitudes at different sound levels followed a similar time course. We compared the CM thresholds before and after urethane application (Figure 1(d)). The CM thresholds were defined as the minimum sound level that evoked a detectable CM response. Consistent with the CM magnitude measurements, the CM thresholds were increased by urethane application at all frequencies examined. The increase of threshold is similar and shows no significance at different sound frequencies ($p > 0.05$, Student's t-test).

3.2. OHC Responses under Current and Voltage Clamp. The CM response is dominated by the OHCs in the organ of Corti [9, 31]. As such, the CM reduction in our experiments represents a significant reduction in OHC activity after urethane application. To determine how urethane alters the responses of OHCs, whole-cell current- and voltage-clamp recordings were performed from OHCs acutely isolated from the middle and apical turns of the rat cochlea. Isolated OHCs can easily be identified based on visual inspection: the OHCs display a cylindrical morphology with a nucleus located near the base, whereas inner hair cells are flask-shaped with an upper nucleus position. Another indication of OHCs is a functional characteristic: the visible motile responses elicited by the rapid membrane potential changes generated during our patch-clamp measurements [22, 32].

The average zero current membrane potential under whole-cell recording conditions was −54 mV (SD = 7 mV, n = 19). To determine the influence of urethane, different concentrations of urethane were applied to the recorded OHC via local perfusion for ~15 s (as shown in Figure 2(a)). As a control, recordings were also performed with L-15 medium: no membrane potential change was detected during L-15 perfusion (0 mM in Figure 2(b)). The stability of this recording indicates that our measurements were not affected by the perfusion flow rate. When 100 mM urethane was delivered to an OHC clamped at 0 nA, the steady-state membrane potential was hyperpolarized by 28.6 mV and was repolarized shortly after drug application (Figure 2(b)). This reversible hyperpolarization was detected in all five OHCs measured (mean ± SD = 27.0 ± 3.9). To rule out the effects of urethane on the OHC membrane potential, we applied several concentrations of urethane. Urethane at a concentration as low as 0.1 mM, which is ~1/100 of the dose typically used to anesthetize animals, elicited a detectable membrane hyperpolarization. Figure 2(c) displays the average membrane potential changes induced by different urethane concentrations. These data also provide the mean normalized response. The smooth curve represents a fit according to the following form of the Hill equation: $V_{Uret} = 100/[(K_D/[Uret])^n + 1]$. A fifty percent reduction in the membrane potential was detected at 15.4 mM (K_D), and the slope (n) of the membrane potential change to the urethane concentration was 0.91. Subsequent experiments

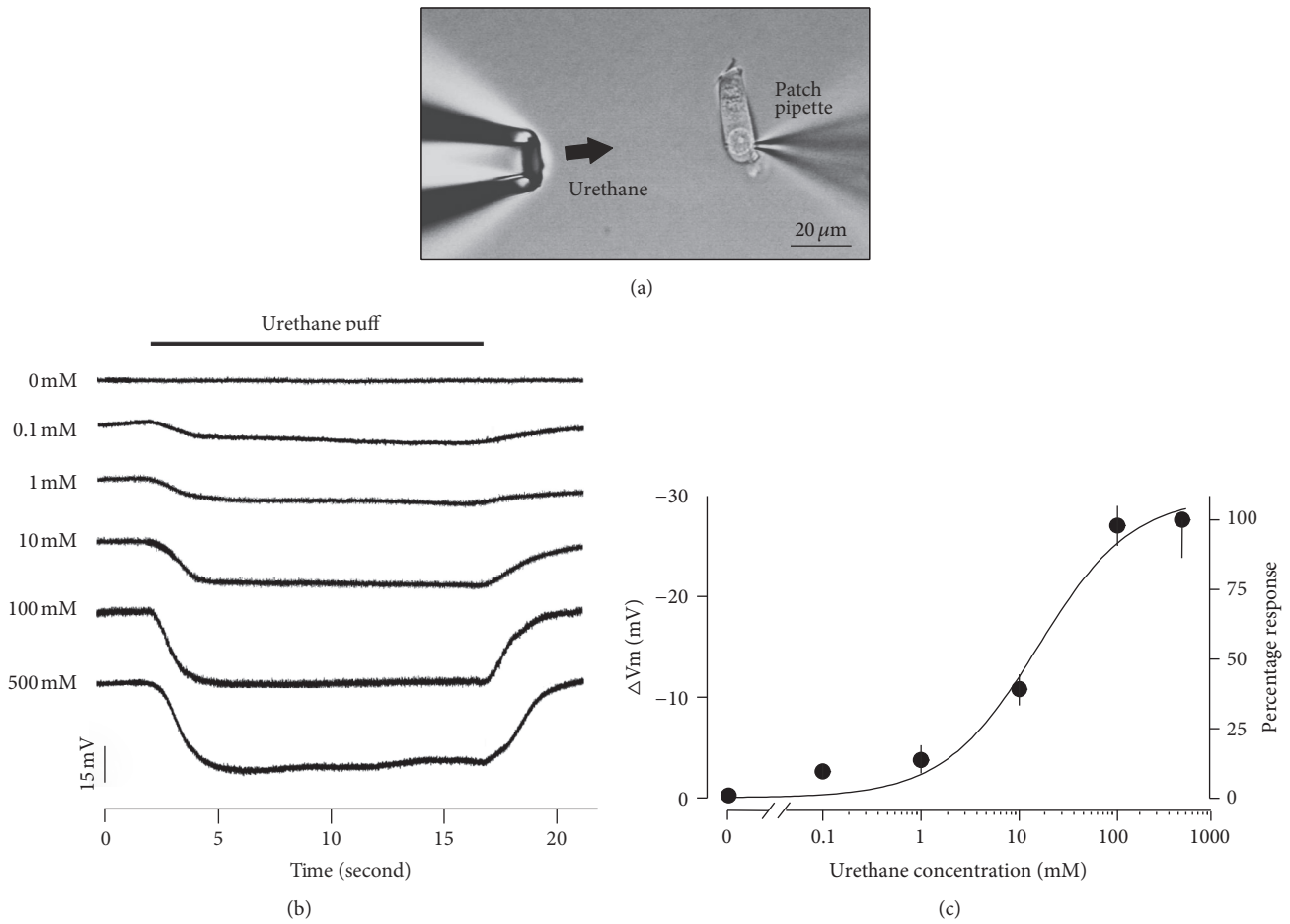

Figure 2: The urethane-induced hyperpolarization of the OHC membrane potential. (a) A photograph showing the experimental setup for the whole-cell patch-clamp recordings. Urethane was delivered via pressure ejection from a micropipette positioned ~50 μm from the cell. The microphotograph was captured using an upright microscope under bright field illumination. The bar represents 20 μm. (b) Examples of membrane potentials recorded from OHCs clamped to zero membrane current during the delivery of a urethane puff (0.1 mM, 1 mM, 10 mM, 100 mM, or 500 mM concentration, timing denoted by the horizontal bar) or standard medium (0 mM). (c) The dose-response curve of the OHC membrane potential evoked by 0 mM (obtained from 4 cells), 0.1 mM (5 cells), 1 mM (3 cells), 10 mM (5 cells), 100 mM (5 cells), or 500 mM (4 cells) urethane. The data are presented as the mean values; the error bars represent the SD. The values are also normalized to the mean reduction evoked by 500 mM urethane. The smooth curve is the Hill equation with a half-activating concentration of 15.4 mM and a slope of 0.91.

used 100 mM urethane because this concentration consistently evoked an apparent response.

We also examined the effects of urethane on the membrane current by using voltage-clamp recordings. A representative example of the whole-cell current recorded from an isolated OHC is shown in Figure 3(a). When the membrane potential was clamped from −140 to +94 mV, the cell currents changed from −445 pA (inward) to +1480 pA (outward), resulting in a dynamic range of 1925 pA. The response measured under control conditions is consistent with results previously published for guinea pig [22, 33] and gerbil OHCs [34]. The local perfusion of 100 mM urethane significantly increased the current magnitudes, especially at potentials greater than −50 mV. Figure 3(b) shows the current-voltage (I-V) curve derived from the steady-state responses shown in Figure 3(a). The dynamic range was approximately 72% larger after urethane application in the example presented. The mean change of I-V curves recorded from 11 OHCs was shown in Figure 3(c). Notably, the increased outward currents occurred at high membrane potentials.

3.3. The Effect of Strychnine on the Urethane-Induced Response. Urethane is not an endogenous neurotransmitter or modulator. Therefore, it is unlikely that the effects of urethane are mediated by a specific urethane receptor. The apparent changes in the OHC current response in the voltage-clamp experiments are most likely due to the effects of urethane on existent ion channels. Acetylcholine is the primary efferent neurotransmitter in the cochlea and is released from the efferent chemical synapses at the base of the OHCs [19, 24]. The α9 subunit of the nicotinic AChR family, which was identified from a rat genomic library, has been demonstrated

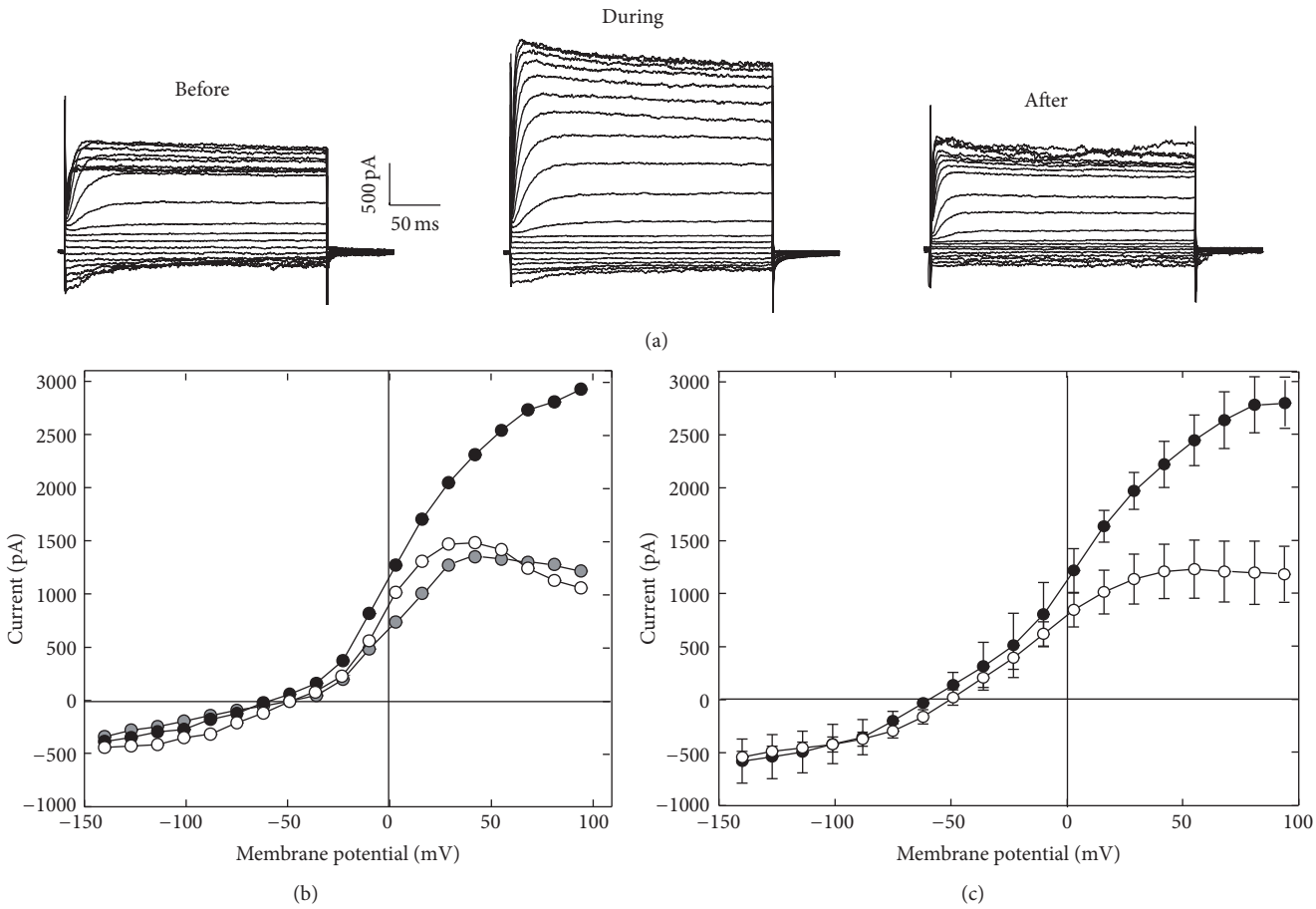

Figure 3: Urethane-induced membrane current changes. (a) Example of the membrane current waveforms recorded from a solitary OHC before, during, and after 100 mM urethane application. The cell was held at −70 mV, and voltage commands varied from −140 to +94 mV in 13 mV steps. (b) The *I-V* curves derived from the steady-state responses shown in (a). The open, black, and gray filled circles represent the responses before, during, and after urethane application, respectively. (c) Plot of the average (±SD) *I-V* curves recorded from OHCs ($n = 11$) before (open circles) and during (filled circles) urethane application.

to play an important role in the ACh-induced responses of OHCs [18, 20, 21]. To determine whether the urethane-induced response occurs via this AChR, we examined the effect of strychnine (a potent antagonist of the $\alpha 9$ AChR subunit) on the urethane-induced responses. Because the membrane current is directly related to nicotinic AChR activity and is easy to record, we measured the urethane-induced current as an indicator of nicotinic AChR activity.

To obtain the urethane-induced current, the membrane potential of isolated OHCs was held at 0 mV. The top trace in Figure 4(a) shows a 280 pA upward change of membrane current that correlated in time to the perfusion of 100 mM urethane onto this cell (~20 s). As indicated in Figure 3(b), urethane increased the outward current at a membrane potential of 0 mV. Therefore, the magnitude of the observed current change reflects the amplitude of the outward current elicited by urethane. Coapplication of 0.01 μM strychnine reduced the amplitude of the urethane-induced current to 114 pA at saturation level (Figure 4(a), middle trace). These data suggest that the urethane-induced response is mediated, at least in part, via AChR assembled from $\alpha 9$ subunits. Then, a higher concentration of strychnine (0.1 μM) was coapplied to examine whether the urethane response was blocked in a dose-dependent manner. To minimize desensitization of the receptor, 3 min washout was set between two concentrations. As shown in the bottom trace (Figure 4(a)), the urethane-induced outward current was further reduced to 48 pA in the presence of 0.1 μM strychnine. In the seven OHCs measured (Figure 4(b)), the magnitude of the urethane-induced response was significantly reduced by the coapplication of both 0.01 μM (by 54 ± 12% on average) and 0.1 μM strychnine (by 79 ± 10% on average) (both $p < 0.001$, Student's t-test).

3.4. NLC Measurement during Urethane Treatment. Mammalian OHCs contract or elongate at acoustic frequencies depending on the membrane potential of the cell [10, 35, 36]. This process, defined as electromotility, is necessary for cochlear amplification [37–39]. Prestin, a unique voltage-dependent motor protein found in the membrane of OHCs, mediates the electromotility of OHCs [11, 40]. The voltage-sensing and motor functions of mammalian prestin manifest as two characteristics: the NLC and electromotility. The NLC

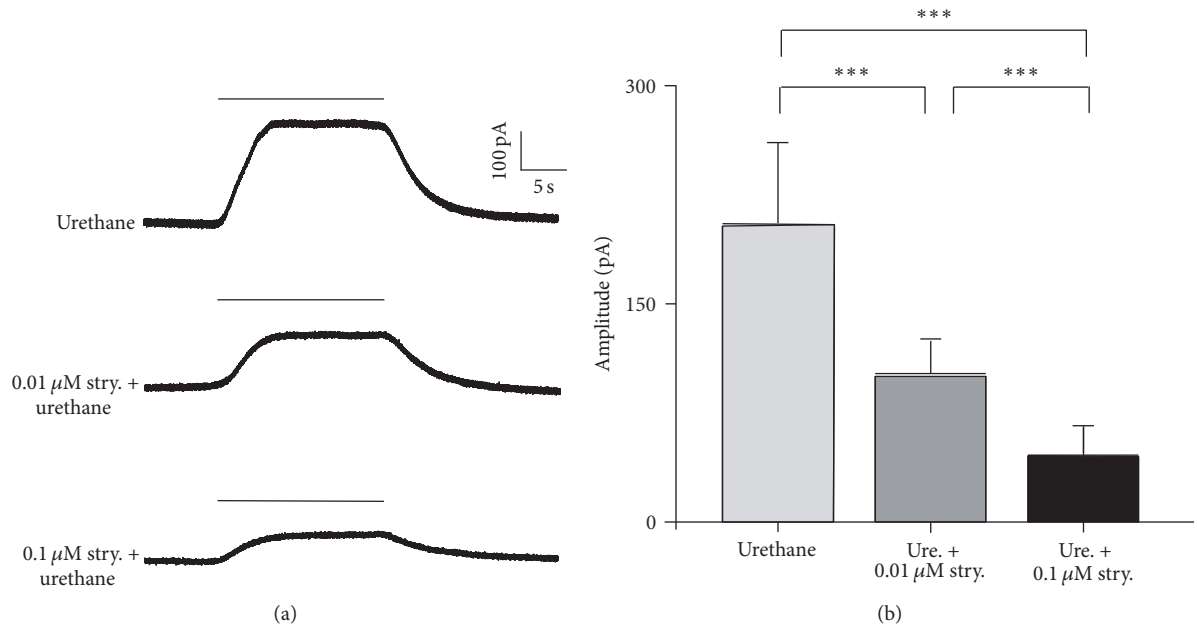

Figure 4: Urethane induces membrane current changes via the nicotinic AChR. (a) Strychnine, an antagonist of α9 AChRs, partially blocked the OHC response to urethane. The cell was held at 0 mV, and 100 mM urethane was pressure-ejected near the cell (timing denoted by the horizontal bar) to obtain the control response (top trace). Either 0.01 (middle trace) or 0.1 μM strychnine (bottom trace) was coapplied with urethane to the OHC. The magnitude of the outward currents decreased as the coapplied strychnine concentration increased. A 3 min waiting period was used between each trial. (b) The average amplitudes of outward current in response to 100 mM urethane or 100 mM urethane coapplied with two different doses of strychnine. Bar = SD. $^{***}p < 0.001$, Student's t-test. $N = 7$.

and electromotility are fully coupled in mammals [30, 41, 42] and can be characterized using a simple two-state Boltzmann function. Because the NLC can be easily and accurately measured experimentally, we measured the NLC to evaluate the effects of urethane on prestin function.

Figure 5(a) shows an example of the NLC obtained from an isolated OHC under the whole-cell patch-clamp configuration. As shown in the control (open circles and gray line) treatment before urethane application, the NLC is characterized by a bell-shaped dependence on the membrane potential and a peak at −54.8 mV for this cell. No clear change was detected in response to application of 100 mM urethane (filled circles and black line). We examined the NLC from a total of 10 OHCs in response to urethane treatment. Figure 5(b) presents the mean and SD of the normalized NLC from these cells. Four parameters (Q_{max}, C_{lin}, $V_{1/2}$, and z) were obtained from a curve fit of the NLC response using the first derivative of the Boltzmann function (heavy lines in Figures 5(a) and 5(b)). The normalized mean values and SDs of the four parameters from the 10 OHCs are plotted in Figure 5(c). No statistically significant difference was found in response to urethane treatment for all parameters ($p > 0.05$, Student's t-test).

4. Discussion

We have shown for the first time that urethane affects the electrical response properties of isolated OHCs. As shown in Figure 2, urethane hyperpolarizes OHCs by approximately 30 mV. Our voltage-clamp data shows that when OHCs were depolarized, the outward current was significantly increased by urethane (Figure 3). This effect was voltage-dependent: it was more pronounced at membrane potentials higher than −50 mV. In mature OHCs, two currents are primarily involved in this process: (1) the voltage activated outward K^+ current and (2) the Ca^{2+}-activated K^+ current. The voltage-dependent K^+ current is activated at membrane potentials from −90 mV to −50 mV, displaying half activation at −80 mV [43]. Because the urethane-induced current change was clearly detected at membrane potentials >−50 mV, its effect is likely not via this channel.

The Ca^{2+}-activated K^+ channel was first reported by Ashmore and Meech [44]. At membrane potentials >−35 mV, this K^+ channel is opened by an influx of Ca^{2+}, leading to K^+ efflux [45]. Under physiological conditions, the activation of AChRs causes an influx of Ca^{2+} [22]. We assumed that the effect of urethane on OHCs involves this process based on our strychnine experiment. The α9 subunit of the nicotinic AChR family has been demonstrated to be the primary nicotinic AChR subunit in OHCs [20]. The α9 subunit displays unique pharmacological properties similar to those detected in cochlear hair cells. We found that strychnine, a potent antagonist of α9-containing AChRs, significantly blocks the urethane-induced outward current (Figure 4). Therefore, we propose that urethane activates α9-containing AChRs and induces a Ca^{2+} influx. Then, this influx of Ca^{2+} leads to the opening of Ca^{2+}-activated K^+ channels and subsequent K^+ efflux, resulting in hyperpolarization of the OHCs. Consistent with our results, a study in *Xenopus* oocytes indicates that urethane enhances the response of nACh receptor [20]. Our

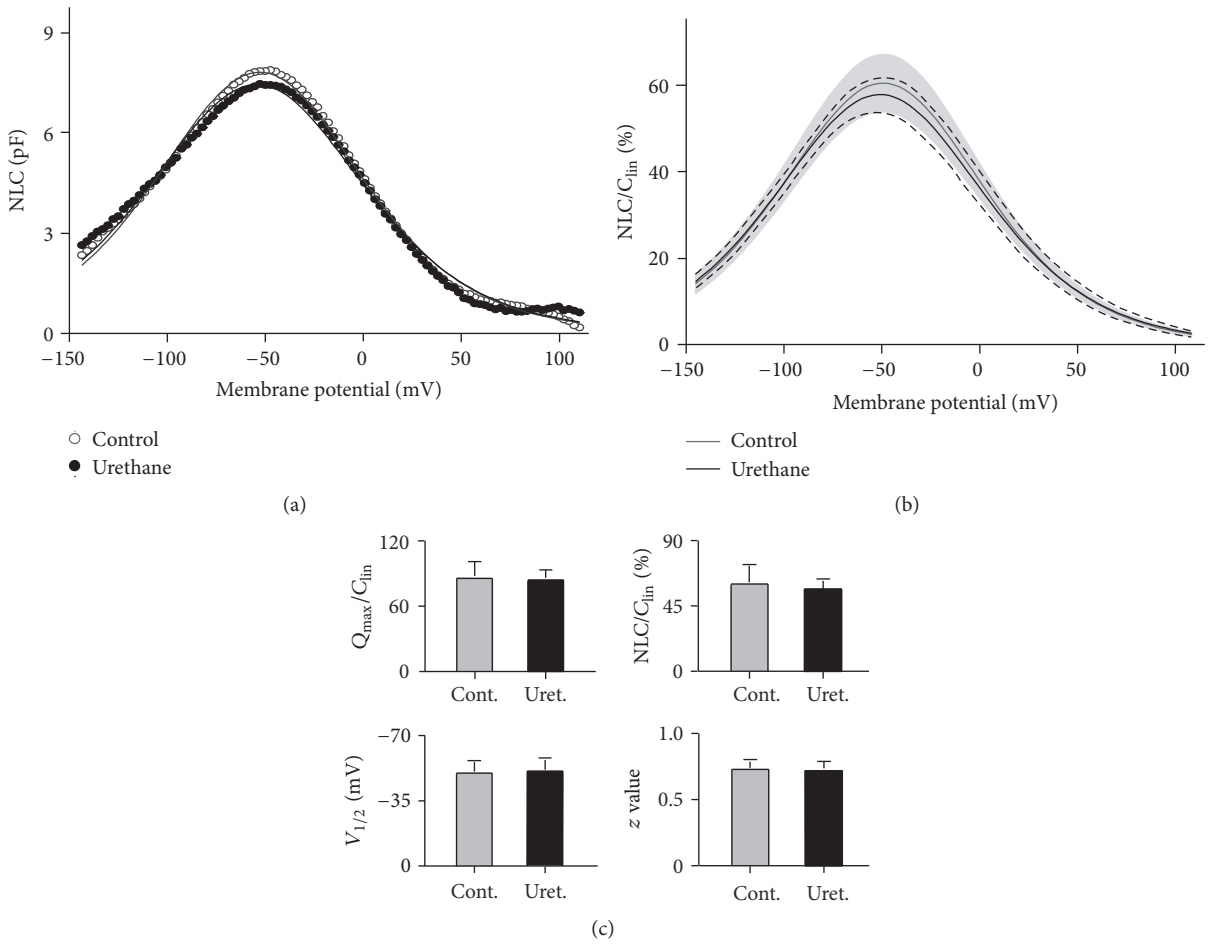

Figure 5: The effects of urethane on the NLC measured from OHCs. (a) The NLC obtained from a representative OHC before (control, open circles) and during (urethane, filled circles) 100 mM urethane application. The capacitance-voltage responses were fitted to the Boltzmann function (shown as the gray and black lines). C_{lin} was subtracted from the NLC. pF, picofarads. (b) Pooled data of the NLCs recorded from 10 OHCs. The NLCs were normalized to the corresponding C_{lin}, and the curves were plotted as the mean NLC ± SD. The SD around the mean is indicated by the shaded region for the control and by dashed lines for urethane treatment. (c) Four parameters derived from the curve fit to the Boltzmann function. The data are expressed as the means and the SDs; $N = 10$. No significant difference was detected between the cases before and during urethane application (Student's t-test, $p > 0.05$).

data is also supported by the urethane effects on cochlear function by measuring DPOAE [46]. Urethane decreases the efferent influence from medial olivocochlear terminus to OHCs via the $\alpha 9$ receptor. The presence of urethane may reduce the effects of ACh release from efferent fibers. However, the direct mechanism underlying nicotinic AChR activation by urethane remains unknown.

The cylindrically shaped OHCs alter their cell length in response to membrane potential changes, exhibited as either a somatic elongation (upon hyperpolarization) or contraction (upon depolarization). This somatic motility of OHCs is responsible for cochlear amplification, which contributes to the exquisite frequency selectivity and sensitivity in mammals [10, 37]. However, this change in length is asymmetric: the magnitude of contraction is much larger than that of elongation [13–15]. Figure 2 shows that urethane hyperpolarizes OHCs by approximately 30 mV. This potential change moves the operating point of the voltage-to-length change conversion function toward lower slope, thereby reducing the overall augmentation of OHC electromotility. Based on the voltage-to-length change conversion function for OHCs in the guinea pig, a 30 mV hyperpolarization reduces the total motility magnitude by approximately 25–35% [15]. We expect a corresponding maximal magnitude change in rat OHCs.

However, *in vitro* acetylcholine application evokes an increase of electromotile responses of isolated OHCs that develops on a time scale of several seconds [22]. It would increase the driving force for the mechanotransduction current, causing the increase of cochlear microphonic potential. It seems a mismatch between our *in vitro* data and *in vivo* CM results. For *in vitro* experiment, a high concentration urethane was applied to isolated OHCs directly. Therefore, the effects were observed in seconds. However, *in vivo*, a safe concentration urethane was injected intraperitoneally. It may take time for urethane to reach and accumulate in the inner ear. The time course for OHCs may differ from that for cardiovascular and respiratory systems. In addition to a change in the membrane potential, mechanical properties of OHCs

could also influence the cochlear amplifier. It is the consensus that normal cell morphology and somatic stiffness of OHCs are essential for cochlear amplification [12, 47]. Acetylcholine decreases the axial stiffness of the OHCs and reduces the overall mechanical load of the aggregate OHC, resulting in the increase of motile magnitude [22]. It has been suggested that the changes of the OHCs stiffness are mediated by Ca^{2+}-dependent phosphorylation of the OHC cortical cytoskeleton [22, 48]. Since urethane would also activate α9-containing AChRs and induce a Ca^{2+} influx, a similar decrease of OHCs axial stiffness and a reduction of global cochlear activity may be induced by urethane application *in vivo*.

The electromotility of OHCs is presumably attributed to the voltage-dependent activity of the motor protein prestin [11, 40]. A generally accepted model for prestin function is that intracellular anions (in most cases Cl^-) move toward the extracellular surface upon hyperpolarization and toward the cytoplasmic side in response to depolarization [40]. This anion translocation produces a nonlinear change in the membrane capacitance and, subsequently, triggers a conformational change in prestin, which ultimately alters the somatic length of the OHC. According to this model, any changes in this voltage-dependent activity of prestin may alter the motility of OHCs and affect the overall level of cochlear amplification. For all measured parameters reflecting the properties of prestin function, we did not observe any significant change in response to urethane in our experiments (Figure 5). Therefore, we assumed that the influence of urethane was not the alteration of the motile activity of prestin. Nonetheless, anion transfer may be significantly reduced by urethane-induced hyperpolarization. In mammalian OHCs, this charge movement is represented as the NLC, which is characterized by a bell-shaped dependence on the membrane potential that peaks between −70 and −20 mV (−50 mV in our results) [30, 41]. The urethane-induced hyperpolarization shifts the operating range of the membrane potential away from this peak, thus reducing the charge movement and the activity of prestin. This effect is a likely mechanism by which urethane reduces OHC motility *in vivo*. Because the electromotility of OHCs feeds a cycle-by-cycle force to the organ of Corti so that the sound vibration is amplified, it is conceivable that even a modest reduction in the motility of OHCs could reduce the overall level of cochlear amplification.

The results from isolated OHCs are consistent with our *in vivo* experimental evidence (Figure 1). Although the time courses of the urethane-induced effects were different, all of the rats examined exhibited a similar reduction in the CM magnitude. Despite the expanding research to awake animal models of monkeys [49, 50], bats [51, 52], mice [28], and rats [53], the majority of auditory studies are based on the results obtained from anesthetized animals. The frequency selectivity of auditory neurons is composed of two elements: the frequency tuning of the cochlea and the refinement of the auditory neural system. The detected anesthesia-induced changes in neural responses involve the effects of the anesthetic on not only the neurons themselves but also the peripheral receptors (hair cells). Therefore, it is critical to identify the influence over hair cells from the integrity. Our data show that urethane elicited a ~10 dB CM threshold lifting (Figure 1(d)), which indicates that the depression of OHCs leads to a reduction in hearing sensitivity. Furthermore, this depression is identical at all sound frequencies, suggesting that urethane affects OHCs along the entire basilar membrane. These results are similar to those of isoflurane and ketamine, which have been assessed using distortion product otoacoustic emissions [1].

5. Conclusions

The present study found that urethane hyperpolarizes outer hair cells, resulting in a reduction in hearing sensitivity without affecting frequency selectivity. Our findings indicate that anesthetics directly affect cochlear hair cells and provide an alternative strategy to modulate cochlear functions.

Competing Interests

The authors declare that they have no competing interests.

Acknowledgments

This work was supported by grants from the National Natural Science Foundation of China (31271179) and a 973 Program (2014CB943002) to Jie Tang and the Science and Technology Planning Project of Guangdong Province (509088405041) to Jinfang Xiao.

References

[1] J. M. E. Cederholm, K. E. Froud, A. C. Y. Wong, M. Ko, A. F. Ryan, and G. D. Housley, "Differential actions of isoflurane and ketamine-based anaesthetics on cochlear function in the mouse," *Hearing Research*, vol. 292, no. 1-2, pp. 71–79, 2012.

[2] R. Santarelli, E. Arslan, L. Carraro, G. Conti, M. Capello, and G. Plourde, "Effects of isoflurane on the auditory brainstem responses and middle latency responses of rats," *Acta Oto-Laryngologica*, vol. 123, no. 2, pp. 176–181, 2003.

[3] M. R. Ruebhausen, T. J. Brozoski, and C. A. Bauer, "A comparison of the effects of isoflurane and ketamine anesthesia on auditory brainstem response (ABR) thresholds in rats," *Hearing Research*, vol. 287, no. 1-2, pp. 25–29, 2012.

[4] J. Astl, J. Popelář, E. Kvašňák, and J. Syka, "Comparison of response properties of neurons in the inferior colliculus of guinea pigs under different anesthetics," *Audiology*, vol. 35, no. 6, pp. 335–345, 1996.

[5] J. W. Schumacher, D. M. Schneider, and S. M. N. Woolley, "Anesthetic state modulates excitability but not spectral tuning or neural discrimination in single auditory midbrain neurons," *Journal of Neurophysiology*, vol. 106, no. 2, pp. 500–514, 2011.

[6] B. Capsius and H.-J. Leppelsack, "Influence of urethane anesthesia on neural processing in the auditory cortex analogue of a songbird," *Hearing Research*, vol. 96, no. 1-2, pp. 59–70, 1996.

[7] B. H. Gaese and J. Ostwald, "Anesthesia changes frequency tuning of neurons in the rat primary auditory cortex," *Journal of Neurophysiology*, vol. 86, no. 2, pp. 1062–1066, 2001.

[8] K. Szalda and R. Burkard, "The effects of nembutal anesthesia on the auditory steady-state response (ASSR) from the inferior colliculus and auditory cortex of the chinchilla," *Hearing Research*, vol. 203, no. 1-2, pp. 32–44, 2005.

[9] P. Dallos, "Overview: cochlear neurobiology," in *The Cochlea*, A. N. P. P. Dallos and R. R. Fay, Eds., vol. 8 of *Springer Handbook*

of Auditory Research, pp. 1–43, Springer, New York, NY, USA, 1996.

[10] W. E. Brownell, C. R. Bader, D. Bertrand, and Y. De Ribaupierre, "Evoked mechanical responses of isolated cochlear outer hair cells," *Science*, vol. 227, no. 4683, pp. 194–196, 1985.

[11] J. Zheng, W. Shen, D. Z. Z. He, K. B. Long, L. D. Madison, and P. Dallos, "Prestin is the motor protein of cochlear outer hair cells," *Nature*, vol. 405, no. 6783, pp. 149–155, 2000.

[12] M. C. Liberman, J. Gao, D. Z. Z. He, X. Wu, S. Jia, and J. Zuo, "Prestin is required for electromotility of the outer hair cell and for the cochlear amplifier," *Nature*, vol. 419, no. 6904, pp. 300–304, 2002.

[13] B. N. Evans, P. Dallos, and R. Hallworth, "Asymmetries in motile responses of outer hair cells in simulated in vivo conditions," in *Cochlear Mechanisms: Structure, Function, and Models*, B. N. Evans, P. Dallos, and R. Hallworth, Eds., NATO ASI Series, pp. 205–206, Plenum, New York, NY, USA, 1989.

[14] B. N. Evans, R. Hallworth, and P. Dallos, "Outer hair cell electromotility: the sensitivity and vulnerability of the DC component," *Hearing Research*, vol. 52, no. 2, pp. 288–304, 1991.

[15] J. Santos-Sacchi, "Asymmetry in voltage-dependent movements of isolated outer hair cells from the organ of Corti," *Journal of Neuroscience*, vol. 9, no. 8, pp. 2954–2962, 1989.

[16] H. Spoendlin, "Innervation densities of the cochlea," *Acta Oto-Laryngologica*, vol. 73, no. 2–6, pp. 235–248, 1972.

[17] W. B. Warr, J. J. Guinan, and J. S. White, "Organization of the efferent fibers: the lateral and medial olivocochlear systems," in *Neurobiology of Hearing: The Cochlea*, R. A. Altschuler, D. W. Hoffmann, and R. P. Bobbin, Eds., pp. 333–348, Raven Press, New York, NY, USA, 1986.

[18] M. Eybalin, "Neurotransmitters and neuromodulators of the mammalian cochlea," *Physiological Reviews*, vol. 73, no. 2, pp. 309–373, 1993.

[19] W. F. Sewell, "Neurotransmitters and synaptic transmission," in *The Cochlea*, P. A. Dallos and R. R. Fay, Eds., pp. 503–533, Springer, New York, NY, USA, 1996.

[20] A. B. Elgoyhen, D. S. Johnson, J. Boulter, D. E. Vetter, and S. Heinemann, "α9: an acetylcholine receptor with novel pharmacological properties expressed in rat cochlear hair cells," *Cell*, vol. 79, no. 4, pp. 705–715, 1994.

[21] R. P. Bobbin, "Chemical receptors on outer hair cells and their molecular mechanisms," in *Hair Cells and Hearing Aids*, C. I. Berlin, Ed., pp. 29–55, Singular Publishing Group, San Diego, Calif, USA, 1996.

[22] P. Dallos, D. Z. Z. He, X. Lin, I. Sziklai, S. Mehta, and B. N. Evans, "Acetylcholine, outer hair cell electromotility, and the cochlear amplifier," *The Journal of Neuroscience*, vol. 17, no. 6, pp. 2212–2226, 1997.

[23] M. L. Wiederhold and N. Y. S. Kiang, "Effects of electric stimulation of the crossed olivocochlear bundle on single auditory–nerve fibers in the cat," *Journal of the Acoustical Society of America*, vol. 48, no. 4, pp. 950–965, 1970.

[24] J. J. Guinan, "Physiology of olivocochlear efferents," in *The Cochlea*, P. Dallos and R. R. Fay, Eds., vol. 8 of *Springer Handbook of Auditory Research*, pp. 435–502, Springer, New York, NY, USA, 1996.

[25] K. Hara and R. A. Harris, "The anesthetic mechanism of urethane: the effects on neurotransmitter-gated ion channels," *Anesthesia and Analgesia*, vol. 94, no. 2, pp. 313–318, 2002.

[26] J. Tang, J. L. Pecka, X. Tan, K. W. Beisel, and D. Z. Z. He, "Engineered pendrin protein, an anion transporter and molecular motor," *Journal of Biological Chemistry*, vol. 286, no. 35, pp. 31014–31021, 2011.

[27] J. Tang, J. L. Pecka, B. Fritzsch, K. W. Beisel, and D. Z. Z. He, "Lizard and frog prestin: evolutionary insight into functional changes," *PLoS ONE*, vol. 8, no. 1, Article ID e54388, 2013.

[28] X. Xiong, F. Liang, H. Li et al., "Interaural level difference-dependent gain control and synaptic scaling underlying binaural computation," *Neuron*, vol. 79, no. 4, pp. 738–753, 2013.

[29] J. Santos-Sacchi, M. Wu, and S. Kakehata, "Furosemide alters nonlinear capacitance in isolated outer hair cells," *Hearing Research*, vol. 159, no. 1-2, pp. 69–73, 2001.

[30] J. Santos-Sacchi, "Reversible inhibition of voltage-dependent outer hair cell motility and capacitance," *The Journal of Neuroscience*, vol. 11, no. 10, pp. 3096–3110, 1991.

[31] P. M. Sellick and I. J. Russell, "The responses of inner hair cells to basilar membrane velocity during low frequency auditory stimulation in the guinea pig cochlea," *Hearing Research*, vol. 2, no. 3-4, pp. 439–445, 1980.

[32] D. Z. Z. He, B. N. Evans, and P. Dallos, "First appearance and development of electromotility in neonatal gerbil outer hair cells," *Hearing Research*, vol. 78, no. 1, pp. 77–90, 1994.

[33] G. D. Housley and J. F. Ashmore, "Direct measurement of the action of acetylcholine on isolated outer hair cells of the guinea pig cochlea," *Proceedings of the Royal Society B: Biological Sciences*, vol. 244, no. 1310, pp. 161–167, 1991.

[34] D. Z. Z. He, J. Zheng, and P. Dallos, "Development of acetylcholine receptors in cultured outer hair cells," *Hearing Research*, vol. 162, no. 1-2, pp. 113–125, 2001.

[35] B. Kachar, W. E. Brownell, R. Altschuler, and J. Fex, "Electrokinetic shape changes of cochlear outer hair cells," *Nature*, vol. 322, no. 6077, pp. 365–368, 1986.

[36] P. Dallos and B. N. Evans, "High-frequency motility of outer hair cells and the cochlear amplifier," *Science*, vol. 267, no. 5206, pp. 2006–2009, 1995.

[37] J. F. Ashmore, "A fast motile response in guinea-pig outer hair cells: the cellular basis of the cochlear amplifier," *The Journal of Physiology*, vol. 388, pp. 323–347, 1987.

[38] J. Ashmore, "Cochlear outer hair cell motility," *Physiological Reviews*, vol. 88, no. 1, pp. 173–210, 2008.

[39] P. Dallos, "The active cochlea," *The Journal of Neuroscience*, vol. 12, no. 12, pp. 4575–4585, 1992.

[40] P. Dallos and B. Fakler, "Prestin, a new type of motor protein," *Nature Reviews Molecular Cell Biology*, vol. 3, no. 2, pp. 104–111, 2002.

[41] J. F. Ashmore, *Cochlear Mechanisms Structure, Function, and Models*, Edited by D. Kemp, and J. P. Wilson, Plenum Press, New York, NY, USA, 1989.

[42] K. Homma and P. Dallos, "Evidence that prestin has at least two voltage-dependent steps," *Journal of Biological Chemistry*, vol. 286, no. 3, pp. 2297–2307, 2011.

[43] G. D. Housley and J. F. Ashmore, "Ionic currents of outer hair cells isolated from the guinea-pig cochlea," *Journal of Physiology*, vol. 448, pp. 73–98, 1992.

[44] J. F. Ashmore and R. W. Meech, "Ionic basis of membrane potential in outer hair cells of guinea pig cochlea," *Nature*, vol. 322, no. 6077, pp. 368–371, 1986.

[45] C. Erostegui, C. H. Norris, and R. P. Bobbin, "In vitro pharmacologic characterization of a cholinergic receptor on outer hair cells," *Hearing Research*, vol. 74, no. 1-2, pp. 135–147, 1994.

[46] A. R. Chambers, K. E. Hancock, S. F. Maison, M. C. Liberman, and D. B. Polley, "Sound-evoked olivocochlear activation in unanesthetized mice," *Journal of the Association for Research in Otolaryngology*, vol. 13, no. 2, pp. 209–217, 2012.

[47] P. Dallos, X. Wu, M. A. Cheatham et al., "Prestin-based outer hair cell motility is necessary for mammalian cochlear amplification," *Neuron*, vol. 58, no. 3, pp. 333–339, 2008.

[48] G. I. Frolenkov, F. Mammano, I. A. Belyantseva, D. Coling, and B. Kachar, "Two distinct Ca^{2+}-dependent signaling pathways regulate the motor output of cochlear outer hair cells," *The Journal of Neuroscience*, vol. 20, no. 16, pp. 5940–5948, 2000.

[49] T. Lu, L. Liang, and X. Wang, "Temporal and rate representations of time-varying signals in the auditory cortex of awake primates," *Nature Neuroscience*, vol. 4, no. 11, pp. 1131–1138, 2001.

[50] S. J. Eliades and X. Wang, "Chronic multi-electrode neural recording in free-roaming monkeys," *Journal of Neuroscience Methods*, vol. 172, no. 2, pp. 201–214, 2008.

[51] J. Tang and N. Suga, "Modulation of auditory processing by cortico-cortical feed-forward and feedback projections," *Proceedings of the National Academy of Sciences of the United States of America*, vol. 105, no. 21, pp. 7600–7605, 2008.

[52] J. Tang, W. Yang, and N. Suga, "Modulation of thalamic auditory neurons by the primary auditory cortex," *Journal of Neurophysiology*, vol. 108, no. 3, pp. 935–942, 2012.

[53] B. D. Richardson, K. E. Hancock, and D. M. Caspary, "Stimulus-specific adaptation in auditory thalamus of young and aged awake rats," *Journal of Neurophysiology*, vol. 110, no. 8, pp. 1892–1902, 2013.

Hindawi Publishing Corporation
Neural Plasticity
Volume 2016, Article ID 1512831, 10 pages
http://dx.doi.org/10.1155/2016/1512831

Research Article

A Novel Nonsense Mutation of *POU4F3* Gene Causes Autosomal Dominant Hearing Loss

Chi Zhang,[1,2] Mingming Wang,[1,2] Yun Xiao,[1,2] Fengguo Zhang,[1,2] Yicui Zhou,[1,2] Jianfeng Li,[1,2] Qingyin Zheng,[3] Xiaohui Bai,[1,2] and Haibo Wang[1,2]

[1]*Department of Otorhinolaryngology Head and Neck Surgery, Shandong Provincial Hospital Affiliated to Shandong University, Jinan, China*
[2]*Shandong Provincial Key Laboratory of Otology, Jinan, China*
[3]*Department of Otolaryngology-Head & Neck Surgery, Case Western Reserve University, Cleveland, OH, USA*

Correspondence should be addressed to Haibo Wang; whboto11@163.com

Received 18 July 2016; Revised 11 October 2016; Accepted 24 October 2016

Academic Editor: Genglin Li

POU4F3 gene encodes a transcription factor which plays an essential role in the maturation and maintenance of hair cells in cochlea and vestibular system. Several mutations of *POU4F3* have been reported to cause autosomal dominant nonsyndromic hearing loss in recent years. In this study, we describe a pathogenic nonsense mutation located in *POU4F3* in a four-generation Chinese family. Target region capture sequencing was performed to search for the candidate mutations from 81 genes related to nonsyndromic hearing loss in this family. A novel nonsense mutation of *POU4F3*, c.337C>T (p. Gln113*), was identified in a Chinese family characterized by late-onset progressive nonsyndromic hearing loss. The novel mutation cosegregated with hearing loss in this family and was absent in 200 ethnicity-matched controls. The mutation led to a stop codon and thus a truncated protein with no functional domains remained. Transient transfection and immunofluorescence assay revealed that the subcellular localization of the truncated protein differed markedly from normal protein, which could be the underlying reason for complete loss of its normal function. Here, we report the first nonsense mutation of *POU4F3* associated with progressive hearing loss and explored the possible underlying mechanism. Routine examination of *POU4F3* is necessary for the genetic diagnosis of hereditary hearing loss in the future.

1. Introduction

Hearing loss is one of the most common sensory disorders in human. Genetic factors account for about 50% of these cases. Nonsyndromic hearing loss has four hereditary patterns: autosomal dominant, autosomal recessive, X-linked, and mitochondrial. Although hundreds of genes have been reported to be associated with nonsyndromic hearing loss, GJB2, SLC26A4, and mtDNA12SrRNA are the major contributors. Sometimes, one deafness gene can exhibit both autosomal dominant and recessive patterns in different mutations, such as *WFS1* [1–3]. To date, there have been 67 loci mapped and related to autosomal dominant nonsyndromic hearing loss (ADNSHL), but only 33 corresponding genes have been identified (http://hereditaryhearingloss.org/). A large proportion of sensorineural hearing loss remains genetically unexplained. The traditional Sanger sequencing method is highly expensive and time-consuming in identifying the pathogenic variants when there are hundreds of candidate genes. In contrast, next-generation sequencing can overcome these shortcomings through its ability to perform parallel sequencing of billions of nucleotides at a low cost and high speed. It has been proven as a powerful tool in identification of novel mutations and genes associated with hereditary hearing loss in recent years.

POU class 4 transcription factor 3 *(POU4F3)*, also known as *BRN3C*, is a POU-domain transcription factor exclusively expressed in both nascent and adult hair cells of cochlear and vestibular system in the inner ear [4, 5]. Brn-3c knockout mice were used to study its function in vivo. The homozygous mice of targeted deletion of *POU4F3*, Brn-3c$^{-/-}$, manifested severe defects in hearing and balance, and they showed a rapid and progressive loss of hair cells during late gestation

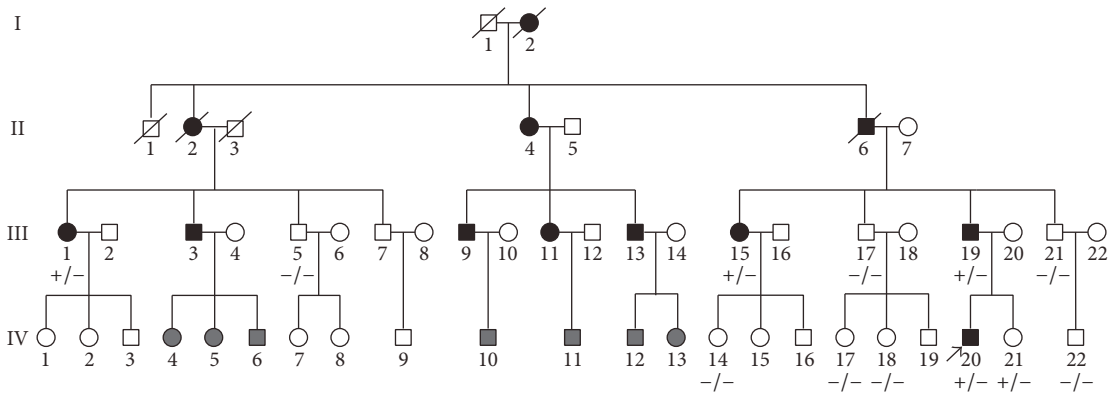

Figure 1: Pedigree of the Chinese family suffering from autosomal dominant hearing loss. Black squares and circles represent members with symptoms of DFNA15. Grey squares and circles represent members with unavailable status. Genotypes are marked below each member (+ means the mutation exists). Arrow shows the proband.

and early postnatal period. In contrast, the heterozygous littermates Brn-3c$^{+/-}$ mice represented normal behaviors. Histological examinations revealed that hair cells were totally absent in the auditory and vestibular systems of Brn-3c$^{-/-}$ adult mice. Loss of hair cells also resulted in a large decrease in the number of neurons and myelinated fibers in the spiral ganglion [6]. Other studies revealed that *POU4F3* was expressed in postmitotic cells committed to hair cell phenotype but not in mitotic progenitors [7] and the expression level of *POU4F3* kept high in both inner and outer hair cells till adulthood in mice [8], which meant *POU4F3* was essential for the maturation and maintenance, but not the fate determination of hair cells. The vital role of *POU4F3* in the development of hair cells indicated that it might be related with some kind of hereditary hearing loss.

The search for pathogenic mutations involved in hereditary hearing loss never ceases. Mutation of *POU4F3* was confirmed to be a causative factor of autosomal dominant nonsyndromic deafness 15 (DFNA15). Thus far, several *POU4F3* mutations were involved in *DFNA15* and mapped to 5q31-33 [9–16]. The main clinical manifestation is bilateral, late-onset, progressive sensorineural hearing loss affecting all frequencies [10, 12–15]. Pauw et al. reported a mean progression rate of 0.8–1.4 dB/year [17]. Vestibular impairments in some patients were also reported in previous studies, but the incidence was low and the symptoms were quite mild and easy to be neglected [17, 18].

In this study, we reported a Chinese family suffering from ADNSHL. All affected members experienced a late-onset progressive hearing loss. A new nonsense mutation in *POU4F3*, c.337C>T (p. Gln113*), was identified to be the causative factor using the method of target region capture sequencing.

2. Materials and Methods

2.1. Subjects and Clinical Examinations. A four-generation Chinese family suffering from hereditary hearing loss was reported here. All 12 patients in this family had a putative autosomal dominant pattern of inheritance according to the participating patient statements. Because of some objective reasons and out of the patients' privacy, we were not able to contact and examine all the members in this family. Only 4 members with impaired hearing (III-1, III-15, III-19, and IV-20) and 8 members with normal hearing (III-5, III-17, III-21, IV-14, IV-17, IV-18, IV-21, and IV-22) participated in our research (Figure 1). They all received clinical examinations in Department of Otorhinolaryngology Head and Neck Surgery, Shandong Provincial Hospital Affiliated to Shandong University. The medical history was obtained from all participants. After physical and otoscopic examinations, all the subjects received auditory tests including pure tone audiometry (PTA), tinnitus examination, acoustic immittance, auditory brainstem response, and distortion product otoacoustic emission according to standard protocols. Vestibular bithermal caloric test and evoked myogenic potentials were performed to the proband (IV-20) due to his complaint of occasional vertigo. Other syndromic or systematic diseases which can influence hearing and past history of ototoxic medication were excluded. Degrees of hearing loss were determined according to the guidelines of American Speech-Language-Hearing Association [19]. Individual was considered affected if PTA thresholds of most frequencies were higher than the 95 percentile thresholds of presbycusis according to the method of ISO 7029-2000 [20]. Before this study, all participants provided written informed consents according to the protocol, which was approved by the ethics committee of the Institutional Review Board of the Shandong Provincial Hospital Affiliated to Shandong University.

2.2. Targeted Next-Generation Sequencing of Deafness Gene. In order to identify the pathogenic mutation underlying the hearing loss in this family, the genomic DNA was extracted from peripheral blood of all the subjects using DNA extraction kit (Axygen, USA). Target region capture sequencing was employed to screen possible mutations of 81 genes (see S1 Table in Supplementary Material available online at http://dx.doi.org/10.1155/2016/1512831) related to nonsyndromic hearing loss in the genome of the proband. This work was done by BGI (Beijing Genomics Institute,

Shenzhen, China) using a standardized next-generation capture sequencing platform. This method can cover all exons and nearby ±10 base pairs of introns of the 81 candidate genes. Data analysis was conducted according to the analysis process for next-generation sequencing, BGIv0.1.0. Reads were aligned to the human reference genome UCSC hg19 Feb.2009 by BWA 0.6.2-r126 software. Mutation detection software was GATK. dbSNP (snp137) was used as a reference for recorded SNPs. The databases including 1000 genome database (phase I), HapMap database (combined data from phases II and III), and own databases of BGI (BGI-DB, HGVD) were used as references to investigate the novelty and possible pathogenicity of the variations detected in the sequencing approach. Guideline of American College of Medical Genetics and Genomics was used as the reference of data interpretation [21].

2.3. Mutation Detection by Sanger Sequencing on Genomic DNA. Sanger sequencing was performed in all the family members participating in our research and 200 ethnicity-matched control subjects. The primers used to amplify the exons and intron-exon boundaries by polymerase chain reaction were as follows: (1) forward 5′-GCAGGCTGCTTGTAAGATGAG-3′ and reverse 5′-AGACAGCGGCGATTGTTC-3′; (2) forward 5′-CTCGGTTGCTTGAAAATGTG-3′ and reverse 5′-GGGGATCTTGAGATTAGCC-3′; (3) forward 5′-AGCTGGAAGCCTTCGCC-3′ and reverse 5′-GGAAAGTCTGTGGCTTCGG-3′. The first pair of primers was for the amplification of exon 1, while the other two were for exon 2. Sequencing reactions were performed by BGI (Beijing Genomics Institute, Shenzhen, China). Data was analyzed using Lasergene-SeqMan software. The sequences were compared with the sequence of *POU4F3* gene (GenBank Accession number NM_002700) and corresponding protein sequence (NP_002691.1).

2.4. Bioinformatics Analysis. Mutation Taster was used to predict the possible pathogenic effect of the candidate mutation (http://www.mutationtaster.org/) [22]. Three-dimensional (3D) modeling of the human wild-type and mutant *POU4F3* protein was carried out using I-TASSER, an automated homology modeling program (http://zhanglab.ccmb.med.umich.edu/). The wild-type POU4F3 protein includes 338 amino acids (NP_002691.1) and the mutant protein includes 112 amino acids. Data obtained from the homology models were visualized using Swiss-Pdb Viewer 4.1 software.

2.5. Cell Culture. HEK293 cells were originally stored in Shandong Provincial Key Laboratory of Otology and then cultured in MEM (Gibco, USA) containing 10% FBS (Gibco, USA) in a sterile environment with 5% CO_2 at 37°C. HEI-OC1 auditory cells, which were given by Dr. Federico Kalinec (University of California, Los Angeles) as a present, were cultured in DMEM (Gibco, USA) containing 10% FBS in a sterile environment with 10% CO_2 at 33°C [23].

2.6. Plasmid Construction. The vector containing human *POU4F3* cDNA was purchased from Cusabio Biotech (Wuhan, China). Sanger sequencing of this cDNA clone confirmed that it is totally consistent with that of *POU4F3* cDNA (accession number: BC112207). We then used this to generate the wild-type expression plasmid. Primers used to amplify the cDNA region were 5′-ATGCAGGATCCATGATGGCCATGAACTCCAAGCAGCCTTTCG-3′ and 5′-ACGCAGAATTCGTGGACAGCCGAATACTTCA-3′. After digestion by restriction enzymes BamH I and EcoR I, the amplified PCR products were then subcloned into the expression vector, pCMV-Tag 2B (Agilent Technologies, USA). To construct the mutant expression vector, we used the QuikChange site-directed mutagenesis kit (Stratagene, USA) to introduce the mutation (c.337C>T) which we identified from targeted next-generation sequencing into the wild-type vector following the manufacturer's protocol.

2.7. Transient Transfection and Immunofluorescence Analysis. HEK 293 and HEI-OC1 cells were cultured on glass coverslips in 24-well plates with the densities of 25×10^4/well and 10×10^4/well, respectively, and were then transfected with either wild-type or mutant expression plasmid using Lipofectamine® 3000 transfection reagent (Invitrogen, USA). Immunofluorescence analysis was performed after 72-hour transfection. Cells were fixed in 4% paraformaldehyde for 15 min, permeabilized in PBS containing 0.3% Triton X-100 for 10 min and then blocked in PBS containing 10% donkey serum for 1 h at 37°C in a humid atmosphere. Subsequently, the cells were incubated for 12–14 h at 4°C with primary anti-FLAG antibody (Ca# F1804, Sigma, USA) at a concentration of 1 : 800 diluted and then stained with secondary goat-anti-mouse antibody (Sigma, USA) and DAPI for 1 h at a concentration of 1 : 1000. Finally, the cells were visualized under confocal microscope for image acquisition.

3. Results

3.1. Clinical Manifestations. A four-generation Chinese family suffered from hereditary progressive hearing loss with an autosomal dominant pattern. The pedigree of this Chinese family was drawn in Figure 1 according to the statements of participants. Totally, there were 12 members suffering from similar symptoms of hearing loss and tinnitus in this family, with 9 of them still alive at the time of investigation. But out of respect for the patients' privacy and some other objective reasons, we only got 12 members to participate in our study. All the members with symptoms in this family represented bilateral late-onset progressive hearing loss, but the onset age (range, 14–40 y) varied a lot from one another. PTA results showed moderate to severe hearing loss in these patients. The audiometric configurations were flat to downsloping (Figure 2). Four of the 12 participating members including III-1, III-15, III-19, and IV-20 were assumed to be affected after PTA test and comparison with 95th percentile thresholds of presbycusis.

The proband (IV-20) developed bilateral hearing loss at the age of 14 and after then, the hearing loss became more and more severe. So he received PTA in our hospital at 17 and 18 years old, respectively. The results showed moderate sensorineural hearing loss of both ears (shown in Figure 2)

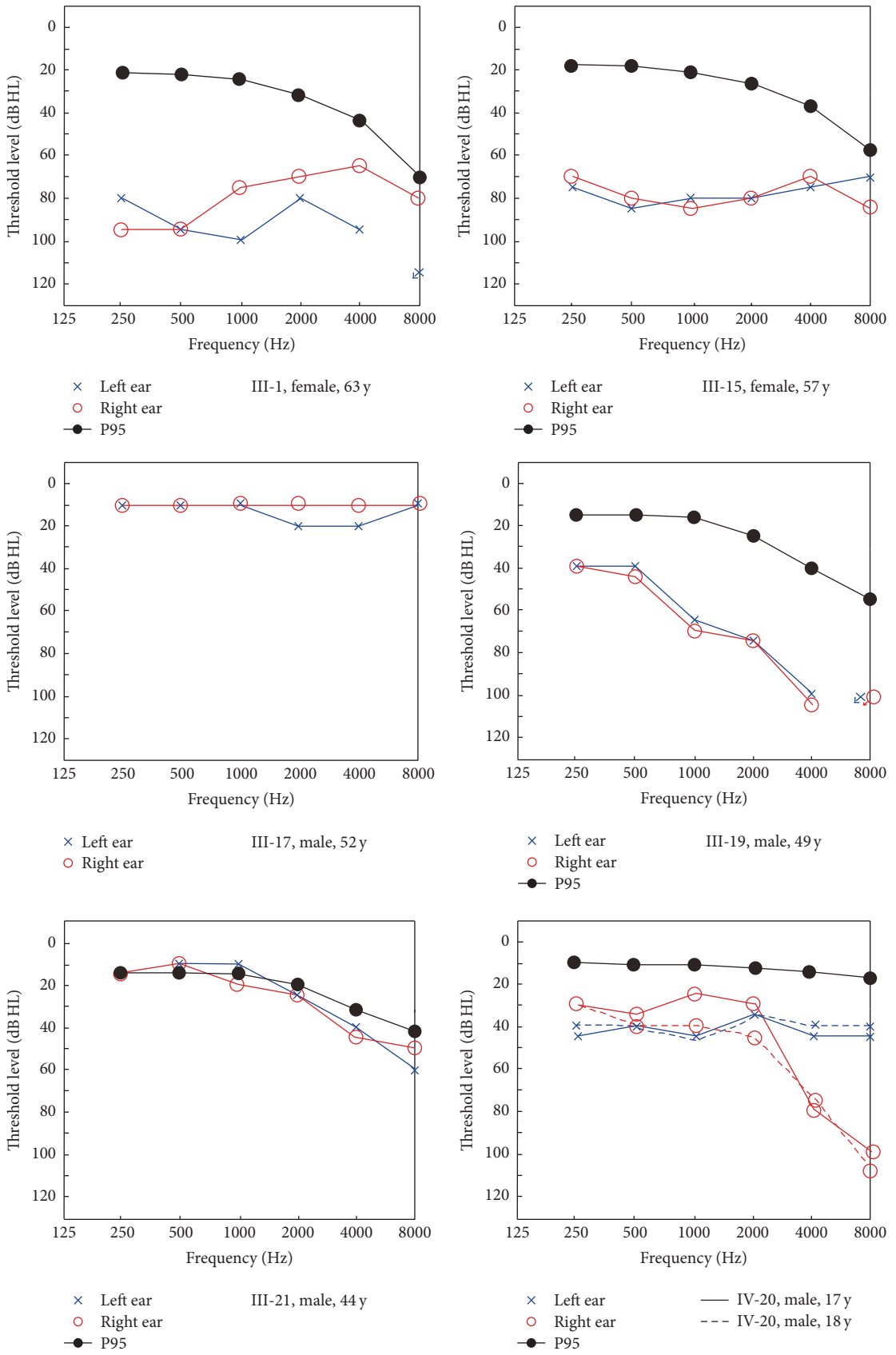

Figure 2: Continued.

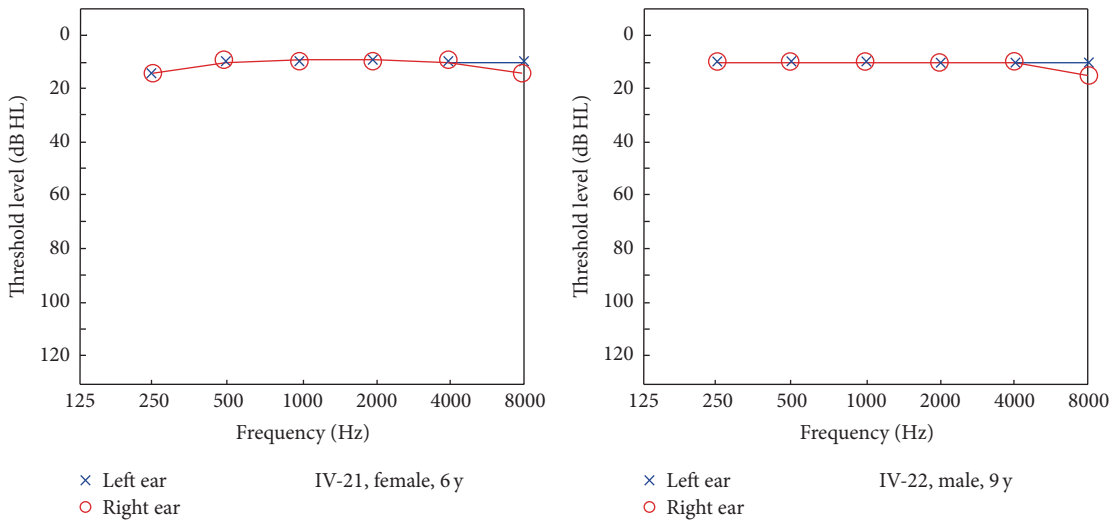

Figure 2: Audiograms of some members participating in our study in the Chinese family. Blue crosses and red circles represent the air conduction hearing threshold levels of left and right ears, respectively. For IV-20, hearing levels of the age of 17 and 18 years are shown in full and broken lines, respectively. Black lines with solid circles represent the 95 percentile air conduction hearing threshold levels of presbycusis with a certain gender and age according to the algorithm of ISO 7029:2000. Pedigree number, gender, and age are shown below the audiogram of each individual. "IV-20, male, 17 y" and "IV-20, male, 18 y" in the keys refer to both red and blue colors.

and an obvious decrease of the right ear in 1 and 2 kHz was observed when comparing these two audiograms. Usually, the configurations of both ears were the same or similar, but the proband showed different configurations on each side of ears.

Tinnitus was a common symptom among these patients. Tinnitus examination revealed a 3 kHz binaural consistent tinnitus in IV-20 (left: 51 dB HL; right: 85 dB HL) and a 6 kHz binaural tinnitus in III-19 (left: 103 dB HL; right: 104 dB HL). Speech recognition scores (SRS) of IV-20 were 88% in left and 80% in right. SRS of III-19 were 52% in left and 48% in right. Results of vestibular bithermal caloric test and VEMP showed no obvious dysfunction although IV-20 mentioned he experienced vertigo sometimes. Tympanometry results of all participants were completely normal. ABR results of those affected members were consistent with results of PTA, showing moderate to severe sensorineural hearing loss. All affected members failed to pass DPOAE test in most or all frequencies bilaterally. Results of all the unaffected members were normal.

3.2. A Novel Nonsense Mutation Was Identified in POU4F3 Gene. Target region capture sequencing was performed to identify the causative mutation underlying this Chinese family. Single-nucleotide variations were filtered in the dbSNP137, the 1000 Genomes Project, and HapMap8 databases with a 0.5% cutoff of minor allele frequency. Ten variations in nine genes *(POU4F3, OTOF, DSPP, DIAPH1, DFNB31, TPRN, TECTA, TMPRSS3,* and *TRIOBP)* were detected to be possible candidates. By considerations of the autosomal dominant pattern and clinical manifestations in this family, five genes were excluded. Sanger sequencing was performed in all the participating members to confirm the remaining four genes *(DSPP, DIAPH1, TECTA,* and *POU4F3)*. Only one heterozygous nonsense mutation, c.337C>T (p. Gln113*), in exon 2 of *POU4F3* was confirmed (Figure 3(a)). c.337C>T leads to a truncated protein comprising only 112 amino acids (the normal protein contains 338 amino acids) (Figure 3(b)). Among the eight normal-hearing members, c.337C>T was also detected in the proband's little sister (IV-21) who was only six years old. Given that hearing loss caused by mutations of *POU4F3* usually occurs at late age, probably it was still too early for her to present with the symptoms. Sanger sequencing was also conducted in 200 ethnicity-matched control subjects and the mutation was absent in all of them.

Prediction made by Mutation Taster about whether this mutation was pathogenic showed a probability value of 1 (value close to 1 indicates a high "security" of the prediction). A molecular model of *POU4F3* was constructed based on the crystal structure (PDB ID: 1gt0A and 1jvrA) (Figure 3(c)). The constructed model of wild-type protein matched the sequence of *POU4F3* (residues 1–338). The sequence identity between the target and template was 53%, higher than the average 25%. The constructed model of mutant protein matched the target sequence of *POU4F3* (residues 1–112). The sequence identity between the target and template was 25%. We analyzed the wild and mutant structure of *POU4F3* proteins with Swiss-Pdb Viewer 4.1 software. Compared with the wild-type Pou4f3 structure, the mutant protein structure is incomplete.

3.3. Effect of the POU4F3 Mutation on the Subcellular Localization of Protein. POU4F3 is a transcription factor and is exclusively located in the nuclei as previously reported [10, 24]. Subcellular localization is vital for a transcription factor to perform its normal function as it requires the protein to combine with the targets on DNA sequences in nuclei. So the wild-type and mutant-type plasmids were constructed using

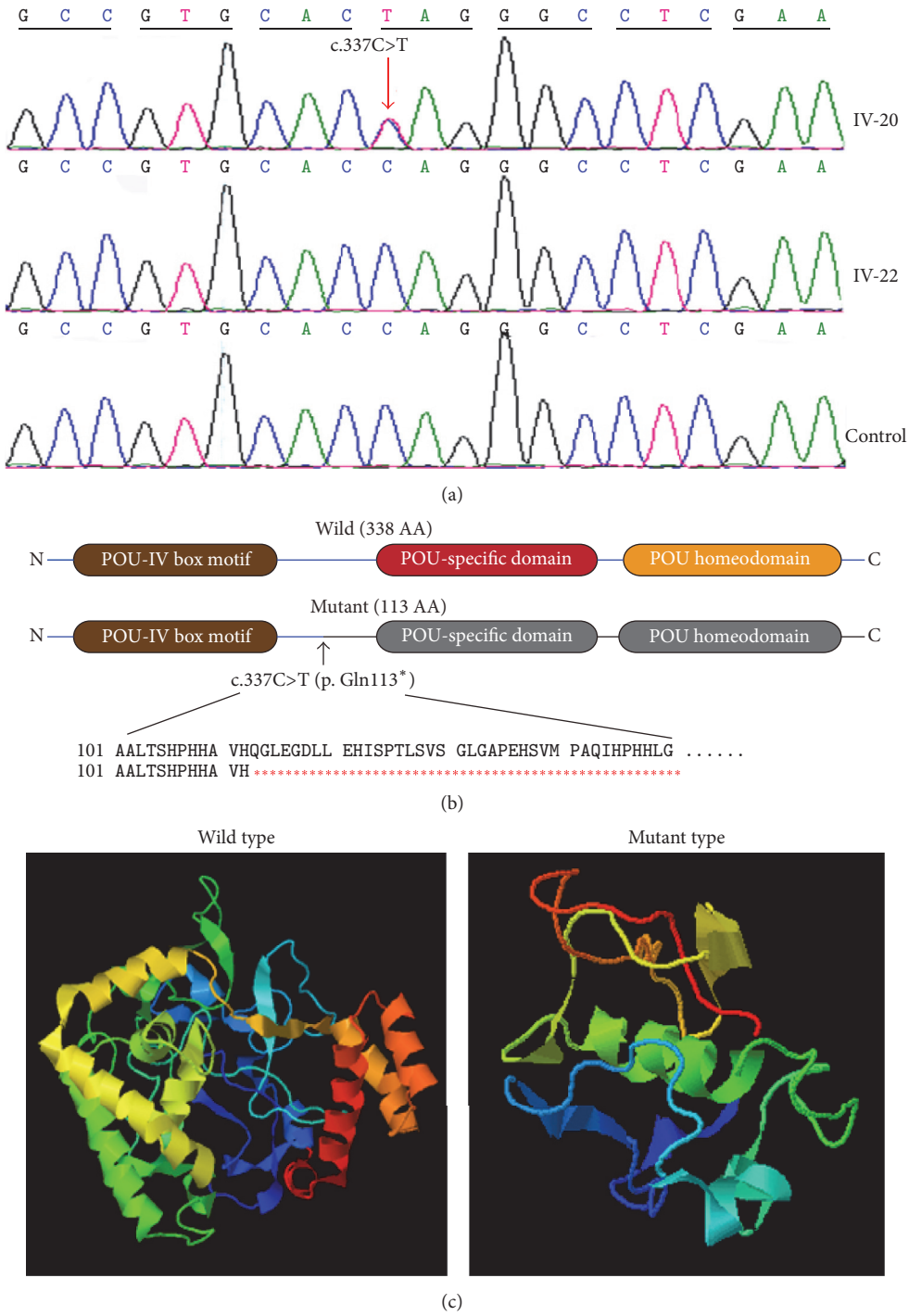

Figure 3: Sanger sequencing confirmation and structural analysis of c.337C>T. (a) Sequencing results of two members in this family and the representative of 200 ethnicity-matched control subjects. Red arrow points to the position of the heterozygous mutation in POU4F3 gene, c.337C>T. (b) The schematic diagram of POU4F3 protein indicating the loss of POU-specific domain and POU homeodomain in mutant protein. (c) Three-dimensional molecular models revealed the incomplete structure of mutant-type protein.

the pCMV-Tag2B plasmid and cDNA of *POU4F3*. These two constructs were transfected into HEK 293 and HEI-OC1 cell lines, respectively. HEI-OC1 cell line is a conditionally immortalized organ of Corti-derived epithelial cell line [23], which has been shown to be an excellent in vitro system to investigate the cellular and molecular mechanisms involved in ototoxicity and otoprotection of new pharmacological drugs. As the *POU4F3* proteins expressed by these two constructs were fused with N-terminal FLAG-tag, we used anti-FLAG antibody to detect its localization

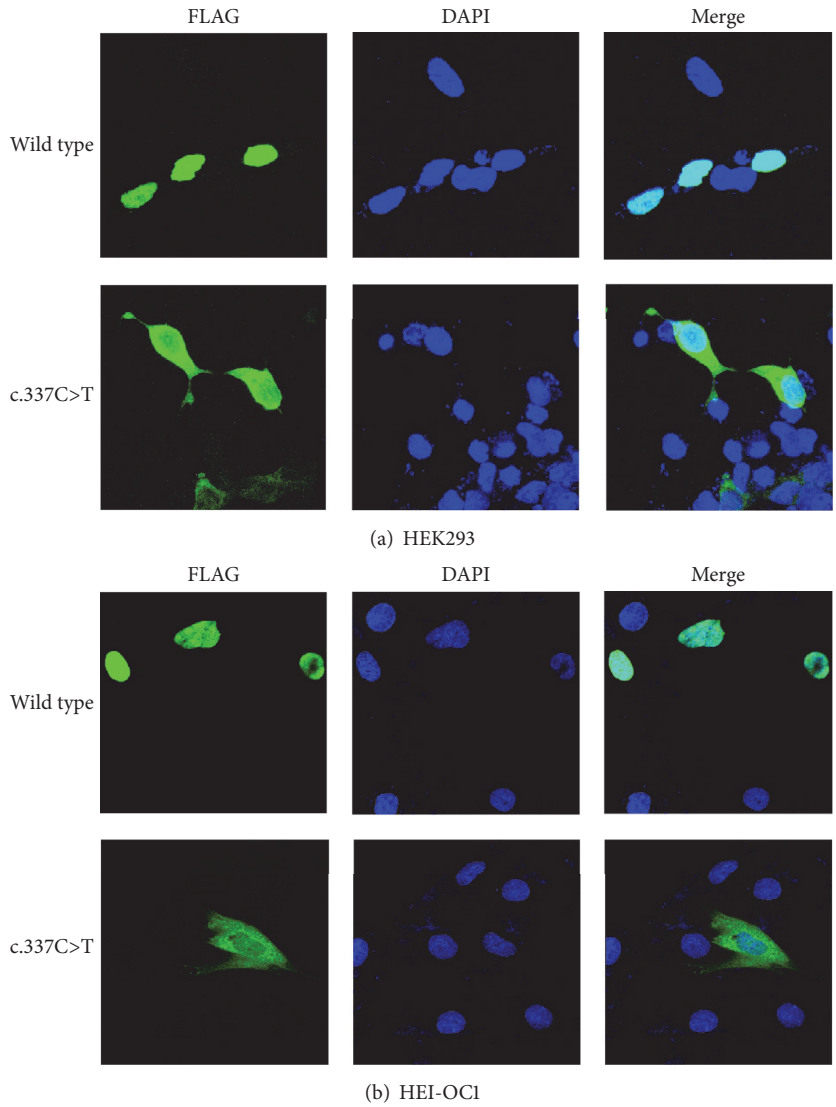

Figure 4: Immunofluorescence analysis after transient transfection in HEK293 and HEI-OC1 cell lines. Images display DAPI in blue, FLAG-tagged protein in green, and merged pictures. (a) In HEK293 cells, mutant protein located mostly in cytoplasm while the wild-type protein was exclusively located in nuclei. (b) Similar results were observed in HEI-OC1 cells.

by immunofluorescence analysis under confocal microscopy. Similar results were observed in both cell lines. The normal *POU4F3* protein was exclusively located in the cell nuclei while most of the mutant *POU4F3* protein was located in the cytoplasm. Even though there was still some mutant *POU4F3* protein in the nuclei, the signal was much weaker than that in the cytoplasm (Figure 4).

4. Discussion

POU4F3, also known as *BRN3C*, is a member of the POU superfamily of transcription factors. Transcription factors bind directly to DNA and regulate the translation of target genes. All 14 members in this superfamily are characterized by comprising two DNA-binding domains, the POU homeodomain, and the POU-specific domain, which are the main functional parts [25]. *POU4F3* protein plays an essential role in the development and maintenance of hair cells in the inner ear sensory epithelia [7]. Targeted null mutation of *POU4F3* resulted in loss of all hair cells in the cochlea and vestibular system of Brn-3c$^{-/-}$ mice and thus led to symptoms of complete hearing loss and severe vestibular dysfunction [6, 26].

In this study, we identified a new nonsense mutation of *POU4F3*, c.337C>T, in a Chinese family which represented progressive hearing loss in an autosomal dominant pattern. This mutation changed the codon CAG to UAG which is a stop codon and thus produces a truncated protein with only 112 amino acids while the normal protein should comprise 338 amino acids. The truncated protein loses the two functional DNA-binding domains, POU-specific domain and POU homeodomain; therefore it might lose its entire

Table 1: Variants of *POU4F3* related to DFNA 15.

Description	Exon	Amino acid change	Type of variant	Ethnicity	Reference
c.884del8	2	Ile295Thrfs*5	Frameshift	Jewish	Vahava et al. (1998) [14]
c.668T>C	2	Leu223Pro	Missense	Dutch	Collin et al. (2008) [10]
c.865C>T	2	Leu289Phe	Missense	Dutch	Collin et al. (2008) [10]
c.662del14	2	Gly221Glufs*77	Frameshift	Korean	Lee et al. (2010) [13]
c.694G>A	2	Glu232Lys	Missense	Korean	Baek et al. (2012) [9]
c.977G>A	2	Arg326Lys	Missense	Korean	Kim et al. (2013) [12]
c.603_604delGG	2	Val203Aspfs*11	Frameshift	Chinese	Yang et al. (2013) [16]
Deletion of entire gene	2		Deletion	Brazilian	Freitas et al. (2014) [11]
c.491C>G	2	Pro164Arg	Missense	Chinese	Wei et al. (2014) [15]
c.337C>T	2	Gln113*	Nonsense	Chinese	This study

function as a transcription factor and result in hair cell apoptosis and progressive hearing loss.

To date, 10 pathogenic variants of *POU4F3* related to DFNA15 have been identified in different countries and ethnicities (Table 1). All the patients were reported to demonstrate the symptoms of postlingual, progressive sensorineural hearing loss and the autosomal dominant pattern of inheritance. The onset age of hearing loss varied a lot from early adult to midlife. All frequencies, especially high frequencies, could be affected resulting in flat to slowly downsloping audiometric configurations in most patients [17]. Interestingly, Brn-3c$^{-/-}$ mice showed severe hearing loss and vestibular dysfunction after birth, while Brn-3c$^{+/-}$ mice showed no auditory and vestibular symptoms [6, 27]. Unlike mice, human would develop late-onset hearing loss when carrying a heterozygous mutation of *POU4F3*. More attention should be paid to *POU4F3* when identifying the cause of a patient with symptoms mentioned above.

No symptoms of vestibular dysfunction were found in the members of this Chinese family. However, the vestibular function in some patients was previously reported to be slightly affected after thorough examinations but the incidence and severity were low [18]. In contrast, distinct vestibular impairment was revealed in Brn-3c$^{-/-}$ mice. The reasons why no obvious vestibular symptoms were found in human are probably that only heterozygous mutations were identified and the normal *POU4F3* allele could produce enough protein to maintain a desirable vestibular function, or functional compensation of vestibular system occurred during the long time span of this disease.

In order to investigate the effect of this novel mutation, we examined the subcellular localization of mutant protein in comparison to a wild-type protein control. The immunofluorescence staining revealed that normal protein was exclusively located in nuclei while mutant protein was located predominantly in cytoplasm in both HEK293 cells and HEI-OC1 cells. Nuclear localization signal (NLS) is an amino acid sequence which plays a key role in guiding transcription factors to cell nucleus and loss of NLS would result in cytoplasmic localization. There are two NLSs in *POU4F3* according to a previous study [28]. One is monopartite NLS (amino acids 274 to 278), and the other is a bipartite NLS (amino acids 314 to 331). The mutation c.337C>T (p. Gln113*) led to the loss of both NLSs which in turn caused the change of localization. Some earlier studies reported that mutant protein produced by transfection could also locate only in nuclei and the difference between normal and mutant protein was the proportion of cells with *POU4F3* protein outside nuclei [10, 13]. We did not discover this phenomenon after repeated experiments. The possible reason may be these reported missense mutations could not fully destroy the function of NLS.

Identification of targets of *POU4F3* is important for understanding its function and the mechanism of *POU4F3*-related hearing loss. There have been several genes verified to be its downstream targets. Growth factor independence 1 (Gfi1), a zinc-finger transcription factor, was the first-identified target gene of *POU4F3* and its loss of expression was presumed to be the main cause of outer hair cell degeneration in *POU4F3* mutant individuals [29]. Clough et al. reported that *POU4F3* was capable of activating both BDNF and NT-3 promoters and might be an important regulator of neurotrophic gene expression [30]. Later, Lhx3, a LIM domain transcription factor, was validated to be regulated by *POU4F3* in auditory but not in vestibular system of hair cells [31]. In 2014, the orphan thyroid nuclear receptor Nr2f2 was identified as a new target gene which might be relevant to the survival and development of hair cells [32]. But still, the *POU4F3*-related mechanism of differentiation and maintenance of hair cells is largely unknown.

5. Conclusions

In this study we identified a new nonsense mutation c.337C>T in *POU4F3* for the first time in a four-generation Chinese family suffering from autosomal dominant nonsyndromic hearing loss. Functional defects of this truncated protein were revealed by structural analysis and in vitro cellular experiments. Thus far, 10 variants of *POU4F3* related to DFNA15 have been reported. Mutation of *POU4F3* may not be a rare cause in ADNSHL and routine examination of *POU4F3* is necessary for the genetic diagnosis of hereditary hearing loss in the future.

Disclosure

Chi Zhang and Mingming Wang should be regarded as co-first authors.

Competing Interests

The authors declare that there is no conflict of interests to report.

Authors' Contributions

Chi Zhang and Mingming Wang contributed to the work equally.

Acknowledgments

This work was supported by grants from the National 973 Basic Research Program of China (2014CB541703), grants from the National Natural Science Foundation of China (81470693 and 81470704), grants from the project funded by China Postdoctoral Science Foundation (2014M560563 and 2015T80726), grants from the Natural Science Foundation of Shandong Province (ZR2014HM022 and ZR2014HP064), and a grant from the Shandong Province Science and Technology Development Plan (no. 2014GSF118109). The authors sincerely thank Dr. Federico Kalinec for his kind providing of the HEI-OC1 cell line and all the family members for their participation and cooperation in this study.

References

[1] X. Bai, H. Lv, F. Zhang et al., "Identification of a novel missense mutation in the *WFS1* gene as a cause of autosomal dominant nonsyndromic sensorineural hearing loss in all-frequencies," *American Journal of Medical Genetics Part A*, vol. 164, no. 12, pp. 3052–3060, 2014.

[2] F. Zhang, Y. Xiao, L. Xu et al., "Mutation analysis of the common deafness genes in patients with nonsyndromic hearing loss in linyi by SNPscan assay," *BioMed Research International*, vol. 2016, Article ID 1302914, 7 pages, 2016.

[3] Y. Ma, Y. Xiao, X. Bai et al., "GJB2, SLC26A4, and mitochondrial DNA12S rRNA hot-spots in 156 subjects with non-syndromic hearing loss in Tengzhou, China," *Acta Oto-Laryngologica*, vol. 136, no. 8, pp. 800–805, 2016.

[4] D. I. Scheffer, J. Shen, D. P. Corey, and Z.-Y. Chen, "Gene expression by mouse inner ear hair cells during development," *Journal of Neuroscience*, vol. 35, no. 16, pp. 6366–6380, 2015.

[5] H. Liu, J. L. Pecka, Q. Zhang, G. A. Soukup, K. W. Beisel, and D. Z. Z. He, "Characterization of transcriptomes of cochlear inner and outer hair cells," *Journal of Neuroscience*, vol. 34, no. 33, pp. 11085–11095, 2014.

[6] M. Xiang, L. Gan, D. Li et al., "Essential role of POU-domain factor Brn-3c in auditory and vestibular hair cell development," *Proceedings of the National Academy of Sciences of the United States of America*, vol. 94, no. 17, pp. 9445–9450, 1997.

[7] M. Xiang, W.-Q. Gao, T. Hasson, and J. J. Shin, "Requirement for Brn-3c in maturation and survival, but not in fate determination of inner ear hair cells," *Development*, vol. 125, no. 20, pp. 3935–3946, 1998.

[8] Y. Li, H. Liu, C. L. Barta et al., "Transcription factors expressed in mouse cochlear inner and outer hair cells," *PLoS ONE*, vol. 11, no. 3, Article ID e0151291, 2016.

[9] J.-I. Baek, S.-K. Oh, D.-B. Kim et al., "Targeted massive parallel sequencing: the effective detection of novel causative mutations associated with hearing loss in small families," *Orphanet Journal of Rare Diseases*, vol. 7, no. 1, article 60, 2012.

[10] R. W. J. Collin, R. Chellappa, R.-J. Pauw et al., "Missense mutations in POU4F3 cause autosomal dominant hearing impairment DFNA15 and affect subcellular localization and DNA binding," *Human Mutation*, vol. 29, no. 4, pp. 545–554, 2008.

[11] É. L. Freitas, J. Oiticica, A. G. Silva, R. S. M. Bittar, C. Rosenberg, and R. C. Mingroni-Netto, "Deletion of the entire POU4F3 gene in a familial case of autosomal dominant non-syndromic hearing loss," *European Journal of Medical Genetics*, vol. 57, no. 4, pp. 125–128, 2014.

[12] H.-J. Kim, H.-H. Won, K.-J. Park et al., "SNP linkage analysis and whole exome sequencing identify a novel POU4F3 mutation in autosomal dominant late-onset nonsyndromic hearing loss (DFNA15)," *PLoS ONE*, vol. 8, no. 11, Article ID e79063, 2013.

[13] H. K. Lee, H. J. Park, K. Y. Lee, R. Park, and U. K. Kim, "A novel frameshift mutation of POU4F3 gene associated with autosomal dominant non-syndromic hearing loss," *Biochemical and Biophysical Research Communications*, vol. 396, no. 3, pp. 626–630, 2010.

[14] O. Vahava, R. Morell, E. D. Lynch et al., "Mutation in transcription factor POU4F3 associated with inherited progressive hearing loss in humans," *Science*, vol. 279, no. 5358, pp. 1950–1954, 1998.

[15] Q. Wei, H. Zhu, X. Qian et al., "Targeted genomic capture and massively parallel sequencing to identify novel variants causing Chinese hereditary hearing loss," *Journal of Translational Medicine*, vol. 12, article 311, 2014.

[16] T. Yang, X. Wei, Y. Chai, L. Li, and H. Wu, "Genetic etiology study of the non-syndromic deafness in Chinese Hans by targeted next-generation sequencing," *Orphanet Journal of Rare Diseases*, vol. 8, no. 1, article 85, 2013.

[17] R. J. Pauw, F. J. W. Van Drunen, R. W. J. Collin, P. L. M. Huygen, H. Kremer, and C. W. R. J. Cremers, "Audiometric characteristics of a Dutch family linked to DFNA15 with a novel mutation (p.L289F) in POU4F3," *Archives of Otolaryngology—Head and Neck Surgery*, vol. 134, no. 3, pp. 294–300, 2008.

[18] F. J. W. van Drunen, R. J. Pauw, R. W. J. Collin, H. Kremer, P. L. M. Huygen, and C. W. R. J. Cremers, "Vestibular impairment in a Dutch DFNA15 family with an L289F mutation in POU4F3," *Audiology and Neurotology*, vol. 14, no. 5, pp. 303–307, 2009.

[19] J. G. Clark, "Uses and abuses of hearing loss classification.," *ASHA*, vol. 23, no. 7, pp. 493–500, 1981.

[20] International Organization for Standardization, "ISO 7029:2000 Acoustics—Statistical distribution of hearing thresholds as a function of age," http://www.iso.org/iso/home/store/catalogue_tc/catalogue_detail.htm?csnumber=26314.

[21] C. S. Richards, S. Bale, D. B. Bellissimo et al., "ACMG recommendations for standards for interpretation and reporting of sequence variations: Revisions 2007," *Genetics in Medicine*, vol. 10, no. 4, pp. 294–300, 2008.

[22] J. M. Schwarz, D. N. Cooper, M. Schuelke, and D. Seelow, "MutationTaster2: mutation prediction for the deep-sequencing age," *Nature Methods*, vol. 11, no. 4, pp. 361–362, 2014.

[23] G. M. Kalinec, P. Webster, D. J. Lim, and F. Kalinec, "A cochlear cell line as an in vitro system for drug ototoxicity screening," *Audiology and Neuro-Otology*, vol. 8, no. 4, pp. 177–189, 2003.

[24] M. Xiang, L. Zhou, J. P. Macke et al., "The Brn-3 family of POU-domain factors: primary structure, binding specificity, and expression in subsets of retinal ganglion cells and somatosensory neurons," *Journal of Neuroscience*, vol. 15, no. 7, part 1, pp. 4762–4785, 1995.

[25] M. Wegner, D. W. Drolet, and M. G. Rosenfeld, "POU-domain proteins: structure and function of developmental regulators," *Current Opinion in Cell Biology*, vol. 5, no. 3, pp. 488–498, 1993.

[26] L. Erkman, R. J. McEvilly, L. Luo et al., "Role of transcription factors Brn-3.1 and Brn-3.2 in auditory and visual system development," *Nature*, vol. 381, no. 6583, pp. 603–606, 1996.

[27] E. M. Keithley, L. Erkman, T. Bennett, L. Lou, and A. F. Ryan, "Effects of a hair cell transcription factor, Brn-3.1, gene deletion on homozygous and heterozygous mouse cochleas in adulthood and aging," *Hearing Research*, vol. 134, no. 1-2, pp. 71–76, 1999.

[28] S. Weiss, I. Gottfried, I. Mayrose et al., "The DFNA15 deafness mutation affects POU4F3 protein stability, localization, and transcriptional activity," *Molecular and Cellular Biology*, vol. 23, no. 22, pp. 7957–7964, 2003.

[29] R. Hertzano, M. Montcouquiol, S. Rashi-Elkeles et al., "Transcription profiling of inner ears from *Pou4f3*$^{ddl/ddl}$ identifies Gfi1 as a target of the Pou4f3 deafness gene," *Human Molecular Genetics*, vol. 13, no. 18, pp. 2143–2153, 2004.

[30] R. L. Clough, R. Sud, N. Davis-Silberman et al., "Brn-3c (POU4F3) regulates BDNF and NT-3 promoter activity," *Biochemical and Biophysical Research Communications*, vol. 324, no. 1, pp. 372–381, 2004.

[31] R. Hertzano, A. A. Dror, M. Montcouquiol et al., "Lhx3, a LIM domain transcription factor, is regulated by Pou4f3 in the auditory but not in the vestibular system," *European Journal of Neuroscience*, vol. 25, no. 4, pp. 999–1005, 2007.

[32] C. Tornari, E. R. Towers, J. E. Gale, and S. J. Dawson, "Regulation of the orphan nuclear receptor Nr2f2 by the DFNA15 deafness gene Pou4f3," *PLoS ONE*, vol. 9, no. 11, Article ID e112247, 2014.

Hindawi Publishing Corporation
Neural Plasticity
Volume 2016, Article ID 3018132, 6 pages
http://dx.doi.org/10.1155/2016/3018132

Research Article

NLRP3 Is Expressed in the Spiral Ganglion Neurons and Associated with Both Syndromic and Nonsyndromic Sensorineural Deafness

Penghui Chen,[1,2,3] Longxia He,[1,2,3] Xiuhong Pang,[4] Xiaowen Wang,[1,2,3] Tao Yang,[1,2,3] and Hao Wu[1,2,3,5]

[1]*Department of Otolaryngology-Head and Neck Surgery, Xinhua Hospital, Shanghai Jiaotong University School of Medicine, Shanghai, China*
[2]*Ear Institute, Shanghai Jiaotong University School of Medicine, Shanghai, China*
[3]*Shanghai Key Laboratory of Translational Medicine on Ear and Nose Diseases, Shanghai, China*
[4]*Department of Otorhinolaryngology-Head and Neck Surgery, Taizhou People's Hospital, Jiangsu Province, China*
[5]*Department of Otorhinolaryngology-Head and Neck Surgery, Shanghai Ninth People's Hospital, Shanghai Jiaotong University School of Medicine, Shanghai, China*

Correspondence should be addressed to Tao Yang; yangtfxl@sina.com and Hao Wu; wuhao622@sina.cn

Received 30 August 2016; Revised 9 October 2016; Accepted 20 October 2016

Academic Editor: Genglin Li

Nonsyndromic deafness is genetically heterogeneous but phenotypically similar among many cases. Though a variety of targeted next-generation sequencing (NGS) panels has been recently developed to facilitate genetic screening of nonsyndromic deafness, some syndromic deafness genes outside the panels may lead to clinical phenotypes similar to nonsyndromic deafness. In this study, we performed comprehensive genetic screening in a dominant family in which the proband was initially diagnosed with nonsyndromic deafness. No pathogenic mutation was identified by targeted NGS in 72 nonsyndromic and another 72 syndromic deafness genes. Whole exome sequencing, however, identified a p.E313K mutation in *NLRP3*, a gene reported to cause syndromic deafness Muckle-Wells Syndrome (MWS) but not included in any targeted NGS panels for deafness in previous reports. Follow-up clinical evaluation revealed only minor inflammatory symptoms in addition to deafness in six of the nine affected members, while the rest, three affected members, including the proband had no obvious MWS-related inflammatory symptoms. Immunostaining of the mouse cochlea showed a strong expression of NLRP3 in the spiral ganglion neurons. Our results suggested that *NLRP3* may have specific function in the spiral ganglion neurons and can be associated with both syndromic and nonsyndromic sensorineural deafness.

1. Introduction

Hearing loss is a common sensory deficit that is genetically heterogeneous. It is estimated that about 70% of all inherited deafness is nonsyndromic, while the remaining 30% is syndromic. To date, more than 100 loci for nonsyndromic deafness have been mapped (http://hereditaryhearingloss.org/) and more than 400 syndromes have been described in which deafness is part of the anomalies. In some cases, mutations in the same gene can cause both nonsyndromic and syndromic deafness. While the number of causative genes is usually limited for each individual case of syndromic deafness, nonsyndromic deafness is often phenotypically similar among cases of different molecular etiologies, rendering the genetic diagnosis difficult for this type of hearing loss.

The advent of next-generation sequencing (NGS) provided an ideal tool to answer this challenge, as combined technologies of targeted genomic enrichment and high-throughput sequencing make it possible to sequence over a hundred deafness genes simultaneously at a reasonable cost [1, 2]. In recent years, a variety of targeted NGS panels have been implemented in genetic screening of deafness.

The number of targeted genes ranged from 50 to over 200, typically including all known nonsyndromic deafness genes up to the date of the design and differing in the number of syndromic deafness genes [3–8]. Though those panels theoretically should able to cover most genes associated with nonsyndromic deafness, it remains possible that some syndromic deafness genes outside the panels may lead to clinical phenotypes similar to nonsyndromic deafness.

In this study, we showed one such example in a dominant family segregated with apparently nonsyndromic deafness. After targeted NGS failed to identify any causative mutation in 144 known deafness genes, an E313K mutation in *NLRP3* was revealed by whole exome sequencing which has been previously linked to syndromic deafness Muckle-Wells Syndrome (MWS, OMIM # 191900) [9]. Reports on such cases may improve the precise genetic diagnosis of deafness.

2. Materials and Methods

2.1. Subjects. A Chinese Han family (Family C277) segregated with autosomal dominant hearing loss was recruited through Xinhua Hospital, Shanghai, China. As shown in Figure 1, this family consisted of 9 affected family members and 1 unaffected family member. All affected members had bilateral, late-onset sensorineural hearing loss. The family members gave written, informed consent to participate in the present study. This study was approved by the ethics committee of Xinhua Hospital, Shanghai Jiaotong University School of Medicine.

2.2. Clinical Characterization. The hearing levels of all affected family members were measured by air and bone conducted pure tone audiometry. After detection of the p.E313K mutation in *NLRP3*, the affected family members received a follow-up clinical evaluation focusing on the MWS-related inflammatory symptoms including chronic fatigue, recurrent fever, headache, ocular symptoms such as conjunctivitis, uveitis, papillary edema, and opticus neuritis, oral ulcers, abdominal pain, proteinuria, musculoskeletal symptoms such as arthralgia, arthritis, and myalgia, and skin symptoms such as erythematous rash and cold-induced urticaria.

2.3. Targeted NGS and Whole Exome Sequencing. Genomic DNAs from the 10 family members were extracted from whole blood using Blood DNA kit (TIANGEN Biotech, Beijing, China). Targeted NGS of 144 known deafness genes (see complete list of the genes in Supplementary Table S1 in Supplementary Material available online at http://dx.doi.org/10.1155/2016/3018132) was performed in proband III-3 using the MyGenotics gene enrichment system (MyGenotics, Boston, MD, USA) and the Illumina HiSeq 2000 sequencer (Illumina, San Diego, CA, USA) as previously described [10]. Whole exome sequencing was performed in family members I2, III2, III4, and I1 using the Agilent SureSelect V5+UTR Exome Enrichment Kit (Agilent, Santa Clara, CA, USA) and the Hiseq X Ten sequencer (Illumina, San Diego, CA, USA) as previously reported [11]. The reads were aligned to HG19 using the BWA software and the variants were called using the Genome Analysis Toolkit (GATK), both with the default parameters. SNVs and indels were presented using Variant Call Format (VCF) version 4.1 and annotated using the ANNOVAR software. To identify the candidate pathogenic mutations, exclusive filtering criteria were applied to the variants including the following: (1) SNVs in nonsplicing region leading to synonymous amino acids; (2) SNVs and indels called in off-target regions; (3) variants with maximum minor allele frequency (MAF) greater than 0.001 in public databases 1000 Genomes Project, NHLBI Exome Sequencing Project (ESP) and the Examination for Architects in Canada (ExAC).

2.4. Immunostaining of the Mouse Cochlea. Immunostaining of the mouse cochlea was performed as previously described [11]. Briefly, P60 mouse cochlea was extracted, perfused, and fixed in PFA overnight. The cochlea was then washed in 0.1 M PBS, incubated in 5% EDTA for 5 days, dehydrated in 30% sucrose, embedded in OCT, and frozen at −20°C. Frozen sections (10 μm) were obtained parallel to the modiolus. The slides were rewarmed at room temperature for 30 minutes, washed in PBS, incubated with a blocking buffer containing 5% donkey serum, 0.3% Triton X-100, and 1% BSA in PBS for 1 hour at room temperature, incubated in the 1 : 500 mouse anti-TUJ1 (MMS435P-250, Covance, Princeton, USA) and 1 : 200 rat anti-NLRP3 (MAB7578-SP, RnD, Minneapolis, USA) primary antibodies at 4°C overnight, and detected with 1 : 500 secondary antibodies conjugated to Alexa 488 and Alexa 594 (Jackson Immunoresearch, West Grove, USA). The slides were mounted in Prolong-Gold Antifade reagent with DAPI (Invitrogen, Carlsbad, USA) and examined with confocal fluorescence microscopy (LSM710, Zeiss, Berlin, Germany).

3. Results

3.1. Auditory Characteristics. The affected members in Family C277 exhibited bilateral, late-onset, slowly progressive hearing impairment (Figure 2). The age at onset was around 20 years. The hearing impairment began in the middle and high frequencies, gradually progressed to all frequencies, and eventually reached profound in the sixth decade. There was no evidence of vestibular dysfunction in any member. Initial clinical evaluation of the proband III3 revealed no significant abnormalities other than the hearing impairment.

3.2. Exclusion of 144 Known Deafness Genes. To identify the genetic cause of the deafness in Family C277, we first screened 144 known deafness genes in proband III3 including 72 nonsyndromic and 72 additional syndromic deafness genes. Targeted NGS generated 2514581 mapped reads with an averaged on-target sequencing depth of 299x. 92.4% of the targeted regions were covered with at least 10x in depth. A total of four heterozygous nonsynonymous candidate variants with MAF of 0.01 or less were identified including p.Q1495fs in *PCDH15* (NM_001142767), p.M1209I in *COL4A3* (NM_000091), p.G204S in *EDN3* (NM_207033), and p.R36H

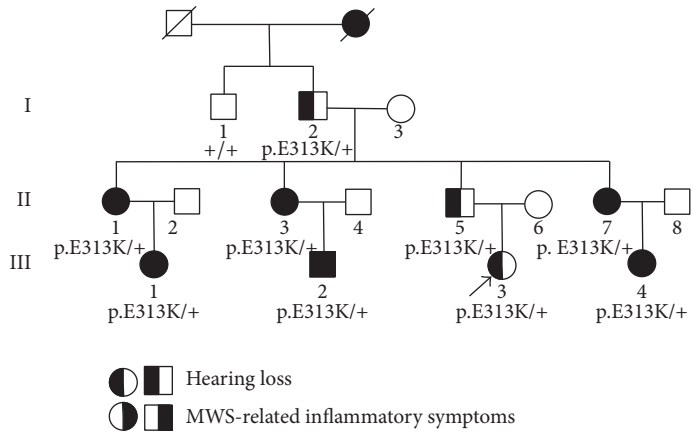

Figure 1: Pedigree of Family C277 with progressive hearing loss and MWS-related inflammatory symptoms. The genotype of the p.E313K mutation in *NLRP3* was marked under the family members. Proband III3 was pointed by an arrow.

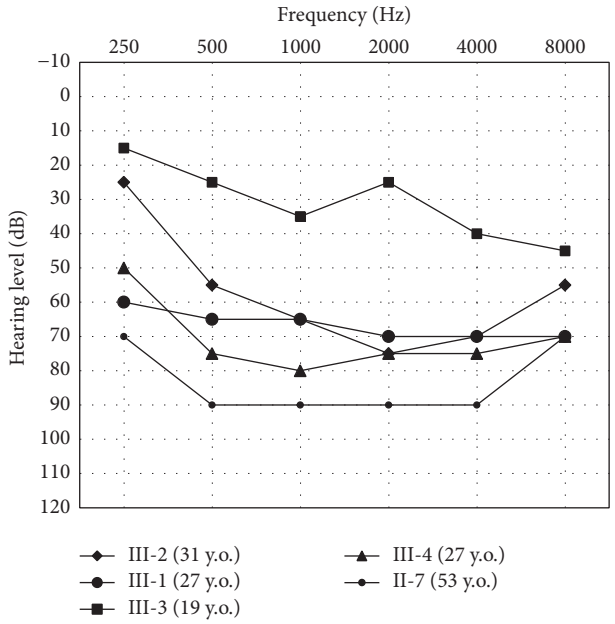

Figure 2: Audiometric features of affected individuals III1, III2, III3, III4, and II7 at age of 19–53 years. Pure tone hearing thresholds were shown as the averages of the left and right sides. The rest of the four affected individuals I2 (80 y.o.), II1 (56 y.o.), II3 (55 y.o.), and II5 (59 y.o.) had hearing thresholds of 90 dB or higher.

in *KCNE1* (NM_001127670). Sanger sequencing in all 10 family members, however, revealed that none of the four variants segregated with the hearing loss phenotype in Family C277.

3.3. Identification of the p.E313K Mutation in NLRP3. To further investigate the genetic cause of the deafness in Family C277, we performed whole exome sequencing in affected family members I2, III2, and III3 and unaffected family member I1. The mean sequencing depth for I2, III2, III3, and I1 was 76.67x, 93.72x, 91.05x, and 98.94x, respectively. An averaged 98% of the targeted region was covered by at least 5x in depth. A total of seven nonsynonymous candidate variants with MAF of 0.01 or less were identified in affected individuals I2, III2, and III3 but not in unaffected individual I1. Sanger sequencing in all 10 family members revealed a p.E313K (NM_001127462: c.G937A) mutation in *NLRP3*, a gene not included in any of the targeted NGS panels for deafness in previous reports (see Section 4 for details), as the only pathogenic mutation segregating with the hearing loss phenotype. The p.E313K mutation is located in the NBS domain of NLRP3 and changed an evolutionary conserved amino acid (Figure 3). This mutation was predicted as pathogenic by computer programs Mutation Taster, SIFT, and PROVEAN (prediction scores of 0.794, 2.80, and −3.02, resp.). It was not seen in 300 Chinese Han normal hearing controls.

3.4. Characteristics of the Autoinflammatory Abnormalities. The p.E313K mutation in *NLRP3* has been previously reported to be associated with inherited autoinflammatory disease Muckle-Wells Syndrome (MWS) [9]. A follow-up clinical evaluation therefore was performed in all 9 affected family members focusing on the MWS-related autoinflammatory features (Table 1). Different from the previous report, in six of the nine affected members only minor inflammatory symptoms were present including conjunctivitis and uveitis ($n = 4$), oral ulcers ($n = 3$), arthralgias and arthritis ($n = 1$), and erythematous rash ($n = 2$). The rest three affected members I2, II5, and III3 had no obvious MWS-related inflammatory symptoms. None of the nine affected members had chronic fatigue, recurrent fever, headache, pericarditis, abdominal pain, and proteinuria. The occurrence of the MWS-related inflammatory symptoms was apparently not associated with age. The affected individual I2 was 80 years old but did not have any inflammatory symptoms. On the contrary, the affected individual III-4 was only 27 years old but showed conjunctivitis, uveitis, and erythematous rash at a quite early age.

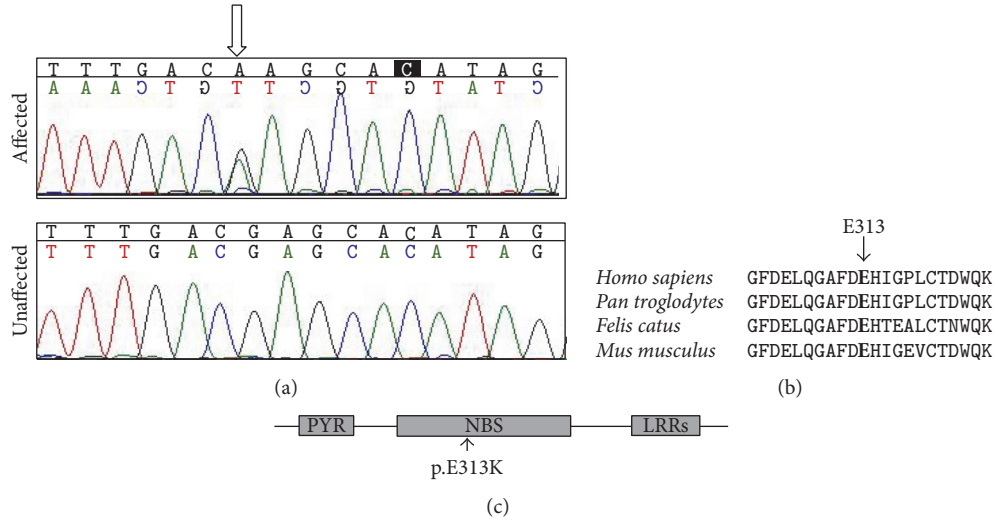

Figure 3: The p.E313K (c.G937A) mutation of *NLRP3*. (a) Chromatograms of the mutant and wild-type sequences. (b) Conservation of the E313 residue of NLRP3 in *Homo sapiens, Pan troglodytes, Felis catus*, and *Mus musculus*. (c) Domain structure of NLRP3 protein with the location of the p.E313K mutation marked by an arrow.

Table 1: Clinical features of the patients with the p.E313K mutation in *NLRP3*.

Clinical symptoms	I2 (80)*	II1 (56)*	II3 (55)*	II5 (59)*	II7 (53)*	III1 (27)*	III2 (31)*	III3 (19)*	III4 (27)*	% in the current study	% in the referenced study [9]
Chronic fatigue	—	—	—	—	—	—	—	—	—	0	100
Recurrent fever	—	—	—	—	—	—	—	—	—	0	31
Headache	—	—	—	—	—	—	—	—	—	0	54
Ocular symptoms											
Conjunctivitis	—	Y	—	—	Y	Y	—	—	Y	44	85
Uveitis	—	Y	—	—	Y	Y	—	—	Y	44	77
Papillary edema	—	—	—	—	—	—	—	—	—	0	15
Hearing loss	Y	Y	Y	Y	Y	Y	Y	Y	Y	100	92
Oral ulcers	—	Y	Y	—	—	—	Y	—	—	33	46
Pericarditis	—	—	—	—	—	—	—	—	—	0	23
Abdominal pain	—	—	—	—	—	—	—	—	—	0	31
Renal amyloidosis	—	—	—	—	—	—	—	—	—	0	77
Musculoskeletal symptoms											
Arthralgias	—	—	Y	—	—	—	—	—	—	11	85
Arthritis	—	—	Y	—	—	—	—	—	—	11	69
Myalgias	—	—	—	—	—	—	—	—	—	0	54
Skin symptoms											
Erythematous rash	—	—	—	—	Y	—	—	—	Y	18	54

*Age (years) when tested.

3.5. Expression of NLRP3 in the Spiral Ganglion Neurons. Immunostaining showed that NLRP3 was strongly expressed in the spiral ganglion neurons of adult (P60) mouse cochlea (Figure 4). Its expression was mainly distributed in the cytoplasm similar to the neural marker Tuj1.

4. Discussion

In this study, we identified a p.E313K mutation in *NLRP3* as the pathogenic cause of the deafness in Family C277. *NLRP3* encodes a pyrin-like protein expressed in innate

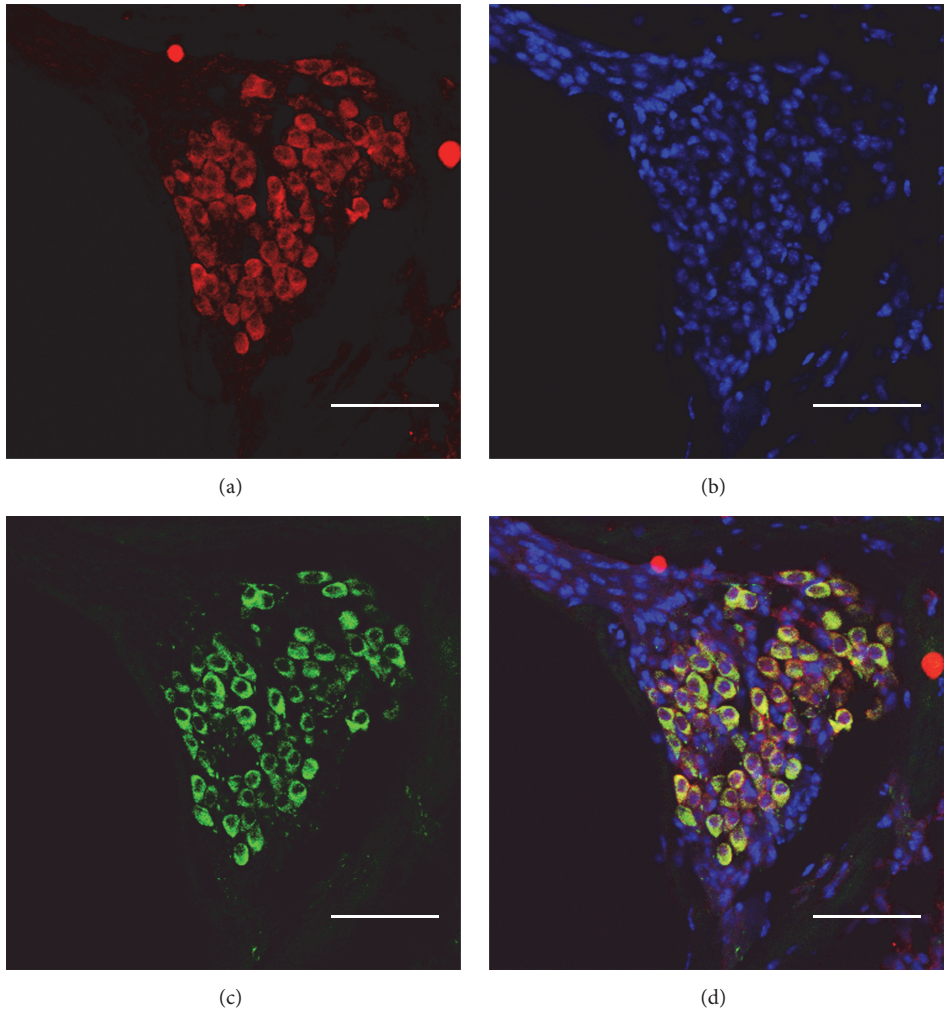

Figure 4: Expression of NLRP3 in the spiral ganglion neurons of the P60 mouse cochlea. ((a)–(c)) NLRP3, cell nucleus, and Tuj1 were stained as red, blue, and green, respectively. (d) Colocalization of NLRP3 and Tuj1 staining. Bars: 50 μm.

immune cells such as neutrophils, monocytes, and dendritic cells [12]. The NLRP3 protein contains a pyrin domain, a nucleotide-binding site (NBS) domain where the E313 amino acid residue resides, and a leucine-rich repeat (LRR) motif (Figure 3(c)). It plays an important role in inflammation, immune response, and apoptosis, while the neurological function of NLRP3 was only implicated in the sensorineural hearing loss [13]. Dominant mutations in *NLRP3* may lead to a spectrum of inflammatory diseases including familial cold autoinflammatory syndrome (FCAS, OMIM # 120100), Muckle-Wells Syndrome (MWS, OMIM # 191900), and chronic infantile neurological cutaneous and articular syndrome (CINCA, OMIM # 607115).

The p.E313K mutation in *NLRP3* has been previously reported to be associated with MWS [9]. MWS is a rare autosomal dominant disorder characterized by episodic skin rash, arthralgias, recurrent fever, and renal amyloidosis as well as late-onset sensorineural hearing loss. In a large dominant family of European descent in the report [12], a majority or all of the thirteen affected family members with the p.E313K mutation in *NLRP3* had MWS-related inflammatory symptoms including chronic fatigue (100%), recurrent fever (31%), headache (54%), ocular symptoms such as conjunctivitis (85%) and uveitis (77%), oral ulcers (46%), pericarditis (23%), abdominal pain (31%), renal amyloidosis (77%), musculoskeletal symptoms such as arthralgias (85%), arthritis (69%), and myalgia (54%), and erythematous rash (54%). On the contrary, Family C277 in our study exhibited a much milder degree of MWS-related inflammatory symptoms, in which only 44% of the nine affected members had conjunctivitis and uveitis, 33% with oral ulcers, 18% with erythematous rash, and 11% with arthralgias and arthritis (Table 1). Chronic fatigue, recurrent fever, headache, pericarditis, abdominal pain, renal amyloidosis, or myalgia was not reported in any of them. Three affected members, I2, II5, and III3, were free of MWS-related inflammatory symptoms other than the hearing loss (i.e., nonsyndromic deafness). The hearing loss in Family C277, therefore, should be regarded as a mixed syndromic (II1, II2, II7, III1, III2, and III4) and nonsyndromic (I2, II5, and III3) deafness depending

on the specific affected individuals. The key symptom in this family overall, however, should be the hearing loss as the inflammatory symptoms were either relatively minor or completely absent. We speculated that the complicate genotype-phenotype correlation of the p.E313K mutation in NLRP3 can be influenced by both genetic and environmental factors. The different genetic background of the ethnicity may explain the phenotypic difference observed between the Chinese and European families with the same mutation. The environmental factors may explain the intrafamilial difference observed in Family C277.

Due to the mild inflammatory symptoms, the disorder of Family C277 was indeed initially diagnosed as nonsyndromic deafness. To our knowledge, however, *NLRP3* was not included in any of the major targeted NGS panels for deafness in the previous and current studies (Supplementary Table S2). The p.E313K pathogenic mutation, therefore, was not identified until whole exome sequencing was performed. On the other hand, our immunostaining results showed that NLRP3 is strongly expressed in the spiral ganglion neurons of mouse cochlea (Figure 4), implicating a specific role of *NLRP3* in the inner ear function. Previous reports showed that early treatment with IL-1 inhibitors Anakinra or Canakinumab in patients with *NLRP3* mutations can improve hearing and prevent irreversible renal damage from amyloidosis [12, 14]. The early genetic diagnosis of *NLRP3* mutations, therefore, is essential for proper clinical intervention. Our study suggested that syndromic deafness genes such as *NLRP3* should be recognized and targeted for genetic screening of nonsyndromic deafness by targeted NGS.

5. Conclusions

NLRP3 may have specific function in the spiral ganglion neurons of the cochlea. Mutations in *NLRP3* can be associated with both syndromic and nonsyndromic sensorineural deafness. Such genes should be recognized and targeted for genetic screening of nonsyndromic deafness.

Competing Interests

The authors declare no competing financial interests.

Authors' Contributions

Penghui Chen and Longxia He contributed equally to this work.

Acknowledgments

This research was supported by grants from National Science Foundation of China (81570930 and 81371101 to Tao Yang; 81330023 to Hao Wu), Shanghai Municipal Science and Technology Commission (14DZ1940102 to Tao Yang; 14DZ2260300 and 14DJ1400201 to Hao Wu), and Shanghai Municipal Education Commission-Gaofeng Clinical Medicine Grant (20152519 to Tao Yang).

References

[1] J. Shendure and H. Ji, "Next-generation DNA sequencing," *Nature Biotechnology*, vol. 26, no. 10, pp. 1135–1145, 2008.

[2] H. L. Rehm, "Disease-targeted sequencing: a cornerstone in the clinic," *Nature Reviews Genetics*, vol. 14, no. 4, pp. 295–300, 2013.

[3] X. Gu, L. Guo, H. Ji et al., "Genetic testing for sporadic hearing loss using targeted massively parallel sequencing identifies 10 novel mutations," *Clinical Genetics*, vol. 87, no. 6, pp. 588–593, 2015.

[4] H. Mutai, N. Suzuki, A. Shimizu et al., "Diverse spectrum of rare deafness genes underlies early-childhood hearing loss in Japanese patients: a cross-sectional, multi-center next-generation sequencing study," *Orphanet Journal of Rare Diseases*, vol. 8, no. 1, article 172, 2013.

[5] J. H. Park, N. K. Kim, A. R. Kim et al., "Exploration of molecular genetic etiology for Korean cochlear implantees with severe to profound hearing loss and its implication," *Orphanet Journal of Rare Diseases*, vol. 9, no. 1, article 167, 2014.

[6] A. E. Shearer, E. A. Black-Ziegelbein, M. S. Hildebrand et al., "Advancing genetic testing for deafness with genomic technology," *Journal of Medical Genetics*, vol. 50, no. 9, pp. 627–634, 2013.

[7] B. Vona, T. Müller, I. Nanda et al., "Targeted next-generation sequencing of deafness genes in hearing-impaired individuals uncovers informative mutations," *Genetics in Medicine*, vol. 16, no. 12, pp. 945–953, 2014.

[8] T. Yang, X. Wei, Y. Chai, L. Li, and H. Wu, "Genetic etiology study of the non-syndromic deafness in Chinese Hans by targeted next-generation sequencing," *Orphanet Journal of Rare Diseases*, vol. 8, no. 1, article 85, 2013.

[9] J. B. Kuemmerle-Deschner, P. Lohse, I. Koetter et al., "NLRP3 E311K mutation in a large family with Muckle-Wells syndrome—description of a heterogeneous phenotype and response to treatment," *Arthritis Research & Therapy*, vol. 13, no. 6, article R196, 2011.

[10] M. Gao, G. Chen, H. Wang et al., "Therapeutic potential and functional interaction of carfilzomib and vorinostat in T-cell leukemia/lymphoma," *Oncotarget*, vol. 7, no. 20, pp. 29102–29115, 2016.

[11] L. Zhang, J. Wang, X. Feng et al., "Multifocal skeletal tuberculosis: a case report," *Experimental and Therapeutic Medicine*, vol. 11, no. 4, pp. 1288–1292, 2016.

[12] G. Guarda, M. Zenger, A. S. Yazdi et al., "Differential expression of NLRP3 among hematopoietic cells," *The Journal of Immunology*, vol. 186, no. 4, pp. 2529–2534, 2011.

[13] J. J. Chae, Y.-H. Cho, G.-S. Lee et al., "Gain-of-Function pyrin mutations induce NLRP3 protein-independent interleukin-1β activation and severe autoinflammation in mice," *Immunity*, vol. 34, no. 5, pp. 755–768, 2011.

[14] I. Koné-Paut and C. Galeotti, "Anakinra for cryopyrin-associated periodic syndrome," *Expert Review of Clinical Immunology*, vol. 10, no. 1, pp. 7–18, 2014.

Hindawi Publishing Corporation
Neural Plasticity
Volume 2016, Article ID 4034218, 10 pages
http://dx.doi.org/10.1155/2016/4034218

Research Article

Protective Effect of Edaravone on Glutamate-Induced Neurotoxicity in Spiral Ganglion Neurons

Xiaohui Bai,[1,2] Chi Zhang,[1,2] Aiping Chen,[1,2] Wenwen Liu,[1,2] Jianfeng Li,[1,2] Qian Sun,[3] and Haibo Wang[1,2]

[1]*Department of Otolaryngology-Head and Neck Surgery, Shandong Provincial Hospital Affiliated to Shandong University, Jinan 250021, China*
[2]*Shandong Provincial Key Laboratory of Otology, Jinan 250022, China*
[3]*Human Genetics Department, Emory University, Atlanta, GA, USA*

Correspondence should be addressed to Haibo Wang; whboto11@163.com

Received 19 July 2016; Accepted 10 October 2016

Academic Editor: Genglin Li

Glutamate is an important excitatory neurotransmitter in mammalian brains, but excessive amount of glutamate can cause "excitotoxicity" and lead to neuronal death. As bipolar neurons, spiral ganglion neurons (SGNs) function as a "bridge" in transmitting auditory information from the ear to the brain and can be damaged by excessive glutamate which results in sensorineural hearing loss. In this study, edaravone, a free radical scavenger, elicited both preventative and therapeutic effects on SGNs against glutamate-induced cell damage that was tested by MTT assay and trypan blue staining. Ho.33342 and PI double staining revealed that apoptosis as well as necrosis took place during glutamate treatment, and apoptosis was the main type of cell death. Oxidative stress played an important role in glutamate-induced cell damage but pretreatment with edaravone alleviated cell death. Results of western blot demonstrated that mechanisms underlying the toxicity of glutamate and the protection of edaravone were related to the PI3K pathway and Bcl-2 protein family.

1. Introduction

Hearing loss is a very common sensory disorder which, to a great extent, influences the quality of patients' life. Sensorineural hearing loss is often associated with the impairment of spiral ganglion neurons (SGNs). SGNs are bipolar neurons that transmit auditory information from the ear to the brain. They are indispensable for the preservation of normal hearing and their survival depends mainly on genetic and environmental interactions [1]. Many disturbances, such as noise exposure, ototoxic medication, and genetic factors, can lead to the loss of SGNs irreversibly and therefore result in sensorineural hearing loss.

It is widely accepted that glutamate is an important excitatory neurotransmitter in mammalian brains, but excessive amount of glutamate can cause "excitotoxicity" and lead to neuronal death in some injuries and diseases, such as cerebral ischemia, traumatic brain disorder, HIV, and neurodegenerative disorders [2, 3]. Treatment with excessive glutamate in rats was found to result in high-frequency hearing loss. And there was a dramatic and selective reduction of neurons in the basal, high-frequency-related portion of the spiral ganglion, but no loss of hair cells was discovered [4]. Traumatic sound exposure, aminoglycoside antibiotics, cochlea ischemia, or traumatic stress leads to an excessive release of glutamate from inner hair cells into the synaptic cleft [5]. Glutamate excitotoxicity causes neuronal cell death primarily through the excessive activation of glutamate receptors which triggers massive Ca^{2+} influx into neurons [6]. Ca^{2+}-loaded mitochondria generate reactive oxygen species (ROS), which comprises superoxide and nitric oxide [7, 8]. And large amount of ROS leads to cell death eventually.

Edaravone (MCI-186, 3-methyl-1-phenyl-2-pyrazolin-5-one) is a potent free radical scavenger which has already been used in the clinical treatment of ischemia impairments, such as acute cerebral infarction, acute myocardial infarction,

and rheumatoid arthritis [9–11]. It can interact with both peroxyl and hydroxyl radicals to form oxidized compounds and thus attenuate ischemic damage [12]. Many studies have revealed that free radical scavengers are also very useful in the treatment of otology disorders, such as inner ear barotrauma, aminoglycoside-induced ototoxicity, and cisplatin-induced ototoxicity [13–15].

So far, few concerns have been focused on the protective effect of edaravone on spiral ganglion neurons against toxicity of glutamate. In this study, we aim to demonstrate whether edaravone, the free radical scavenger, can protect SGNs from glutamate-induced cytotoxicity and the possible underlying mechanism.

2. Materials and Methods

2.1. Materials. Dulbecco's Modified Eagle's Medium (DMEM) with high-glucose and fetal bovine serum were purchased from GIBCO (USA). Anti-NSE antibody was obtained from Abcam (USA); other antibodies including anti-Bcl-2, anti-Bax, anti-AKT, anti-p-AKT, and anti-β-actin were purchased from Santa Cruz Biotechnology (USA). Glutathione (GSH), superoxide dismutase (SOD), and malonaldehyde (MDA) assay kits (A006-1, A001-3, and A003-1, resp.) were all purchased from Nanjing Jiancheng Bioengineering Institute (China). BCA protein assay kit was a product from Shenergy Biocolor Bioscience & Technology Company (China). Glutamate (Glu), edaravone (Ed), 3-(4,5-dimethylthiazol-2-yl)-2,5-diphenyltetrazolium bromide (MTT), trypan blue solution, and other agents were obtained from Sigma (USA).

2.2. Primary Cultures of Rat SGNs. As our previous protocol [1], the SGNs cells were isolated from rats at age less than 5 postnatal days. After anesthesia with pentobarbital sodium, the rats were decapitated at the base of the foramen magnum, the epidermis was removed, cranium was opened along the sagittal suture, and the brain halves were removed. The following steps were carried out under the microscope and in phosphate buffered solution (PBS). The bulla of the temporal bone was opened, and then the capsule of the inner ear, the stria vascularis, and the organ of corti were removed. Rosenthal's canal was isolated and placed into Ca^{2+}–Mg^{2+}-free Hank's balanced salt solution containing 0.125% trypsinase. After digesting for 15 min at 37°C, the tissue was eluted with the plating medium DMEM supplemented with 10% fetal bovine serum. Then the cells were collected by centrifugation at 1000 rpm for 8 min, resuspended, and plated in poly-L-lysine-coated 24-well culture plates at a density of 1.0×10^5 cells/mL at 37°C in a humid atmosphere of 5% CO_2.

Next, primary SGNs were identified by immunocytochemistry staining. SGNs (1.0×10^5/mL) were inoculated in 24-well plate, rinsed three times with PBS, and then stained with primary anti-NSE antibody (1 : 400) and secondary goat-anti-rabbit Cy3 antibody.

2.3. Drug Treatment. SGNs (1.0×10^5/mL) subcultured in 96-well or 24-well plate were treated with 2 mM glutamate for 10 minutes. Then the medium was replaced by normal DMEM. Different concentrations of edaravone were added to the medium either 20 min before or 2 h, 6 h, and 12 h after glutamate treatment. All the doses and time points were determined by preliminary experiments (data not shown).

2.4. Assessment of Cell Viability by MTT and Trypan Blue Staining. Cell viability was quantified by MTT assay and trypan blue staining. MTT (5 mg/mL, 20 μL) was added to each well and incubated for 4 h at 37°C after the drug treatments as described above. The medium was removed and the cell pellet was dissolved in DMSO. Then, the optical density (OD) values were measured at 570 nm using an ELISA reader. All experiments were repeated three times. Cell relative viability was calculated according to the following formula:

$$\text{Cell relative viability } (\%) = \frac{\text{OD}_{\text{experiment}}}{\text{OD}_{\text{control}}} \times 100\%. \quad (1)$$

OD_{blank} was used as zero.

In trypan blue staining, SGNs were stained with 0.4% trypan blue for 5 min after the drug treatments as described above. Pictures were taken by microscope and trypan blue positive and negative cells were counted afterwards. Cell survival rate was defined as the percentage of negative cells.

2.5. Detection of Apoptosis and Necrosis by Ho.33342 and Propidium Iodide (PI) Double Staining. SGNs were incubated with glutamate with or without edaravone (500 μM). Control cells were without any treatment. Cells were washed twice by PBS, fixed with 95% alcohol for 10 min, and then stained by Ho.33342 (10 mg/mL) and PI (50 mg/mL) at 37°C for 30 min. Morphological changes were examined by fluorescence microscope under green light (515–560 nm) and ultraviolet (UV) light (340–380 nm), respectively. At least 500 cells were counted in 5 randomly selected fields per group. All treatments were repeated three times.

2.6. Detection of GSH Content, SOD Activity, and MDA Level by Spectrophotometer. SGNs were incubated with 2 mM glutamate for 10 min with or without the pretreatment of 500 μM edaravone 2 h ahead. Control cells were without any treatment. Then cells were washed twice with ice-cold PBS, sonicated, and harvested for the following assays. Intracellular GSH content, SOD activity, and MDA level in all groups were measured by commercial assay kits according to the manufacturer's instructions. OD values at optimal wavelengths were measured using spectrophotometer and the relative levels comparing with control cells were calculated. All experiments were repeated three times.

2.7. Protein Extraction and Western Blot Analysis. After SGNs were treated by 2 mM glutamate with or without pretreatment of 500 μM edaravone, the proteins were collected and the expressions of AKT, p-AKT, Bax, and Bcl-2 genes were examined by western blot after 24 hours' normal culture. Briefly, total protein was extracted from SGNs using lysis buffer (containing 50 mM Tris-Cl, pH 8.0, 150 mM NaCl, 0.1% SDS, 1% NP-40, and 100 mg/mL PMSF). The protein

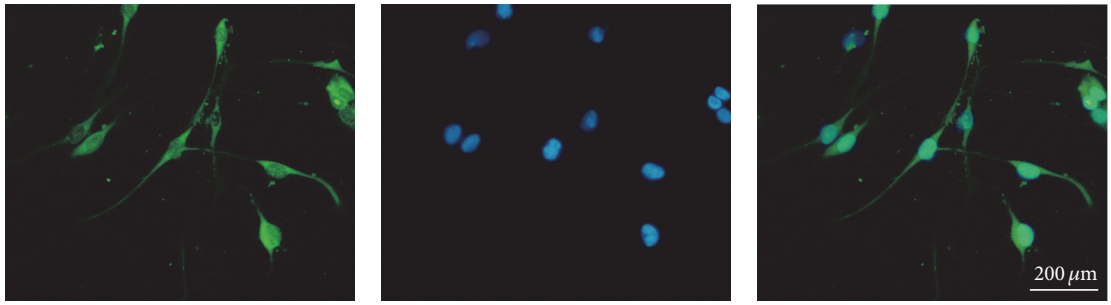

(a) (b) (c)

Figure 1: Identification of SGNs by anti-NSE antibody. (a) Corresponding NSE-Cy3 field to identify NSE positive cells. (b) Corresponding DAPI field, showing all nucleoli in the field. (c) (a), and (b) merged.

concertation of each sample was measured by BCA protein assay kit. Total protein 40 mg of each sample was loaded in 10% SDS-PAGE gels and electrically transferred onto polyvinylidene difluoride membranes. After that, the membranes were blocked in 5% nonfat dried milk/Tris-buffered Saline-Tween for 2 h at room temperature. Subsequently, the membranes were incubated with primary antibodies for 2 h at room temperature (anti-AKT: 1 : 500, anti-p-AKT: 1 : 400, anti-Bcl-2: 1 : 400, anti-Bax: 1 : 400, and anti-β-actin: 1 : 2000). Following three washes with TBST, the blots were incubated with the secondary goat-anti-mouse or goat-anti-rabbit IgG antibody (1 : 2000) at room temperature for 2 h. Finally, the immunoblots were detected by an ECL kit and visualized after exposure to X-ray film. Densitometer was used to quantitate the immunoreactive bands. The ratios of AKT, p-AKT, Bcl-2, and Bax toβ-actin were then determined.

2.8. Statistical Analysis. Data were presented as mean ± standard error on the mean (SEM). Statistical calculations were performed using SPSS19.0 software. One-way analysis of variance (ANOVA) was applied to analyze data. $p < 0.05$ was considered statistically significant.

3. Results

3.1. SGNs Were Identified by Anti-NSE Antibody. Figure 1 showed all nuclei stained by DAPI presented blue florescence; meanwhile, the cells stained by NSE presented green fluorescence. Merging of the stained images showed the cells with blue-green fluorescence, which were identified as SGNs.

3.2. Edaravone Performed Both Preventative and Therapeutic Effects against Toxicity of Glutamate. To determine whether edaravone has preventative effect on glutamate-induced cell damage, 4 experimental groups of SGNs were arranged. One group was treated with 2 mM glutamate alone for 10 min while the other three groups were pretreated with edaravone at different concentrations (250 μM, 500 μM, and 750 μM) for 20 min before glutamate treatment. Then the medium was changed to normal medium (Figure 2(a)). For the control group, SGNs were cultured in normal medium without any treatments. SGNs treated with glutamate appeared obvious morphological changes compared with control group when observed under phase contrast microscope. In addition, with glutamate treatment, the number of cells was significantly decreased, many cells were dying, lost the fusiform shape, and became round or elliptical, and large quantities of dead cells were also observed. Pretreatment of edaravone reversed these changes resulting from glutamate treatment, and at the dose of 500 μM and 750 μM, SGNs showed favorable growth without distinct cell death (Figure 2(b)).

Based on the result, we considered the 500 μM concentration of edaravone to be desirable and chose it to do the following experiments. In order to make sure that edaravone also had therapeutic effect on glutamate-induced toxicity, all the groups of SGNs were treated with glutamate for 10 min first, and then the medium was changed to normal medium. 500 μM edaravone was added to the medium 2 h, 6 h, or 12 h after glutamate treatment (Figure 3(a)). Cell death decreased with the treatment of edaravone. 2 h after glutamate treatment or even earlier time point was the most suitable time point for administering edaravone to reach the maximal protection effect among these groups. At later time points, the cell death could not be reduced effectively (Figure 3(b)). In short, these results showed that edaravone performed both preventative and therapeutic effects on the glutamate-induced toxicity in SGNs.

3.3. Edaravone Alleviated the Decrease of Cell Viability Caused by Glutamate. In order to estimate the protective effect of edaravone, MTT assay and trypan blue staining were performed to measure cell viability. The cell viability of control group was considered as 100%. Figure 4 showed that one group of SGNs was treated with glutamate alone, while the other three groups were pretreated with edaravone at different concentrations (250 μM, 500 μM, and 750 μM) for 20 min before glutamate treatment. The cell viabilities of MTT test were 32%, 48%, 75%, and 78% for each group, respectively (Figure 4(a)), and those of trypan blue staining were 30%, 45%, 72%, and 70% (Figure 4(b)). These results revealed that pretreatment with edaravone increased the cell viability of SGNs and the protective effect was presented in a dose-dependent manner. The protection reached the peak at the concentration of 500 μM and no obvious benefits were observed by further elevating the concentration. Figure 5 showed that one group of SGNs was treated with glutamate

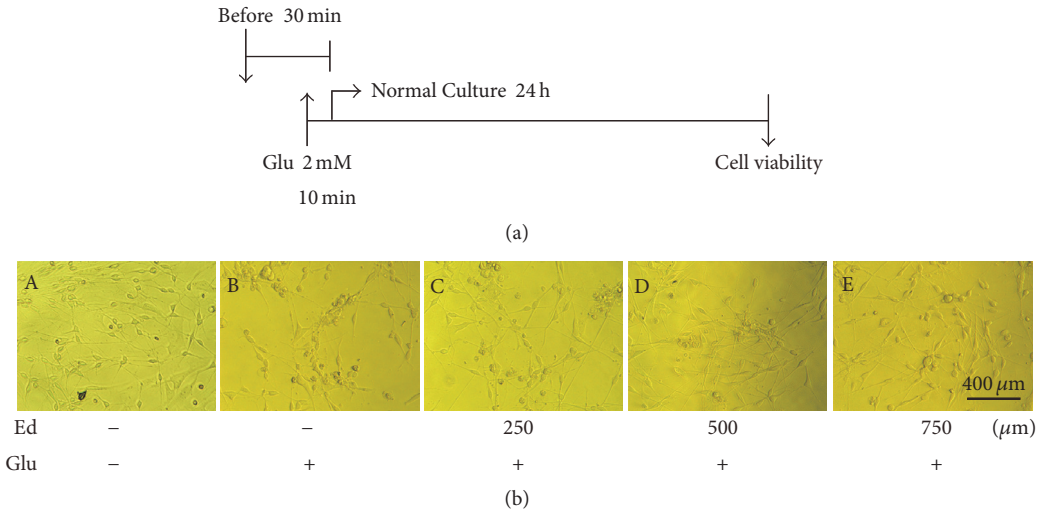

Figure 2: Preventative effect of edaravone on toxicity of glutamate in cultures of SGNs. (a) Illustration of drug treatment. SGNs were treated with edaravone first and 2 mM glutamate 20 min later. Then the medium was changed to normal medium 10 min after that. Cell viability was observed after normal culture for 24 h. (b) Pretreatment with edaravone mitigated cell death and morphological changes caused by glutamate. (A) The normal-cultured control cells. (B, C, D, and E) Morphological changes in SGNs treated with glutamate and different concentrations of edaravone (0, 250, 500, and 750 μM) were observed, respectively.

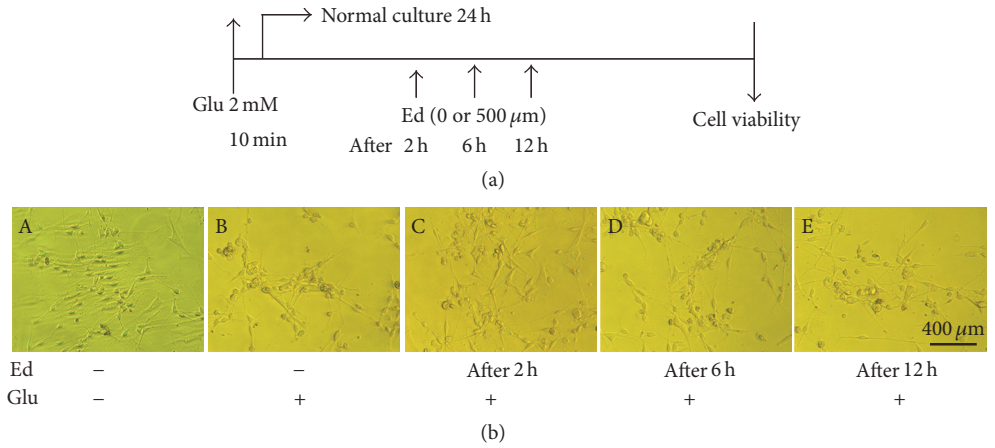

Figure 3: Therapeutic effect of edaravone on toxicity of glutamate in cultures of SGNs. (a) Illustration of drug treatment. SGNs were treated with 2 mM glutamate for 10 min; then the medium was changed to normal medium. 500 μM edaravone was added to the medium at different time points (2 h, 6 h, and 12 h later), respectively. Cell viability was observed after normal culture for 24 h. (b) Treatment with edaravone reduced cell death and morphological changes of SGNs caused by glutamate. (A) The control cells. (B, C, D, and E) Morphological changes in SGNs treated with glutamate and 500 μM edaravone added at different time point.

alone, while the other three were treated with 500 μM edaravone 2 h, 6 h, or 12 h after glutamate treatment, respectively. The cell viabilities of MTT test were 25%, 49%, 35%, and 33%, respectively (Figure 5(a)), and those of trypan blue staining were 22%, 40%, 32%, and 30% (Figure 5(b)). Treatment of edaravone at the time point of 2 h after glutamate achieved satisfying protection for SGNs against glutamate-induced cytotoxicity. But there was no significant improvement in cell viability when treated at later time points.

3.4. Edaravone Reduced Apoptosis and Necrosis Caused by Glutamate. Apoptosis and necrosis were detected using Ho.33342 and PI. Nuclei of apoptotic cells would be stained with brilliant-blue fluorescence by Ho.33342, while nuclei of necrotic cells would be stained with red fluorescence by PI. After treatment with 2 mM glutamate for 10 min, the cells were changed to normal medium and culture for additional 24 h. Then SGNs were fixed and stained with Ho.33342 and PI. Nuclei which were dyed brilliant-blue or red demonstrated the occurrence of apoptosis or necrosis. The percentages of necrotic cells and apoptotic cells with glutamate treatment were higher than those of the control group without any treatment. On the contrary, SGNs pretreated with edaravone compared to control group showed no obvious apoptosis

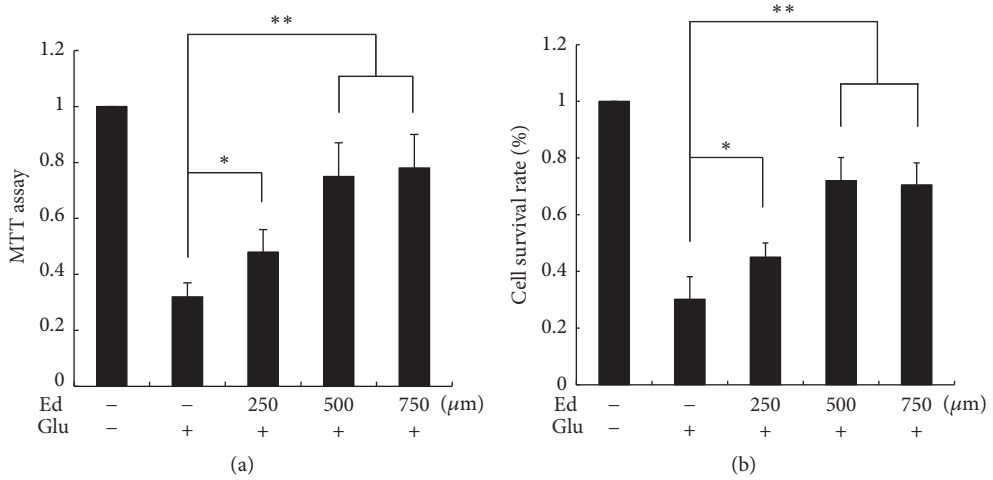

Figure 4: Pretreatment of edaravone reduced the toxicity of glutamate towards SGNs. Cell viability was detected by MTT assay (a) and trypan blue staining (b). Three groups were pretreated with 250 μM, 500 μM, and 750 μM edaravone, respectively. $^{*}p < 0.05$, $^{**}p < 0.01$, versus glutamate-treated group. The data shown here was the mean ± SEM of three separate experiments.

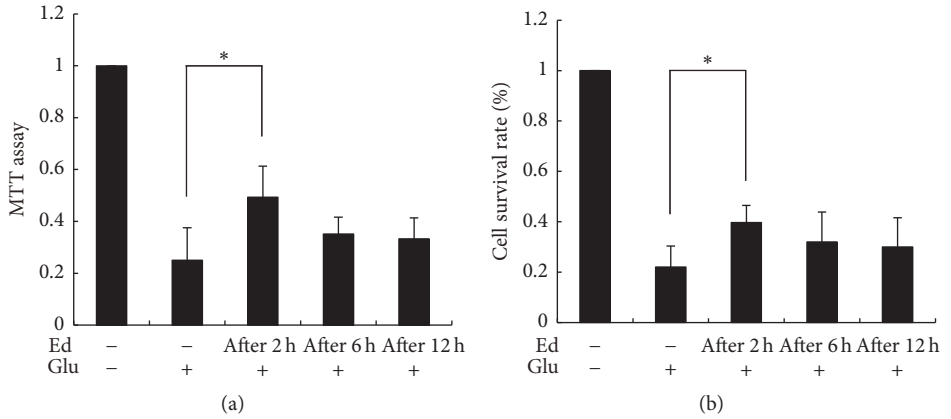

Figure 5: Treatment of edaravone buffered the toxicity of glutamate towards SGNs. Cell viability was detected by MTT assay (a) and trypan blue staining (b). Three groups were treated with 500 μM edaravone 2 h, 6 h, and 12 h after administration of glutamate, respectively. $^{*}p < 0.05$, versus glutamate-treated group. The data shown here was the mean ± SEM of three separate experiments.

and necrosis (Figure 6). So we came to the conclusion that glutamate could induce apoptosis and necrosis of SGNs, but edaravone could effectively alleviate cell death.

3.5. Edaravone Reversed Decrease of SOD Activity, MDA Elevation, and GSH Reduction Caused by Glutamate. By taking control as 100%, treatment of SGNs with 2 mM glutamate decreases activity of SOD to 35% and level of GSH to 30% and increased content of MDA to 190%. Pretreatment of edaravone (500 μM) reversed these changes to approximately normal levels, with activity of SOD to 90%, level of GSH to 115%, and content of MDA to 105% (Figure 7). These changes were all statistically significant ($^{*}p < 0.05$).

3.6. Edaravone Protected SGNs from Glutamate-Induced Apoptosis through PI3K/Akt Pathway. As shown in Figure 8, western blot analysis was performed in order to demonstrate the mechanism of edaravone's antiapoptotic effect. Representative blots showed the amount of p-AKT, AKT, Bcl-2, and Bax in SGNs (Figure 8(a)) and densitometer was used to quantitate the immunoreactive bands (Figures 8(b), 8(c), 8(d), and 8(e)). Treatment of SGNs with glutamate reduced AKT phosphorylation significantly. Moreover, the expression of antiapoptotic protein Bcl-2 was increased and the apoptotic protein Bax was decreased. Pretreatment of SGNs with 500 μM edaravone reversed these changes. The protection of edaravone could be blocked by the PI3K inhibitor, LY294002. Therefore, the protective effect of edaravone on SGNs against glutamate-induced apoptosis was associated with PI3K/Akt pathway and Bcl-2 protein family.

4. Discussion

Ischemic brain injury can cause glutamate accumulation, and then postsynaptic glutamate receptors are overstimulated and

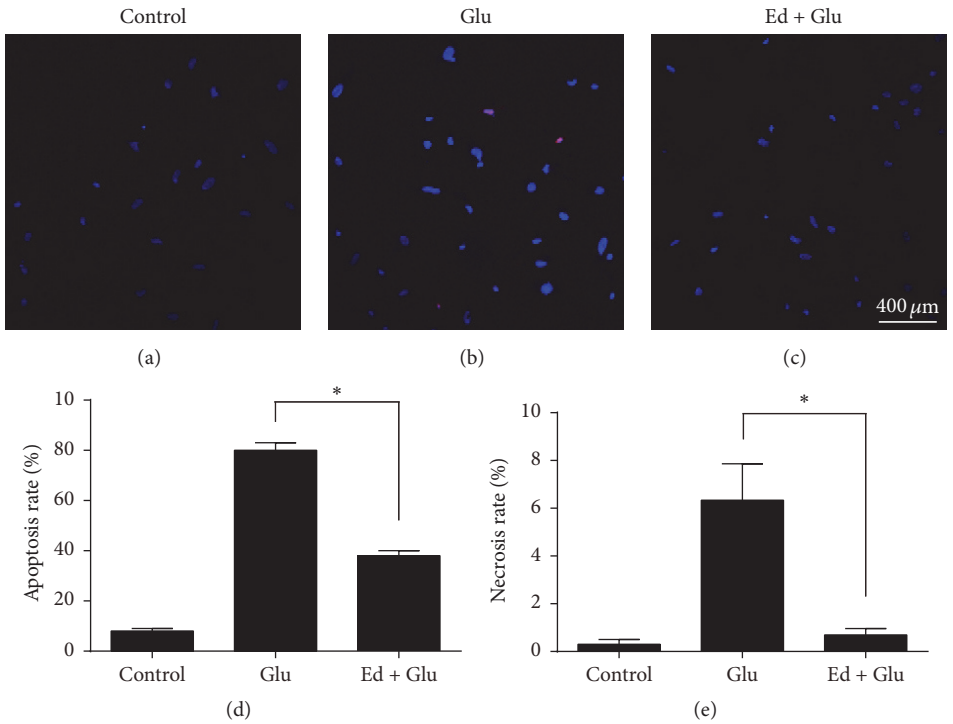

Figure 6: Cytoprotection of edaravone on glutamate-induced apoptosis and necrosis in SGNs. (a) Untreated SGNs appeared blue intact nuclei. (b) SGNs were treated with glutamate for 10 min and then cultured for 24 h. Nuclei of apoptotic SGNs were obvious and stained brilliant-blue by Ho.33342. Nuclei of necrotic cells were labeled red by PI. (c) SGNs were pretreated with 500 μM edaravone 20 min before glutamate. (d and e) Apoptosis and necrosis rates of SGNs. $^{*}p < 0.05$, versus glutamate-treated group.

intracellular Ca^{2+} overload occurs. This succession leads to the generation of free radicals and finally cell death. Since administration of glutamate in rats led to high-frequency hearing loss [4] and glutamate might be an important neurotransmitter in cochlea [16], in some cases glutamate accumulation may be a pathogenic mechanism of some otology disorders. Thus, whether free radical scavengers, such as edaravone, can protect SGNs from glutamate-induced cell damage is a meaningful question to be solved. Edaravone was the first free radical scavenger that has provided clinical evidence for therapeutic effects on ischemic stroke and it has been used clinically since 2001 [17]. Edaravone has been previously reported to protect several organs, such as the brain [18], kidney [19], liver [20], and retina [21] from free radical-induced damage. It has also been proven to be useful in otology disorders. Streptomycin-induced vestibulotoxicity in guinea pig could be attenuated by edaravone [22]. And edaravone could protect cochlea from acoustic trauma induced by reactive oxygen species [23]. In this study, we discovered that edaravone could protect spiral ganglion neurons from glutamate-induced cell damage, and the underlying mechanism was related to PI3K pathway and proteins of Bcl-2 family.

SGNs were identified first by NSE antibody through immunofluorescence analysis. Treatment of SGNs with glutamate induced obvious morphological changes and large percentage of cell death, and these changes were reversed by edaravone administration both before and after glutamate treatment (Figures 2 and 3). This phenomenon gave us the clue that edaravone could elicit both preventative and therapeutic effects against glutamate-induced cell damage.

In order to further clarify the protective effect of edaravone, MTT assay and trypan blue staining were performed to examine the cell viability of glutamate-treated SGNs with or without combining with edaravone treatment. In the living cells, the mitochondria can change MTT into blue crystal and trypan blue cannot pass the intact cell membrane, while the opposite happens in the damaged cells. The results showed that treatment with glutamate resulted in severe reduction of cell viability indicating massive cell death. Pretreatment of edaravone significantly decreased the glutamate-induced toxicity and elevated the cell viability markedly in a dose-dependent manner. The protection reached the peak at the concentration of 500 μM and no obvious improvement was observed at higher concentrations (Figure 4(a)). Treatment with edaravone 2 hours after glutamate also reduced cell death significantly but no obvious differences were observed in later time points. These results demonstrated that treatment with edaravone before or after glutamate can decrease glutamate-induced cell death significantly in SGNs. The preventative effect of edaravone at 500 μM was quite satisfying and this management was employed in the following experiments.

Apoptosis and necrosis are two typical forms of cell death. Ankarcrona et al. discovered that glutamate-induced neuronal death was a succession of necrosis or apoptosis

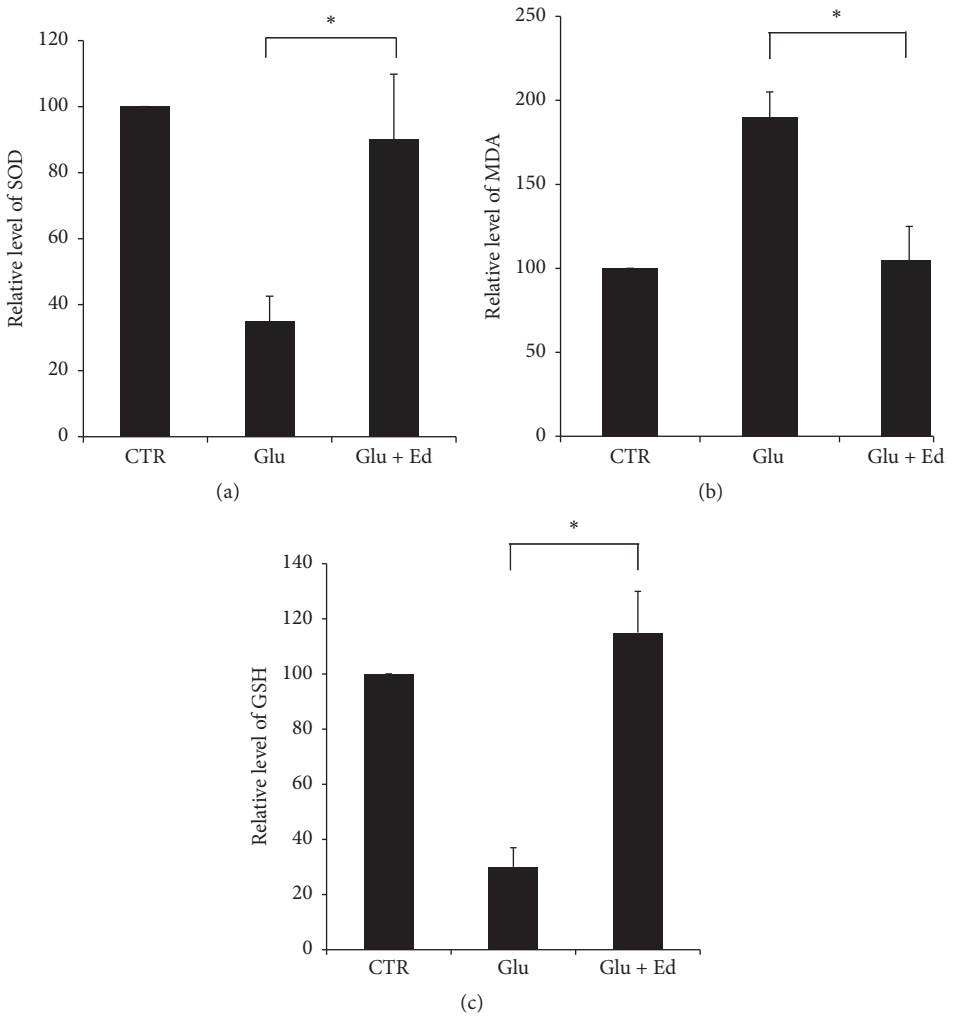

Figure 7: Changes of SOD activity, MDA level, and GSH content in different groups. Compared with the control group, glutamate decreased activity of SOD, content of SOD, and elevated level of MDA markedly. Edaravone protected SGNs by reversing these changes. $^{*}p < 0.05$. The data shown here was the mean ± SEM of three separate experiments.

depending on mitochondrial function [3]. Glutamate also induced apoptosis in spiral ganglion explants and the apoptosis could be prevented by a caspase-3 inhibitor [5]. In this study, Ho.33342 and PI staining revealed that both apoptosis and necrosis took place after administrating glutamate. Furthermore, apoptotic cells which were stained with brilliant blue color accounted for the majority of cell death indicating that apoptosis was the predominant form of cell damage induced by glutamate in SGNs. Pretreatment with edaravone reduced the glutamate-induced apoptosis and necrosis.

Next, we investigated the possible mechanism underlying glutamate's excitotoxicity and edaravone's protection on SGNs. Oxidative stress is a common underlying process related to a variety of disorders, such as ischemia-reperfusion disorders, cardiovascular diseases, cancer, and diabetes mellitus. It is well known that GSH and SOD are critical components in fighting against oxidative stress. MDA is the product of lipid peroxidation which is initiated in the presence of hydroxyl radicals. These are all important indicators of oxidative stress. So we then measured the changes of SOD activity, MDA level, and GSH content in different experimental groups. The results showed that, after treatment of glutamate, SOD activity and GSH content were reduced, while MDA level was elevated significantly, which meant oxidative stress played an important role in glutamate-induced cell damage. Meanwhile, pretreatment of edaravone reversed these changes to almost normal levels.

PI3K/Akt pathway is an important antiapoptotic pathway. Results of western blot showed that treatment of SGNs with glutamate inhibited the phosphorylation of Akt, when the level of total Akt remained constant. Bcl-2 and Bax were considered to be involved in the antiapoptotic effect and neural protection of edaravone [24, 25]. Treatment of SGNs with glutamate resulted in the elevation of the apoptotic protein Bax and the reduction of antiapoptotic protein Bcl-2. Pretreatment with edaravone eliminated all of these phenomena above. In addition, LY294002, the PI3K inhibitor, was used to block PI3K pathway and eventually

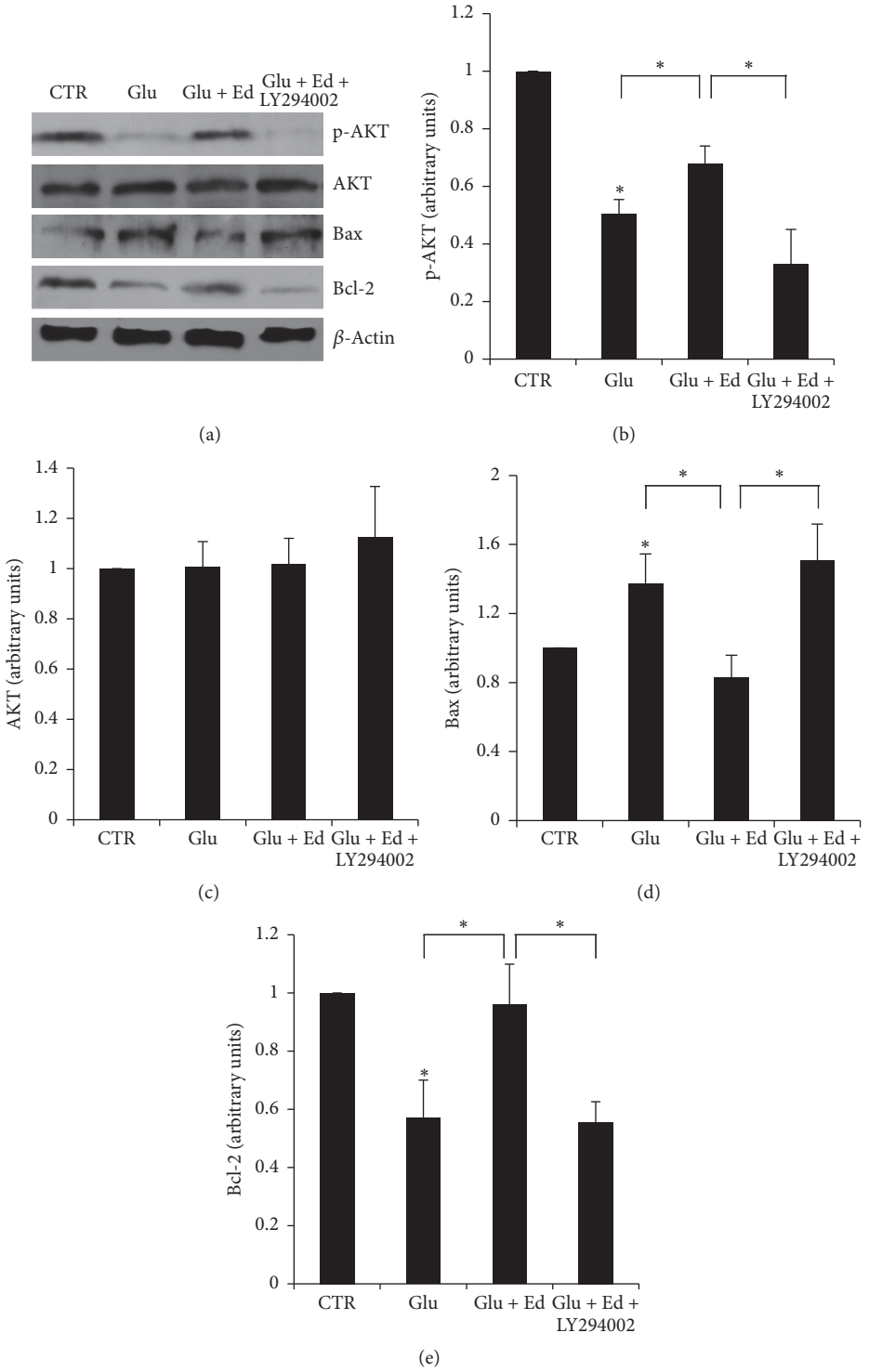

Figure 8: Detection of expression of p-AKT, AKT, Bax, and Bcl-2 by western blot. (a) Representative blots. (b, c, d, and e) Quantification of immunoreactive bands by densitometer. Treatment with glutamate resulted in the reduction of p-AKT, Bcl-2, and elevation of Bax. Pretreatment with 500 μM edaravone protected SGNs by reversing these changes. Meanwhile, LY294002 eliminated the protection effect of edaravone. Statistical analyses were carried out among different groups. $^{*}p < 0.05$.

erased the protection of edaravone. This result indicated that PI3K pathway and Bcl-2 protein family were related to the protection effect of edaravone in glutamate-induced cytotoxicity of SGNs.

Therapies against glutamate-induced cell damage have been discussed widely. Local application of glutamate receptor antagonists, such as caroverine, showed a therapeutic effect when applying 1 h after noise exposure but not 24 h afterwards [26]. Glutamate-induced apoptosis could be blocked selectively by a caspase-3 inhibitor in cultured spiral ganglion explants [5]. In this study, administration of edaravone before or after glutamate presented desirable protective effects in SGNs. It reduced apoptosis and necrosis significantly and reversed the changes of SOD, GSH, and MDA measurements. So, we believe edaravone or other free radical scavengers could be an option in the treatment of sensorineural hearing disorders related to glutamate accumulation.

5. Conclusion

In this study, we discovered that glutamate induces both apoptosis and necrosis in spiral ganglion neurons in vitro, but apoptosis is the main form of cell death. Edaravone is a potent free radical scavenger and can elicit salient protective effect against glutamate-induced cell damage in SGNs. The underlying mechanism is associated with the PI3K pathway and Bcl-2 protein family. The combination of free radical scavenger, such as edaravone, glutamate antagonist, and caspase-3 inhibitor, may be a desirable treatment of hearing disorders induced by an excessive release of glutamate.

Competing Interests

The authors declare that they have no competing interests.

Authors' Contributions

Xiaohui Bai and Chi Zhang contributed equally to this work.

Acknowledgments

This work was supported by grants from the National 973 Basic Research Program of China (2014CB541703), grants from the National Natural Science Foundation of China (81470693, 81470704), and grants from the Natural Science Foundation of Shandong Province (ZR2014HM022).

References

[1] W. Liu, Z. Fan, Y. Han et al., "Curcumin attenuates peroxynitrite-induced neurotoxicity in spiral ganglion neurons," *NeuroToxicology*, vol. 32, no. 1, pp. 150–157, 2011.

[2] J. Wang, T. Pang, R. Hafko, J. Benicky, E. Sanchez-Lemus, and J. M. Saavedra, "Telmisartan ameliorates glutamate-induced neurotoxicity: roles of AT_1 receptor blockade and PPARγ activation," *Neuropharmacology*, vol. 79, pp. 249–261, 2014.

[3] M. Ankarcrona, J. M. Dypbukt, E. Bonfoco et al., "Glutamate-induced neuronal death: a succession of necrosis or apoptosis depending on mitochondrial function," *Neuron*, vol. 15, no. 4, pp. 961–973, 1995.

[4] R. Janssen, L. Schweitzer, and K. F. Jensen, "Glutamate neurotoxicity in the developing rat cochlea: physiological and morphological approaches," *Brain Research*, vol. 552, no. 2, pp. 255–264, 1991.

[5] S. Steinbach and J. Lutz, "Glutamate induces apoptosis in cultured spiral ganglion explants," *Biochemical and Biophysical Research Communications*, vol. 357, no. 1, pp. 14–19, 2007.

[6] J. T. Coyle and P. Puttfarcken, "Oxidative stress, glutamate, and neurodegenerative disorders," *Science*, vol. 262, no. 5134, pp. 689–695, 1993.

[7] T. M. Dawson, V. L. Dawson, and S. H. Snyder, "A novel neuronal messenger molecule in brain: the free radical, nitric oxide," *Annals of Neurology*, vol. 32, no. 3, pp. 297–311, 1992.

[8] M. Lafon-Cazal, S. Pietri, M. Culcasi, and J. Bockaert, "NMDA-dependent superoxide production and neurotoxicity," *Nature*, vol. 364, no. 6437, pp. 535–537, 1993.

[9] K. Tsujita, H. Shimomura, H. Kawano et al., "Effects of edaravone on reperfusion injury in patients with acute myocardial infarction," *American Journal of Cardiology*, vol. 94, no. 4, pp. 481–484, 2004.

[10] Y. Higashi, D. Jitsuiki, K. Chayama, and M. Yoshizumi, "Edaravone (3-methyl-1-phenyl-2-pyrazolin-5-one), a novel free radical scavenger, for treatment of cardiovascular diseases," *Recent Patents on Cardiovascular Drug Discovery*, vol. 1, no. 1, pp. 85–93, 2006.

[11] M. Mishina, Y. Komaba, S. Kobayashi et al., "Efficacy of edaravone, a free radical scavenger, for the treatment of acute lacunar infarction," *Neurologia Medico-Chirurgica*, vol. 45, no. 7, pp. 344–348, 2005.

[12] M. S. Asplund, A. Lidian, B. Linder, M. Takumida, and M. Anniko, "Protective effect of edaravone against tobramycin-induced ototoxicity," *Acta Oto-Laryngologica*, vol. 129, no. 1, pp. 8–13, 2009.

[13] H. Maekawa, T. Matsunobu, H. Tsuda et al., "Therapeutic effect of edaravone on inner ear barotrauma in the guinea pig," *Neurochemistry International*, vol. 54, no. 8, pp. 513–518, 2009.

[14] S. L. Garetz, R. A. Altschuler, and J. Schacht, "Attenuation of gentamicin ototoxicity by glutathione in the guinea pig in vivo," *Hearing Research*, vol. 77, no. 1-2, pp. 81–87, 1994.

[15] A. R. Fetoni, B. Sergi, A. Ferraresi, G. Paludetti, and D. Troiani, "Protective effects of α-tocopherol and tiopronin against cisplatin-induced ototoxicity," *Acta Oto-Laryngologica*, vol. 124, no. 4, pp. 421–426, 2004.

[16] R. Janssen, "Glutamate neurotoxicity in the developing rat cochlea is antagonized by kynurenic acid and MK-801," *Brain Research*, vol. 590, no. 1-2, pp. 201–206, 1992.

[17] H. Yoshida, H. Yanai, Y. Namiki, K. Fukatsu-Sasaki, N. Furutani, and N. Tada, "Neuroprotective effects of edaravone: a novel free radical scavenger in cerebrovascular injury," *CNS Drug Reviews*, vol. 12, no. 1, pp. 9–20, 2006.

[18] H. Shichinohe, S. Kuroda, H. Yasuda et al., "Neuroprotective effects of the free radical scavenger Edaravone (MCI-186) in mice permanent focal brain ischemia," *Brain Research*, vol. 1029, no. 2, pp. 200–206, 2004.

[19] M. Matsuyama, T. Hayama, K. Funao et al., "Treatment with edaravone improves the survival rate in renal warm ischemia-reperfusion injury using rat model," *Transplantation Proceedings*, vol. 38, no. 7, pp. 2199–2200, 2006.

[20] M. Taniguchi, M. Uchinami, K. Doi et al., "Edaravone reduces ischemia-reperfusion injury mediators in rat liver," *Journal of Surgical Research*, vol. 137, no. 1, pp. 69–74, 2007.

[21] Y. Inokuchi, S. Imai, Y. Nakajima et al., "Edaravone, a free radical scavenger, protects against retinal damage in vitro and in vivo," *Journal of Pharmacology and Experimental Therapeutics*, vol. 329, no. 2, pp. 687–698, 2009.

[22] O. Horiike, H. Shimogori, T. Ikeda, and H. Yamashita, "Protective effect of edaravone against streptomycin-induced vestibulotoxicity in the guinea pig," *European Journal of Pharmacology*, vol. 464, no. 1, pp. 75–78, 2003.

[23] T. Takemoto, K. Sugahara, T. Okuda, H. Shimogori, and H. Yamashita, "The clinical free radical scavenger, edaravone, protects cochlear hair cells from acoustic trauma," *European Journal of Pharmacology*, vol. 487, no. 1–3, pp. 113–116, 2004.

[24] Y. Song, M. Li, J.-C. Li, and E.-Q. Wei, "Edaravone protects PC12 cells from ischemic-like injury via attenuating the damage to mitochondria," *Journal of Zhejiang University SCIENCE B*, vol. 7, no. 9, pp. 749–756, 2006.

[25] S. Amemiya, T. Kamiya, C. Nito et al., "Anti-apoptotic and neuroprotective effects of edaravone following transient focal ischemia in rats," *European Journal of Pharmacology*, vol. 516, no. 2, pp. 125–130, 2005.

[26] Z. Chen, M. Ulfendahl, R. Ruan, L. Tan, and M. Duan, "Acute treatment of noise trauma with local caroverine application in the guinea pig," *Acta Oto-Laryngologica*, vol. 123, no. 8, pp. 905–909, 2003.

Hindawi Publishing Corporation
Neural Plasticity
Volume 2016, Article ID 8580675, 9 pages
http://dx.doi.org/10.1155/2016/8580675

Research Article

Plasma Membrane Targeting of Protocadherin 15 Is Regulated by the Golgi-Associated Chaperone Protein PIST

Hongyun Nie,[1] Yueyue Liu,[1] Xiaolei Yin,[2] Huiren Cao,[1] Yanfei Wang,[1] Wei Xiong,[3] Yushuang Lin,[1] and Zhigang Xu[1]

[1]*Shandong Provincial Key Laboratory of Animal Cells and Developmental Biology, Shandong University School of Life Sciences, Jinan, Shandong 250100, China*
[2]*Taishan Medical University, Tai'an, Shandong 271000, China*
[3]*School of Life Sciences, Tsinghua University, Beijing 100084, China*

Correspondence should be addressed to Yushuang Lin; linyushuang@sdu.edu.cn and Zhigang Xu; xuzg@sdu.edu.cn

Received 18 July 2016; Accepted 26 September 2016

Academic Editor: Renjie Chai

Protocadherin 15 (PCDH15) is a core component of hair cell tip-links and crucial for proper function of inner ear hair cells. Mutations of *PCDH15* gene cause syndromic and nonsyndromic hearing loss. At present, the regulatory mechanisms responsible for the intracellular transportation of PCDH15 largely remain unknown. Here we show that PIST, a Golgi-associated, PDZ domain-containing protein, interacts with PCDH15. The interaction is mediated by the PDZ domain of PIST and the C-terminal PDZ domain-binding interface (PBI) of PCDH15. Through this interaction, PIST retains PCDH15 in the trans-Golgi network (TGN) and reduces the membrane expression of PCDH15. We have previously showed that PIST regulates the membrane expression of another tip-link component, cadherin 23 (CDH23). Taken together, our finding suggests that PIST regulates the intracellular trafficking and membrane targeting of the tip-link proteins CDH23 and PCDH15.

1. Introduction

Inner ear hair cells are responsible for mechanoelectrical transduction (MET) that converts mechanical stimuli into electrical signals. MET occurs within stereocilia, the F-actin-based, and microvilli-like protrusions on the apical surface of hair cells [1]. Stereocilia are organized into several rows of increasing heights, forming a staircase-like structure. Several types of extracellular links, including tip-links, top-connectors, lateral-links, ankle-links, and kinociliary-links, connect stereocilia with each other and with the microtubule-based kinocilium [2]. Among these extracellular links, tip-links are of great importance. Tip-links connect the tip of each stereocilium to the side of its taller neighboring stereocilium and are directly involved in the MET process [3]. The yet unidentified MET channels localize at the lower end of tip-links and form the so-called MET machinery together with the lower end of tip-links as well as other proteins [4]. When stereocilia are deflected in the excitatory direction, the tension of tip-links increases and the open probability of MET channels also increases, resulting in the influx of cations into hair cells [1].

Protocadherin 15 (PCDH15) is an atypical cadherin that contains eleven extracellular cadherin (EC) repeats, whereas classical cadherins usually have only five EC repeats. Genetic, biochemical, immunochemical, and structural evidence indicated that PCDH15 and cadherin 23 (CDH23), another atypical cadherin, form the lower and higher part of tip-links, respectively [5–7]. PCDH15 and CDH23 interact with each other via the most N-terminal two EC repeats and create a ~ 170 nm long extracellular link under endolymph-like calcium levels [7–9]. Mutations of *PCDH15* gene are responsible for syndromic hearing loss Usher 1F or nonsyndromic hearing loss DFNB23 [10–12]. *Pcdh15* mutations are also responsible for the hearing and balancing deficits of Ames waltzer (av) mice [13, 14]. In av mice, stereociliary tip-links are reduced or

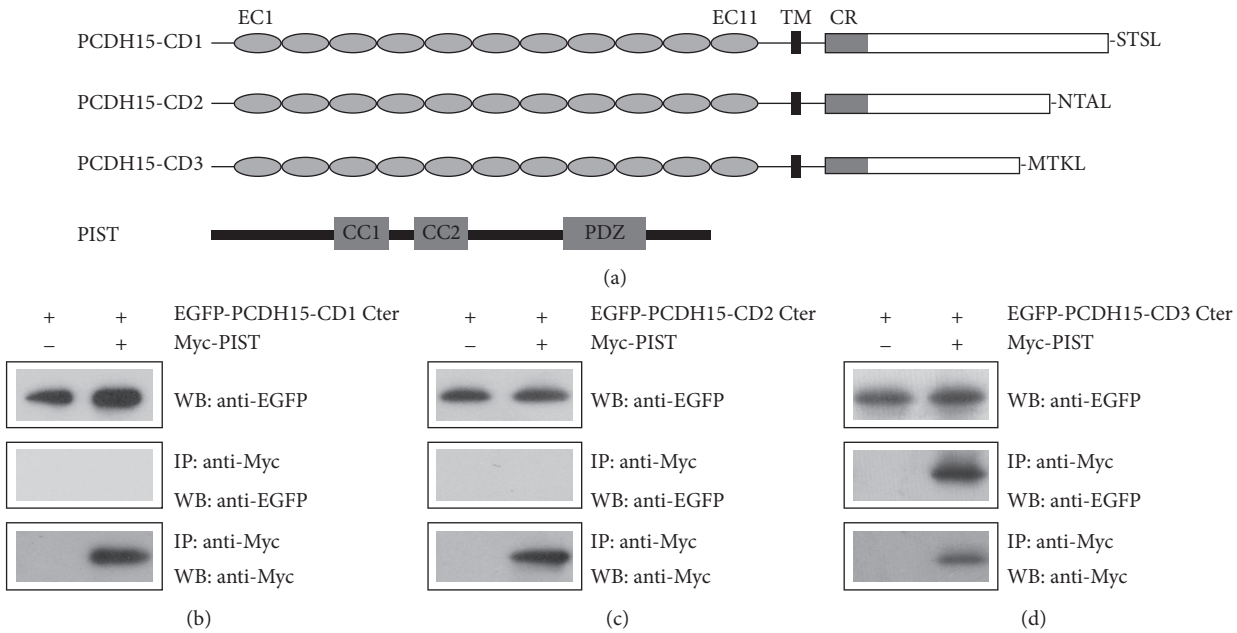

Figure 1: PCDH15-CD3 interacts with PIST. (a) Schematic diagram of PCDH15 and PIST domain structure. EC, extracellular cadherin repeats; TM, transmembrane domain; CR, common region; CC1, coiled-coil domain 1; CC2, coiled-coil domain 2; PDZ, PSD-95/discs large/ZO-1 domain. The C-terminal PBI of PCDH15 isoforms (STSL, NTAL, and MTKL) is also indicated. (b) Western blots showing coimmunoprecipitation (co-IP) of EGFP-tagged mouse PCDH15-CD1 cytoplasmic domain with Myc-tagged human PIST. (c) Western blots showing co-IP of EGFP-tagged mouse PCDH15-CD2 cytoplasmic domain with Myc-tagged human PIST. (d) Western blots showing co-IP of EGFP-tagged mouse PCDH15-CD3 cytoplasmic domain with Myc-tagged human PIST. IP indicates antibody used for immunoprecipitation and WB indicates antibody used for detection.

even absent, depending on the nature of the mutations, and hair cells are degenerated eventually, resulting in deafness and vestibular dysfunction [15].

Three prominent PCDH15 isoforms are generated by alternative pre-mRNA splicing, which are PCDH15-CD1, PCDH15-CD2, and PCDH15-CD3 [6]. These PCDH15 isoforms differ in their cytoplasmic domains (Figure 1(a)) and show different spatiotemporal expression pattern in the developing and mature inner ear [6]. Noticeably, different PCDH15 isoforms contain different PDZ binding interfaces (PBI) at their C-termini, which consist of the last four amino acids and are responsible for binding to PDZ domains. Different PCDH15 isoforms function redundantly during hair cell development, whereas PCDH15-CD2 was shown to be essential for tip-links in mature auditory hair cells [16, 17]. All PCDH15 isoforms could interact with TMHS (also called LHFPL5), an integral component of MET machinery of cochlear hair cells [18]. PCDH15-CD2, but not PCDH15-CD1 or PCDH15-CD3, also binds TMIE, another MET machinery component [19]. Furthermore, all PCDH15 isoforms directly interact with TMC1 and TMC2, the candidate MET channels, and core component of MET machinery [20, 21]. These data suggest that PCDH15 is an important component of the MET machinery.

Several other PCDH15-binding proteins have also been identified so far. PCDH15-CD1 was shown to interact with PDZ domain-containing protein harmonin via its C-terminal PBI [22, 23]. Further investigation showed that the stereociliary localization of PCDH15 is affected in *harmonin* knockout mice [24]. PCDH15-CD1 also interacts with Myosin VIIA, and the stereociliary localization of PCDH15 is perturbed in *myosin VIIA* mutant mice [25]. Recently, PCDH15-CD2 was shown to interact with Myosin 3A, which might regulate the transportation of PCDH15 to stereociliary tips [26]. In the present work, we show that PCDH15-CD3, but not PCDH15-CD1 or PCDH15-CD2, interacts with PDZ domain-containing protein PIST, which might play an important role in the intracellular trafficking and plasma membrane targeting of PCDH15-CD3.

2. Materials and Methods

2.1. DNA Constructs and Antibodies. Chicken *Pcdh15-CD3* cDNA was inserted into pBD-GAL4 Cam vector (Stratagene) to express the C-terminal 106 amino acids of chicken PCDH15-CD3 as bait protein. Mouse *Pcdh15* cDNAs were inserted into pcDNA3.1(+) to express full length PCDH15 isoforms with a Myc tag between the N-terminal signal peptide and the first EC repeat. Mouse *Pcdh15* cDNAs were inserted into pEGFP-C2 or modified pEGFP-C2 (EGFP replaced with Myc) to express EGFP-tagged or Myc-tagged PCDH15 cytoplasmic domains. The cDNA encoding mouse PCDH15-CD3 missing the last 4 aa (MTKL) at the C-terminus was inserted into the same vectors to express Myc-PCDH15-CD3 (-MTKL) and Myc-PCDH15-CD3 Cter (-MTKL). Human *PIST* cDNA was inserted into pEGFP-C2

or modified pEGFP-C2 to express full length PIST, PIST CC2-plus domain (146-274aa), and PIST PDZ domain (276-366aa) as EGFP-fusion or Myc-fusion proteins. Mouse monoclonal anti-EGFP antibody (Cat. number M20004) was from Abmart. Mouse monoclonal anti-Myc antibody (Cat. number M4439) was from Sigma-Aldrich.

2.2. Yeast Two-Hybrid Screen. The yeast two-hybrid screen was performed as previously described [27, 28]. Briefly, yeast strain AH109 (Clontech) was sequentially transformed with the bait plasmid and a chicken cochlear cDNA library in the HybriZAP two-hybrid vector [29]. Totally 2.4×10^6 transformants were selectively screened using *HIS3* (at the presence of 2.5 mM of 3-amino-1,2,4-triazole) as the primary reporter gene. The positive colonies were further examined using two more reporter genes *ADE2* and *lacZ*. The prey vectors in triple-positive yeast colonies were recovered and the sequence of cDNA inserts was determined by Sanger sequencing.

2.3. Coimmunoprecipitation (Co-IP). HEK293T cells were transfected with the expression vectors using jetPRIME Transfection Agent (Polyplus, Cat. number PT-114-15) according to the manufacturer's instructions. Transfected cells were washed with phosphate-buffered saline (PBS) 24 hours after transfection and lysed in ice-cold lysis buffer consisting of 150 mM NaCl, 50 mM Tris at pH 7.5, 1% (vol/vol) Triton X-100, 1 mM PMSF, and 1 × protease inhibitor cocktail (Roche). After centrifugation at 4°C, the supernatant was collected and incubated with immobilized anti-Myc antibody (Sigma-Aldrich, Cat. number E6654) at 4°C overnight. After washing five times with washing buffer (a modified lysis buffer containing 500 mM NaCl instead of 150 mM), the immunoprecipitated proteins were separated by polyacrylamide gel electrophoresis (PAGE) and then transferred to PVDF membrane. The blot was incubated with corresponding primary antibodies, followed by incubation with secondary antibodies (Bio-Rad), and the signals were detected with the ECL system (Cell Signaling Technology).

2.4. Immunofluorescence. COS-7 cells were grown on Gelatin-coated glass cover slips and transfected with the expression vectors. Transfected cells were fixed with 4% paraformaldehyde (PFA) in PBS for 15 minutes and then permeabilized and blocked with PBT1 (0.1% Triton X-100, 1% BSA, 5% heat-inactivated goat serum in PBS, pH 7.3) for 30 minutes, followed by incubation with primary antibody diluted in PBT1 over night at 4°C. After washing twice with PBT1 for 10 minutes and twice with PBT2 (0.1% Triton X-100, 0.1% BSA in PBS) for 5 minutes, cells were incubated with fluorescence-conjugated secondary antibody (Life Tech) in PBT2 for 1 hour, followed by two 5-minute PBT2 washes and two 5-minute PBS washes. For nuclei staining, cells were incubated with DAPI (Gen-View Scientific Inc.) for 15 minutes, followed by four 5-minute PBS washes and then mounted in Glycerol/PBS (1 : 1). The cells were imaged with a confocal microscope (LSM 700, Zeiss).

3. Results

To identify proteins that interact with PCDH15, we performed yeast two-hybrid screens of a chicken cochlear cDNA library using PCDH15 as bait. *HIS3* gene was used as the primary reporter gene for the screen in the presence of 3-amino-1,2,4-triazole (3-AT) that inhibits the autoactivation of *HIS3* reporter gene. When the intact cytoplasmic domain of chicken PCDH15-CD3 was used as bait, it autoactivated the *HIS3* reporter gene at the highest 3-AT concentration (15 mM) tested. Then various regions within the PCDH15-CD3 cytoplasmic domain were tested for autoactivation. The results showed that the fragment containing the C-terminal 106 amino acids does not activate *HIS3* reporter gene at the presence of 2.5 mM 3-AT, and this fragment was used in the following yeast two-hybrid screen. Among the positive clones that activate all the three reporter genes (*HIS3*, *ADE2*, and l*acZ*), several clones encode the PDZ-containing, Golgi-associated chaperone protein PIST. PIST has been shown to play important roles in regulating the membrane targeting of several transmembrane proteins such as frizzled, somatostatin receptor subtype 5 (SSTR5) and β1-adrenergic receptor (β1AR) [30–32].

We then performed coimmunoprecipitation (co-IP) experiments to verify the interaction between PCDH15 and PIST. From here on in the rest of our investigation, we focused on mammalian proteins. Our data showed that when overexpressed in HEK293T cells, EGFP-tagged cytoplasmic domain of mouse PCDH15-CD3 was co-IPed with Myc-tagged human PIST, whereas PCDH15-CD1 and PCDH15-CD2 were not (Figures 1(b)–1(d)). This result suggests that PCDH15-CD3, but not PCDH15-CD1 or PCDH15-CD2, interacts with PIST.

Previously we have shown that PIST binds to cadherin 23 (CDH23), the upper tip-link component, and retains CDH23 in the trans-Golgi network (TGN) in cultured cells [33]. To test whether this also applies to PCDH15, we analyzed the subcellular distribution of PCDH15 and PIST in cultured cells by immunofluorescence and confocal microscopy. The results showed that when coexpressed in COS-7 cells, EGFP-PIST mainly localizes in the TGN, whereas Myc-PCDH15-CD1 or Myc-PCDH15-CD2 localizes in the cytoplasm as well as on the plasma membrane, consistent with the fact that PCDH15-CD1 or PCDH15-CD2 does not interact with PIST (Figures 2(a) and 2(b)). In contrast, when cotransfected with EGFP-PIST and Myc-PCDH15-CD3, most (70.24%) cells show colocalization of PCDH15-CD3 with PIST in the TGN (Figure 2(c)).

We then performed co-IP experiments to explore which regions/motifs in PCDH15-CD3 and PIST are responsible for the interaction between them. PIST contains a PDZ domain near the C-terminus and two coiled-coil (CC) domains in the middle part (Figure 3(a)). Co-IP experiments with EGFP-tagged PIST PDZ domain (276-366aa) or the second CC domain (CC2) plus the amino acids between CC2 and PDZ domain (CC2-plus, 146-274aa) revealed that both domains could be co-IPed with Myc-PCDH15-CD3 cytoplasmic domain (Figures 3(b) and 3(c)). PCDH15-CD1, PCDH15-CD2, and PCDH15-CD3 have unique C-termini

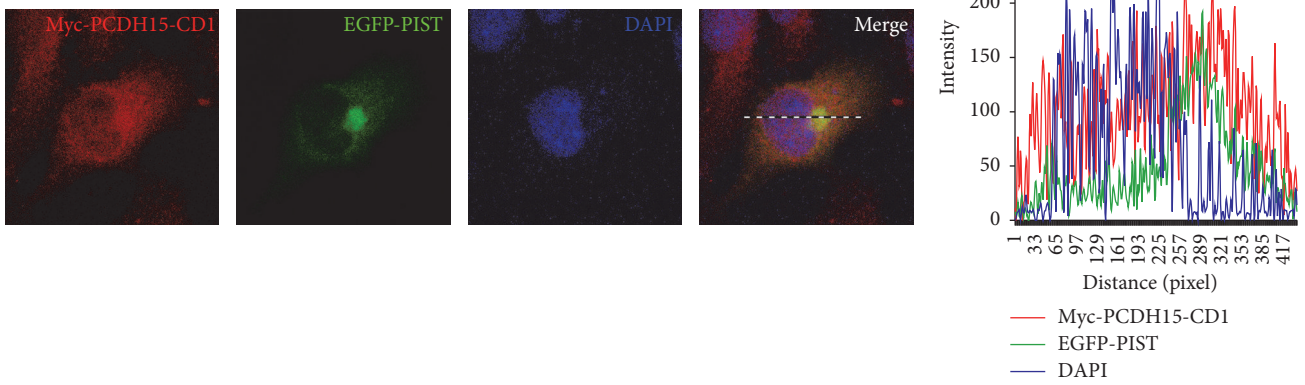

(a)

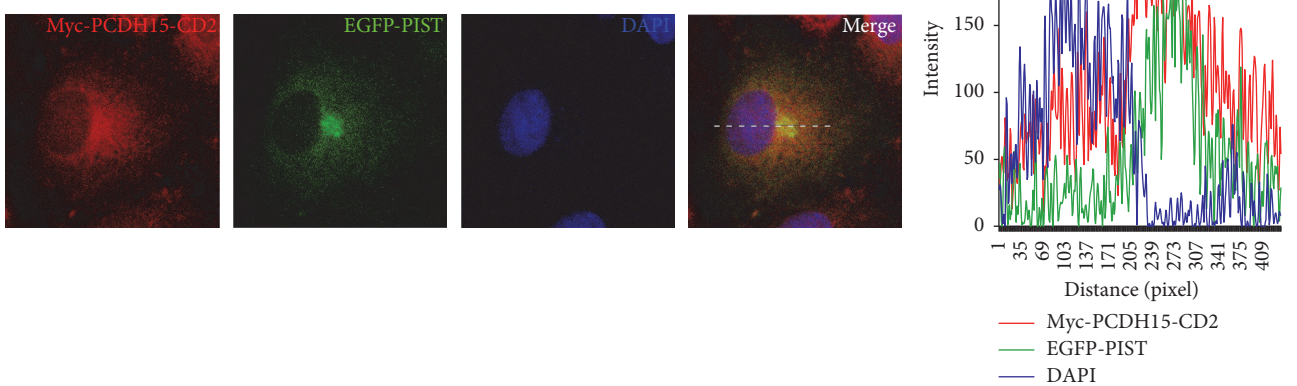

(b)

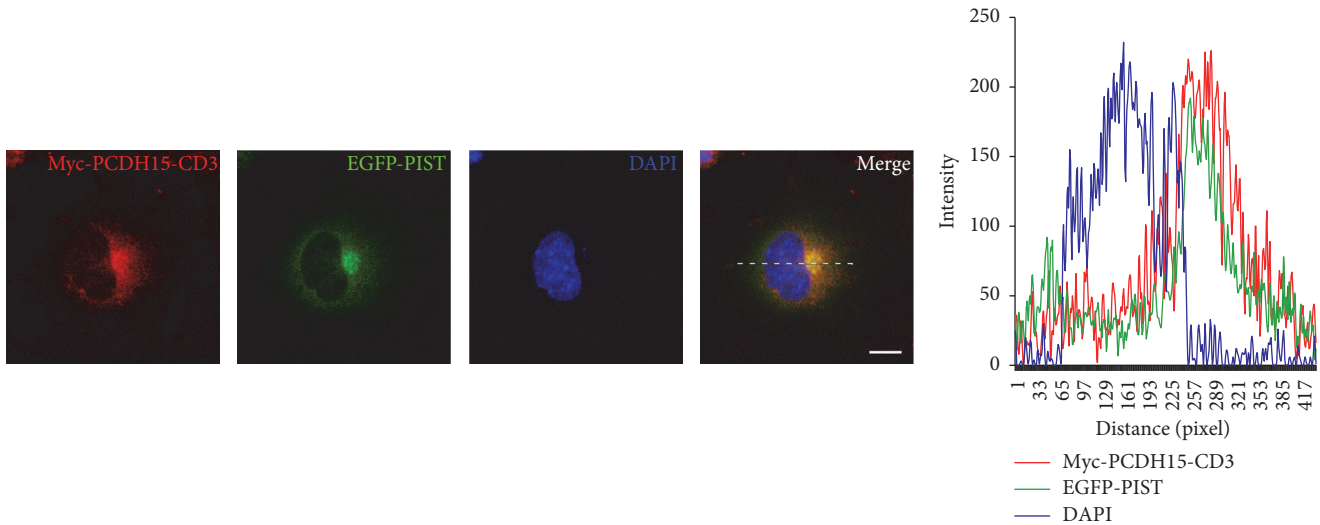

(c)

Figure 2: Colocalization of PCDH15-CD3 with PIST in COS-7 cells. (a) In the presence of EGFP-PIST, Myc-PCDH15-CD1 localizes in the cytoplasm as well as on the cell membrane. (b) In the presence of EGFP-PIST, Myc-PCDH15-CD2 localizes in the cytoplasm as well as on the cell membrane. (c) In the presence of EGFP-PIST, Myc-PCDH15-CD3 colocalizes with EGFP-PIST in the TGN. Myc-PCDH15 was stained with mouse anti-Myc antibody and then TRITC-conjugated goat anti-mouse secondary antibody. Nuclei were stained with DAPI. The fluorescent intensity was quantified using Image J. Scale bars, 10 μm.

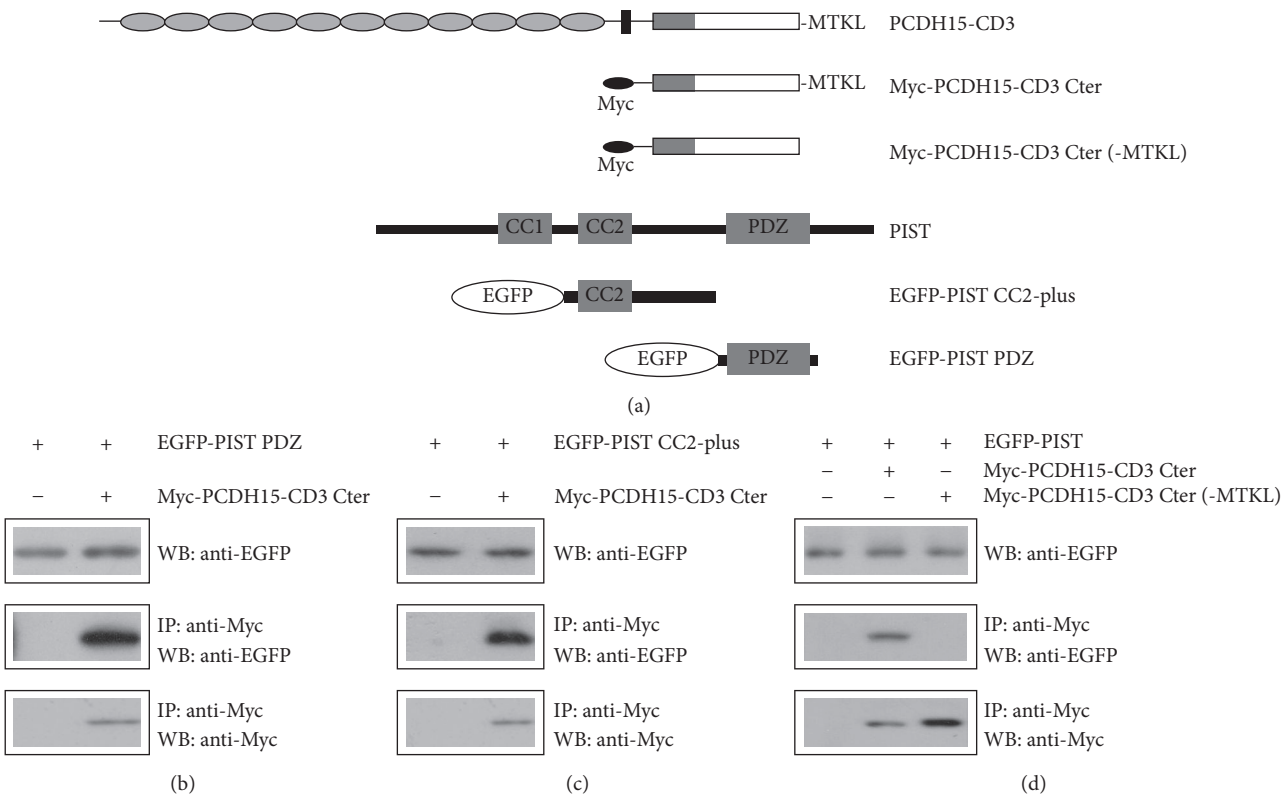

Figure 3: The C-terminal PBI of PCDH15-CD3 is necessary for the interaction with PIST. (a) Schematic diagram of PCDH15 and PIST domains used in this experiment. (b) Western blots showing coimmunoprecipitation (co-IP) of EGFP-tagged human PIST PDZ domain with Myc-tagged mouse PCDH15-CD3 cytoplasmic domain. (c) Western blots showing co-IP of EGFP-tagged human PIST CC2-plus region with Myc-tagged mouse PCDH15-CD3 cytoplasmic domain. (d) Western blots showing co-IP of EGFP-tagged human PIST with Myc-tagged mouse PCDH15-CD3 cytoplasmic domain with or without the C-terminal PBI (MTKL). IP indicates antibody used for immunoprecipitation and WB indicates antibody used for detection.

(STSL, NTAL, and MTKL, resp.), which belong to type I PBI [34]. We found that when the C-terminal MTKL of PCDH15-CD3 was removed, EGFP-PIST could not be co-IPed with Myc-tagged PCDH15-CD3 cytoplasmic domain anymore (Figure 3(d)). In line with this, Myc-tagged PCDH15-CD3 lacking the C-terminal MTKL is not retained in the TGN by EGFP-PIST anymore (Figures 4(a) and 4(b)). These data suggest that the principal interaction between PCDH15-CD3 and PIST utilizes the PDZ binding interface.

Finally, we examined whether the association with PIST affects the membrane targeting of PCDH15-CD3. When coexpressed with EGFP, Myc-PCDH15-CD3 mainly localizes in the cytoplasm and on the plasma membrane (Figure 5(a)). The plasma membrane localization of Myc-PCDH15-CD3 could be observed more clearly when the extracellular Myc epitope was labeled by anti-Myc antibody without cell permeabilization (Figure 5(a′)). In contrast, when EGFP-PIST is present, Myc-PCDH15-CD3 colocalizes with EGFP-PIST in the TGN, and the membrane labelling in nonpermeabilized cells disappeared completely (Figures 5(b) and 5(b′)). These data suggest that PIST retains PCDH15-CD3 in the TGN and reduces the membrane expression of PCDH15-CD3.

4. Discussion

PCDH15 and CDH23 form the lower and upper part of tip-links, respectively, and are indispensable for hearing transduction. Besides tip-links, PCDH15 and CDH23 also localize at kinociliary-links, transient lateral-links, and ribbon synapse of hair cells [6, 7, 35–37]. It has been suggested that the transportation of PCDH15 to apical (stereociliary bundle) and basal (ribbon synapses) poles depends on distinct trafficking mechanisms. Apically transported PCDH15 was shown to associate with the Arf1-positive early endosomal vesicles and colocalize with the early endosomal marker Rab5, whereas basally transported PCDH15 was shown to associate with AP-1-positive post-trans-Golgi vesicles [38]. The detailed mechanism of PCDH15 transportation remains elusive.

In the present work we show that PIST might play an important role in regulating the intracellular traffic and membrane targeting of PCDH15. Previously we have shown that PIST regulates the membrane expression of CDH23 [33]. Taken together, our work suggests that PIST regulates the intracellular transportation of both tip-link components,

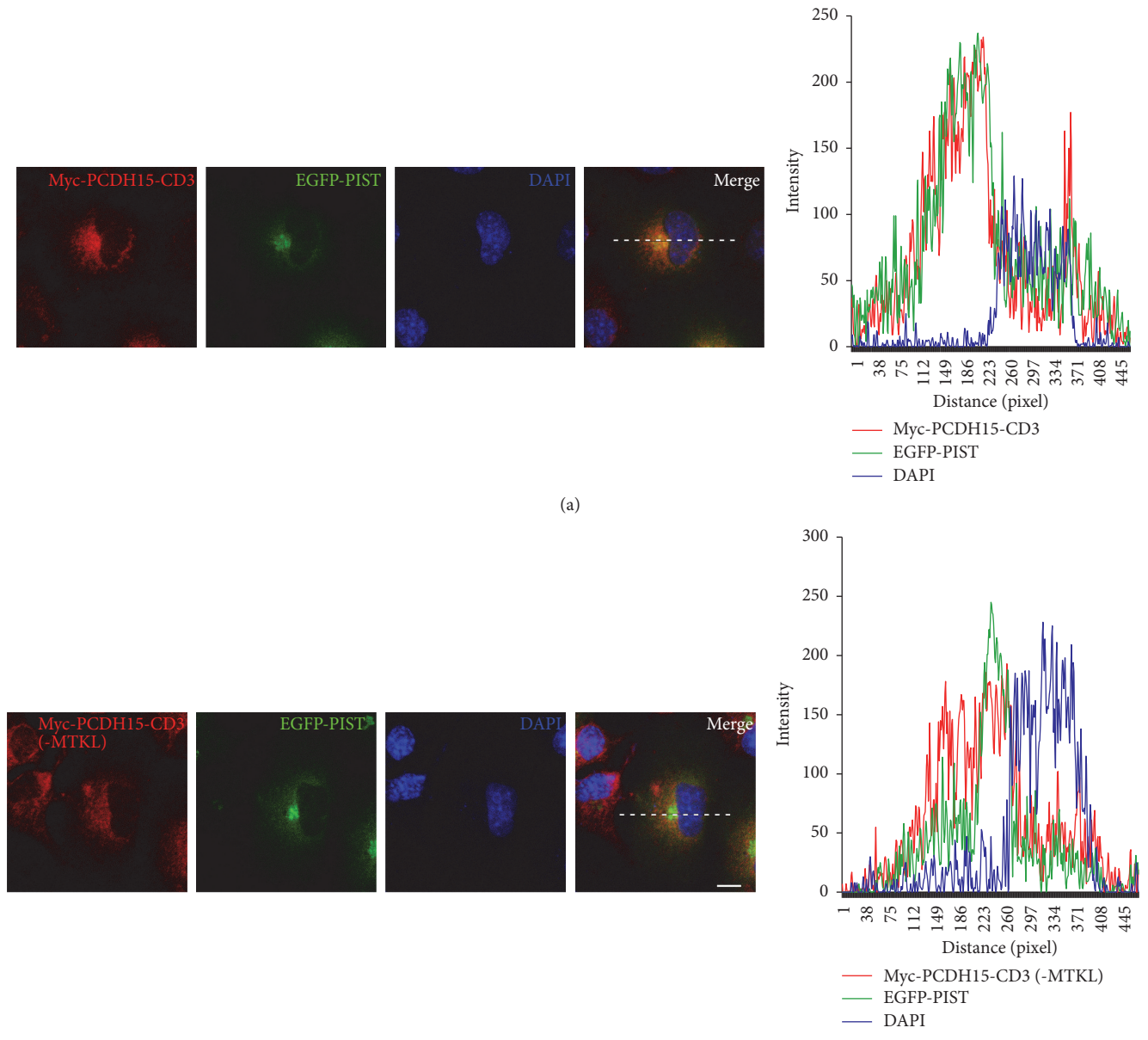

Figure 4: The C-terminal PBI of PCDH15-CD3 is necessary for its retention in the TGN of COS-7 cells by PIST. (a) In the presence of EGFP-PIST, Myc-PCDH15-CD3 colocalizes with EGFP-PIST in the TGN. (b) In the presence of EGFP-PIST, Myc-PCDH15-CD3 lacking the C-terminal PBI (MTKL) localizes in the cytoplasm as well as on the cell membrane. Myc-PCDH15 was stained with mouse anti-Myc antibody and then TRITC-conjugated goat anti-mouse secondary antibody. Nuclei were stained with DAPI. The fluorescent intensity was quantified using Image J. Scale bars, 10 μm.

PCDH15 and CDH23. PIST is a PDZ-containing, Golgi-associated chaperone protein, also named as FIG, GOPC, or CAL. PIST plays important roles in regulating the membrane targeting of transmembrane proteins [30–32]. Notably, PIST was shown to colocalize with the early endosome marker Rab5 and the TGN/endosome marker Rab14 [39]. Our data reveal that PCDH15-CD3 and CDH23 bind PIST via their C-terminal PBI and colocalize with PIST in the TGN, which might regulate the transportation of PCDH15 and CDH23 to the apical surface of hair cells.

Interestingly, we found that, besides the PDZ domain, the CC2 domain and its downstream amino acids (CC2-plus) of PIST also interact with PCDH15-CD3. This was also observed in the interaction between PIST and CDH23 [33]. Nevertheless, it seems that PDZ/PBI mediate the principal interaction between PIST and PCDH15-CD3 or CDH23 because deletion of the C-terminal PBI abolishes the interaction completely. PCDH15-CD1, PCDH15-CD2, and PCDH15-CD3 all contain a type I PBI, but only PCDH15-CD3 binds PIST and colocalizes with PIST in the TGN.

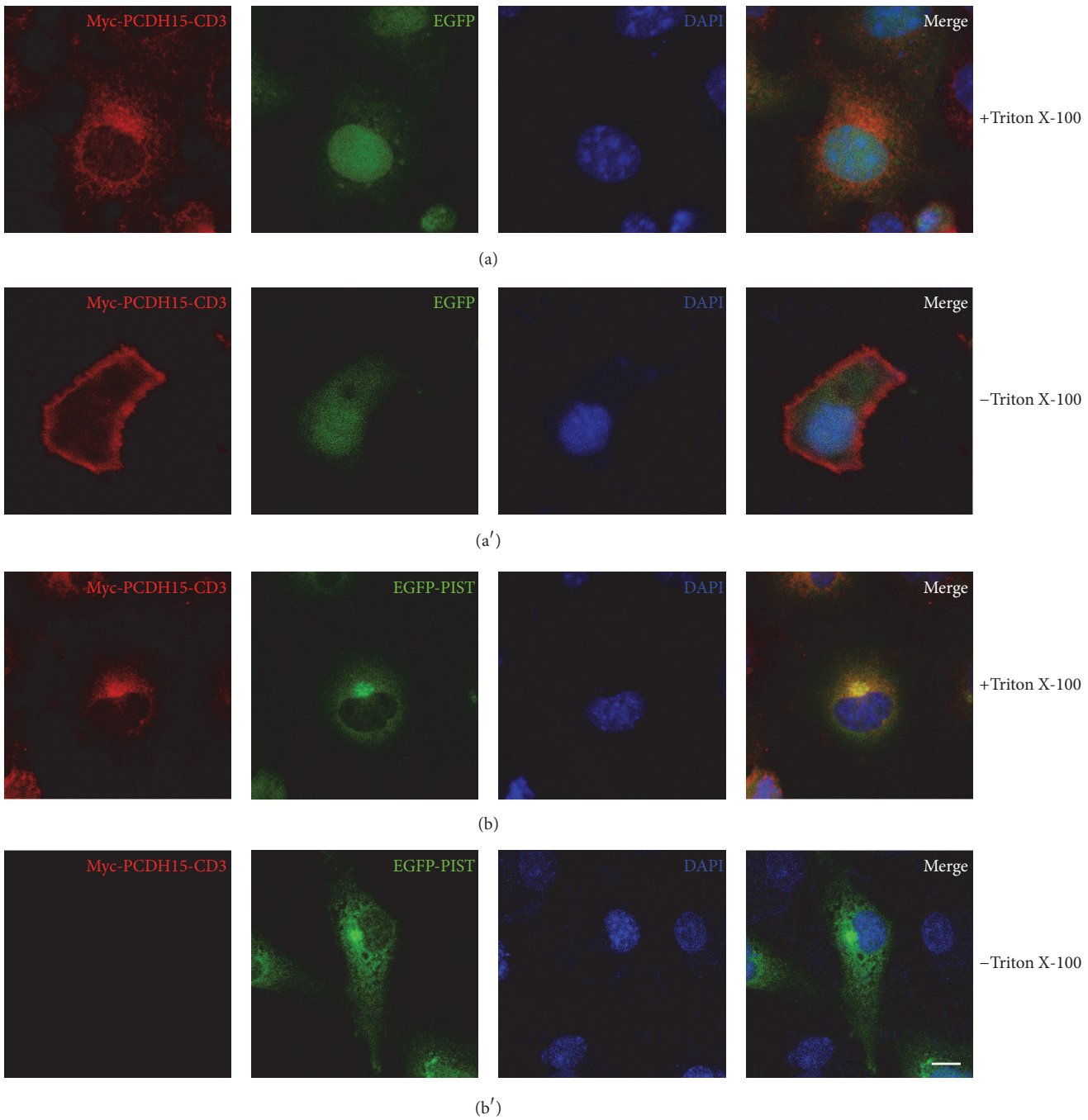

Figure 5: PIST reduces the membrane expression of PCDH15-CD3 in COS-7 cells. (a) Myc-PCDH15-CD3 immunoreactivity shows cytoplasmic and plasma membrane localization when coexpressed with EGFP. (a′) Myc-PCDH15-CD3 immunoreactivity using a nonpermeable protocol shows clear plasma membrane localization when coexpressed with EGFP. (b) Myc-PCDH15-CD3 immunoreactivity colocalizes with EGFP-PIST in the TGN. (b′) The plasma membrane localization of Myc-PCDH15-CD3 immunoreactivity examined using a nonpermeable protocol disappears when EGFP-PIST is present. For the nonpermeable protocol, staining was performed as normal except that Triton X-100 was excluded. Myc-PCDH15 was stained with mouse anti-Myc antibody and then TRITC-conjugated goat anti-mouse secondary antibody. Nuclei were stained with DAPI. Scale bar, 10 μm.

Previously, PCDH15-CD1 has been shown to interact with PDZ domain-containing protein harmonin [22, 23]. The different C-terminal PBI of the three PCDH15 isoforms might mediate interaction with different PDZ domain-containing proteins and render the PCDH15 isoforms different function or regulation.

Competing Interests

The authors declare that there is no conflict of interests regarding the publication of this paper.

Acknowledgments

The authors thank Dr. W. B. Guggino (Johns Hopkins Medical Institute, Baltimore, MD) for providing the PIST cDNA. This work is supported by grants from the National Basic Research Program of China (2013CB967700 to Zhigang Xu), the National Natural Science Foundation of China (31371355 to Zhigang Xu and 31401007 to Yanfei Wang), the China Postdoctoral Science Foundation (2014M560550 to Yanfei Wang), Shandong Provincial Natural Science Foundation (ZR2011CQ034 to Huiren Cao), and the Fundamental Research Funds of Shandong University (2014HW011 to Yanfei Wang).

References

[1] P. G. Gillespie and U. Müller, "Mechanotransduction by hair cells: models, molecules, and mechanisms," *Cell*, vol. 139, no. 1, pp. 33–44, 2009.

[2] R. J. Goodyear, W. Marcotti, C. J. Kros, and G. P. Richardson, "Development and properties of stereociliary link types in hair cells of the mouse cochlea," *Journal of Comparative Neurology*, vol. 485, no. 1, pp. 75–85, 2005.

[3] J. A. Assad, G. M. Shepherd, and D. P. Corey, "Tip-link integrity and mechanical transduction in vertebrate hair cells," *Neuron*, vol. 7, no. 6, pp. 985–994, 1991.

[4] M. Beurg, R. Fettiplace, J.-H. Nam, and A. J. Ricci, "Localization of inner hair cell mechanotransducer channels using high-speed calcium imaging," *Nature Neuroscience*, vol. 12, no. 5, pp. 553–558, 2009.

[5] J. Siemens, C. Lillo, R. A. Dumont et al., "Cadherin 23 is a component of the tip link in hair-cell stereocilla," *Nature*, vol. 428, no. 6986, pp. 950–955, 2004.

[6] Z. M. Ahmed, R. Goodyear, S. Riazuddin et al., "The tip-link antigen, a protein associated with the transduction complex of sensory hair cells, is protocadherin-15," *The Journal of Neuroscience*, vol. 26, no. 26, pp. 7022–7034, 2006.

[7] P. Kazmierczak, H. Sakaguchi, J. Tokita et al., "Cadherin 23 and protocadherin 15 interact to form tip-link filaments in sensory hair cells," *Nature*, vol. 449, no. 7158, pp. 87–91, 2007.

[8] D. N. Furness, Y. Katori, B. Nirmal Kumar, and C. M. Hackney, "The dimensions and structural attachments of tip links in mammalian cochlear hair cells and the effects of exposure to different levels of extracellular calcium," *Neuroscience*, vol. 154, no. 1, pp. 10–21, 2008.

[9] M. Sotomayor, W. A. Weihofen, R. Gaudet, and D. P. Corey, "Structure of a force-conveying cadherin bond essential for inner-ear mechanotransduction," *Nature*, vol. 492, no. 7427, pp. 128–132, 2012.

[10] Z. M. Ahmed, S. Riazuddin, S. L. Bernstein et al., "Mutations of the protocadherin gene PCDH15 cause usher syndrome type 1F," *The American Journal of Human Genetics*, vol. 69, no. 1, pp. 25–34, 2001.

[11] K. N. Alagramam, H. Yuan, M. H. Kuehn et al., "Mutations in the novel protocadherin PCDH15 cause Usher syndrome type 1F," *Human Molecular Genetics*, vol. 10, no. 16, pp. 1709–1718, 2001.

[12] Z. M. Ahmed, S. Riazuddin, J. Ahmad et al., "PCDH15 is expressed in the neurosensory epithelium of the eye and ear and mutant alleles are responsible for both USH1F and DFNB23," *Human Molecular Genetics*, vol. 12, no. 24, pp. 3215–3223, 2003.

[13] K. N. Alagramam, C. L. Murcia, H. Y. Kwon, K. S. Pawlowski, C. G. Wright, and R. P. Woychik, "The mouse Ames waltzer hearing-loss mutant is caused by mutation of Pcdh15, a novel protocadherin gene," *Nature Genetics*, vol. 27, no. 1, pp. 99–102, 2001.

[14] Q. Y. Zheng, H. Yu, J. L. Washington III et al., "A new spontaneous mutation in the mouse protocadherin 15 gene," *Hearing Research*, vol. 219, no. 1-2, pp. 110–120, 2006.

[15] K. N. Alagramam, R. J. Goodyear, R. Geng et al., "Mutations in protocadherin 15 and cadherin 23 affect tip links and mechanotransduction in mammalian sensory hair cells," *PLoS ONE*, vol. 6, no. 4, Article ID e19183, 2011.

[16] S. W. Webb, N. Grillet, L. R. Andrade et al., "Regulation of PCDH15 function in mechanosensory hair cells by alternative splicing of the cytoplasmic domain," *Development*, vol. 138, no. 8, pp. 1607–1617, 2011.

[17] E. Pepermans, V. Michel, R. Goodyear et al., "The CD2 isoform of protocadherin-15 is an essential component of the tip-link complex in mature auditory hair cells," *EMBO Molecular Medicine*, vol. 6, no. 7, pp. 984–992, 2014.

[18] W. Xiong, N. Grillet, H. M. Elledge et al., "TMHS is an integral component of the mechanotransduction machinery of cochlear hair cells," *Cell*, vol. 151, no. 6, pp. 1283–1295, 2012.

[19] B. Zhao, Z. Wu, N. Grillet et al., "TMIE is an essential component of the mechanotransduction machinery of cochlear hair cells," *Neuron*, vol. 84, no. 5, pp. 954–967, 2014.

[20] R. Maeda, K. S. Kindt, W. Mo et al., "Tip-link protein protocadherin 15 interacts with transmembrane channel-like proteins TMC1 and TMC2," *Proceedings of the National Academy of Sciences of the United States of America*, vol. 111, no. 35, pp. 12907–12912, 2014.

[21] M. Beurg, W. Xiong, B. Zhao, U. Müller, and R. Fettiplace, "Subunit determination of the conductance of hair-cell mechanotransducer channels," *Proceedings of the National Academy of Sciences of the United States of America*, vol. 112, no. 5, pp. 1589–1594, 2015.

[22] A. Adato, V. Michel, Y. Kikkawa et al., "Interactions in the network of Usher syndrome type 1 proteins," *Human Molecular Genetics*, vol. 14, no. 3, pp. 347–356, 2005.

[23] J. Reiners, T. Märker, K. Jürgens, B. Reidel, and U. Wolfrum, "Photoreceptor expression of the Usher syndrome type 1 protein protocadherin 15 (USH1F) and its interaction with the scaffold protein harmonin (USH1C)," *Molecular Vision*, vol. 11, pp. 347–355, 2005.

[24] D. Yan, K. Kamiya, X. M. Ouyang, and X. Z. Liu, "Analysis of subcellular localization of Myo7a, Pcdh15 and Sans in Ush1c knockout mice," *International Journal of Experimental Pathology*, vol. 92, no. 1, pp. 66–71, 2011.

[25] M. Senften, M. Schwander, P. Kazmierczak et al., "Physical and functional interaction between protocadherin 15 and myosin VIIa in mechanosensory hair cells," *The Journal of Neuroscience*, vol. 26, no. 7, pp. 2060–2071, 2006.

[26] M. Grati, D. Yan, M. H. Raval et al., "MYO3A causes human dominant deafness and interacts with protocadherin 15-CD2 isoform," *Human Mutation*, vol. 37, no. 5, pp. 481–487, 2016.

[27] Z. Xu, A. W. Peng, K. Oshima, and S. Heller, "MAGI-1, a candidate stereociliary scaffolding protein, associates with the tip-link component cadherin 23," *Journal of Neuroscience*, vol. 28, no. 44, pp. 11269–11276, 2008.

[28] H. Cao, X. Yin, Y. Cao et al., "FCHSD1 and FCHSD2 are expressed in hair cell stereocilia and cuticular plate and regulate actin polymerization in vitro," *PLoS ONE*, vol. 8, no. 2, Article ID e56516, 2013.

[29] S. Heller, C. A. Sheane, Z. Javed, and A. J. Hudspeth, "Molecular markers for cell types of the inner ear and candidate genes for hearing disorders," *Proceedings of the National Academy of Sciences of the United States of America*, vol. 95, no. 19, pp. 11400–11405, 1998.

[30] R. Yao, T. Maeda, S. Takada, and T. Noda, "Identification of a PDZ domain containing golgi protein, GOPC, as an interaction partner of frizzled," *Biochemical and Biophysical Research Communications*, vol. 286, no. 4, pp. 771–778, 2001.

[31] W. Wente, T. Stroh, A. Beaudet, D. Richter, and H.-J. Kreienkamp, "Interactions with PDZ domain proteins PIST/GOPC and PDZK1 regulate intracellular sorting of the somatostatin receptor subtype 5," *The Journal of Biological Chemistry*, vol. 280, no. 37, pp. 32419–32425, 2005.

[32] J. Koliwer, M. Park, C. Bauch, M. Von Zastrow, and H.-J. Kreienkamp, "The golgi-associated PDZ domain protein PIST/GOPC stabilizes the β1-Adrenergic receptor in intracellular compartments after internalization," *Journal of Biological Chemistry*, vol. 290, no. 10, pp. 6120–6129, 2015.

[33] Z. Xu, K. Oshima, and S. Heller, "PIST regulates the intracellular trafficking and plasma membrane expression of cadherin 23," *BMC Cell Biology*, vol. 11, article 80, 2010.

[34] M. Sheng and C. Sala, "PDZ domains and the organization of supramolecular complexes," *Annual Review of Neuroscience*, vol. 24, pp. 1–29, 2001.

[35] V. Michel, R. J. Goodyear, D. Weil et al., "Cadherin 23 is a component of the transient lateral links in the developing hair bundles of cochlear sensory cells," *Developmental Biology*, vol. 280, no. 2, pp. 281–294, 2005.

[36] A. Lagziel, Z. M. Ahmed, J. M. Schultz, R. J. Morell, I. A. Belyantseva, and T. B. Friedman, "Spatiotemporal pattern and isoforms of cadherin 23 in wild type and waltzer mice during inner ear hair cell development," *Developmental Biology*, vol. 280, no. 2, pp. 295–306, 2005.

[37] M. Zallocchi, D. T. Meehan, D. Delimont et al., "Role for a novel Usher protein complex in hair cell synaptic maturation," *PLoS ONE*, vol. 7, no. 2, Article ID e30573, 2012.

[38] M. Zallocchi, D. Delimont, D. T. Meehan, and D. Cosgrove, "Regulated vesicular trafficking of specific PCDH15 and VLGR1 variants in auditory hair cells," *Journal of Neuroscience*, vol. 32, no. 40, pp. 13841–13859, 2012.

[39] R. Lu, L. Stewart, and J. M. Wilson, "Scaffolding protein GOPC regulates tight junction structure," *Cell and Tissue Research*, vol. 360, no. 2, pp. 321–332, 2015.

Hindawi Publishing Corporation
Neural Plasticity
Volume 2016, Article ID 2814056, 6 pages
http://dx.doi.org/10.1155/2016/2814056

Research Article

Factor Analysis of Low-Frequency Repetitive Transcranial Magnetic Stimulation to the Temporoparietal Junction for Tinnitus

Hui Wang,[1] Bei Li,[1] Meiye Wang,[1] Ming Li,[2] Dongzhen Yu,[1] Haibo Shi,[1] and Shankai Yin[1]

[1]*Department of Otolaryngology Head and Neck Surgery, Shanghai Jiao Tong University Affiliated Sixth People's Hospital, Shanghai 200233, China*
[2]*Department of Otolaryngology, Tinnitus and Hyperacusis Center Yueyang Hospital of Integrated Traditional Chinese and Western Medicine Affiliated to Shanghai University of Traditional Chinese Medicine, Shanghai 200437, China*

Correspondence should be addressed to Dongzhen Yu; doctor.yu@126.com and Haibo Shi; haibo99@hotmail.com

Received 5 July 2016; Revised 16 September 2016; Accepted 3 October 2016

Academic Editor: Genglin Li

Objectives. We investigated factors that contribute to suppression of tinnitus after repetitive transcranial magnetic stimulation (rTMS). *Methods*. A total of 289 patients with tinnitus underwent active 1 Hz rTMS in the left temporoparietal region. A visual analog scale (VAS) was used to assess tinnitus loudness. All participants were interviewed regarding age, gender, tinnitus duration, laterality and pitch, audiometric parameters, sleep, and so forth. The resting motor thresholds (RMTs) were measured in all patients and 30 age- and gender-matched volunteers. *Results*. With respect to different factors that contribute to tinnitus suppression, we found improvement in the following domains: shorter duration, normal hearing (OR: 3.25, 95%CI: 2.01–5.27, $p = 0.001$), and without sleep disturbance (OR: 2.51, 95%CI: 1.56–4.1, $p = 0.005$) adjusted for age and gender. The patients with tinnitus lasting less than 1 year were more likely to show suppression of tinnitus (OR: 2.77, 95%CI: 1.48–5.19, $p = 0.002$) compared to those with tinnitus lasting more than 5 years. Tinnitus patients had significantly lower RMTs compared with healthy volunteers. *Conclusion*. Active low-frequency rTMS results in a significant reduction in the loudness of tinnitus. Significant tinnitus suppression was shown in subjects with shorter tinnitus duration, with normal hearing, and without sleep disturbance.

1. Introduction

Tinnitus is a subjective, mostly transitory, phantom auditory perception of sound that affects millions of people at some point in their lives [1]. It is estimated that tinnitus will become chronic and severely affect the quality of life in 1%–3% of the general population [2]. About 20% of adults that experience tinnitus will require clinical intervention [3]. Tinnitus can occur constantly or intermittently in one or both ears or centrally in the head and can be perceived as coming from within the head. There is convincing evidence from functional imaging and neurophysiological studies that central mechanisms are responsible for most cases of tinnitus [4–6], which may be caused by (1) changes in the firing pattern of neurons in the central auditory system, (2) changes in burst firing and neural synchrony, and (3) cortical tonotopic map reorganization [7]. All of the above may occur due to alterations in neuronal activity in the brain cortex, which suggests promising treatment strategies for tinnitus.

Based on the above findings, repetitive transcranial magnetic stimulation (rTMS) of the temporal and temporoparietal cortex has been proposed as a promising treatment for chronic tinnitus. Its mechanism of action involves targeting the hyperactivity/abnormal synchronization within the auditory cortex to suppress tinnitus [8–10]. rTMS temporarily disrupts a circumspect area of the cortex that interrupts normal functioning and has acute and chronic effects in tinnitus patients. Several clinical studies consistently showed a reduction of tinnitus severity after application of rTMS to the left temporoparietal region of the cortex [11–13]. However, the treatment results showed high interindividual variability [14, 15], indicating the need for optimization of the

indications. This variability also indicates that a large sample study is needed.

The present study was using active rTMS performed to investigate optimization of the indications by evaluating the different factors that contribute to tinnitus suppression after low-frequency rTMS for the treatment of chronic tinnitus.

2. Methods

2.1. Subjects. Patients suffering from nonpulsatile and constant tinnitus examined and treated at the Affiliated Sixth People's Hospital Otolaryngology Department, Shanghai Jiao Tong University, between December 2014 and December 2015, were included in this study. With local ethics committee approval, written informed consent was obtained from all subjects prior to enrollment, and the possible consequences of the study were explained. Our registration number is ChiCTR-INR-16008092. Upon recruitment, the subjective tinnitus loudness perception in patients was determined using a visual analog scale (VAS) ranging from 0 to 10, where 0 indicates no tinnitus and 10 indicates the worst possible tinnitus-related discomfort. VAS improvement in responders decreased to 20% of the basal score indicating no reduction, 40%, 60%, and 80% of the basal score indicating slight, marked, and strong reduction, and 100% reduction indicating complete suppression of tinnitus immediately after stimulation. The reduction range from 40% to 100% is considered as "good effect." Measurements were made before, immediately, and 2 weeks after the last intervention session.

Detailed histories were obtained from all patients, including a clinical examination and audiogram. Hearing level was assessed by using an audiometer in a soundproof room, and the loudness and pitch of tinnitus were evaluated with a TinniTest audiometer. Normal hearing was defined as normal audiogram (threshold < 25 dB HL at all frequencies from 0.25 to 8 kHz) as well as a normal tympanometric curve of type A. The ipsilateral and contralateral stapedial reflexes were also included. All participants were comprehensively interviewed for information regarding their age, gender, tinnitus duration, tinnitus laterality, pitch of tinnitus, sleep quality, accompanying symptoms, and so forth.

2.2. rTMS Procedure. All of the patients underwent rTMS over the left temporoparietal cortex region. As described in our previous study [6], rTMS consisted of 1000 stimuli at 1 Hz daily and 110% of the motor cortex threshold for 5 consecutive days per week (Monday to Friday) for 2 weeks. For repetitive pulses, TMS was delivered through a focal figure-eight magnetic coil connected to a magnetic stimulator (MagPro R30; MagVenture, Farum, Denmark). The resting motor threshold (RMT) was defined as the lowest stimulator output intensity capable of inducing motor evoked potentials (MEPs) of at least 50 μV peak-to-peak amplitude in the relaxed state in at least 5 of 10 consecutive trials. Thirty volunteers with normal hearing served as controls, whose RMTs were obtained. The tinnitus subjects and controls were age- and gender-matched.

2.3. Statistical Analysis. All statistical analyses were performed using SPSS v 16.0 (SPSS, Chicago, IL, USA). Prior to analysis, all variables were examined for their normality. All categorical variables were analyzed by the Chi-square test. We calculated the odds ratio (OR) and associated 95% confidence interval (CI) for demographic factors using the Mantel–Haenszel method. Logistic regression was performed to identify the factors contributing to tinnitus suppression after the intervention. In all analyses, $p < 0.05$ was taken to indicate statistical significance.

3. Results

The stimulation protocols were well tolerated, and all the patients completed the treatment except three patients who reported transient mild to moderate headache, two patients who reported transient worsening of their tinnitus, and two patients that complained of vertigo. None of the patients developed seizures or other serious side effects or adverse effects. A total of 289 patients with chronic unilateral or bilateral tinnitus (137 male, 182 female, age range: 19–87 years, mean 57 ± 14.7 years) were included in the study. In the active stimulation group, 76 (26.3%) patients reported purely left-sided tinnitus, 50 (17.3%) patients reported purely right-sided tinnitus, 129 (44.6%) patients described their tinnitus as bilateral, and 34 (11.8%) patients described their tinnitus as originating within the head. The duration of tinnitus ranged from 7 months to 40 years, with a median of 5.8 years, and approximately 15.2% of the subjects had experienced tinnitus for more than 5 years. The patients rated their tinnitus loudness on the VAS, and the median score was 6.5 (range, 4–10). A total of 169 (58.5%) of the 289 patients reported tonal tinnitus and 108 (37.4%) patients described noisiform tinnitus. Twelve (4.2%) patients could not determine the pitch of tinnitus or their pitch of tinnitus was unmatchable. Audiometric assessment showed normal hearing in 143 of 289 subjects (49.5%) and hearing loss in 146 (50.5%). Tinnitus interfered with sleep in 129 of the 289 patients.

The clinical characteristics of the tinnitus patients are shown in Table 1. Participants completed a questionnaire assessment of medical history before and immediately after the last intervention. Information on age, gender, tinnitus laterality, duration of tinnitus, hearing level, pitch of tinnitus, accompanying symptoms, underlying diseases, and sleep quality was included in the analyses.

rTMS showed a good effect in 138 of the patients included in the study (47.8%) and no effect in 151 patients (52.2%) in the active group. With respect to different factors contributing to tinnitus suppression, we observed improvement after active rTMS in the following domains: age, gender, duration of tinnitus, tinnitus laterality, audiometric parameters, and sleep. Significant tinnitus suppression was associated with younger age, male gender, shorter duration of tinnitus, tinnitus located centrally in the head, normal hearing, and no sleep disturbance at night ($p < 0.05$). These patients showed no significant differences in pitch of tinnitus, accompanying symptoms, such as headache and vertigo, and underlying diseases, such as hypertension, diabetes, and heart disease ($p > 0.05$) (Table 1).

Before the intervention, the average baseline VAS score in patients with active stimulation was 5.5. The score was

Table 1: Clinical characteristics of the patients suffering from tinnitus.

Independent variables	Active group		N	p value
	No effect%	Improved%		
Age (yrs)				
<30	5 (29.41)	12 (70.59)	17	0.012
31–50	30 (48.39)	32 (51.61)	62	
51–70	88 (51.16)	84 (48.84)	172	
>70	28 (73.68)	10 (26.32)	38	
Gender				
Male	56 (45.16)	68 (54.84)	124	0.043
Female	95 (57.58)	70 (42.42)	165	
Underlying diseases				
Good condition	121 (50.21)	120 (49.79)	241	0.154
Underlying diseases	30 (62.50)	18 (37.50)	48	
Accompanied symptoms				
No accompanied symptoms	95 (47.74)	104 (52.26)	199	0.052
Headache	18 (69.23)	8 (30.77)	26	
Dizziness	38 (59.38)	26 (40.62)	64	
Pitch of tinnitus				
Tone	79 (46.75)	90 (53.25)	169	0.06
Noise	66 (61.11)	42 (38.89)	108	
Uncertainty	6 (50.00)	6 (50.00)	12	
Tinnitus laterality				
Left ear	38 (50.00)	38 (50.00)	76	0.025
Right ear	28 (56.00)	22 (44.00)	50	
Bilateral	75 (58.14)	54 (41.86)	129	
Ringing in the head	10 (29.41)	24 (70.59)	34	
Audiometric parameters				
Normal hearing	53 (37.59)	88 (62.41)	141	0.001
Sensorineural hearing loss	98 (66.22)	50 (33.78)	148	
Tinnitus duration				
≤1 yr	29 (39.73)	44 (60.27)	73	0.013
1 yr < x ≤ 2 yrs	26 (48.15)	28 (51.85)	54	
2 yrs < x ≤ 5 yrs	62 (64.58)	34 (35.42)	96	
>5 yrs	34 (51.51)	32 (48.49)	66	
Sleep				
Sleep disturbance	84 (64.62)	46 (35.38)	130	0.005
Sleep well	67 (42.14)	92 (57.86)	159	

Table 2: Multivariate stepwise logistic regression analyses models for different factors that contribute to tinnitus suppression.

Independent variables	Odds ratio	95% Confidence interval	p value
Age (yrs)			
<30	0.24	0.06–1.07	$p = 0.061$
31–50	0.48	0.14–1.69	$p = 0.255$
51–70	0.29	0.08–1.12	$p = 0.072$
>70	1		
Gender			
Female	1		
Male	1.57	0.88–2.76	$p = 0.122$
Tinnitus laterality			
Left ear	1		
Right ear	0.81	0.36–1.81	$p = 0.602$
Bilateral	0.85	0.45–1.60	$p = 0.613$
Ringing in the head	1.63	0.62–4.31	$p = 0.324$
Hearing level			
Normal hearing	3.25	2.01–5.27	$p = 0.001$
Sensorineural hearing loss	1		
Duration of tinnitus			
>5 yrs	1		
2 yrs < x ≤ 5 yrs	1.52	0.70–3.10	$p = 0.441$
1 yr < x ≤ 2 yrs	1.61	0.82–3.20	$p = 0.731$
≤1 yrs	2.77	1.48–5.19	$p = 0.002$
Sleep			
Sleep disturbance	1		
Without sleep disturbance	2.51	1.56–4.10	$p = 0.005$

decreased to 2.7 immediately after the last active intervention. After active rTMS, 51.3% (SD = 20.6%) patients experienced a significant reduction in tinnitus loudness, as evidenced by VAS scale.

In the present study, the duration of tinnitus was correlated with tinnitus suppression by rTMS. The intervention was more effective in suppressing tinnitus in patients that had suffered from tinnitus for only a short time. Multinomial logistic regression analysis was performed with tinnitus duration as a dependent variable and the change in VAS score before and after stimulation as a predictor variable. There was a linear (negative) correlation between the duration of tinnitus and the degree of tinnitus suppression by rTMS ($p = 0.013$). Patients with tinnitus lasting less than 1 year were more likely to show suppression of tinnitus (OR: 2.77, 95% CI: 1.48–5.19, $p = 0.002$) immediately after the last intervention compared to those with tinnitus lasting more than 5 years (Table 2). Tinnitus could be suppressed, on average, in 60.2% of patients with tinnitus lasting less than 1 year but only in 51.8% of those with symptom duration of less than 2 years and only in 40.7% of those with symptoms lasting for more than 2 years.

When compared to patients with sensorineural hearing loss, those with normal hearing were more likely to show suppression of tinnitus (OR: 3.25, 95% CI: 2.01–5.27, $p = 0.001$) immediately after the last intervention. In addition, the rTMS treatment showed a significant effect in patients that reported no sleep disturbance (OR: 2.51, 95% CI: 1.56–4.10, $p = 0.005$). Patients with tinnitus located centrally in the head often reported a reduction in tinnitus after the rTMS procedure in contrast to those with left or right tinnitus (OR: 1.63, 95% CI: 0.62–4.31 $p = 0.324$). Although rTMS was

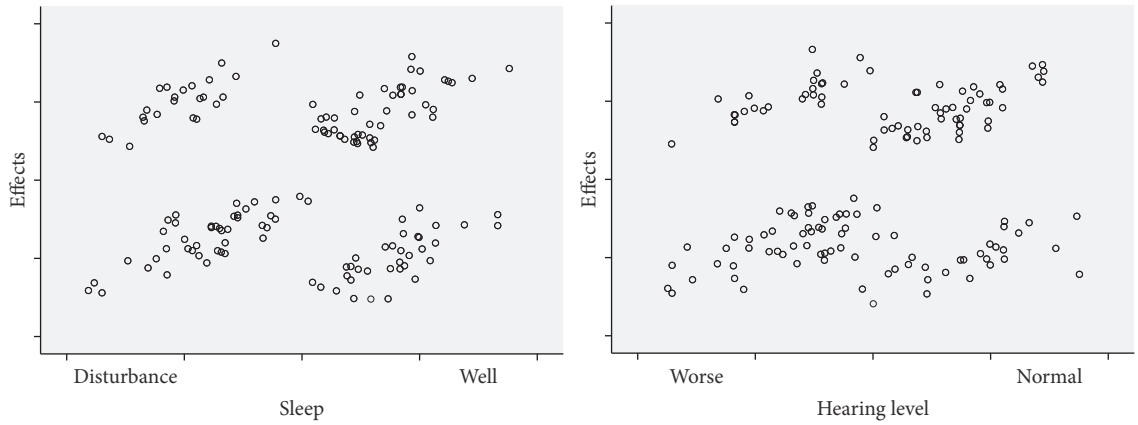

Figure 1: Correlations were observed between sleep and hearing level and efficacy of rTMS. The intervention was more likely to suppress tinnitus in subjects with normal hearing and those without sleep disturbance.

only applied over the left temporoparietal cortex, tinnitus was decreased equally well regardless of whether it was predominantly experienced in the left or right ear. There was no significant difference in the outcome between ipsilateral and contralateral rTMS. There was no significant difference in the outcome between bilateral and left-sided stimulation either (Table 2).

To investigate the major determinants of the effects of rTMS on tinnitus, we performed stepwise linear regression analyses between baseline characteristics, such as age, sex, duration of tinnitus, tinnitus laterality, hearing level, sleep quality, and efficacy of treatment. Age, gender, duration of tinnitus, hearing level, and sleep quality showed significant associations with the efficacy of rTMS, while tinnitus laterality showed no considerable effect ($p = 0.233$). On multiple regression analysis adjusted for age and gender, the patients with shorter tinnitus duration and normal hearing and without sleep disturbance showed maximal induction of tinnitus suppression by rTMS (Figure 1).

Baseline RMT in tinnitus patients was 48.5%, and that in healthy controls was 53.1%, indicating that tinnitus patients had significantly lower RMTs (Figure 2) than healthy volunteers ($t = 2.926$, $p = 0.004$).

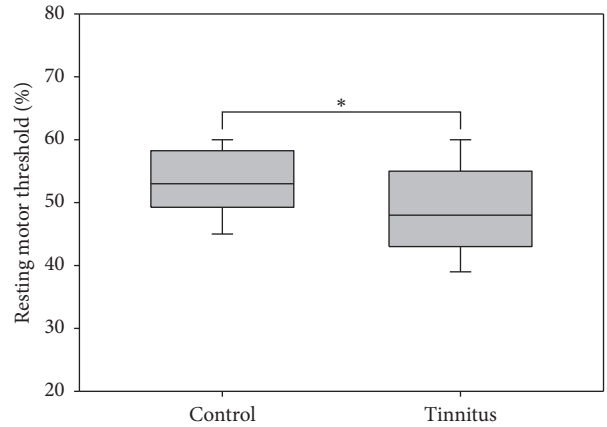

Figure 2: The resting motor threshold was significantly lower in tinnitus patients compared with healthy volunteers.

4. Discussion

The present study demonstrated that active low-frequency rTMS results in a significant decrease in the loudness of tinnitus. With respect to different factors that contribute to tinnitus suppression, active rTMS induces maximal tinnitus suppression in subjects with shorter tinnitus duration, normal hearing, and without sleep disturbance. The tinnitus patients have enhanced brain excitability compared with the controls.

The use of rTMS in the treatment of tinnitus stems from the development of models of central generation induced by auditory deafferentation (neural plasticity with hypersynchrony or hyperactivity of cortical and subcortical auditory and nonauditory areas) [16–19]. The results of the present study showed that tinnitus can be transiently suppressed partially or completely by rTMS in approximately 47.8% of tinnitus patients. Tinnitus duration, hearing level, and sleep quality were identified as positive predictors, in agreement with previous studies [20]. The amount of tinnitus suppression by rTMS was inversely correlated with the duration of symptoms; that is, shorter duration of tinnitus was associated with a greater suppressive effect. Two years seems to be an important turning point for obtaining a beneficial outcome. Tinnitus lasting less than 1 year could be suppressed on average in 60.2% of responding patients, decreasing to 51.8% of those with a symptom duration of less than 2 years and 40.7% after more than 2 years. It is possible that the central network involved in tinnitus becomes less plastic and less responsive to rTMS intervention over time. In addition, the degree of tinnitus suppression achieved through rTMS depended on the hearing of the patients. Hearing impairment was also identified as a negative predictor in our study. When compared to patients with sensorineural hearing loss, those with normal hearing were more likely to show suppression of tinnitus immediately after the last intervention. These observations suggested that hearing loss may represent an ongoing trigger for the generation of tinnitus and both reduce and

shorten the TMS treatment effects. In addition, the deprivation of auditory input may lead to disinhibition in the central auditory system, which in turn may exacerbate the plastic changes in neural functioning that could underlie tinnitus [21]. In addition, the reduction of inhibition in central auditory structures leads to hyperexcitability of circumscribed regions of the central auditory system, as evidenced by the enhanced brain excitability indicated in the present study. Moreover, rTMS treatment had a significant effect in patients without sleep disturbance. Nonauditory areas, such as the frontoparietal areas and limbic areas, have been suggested to be involved in the pathophysiology of tinnitus, as evidenced by the functional imaging data in our previous study [6]. These interactions between auditory and nonauditory brain regions may explain why tinnitus is perceived as bothersome. These mechanisms can lead to comorbid conditions, such as concentration problems, depression, and sleep disturbances [22]. Accordingly, impaired sleep quality shows an increased prevalence in cases of chronic tinnitus. In addition, patients frequently report that tinnitus prevents them from falling asleep.

Low-frequency rTMS, which is known to suppress cortical excitability, has been used successfully to interfere with neural functioning in the temporoparietal cortical region as the magnetic field passes through the skull and induces a small secondary current in the cortex [9, 23]. Accordingly, low-frequency rTMS has been used to treat tinnitus [24, 25]. In addition, TMS can also be used as a diagnostic tool for the assessment of motor cortex excitability by quantifying contractions of peripheral muscles induced by stimulation of the corresponding motor cortex representation. In the present study, tinnitus patients were shown to have enhanced brain excitability compared with controls, which was consistent with previous studies suggesting that central mechanisms are responsible for at least some cases of tinnitus [26]. The enhanced brain excitability was accompanied by a decrease in glucose metabolism and inhibitory-acting γ-aminobutyric acid (GABA) in the stimulated temporal cortex and an increase in cingulate and frontal areas but also in motor cortex, as evidenced by the previous study [27–29]. Many efforts have been made to gain insight into the neurophysiological mechanisms of tinnitus [30]. This knowledge can contribute to investigations into the pathophysiology of tinnitus.

Evidence from previous studies suggested that a functional network of several cortical areas may be responsible for tinnitus, but the precise region affected remains unclear [31, 32]. Using PET imaging, Plewnia et al. [33] found greater activity in the left auditory cortex of chronic tinnitus patients, regardless of the side of symptoms, or centrally within the head. Although rTMS was only applied over the left temporoparietal cortex in the present study, patients responded equally well regardless of whether their symptoms were predominantly in the left or right ear. The rate of response in tinnitus located centrally in the head was even higher than that for tinnitus located predominantly in the ears. However, on multiple regression analysis adjusted for age and gender, tinnitus laterality had no considerable effect.

In conclusion, active low-frequency rTMS resulted in significant suppression of the loudness of tinnitus, especially in patients with a shorter tinnitus duration and normal hearing and without sleep disturbance. Tinnitus patients showed enhanced brain excitability compared with controls. Future studies may significantly benefit from emerging imaging techniques to identify the mechanisms underlying tinnitus and from stimulation protocols that will together determine the optimal site for targeting rTMS stimulation.

Competing Interests

The authors declare that there are no competing interests.

Authors' Contributions

Hui Wang, Bei Li, and Meiye Wang have contributed equally to this work.

Acknowledgments

This study was supported by grants from Excellent Academic Leader Training Program of Shanghai Municipal Health System (XBR2013085), cooperation projects of new perspectives and advanced technology based on shanghai hospitals (SHDC 12014125), and National Natural Science Foundation of China (81570908/H1304).

References

[1] C. P. Lanting, E. de Kleine, and P. van Dijk, "Neural activity underlying tinnitus generation: results from PET and fMRI," *Hearing Research*, vol. 255, no. 1-2, pp. 1–13, 2009.

[2] D. E. Tunkel, C. A. Bauer, G. H. Sun et al., "Clinical practice guideline: tinnitus," *Otolaryngology—Head and Neck Surgery*, vol. 151, no. 2, supplement, pp. S1–S40, 2014.

[3] C. W. Newman, S. A. Sandridge, and G. P. Jacobson, "Assessing outcomes of tinnitus intervention," *Journal of the American Academy of Audiology*, vol. 25, no. 1, pp. 76–105, 2014.

[4] A. Crippa, C. P. Lanting, P. V. Dijk, and J. B. Roerdink, "A diffusion tensor imaging study on the auditory system and tinnitus," *The Open Neuroimaging Journal*, vol. 4, pp. 16–25, 2010.

[5] C. P. Lanting, E. de Kleine, R. N. Eppinga, and P. van Dijk, "Neural correlates of human somatosensory integration in tinnitus," *Hearing Research*, vol. 267, no. 1-2, pp. 78–88, 2010.

[6] H. Wang, B. Li, Y. Feng et al., "A pilot study of EEG source analysis based repetitive transcranial magnetic stimulation for the treatment of tinnitus," *PLoS ONE*, vol. 10, no. 10, Article ID e0139622, 2015.

[7] A. J. Norena, "Revisiting the cochlear and central mechanisms of tinnitus and therapeutic approaches," *Audiology and Neurotology*, vol. 20, supplement 1, pp. 53–59, 2015.

[8] O. M. Meeus, D. De Ridder, and P. H. Van de Heyning, "Transcranial magnetic stimulation (TMS) in tinnitus patients," *B-ENT*, vol. 5, no. 2, pp. 89–100, 2009.

[9] I. Lorenz, N. Müller, W. Schlee, B. Langguth, and N. Weisz, "Short-term effects of single repetitive TMS sessions on auditory evoked activity in patients with chronic tinnitus," *Journal of Neurophysiology*, vol. 104, no. 3, pp. 1497–1505, 2010.

[10] J. P. Lefaucheur, N. André-Obadia, A. Antal et al., "Evidence-based guidelines on the therapeutic use of repetitive transcranial magnetic stimulation (rTMS)," *Clinical Neurophysiology*, vol. 125, no. 11, pp. 2150–2206, 2014.

[11] S. Vanneste and D. De Ridder, "The involvement of the left ventrolateral prefrontal cortex in tinnitus: a TMS study," *Experimental Brain Research*, vol. 221, no. 3, pp. 345–350, 2012.

[12] S. Rossi, A. De Capua, M. Ulivelli et al., "Effects of repetitive transcranial magnetic stimulation on chronic tinnitus: a randomised, crossover, double blind, placebo controlled study," *Journal of Neurology, Neurosurgery and Psychiatry*, vol. 78, no. 8, pp. 857–863, 2007.

[13] A. Lehner, M. Schecklmann, T. B. Poeppl et al., "Multisite rTMS for the treatment of chronic tinnitus: stimulation of the cortical tinnitus network—a pilot study," *Brain Topography*, vol. 26, no. 3, pp. 501–510, 2013.

[14] A. Londero, B. Langguth, D. De Ridder, P. Bonfils, and J.-P. Lefaucheur, "Repetitive transcranial magnetic stimulation (rTMS): a new therapeutic approach in subjective tinnitus?" *Neurophysiologie Clinique*, vol. 36, no. 3, pp. 145–155, 2006.

[15] J. Burger, E. Frank, P. Kreuzer et al., "Transcranial magnetic stimulation for the treatment of tinnitus: 4-year follow-up in treatment responders—a retrospective analysis," *Brain Stimulation*, vol. 4, no. 4, pp. 222–227, 2011.

[16] B. Langguth, P. Eichhammer, R. Wiegand et al., "Neuronavigated rTMS in a patient with chronic tinnitus. Effects of 4 weeks treatment," *NeuroReport*, vol. 14, no. 7, pp. 977–980, 2003.

[17] C. Plewnia, M. Bartels, and C. Gerloff, "Transient suppression of tinnitus by transcranial magnetic stimulation," *Annals of Neurology*, vol. 53, no. 2, pp. 263–266, 2003.

[18] J. J. Eggermont, "Pathophysiology of tinnitus," *Progress in Brain Research*, vol. 166, pp. 19–543, 2007.

[19] D. De Ridder, A. B. Elgoyhen, R. Romo, and B. Langguth, "Phantom percepts: tinnitus and pain as persisting aversive memory networks," *Proceedings of the National Academy of Sciences of the United States of America*, vol. 108, no. 20, pp. 8075–8080, 2011.

[20] D. De Ridder, E. Verstraeten, K. Van Der Kelen et al., "Transcranial magnetic stimulation for tinnitus: influence of tinnitus duration on stimulation parameter choice and maximal tinnitus suppression," *Otology and Neurotology*, vol. 26, no. 4, pp. 616–619, 2005.

[21] C. P. Lanting, E. De Kleine, H. Bartels, and P. Van Dijk, "Functional imaging of unilateral tinnitus using fMRI," *Acta Oto-Laryngologica*, vol. 128, no. 4, pp. 415–421, 2008.

[22] B. Langguth, "A review of tinnitus symptoms beyond 'ringing in the ears': a call to action," *Current Medical Research and Opinion*, vol. 27, no. 8, pp. 1635–1643, 2011.

[23] B. Langguth, T. Kleinjung, M. Landgrebe, D. de Ridder, and G. Hajak, "rTMS for the treatment of tinnitus: the role of neuronavigation for coil positioning," *Neurophysiologie Clinique*, vol. 40, no. 1, pp. 45–58, 2010.

[24] G. Frank, T. Kleinjung, M. Landgrebe et al., "Left temporal low-frequency rTMS for the treatment of tinnitus: clinical predictors of treatment outcome—a retrospective study," *European Journal of Neurology*, vol. 17, no. 7, pp. 951–956, 2010.

[25] J. F. Piccirillo, D. Kallogjeri, J. Nicklaus et al., "Low-frequency repetitive transcranial magnetic stimulation to the temporoparietal junction for tinnitus: four-week stimulation trial," *JAMA Otolaryngology—Head and Neck Surgery*, vol. 139, no. 4, pp. 388–395, 2013.

[26] J. A. Henry, L. E. Roberts, D. M. Caspary, S. M. Theodoroff, and R. J. Salvi, "Underlying mechanisms of tinnitus: review and clinical implications," *Journal of the American Academy of Audiology*, vol. 25, no. 1, pp. 5–22, quiz 126, 2014.

[27] M. Lee, S. E. Kim, W. S. Kim et al., "Cortico-cortical modulation induced by 1-Hz repetitive transcranial magnetic stimulation of the temporal cortex," *Journal of Clinical Neurology*, vol. 9, no. 2, pp. 75–82, 2013.

[28] U. Ziemann, F. Meintzschel, A. Korchounov, and T. V. Ilić, "Pharmacological modulation of plasticity in the human motor cortex," *Neurorehabilitation and Neural Repair*, vol. 20, no. 2, pp. 243–251, 2006.

[29] V. Di Lazzaro, F. Pilato, M. Dileone et al., "GABAA receptor subtype specific enhancement of inhibition in human motor cortex," *Journal of Physiology*, vol. 575, no. 3, pp. 721–726, 2006.

[30] P. Eichhammer, T. Kleinjung, M. Landgrebe, G. Hajak, and B. Langguth, "TMS for treatment of chronic tinnitus—neurobiological effects," *Progress in Brain Research*, vol. 166, pp. 369–375, 2007.

[31] H. Burton, A. Wineland, M. Bhattacharya, J. Nicklaus, K. S. Garcia, and J. F. Piccirillo, "Altered networks in bothersome tinnitus: a functional connectivity study," *BMC Neuroscience*, vol. 13, no. 1, article 3, 2012.

[32] M. R. Laureano, E. T. Onishi, R. A. Bressan et al., "Memory networks in tinnitus: a functional brain image study," *PLoS ONE*, vol. 9, no. 2, article e87839, 2014.

[33] C. Plewnia, M. Reimold, A. Najib, G. Reischl, S. K. Plontke, and C. Gerloff, "Moderate therapeutic efficacy of positron emission tomography-navigated repetitive transcranial magnetic stimulation for chronic tinnitus: A Randomised, Controlled Pilot Study," *Journal of Neurology, Neurosurgery and Psychiatry*, vol. 78, no. 2, pp. 152–156, 2007.

Hindawi Publishing Corporation
Neural Plasticity
Volume 2016, Article ID 6143164, 9 pages
http://dx.doi.org/10.1155/2016/6143164

Review Article

Cochlear Synaptopathy and Noise-Induced Hidden Hearing Loss

Lijuan Shi,[1] Ying Chang,[1] Xiaowei Li,[1] Steve Aiken,[2] Lijie Liu,[1] and Jian Wang[1,2]

[1]*Department of Physiology, Medical College of Southeast University, 87 Dingjiaoqiao Road, Nanjing 210009, China*
[2]*School of Human Communication Disorders, Dalhousie University, 1256 Barrington St. Dalhousie University, Halifax, NS, Canada B3J 1Y6*

Correspondence should be addressed to Lijie Liu; liulj321liulj321@163.com and Jian Wang; jian.wang@dal.ca

Received 30 May 2016; Revised 9 August 2016; Accepted 21 August 2016

Academic Editor: Preston E. Garraghty

Recent studies on animal models have shown that noise exposure that does not lead to permanent threshold shift (PTS) can cause considerable damage around the synapses between inner hair cells (IHCs) and type-I afferent auditory nerve fibers (ANFs). Disruption of these synapses not only disables the innervated ANFs but also results in the slow degeneration of spiral ganglion neurons if the synapses are not reestablished. Such a loss of ANFs should result in signal coding deficits, which are exacerbated by the bias of the damage toward synapses connecting low-spontaneous-rate (SR) ANFs, which are known to be vital for signal coding in noisy background. As there is no PTS, these functional deficits cannot be detected using routine audiological evaluations and may be unknown to subjects who have them. Such functional deficits in hearing without changes in sensitivity are generally called "noise-induced hidden hearing loss (NIHHL)." Here, we provide a brief review to address several critical issues related to NIHHL: (1) the mechanism of noise induced synaptic damage, (2) reversibility of the synaptic damage, (3) the functional deficits as the nature of NIHHL in animal studies, (4) evidence of NIHHL in human subjects, and (5) peripheral and central contribution of NIHHL.

1. Noise-Induced Hidden Hearing Loss (NIHHL)

Noise-induced hidden hearing loss (NIHHL) refers to any functional impairment seen in subjects with noise exposing history but no permanent threshold shift (PTS). This is different from the conventional definition of noise-induced hearing loss (NIHL), which is based on changes in auditory sensitivity or threshold shift [1]. Therefore, noise exposure recommendations are based on the likelihood that a particular dose of exposure will result in a PTS. Noise exposures that are not expected to cause PTS are thus considered safe.

Physiologically, variations in auditory sensitivity following exposure to noise are largely due to the functional status of outer hair cells (OHCs) in the cochlea, which provide mechanical amplification of soft sounds [2, 3]. Noise exposures that result in only a temporary threshold shift (TTS) have a reversible impact on OHC function, which is manifested by the recovery of otoacoustic emissions (OAE) [4–6] and cochlear microphonics (CM) [7–11]. The functional changes in these measures parallel the recovery of hearing thresholds, as well as the repair of structures such as stereocilia and the tectorial membrane [7, 12]. By contrast, noise exposure at higher levels and/or for longer durations can cause permanent damage to, or even the death of, OHCs and, hence, lead to PTS. Therefore, the OHCs and the structures surrounding them, including the tectorial membrane and the supporting cells, are considered to be the major loci of cochlear damage that result in noise-induced threshold shifts [13, 14].

Although some early reports claimed that reversible noise-induced IHC pathologies were responsible for TTS [15, 16], IHCs are relatively insensitive to noise-induced cell death. However, it has long been recognized that the synapse between IHCs and primary spiral ganglion neurons (SGNs) can be damaged by noise [17–19]. These early studies showed that this manifests mainly as damage to the postsynaptic terminals; however, there is clear evidence from more recent studies that noise induces damage to both pre- and postsynaptic structures. More importantly, disruption of the synapses can be permanent, resulting in degenerative death of SGNs [6]. The finding that damage to ribbon synapses

can occur without PTS is significant because of the potential impact of such damage on hearing function. Because the physiological damage is not accompanied by a permanent shift in hearing threshold, it would likely be missed by a standard (i.e., threshold-based) hearing assessment and has thus been referred to as NIHHL.

NIHHL first manifests as reduced output of the auditory nerve at high sound levels, without affecting the hearing threshold. This reduction has been found in both animals [6, 20–23] and human subjects with a history of noise exposure but with normal audiograms [24]. Since the thresholds of the auditory nerve remain unchanged, the function relating compound action potentials (CAP) amplitude with sound levels in NIHHL animal is different from that in animals with threshold changes. Schematic curves of CAP input/output functions are presented in Figure 1 for a comparison across normal control and those with different pathologies. Theoretically, if the damage is restricted to OHCs, the major change in CAP input/output (I/O) curve is restricted around threshold and the amplitude reaches the control value at high sound levels. In the case of NIHHL, CAP reduction is mainly at high sound level, with no difference at low sound level, suggesting a suprathreshold deficit. When the damage occurs at both OHCs and the IHC-SGN synapses, the reduction of CAP amplitude is seen across all sound levels.

As NIHHL is initiated at the synapse between the IHCs and SGNs, which silences the auditory nerve fibers (ANFs) that extend from them, the corresponding disorder is categorized as a cochlear neuropathy (i.e., cochlear synaptopathy) [25, 26]. Presumably, the reduction in the amplitude of the auditory nerve response without threshold elevation is due to selective loss of ANFs that have high thresholds, which is supported by single-unit recording studies [20, 27]. Given the important features of those low-spontaneous-rate ANFs in auditory coding, the neuropathy or synaptopathy in hidden hearing loss is not simply a reduction in the number of functional ANFs. Furthermore, the synaptopathy in NIHHL is likely to be related to the synaptic repair after initial damage by noise [20], rather than a simple initial loss. In addition, the functional deficits seen in NIHHL may also involve the contribution from central auditory plasticity [26, 28–32]. In this review, we summarize the available data for noise-induced damage and repair around IHC–SGN synapses and discuss the evidence for the contributions of cochlear malfunction and central plasticity to NIHHL.

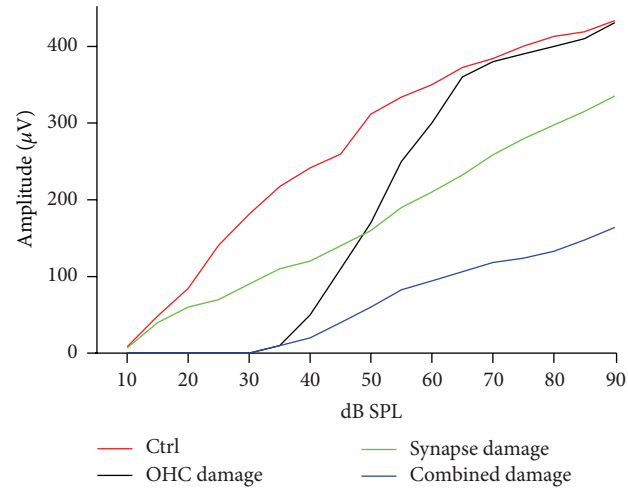

Figure 1: Schematic curves of CAP I/O functions under different conditions. As compared with the control behavior, restricted OHC lesion results in an elevation of CAP threshold, but no reduction of CAP amplitude at high sound levels, while the restricted synapse damage results in the reduction of CAP amplitude largely at high sound levels.

2. Noise-Induced Damage and Repair around Cochlear Ribbon Synapses

Accumulated evidence has shown that the synapses between IHCs and type-I SGNs are sensitive to noise and the damage to this synapse is likely to be the bases for NIHHL. The synapse is characterized by presynaptic dense bodies termed ribbons [33–35], which are spherical or ellipsoidal in shape, 100–200 nm in diameter [36], and surrounded by synaptic vesicles. The ribbons are built up from RIBEYE protein subunits [37, 38] and anchored to the active zone of the presynaptic membrane via Bassoon proteins [39–41]. The functional role of ribbons has been recognized as tethering and conveying synaptic vesicles to the active zones [42, 43], where the release of neurotransmitters at these synapses is modulated by a specific L-type calcium ion channel (i.e., CaV1.3) [44, 45].

Noise exposure causes damage to both the presynaptic ribbons and postsynaptic nerve terminals of the ribbon synapses [6, 22, 23, 46–48]. The damaged synapses exhibit various degrees of swelling of the terminals, resulting in disruption of the synaptic connections between IHCs and SGNs [20, 46, 48]. Immunohistological staining has revealed similar losses for ribbons and terminals [6, 22, 23, 49]. The mechanism for the damage to the postsynaptic terminal is glutamate-mediated excitotoxicity (reviewed in [46]). However, it is unclear how the presynaptic ribbons are damaged. One possible mechanism of ribbon loss is the loss of cell-cell contact that is required for the maintenance of the pre- and postsynaptic complexes [50–53]. Our electron microscopy evaluations did not reveal any residual presynaptic complexes without ribbon and postsynaptic terminals [20]. Therefore, it is likely that the entire presynaptic structure breaks down when the postsynaptic terminal is damaged.

Another possibility is that ribbon loss results from a breakdown of ribbon building units. A brick assembly model, in which a ribbon is built up from multiple Ribeye subunits, has been proposed for ribbon construction in retina photoreceptor cells [37]. Moreover, the ribbons in retina sensorial cells can be partially broken down by light, but they rapidly reassemble in the dark, probably serving as a mechanism of adaption to bright light [54–58]. In the retina, the ribbon size appears to be a determining factor for the quantity of neurotransmitter released. However, the dynamic disassembling/reassembling process has not been identified in the cochlea, and changes in the ribbon size and the

relationship with the release of neurotransmitters have not been investigated in the cochlea. Additionally, disassembly and reassembly, as well as ribbon size, are modulated by Ca^{2+} signaling involving CaV-channels, presynaptic Ca^{2+} levels and storage, and guanylate cyclase-activating protein-2 (GCAP2; see the review by Schmitz [59]). Interestingly, optical stimulation of photoreceptors causes hyperpolarization of the presynaptic membrane and a decrease in $[Ca^{2+}]_i$, as opposed to depolarization and the large increase in $[Ca^{2+}]_i$ in IHCs in response to sound. The decrease in $[Ca^{2+}]_i$ in photoreceptor cells is followed by a conformational change of GCAP2, which results in the disassembly of the ribbons. In the cochlea, it is not known whether there is a GCAP-mediated pathway that controls ribbon size. As the membrane potential of IHCs is depolarized with increasing sound levels, resulting in an influx of Ca^{2+}, the role of Ca in ribbon assembly is unlikely to be the same as it is in the retina.

2.1. Is the Synaptic Damage Reversible? There is some debate about whether noise-induced ribbon synapse damage is reversible. The first quantitative study of noise-induced ribbon synapse damage in CBA mice [6] reported that the number of ribbon synapses was reduced to 40% compared with the control 1 day after brief noise exposure that did not lead to PTS. The synapse count recovered to 50% within 1 week, but no further recovery was observed, and this 50% loss of synapses was considered permanent. SGN death observed 2 years after the noise was found to match the 50% permanent loss of synapses [6]. However, a study on guinea pigs carried out by the same research group found a similar loss of ribbon synapses 2 weeks after exposure to noise that did not cause PTS [49], but this study found a much smaller final loss of SGNs. This suggests that some SGNs, which had originally lost their synapses with IHCs, survived and reestablished synapses with IHCs.

Our studies on guinea pigs have revealed a clear recovery in the synapse count following a massive initial loss induced by noise exposure that did not lead to PTS [22, 23]. Although this recovery was not complete, approximately 50% of the initial loss of paired ribbon and postsynaptic density (PSD) puncta in the basal half of the cochleae was seen 1 day after noise, and the loss was recovered to <20% within 1 month. Comparing the aforementioned data from mice and guinea pigs, it appears that there may be some species difference in the ability to regenerate synapses following noise-induced hearing damage. However, a recent study of C57 mice reported that the loss of ribbon synapses induced by non-PTS-inducing noise was largely reversible [60]. This discrepancy in synapse regeneration following noise exposure requires further investigation.

In a recent review, it was argued that the recovery of CtBP2/PSD counts in guinea pig cochleae following noise exposure reported in our studies may be attributable to up/downregulation of the synaptic protein rather than regeneration of synaptic connections [25]. However, there are several lines of evidence for the possibility of synapse repair following noise-induced damage. First, it has been reported that plastic changes occur in the presynaptic component, including the existence of multiple presynaptic ribbons around an active zone [61] and the changes in the size and location of ribbons following noise exposure [22]. Second, the change in the amplitude of the compound action potential (CAP) corresponded to the changes in ribbon/PSD counts: a large initial reduction in CAP amplitude and synapse counts were followed by a significant recovery after the noise exposure [20]. Third, changes in many single-ANF coding activities were not seen at the time that the synapses were damaged but rather manifested later (see Section 3) with the recovery in both the CAP and synapse number, suggesting that those changes occurred in the ANFs that connect IHCs via repaired/reestablished synapses [20]. Further work is required to determine the mechanisms and factors that influence the repair of both pre- and postsynaptic components.

3. Cochlear Coding Deficits in Hidden Hearing Loss

Ribbon synapses exhibit spatial differences around IHCs; that is, the synapses at the modiolar side of an IHC have relatively small ribbons but larger postsynaptic terminals, whereas those at the pillar side have relatively large ribbons but smaller terminals [62]. This spatial variation in synapse morphology has been linked to functional variations across ANFs. Liberman et al. reported that ANFs are functionally categorized by their spontaneous rate (SR), which is inversely related to the fiber's threshold and dynamic range [63–65]. It is widely accepted that low-SR ANFs exhibit synapses with IHCs on their modiolar side, whereas high-SR units exhibit synapses on the pillar side (this is based on data obtained using intracellular tracer injections) [66]. The low-SR units are considered critical for hearing in noisy environments due to their larger dynamic range, higher thresholds, and the ability to follow the quick change of the amplitude of acoustic signals. By contrast, high-SR units are responsible for the sensitivity to quiet sounds and are saturated by high-level background noise [26, 63, 64, 67, 68].

In NIHHL, low-SR ANFs appear to be more vulnerable to noise than high-SR units. Selective loss of low-SR ANFs has been found following exposure to noise that did not lead to PTS [27]. Presumably, this selective loss of low-SR units should produce coding deficits, which can be predicted based on the unique features of those units [26]. However, no coding deficits were examined and reported in this study [27]. On the other hand, we reported a time delay in the development of coding deficits by single ANFs in guinea pigs following a similar noise exposure that did not cause PTS [20]; these deficits were attributed to intensity coding and temporal coding as summarized in Sections 3.1 and 3.2.

3.1. Intensity Coding Deficits in NIHHL. Intensity coding in the cochlea is defined as the ability of ANFs to encode the sound intensity or the change of sound intensity. This ability is determined primarily by the spike rate (or the change of spike rate) of individual ANF in response to sound intensity change and the number of functional ANFs. Therefore, the intensity coding deficits can be evaluated in both evoked field potential

and single-unit recordings. Deficits in intensity coding were first suggested by a reduction in wave I of the auditory brainstem response (ABR) [6, 49], as well as a reduction in the amplitude of the CAP [20], as this is likely due to the loss of functional ANFs following synapse disruption. The fact that the reduction is more significant at higher sound levels has been considered evidence for selective damage to low-SR fibers, which have higher thresholds [25, 26, 69].

The deterioration in intensity coding following no-PTS noise exposure was manifested as a reduction in the driven spike rates (peak, sustained, and total rates) of ANF units that were tested only at one sound level [20]. Such changes are significant only in low-SR ANF units and are seen at a later time rather than immediately following exposure. This time delay in the development of coding deficits suggests that (1) the reduction in driven spike rates occurs in the ANFs to which the synaptic connections to the IHCs are reestablished following the initial disruption and (2) the repaired synapses are functionally abnormal, with less efficient neurotransmitter release.

3.2. Temporal Coding Deficits in NIHHL. Temporal processing ability in the cochlea as well as in the whole auditory pathway is defined as the ability to follow the quick change of acoustic signals. In human subjects, the process involves both bottom-up and top-down mechanisms; but in animal models, only bottom-up mechanisms are tested (see reviewed by [67]). Many different tests have been used to detect the bottom-up mechanisms of temporal coding, some of them based on the peristimulatory changes of firing rate showing latency and adaptation. As reviewed above, the major function of presynaptic ribbons in IHCs is to facilitate the synaptic transmission. Therefore, the damage to this synapse likely produces temporal coding deficits in ANFs. Indeed, such deficits were manifested as an increase in response latency of ANFs in animals with NIHHL. This was first demonstrated as a significant delay in CAP peak latency [21] and then further supported by the delayed latency of peak in PSTH (or peak latency) of ANFs in our single-unit study [20]. In another very recent report, such delay was reported in ABR as the marker of cochlear synaptopathy [70]. We also found a reduction in the ratio of peak to sustained rates in animals that were exposed to noise. This ratio is considered an index of the ability of a neuron to encode dynamic signal changes (see review by [68]). Using a paired-click paradigm, we found that the ANF response of noise-exposed animals to the second click recovered more slowly from the masking effect of the first click. These results reveal poorer coding to the transient features of acoustic signals by ANFs, which were examined in previous studies to show the deterioration in of temporal coding in animals with Bassoon mutation [39, 41]. Whereas an increase in peak latency was seen shortly after exposure to noise, changes in the peak rate and the peak/sustained spike ratio, as well as a slower recovery of the spike rate to the second click, were not seen until later, suggesting an association between the deficits and the synapse repair.

Phase locking is a mechanism for the auditory coding of temporal envelopes. A temporal deficit in phase-locking responses has been proposed based on selective loss of low-SR units and the functional features of this group of ANFs [25, 26, 69], but it has not been tested at the single-unit level.

4. Association of Coding Deficits with Unhealthy Synaptic Repair

So far, there appear to be two models for the development of coding deficits in NIHHL. One model suggests that the coding deficit or synaptopathy is simply due to the loss of low-SR ANFs. Since those units have unique functions in signal coding, the loss of those functions is predicted as the consequences. Evidence from our own laboratory suggests another model. That is, the coding deficits are developed as the result of unhealthy synaptic repair after initial disruption. We found that the noise-induced synaptic damage in guinea pigs under NIHHL is largely repairable, leaving only a small amount of synapses not being reestablished. Therefore, the coding deficits or synaptopathy cannot be simply attributed to the loss of SR units. Since the coding deficits are seen at the time when the synapse counts are largely recovered, we believe that the coding deficits likely occur in the repaired synapses (most of them innervating low-SR ANFs). Studies are needed to verify which model is more likely the case in human subjects.

5. Central and Peripheral Contributions to NIHHL

Hearing loss impacts auditory perception. It has long been recognized that subjects with normal audiograms may have perceptual difficulties, and this is especially true in the elderly. Age-related hearing loss with threshold elevation is termed peripheral presbycusis, whereas the perceptual difficulties seen in the elderly without threshold shift are usually termed central presbycusis [71]. For example, temporal processing deficits and difficulties of hearing in noisy environments are two major problems experienced by the elderly. These problems were recognized long before the discovery of cochlear damage associated with NIHHL and were considered to be the result of "central auditory processing disorders" [71–75]. It was generally accepted that any perceptual deficits observed without changes to hearing thresholds and cognitive functioning can be attributed to central dysfunctions.

Based on recent progress in functional deficits in cochlear coding, such separation between peripheral and central presbycusis is likely to be incorrect. The so-called central presbycusis may, at least in part, result from disorders in the auditory periphery. The coding deficits related to the loss of low-SR ANFs had been described as a type of auditory neuropathy and/or synaptopathy even before any of the predicted deficits were identified. Data on changes in the SR distributions of ANFs suggest the reestablishment of synapses following an initial disruption that was selective to low-SR units [20]. Although our data revealed abnormalities in some aspects of coding in the auditory nerve, further work is required to investigate coding deficits in NIHHL. Such studies cannot be replaced by speculation based on

the selective loss of low-SR fibers; for example, one cannot be certain how the auditory nerve changes its response to amplitude modulation until it is measured at the single-unit level. Two possibilities must be considered: (1) the surviving ANFs may change their function and (2) the initially lost low-SR fibers may be repaired but with changed function.

It should be noted that there is now a tendency in the literature to consider NIHHL to be a purely peripheral issue, a result of the overcorrection of the "central presbycusis." However, despite the strong evidence for a peripheral contribution, the central contribution to the problems seen in NIHHL should not be neglected. In other words, it may be more constructive to assume that there are both peripheral and central contributions to NIHHL. It is well known that hearing loss (with elevated threshold) can induce central changes, which can result in deteriorations in signal processing. Studies aiming to distinguish the role of central plasticity from that of ribbon synapse damage are rare. One such report found that an increase in central gain was responsible for tinnitus in human subjects with typical damage seen in NIHHL (i.e., reduced auditory nerve input to the brain (measured as a smaller ABR wave I)) but normal hearing threshold [24]. In an earlier study in rats, tinnitus was found 6 months after exposure to noise that caused minimal loss of hair cells and PTS but significant loss of ANFs [76].

One of the central impacts of hearing loss due to damage to peripheral auditory organ is imbalance between excitation and inhibition, resulting in hyperactivity and/or hyperresponsiveness in the central auditory system (see reviews in [77–80]). The types of hearing loss producing such central enhancement include cochlear ablation, drug- and noise-induced damage. While direct effect of drugs and noise on central neurons needs to be differentiated, a similarity across those hearing loss models is the reduction of cochlea output to the auditory brain, which may be the main initial factor causing the imbalance between excitation and inhibition. In this sense, central plasticity should also be seen in subjects with NIHHL. While most of studies in central plasticity using NIHL model correlated the central enhancement with the amount of threshold shifts [29, 81–85], at least one study has reported central enhancement in mice exposed briefly to noise at a moderate level that did not cause PTS, presumably producing only NIHHL [30]. Unfortunately, the reduction in auditory input from the cochlea was not quantified in this study. Taken together, available data suggest that cochlear damage, with or without threshold elevation, can lead to central plasticity by reducing input from the auditory nerve. Further work is required to establish the central contribution to coding/perception difficulties in NIHHL, and previous studies on central processing disorders in subjects with NIHL should be reevaluated to differentiate the central contributions from the peripheral ones.

In a brief summary, we use Figure 2 to summarize the available data for the mechanisms of perception difficulty experienced by subjects with history of noise exposure but normal or near normal thresholds. In this schematic diagram, we include the two potential models of noise-induced synaptopathy in cochleae. In model 1, the coding deficits are speculated based on the role of low-SR ANFs in signal coding. Further evaluation is needed to validate this model. Both models result in a reduction in the cochlear output to the auditory brain, which in turn will result in plastic reorganization of the brain. Auditory signal processing disorders experienced by subjects with long-term NIHHL should include what are inherited from the coding deficits developed in the auditory peripheral and those associated with the plastic changes of auditory brain.

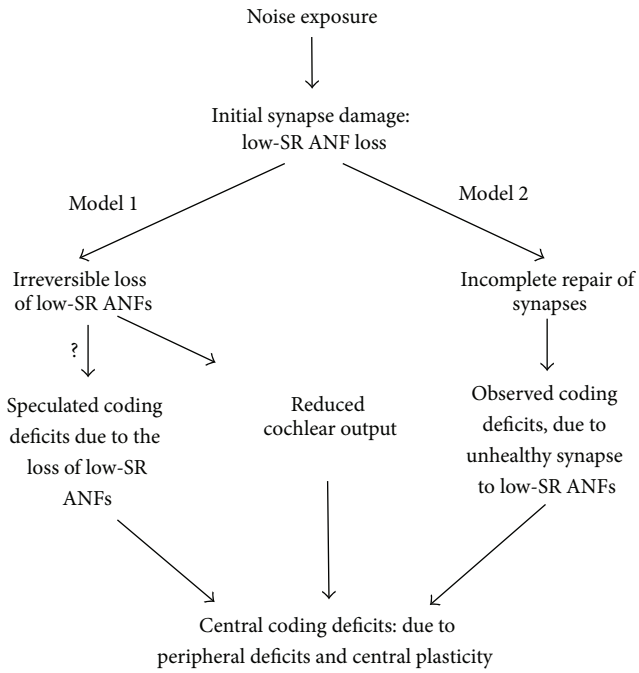

Figure 2: Diagram for the hypothesis of coding deficits in NIHHL.

6. Clinical Implications and Future Directions

6.1. Evidence of NIHHL in Human Subjects. Although more studies on the impact of noise on human hearing showing no changes in auditory sensitivity are required, evidence suggesting the occurrence of NIHHL in human subjects is being accumulated. This is supported by thorough research on the signal perception deficits experienced by subjects with a history of noise exposure but normal thresholds [26]. Since the deficits are demonstrated at suprathreshold levels, it is clear that normal hearing thresholds do not guarantee normal hearing functions, especially in subjects with history of noise exposure [24, 86]. The second line of evidence is the reduction in the output of the auditory nerve in subjects with a history of exposure to noise. This manifests as a reduction in wave I in the ABR at suprathreshold levels [24]. Interestingly, the combination of a reduction in wave I and an increase in wave V/I ratio may be considered evidence of increased central gain and is likely responsible for the generation of tinnitus in hidden hearing loss [32, 87, 88]. The third line of evidence comes from the age-related SGN degeneration seen in the examination of human temporal bones [89]. Unfortunately, there is, as yet, no clear human evidence that degeneration of

SGNs is expedited by exposure to noise that does not cause threshold elevation.

6.2. Significance of NIHHL. The clinical implications of NIHHL are manifested by the fact that noise exposure causing NIHHL occurs frequently in daily life and impacts much more general population [90]. Such noise exposure has been generally considered to be safe according to current safety standards for exposure to noise. The evidence from the studies reviewed here indicates that the resulting damage to the ribbon synapses from noise that did not induce PTS can be repaired even though the repair is incomplete. More importantly, the signal coding deficits are developed in association with the synapse repair. Since the damage and repair occur repeatedly, the damage on signal coding can be accumulated during aging and likely contributes to the perceptual difficulties experienced by the elderly [26]. This impact of noise exposure on signal coding is obviously different from the contribution made by the hearing loss defined by threshold shifts.

6.3. Future Direction. In future, the coding deficits and related synaptic repair in NIHHL should be further investigated in a laboratory setting. Since the ribbon synapse is the first gating point for temporal processing in auditory pathway, the observed coding deficits suggest a clear peripheral origin for the decline in temporal processing and perceptual difficulties during aging. Whether and how the synaptic damage will impact the central auditory processing need to be investigated in a manner that is clearly differentiated from the impact of hearing threshold shift. Moreover, the coding function of ANFs should be observed over a long period of time following exposure to noise to determine whether the coding deficits are temporary or persistent. We are currently collecting data using electron microscopy, as well as conducting an analysis on the potential changes of the molecular structures of ribbons and PSDs, in an attempt to elucidate the morphological/molecular mechanisms responsible for functional changes of repaired ribbon synapses. It would also be interesting to understand the reasons for the extreme sensitivity of low-SR synapses to noise, as well as elucidate possible methods to prevent damage. Laboratory studies should also aim to explore the mechanisms of synaptic repair in the cochlea, as well as reveal the factors that influence repair in order to promote it.

To translate the knowledge to clinic, investigation is needed to establish good measures for detecting NIHHL in human subjects. Although ABR wave I is useful for evaluating synaptopathy caused by noise that does not induce PTS, its reliability and sensitivity are questionable in human subjects where the ABR amplitude is small, and other methods should be explored. A very recent report suggests the use of ABR latency as the marker of NIHHL [70]. The study tested human subjects with normal hearing thresholds and reported a big variation in the threshold of envelope interaural timing difference, which was negatively correlated with the shift of ABR wave V latency by background noise: the higher the threshold (poorer sensitivity), the smaller the shift. The observation of the latency shift with masking is supported by the fact that the low-SR ANFs have longer latency than high-SR fibers and are resistant to background noise [91, 92]. It is not clear why the study did not report the change in wave V amplitude by masking. Theoretically, the masking should produce greater reduction in wave V amplitude in subjects with selective loss of low-SR units. Moreover, no information about the history of noise exposure was reported and it is not clear whether the poorer performance in temporal cue detection was due to noise-induced synaptopathy or other reasons.

To date, the most promising methods for diagnosing cochlear synaptopathy are related to selective loss of low-SR ANFs, the subcortical steady state responses (SSSR) [93, 94]. Based on the animal studies, this test should be carried out using amplitude-modulated signals at relatively high intensity and a shallow modulation depth [95]. The input intensity of the driving signal should fall within the saturation range of the high-SR fibers. High frequency carrier waves with a high intensity and with shallow amplitude modulation are especially useful for evaluating the function of low-SR fibers. This is supported by modeling the loss of low-SR fibers. To differentiate the SSSR contribution from the auditory nerve from that of central neurons, a higher modulation frequency should be used. The optimal modulation frequency is likely to differ across species [96–98]. A recent mouse study found that the modulation frequency close to 1 kHz was optimum with a high frequency carrier without concern of modulation depth [99]. However, a recent human study reported a successful detection of the low-SR unit loss using off-frequency maskers and a shallow modulation depth [95].

Competing Interests

The authors declare that they have no competing interests.

Acknowledgments

This study was supported by grants from Natural Science and Engineering Research Council of Canada (RGPIN-2014-05437) and from Natural Science Foundation of China (81271086 and 81400464). The English in this document has been checked by at least two professional editors, both native speakers of English. For a certificate, please see http://www.textcheck.com/certificate/g8RpDT/.

References

[1] E. Borg, B. Canlon, and B. Engstrom, "Noise-induced hearing loss: literature review and experiments in rabbits. Morphological and electrophysiological features, exposure parameters and temporal factors, variability and interactions," *Scandinavian Audiology*, vol. 40, supplement, pp. 4–146, 1995.

[2] R. Szalai, K. Tsaneva-Atanasova, M. E. Homer, A. R. Champneys, H. J. Kennedy, and N. P. Cooper, "Nonlinear models of development, amplification and compression in the mammalian cochlea," *Philosophical Transactions of the Royal Society of London, Series A: Mathematical, Physical and Engineering Sciences*, vol. 369, no. 1954, pp. 4183–4204, 2011.

[3] A. J. Hudspeth, "Mechanical amplification of stimuli by hair cells," *Current Opinion in Neurobiology*, vol. 7, no. 4, pp. 480–486, 1997.

[4] K. W. Chang and S. J. Norton, "The effects of continuous versus interrupted noise exposures on distortion product otoacoustic emissions in guinea pigs," *Hearing Research*, vol. 96, no. 1-2, pp. 1–12, 1996.

[5] M. Subramaniam, D. Henderson, and V. Spongr, "The relationship among distortion-product otoacoustic emissions, evoked potential thresholds, and outer hair cells following interrupted noise exposures," *Ear & Hearing*, vol. 15, no. 4, pp. 299–309, 1994.

[6] S. G. Kujawa and M. C. Liberman, "Adding insult to injury: cochlear nerve degeneration after 'temporary' noise-induced hearing loss," *The Journal of Neuroscience*, vol. 29, no. 45, pp. 14077–14085, 2009.

[7] H. Wang, S. Yin, Z. Yu, Y. Huang, and J. Wang, "Dynamic changes in hair cell stereocilia and cochlear transduction after noise exposure," *Biochemical and Biophysical Research Communications*, vol. 409, no. 4, pp. 616–621, 2011.

[8] G.-D. Chen and H.-B. Zhao, "Effects of intense noise exposure on the outer hair cell plasma membrane fluidity," *Hearing Research*, vol. 226, no. 1-2, pp. 14–21, 2007.

[9] G.-D. Chen and Y. Liu, "Mechanisms of noise-induced hearing loss potentiation by hypoxia," *Hearing Research*, vol. 200, no. 1-2, pp. 1–9, 2005.

[10] C. Chen, A. Nenov, and R. P. Bobbin, "Noise exposure alters the response of outer hair cells to ATP," *Hearing Research*, vol. 88, no. 1-2, pp. 215–221, 1995.

[11] J. Wang, Q. Li, W. Dong, and J. Chen, "Effects of various noise exposures on endocochlear potentials correlated with cochlear gross responses," *Hearing Research*, vol. 59, no. 1, pp. 31–38, 1992.

[12] Y. Wang, K. Hirose, and M. C. Liberman, "Dynamics of noise-induced cellular injury and repair in the mouse cochlea," *Journal of the Association for Research in Otolaryngology*, vol. 3, no. 3, pp. 248–268, 2002.

[13] D. Henderson and M. Subramaniam, "Advances in our understanding of noise-induced hearing loss," *Applied Occupational and Environmental Hygiene*, vol. 11, no. 4, pp. 255–260, 1996.

[14] H. Sohmer, "Pathophysiological mechanisms of hearing loss," *Journal of Basic and Clinical Physiology and Pharmacology*, vol. 8, no. 3, pp. 113–125, 1997.

[15] W. R. Henry and M. J. Mulroy, "Afferent synaptic changes in auditory hair cells during noise-induced temporary threshold shift," *Hearing Research*, vol. 84, no. 1-2, pp. 81–90, 1995.

[16] M. J. Mulroy, R. F. Fromm, and S. Curtis, "Changes in the synaptic region of auditory hair cells during noise-induced temporary threshold shift," *Hearing Research*, vol. 49, no. 1–3, pp. 79–87, 1990.

[17] D. Robertson, "Functional significance of dendritic swelling after loud sounds in the guinea pig cochlea," *Hearing Research*, vol. 9, no. 3, pp. 263–278, 1983.

[18] M. C. Liberman and M. J. Mulroy, "Acute and chronic effects of acoustic trauma: cochlear pathology and auditory nerve pathophysiology," in *New Perspectives on Noise-Induced Hearing Loss*, R. P. Henderson, D. Henderson, and R. J. Salvi, Eds., pp. 105–135, Raven Press, New York, NY, USA, 1982.

[19] H. Spoendlin, "Primary structural changes in the organ of corti after acoustic overstimulation," *Acta Oto-Laryngologica*, vol. 71, no. 1-6, pp. 166–176, 1971.

[20] Q. Song, P. Shen, X. Li et al., "Coding deficits in hidden hearing loss induced by noise: the nature and impacts," *Scientific Reports*, vol. 6, Article ID 25200, 2016.

[21] L. Shi, X. Guo, P. Shen et al., "Noise-induced damage to ribbon synapses without permanent threshold shifts in neonatal mice," *Neuroscience*, vol. 304, pp. 368–377, 2015.

[22] L. Shi, L. Liu, T. He et al., "Ribbon synapse plasticity in the cochleae of guinea pigs after noise-induced silent damage," *PLoS ONE*, vol. 8, no. 12, Article ID e81566, 2013.

[23] L. Liu, H. Wang, L. Shi et al., "Silent damage of noise on cochlear afferent innervation in guinea pigs and the impact on temporal processing," *PLoS ONE*, vol. 7, no. 11, Article ID e49550, 2012.

[24] G. C. Stamper and T. A. Johnson, "Auditory function in normal-hearing, noise-exposed human ears," *Ear and Hearing*, vol. 36, no. 2, pp. 172–184, 2015.

[25] S. G. Kujawa and M. C. Liberman, "Synaptopathy in the noise-exposed and aging cochlea: primary neural degeneration in acquired sensorineural hearing loss," *Hearing Research*, vol. 330, pp. 191–199, 2015.

[26] C. J. Plack, D. Barker, and G. Prendergast, "Perceptual consequences of 'hidden' hearing loss," *Trends in Hearing*, vol. 18, 2014.

[27] A. C. Furman, S. G. Kujawa, and M. C. Liberman, "Noise-induced cochlear neuropathy is selective for fibers with low spontaneous rates," *Journal of Neurophysiology*, vol. 110, no. 3, pp. 577–586, 2013.

[28] W. Singer, A. Zuccotti, M. Jaumann et al., "Noise-induced inner hair cell ribbon loss disturbs central arc mobilization: a novel molecular paradigm for understanding tinnitus," *Molecular Neurobiology*, vol. 47, no. 1, pp. 261–279, 2013.

[29] D. Robertson, C. Bester, D. Vogler, and W. H. A. M. Mulders, "Spontaneous hyperactivity in the auditory midbrain: relationship to afferent input," *Hearing Research*, vol. 295, pp. 124–129, 2013.

[30] Y. Niu, A. Kumaraguru, R. Wang, and W. Sun, "Hyperexcitability of inferior colliculus neurons caused by acute noise exposure," *Journal of Neuroscience Research*, vol. 91, no. 2, pp. 292–299, 2013.

[31] K.-Y. Lee, "Pathophysiology of age-related hearing loss (peripheral and central)," *Korean Journal of Audiology*, vol. 17, no. 2, pp. 45–49, 2013.

[32] R. Schaette and D. McAlpine, "Tinnitus with a normal audiogram: physiological evidence for hidden hearing loss and computational model," *The Journal of Neuroscience*, vol. 31, no. 38, pp. 13452–13457, 2011.

[33] R. Nouvian, D. Beutner, T. D. Parsons, and T. Moser, "Structure and function of the hair cell ribbon synapse," *Journal of Membrane Biology*, vol. 209, no. 2-3, pp. 153–165, 2006.

[34] T. Moser, A. Brandt, and A. Lysakowski, "Hair cell ribbon synapses," *Cell and Tissue Research*, vol. 326, no. 2, pp. 347–359, 2006.

[35] P. A. Fuchs, E. Glowatzki, and T. Moser, "The afferent synapse of cochlear hair cells," *Current Opinion in Neurobiology*, vol. 13, no. 4, pp. 452–458, 2003.

[36] A. Merchan-Perez and M. C. Liberman, "Ultrastructural differences among afferent synapses on cochlear hair cells: correlations with spontaneous discharge rate," *Journal of Comparative Neurology*, vol. 371, no. 2, pp. 208–221, 1996.

[37] V. G. Magupalli, K. Schwarz, K. Alpadi, S. Natarajan, G. M. Seigel, and F. Schmitz, "Multiple RIBEYE-RIBEYE interactions create a dynamic scaffold for the formation of synaptic ribbons," *The Journal of Neuroscience*, vol. 28, no. 32, pp. 7954–7967, 2008.

[38] R. C. Uthaiah and A. J. Hudspeth, "Molecular anatomy of the hair cell's ribbon synapse," *The Journal of Neuroscience*, vol. 30, no. 37, pp. 12387–12399, 2010.

[39] Z. Jing, M. A. Rutherford, H. Takago et al., "Disruption of the presynaptic cytomatrix protein bassoon degrades ribbon anchorage, multiquantal release, and sound encoding at the hair cell afferent synapse," *The Journal of Neuroscience*, vol. 33, no. 10, pp. 4456–4467, 2013.

[40] D. Khimich, R. Nouvtan, R. Pujol et al., "Hair cell synaptic ribbons are essential for synchronous auditory signalling," *Nature*, vol. 434, no. 7035, pp. 889–894, 2005.

[41] B. N. Buran, N. Strenzke, A. Neef, E. D. Gundelfinger, T. Moser, and M. C. Liberman, "Onset coding is degraded in auditory nerve fibers from mutant mice lacking synaptic ribbons," *The Journal of Neuroscience*, vol. 30, no. 22, pp. 7587–7597, 2010.

[42] T. D. Parsons and P. Sterling, "Synaptic ribbon: conveyor belt or safety belt?" *Neuron*, vol. 37, no. 3, pp. 379–382, 2003.

[43] C. Vogl, B. H. Cooper, J. Neef et al., "Unconventional molecular regulation of synaptic vesicle replenishment in cochlear inner hair cells," *Journal of Cell Science*, vol. 128, no. 4, pp. 638–644, 2015.

[44] R. M. Nemzou N, A. V. Bulankina, D. Khimich, A. Giese, and T. Moser, "Synaptic organization in cochlear inner hair cells deficient for the $Ca_V1.3$ (α1D) subunit of L-type Ca^{2+} channels," *Neuroscience*, vol. 141, no. 4, pp. 1849–1860, 2006.

[45] A. Brandt, D. Khimich, and T. Moser, "Few CaV1.3 channels regulate the exocytosis of a synaptic vesicle at the hair cell ribbon synapse," *The Journal of Neuroscience*, vol. 25, no. 50, pp. 11577–11585, 2005.

[46] R. Pujol and J.-L. Puel, "Excitotoxicity, synaptic repair, and functional recovery in the mammalian cochlea: a review of recent findings," *Annals of the New York Academy of Sciences*, vol. 884, pp. 249–254, 1999.

[47] J.-L. Puel, C. d'Aldin, J. Ruel, S. Ladrech, and R. Pujol, "Synaptic repair mechanisms responsible for functional recovery in various cochlear pathologies," *Acta Oto-Laryngologica*, vol. 117, no. 2, pp. 214–218, 1997.

[48] R. Pujol, J.-L. Puel, C. Gervais d'Aldin, and M. Eybalin, "Pathophysiology of the glutamatergic synapses in the cochlea," *Acta Oto-Laryngologica*, vol. 113, no. 3, pp. 330–334, 1993.

[49] H. W. Lin, A. C. Furman, S. G. Kujawa, and M. C. Liberman, "Primary neural degeneration in the guinea pig cochlea after reversible noise-induced threshold shift," *Journal of the Association for Research in Otolaryngology*, vol. 12, no. 5, pp. 605–616, 2011.

[50] A. M. Craig, E. R. Graf, and M. W. Linhoff, "How to build a central synapse: clues from cell culture," *Trends in Neurosciences*, vol. 29, no. 1, pp. 8–20, 2006.

[51] Y. Jin, "Synaptogenesis," in *WormBook*, pp. 1–11, 2005.

[52] L. Abbas, "Synapse formation: let's stick together," *Current Biology*, vol. 13, no. 1, pp. R25–R27, 2003.

[53] S. Okabe, "Birth, growth and elimination of a single synapse," *Anatomical Science International*, vol. 77, no. 4, pp. 203–210, 2002.

[54] M. A. Adly, I. Spiwoks-Becker, and L. Vollrath, "Ultrastructural changes of photoreceptor synaptic ribbons in relation to time of day and illumination," *Investigative Ophthalmology & Visual Science*, vol. 40, no. 10, pp. 2165–2172, 1999.

[55] F. Schmitz and D. Drenckhahn, "Intermediate stages in the disassembly of synaptic ribbons in cone photoreceptors of the crucian carp, *Carassius carassius*," *Cell & Tissue Research*, vol. 272, no. 3, pp. 487–490, 1993.

[56] F. Schmitz, "The making of synaptic ribbons: how they are built and what they do," *Neuroscientist*, vol. 15, no. 6, pp. 611–624, 2009.

[57] I. Spiwoks-Becker, M. Glas, I. Lasarzik, and L. Vollrath, "Mouse photoreceptor synaptic ribbons lose and regain material in response to illumination changes," *European Journal of Neuroscience*, vol. 19, no. 6, pp. 1559–1571, 2004.

[58] H. Regus-Leidig, D. Specht, S. Tom Dieck, and J. H. Brandstätter, "Stability of active zone components at the photoreceptor ribbon complex," *Molecular Vision*, vol. 16, pp. 2690–2700, 2010.

[59] F. Schmitz, "Presynaptic [Ca^{2+}] and GCAPs: aspects on the structure and function of photoreceptor ribbon synapses," *Frontiers in Molecular Neuroscience*, vol. 7, article 3, 2014.

[60] L. Shi, K. Liu, H. Wang et al., "Noise induced reversible changes of cochlear ribbon synapses contribute to temporary hearing loss in mice," *Acta Oto-Laryngologica*, vol. 135, no. 11, pp. 1093–1102, 2015.

[61] J. Ruel, J. Wang, G. Rebillard et al., "Physiology, pharmacology and plasticity at the inner hair cell synaptic complex," *Hearing Research*, vol. 227, no. 1-2, pp. 19–27, 2007.

[62] L. D. Liberman, H. Wang, and M. C. Liberman, "Opposing gradients of ribbon size and AMPA receptor expression underlie sensitivity differences among cochlear-nerve/hair-cell synapses," *The Journal of Neuroscience*, vol. 31, no. 3, pp. 801–808, 2011.

[63] E. D. Young and P. E. Barta, "Rate responses of auditory nerve fibers to tones in noise near masked threshold," *Journal of the Acoustical Society of America*, vol. 79, no. 2, pp. 426–442, 1986.

[64] J. A. Costalupes, "Representation of tones in noise in the responses of auditory nerve fibers in cats. I. Comparison with detection thresholds," *The Journal of Neuroscience*, vol. 5, no. 12, pp. 3261–3269, 1985.

[65] M. C. Liberman, "Auditory-nerve response from cats raised in a low-noise chamber," *Journal of the Acoustical Society of America*, vol. 63, no. 2, pp. 442–455, 1978.

[66] M. C. Liberman, "Single-neuron labeling in the cat auditory nerve," *Science*, vol. 216, no. 4551, pp. 1239–1241, 1982.

[67] J. J. Eggermont, "Animal models of auditory temporal processing," *International Journal of Psychophysiology*, vol. 95, no. 2, pp. 202–215, 2015.

[68] P. Heil and A. J. Peterson, "Basic response properties of auditory nerve fibers: a review," *Cell and Tissue Research*, vol. 361, no. 1, pp. 129–158, 2015.

[69] L. D. Liberman and M. C. Liberman, "Dynamics of cochlear synaptopathy after acoustic overexposure," *Journal of the Association for Research in Otolaryngology*, vol. 16, no. 2, pp. 205–219, 2015.

[70] G. Mehraei, A. E. Hickox, H. M. Bharadwaj et al., "Auditory brainstem response latency in noise as a marker of cochlear synaptopathy," *The Journal of Neuroscience*, vol. 36, no. 13, pp. 3755–3764, 2016.

[71] L. E. Humes, J. R. Dubno, S. Gordon-Salant et al., "Central presbycusis: a review and evaluation of the evidence," *Journal of the American Academy of Audiology*, vol. 23, no. 8, pp. 635–666, 2012.

[72] J. P. Walton, "Timing is everything: temporal processing deficits in the aged auditory brainstem," *Hearing Research*, vol. 264, no. 1-2, pp. 63–69, 2010.

[73] S. Bertoli, J. Smurzynski, and R. Probst, "Effects of age, age-related hearing loss, and contralateral cafeteria noise on the

discrimination of small frequency changes: psychoacoustic and electrophysiological measures," *Journal of the Association for Research in Otolaryngology*, vol. 6, no. 3, pp. 207–222, 2005.

[74] K. B. Snell, F. M. Mapes, E. D. Hickman, and D. R. Frisina, "Word recognition in competing babble and the effects of age, temporal processing, and absolute sensitivity," *Journal of the Acoustical Society of America*, vol. 112, no. 2, pp. 720–727, 2002.

[75] D. R. Frisina and R. D. Frisina, "Speech recognition in noise and presbycusis: relations to possible neural mechanisms," *Hearing Research*, vol. 106, no. 1-2, pp. 95–104, 1997.

[76] C. A. Bauer, T. J. Brozoski, and K. Myers, "Primary afferent dendrite degeneration as a cause of tinnitus," *Journal of Neuroscience Research*, vol. 85, no. 7, pp. 1489–1498, 2007.

[77] J. J. Eggermont, "Acquired hearing loss and brain plasticity," *Hearing Research*, 2016.

[78] Y. Zhao, Q. Song, X. Li, and C. Li, "Neural hyperactivity of the central auditory system in response to peripheral damage," *Neural Plasticity*, vol. 2016, Article ID 2162105, 9 pages, 2016.

[79] P. O. Laugen Heggdal, J. Brännström, H. J. Aarstad, F. S. Vassbotn, and K. Specht, "Functional-structural reorganisation of the neuronal network for auditory perception in subjects with unilateral hearing loss: review of neuroimaging studies," *Hearing Research*, vol. 332, pp. 73–79, 2016.

[80] A. R. Fetoni, D. Troiani, L. Petrosini, and G. Paludetti, "Cochlear injury and adaptive plasticity of the auditory cortex," *Frontiers in Aging Neuroscience*, vol. 7, article 8, 2015.

[81] J. Syka and N. Rybalko, "Threshold shifts and enhancement of cortical evoked responses after noise exposure in rats," *Hearing Research*, vol. 139, no. 1-2, pp. 59–68, 2000.

[82] J. F. Willott and S. M. Lu, "Noise-induced hearing loss can alter neural coding and increase excitability in the central nervous system," *Science*, vol. 216, no. 4552, pp. 1331–1334, 1982.

[83] S. Yang, W. Su, and S. Bao, "Long-term, but not transient, threshold shifts alter the morphology and increase the excitability of cortical pyramidal neurons," *Journal of Neurophysiology*, vol. 108, no. 6, pp. 1567–1574, 2012.

[84] W. H. A. M. Mulders and D. Robertson, "Hyperactivity in the auditory midbrain after acoustic trauma: dependence on cochlear activity," *Neuroscience*, vol. 164, no. 2, pp. 733–746, 2009.

[85] W. Sun, A. Deng, A. Jayaram, and B. Gibson, "Noise exposure enhances auditory cortex responses related to hyperacusis behavior," *Brain Research*, vol. 1485, pp. 108–116, 2012.

[86] D. Ruggles, H. Bharadwaj, and B. G. Shinn-Cunningham, "Normal hearing is not enough to guarantee robust encoding of suprathreshold features important in everyday communication," *Proceedings of the National Academy of Sciences of the United States of America*, vol. 108, no. 37, pp. 15516–15521, 2011.

[87] J. W. Gu, B. S. Herrmann, R. A. Levine, and J. R. Melcher, "Brainstem auditory evoked potentials suggest a role for the ventral cochlear nucleus in tinnitus," *Journal of the Association for Research in Otolaryngology*, vol. 13, no. 6, pp. 819–833, 2012.

[88] M. Knipper, P. Van Dijk, I. Nunes, L. Rüttiger, and U. Zimmermann, "Advances in the neurobiology of hearing disorders: recent developments regarding the basis of tinnitus and hyperacusis," *Progress in Neurobiology*, vol. 111, pp. 17–33, 2013.

[89] C. A. Makary, J. Shin, S. G. Kujawa, M. C. Liberman, and S. N. Merchant, "Age-related primary cochlear neuronal degeneration in human temporal bones," *Journal of the Association for Research in Otolaryngology*, vol. 12, no. 6, pp. 711–717, 2011.

[90] R. Ivory, R. Kane, and R. C. Diaz, "Noise-induced hearing loss: a recreational noise perspective," *Current Opinion in Otolaryngology & Head & Neck Surgery*, vol. 22, no. 5, pp. 394–398, 2014.

[91] J. Bourien, Y. Tang, C. Batrel et al., "Contribution of auditory nerve fibers to compound action potential of the auditory nerve," *Journal of Neurophysiology*, vol. 112, no. 5, pp. 1025–1039, 2014.

[92] W. S. Rhode and P. H. Smith, "Characteristics of tone-pip response patterns in relationship to spontaneous rate in cat auditory nerve fibers," *Hearing Research*, vol. 18, no. 2, pp. 159–168, 1985.

[93] A. Krishnan, G. M. Bidelman, C. J. Smalt, S. Ananthakrishnan, and J. T. Gandour, "Relationship between brainstem, cortical and behavioral measures relevant to pitch salience in humans," *Neuropsychologia*, vol. 50, no. 12, pp. 2849–2859, 2012.

[94] H. M. Bharadwaj and B. G. Shinn-Cunningham, "Rapid acquisition of auditory subcortical steady state responses using multichannel recordings," *Clinical Neurophysiology*, vol. 125, no. 9, pp. 1878–1888, 2014.

[95] H. M. Bharadwaj, S. Masud, G. Mehraei, S. Verhulst, and B. G. Shinn-Cunningham, "Individual differences reveal correlates of hidden hearing deficits," *The Journal of Neuroscience*, vol. 35, no. 5, pp. 2161–2172, 2015.

[96] D. W. Purcell, S. M. John, B. A. Schneider, and T. W. Picton, "Human temporal auditory acuity as assessed by envelope following responses," *Journal of the Acoustical Society of America*, vol. 116, no. 6, pp. 3581–3593, 2004.

[97] S. Kuwada, J. S. Anderson, R. Batra, D. C. Fitzpatrick, N. Teissier, and W. R. D'Angelo, "Sources of the scalp-recorded amplitude-modulation following response," *Journal of the American Academy of Audiology*, vol. 13, no. 4, pp. 188–204, 2002.

[98] D. Pauli-Magnus, G. Hoch, N. Strenzke, S. Anderson, T. J. Jentsch, and T. Moser, "Detection and differentiation of sensorineural hearing loss in mice using auditory steady-state responses and transient auditory brainstem responses," *Neuroscience*, vol. 149, no. 3, pp. 673–684, 2007.

[99] L. A. Shaheen, M. D. Valero, and M. C. Liberman, "Towards a diagnosis of cochlear neuropathy with envelope following responses," *Journal of the Association for Research in Otolaryngology*, vol. 16, no. 6, pp. 727–745, 2015.